



## CONTINUATION PAGE

Form Approved  
GSAE No. 8704-0188

2

Please refer to the instructions on the reverse side of this form for information regarding the use of this form for reporting individual, marriage, family and social, scientific and educational research projects, and continuing the research of individual investigators. Some questions regarding the Bureau's policies of any other agency of the Department concerning reporting requirements for continuing the research of individual investigators should be referred to the Director, Office of Management and Administration, 1215 Jefferson Davis Highway, Suite 1204, Arlington, VA 22202-4302, and to the Office of Management and Administration, Personnel Administration Project #704-1182, Washington, DC 20503.

1. AGENCY USE ONLY (Leave blank)	2. REPORT DATE February 1994	3. REPORT TYPE AND DATES COVERED FINAL 3/15/89 - 7/15/93
4. TITLE AND SUBTITLE NEW MECHANISMS FOR TOUGHENING CERAMIC MATERIALS		5. FUNDING NUMBERS F49620-89-C-0054 DARPA Order No. 5994.
6. AUTHOR(S) Raymond A. Cutler, Anil V. Virkar, L.E. Cross, Fred F. Lange		
7. PERFORMING ORGANIZATION NAME(S) AND ADDRESS(ES) Ceramatec, Inc. Pennsylvania State Univ. Salt Lake City, UT University Park, PA University of Utah University of California at Salt Lake City, UT Santa Barbara, CA		8. PERFORMING ORGANIZATION REPORT NUMBER AFOSR-TR-94 0152 PROG: 94640001
9. SPONSORING/MONITORING AGENCY NAME(S) AND ADDRESS(ES) USAF, AFSC DARPA Air Force Office of 3701 N. Fairfax Dr. Scientific Research Arlington, VA 22203-1714 Bolling AFB, DC 20332-6448		10. SPONSORING/MONITORING AGENCY REPORT NUMBER F49620-89-C-0054

11. SUPPLEMENTARY NOTES	<p><b>DTIC</b> ELECTE DISTRIBUTION CODE <b>S F D</b> APR 21 1994</p>
12. DISTRIBUTION/AVAILABILITY STATEMENT Approved for public release; distribution unlimited.	

13. ABSTRACT (Maximum 200 words)  
Ferroelastic toughening was identified as a viable mechanism for toughening ceramics. Domain structure and domain switching was identified by x-ray diffraction, transmission optical microscopy, and transmission electron microscopy in zirconia, lead zirconate titanate and gadolinium molybdate. Switching in compression was observed at stresses greater than 600 MPa and at 400 MPa in tension for polycrystalline t'-zirconia. Domain switching contributes to toughness, as evidenced by data for monoclinic zirconia, t'-zirconia, PZT and GZO. The magnitude of toughening varied between 0.6 MPa·m<sup>1/2</sup> for GZO to 2-6 MPa·m<sup>1/2</sup> for zirconia. Polycrystalline monoclinic and t'-zirconias, which showed no transformation toughening, had similar toughness values as Y-TZP which exhibits transformation. Coarse-grained monoclinic and tetragonal (t') zirconia samples could be cooled to room temperature for mechanical property evaluation since fine domain size, not grain size, controlled transformation for t'-zirconia and minimized stress for m-ZrO<sub>2</sub>. LnAlO<sub>3</sub>, LnNbO<sub>4</sub>, and LnCrO<sub>3</sub> were among the materials identified as high temperature ferroelastics.

14. SUBJECT TERMS Ferroelastic toughening, twinning, domain switching		15. NUMBER OF PAGES
17. SECURITY CLASSIFICATION OF REPORT		16. PRICE CODE
18. SECURITY CLASSIFICATION OF THIS PAGE	19. SECURITY CLASSIFICATION OF ABSTRACT	20. LIMITATION OF ABSTRACT

**FINAL REPORT**

Approved for public release;  
distribution unlimited.

February 1994

**NEW MECHANISM FOR TOUGHENING CERAMIC MATERIALS**

Submitted by  
Ceramatec, Inc.  
2425 South 900 West  
Salt Lake City, Utah 84119

Contract No. F49620-89-C-0054  
ARPA Order 5994, Program Code 7Y10  
March 15, 1989-July 15, 1993  
Contract Amount: \$928,060  
Contractor: Ceramatec, Inc.

Principal Investigator: Dr. Raymond A. Cutler (801) 972-2455  
Subcontractor: University of Utah

Principal Investigator: Prof. Anil V. Virkar (801) 581-5396  
Subcontractor: Pennsylvania State University

Principal Investigator: Prof. L. E. Cross (814) 865-1154  
Subcontractor: University of California at Santa Barbara

Principal Investigator: Prof. F. F. Lange (805) 893-8248

Sponsored by  
Advanced Research Projects Agency  
ARPA Order No. 5994

Monitored by AFOSR under Contract No. F496-89-C-0054  
Program Manager: Lt. Col. Larry W. Burggraf (202) 767-4933

The views and conclusions contained in this document are those of the authors and should not be interpreted as necessarily representing the official policies or endorsements, either expressed or implied, of the Advanced Research Projects Agency or the U. S. Government.

DTIC QUALITY INSPECTED 3

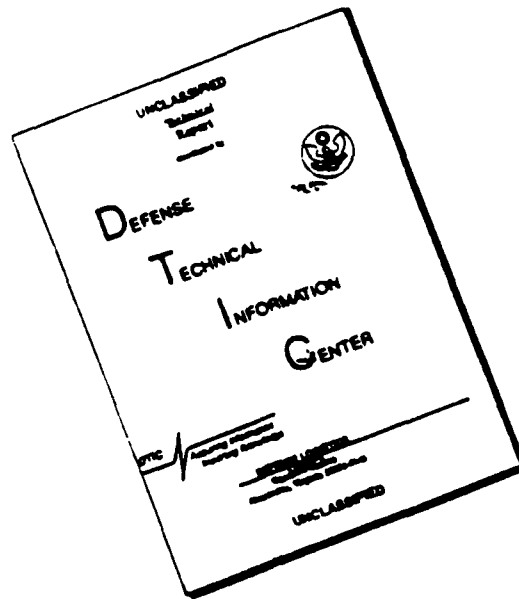
**Ceramatec**

94 - 20 117

397274  
94-12044  
26410x



# DISCLAIMER NOTICE



THIS DOCUMENT IS BEST QUALITY AVAILABLE. THE COPY FURNISHED TO DTIC CONTAINED A SIGNIFICANT NUMBER OF PAGES WHICH DO NOT REPRODUCE LEGIBLY.





mechanical deformation and fracture using a variety of characterization techniques, (2) Isolate the ferroelastic effects from transformation in  $ZrO_2$ , (3) Determine the potential magnitude of toughening in  $ZrO_2$ , (4) Determine if ferroelastic toughening can occur in other materials, and (5) Identify other ferroelastics with potential for ferroelastic toughening.

The approach applied included fabrication of ferroelastic ceramic materials, characterization by x-ray diffraction, mechanical properties, transmission optical and electron microscopy, Raman spectroscopy, Perturbed-angular-correlation (PAC) measurements, hot grinding, and ageing experiments.

The program has met all of the objectives. It demonstrated that ferroelastic toughening occurs in monoclinic and tetragonal  $ZrO_2$ ,  $Gd_2(MoO_4)_3$  (GMO) and lead-zirconate-titanate (PZT). Domain switching was affected by the application of an external uniform stress as well as in the near stress field of a crack tip. Its occurrence in the near stress field of a crack tip implies that domain switching in a natural manner provides a mechanism for toughening. Toughness enhancement on the order of two to three times is possible. Rare earth aluminates, niobates and chromates were identified as high temperature ferroelastics and TiAl has been identified as a possible high temperature ferroelastic.

The implications of the research are significant since they suggest that as we gain further insight into ferroelasticity we may be able to engineer the properties of materials through understanding the crystallography and the characteristics of the phase transition.

The principal outcome of the work done is that ferroelastic domain switching is a viable toughening mechanism and a significant amount of toughness in tetragonal zirconia is due to ferroelastic effects (on the order of  $\approx 2$ - $6$  MPa $\sqrt{m}$ ). Eighteen papers, listed below, have resulted from this funding. The papers below are the body of the report.

## II. A BRIEF SUMMARY OF THE RESULTS

### Refereed Publications:

1. G. V. Srinivasan, J. F. Jue, S. Y. Kuo and A. V. Virkar, "Ferroelastic Domain Switching in Polydomain Tetragonal Zirconia Single Crystals," *J. Am. Ceram. Soc.*, **72**[11] 2098-103 (1989).
2. K. Mehta and A. V. Virkar, "Fracture Mechanisms in Ferroelectric-Ferroelastic Lead Zirconate Titanate (Zr:Ti=0.54:0.46) Ceramics," *J. Am. Ceram. Soc.*, **73**[3] 567-74 (1990).
3. K. Mehta, J. F. Jue and A. V. Virkar, "Grinding-Induced Texture in Ferroelastic Tetragonal Zirconia," *J. Am. Ceram. Soc.*, **73**[6] 1777-79 (1990).
4. J. F. Jue and A. V. Virkar, "Fabrication, Microstructural Characterization and Mechanical Properties of Polycrystalline  $t'$ -Zirconia," *J. Am. Ceram. Soc.*, **73**[12] 3650-57 (1990).

5. R. A. Cutler, R. J. Mayhew, K. M. Prettyman and A. V. Virkar, "High Toughness Ce-TZP/ $\text{Al}_2\text{O}_3$  Ceramics With Improved Hardness and Strength," *J. Am. Ceram. Soc.*, **74**[1] 179-86 (1991).
6. C. J. Chan, F. F. Lange, M. Rühle, J. F. Jue and A. V. Virkar, "Ferroelastic Domain Switching in Tetragonal Zirconia," *MRS Proceedings* (1991).
7. C. J. Chan, F. F. Lange, M. Rühle, J. F. Jue and A. V. Virkar, "Ferroelastic Domain Switching in Tetragonal Zirconia-Microstructural Aspects," *J. Am. Ceram. Soc.*, **74**[4] 807-13 (1991).
8. G. L. Gatchen, I. D. Williams, D. M. Spaar, S. J. Wukitch and J. M. Adams, "Highly Asymmetric Electric-Field Gradients at the Nb Sites in Ferroelastic  $\text{GdNbO}_4$  and  $\text{NdNbO}_4$ ," *Phys. Rev. B*, **43** 1138-41 (1991).
9. A. V. Virkar, J. F. Jue, P. Smith, K. Mehta and K. Prettyman, "The Role of Ferroelasticity in Toughening of Brittle Materials," *Phase Transitions*, **35** 27-46 (1991).
10. J. F. Jue, J. Chen and A. V. Virkar, "Low-Temperature Aging of  $t'$ -Zirconia: The Role of Microstructure on Phase Stability," *J. Am. Ceram. Soc.*, **74**[8] 1811-20 (1991).
11. K. M. Prettyman, J-F. Jue and A. V. Virkar, "Hysteresity Effects in Three Mole Percent Ytria-Doped Zirconia ( $t'$  phase)," *J. Mater. Sci.*, **27**[4] 4167-74 (1992).
12. R. A. Cutler, J. R. Reynolds, and A. Jones, "Sintering and Characterization of Polycrystalline Monoclinic, Tetragonal, and Cubic Zirconia," *J. Am. Ceram. Soc.*, **75**[8] 2137-83 (1992).
13. A. Seifert, F. F. Lange and J. S. Speck, "Liquid Precursor Route for Hetero-epitaxy of  $\text{Zr}(\text{Y})\text{O}_2$  Thin Films on (001) Cubic Zirconia," *J. Am. Ceram. Soc.*, **76**[2] 443-48 (1993).
14. T. Log, R. A. Cutler, J. F. Jue and A. V. Virkar, "Polycrystalline  $t'$ - $\text{ZrO}_2(\text{LnO}_2)$  Formed by Displacive Transformations," *J. Mater. Sci.*, **28**, 4503-09 (1993).
15. R. A. Cutler, J. M. Lindemann, J. H. Ulvensøen and H. I. Lange, "Damage-Resistant SrO-Doped Ce-TZP/ $\text{Al}_2\text{O}_3$  Composites," to appear in *Materials & Design*, **15** (1994).

Publications to be published in referred journals:

16. P. C. Smith and A. V. Virkar, "Ferroelastic Fracture Properties of Gadolinium Molybdate and Isotypic Compounds," to be submitted to *J. Am. Ceram. Soc.*
17. J. Fong, J. Chen and A. V. Virkar, "Characterization of  $t'$  Phase in Ce-TZP Materials," to be submitted to *J. Am. Ceram. Soc.*

18. J. Chen, A. V. Virkar and R. A. Cutler, "Polycrystalline Polydomain Monoclinic Zirconia," to be submitted to *J. Am. Ceram. Soc.*

Graduate Student Theses and Dissertations:

19. P. C. Smith, "Fracture of Ferroelastic Gadolinium Molybdate," Master's Thesis, University of Utah (1990).

20. J. F. Jue, "Fabrication and Characterization of t'-Zirconia," Ph.D. Dissertation, University of Utah (1991).

21. K. M. Prettyman, "Ferroelastic Domain Formation and Switching as a Toughening Mechanism in Ceria-Doped Zirconia," Ph.D. Dissertation, University of Utah (1991).

22. K. Mehta, "Fracture of Ferroelectric-Ferroelastic Lead Zirconate Titanate Ceramics," Master's Thesis, University of Utah (1994).

Important Conclusions of the Work

1. Domain structure and domain switching were identified by XRD, TOM, and TEM in ZrO<sub>2</sub>, PZT and GMO. Switching in compression was observed at stresses > 600 MPa and at 400 MPa in tension for polycrystalline t'-ZrO<sub>2</sub>.

2. Domain switching contributes to toughness, as evidenced by data for m-ZrO<sub>2</sub>, t'-ZrO<sub>2</sub>, PZT and GMO. The magnitude of toughening varied between ≈0.6 MPa√m for GMO to 2-6 MPa√m for ZrO<sub>2</sub>.

3. Single crystal t'-ZrO<sub>2</sub> had a SENB toughness of 8 MPa√m at 1000°C. This value is similar to Y-TZP at room temperature. Polycrystalline m-ZrO<sub>2</sub> and t'-ZrO<sub>2</sub>, which show no transformation toughening, had similar toughness values as Y-TZP which exhibits transformation.

4. Coarse-grained polycrystalline m and t'-ZrO<sub>2</sub> samples could be cooled to room temperature for mechanical property evaluation since fine domain size, not grain size, controlled transformation for t'-ZrO<sub>2</sub> and minimized stress during the t-->m transformation for m-ZrO<sub>2</sub>.

5. Relaxation experiments on PZT showed that switching is rate-dependent (is expected to occur only near the crack tip in tension in many materials). Fracture toughness decreases as T<sub>c</sub> is approached. Switching on fracture surfaces was observed in ZrO<sub>2</sub>, PZT and GMO.

6. Hot grinding showed that transformation, reversible or otherwise, is not responsible for texture, and in-situ tension XRD showed it does not contribute to toughness.

7.  $\text{LnAlO}_3$ ,  $\text{LnNbO}_4$ , and  $\text{LnCrO}_3$  materials have been identified as high temperature ferroelastics.  $\text{TiAl}$  has been identified as a possible high temperature ferroelastic.

8. Multi-variant  $\text{ZrO}_2$ (3 mol. %  $\text{Y}_2\text{O}_3$ ) thin films were epitaxially formed on cubic single crystal substrates. The two variants with the  $c_t$ -axis parallel the substrate/thin film interface are energetically more favorable than the variant with  $c_t$  normal to the interface.

9. Polycrystalline  $t'$ - $\text{ZrO}_2$  was fabricated by heat treating presintered Ce-TZP materials at  $2050^\circ\text{C}$  in air. The existence of  $t'$  phase was confirmed by TOM, SEM and TEM. Fracture toughness is similar between  $t'$  and  $t$  materials despite significantly lower  $t \rightarrow m$  transformation during fracture. Under mechanical stress, both  $t$  and  $t'$  materials can create and annihilate tetragonal variants in order to accommodate the mechanical stresses.

10. Transmission electron microscopy of monoclinic zirconia cooled from the cubic stability regime shows 12 variants, as expected from group theory. These variants accommodate stress and allow polycrystalline materials to be cycled through the  $m \leftrightarrow t$  transformations without catastrophic failure.

#### REFERENCES

1. R. P. Ingel, D. Lewis, B. A. Bender, and R. W. Rice, "Temperature Dependence of Strength and Fracture Toughness of  $\text{ZrO}_2$  Single Crystals," *J. Am. Ceram. Soc.*, **65** C-150-52 (1982).
2. T. C. Yuan, G. V. Srinivasan, J. F. Jue and A. V. Virkar, "Dual-Phase Magnesia-Zirconia Ceramics with Strength Retention at Elevated Temperature," *J. Mater. Sci.* **24** 3855-64 (1989).
3. D. Michel, L. Mazerolles, and M. Perez y Jorba, "Fracture of Metastable Tetragonal Zirconia Crystals," *J. Mater. Sci.*, **18** 2618-28 (1983).
4. K. Aizu, *Phys. Rev. Condensed Matter*, **2**[3] 754-72 (1970).
5. A. V. Virkar and R. L. K. Matsumoto, "Ferroelastic Domain Switching as a Toughening Mechanism in Tetragonal Zirconia," *J. Am. Ceram. Soc.* **69**[10] C-224-26 (1986).

# Ferroelastic Domain Switching in Polydomain Tetragonal Zirconia Single Crystals

Gajawalli V. Srinivasan, Jan-Fong Jue,\* Shih-Yee Kuo,\* and Anil V. Virkar\*

Department of Materials Science and Engineering, University of Utah, Salt Lake City, Utah 84112

As-received, yttria-doped (4.2 wt%  $Y_2O_3$ ) single crystals of zirconia were heated to  $\geq 2100^\circ C$  in air. Cube-shaped samples with faces perpendicular to  $\langle 100 \rangle$  axes on the basis of the pseudocubic symmetry were cut from the crystals. X-ray and electron diffraction indicated that the crystals are polydomain with  $[001]$  axes, on the basis of the tetragonal symmetry, in three mutually orthogonal directions (perpendicular to the cube faces). The cube-shaped crystals were tested in compression at temperatures as high as  $1400^\circ C$ . X-ray diffraction indicated that ferroelastic domains underwent reorientation (switching) in compression. Subsequently, notched samples with the long direction of the beams along  $\langle 100 \rangle$  on the basis of the pseudocubic symmetry were fractured in three-point bending at temperatures as high as  $1000^\circ C$ . X-ray diffraction from fracture surfaces showed that domain reorientation had occurred and that no monoclinic phase was observed on fracture or ground surfaces. The fracture toughness at room temperature and at  $1000^\circ C$  was  $\sim 12$  and  $\sim 8 \text{ MPa} \cdot \text{m}^{1/2}$ , respectively. Preliminary experiments on polycrystalline tetragonal zirconia samples containing 5.4 wt%  $Y_2O_3$  and sintered at  $\geq 2100^\circ C$  also showed no evidence of the monoclinic phase on fracture or ground surfaces. The toughness of the polycrystalline samples was typically  $7.7 \text{ MPa} \cdot \text{m}^{1/2}$ . These results indicate that ferroelastic domain switching can occur during fracture and may contribute to toughness. [Key words: zirconia, ferroelastic materials, single crystals, domains, fracture toughness.]

## I. Introduction

HIGH toughness and/or strength of many zirconia-based ceramics are known to be due to transformation toughening. In these materials, the toughness and the strength decrease with increasing temperature, since the thermodynamic driving force for transformation of the metastably retained tetragonal phase into the stable monoclinic polymorph decreases with increasing temperature. As a result, above about  $800^\circ$  to  $900^\circ C$ , no contribution to transformation to the overall toughness is expected. Indeed, numerous zirconia-based materials do exhibit loss of strength and toughness with increasing temperature. There are, however, some tetragonal zirconia materials in which high strength and toughness can be retained to temperatures above the monoclinic  $\rightarrow$  tetragonal transition temperature. Also, there are materials in which the toughness and the strength do not decrease with increasing temperature. The data of Ingel *et al.*<sup>1,2</sup> on yttria-stabilized tetragonal zirconia single crystals showed a strength of  $\sim 700 \text{ MPa}$  up to  $1600^\circ C$ . By contrast, the strength of the corresponding cubic crystals was only  $350 \text{ MPa}$ . In a study by Michel *et al.*,<sup>3</sup> the toughnesses of tetragonal and cubic crystals were  $\sim 6$  and  $\sim 1.8 \text{ MPa} \cdot \text{m}^{1/2}$ , respectively. Similarly, the work of Yuan *et al.*<sup>4</sup> on polycrystalline ceramics containing 40 vol%  $ZrO_2$  and 60 vol%  $MgO$  shows that the strength is independent of tempera-

ture up to the maximum testing temperature of  $1000^\circ C$ . X-ray diffraction from fracture surfaces of either the single crystals or the  $MgO-ZrO_2$  ceramics failed to reveal the existence of the monoclinic phase. Failure to observe the monoclinic phase could possibly be explained on the premise that reverse transformation to the tetragonal phase may have occurred during the fracture process, as observed in some other polycrystalline zirconia materials. However, the high strength of tetragonal zirconia single crystals above  $1000^\circ C$  in the study by Ingel *et al.*<sup>1,2</sup> cannot be explained on the basis of reverse transformation, as the  $m \rightarrow t$  transition in zirconia containing 4.2 wt%  $Y_2O_3$  is  $\leq 700^\circ C$ . Also, the constancy of strength and toughness up to  $1000^\circ C$ , the maximum test temperature, in a study by Yuan *et al.*<sup>4</sup> cannot be explained on the basis of transformation toughening.

During an investigation of a polycrystalline ceria-stabilized, tetragonal zirconia (Ce-TZP) ceramic, no monoclinic phase was observed on ground surfaces.<sup>5</sup> However, surface grinding led to the development of crystallographic texture.<sup>5</sup> After surface grinding, the X-ray peak intensity of the (002) peak increased significantly, while that of the (200) peak decreased. Similar effects were observed for the (113) and (131) peaks. The enhancement of the intensity of the (002) peak indicates that many of the crystallites in the near-surface region reoriented themselves upon grinding in such a way that their  $c$  axes became orthogonal to the surface. According to Michel *et al.*,<sup>3</sup> the cubic  $\rightarrow$  tetragonal displacive transformation in zirconia is a ferroelastic transition. Using Aizu's<sup>6,7</sup> notations, the representative species is given by  $m3mF4/mmm$ . Based on group theory considerations, the tetragonal phase is expected to be a ferroelastic phase. For a material to be ferroelastic, the crystal must exist in at least two energetically equivalent orientational states and it must be possible, at least in principle, to shift the crystal from one state into the other by the application of an external stress. The development of texture upon grinding is consistent with the existence of ferroelasticity in tetragonal zirconia. Later work showed that similar texture can be developed in  $BaTiO_3$  and PZT, which are known to be simultaneously ferroelectric-ferroelastic materials.<sup>8,9</sup>

The objective of the present work was to examine the role of ferroelasticity in zirconia ceramics. The majority of zirconia ceramics do exhibit transformation, which makes unequivocal identification of ferroelastic effects difficult. Published information on tetragonal zirconia single crystals indicates that these crystals do not readily undergo transformation to the monoclinic phase.<sup>3</sup> This suggests that tetragonal single crystals are ideally suited to examine the ferroelastic behavior. For this reason, the experimental part of this investigation was primarily confined to single crystals of tetragonal zirconia stabilized by the addition of 4.2 wt%  $Y_2O_3$ , although a few experiments were conducted on sintered, polycrystalline zirconia ceramics.

## II. Experimental Procedure

As-received crystals\* (4.2 wt%  $Y_2O_3$ ) were mounted on a two-axis goniometer and oriented using Laue back reflection. Cube-shaped crystals, approximately  $3 \text{ mm} \times 3 \text{ mm} \times 3 \text{ mm}$ , were cut out of the crystals in such a way that the  $\langle 100 \rangle$  axes on the basis of the pseudocubic symmetry were orthogonal to the surfaces of the cubes. Bar-shaped samples,  $3 \text{ mm} \times 3 \text{ mm} \times 25 \text{ mm}$ , were also cut in such a way that the long direction of the bar was along

Manuscript No. 199030. Received July 1, 1988; approved April 14, 1989.

Supported by DARPA through AFOSR under Contract No. F49620-87-C-0077 through a subcontract from Ceramtec to the University of Utah.

\*Member, American Ceramic Society.

\*Ceres Corp., Waltham, MA.

(100). Some of the samples were then heated in a gas-fired furnace to a temperature  $\geq 2100^\circ\text{C}$  in air. The exact temperature could not be accurately determined for lack of a direct view of the hot zone. The temperature at the flame entry tube was as high as  $\sim 2400^\circ\text{C}$ . It is believed that the actual sample temperature was  $\geq 2100^\circ\text{C}$ . The hold time at temperature was about 10 min. However, about 2 h was necessary to raise the temperature from  $\sim 1600^\circ$  to  $\geq 2100^\circ\text{C}$ . After 10 min at  $\geq 2100^\circ\text{C}$ , the platform containing the samples was immediately lowered to a region in the furnace where the temperature was  $\sim 1400^\circ\text{C}$ . The reason for relatively rapid cooling to  $1400^\circ\text{C}$  was to prevent (or minimize) the precipitation of tetragonal phase by a diffusive process. Subsequently, the crystals were furnace-cooled to room temperature. A few polycrystalline zirconia samples containing 5.4 wt%  $\text{Y}_2\text{O}_3$  (Tosoh powder), prepared at  $1500^\circ\text{C}/2$  h, were heat-treated in the gas-fired furnace at  $\geq 2100^\circ\text{C}$ . The objective of this work was to determine if nontransformable polycrystalline zirconia samples can be fabricated by heating them in the stability range of the cubic phase field.

The cube-shaped samples were subjected to compressive loading at room temperature as well as at temperatures up to  $1400^\circ\text{C}$ . Compressive testing at elevated temperatures was conducted using a silicon carbide loading fixture heated by molybdenum disilicide heating elements. At room temperature, the applied stresses were as high as  $\sim 2.25$  GPa. At elevated temperatures, the maximum applied stress was on the order of 300 MPa. The objective of the compression tests was to determine if domain reorientation (switching) can be effected by compressive loading. Thin notches were machined in the bar-shaped samples for the measurement of fracture toughness,  $K_{Ic}$ , using the single-edge notched-beam (SENB) technique in three-point bending. The samples were broken at room temperature and at  $1000^\circ\text{C}$ .

X-ray diffraction traces using  $\text{CuK}\alpha$  radiation were obtained from (1) ground surfaces, (2) fracture surfaces, and (3) surfaces of the cube-shaped crystals subjected to compression testing. The objective was to determine if domain reorientation occurred in any of the samples, and if any monoclinic phase was present in these crystals.

For examination in a scanning transmission electron microscope, samples were prepared by dimple grinding followed by ion-milling to perforation. Samples were oriented in such a way that the foil surfaces were orthogonal to the (001) axis on the basis of the pseudocubic symmetry. Polycrystalline samples were polished and etched in HF to reveal the grain structure.

### III. Results

#### (1) X-ray Diffraction

In the range of  $2\theta$  from  $33^\circ$  to  $37^\circ$  and from  $72^\circ$  to  $76^\circ$ , generally either two, three, or even four peaks were observed from the surfaces of the cube-shaped samples cut from the as-received single crystals. A typical X-ray diffractometer trace in the  $2\theta$  range between  $72^\circ$  and  $76^\circ$  from the as-received crystal is shown in Fig. 1(A). In the same ranges of  $2\theta$ , only two peaks were observed in samples that had been annealed at  $\geq 2100^\circ\text{C}$ , as shown in Fig. 1(B). X-ray traces shown in Figs. 1(A) and (B) are typical of the traces obtained from any of the six cube surfaces. The peaks in the annealed sample are identified as (400)*d* and (004)*d* of the single-phase tetragonal crystals. The corresponding *c/a* is about 1.015. Of the four peaks observed in the X-ray traces from the as-received crystal, the inner two and the outer two are labeled (400)*d* and (004)*d*, and (400)*p* and (004)*p*, respectively. The *c/a* ratios corresponding to the inner and outer sets of peaks are 1.006 and 1.0215, respectively.

X-ray diffraction traces from cube-shaped samples that had been annealed at  $\geq 2100^\circ\text{C}$  (and polished) show (002) and (004) peaks of lower intensities than the (200) and (400) peaks, respectively. This result is consistent with an X-ray diffraction trace from a powder of the tetragonal phase. After surface grinding and/or cutting, however, the intensities of the (002) and (004) peaks were invariably greater than those of the (200) and (400) peaks, respectively. The sample whose X-ray trace is

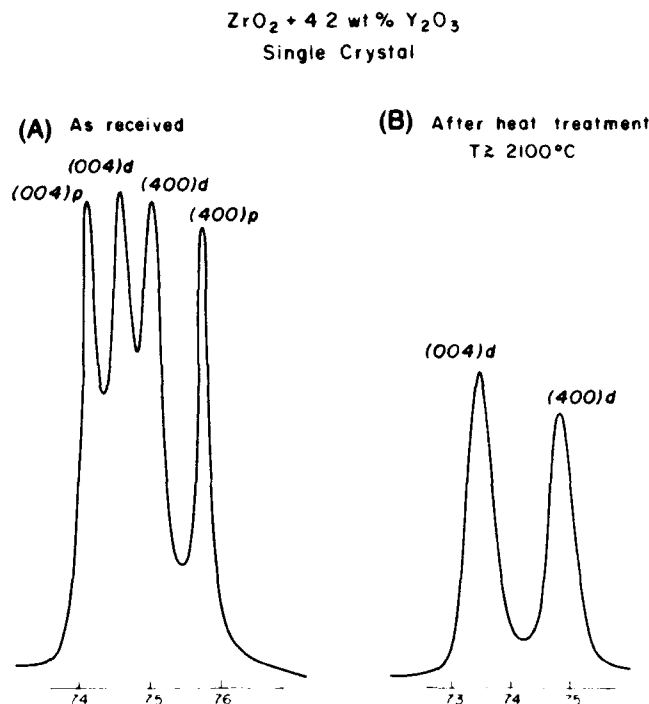


Fig. 1. (A) X-ray diffraction trace in the  $2\theta$  range between  $72^\circ$  and  $76^\circ$  from an as-received crystal (cube faces orthogonal to (100) on the basis of the pseudocubic symmetry) showing peaks from the displacively formed and precipitated tetragonal phases. (B) X-ray diffraction trace in the  $2\theta$  range between  $72^\circ$  and  $76^\circ$  from an annealed ( $\geq 2100^\circ\text{C}$ ) crystal (cube faces orthogonal to (100) on the basis of the pseudocubic symmetry) showing peaks from the displacively formed tetragonal phase.

shown in Fig. 1(B) was ground. After polishing the ground sample, the intensity of the (002) peak decreased and that of the (200) peak increased. However, even after removing the surface layer to a depth of  $\sim 15 \mu\text{m}$ , the intensity ratio of (002) to (200) was greater than the one corresponding to the powder pattern. This suggests that the depth of the texture developed by grinding was at least  $15 \mu\text{m}$ .

Polycrystalline zirconia samples fabricated by first sintering at  $1500^\circ\text{C}$  followed by heating to  $\geq 2100^\circ\text{C}$  were also examined by X-ray diffraction. Samples were found to be of the tetragonal symmetry. No monoclinic phase was observed in the X-ray diffraction traces from ground and fracture surfaces. However, increase in the intensities of (002) and (004) peaks readily occurred upon surface grinding.

Prior to compression testing of cube-shaped crystals, X-ray diffraction traces were obtained from two surfaces: the surface upon which compressive loads were to be applied and one of the side surfaces. After compression testing, X-ray diffraction traces were again obtained from the same two surfaces. Figure 2 shows X-ray diffraction traces from the surface of an annealed and ground sample subjected to compression ( $\sim 2.25$  GPa) at room temperature, before and after the test. As shown in the figure, the intensities of (002) and (004) peaks decrease and those of (200) and (400) peaks increase after compression testing. Figure 3 shows X-ray traces from the side subjected to compression ( $\sim 300$  MPa) at  $1400^\circ\text{C}$  and from one of the side faces, both before and after the test. After compression testing, the intensity of the (002) peak decreased and that of the (200) peak increased from the surface that was subjected to compressive stress. This observation is consistent with that at room temperature (Fig. 2). By contrast, the intensity of the (002) peak increased and that of (200) decreased from the side surfaces. Similar results were obtained from samples tested at  $1000^\circ$  and  $1200^\circ\text{C}$ . Samples tested at  $1000^\circ$  and  $1200^\circ\text{C}$  were subjected to compressive stresses of 450 and 300 MPa, respectively.

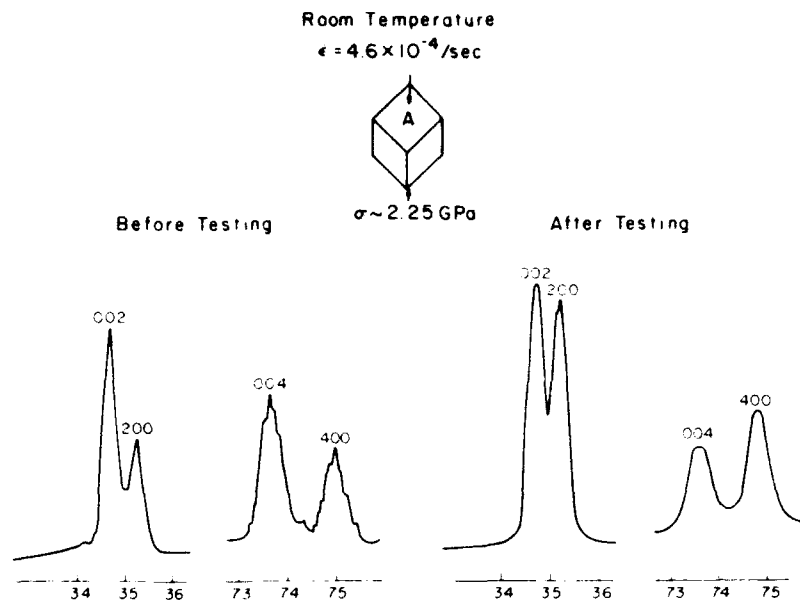


Fig. 2. X-ray diffraction traces from an annealed, cube-shaped sample subjected to compressive loading at room temperature, showing ferroelastic domain switching.

## (2) Microscopy

Figures 4(A) and (B) show electron diffraction patterns of the as-received and annealed samples, respectively. As seen in Fig. 4(B), higher-order spots are split. The diffraction pattern from the as-received crystal is similar to that from the annealed sample except that there are several additional spots (Fig. 4(A)). These additional spots are due to the tetragonal precipitates, some of which transformed to the monoclinic phase. These precipitates are formed by a diffusional process during the presumably slow cool-down after the crystal growth. An electron micrograph of the annealed sample for zone axis (001) is shown in Fig. 5. This structure is similar to the one reported by Lanteri and co-workers<sup>10</sup> and Sakuma.<sup>11</sup>

An optical micrograph of a polycrystalline sample annealed at  $\geq 2100^\circ\text{C}$  is shown in Fig. 6. The sample was etched in HF. The

grain size of the sample is  $\geq 100 \mu\text{m}$ . The density of the sample was  $6.05 \text{ g/mL}$ .

## (3) Fracture Toughness Measurements

The toughness values of the single crystals at room temperature and at  $1000^\circ\text{C}$  were  $\sim 12$  and  $\sim 8 \text{ MPa} \cdot \text{m}^{1/2}$ , respectively. As mentioned previously, no monoclinic phase was observed on the fracture surfaces. As indicated by Michel *et al.*,<sup>3</sup> two peaks corresponding to the monoclinic phase, if present, are expected on the low-angle side of the (004) peak. No such peaks were observed. On the other hand, an enhancement of the (002) peak intensity was observed. X-ray diffraction traces obtained from samples fractured at room temperature and at  $1000^\circ\text{C}$  are shown in Figs. 7(A) and (B), respectively. As seen in these figures, the intensity of the (002) peak increased and that of the (200) peak

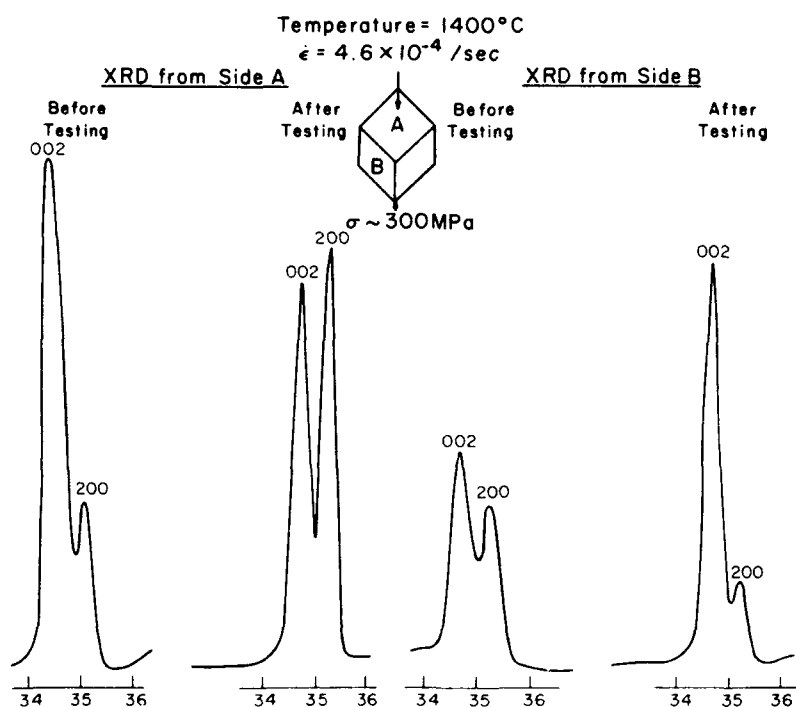
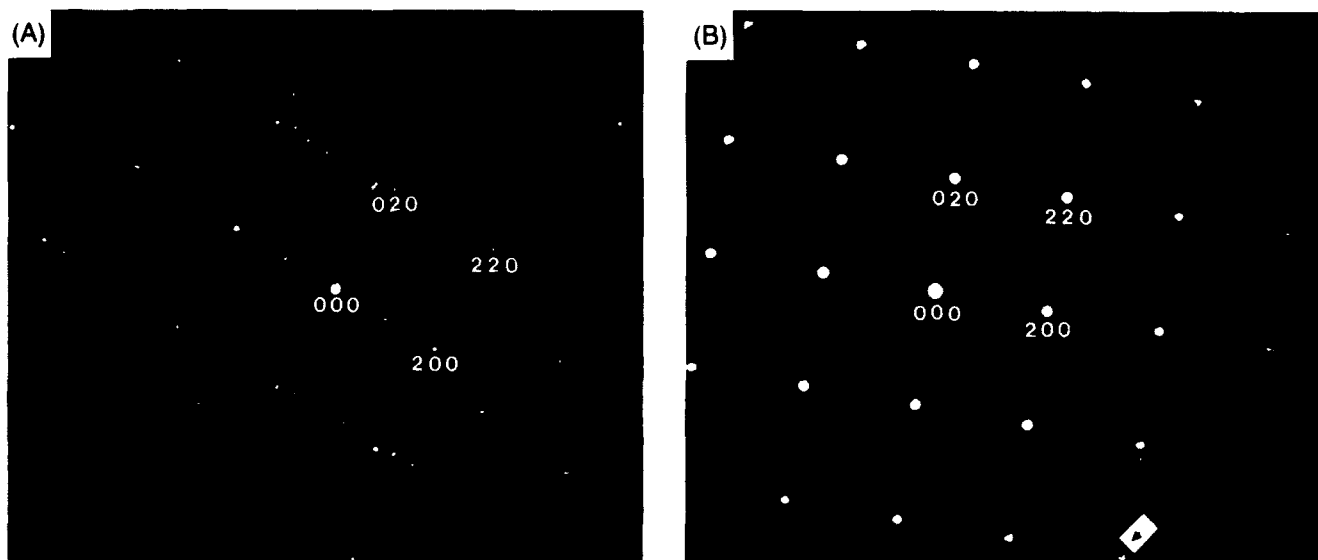


Fig. 3. X-ray diffraction traces from an annealed, cube-shaped sample subjected to compressive loading at  $1400^\circ\text{C}$ , showing ferroelastic domain switching.



**Fig. 4.** (A) Electron diffraction pattern from an as-received crystal along zone axis (100) on the basis of the pseudocubic symmetry. The labeled spots correspond to the tetragonal symmetry. Additional spots are due to the monoclinic phase. (B) Electron diffraction pattern from an annealed crystal zone axis (100) on the basis of a pseudocubic symmetry. The presence of the three variants of the displacively formed tetragonal phase is evidenced by the existence of additional spots indicated by the arrow.

decreased for the sample fractured at 1000°C. For the sample fractured at room temperature also, the intensity of the (002) peak is greater than that from the pristine surface. Toughness of the polycrystalline zirconia samples sintered at  $\geq 2100^\circ\text{C}$ , measured by the SENB technique, was typically  $7.7 \text{ MPa} \cdot \text{m}^{1/2}$ .

#### IV. Discussion

##### (1) Structure of Single Crystals

As shown in Fig. 1(A), between  $2\theta = 73^\circ$  to  $77^\circ$ , four peaks were observed in the X-ray diffraction traces from the as-received crystals. These peaks are labeled (400)*d*, (004)*d*, (400)*p*, and (004)*p*. The letter *d* indicates that the peaks correspond to the tetragonal phase formed by  $c \rightarrow t$  displacive transformation (the so-called *t'*-phase).<sup>10</sup> The letter *p* indicates that the peaks correspond to the tetragonal phase which precipitated out of the cubic phase by a diffusive process. As the tetragonal phase formed by a

diffusive process has a lower yttria content in accordance with the phase diagram, the corresponding  $c/a$  ratio is larger.

X-ray diffraction from surfaces of cube-shaped crystals annealed at  $\geq 2100^\circ\text{C}$  gave identical patterns consisting of two peaks each in the  $2\theta$  ranges between  $33^\circ$  and  $37^\circ$  and between  $72^\circ$  and  $76^\circ$ . The two sets of peaks are (002) and (200), and (400) and (004), corresponding to the tetragonal phase formed displacively. The presence of doublets indicates that the crystal is not a true single crystal, but is a polydomain crystal. If it were a true single crystal, it should yield only one peak in each of the ranges. The corresponding peaks would be (002) and (004), or (200) and (400), depending upon the crystal orientation. Thus, X-ray diffraction alone shows that the crystal must be a polydomain crystal.

##### (2) Ferroelasticity and Zirconia

According to the group theory, for a transition to be ferroelastic, it must satisfy the following criteria:<sup>12</sup> (1) Reduction in the



**Fig. 5.** Bright-field image of a single-phase, annealed crystal, showing the presence of  $90^\circ$  domains.

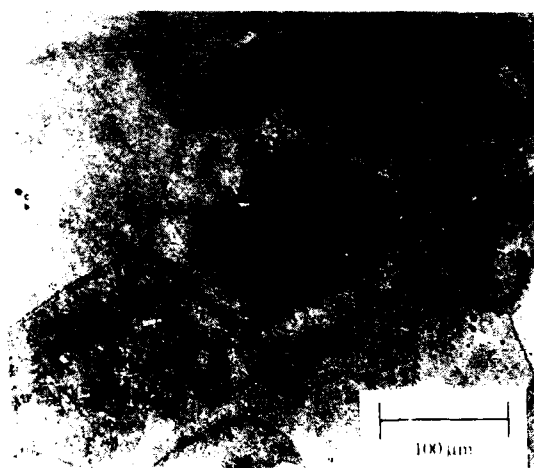


**Fig. 6.** An optical micrograph of a polycrystalline sample (5.4 wt% or 3 mol%  $\text{Y}_2\text{O}_3$ ) heat-treated at  $\geq 2100^\circ\text{C}$ . The sample was etched using HF. X-ray diffraction shows only the presence of the tetragonal phase.

point group symmetry must occur for a transition to be ferroic. (2) A change in the crystal system must occur for the ferroic transition to be ferroelastic. The point groups of cubic and tetragonal zirconia are  $m\bar{3}m$  and  $4/mmm$ , respectively. The change from cubic ( $m\bar{3}m$ ) to tetragonal ( $4/mmm$ ) is accompanied by a reduction in the order of symmetry from 48 to 16. Thus, in accordance with the above criteria, this transition is ferroelastic and may be represented by Aizu's notation,  $m\bar{3}mF4/mmm$ .<sup>6</sup> The number of possible variants may be deduced by simply dividing the order of symmetry in the prototype by that in the ferroelastic phase.<sup>7</sup> Thus, in cubic  $\rightarrow$  tetragonal transition in zirconia,  $48/16 = 3$  variants are expected. Negita<sup>15</sup> has shown that in zirconia the cubic  $\rightarrow$  tetragonal is a first-order transition and tetragonal zirconia is an improper ferroelastic.

As shown by Tendeloo *et al.*,<sup>14</sup> based on the space group considerations (cubic ( $Fm\bar{3}m$ )  $\rightarrow$  tetragonal ( $P4_2/nmc$ )), upon transition a doubling of primitive cells is expected with the occurrence of two types of antiphase domains separated by APB's.

The formation of the three variants and the anti-phase boundary (APB) has been experimentally confirmed by Heuer and co-workers<sup>10,15</sup> and Sakuma.<sup>16</sup> These authors have imaged the three variants by choosing  $\{112\}$  type of reflections with  $\langle 111 \rangle$  zone axis. The electron diffraction pattern shown in Fig. 4 is consistent with the presence of the three variants. The fact that only two peaks were observed in X-ray diffraction patterns in a given  $2\theta$  range suggests that the split spots seen in Fig. 4 cannot be due to tetragonal precipitates. If tetragonal precipitates are present, X-ray diffraction traces should contain four peaks since the  $c/a$  ratio of the precipitates is different from that of the displacively formed tetragonal ( $t'$ ) phase.

### (3) Ferroelastic Domain Switching in Compression

An important characteristic of a ferroic material is that by the application of the pertinent field, it should in principle be possible to shift the crystal from one state into another energetically equivalent state.<sup>6</sup> In the present experiments, when a compressive stress was applied along  $\langle 100 \rangle$  (on the basis of the pseudocubic symmetry), the intensity of the (002) peak decreased and that of the (200) peak increased on the face that was subjected to compression (Figs. 2 and 3). By contrast, the change in the intensities of the two peaks on faces parallel to the compression direction was in the opposite direction (Fig. 3). This is consistent with the expectation that the  $c$  axes of the domains should switch to direc-

tions orthogonal to the compressive loading direction. Lankford *et al.*,<sup>17</sup> observed a step in load-deflection traces of single crystals compressed along  $\langle 100 \rangle$  direction but not when compressed along  $\langle 110 \rangle$  direction. The step observed by Lankford *et al.* is consistent with the occurrence of ferroelastic domain switching.

It could be argued that the changes in the intensities observed in the present studies can be explained on the basis of reversible  $t \rightarrow m$  transition. In ceria-doped polycrystalline tetragonal zirconia, tested in compression, this has been documented.<sup>18</sup> Samples in the present work were compression-tested at temperatures as high as 1400°C. For zirconia containing 2.4 mol% (4.2 wt%)  $Y_2O_3$ , the  $t \rightarrow m$  transition temperature is  $\leq 700^\circ C$ .<sup>19</sup> As the volume change from  $m \rightarrow t$  is negative, according to the Clausius-Clapeyron relation, hydrostatic pressure ( $1/3$  uniaxial compression) decreases the  $t \rightarrow m$  transition temperature.<sup>20</sup> Clearly, the changes in the intensities of the (002) and the (200) peaks observed at temperatures  $\geq 1000^\circ C$  cannot be explained on the basis of  $t \rightarrow m$  reversible transition. Michel *et al.* reported that even after the single crystal (3 mol%  $Y_2O_3$ ) used in their study was crushed to a powder of size less than  $1 \mu m$ , the amount of the monoclinic phase was less than 1%. These results also suggest that the changes in the intensities of the (002) and the (200) peaks observed in our studies at room temperature are probably not due to reversible  $t \rightarrow m$  transition, but are due to domain switching.

### (4) Toughening Mechanisms

The higher toughness of tetragonal single crystals in comparison to cubic crystals in the work by Ingel *et al.*<sup>1,2</sup> was attributed to crack deflection. Similarly, Michel *et al.*<sup>3</sup> also suggested crack deflection by domain boundaries as the probable toughening mechanism. In a recent paper, Heuer *et al.*<sup>11</sup> have suggested that at elevated temperatures precipitation strengthening in tetragonal single crystals containing 4.5 mol%  $Y_2O_3$  can occur. In the present work, toughness of tetragonal single crystals was 12 and 8  $MPa \cdot m^{1/2}$  at room temperature and at 1000°C, respectively. These mechanisms of toughening are probably operative in the single crystals studied in the present work. Wadhavan<sup>22</sup> has suggested ferroelastic domain switching as a possible toughening mechanism. Changes in the intensities of the (002) and (200) peaks observed in compression tests as well as on fracture surfaces suggest that the phenomenon of domain switching can contribute to the overall toughness. At 1000°C, no contribution of transformation toughening is expected, for the reasons mentioned

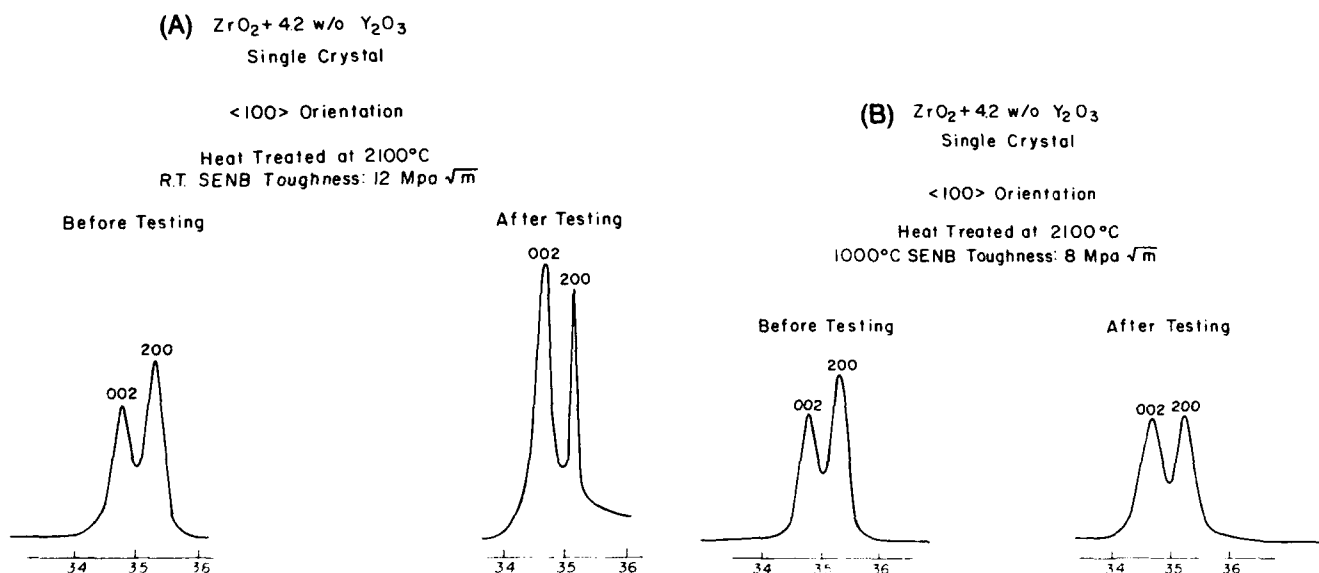


Fig. 7. X-ray diffraction traces from pristine and fracture surfaces of an SENB sample broken at (A) room temperature and (B)  $1000^\circ C$ , showing the occurrence of ferroelastic domain switching during fracture.

previously. At room temperature also, no monoclinic phase was observed on ground or fracture surfaces of single crystals annealed at  $\geq 2100^\circ\text{C}$ . Yet, changes in the intensities of (002) and (200) peaks occurred, consistent with the occurrence of domain switching. This suggests that toughening by ferroelastic domain switching is probably operative at room temperature also. However, the possible contribution of reversible  $t \rightarrow m$  transition at room temperature in toughening cannot be ruled out. In materials such as lead zirconate titanate (PZT), on the other hand, the contributions of the domain switching can be clearly identified, as no transformation toughening is possible.<sup>9</sup>

### V. Summary and Conclusions

Group theoretical considerations suggest that tetragonal zirconia is a ferroelastic material.<sup>6,7,12-14</sup> An important characteristic of a ferroelastic material is that it should be possible, at least in principle, to change domain orientation by the application of an external stress. In the present work, X-ray diffraction evidence was presented in support of the contention that domain switching occurred during compression testing and fracture. The observation that high toughness can be retained far above the  $t \rightarrow m$  transition temperature suggests that there is little contribution from transformation toughening. By contrast, the occurrence of domain switching indicates that ferroelastic domain switching can contribute to toughening. Finally, nontransformable tetragonal zirconia polycrystalline samples containing 5.4 wt% (3 mol%)  $\text{Y}_2\text{O}_3$  with grain size  $\geq 100 \mu\text{m}$  can be fabricated by annealing the samples in the stability range of cubic zirconia ( $\geq 2100^\circ\text{C}$ ).

### References

- <sup>1</sup>R. P. Ingel, D. Lewis, B. A. Bender, and R. W. Rice, "Temperature Dependence of Strength and Fracture Toughness of  $\text{ZrO}_2$  Single Crystals," *J. Am. Ceram. Soc.*, **65** [9] C-150-C-151 (1982).
- <sup>2</sup>R. P. Ingel, D. Lewis, B. A. Bender, and R. W. Rice, "Physical, Microstructural and Thermomechanical Properties of  $\text{ZrO}_2$  Single Crystals": pp. 408-14 in *Advances in Ceramics*, Vol. 12, Science and Technology of Zirconia II, Edited by N. Clausen, M. Rühle, and A. H. Heuer, American Ceramic Society, Columbus, OH, 1985.
- <sup>3</sup>D. Michel, L. Mazerolles, and M. Perez y Jorba, "Fracture of Metastable Tetragonal Zirconia Crystals," *J. Mater. Sci.*, **18**, 2618-28 (1983).
- <sup>4</sup>T. C. Yuan, G. V. Srinivasan, J. F. Jue, and A. V. Virkar, "Dual Phase Magnesia-Zirconia Ceramics with Strength Retention at Elevated Temperatures": to be published in *J. Mater. Sci.*
- <sup>5</sup>A. V. Virkar and R. L. K. Matsumoto, "Ferroelastic Domain Switching as a Toughening Mechanism in Tetragonal Zirconia," *J. Am. Ceram. Soc.*, **69** [10] C-224-C-226 (1986).
- <sup>6</sup>K. Aizu, "Possible Species of 'Ferroelastic' Crystals and of Simultaneously Ferroelectric and Ferroelastic Crystals," *J. Phys. Soc. Jpn.*, **27**, 387 (1969).
- <sup>7</sup>K. Aizu, "Possible Species of Ferromagnetic, Ferroelectric and Ferroelastic Crystals," *Phys. Rev. B: Solid State*, **2** [3] 754-72 (1970).
- <sup>8</sup>A. V. Virkar and R. L. K. Matsumoto, "Toughening Mechanism in Tetragonal Zirconia Polycrystalline (TZP) Ceramics": pp. 653-62 in *Advances in Ceramics*, Vol. 24, Science and Technology of Zirconia III, Edited by S. Somiya, N. Yamamoto, and H. Yanagida, American Ceramic Society, Westerville, OH, 1988.
- <sup>9</sup>K. Mehta and A. V. Virkar, "Fracture Mechanisms in Ferroelectric-Ferroelastic Lead Zirconate Titanate Ceramics": to be published in *J. Am. Ceram. Soc.*
- <sup>10</sup>V. Lanteri, R. Chaim, and A. H. Heuer, "On Microstructure Resulting from the Diffusionless Cubic  $\rightarrow$  Tetragonal Transformation in  $\text{ZrO}_2\text{-Y}_2\text{O}_3$  Alloys," *J. Am. Ceram. Soc.*, **69** [10] C-258-C-261 (1986).
- <sup>11</sup>T. Sakuma, Y. A. Yoshizawa, and H. Suto, "The Microstructure and Mechanical Properties of Ytria-Stabilized Zirconia Prepared by Arc-Melting," *J. Mater. Sci.*, **20** [10] 2399-407 (1985).
- <sup>12</sup>J. C. Tolenado, "Symmetry-Determined Phenomena at Crystalline Phase Transitions," *J. Solid State Chem.*, **27**, 41-49 (1979).
- <sup>13</sup>K. Nagita, "Lattice Vibrations and Cubic to Tetragonal Phase Transition in  $\text{ZrO}_2$ ," *Acta Metall.*, **37** [1] 313-17 (1989).
- <sup>14</sup>G. V. Tendeloo and S. Amelinckx, "Group-Theoretical Considerations Concerning Domain Formation in Ordered Alloys," *Acta Crystallogr.*, **A30**, 431-40 (1974).
- <sup>15</sup>A. H. Heuer, R. Chaim, and V. Lanteri, "The Displacive Cubic  $\rightarrow$  Tetragonal Transformation in  $\text{ZrO}_2$  Alloys," *Acta Metall.*, **35** [3] 661-66 (1987).
- <sup>16</sup>T. Sakuma, "Development of Domain Structure Associated with the Diffusionless Cubic-to-Tetragonal Transition in  $\text{ZrO}_2\text{-Y}_2\text{O}_3$  Alloys," *J. Mater. Sci.*, **22**, 4470-75 (1987).
- <sup>17</sup>J. Lankford, L. Rabenberg, and R. A. Page, "Deformation Mechanisms in Ytria-Stabilized Zirconia," *J. Mater. Sci.*, **23**, 4144-56 (1988).
- <sup>18</sup>P. E. Reyes-Morel, J.-S. Cherng, and I.-W. Chen, "Transformation Plasticity of  $\text{CeO}_2$ -Stabilized Tetragonal Zirconia Polycrystals. II. Pseudoelasticity and Shape Memory Effect," *J. Am. Ceram. Soc.*, **71** [8] 648-57 (1988).
- <sup>19</sup>H. G. Scott, "Phase Relations in the Zirconia-Ytria System," *J. Mater. Sci.*, **10** [9] 1527-35 (1975).
- <sup>20</sup>E. D. Whitney, "Effect of Pressure on Monoclinic-Tetragonal Transition of Zirconia: Thermodynamics," *J. Am. Ceram. Soc.*, **45** [12] 612-13 (1962).
- <sup>21</sup>A. H. Heuer, V. Lanteri, and A. Dominguez-Rodriguez, "High Temperature Precipitation Hardening on  $\text{Y}_2\text{O}_3$  Partially-Stabilized  $\text{ZrO}_2$  (Y-PSZ) Single Crystals," *Acta Metall.*, **37** [2] 559-67 (1989).
- <sup>22</sup>V. K. Wadhavan, "Ferroelasticity and Related Properties of Crystals," *Phase Transitions*, **3**, 3-103 (1982). □

## Fracture Mechanisms in Ferroelectric-Ferroelastic Lead Zirconate Titanate (Zr:Ti = 0.54:0.46) Ceramics

Karun Mehta\* and Anil V. Virkar\*

Department of Materials Science and Engineering, University of Utah, Salt Lake City, Utah 84112

Fracture toughness,  $K_{IC}$ , of a single-phase commercial lead zirconate titanate (PZT) ceramic (Zr/Ti = 0.54/0.46) of tetragonal structure ( $c/a \approx 1.019$ ) was measured using the single edge notched beam method above and below the Curie temperature. Domain switching (poling) under electrical and mechanical loading was examined using X-ray diffraction. Surface grinding, electrical poling, and mechanical poling caused crystallographic texture. Similar texture, indicative of domain switching, was also observed on fracture surfaces of some samples fractured at room temperature. At room temperature, the highest  $K_{IC}$  measured was  $1.85 \text{ MPa} \cdot \text{m}^{1/2}$ , while above the Curie temperature it was about  $1.0 \text{ MPa} \cdot \text{m}^{1/2}$ . Cracks emanating from Vickers indents in poled samples were different in the poling and the transverse directions. The difference in crack sizes is explained on the basis of domain switching during crack growth. These results indicate that ferroelastic domain switching (twinning) is a viable toughening mechanism in the PZT materials tested. [Key words: mechanical properties, lead zirconate titanate, ferroelastic materials, ferroelectric materials, fracture toughness.]

### I. Introduction

LEAD ZIRCONATE TITANATES ( $\text{PbZr}_x\text{Ti}_{(1-x)}\text{O}_3$ ) or PZT are known to be simultaneously ferroelectric-ferroelastic<sup>1,2</sup> materials. The mechanical behavior of these materials has received considerable attention. Fracture of ferroelectric-ferroelastic materials as a function of composition and grain size has been examined by Pohanka and co-workers.<sup>3-6</sup> These authors identified microcracking and twinning as toughening mechanisms. Scanning electron micrographs of samples fractured at room temperature (in the ferroelectric state) exhibited twins (domains), while no twins were observed in samples fractured at  $150^\circ\text{C}$ , which is above the Curie temperature. The ferroelectric phase exhibited significantly higher fracture energy. It was also observed that pressure-depoled PZT exhibited higher fracture energy. McHenry and Koepke<sup>7</sup> examined the effect of applied ac electric fields of various frequencies on slow crack growth of unpoled PZT ceramics and noted that the application of an electric field enhanced the propensity to crack growth. Cook *et al.*<sup>8</sup> examined the strength of fine-grained  $\text{BaTiO}_3$  containing controlled flaws as a function of temperature. The strength decreased from room temperature to  $150^\circ\text{C}$  (Curie temperature), above which it remained constant. The phenomenon of ferroelasticity suggests that absorption of mechanical energy in domain switching (twinning) in the near stress field of a crack tip is a possible toughening mechanism, as recognized by Pohanka and co-workers.<sup>3-6</sup> The mechanics of toughening by domain switching has been recently examined by Pisarenko *et al.*<sup>9</sup>

T. Michalske—contributing editor

Manuscript No. 198781. Received November 21, 1988; approved August 10, 1989.

Supported by DARPA (Contract No. F49620-87-C-0077) through a sub-contract from Ceramtec, Inc., to the University of Utah.

\*Member, American Ceramic Society.

Although domain switching as a toughening mechanism has been suggested, with the exception of optical microscopic observation of fracture surfaces of  $\text{BaTiO}_3$ ,<sup>4</sup> no experimental evidence has been presented in support of it. The present work was undertaken with the following objectives: (1) to determine if domain switching can occur during fracture, (2) to assess the contribution of domain switching to toughness, and (3) to identify parameters which affect domain switching. PZT was chosen as a model material for the present study since it has been extensively characterized with regards to its electrical and electromechanical properties. Also, being simultaneously ferroelectric-ferroelastic, domain switching can be caused by the application of either an electric field or a mechanical stress or a combination of the two.

The experimental work included (1) the measurement of fracture toughness of commercial PZT ceramics with Zr/Ti = 0.54/0.46 and the determination of the degree of texture caused during fracture using X-ray diffraction, (2) characterization of texture due to the reorientation of the  $90^\circ$  degree domains under an applied electric field or a mechanical stress, (3) a study of the kinetics of the domain switching process under an applied electric field, and (4) a study of the anisotropy in indentation crack lengths in mechanically and electrically poled materials.

### II. Experimental Procedure

#### (1) Grinding and Annealing Studies

Some of the as-received samples were diamond ground. Subsequently, a few of the samples were annealed at  $500^\circ\text{C}$  for up to 4 h. X-ray diffraction traces using  $\text{CuK}\alpha$  radiation were obtained from the as-received, as-ground, and ground and annealed surfaces. The objective was to determine if grinding creates surface texture and whether the texture can be removed by annealing above the Curie temperature.

#### (2) Measurement of Fracture Toughness

The as-received, unpoled PZT samples were machined as single edge notched beam (SENB) specimens for the measurement of fracture toughness. The typical dimensions were  $35 \text{ mm} \times 6.5 \text{ mm} \times 3 \text{ mm}$ . A notch of 0.25-mm width and 3-mm depth was machined into every sample. After machining, the samples were annealed at  $500^\circ\text{C}$  for 4 h to ensure that the texture caused by machining a notch was removed. The samples were then fractured in four-point bending under a crosshead speed of 0.125 mm/min between room temperature and  $500^\circ\text{C}$ . Some of the notched and annealed samples were electrically poled for 30 min at  $100^\circ\text{C}$  in a dielectric oil. An electric field of 15.7 kV/cm was applied either perpendicular to the notch surface (along the long direction of the sample) or parallel to the notch surface. Samples were fractured at room temperature, and X-ray diffraction traces were obtained from fracture surfaces to determine the degree of texture, if any.

A few samples in the double cantilever beam (DCB) geometry of dimensions  $74 \text{ mm} \times 15 \text{ mm} \times 3.5 \text{ mm}$  were also tested. In these experiments, the samples were fractured in such a way that the crack propagated very slowly ( $\sim 100 \mu\text{m/s}$ )

for the first 2 to 3 cm, after which rapid fracture occurred. X-ray diffraction traces were obtained from fracture surfaces in the slow as well as rapid fracture regime.

### (3) Switching under the Application of an Electric Field and Relaxation Experiments

The objective of these experiments was to examine the kinetics of switching of  $90^\circ$  domains. The following experiments were designed, using a universal testing machine. Thin rectangular-shaped samples of dimensions  $10\text{ mm} \times 6\text{ mm} \times \sim 400\text{ }\mu\text{m}$  were machined from the as-received, unpoled PZT and annealed at  $500^\circ\text{C}$  for 4 h to ensure complete randomness of domains. Two large faces ( $10\text{ mm} \times 6\text{ mm}$ ) of each sample were silver painted, which served as the electrodes. A loading (actually load sensing) fixture was designed and built with fused quartz rods of 2.5-cm diameter. The quartz rod assembly was mounted on a universal testing machine and an electroded sample was secured between the two rods under a very light load (typically  $\leq 4\text{ N}$ ). The corresponding mechanical stress was on the order of 1.6 MPa or less, which is far below the switching stress. The two electrodes were connected to a regulated dc power supply. Figure 1 shows a schematic of the assembly. Subsequently, a dc voltage was applied across the two electrodes. The corresponding field across the sample was  $\sim 10\text{ kV/cm}$ . The load began to drop (relax) as soon as the voltage was applied. The load relaxation data were analyzed using a first-order kinetic equation. After the relaxation experiments, the silver electrodes were dissolved in  $\text{HNO}_3$ . Subsequently, X-ray diffraction traces were obtained from the large faces to determine the degree of texture developed by domain switching.

### (4) Switching under the Application of a Mechanical Stress

Bar-shaped specimens of dimensions  $3\text{ mm} \times 3\text{ mm} \times 5\text{ mm}$  were machined from the as-received samples and were annealed at  $500^\circ\text{C}$  for 4 h. The specimens were subjected to a compressive stress as high as about 300 MPa between room temperature and  $200^\circ\text{C}$ . The procedure consisted of loading the samples to  $\sim 300\text{ MPa}$  at a crosshead speed of 0.125 mm/min, followed by arresting the crosshead. As soon as the deflection was arrested, the load began to drop. The drop in the load was much slower than switching under an

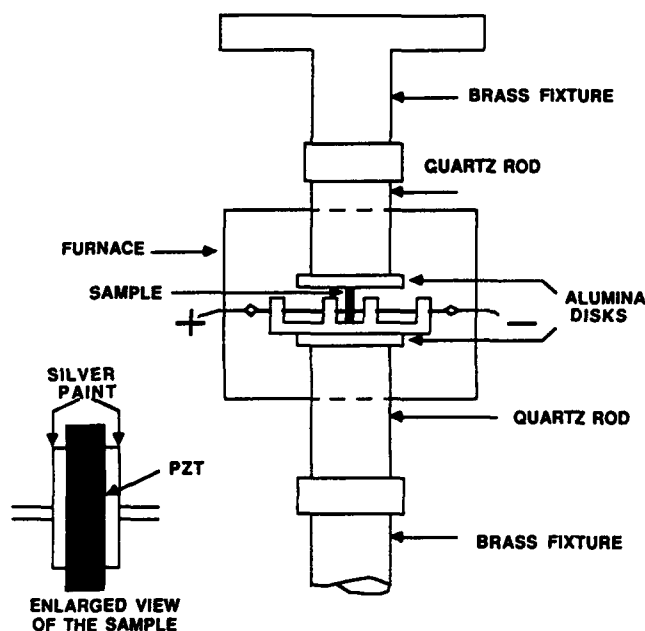


Fig. 1. Schematic of the load recording assembly used for relaxation studies under the application of an electric field. The enlarged view in the inset shows a sample with silver electrodes.

electric field. Specimens were examined using X-ray diffraction in order to determine the degree of texture.

### (5) Indentation Experiments on Mechanically and Electrically Poled Specimens

Bar-shaped specimens of dimensions  $3\text{ mm} \times 3\text{ mm} \times 6\text{ mm}$  were machined out of the as-received PZT, were polished to a  $1\text{-}\mu\text{m}$  finish, and annealed at  $500^\circ\text{C}$  for 4 h. Some of the samples were subjected to a compressive stress of 250 MPa at room temperature with the polished surface parallel to the loading direction. X-ray diffraction traces were obtained from polished surfaces before and after compression testing. Vickers hardness indentations were introduced on the polished surface, with one of the pyramid diagonals parallel to the compression loading axis. Some of the samples were electrically poled, with the polished surface parallel to the poling direction. After poling, indentations were introduced on the polished surface, with one of the pyramid diagonals parallel to the poling direction.

## III. Results

### (1) Grinding and Annealing Studies

Figure 2(a) shows the (002) and the (200) X-ray diffraction peaks of an as-received sample between  $2\theta = 43^\circ$  and  $2\theta = 46^\circ$ . The ratio of the two intensities, i.e.,  $I_{(002)}/I_{(200)}$ , is approximately 0.52. Figure 2(b) shows a trace of a surface-ground sample in which the corresponding ratio  $I_{(002)}/I_{(200)}$  is  $\sim 1.82$ . An X-ray diffraction trace of the same surface-ground sample after annealing at  $500^\circ\text{C}$  is shown in Fig. 2(c). The corresponding intensity ratio is  $\sim 0.57$ , which is about the same as that from the as-received samples.

### (2) Fracture Toughness

Figure 3 shows that the fracture toughness,  $K_{IC}$ , of unpoled samples decreases with increasing temperature. Between room temperature and the Curie temperature ( $\sim 350^\circ\text{C}$ ), the  $K_{IC}$  decreases from a maximum of  $\sim 1.85$  to  $\sim 1.0\text{ MPa}\cdot\text{m}^{1/2}$  and remains constant thereafter up to  $500^\circ\text{C}$ , the maximum test temperature. X-ray diffraction from fracture surfaces showed that the ratio  $I_{(002)}/I_{(200)}$  was typically greater for samples fractured at room temperature compared to that from pristine (annealed) surfaces. By contrast, the intensity ratio for those fractured near or above the Curie temperature was about the same as from pristine surfaces ( $\sim 0.5$ ). In some cases, however, the ratio  $I_{(002)}/I_{(200)}$  for samples fractured at room temperature was the same as that from pristine surfaces. The significance of this will be discussed later. Figure 4 shows X-ray diffraction traces from fracture surfaces of one of the SENB samples that did exhibit an increase in  $I_{(002)}$ . X-ray diffraction traces were also obtained from fracture surfaces of DCB samples. Figure 5 shows these from the slow as well as rapid crack growth regimes. As seen in the figure,  $I_{(002)}/I_{(200)}$  is much greater than 0.5 in the slow crack regime. Actually, in this case  $I_{(002)}$  is even greater than  $I_{(200)}$ . However, traces from the rapid regime of fracture showed that  $I_{(002)}/I_{(200)}$  was about the same as that from pristine surfaces. This shows that the development of texture occurs during slow fracture but not during rapid fracture.

Fracture toughness of electrically poled samples was also measured using the SENB technique. The  $K_{IC}$  of samples poled along a direction perpendicular to the notch was  $\sim 0.98\text{ MPa}\cdot\text{m}^{1/2}$  compared to  $\sim 1.2\text{ MPa}\cdot\text{m}^{1/2}$  for samples poled along the notch surface. The  $K_{IC}$  of unpoled samples from the same set was  $\sim 1.45\text{ MPa}\cdot\text{m}^{1/2}$ .

### (3) Switching under an Electric Field

A typical load-time trace for a sample under an applied electric field of  $10\text{ kV/cm}$  is shown in Fig. 6. As soon as the field was applied, the load rapidly dropped, indicating a decrease in the vertical dimension of the sample. The rate of decrease continuously diminished with time. About 90% of the

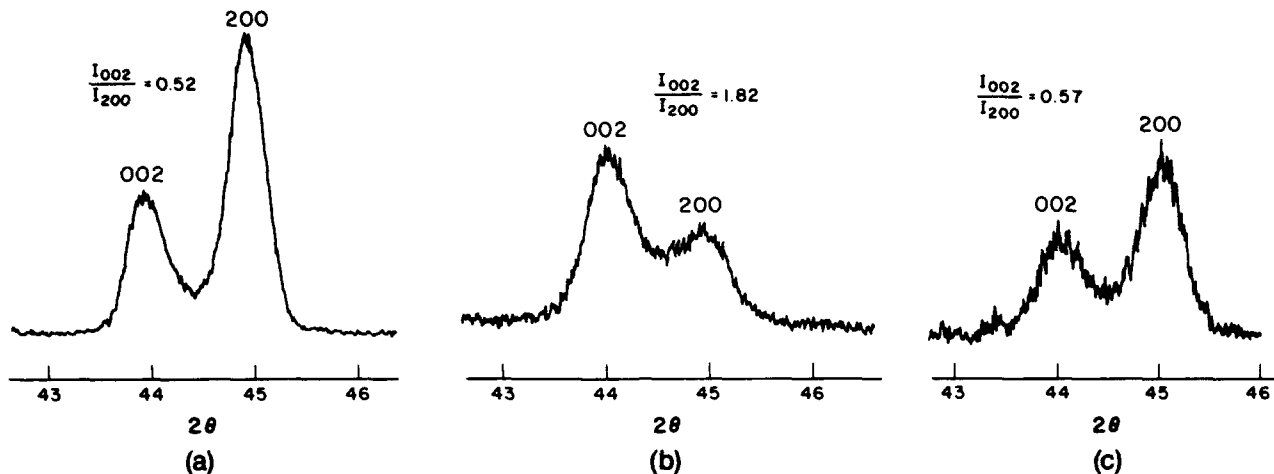


Fig. 2. (a) X-ray diffraction (XRD) trace of an as-received sample showing the (002) and (200) peaks. Note that the peak intensity,  $I_{(002)}$ , is less than  $I_{(200)}$ . The ratio of the intensities, namely  $I_{(002)}/I_{(200)}$ , is about 0.52. (b) XRD trace of the same sample after surface grinding showing  $I_{(002)} > I_{(200)}$  ( $I_{(002)}/I_{(200)} \approx 1.82$ ). This shows that domain switching occurred during grinding. (c) XRD trace of the same (surface-ground) sample which was annealed at 500°C for 4 h after grinding. Note that the texture induced during grinding has disappeared after annealing ( $I_{(002)}/I_{(200)} \approx 0.57$ ).

total load drop occurred in approximately the first 2 to 4 s. Over this range, the data could be described by a first-order equation with a relaxation time,  $\tau$ . In terms of the initial load,  $P(0)$ , and load after infinite time,  $P(\infty)$ , the relaxation time,  $\tau$ , and the time,  $t$ , the instantaneous load,  $P(t)$ , may be given by

$$P(t) = P(\infty) + [P(0) - P(\infty)] \exp\left(-\frac{t}{\tau}\right) \quad (1)$$

Equation (1) shows that a plot of  $\ln(-dP(t)/dt)$  vs  $t$  should yield a straight line with  $-1/\tau$  as the slope and  $\ln\{[P(0) - P(\infty)]/\tau\}$  as the intercept.

After the electric field was removed, a slight increase in the load was noted, indicative of some reverse switching. A typical plot of the logarithm of the rate of load relaxation vs time is shown in Fig. 7. X-ray diffraction traces of the poled samples (after dissolution of silver electrodes) exhibited an increase in

$I_{(002)}/I_{(200)}$  relative to that from pristine surfaces, as shown in Fig. 8. The increase in  $I_{(002)}/I_{(200)}$  indicates that the 90° domains aligned along the poling direction. Under an applied electric field, both the 90° and the 180° domains will align. There, however, is no dimensional change due to the alignment of the 180° domains. That is, the 180° domain switching is not expected to affect the load relaxation. Thus, the relaxation studies represent the alignment kinetics of the 90° domains only.

(4) Switching under a Mechanical Stress

Mechanical tests involved loading samples in a universal testing machine to a predetermined load followed by arresting the crosshead. As soon as the crosshead was arrested, the load began to relax. However, in these tests the load relaxed at a much lower rate compared to the corresponding electrical tests in which loading (application of electrical potential) was almost instantaneous. By contrast, it took several seconds to load the samples to the final desired stress. Electrical poling tests showed that much of the 90° domain switching occurred in the first couple of seconds. Therefore, the early stages of 90° domain switching could not be studied in mechanical relaxation experiments. After relaxation under a fixed deflection, X-ray diffraction traces were obtained from surfaces parallel to the loading axis. An enhancement of the  $I_{(002)}$  (with simultaneous reduction in  $I_{(200)}$ ) was observed, indicating the occurrence of domain reorientation. The intensity ratio,  $I_{(002)}/I_{(200)}$  was, however, lower than in the case of electrically poled samples. The stress required for domain reorientation was observed to be less than 50 MPa. In another experiment, a sample with a strain gauge mounted on it was stressed to 250 MPa. Three important features were observed: (i) The stress-strain trace exhibited a permanent retained strain (on the order of  $4.6 \times 10^{-4}$ ) upon unloading, (ii) there was no unique yield stress (i.e., there is no unique switching stress), and (iii) nonlinearity set in at stresses as low as about 25 to 30 MPa.

(5) Indentation Experiments on Mechanically and Electrically Poled PZT

A few samples were compressed to a stress of 250 MPa. After unloading, indentations were introduced with one of the indent diagonals along the loading (compression) direction. The crack lengths were observed to be longer in the direction of the loading compared to the orthogonal direction. By contrast, in the electrically poled samples, the crack

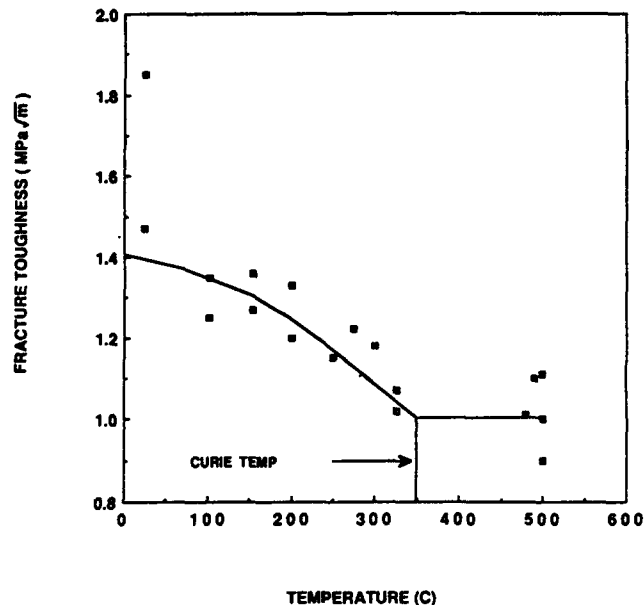


Fig. 3. Fracture toughness,  $K_{Ic}$ , of unpoled samples as a function of temperature.

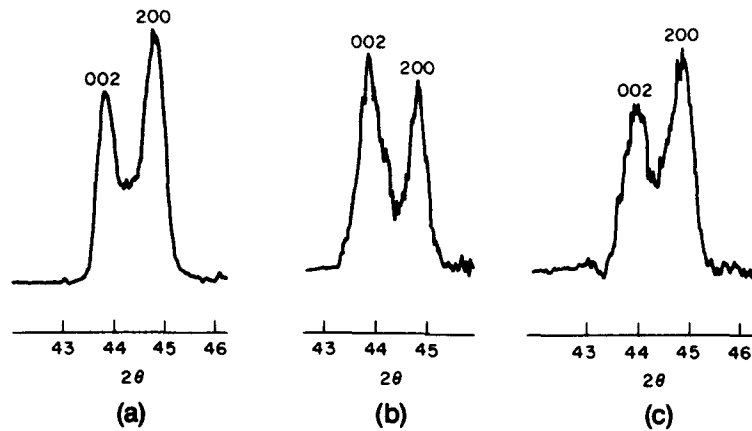


Fig. 4. (a) XRD trace of a sample that was first polished and then annealed at 500°C for 4 h. The figure shows that  $I_{(002)} < I_{(200)}$  as expected for near random orientation of domains. The typical ratio of the intensities is  $\sim 0.57$ . (b) XRD trace from the fracture surface of a single edge notched beam sample broken in four-point bending at room temperature. Note that  $I_{(002)}/I_{(200)}$  is substantially greater than 0.5, showing that domain switching occurred during fracture. In this case,  $I_{(002)}$  is actually greater than  $I_{(200)}$ . (c) XRD trace of the same fracture surface after annealing at 500°C for 4 h. The figure shows that  $I_{(002)} < I_{(200)}$  with  $I_{(002)}/I_{(200)} \sim 0.5$ , showing that the domains are again randomly oriented after annealing above the Curie temperature.

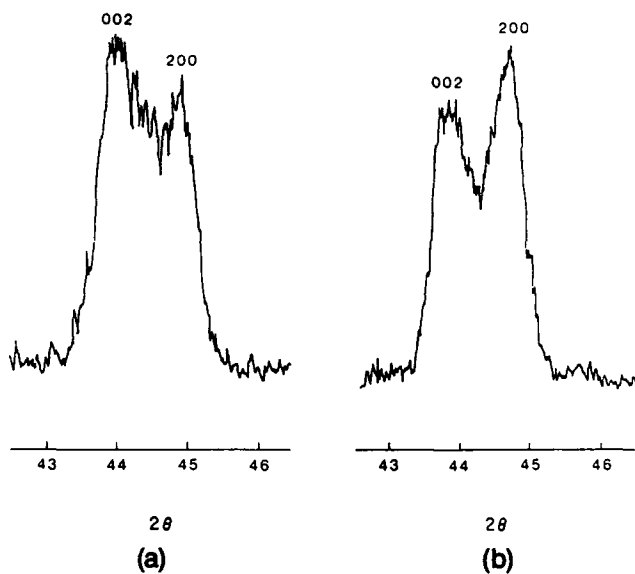


Fig. 5. (a) XRD trace of a fracture surface from the stable crack region of a DCB sample; crack velocity  $\sim 100 \mu\text{m/s}$ . Note that  $I_{(002)} > I_{(200)}$ , showing clearly that domain switching occurred during fracture. (b) XRD trace of fracture surface from the rapid crack growth region of the same DCB sample. Note that  $I_{(002)} < I_{(200)}$  with  $I_{(002)}/I_{(200)} \sim 0.5$ , indicating that very little domain switching occurred during fast crack growth.

lengths were shorter in the poling direction. Figure 9 shows a typical photomicrograph of an indented sample that was mechanically poled. The length of the crack in the loading direction (compression) is  $\sim 105 \mu\text{m}$ , while that in the orthogonal direction is  $\sim 67 \mu\text{m}$ . The corresponding anisotropic toughnesses were determined to be  $\sim 0.35$  and  $\sim 0.73 \text{ MPa} \cdot \text{m}^{1/2}$ , respectively. Similar results were obtained by Yamamoto *et al.*<sup>10</sup> on lanthanated  $\text{PbTiO}_3$  and by Okazaki<sup>11</sup> on PLZT.

#### IV. Discussion

##### (1) Domain Switching as a Toughening Mechanism

The fracture toughness,  $K_{IC}$ , decreased with increasing temperature up to the Curie temperature ( $\sim 350^\circ\text{C}$ ) and remained constant thereafter. Unidirectional compression tests indicated that domain switching can occur at stresses lower than 50 MPa. X-ray diffraction patterns taken from fracture surfaces of DCB samples in the slow regime of fracture and

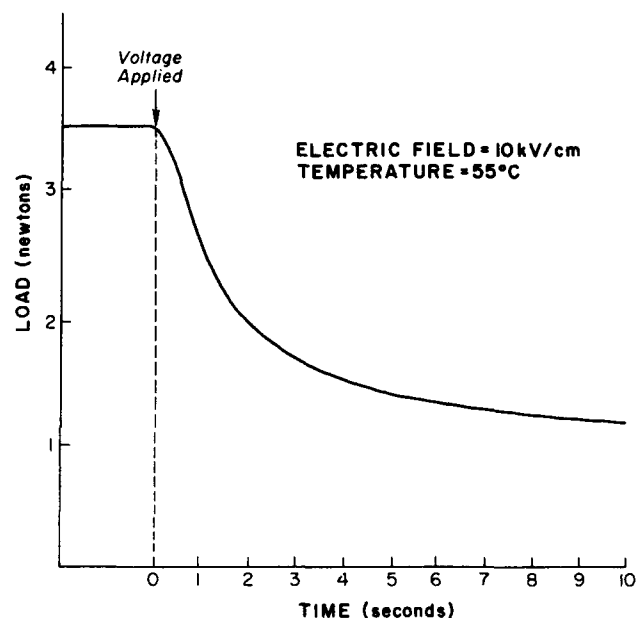


Fig. 6. Load vs time trace for a sample under the application of an electric field of magnitude 10 kV/cm.

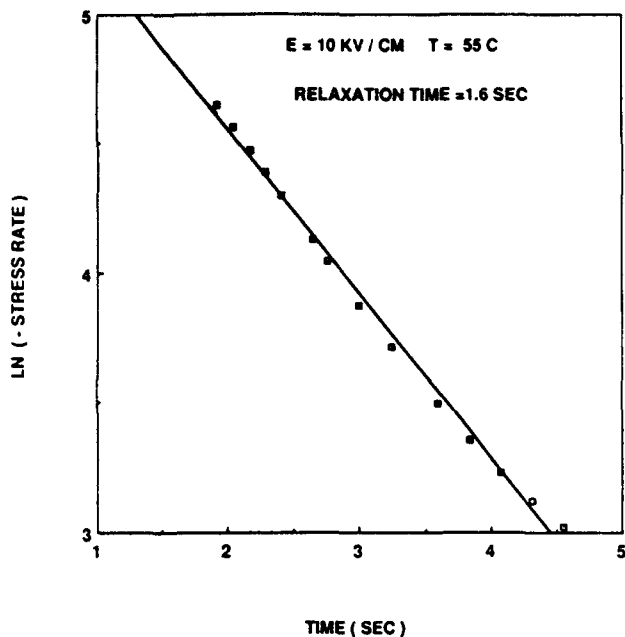


Fig. 7. Plot of  $\ln(-dP/dt)$  vs time for the trace shown in Fig. 6. Note that the data can be described by first-order kinetics.

some of the SENB samples showed that  $I_{(002)}/I_{(200)}$  was greater than that from the pristine surfaces. This indicates that domain reorientation occurred during fracture such that the  $c$  axes of many of the domains became orthogonal to the fracture surfaces. Let us identify the crack surface with the  $xz$  plane and the crack front parallel to the  $z$  axis. Then, for  $\theta = 0$  and  $r \rightarrow 0$ ,  $\sigma_{rr} = \sigma_{\theta\theta} = \sigma_{yy} = \sigma_{zz}$ , where  $(r, \theta)$  are polar coordinates and  $\sigma_{ij}$  denote stresses. It is well-known<sup>12</sup> that for  $\theta = \pi/2$ ,  $\sigma_{rr} = \sigma_{yy} = 3\sigma_{\theta\theta} = 3\sigma_{zz}$ . Thus, just off the crack plane,  $\sigma_{yy}$  is 3 times  $\sigma_{zz}$ . In plane strain, the normal stress in the  $z$  direction is given by  $\sigma_{zz} = \nu(\sigma_{yy} + \sigma_{xx})$ . For a Poisson's

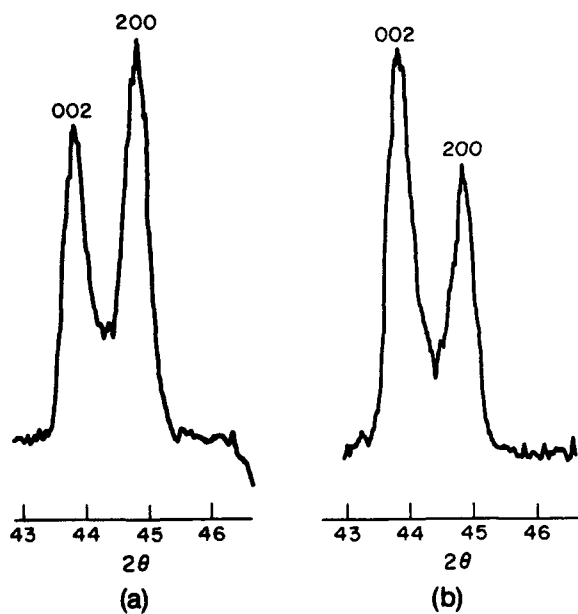


Fig. 8. XRD traces of the (a) as-annealed and (b) electrically poled samples. The trace of the poled sample, which was taken on one of the surfaces perpendicular to the poling direction, clearly shows the occurrence of domain switching.

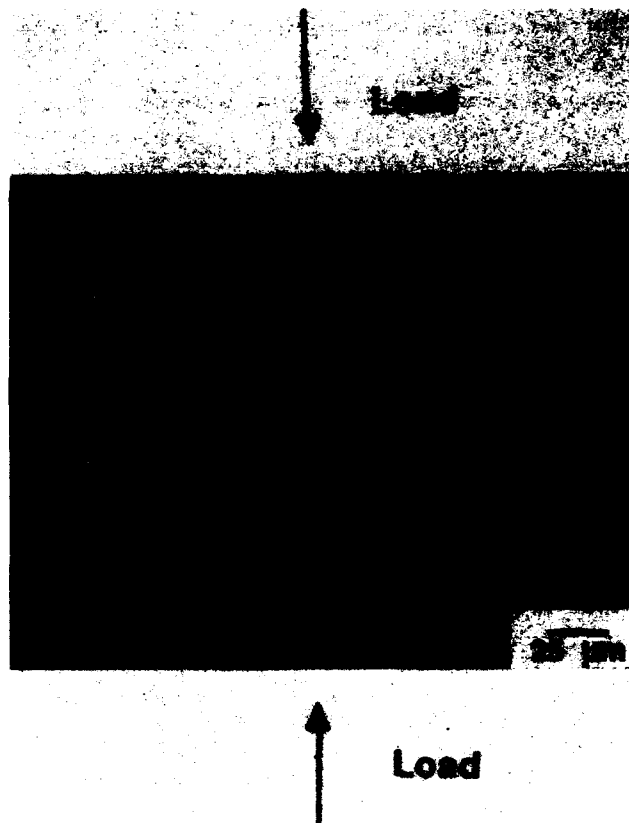


Fig. 9. Photomicrograph showing a microindent (500 g for 10 s) introduced in a mechanically poled sample. Note the anisotropy in crack lengths. The arrows indicate the direction of compression.

ratio of 0.25,  $\sigma_{zz}$  would be the same as  $\sigma_{xx}$ . The net tensile stress experienced by an element of material just ahead and off the crack tip is given by  $2\sigma_{xx}$  or  $(2/3)\sigma_{yy}$ . If this stress exceeds the coercive stress,  $\sigma_c$ ,  $90^\circ$  domain switching can occur during fracture. That is, domain switching will occur in the near crack tip region if  $\sigma_{yy} \geq 1.5\sigma_c$ . An increase in the ratio  $I_{(002)}/I_{(200)}$  from fracture surfaces is in accord with this expectation.

Pisarenko *et al.*<sup>9</sup> analyzed fracture anisotropy in poled PZT using an approach similar to transformation toughening. The depth of the switched zone was estimated using a finite element analysis. The differences in  $K_{IC}$  observed in the two directions, crack plane parallel and orthogonal to the poling direction, were explained on the basis of domain switching. In their analysis, however, an explicit relation between toughness and coercive stress was not derived. An approximate, semiquantitative treatment of toughening due to domain switching is given below.

If the depth to which domain switching occurs is given by  $h$ , the elastic energy release rate,  $G_{IC}$ , is given by

$$G_{IC} \approx G_{IC}^0 + 2h\sigma_c \epsilon_s \quad (2)$$

where  $\epsilon_s$  is the switching strain and  $G_{IC}^0$  is the elastic energy release rate in the paraelastic state. The depth to which switching occurs,  $h$ , is related to the fracture toughness,  $K_{IC}$ , by

$$h \approx \alpha \left( \frac{K_{IC}}{\sigma_{yy}^c} \right)^2 \quad (3)$$

where  $\alpha$  is a constant and  $\sigma_{yy}^c$  is the magnitude of  $\sigma_{yy}$  corresponding to  $\sigma_c$ .

This equation is essentially the same as used for estimating crack tip plastic zone sizes.<sup>12</sup> A similar approach has been used for the estimation of process zone sizes in other toughening mechanisms. The near tip stress field is given by

$$\sigma_{yy} = \frac{K_I}{\sqrt{2\pi r}} \cos\left(\frac{\theta}{2}\right) \left[ 1 + \sin\left(\frac{\theta}{2}\right) \sin\left(\frac{3\theta}{2}\right) \right] \quad (4)$$

For  $\theta = \pi/2$ , with  $K_I = K_{IC}$ , the zone depth,  $h$ , is given by

$$h \approx 0.179 \left( \frac{K_{IC}}{\sigma_c} \right)^2 \approx 0.08 \left( \frac{K_{IC}}{\sigma_c} \right)^2 \quad (5)$$

Substituting into Eq. (2) gives

$$K_{IC} \approx \frac{K_{IC}^2}{\sqrt{1 - \frac{0.16\epsilon_s E}{\sigma_c}}} \quad (6)$$

in which the relation  $K_{IC}^2 = G_{IC}E$  has been used. In Eq. (6),  $K_{IC}^2$  denotes toughness in the absence of domain switching, i.e., in the paraelectric state. In a polycrystalline material with domains randomly distributed, the maximum possible value of  $\epsilon_s$  is given by  $\epsilon_s \approx (2/3)(c/a - 1)$ . For the PZT studied here,  $\epsilon_s \approx 0.0127$ . In a compression test, however, the remnant strain was  $4.6 \times 10^{-4}$ . Thus, in a tensile test it would be  $\sim 9.2 \times 10^{-4}$ . Young's modulus,  $E$ , of this material is  $\approx 6.6 \times 10^{10}$  N/m<sup>2</sup>. The nonlinearity in stress-strain curves sets in at  $\sim 25$  MPa. Thus, the lower estimate of  $\sigma_c$  in compression is  $\approx 25$  MPa. Assuming it to be the same in tension and noting that  $K_{IC}^2$  (above the Curie temperature)  $\approx 1.0$  MPa $\cdot$ m<sup>1/2</sup>,  $K_{IC}$  calculated using Eq. (6) in the ferroic state is  $\approx 1.28$  MPa $\cdot$ m<sup>1/2</sup>. The measured  $K_{IC}$  at room temperature is between 1.3 and 1.85 MPa $\cdot$ m<sup>1/2</sup>. This suggests that a part of the enhancement in fracture toughness must be due to ferroelastic domain switching, with the remaining being due to other mechanisms such as microcracking. The preceding gives only an approximate estimate of domain switching contribution to toughening. A more realistic estimate must await the determination of the depth to which switching occurs as well as the degree of switching.

As discussed in the following, indentation experiments on mechanically poled samples are also in accord with domain switching. X-ray diffraction showed that  $I_{(002)}/I_{(200)}$  decreased from the face subjected to compression while it increased from the faces parallel to the loading axis. This suggests that a compressive stress caused domains to align with  $c$  axes perpendicular to the loading axis. After compression testing, indentations were introduced with one of the diagonals along the loading axis. Crack lengths along the loading axis were longer than in the orthogonal direction (see Fig. 9). This observation can be rationalized as follows.

Many of the domains reorient during compression testing, with their  $c$  axes orthogonal to the loading direction. During fracture, domains in the crack tip region with  $c$  axes parallel to the crack surface should reorient orthogonal to the crack plane. This process is expected to absorb energy which should reflect as enhanced toughness. By contrast, domains that are already orthogonal to the crack surface should remain unaltered. Thus, no energy is absorbed by these domains. When indented with one of the diagonals parallel to the compression loading direction, no switching is expected for a crack along the loading direction, as the domains are already oriented perpendicular to the prospective crack. By contrast, for a crack orthogonal to the loading direction, a large number of domains have their  $c$  axes parallel to the prospective crack. Thus, as a crack is formed by indentation, domain reorienta-

tion near the tip can occur such that their  $c$  axes become perpendicular to the crack surface. This is shown schematically in Fig. 10, in which the arrows A and B indicate the orientations of domains before and after the introduction of the crack. Since energy is absorbed in the switching process, it is expected that the crack will be shorter in the direction perpendicular to the loading direction. This is precisely what was observed. Similar effects were also observed in electrically poled samples in which indentation cracks were shorter in the direction of poling as domains aligned along the field. The  $K_{IC}$  determined by indentation for a crack parallel to the loading direction was  $\sim 0.35$  MPa $\cdot$ m<sup>1/2</sup> compared to  $\sim 0.73$  MPa $\cdot$ m<sup>1/2</sup> in the orthogonal direction, indicating a substantial contribution of domain switching to the overall toughness. The indentation toughnesses are considerably lower than those obtained by SENB technique. However, their relative magnitudes are in accord with the analysis presented here.

SENB testing showed that the toughness of samples electrically poled in a direction along the notch surface was  $\sim 1.2$  MPa $\cdot$ m<sup>1/2</sup> while of the samples poled in a direction perpendicular to the notch surface was  $\sim 0.98$  MPa $\cdot$ m<sup>1/2</sup>. This observation again is in accord with the preceding analysis. The unpoled samples, however, exhibited toughness  $\sim 1.45$  MPa $\cdot$ m<sup>1/2</sup>. This result suggests that domain switching in unpoled samples is apparently easier. Further work is needed to explore this effect.

Okazaki and co-workers<sup>10,11</sup> also observed anisotropy of indentation crack lengths in electrically poled PbTiO<sub>3</sub> and PLZT polycrystalline ceramics. However, they interpreted the results on the basis of an internal stress. In analogy with the indentation work on tempered glass<sup>13</sup> and surface-ground zirconia ceramics<sup>14</sup> in which the apparent toughness  $K_{IC}$  de-

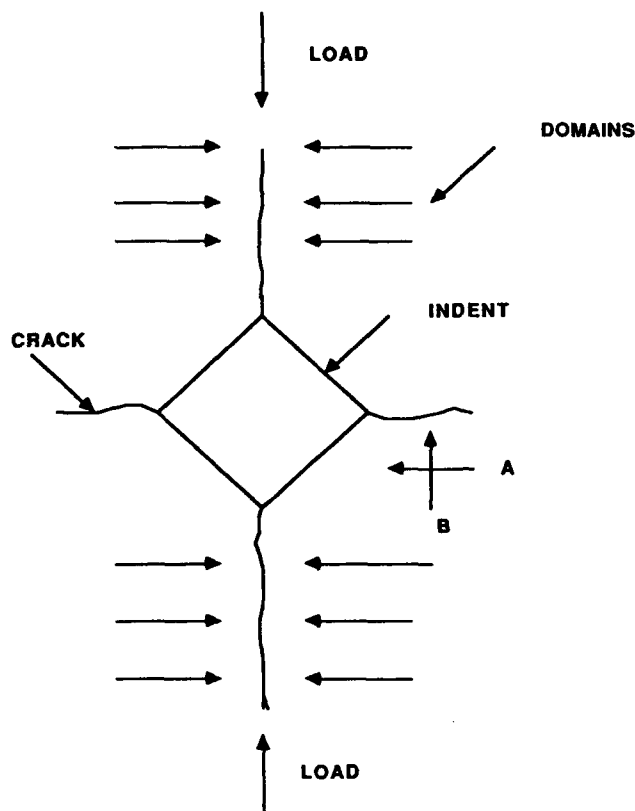


Fig. 10. Schematic showing the anisotropy of crack lengths in a mechanically poled sample. The horizontal cracks are shorter because domain reorientation is expected to occur once the indentation is introduced. The arrows A and B indicate the orientations of the domains before and after introduction of the indent. By contrast, for the vertical cracks, no reorientation is expected, since the domains are already oriented in the prospective direction.

\*In a tensile test, domains from two orthogonal directions orient along the stress axis. By contrast, in a compression test, domains initially along the stress axis reorient in two directions orthogonal to the stress axis. Thus, the switching strain in a tensile test is twice that in a compression test.

pends upon the true toughness  $K_{IC}^0$ , the crack length (radius)  $c$ , and uniform residual stress,  $\sigma_i$ , in the vicinity of the crack tip, via

$$K_{IC} = K_{IC}^0 - \frac{2}{\sqrt{\pi}} \sigma_i \sqrt{c} \quad (7)$$

Okazaki *et al.*<sup>10,11</sup> deduced that there must be a uniform stress in their poled and unpoled samples. In Eq. (7), for a compressive stress,  $\sigma_i < 0$ . Thus, if a surface compressive stress exists, the apparent toughness will be higher. Okazaki *et al.*<sup>10,11</sup> observed that the crack sizes were of the same lengths in unpoled samples (similar to the present work) but were different in the two directions in the poled samples. They suggested that there must be an internal stress in the ferroic samples used in their study and that stresses must be anisotropic, macroscopically, in the poled samples.

Residual stresses determined by Okazaki<sup>11</sup> in PLZT ceramics were as high as 14.5 GPa, while the hardness was only 0.47 GPa. Clearly, such high stresses cannot be sustained by the material. More importantly, it can be shown that their interpretation based on residual stresses is incorrect. It is to be noted that a uniform stress cannot be present in either unpoled or poled samples, since this violates mechanical equilibrium. A periodic internal stress whose wavelength is on the order of twice the grain size, however, does exist because of the tetragonality induced by the cubic  $\rightarrow$  tetragonal transition. To a first approximation, some of the grains are under compression while the others are under tension, with the spatial average of the stress being zero. If the amplitude of the periodic internal stress is  $\sigma_i$ , then the additional toughening that can be realized is  $\sim 1.22\sigma_i d^{1/2}$  where  $d$  is the grain size.<sup>15-17</sup> According to the work of Freiman and co-workers,<sup>18</sup> the magnitude of the internal stress is on the order of 25 MPa. The linear dependence of  $K_{IC}$  on  $c^{1/2}$  with positive slope observed in the work of Okazaki *et al.*<sup>10,11</sup> is probably due to an *R*-curve behavior and cannot be due to residual stress. In tempered glass plates<sup>13</sup> and surface-ground zirconia ceramics,<sup>14</sup> the slope is identified with the surface stress, since the surface is under a uniform stress, unlike the PbTiO<sub>3</sub> and PLZT materials used by Okazaki *et al.*<sup>10,11</sup>

Pisarenko *et al.*<sup>9</sup> have also attributed the anisotropy in fracture toughness of piezoelectric ceramics to the concept of domain reorientation and have further pointed out the errors in the interpretation based on an internal stress. Freiman *et al.*<sup>18</sup> have suggested microcracking and crack/twin interactions as possible mechanisms of toughening. However, no evidence of microcracking was presented. Also, the nature of crack/twin interaction was not suggested. Further, the enhanced toughness of pressure-depoled PZT ceramics was interpreted on the basis of antiferroelectric domains transforming into ferroelectric domains, although no supporting evidence was presented.

## (2) Kinetics of Domain Switching

Based on X-ray diffraction, domain switching was detected on fracture surfaces of some of the samples tested at room temperature, but not all. Failure to observe domain switching in some of the samples does not imply that it did not occur, as discussed below.

In transformation-toughened materials, it is a common practice to determine the monoclinic content on fracture surfaces using X-ray diffraction. Appearance of the monoclinic phase on fracture surfaces in many zirconia ceramics is indeed a unique characteristic of transformation-toughened materials. In most martensitic transformations, the parent phase/martensite boundary can propagate at velocities on the order of the sound velocity. Thus, when a crack propagates through such a body, a high stress is experienced by regions near the crack surfaces for a long enough time for transformation to occur. By contrast, plastic or viscous deformation is time dependent over the ranges of strain rates experienced in typical experiments. If a material such as a hard metal

(high carbon steel) containing a crack is subjected to external loads, a plastic zone develops at the crack tip. Once the stress intensity factor exceeds the quasi-static fracture toughness, the crack begins to propagate in a brittle manner. Thus, plastic deformation contributes to the quasi-static fracture toughness even though rapid fracture occurs in a brittle manner. It is well-known that in steels the critical  $K_I$  for crack propagation is considerably lower than for the initiation of crack propagation.

Domain switching is also known to be time dependent and can be described as a relaxative phenomenon. Recently, Rudyak<sup>19</sup> has examined domain switching and viscosity phenomena in ferroelectric and ferroelastic materials. For many ferroelastics, Rudyak<sup>19</sup> has shown that the characteristic relaxation times,  $\tau_r$ , can be on the order of several seconds. For example, in Gd<sub>2</sub>(MoO<sub>4</sub>) (GMO) and KH<sub>2</sub>(SeO<sub>3</sub>)<sub>2</sub>, the  $\tau_r$  is on the order of several seconds. For simultaneously ferroelectric-ferroelastic materials, there is a one-to-one correspondence between switching by stress and electrical field. The 90° domain switching in PZT is identical with ferroelastic domain switching.<sup>†</sup> Since the electric field can be applied almost instantaneously, experiments on the kinetics of switching were performed under an applied electric field.

When an electric field is applied, two relaxative processes occur: (1) domain switching with relaxation time  $\tau_s$  and (2) charging of the capacitor with a relaxation time  $\tau_c$ .<sup>20</sup> The relaxation experiments conducted in the present study cannot distinguish between the two processes. The process with the larger relaxation time will be reflected in these experiments. Figure 7 shows the data can be adequately represented by a first-order kinetic equation. The  $\tau$  measured was typically between 0.3 to 3 s. This implies that the  $\tau_s \leq 0.3$  to 3 s.

In order to determine how fast 90° domain switching can occur in mechanical loading, some of the samples were rapidly (within 3 to 5 s) loaded to 250 MPa in compression and instantaneously unloaded. X-ray diffraction traces (Fig. 11) before and after loading clearly show that domain switching did occur. These results are in accord with those of electrical experiments in that 90° domain switching occurs in less than a couple of seconds.

Recently, Arlt *et al.*<sup>21</sup> examined frequency response of 90° domain wall motion in PZT under small fields (so that irreversible wall motions do not occur). Under these conditions, the domain walls could be vibrated at frequencies as high as 100 kHz. Thus, the  $\tau_r$  for relaxation may be as small as  $1 \times 10^{-5}$  s. In rapid crack growth, crack velocity,  $v$ , is typically in excess of 10 m/s. If the typical domain size,  $\lambda$ , is, say, 1  $\mu$ m, a domain close to the crack tip experiences a high stress (greater than  $\sigma_c$ ) for time  $\approx \lambda/v$  or on the order of  $1 \times 10^{-7}$  s. This is considerably lower than  $\tau_r$ . The implication is that domain switching is not expected to occur when a crack is rapidly growing. In order to verify this hypothesis, DCB samples were tested in such a way that initially the crack was allowed to grow slowly ( $v \sim 100 \mu$ m/s) but later the samples fractured rapidly. X-ray diffraction from fracture surfaces (Fig. 5) clearly shows that domain switching occurred in the slow crack regime but not in the fast crack regime.

It is instructive to make a similar calculation for transformation-toughened materials. As mentioned previously, in martensitic transformations, the parent phase/martensite boundary moves with a velocity on the order of the sound velocity, which in zirconia is  $\sim 6 \times 10^3$  m/s. The highest velocity that a crack can move is less than the sound velocity. According to Roberts and Wells,<sup>22</sup> this is  $0.38 \times$  longitudinal wave velocity. As the parent phase/martensite boundary can move faster than the ultimate crack velocity, the implication is that, in transformation-toughened materials,

<sup>†</sup>This, however, is not the case with 180° domain switching, during which no dimensional or shape changes occur. Consequently, these are not important from the standpoint of toughening.

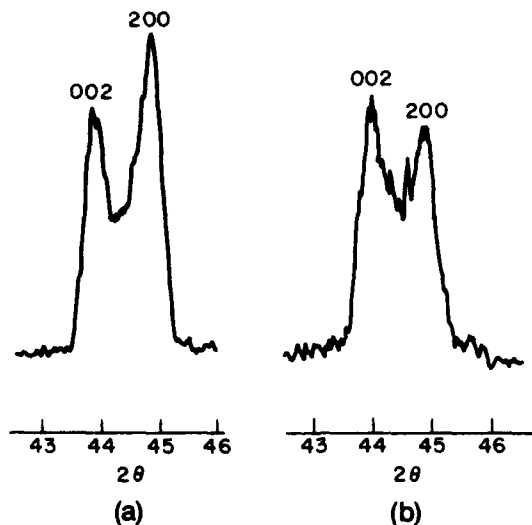


Fig. 11. XRD traces of (a) as-annealed and (b) rapidly loaded (in compression) and unloaded sample, showing the occurrence of domain switching. The entire loading and unloading was done in about 5 s. The figure shows that domain switching occurs relatively quickly and that slow relaxation, such as that observed by Esaklul *et al.*,<sup>21</sup> does not represent the early stages of domain switching.

one would always observe monoclinic phase on fracture surfaces except, of course, when reverse transformation occurs.

The relaxation phenomenon in ferroic materials has been investigated by many researchers. For example, Esaklul *et al.*<sup>23</sup> studied relaxation in PZT under mechanical loading and found that a first-order kinetic equation did not describe the relaxation behavior. The load relaxation was very sluggish. In the present work also, relaxation under mechanical load was slow. Clearly, this phenomenon is different from 90° domain switching. Similar observations were made by Syrkin and Elgard<sup>24</sup> on BaTiO<sub>3</sub>, who measured a relaxation time ~10 min. The slowness of this relaxation phenomenon suggests that it is not relevant from the standpoint of toughening. The present work shows that 90° domain switching, which contributes to toughness, can be examined by electrically poling the sample, as discussed here.

## V. Summary and Conclusions

(1) The  $K_{IC}$  of the commercial PZT ceramics tested decreased with increasing temperature up to the Curie temperature (350°C), beyond which it remained constant up to the maximum test temperature of 500°C.

(2) X-ray diffraction traces from fracture surfaces of samples tested at room temperature often showed that the ratio  $I_{(002)}/I_{(200)}$  was greater than from pristine surfaces. This suggests that domain switching can occur during fracture.

(3) The fact that an increase in the ratio  $I_{(002)}/I_{(200)}$  is sometimes not observed on fracture surfaces of samples rapidly fractured in the ferroic state is attributed to the slowness of the kinetics of switching in comparison to crack growth. However, during the quasi-static loading of a crack, domain switching occurs near the crack tip, thus contributing to toughness.

(4) Indentation experiments on mechanically and electrically poled samples exhibited an anisotropy in crack lengths.

The crack length was shorter in the direction in which the 90° domains align during poling (mechanical and electrical). The alignment of the domains during the poling process was confirmed by X-ray diffraction.

(5) On the basis of these observations, it is proposed that ferroelastic domain switching in the stress field of a crack tip is a viable toughening mechanism in PZT ceramics.

**Acknowledgment:** Ms. Angella Richardson of Edowestern, Inc. of Salt Lake City is gratefully acknowledged for providing the samples used in this study as well as electrical poling of the samples used in the indentation work.

## References

- S. C. Abrahams and E. T. Keve, "Structural Basis of Ferroelectricity and Ferroelasticity," *Ferroelectrics*, **2**, 129–54 (1971).
- K. Aizu, "Possible Species of Ferromagnetic, Ferroelectric and Ferroelastic Crystals," *Phys. Rev. B: Condens. Matter*, **2** [3] 754–72 (1970).
- R. C. Pohanka, S. W. Freiman, K. Okazaki, and S. Tashiro, "Fracture of Piezoelectric Materials"; pp. 353–64 in *Fracture Mechanics of Ceramics*, Vol. 5. Edited by R. C. Bradt, A. G. Evans, D. P. H. Hasselman, and F. F. Lange. Plenum Press, New York, 1983.
- R. C. Pohanka, S. W. Freiman and B. A. Bender, "Effect of Phase Transformation on the Fracture Behavior of BaTiO<sub>3</sub>," *J. Am. Ceram. Soc.*, **61** [1–2] 72–75 (1978).
- R. C. Pohanka, S. W. Freiman, and R. W. Rice, "Fracture Processes in Ferroic Materials," *Ferroelectrics*, **28**, 337 (1980).
- R. C. Pohanka, R. W. Rice, and B. E. Walker, Jr., "Effect of Internal Stress on the Strength of BaTiO<sub>3</sub>," *J. Am. Ceram. Soc.*, **59** [1–2] 71–74 (1976).
- K. D. McHenry and B. G. Koepke, "Electric Field Effects on Subcritical Crack Growth in PZT"; pp. 337–52 in *Fracture Mechanics of Ceramics*, Vol. 5. Edited by R. C. Bradt, A. G. Evans, D. P. H. Hasselman, and F. F. Lange. Plenum Press, New York, 1983.
- R. F. Cook, S. W. Freiman, B. R. Lawn, and R. C. Pohanka, "Fracture of Ferroelectric Ceramics," *Ferroelectrics*, **50**, 267–72 (1983).
- G. G. Pisarenko, V. M. Chushko, and S. P. Kovalev, "Anisotropy of Fracture Toughness of Piezoelectric Ceramics," *J. Am. Ceram. Soc.*, **68** [5] 259–65 (1985).
- T. Yamamoto, H. Igarashi, and K. Okazaki, "Internal Stress Anisotropies Induced by Electric Field in Lanthanum Modified PBTiO<sub>3</sub> Ceramics," *Ferroelectrics*, **50**, 273–78 (1983).
- K. Okazaki, "Mechanical Behavior of Ferroelectric Ceramics," *Bull. Am. Ceram. Soc.*, **63** [9] 1150–52, 57 (1984).
- Kare Hellan, *Introduction to Fracture Mechanics*. McGraw-Hill, New York, 1984.
- D. B. Marshall and B. R. Lawn, "An Indentation Technique for Measuring Stress in Tempered Glass Surfaces," *J. Am. Ceram. Soc.*, **60** [1–2] 86–87 (1977).
- Y. Ikuma and A. V. Virkar, "Crack Size Dependence of Fracture Toughness in Transformation Toughened Ceramics," *J. Mater. Sci.*, **19**, 2233 (1984).
- A. V. Virkar and D. L. Johnson, "Fracture Behavior of ZrO<sub>2</sub>-Zr(O) Composites," *J. Am. Ceram. Soc.*, **60** [11–12] 514–19 (1977).
- R. A. Cutler and A. V. Virkar, "The Effect of Binder Thickness and Residual Stresses on the Fracture Toughness of Cemented Carbides," *J. Mater. Sci.*, **20**, 3557–73 (1985).
- A. G. Evans, A. H. Heuer, and D. L. Porter, "Fracture Toughness of Ceramics," *Adv. Res. Strength Fract. Mater., Int. Conf. Fract.*, **4th**, 1, 529 (1977).
- S. W. Freiman, L. Chuck, J. J. Mecholsky, D. L. Shelleman, and L. J. Storz, "Fracture Mechanisms in Lead Zirconate Titanate Ceramics"; pp. 175–85 in *Fracture Mechanics of Ceramics*, Vol. 8. Edited by R. C. Bradt, A. G. Evans, D. P. H. Hasselman, and F. F. Lange. Plenum Press, New York, 1986.
- V. M. Rudyak, "Viscosity Phenomenon and Switching Processes in Ferroelastics," *Ferroelectrics*, **48**, 131–41 (1983).
- A. K. Jonscher, *Dielectric Relaxation in Solids*. Chelsea Dielectric Press, London, U.K., 1983.
- G. Arlt, H. Dederichs, and R. Herbiet, "90°-Domain Wall Relaxation in Tetragonally Distorted Ferroelectric Ceramics," *Ferroelectrics*, **74**, 37–53 (1987).
- D. K. Roberts and A. A. Wells, "The Velocity of Brittle Fracture," *Engineering (London)*, **178**, 820–21 (1954).
- K. A. Esaklul, W. W. Gerberich, and B. G. Koepke, "Stress Relaxation in PZT," *J. Am. Ceram. Soc.*, **63** [1–2] 25–30 (1980).
- L. N. Syrkin and A. M. Elgard, "Influence of the Domain Structure of Ceramic Ferroelectrics on Their Mechanical Properties," *Sov. Phys.—Solid State (Engl. Trans.)*, **7** [4] 967–71 (1965). □

## Grinding-Induced Texture in Ferroelastic Tetragonal Zirconia

Karun Mehta,\* Jan Fong Jue,\* and Anil V. Virkar\*

Department of Materials Science and Engineering, University of Utah, Salt Lake City, Utah 84112.

Ceria- and yttria-doped tetragonal polycrystalline zirconia ceramics were ground at temperatures as high as 1100°C. X-ray diffraction revealed that the intensity ratio  $I_{(002)}/I_{(200)}$  increased (to as high as  $\approx 4.5$ ) compared with that from the as-sintered surfaces ( $\approx 0.55$ ). The enhancement in  $I_{(002)}/I_{(200)}$  at temperatures well above the  $m \rightarrow t$  transition temperature shows that it is not related to transformation, reversible or otherwise, but can be explained by ferroelastic domain switching. [Key words: tetragonal zirconia, ferroelastic materials, domains, grinding, texture.]

In a study of the mechanical properties of ceria-stabilized tetragonal zirconia, C<sub>2</sub>TZP, Virkar and Matsumoto<sup>1,2</sup> observed that, upon surface grinding, the intensity of the (002) peak ( $I_{(002)}$ ) increases while that of the (200) peak ( $I_{(200)}$ ) decreases without the formation of a monoclinic phase. The increase in  $I_{(002)}$  on ground surfaces implies that the state of stress in the surface region must be conducive to orienting domains with their c axes orthogonal to the surface;<sup>1</sup> that is, the state of stress must be biaxial compressive.<sup>3</sup> Prior work by Michel *et al.*<sup>4</sup> identified tetragonal zirconia as a ferroelastic material. On the basis of this information, Virkar and Matsumoto<sup>1,2</sup> suggested that the changes in intensities of the (200) and the (002) peaks upon grinding must have occurred by ferroelastic domain switching. In support of this contention, additional data on the grinding behavior of BaTiO<sub>3</sub> and lead zirconate titanate were presented which showed that similar texture can also be introduced in these materials.<sup>2</sup> This information was deemed particularly important since no transformation is expected in these materials.

Explanations of grinding-induced texture in tetragonal zirconia based on tetragonal to monoclinic ( $t \rightarrow m$ ) transformation have also been presented.<sup>5</sup> Swain and Hannink,<sup>5</sup> for example, proposed that the texture is introduced by a reversible  $t \rightarrow m \rightarrow t$  transformation. In their hypothesis, during grinding,  $t \rightarrow m$  transformation occurs in some of the grains. Then, with continued grinding the temperature of the surface exceeds the  $A_f$  temperature thereby effecting the reverse  $m \rightarrow t$  transformation. This explanation is incorrect since, during grinding (in hand grinding, for example), a steady state of temperature will be reached after some initial time. If this temperature is above the  $A_f$  temperature, actual grinding itself is done above  $A_f$ . Thus, no  $t \rightarrow m$  can occur. If the temperature is below  $A_f$ ,  $t \rightarrow m$  will occur, but then the reverse transformation cannot occur. For these reasons, the explanation given by Swain and Hannink<sup>5</sup> is incorrect. Further, their own data are not in accord with their model. Specifically their Table I shows that, after annealing the ground samples (for effecting  $m \rightarrow t$  transformation), the

$I_{(002)}/I_{(200)}$  decreased instead of increasing as their model would predict.

The objective of the present work was to demonstrate that the increase in the intensity ratio,  $I_{(002)}/I_{(200)}$ , upon grinding, is not related to transformation, reversible or otherwise. Instead, ferroelastic domain switching explains this phenomenon in a natural way. In the present work, ceria- and yttria-stabilized tetragonal polycrystalline samples were ground at temperatures as high as 1100°C so that transformation effects can be eliminated. These experiments are described in the following paragraphs.

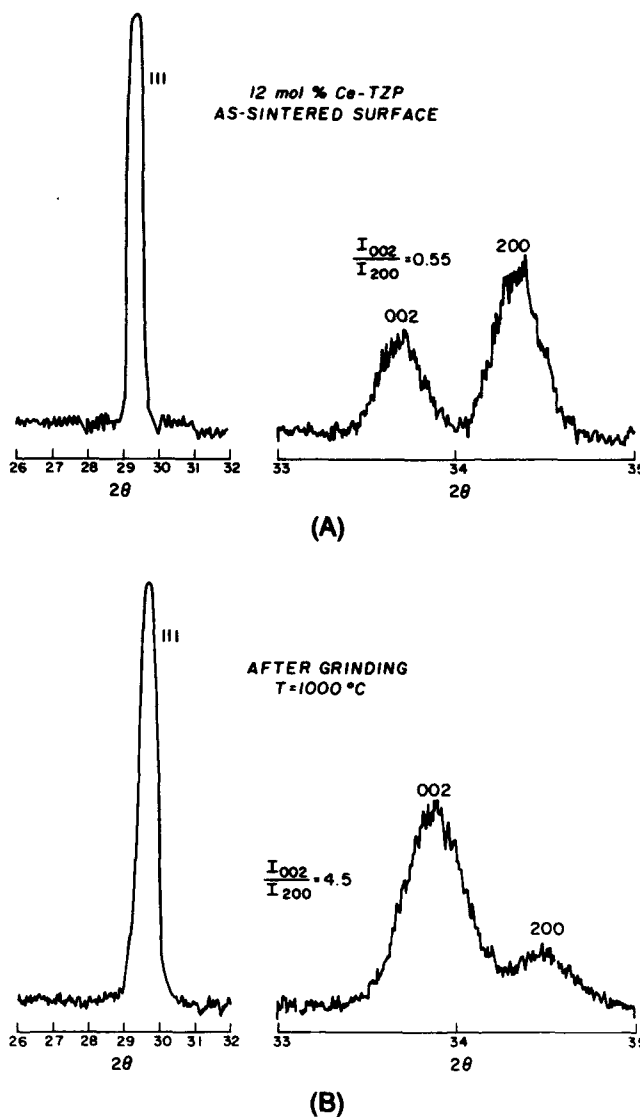


Fig. 1. XRD peaks of 12 mol% C<sub>2</sub>TZP: (A) XRD peaks of an as-fired surface showing the presence of tetragonal single phase with near random orientation,  $I_{(002)}/I_{(200)} \approx 0.55$  and (B) XRD trace of the same sample after grinding at 1000°C showing the presence of tetragonal single phase with  $I_{(002)}/I_{(200)} \approx 4.5$ .

I-W. Chen—contributing editor

Manuscript No. 197962. Received November 16, 1989; approved February 7, 1990.

Supported by DARPA through AFOSR under Contract No. F49620-89-C-0054; subcontract from Ceramtec, Inc., to the University of Utah.

\*Member, American Ceramic Society.

## II. Experimental Procedure, Results, and Discussion

Ceria-doped zirconia polycrystalline ceramics containing 12 and 16 mol%  $\text{CeO}_2$  were fabricated by pressureless sintering of isostatically pressed compacts in air at  $1550^\circ\text{C}$  for 2 h. Similarly, yttria-doped polycrystalline samples containing 2.5 mol%  $\text{Y}_2\text{O}_3$  were also fabricated by sintering in air at  $1450^\circ\text{C}$  for 2 h. The sample surfaces were examined by X-ray diffraction (XRD) using  $\text{CuK}\alpha$  radiation. All the samples contained only the tetragonal phase with no detectable amount of the monoclinic phase. The  $I_{(002)}/I_{(200)}$  ratio from the surfaces of all as-sintered samples was about 0.55, indicative of a near random orientation of the tetragonal phase. Subsequently, the samples were preheated to various temperatures, up to a maximum of  $1100^\circ\text{C}$ . A bonded SiC grinding wheel was kept

next to the furnace. Once the samples were equilibrated at the desired temperature, they were removed from the furnace one at a time and *hot-ground on the uncooled wheel*. The actual grinding operation lasted less than 1 min, typically 30 s. Two factors tend to lower the temperature—loss of heat to the atmosphere and loss of heat to the wheel. One factor tends to raise the temperature—heat generation by grinding. All prior studies on grinding would suggest that the rate of heat generation at the surface being ground exceeds heat dissipation thus resulting in an increase in the temperature of the surface being ground. Therefore, because the samples were heated and the wheel was uncooled, it is expected that the temperature of the surface being ground must have been at least as high as the preheat temperature.

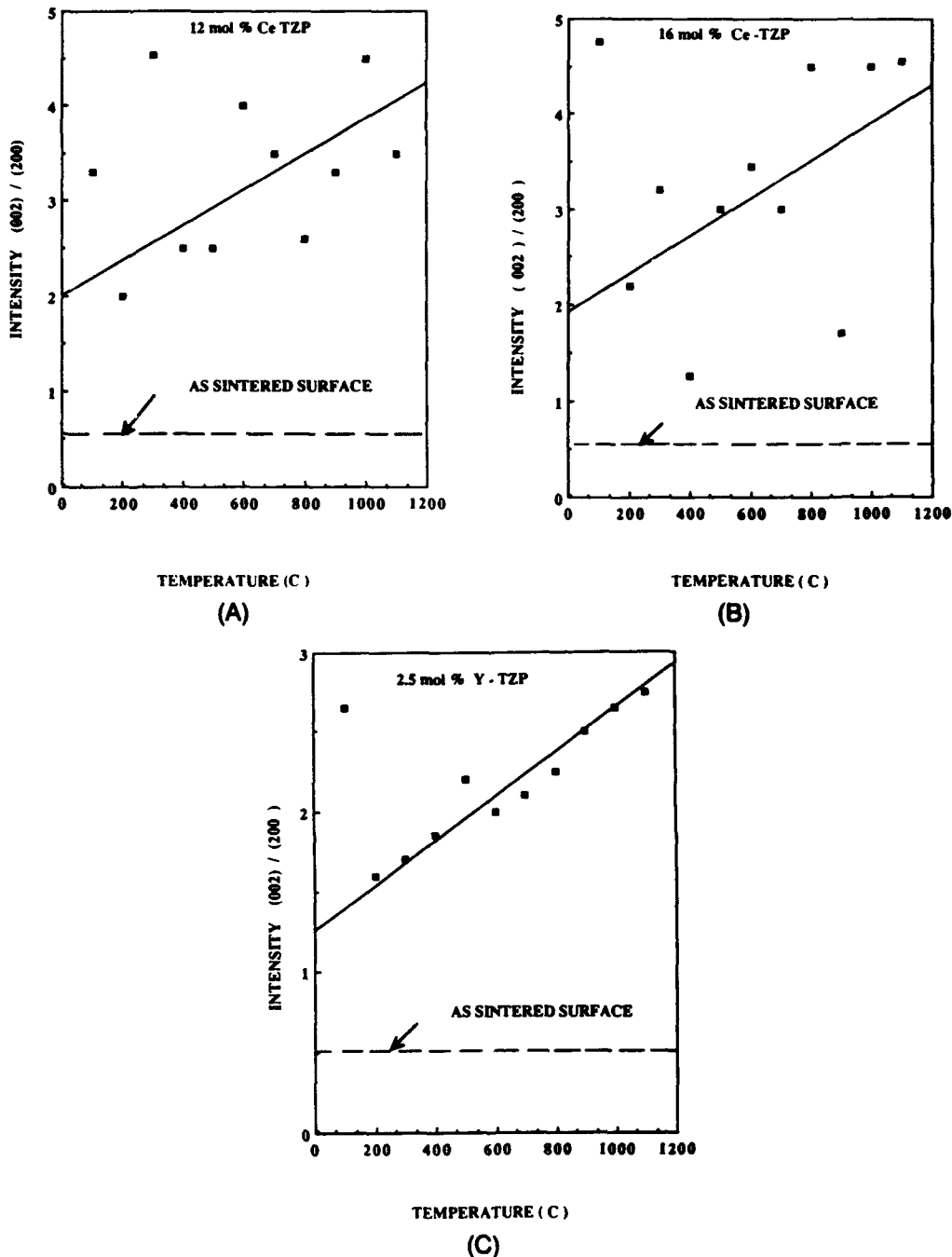


Fig. 2. (A)  $I_{(002)}/I_{(200)}$  ratio as a function of (preheat) temperature at which 12 mol% CeTZP samples were ground. (B)  $I_{(002)}/I_{(200)}$  ratio as a function of (preheat) temperature at which 16 mol% CeTZP samples were ground. (C)  $I_{(002)}/I_{(200)}$  ratio as a function of (preheat) temperature at which 2.5 mol% YTZP samples were ground.

After grinding, the surfaces were again examined by XRD. In all cases the  $I_{(002)}/I_{(200)}$  ratio was considerably greater than 0.5, often as high as 4.5. No monoclinic phase was observed in any of the ground surfaces of 16 mol% CeTZP and YTZP samples at any temperature. Some monoclinic phase was observed in 12 mol% CeTZP samples when ground at room temperature. No monoclinic phase was observed in these samples when ground at temperatures  $\geq 100^\circ\text{C}$ . Figures 1(A) and (B) show XRD peaks of a 12 mol% CeTZP sample from the as-fired surface and from the surface that was ground at  $1000^\circ\text{C}$ , respectively. Note that no monoclinic phase is formed and that the  $I_{(002)}$  is considerably greater than  $I_{(200)}$  from the ground surface. Figures 2(A), (B), and (C) show the ratio  $I_{(002)}/I_{(200)}$  as a function of the temperature at which samples were ground for 12 mol% CeTZP, 16 mol% CeTZP, and 2.5 mol% YTZP, respectively. Because the samples were held in a pair of tongs and ground, it is anticipated that the pressure during grinding must have varied from test to test. Despite this, it is of interest to note that the ratio  $I_{(002)}/I_{(200)}$  actually increases with increasing temperature. With increasing temperature, the tendency of the tetragonal phase to transform into the monoclinic phase decreases, and above  $A_f$  it should be actually zero. If the scenario suggested by Swain and Hannink<sup>5</sup> were operative, the  $I_{(002)}/I_{(200)}$  ratio for samples ground above  $A_f$  would be about 0.5, which is not the case. By contrast, it is well-known that the coercive stress for ferroelastic domain switching usually decreases with increasing temperature (with temperature much below the Curie temperature ( $T_c$ )). Thus, the  $I_{(002)}/I_{(200)}$  ratio is expected to increase with increasing temperature if the texture is caused by ferroelastic domain switching. This is precisely what is observed.

If a ferroelastic material is ground in its paraelastic state (above  $T_c$ ), no texture is to be expected. For the zirconia ceramics used in the present study, the  $T_c$  (for the  $c \rightarrow t$  displacive transition) is above  $\approx 2000^\circ$  to  $2100^\circ\text{C}$ . Thus, all of the grinding experiments were well below the  $T_c$ . To examine the effect of grinding above and below the  $T_c$ , samples of commercial  $\text{PbTiO}_3$  ceramics\* with  $T_c$  of  $\approx 240^\circ\text{C}$  were ground on

a SiC-bonded wheel with and without coolant. After grinding with coolant, the  $I_{(002)}/I_{(200)}$  was about 1.3 compared with 0.5 from pristine, as-fired surfaces. However, when ground without the coolant, the  $I_{(002)}/I_{(200)}$  was  $\approx 0.5$ , the same as from pristine surfaces. No direct measurement of the surface temperature was possible. However, published literature<sup>6</sup> suggests that the surface temperature in dry grinding must have been  $> 240^\circ\text{C}$ . Thus, no texture is developed when samples are ground in the paraelastic state. Such effects of grinding above and below  $T_c$  cannot be observed in zirconia because of the very high  $T_c$ . Consequently, grinding of tetragonal zirconia invariably introduces some texture. This texture can be removed by annealing the samples above  $T_c$  ( $\geq 2100^\circ\text{C}$ ).

### III. Conclusion

Enhancement in the intensity ratio,  $I_{(002)}/I_{(200)}$ , upon grinding of tetragonal zirconia is due to ferroelastic domain switching and not due to reverse transformation.

**Acknowledgment:** Discussions with Dr. Raymond Cutler of Ceramtec, Inc., are gratefully acknowledged.

### References

- <sup>1</sup>A. V. Virkar and R. L. K. Matsumoto, "Ferroelastic Domain Switching as a Toughening Mechanism in Tetragonal Zirconia," *J. Am. Ceram. Soc.*, **69** [10] C-224-C-226 (1986).
- <sup>2</sup>A. V. Virkar and R. L. K. Matsumoto, "Toughening Mechanism in Tetragonal Zirconia Polycrystalline (TZP) Ceramics"; p. 653-62, in *Advances in Ceramics*, Vol. 24, Science and Technology of Zirconia III. Edited by S. Somiya, N. Yamamoto, and H. Yanagida. American Ceramic Society, Inc., Westerville, OH 1988.
- <sup>3</sup>B-S. Li, J-S. Cherng, K. J. Bowman, and I-W. Chen, "Domain Switching as a Toughening Mechanism in Tetragonal Zirconia," *J. Am. Ceram. Soc.*, **71** [7] C-361-C-364 (1988).
- <sup>4</sup>D. Michel, L. Mazerolles, and M. Perez y Jorba, "Fracture of Metastable Tetragonal Crystals," *J. Mater. Sci.*, **18**, 2618-28 (1983).
- <sup>5</sup>M. V. Swain and R. H. J. Hannink, "Metastability of the Martensitic Transformation in a 12 mol% Ceria-Zirconia Alloy: II, Grinding Studies," *J. Am. Ceram. Soc.*, **72** [8] 1358-64 (1989).
- <sup>6</sup>R. J. Lokken and E. J. Duwell, "Grinding Stone, Concrete, and Ceramics with Coated Abrasives"; pp. 201-208 in NBS Special Publication Number 562, *The Science of Ceramic Machining and Surface Finishing II*. Edited by B. J. Hockey and R. W. Rice. National Bureau of Standards, Washington, DC, 1979. □

\*Supplied by Ms. Angela Richardson of Edo Western, Salt Lake City, UT.

# Fabrication, Microstructural Characterization, and Mechanical Properties of Polycrystalline *t'*-Zirconia

Jan Fong Jue\* and Anil V. Virkar\*

Department of Materials Science and Engineering, University of Utah, Salt Lake City, Utah 84112

Large-grained (100- to 200- $\mu\text{m}$ ), yttria-doped, polycrystalline *t'*-zirconia ceramics were fabricated by heat-treating presintered samples at temperatures  $\geq 2100^\circ\text{C}$ . Polarized light microscopy revealed the ferroelastic domain structure in the *t'* samples. XRD showed that no monoclinic phase was detected on as-polished, ground and fracture surfaces, or on surfaces while under a tensile stress as high as 400 MPa. By contrast, relative changes occurred in the tetragonal peak intensities, which were attributed to ferroelastic domain switching. The higher toughness of 3-mol%- $\text{Y}_2\text{O}_3$ -doped *t'* samples ( $7.7 \text{ MPa}\cdot\text{m}^{1/2}$ ) compared to that of 8 mol%  $\text{Y}_2\text{O}_3$  cubic samples ( $2.4 \text{ MPa}\cdot\text{m}^{1/2}$ ) was explained in part by ferroelastic domain switching. [Key words: zirconia—yttria stabilized tetragonal polycrystals, mechanical properties, microscopy, ferroelastic materials, fracture mechanics.]

## I. Introduction

TETRAAGONAL zirconia stabilized with  $\text{Y}_2\text{O}_3$  or other oxides can be fabricated via three different routes: (1) sintering in the stability range of the tetragonal phase field (TZP); (2) sintering in the stability range of the cubic field followed by slow cooling, which leads to the precipitation of the tetragonal phase (PSZ);<sup>2,3</sup> (3) sintering in the cubic phase field followed by rapid cooling, which leads to the displacive, composition-invariant transformation of the cubic phase into the tetragonal phase.<sup>4-6</sup> The former two are referred to as the *t*-phase in the literature, while the latter is referred to as the *t'*-phase. Crystallographically there is no difference between the *t*- and the *t'*-phases. That is, for a given composition, the atomic positions and the unit cell parameters are the same in both phases. However, there are some characteristic morphological differences between the *t* and *t'* phases. Research conducted over the past decade has shown that the stability of the *t* and the *t'* phases may be very different. For example, it is known that the *t*-phase generally transforms into the monoclinic phase under the application of stress. By contrast, the *t'*-phase has been often referred to as a nontransformable phase because it is often resistant to transformation even after severe grinding. It appears that this difference in the behavior of the *t*- and the *t'*-phases must be somehow related to the morphological aspects. It has also been proposed that the transformability of the tetragonal phase depends upon the degree of tetragonality.<sup>7</sup> From the standpoint of morphological features, the *t'*-phase is characterized by the presence of heringbone structure<sup>8</sup> and the three tetragonal variants.<sup>9</sup> Further, the *t'*-phase also exhibits antiphase boundaries (APB's) when imaged through {112} fluorite-forbidden reflection in dark-field TEM.<sup>6,8,9</sup>

I-W. Chen—contributing editor

Manuscript No. 197669. Received April 5, 1990; approved August 27, 1990.

Supported by the Defense Advanced Research Projects Agency (DARPA) through AFOSR under Contract No. F49620-89-C-0054 at the University of Utah through a subcontract from Ceramtec, Inc.

\*Member, American Ceramic Society.

According to the notation introduced by Aizu,<sup>10</sup> the cubic  $\rightarrow$  tetragonal transition in zirconia is of the paraelastic  $\rightarrow$  ferroelastic type with tetragonal zirconia as a ferroelastic phase. Michel *et al.*<sup>11</sup> were the first to recognize that tetragonal zirconia is a ferroelastic material. Recent work by Negita<sup>12</sup> has further shown that the cubic  $\rightarrow$  tetragonal is a first-order transition and the tetragonal zirconia is an improper ferroelastic. According to group theory, the cubic phase of zirconia has  $m\bar{3}m$  point group and  $Fm\bar{3}m$  space group. The tetragonal phase has  $4/mmm$  as the point group and  $P4_2/nmc$  as the space group. The cubic-to-tetragonal transformation is expected to form two types of domains: (1) Twin domains with three variants are due to symmetry reduction from order 48 to 16. The twin domains are, in fact, ferroelastic domains.<sup>10</sup> (2) Antiphase domains are formed because of the primitive cell doubling.<sup>13</sup> The observation of the three variants and the APB's is consistent with group theoretic considerations of the cubic  $\rightarrow$  tetragonal transformation. More details regarding ferroelasticity in zirconia are given in Refs. 14 and 15.

Ingel and co-workers<sup>16,17</sup> studied strength and toughness of tetragonal zirconia single crystals as a function of composition and temperature. Since the single crystals were grown from the melt, the cubic  $\rightarrow$  tetragonal transformation occurred during the cool-down. Thus, effectively the material studied by Ingel *et al.*<sup>16,17</sup> contained *t*-phase in addition to the *t'*-phase. These authors observed that the strength and the toughness could be retained to  $\geq 1000^\circ\text{C}$ , well above the tetragonal  $\rightarrow$  monoclinic transition temperature. The tetragonal crystals exhibited considerably higher strength and toughness in comparison to the cubic crystals. Similarly, in the work of Michel *et al.*,<sup>11</sup> the tetragonal crystals exhibited higher toughness and strength compared to the cubic phase despite the fact that no transformation of the tetragonal to the monoclinic phase occurred. Sakuma *et al.*<sup>8</sup> fabricated *t'*-phase by arc melting. The toughness of arc-melted samples was determined using an indentation technique in which indentations were introduced within a single grain. The results were in accord with the observations of Ingel *et al.*<sup>16,17</sup> In plasma spray coatings, the principal zirconia phase has been identified to be the *t'*-phase.<sup>18</sup> The performance of the *t'* coating with 7 wt%  $\text{Y}_2\text{O}_3$  is considerably superior to the cubic phase coating.<sup>18</sup>

The potential applications of *t'*-zirconia are expected to be in a polycrystalline form. However, to the authors' knowledge, no information on the mechanical properties of polycrystalline, *t'*-zirconia is available. This is probably due to the fact that samples must be heated into the stability range of the cubic phase, which for samples containing 3 mol%  $\text{Y}_2\text{O}_3$  is  $\approx 2100^\circ\text{C}$ . The objective of the present work was to fabricate dense, polycrystalline, *t'*-zirconia ceramics, measure their mechanical properties, and relate them to microstructure. It was also the objective to elucidate the role of ferroelasticity and transformation on fracture mechanisms.

## II. Experimental Procedure

### (D) Sample Fabrication

Bar-shaped samples containing between 3 and 8 mol%  $\text{Y}_2\text{O}_3$  were green formed by die pressing followed by isostatic

pressing (210 MPa) using commercial powder.\* Green formed samples were then sintered in air at 1450°C/2 h or 1500°C/2 h. The resulting samples were typically  $\geq 99\%$  of the theoretical density. The as-sintered samples were then placed inside a gas-fired furnace which was subsequently heated to  $\geq 2100^\circ\text{C}$  in air. After holding the samples at temperature for 15 min, the platform of the furnace was lowered to a cooler portion of the furnace. It is estimated that the temperature of this zone was  $\approx 1200^\circ\text{C}$  and that the samples cooled to a temperature below 1400°C within a few minutes. The samples were cooled to this temperature rather rapidly in order to prevent or minimize phase separation by a diffusional mechanism. After this initial rapid cooling, the samples were slowly (over 6 to 7 h) cooled to room temperature. Density of the samples was measured by a conventional fluid immersion method.

## (2) Sample Characterization

(A) *X-ray Diffraction*: X-ray diffraction<sup>†</sup> (XRD) with  $\text{CuK}\alpha$  radiation was used for the determination of the phases present as well as for the estimation of texture in the tetragonal phase on as-fired surfaces, ground surfaces, fracture surfaces, and on surfaces of samples subjected to bending and/or compressive stresses. The accelerating voltage was 30 kV and the tube current was 30 mA.

(B) *Optical Microscopy*: The as-fired and heat-treated samples were examined under an optical microscope to determine the grain size. One surface of each sample was polished prior to the high-temperature thermal treatment. Observation of this surface after treatment revealed that the grain boundaries were well etched due to thermal grooving. A few samples were also etched using concentrated HF acid. Some of the samples were mechanically thinned down to  $\sim 150\text{-}\mu\text{m}$  thickness using  $1\text{-}\mu\text{m}$  diamond paste. Subsequently, the samples were dimple ground to a minimum thickness of  $\sim 30\text{-}\mu\text{m}$ . These samples were examined under cross-polarized, transmitted light to reveal the microstructure.

After mechanical testing, many of the samples were examined under a microscope equipped with Nomarsky interference contrast. The objective was to determine the surface features formed due to transformation and/or the formation and the movement of ferroelastic domains or twins.

(C) *Electron Microscopy*: Scanning electron microscopy<sup>‡</sup> was used to examine the fracture morphology. Samples for transmission electron microscopy<sup>§</sup> were prepared by dimple grinding of thin sections followed by ion beam thinning to perforation. They were examined under both bright-field and dark-field conditions.

(D) *Mechanical Testing*: Strength was measured in four-point bending on a universal testing machine<sup>¶</sup> under a deflection rate of 0.127 mm/min. Typical sample dimensions were 3 mm  $\times$  3 mm  $\times$  40 mm. The inner and the outer loading spans were 20 and 30 mm, respectively. The toughness was measured using a single-edge notched beam (SENB) technique. A notch of  $\sim 0.15$  mm in width and 1.5 mm in depth was machined using a diamond blade. Thus, the crack length to specimen height ratio was 0.5. Samples were broken in three-point bending.

Several parallelepipeds of dimensions 3 mm  $\times$  3 mm  $\times$  8 mm were subjected to a unidirectional compression test along the long direction. The samples were subjected to a stress as high as 1.2 GPa. After the compression test, one of the faces parallel to the stressing direction was examined by XRD. The resulting XRD pattern was compared with the sample prior to the compression test. The objective of this work was to determine the amount of monoclinic phase formed, if any, and for the estimation of the degree of texture

introduced in the tetragonal phase due to domain switching, if any, by compression testing. After the compression testing, the samples were also examined under Nomarsky microscope.

For the in situ tests, thin ( $\sim 0.7\text{-mm}$ ) samples were machined from the heat-treated bars. A strain gage was mounted on one of the broad faces. The sample was then mounted on a fixture in which it could be stressed in bending by tightening a set of screws. The corresponding strain was recorded using a strain indicator. Using the measured strain and the Young's modulus, the magnitude of the tensile stress on the broad surface was estimated. The maximum stress the samples were subjected to was on the order of 400 MPa. The sample, while still under stress, was placed in a diffractometer and XRD patterns were obtained using  $\text{CuK}\alpha$  radiation. The objective of this experiment was to determine the amount of monoclinic phase formed, if any, and the degree of texture in the tetragonal phase caused by domain switching, if any, due to the application of bending stresses.

## III. Results

### (1) Microstructures and Phases

Figures 1(a) and (b) show optical micrographs of samples with  $\text{Y}_2\text{O}_3$  content 5 and 8 mol% after heat-treating at  $\geq 2100^\circ\text{C}$ . The typical grain size of samples with  $\text{Y}_2\text{O}_3$  content between 3 and 8 mol% was on the order of 100  $\mu\text{m}$ . Densities of the samples determined by the fluid immersion method was 5.99 g/mL for 8 mol%  $\text{Y}_2\text{O}_3$  samples to 6.07 g/mL for 3 mol%  $\text{Y}_2\text{O}_3$  samples. Optical micrographs show that the samples are essentially fully dense and that no macrocracking is evident. XRD showed that all of the samples were essentially single phase either tetragonal or cubic depending upon the  $\text{Y}_2\text{O}_3$  content. The grain size of a sample with 3 mol%  $\text{Y}_2\text{O}_3$  shown in Fig. 1(a) is  $\sim 200\text{-}\mu\text{m}$ . XRD showed it to be tetragonal, with  $c/a \approx 1.013$ . No monoclinic phase was detected. Ordinarily, the critical grain size for the spontaneous transformation of tetragonal  $\rightarrow$  monoclinic is on the order of 1 to 2  $\mu\text{m}$ . XRD patterns showed that the samples heat-treated at  $\geq 2100^\circ\text{C}$  are fully tetragonal (except samples with 8 mol%  $\text{Y}_2\text{O}_3$ , which were cubic) and do not transform into monoclinic phase despite the large grain size.

Figure 2(a) shows an XRD pattern of a 4 mol%  $\text{Y}_2\text{O}_3$  sample after sintering at 1450°C/2 h in which both the cubic and the tetragonal phases are present consistent with the known phase diagram. Prior work has shown that at 1450°C, the single-phase tetragonal field extends to about  $\sim 2.4$  mol%  $\text{Y}_2\text{O}_3$ . The corresponding  $c/a$  is about 1.015. Figure 2(b) shows an XRD pattern of the same sample after heat-treating at  $\geq 2100^\circ\text{C}$ . As seen in the figure, the only peaks observed correspond to the tetragonal phase. The  $c/a$  is on the order of 1.010. The decrease in  $c/a$  is in accordance with an increase in the concentration of dissolved  $\text{Y}_2\text{O}_3$ . These results are in agreement with the work on arc-melted<sup>8</sup> and plasma-sprayed samples.<sup>5</sup> This sample was further crushed to powder ( $\sim 196$  mesh). XRD showed that no monoclinic phase formed. Similar results were noted by Michel *et al.*,<sup>11</sup> who examined crushed powder of a 3 mol%  $\text{Y}_2\text{O}_3$  single crystal. Transmission electron microscopy of the samples heat-treated at  $\geq 2100^\circ\text{C}$  showed characteristics of the  $t'$ -phase, namely, the presence of a herringbone structure in bright field, the presence of three variants when imaged through  $\{112\}$  fluorite-forbidden reflections in dark field, and the presence of anti-phase boundaries in accordance with prior work reported in the literature.<sup>8,9</sup>

Figure 3(a) shows a transmission optical micrograph (TOM) using cross-polarized light of a sample of 3 mol%  $\text{Y}_2\text{O}_3$  heat-treated at  $\geq 2100^\circ\text{C}$ . The domain structure observed in the micrograph is typical of several other ferroelastics. For example, recent work by Schmid *et al.*<sup>19</sup> on 1-2-3 superconductor, which also undergoes paraelastic  $\rightarrow$  ferroelastic transition at  $\sim 700^\circ\text{C}$ , shows the presence of domains when viewed under

\*Tosoh, Atlanta, GA.

†XRD-8000, Diano, Woburn, MA.

‡S-450, Hitachi, Danbury, CT.

§JEM-200CX, JEOL USA, Peabody, MA.

¶Model 1125, Instron, Canton, MA.

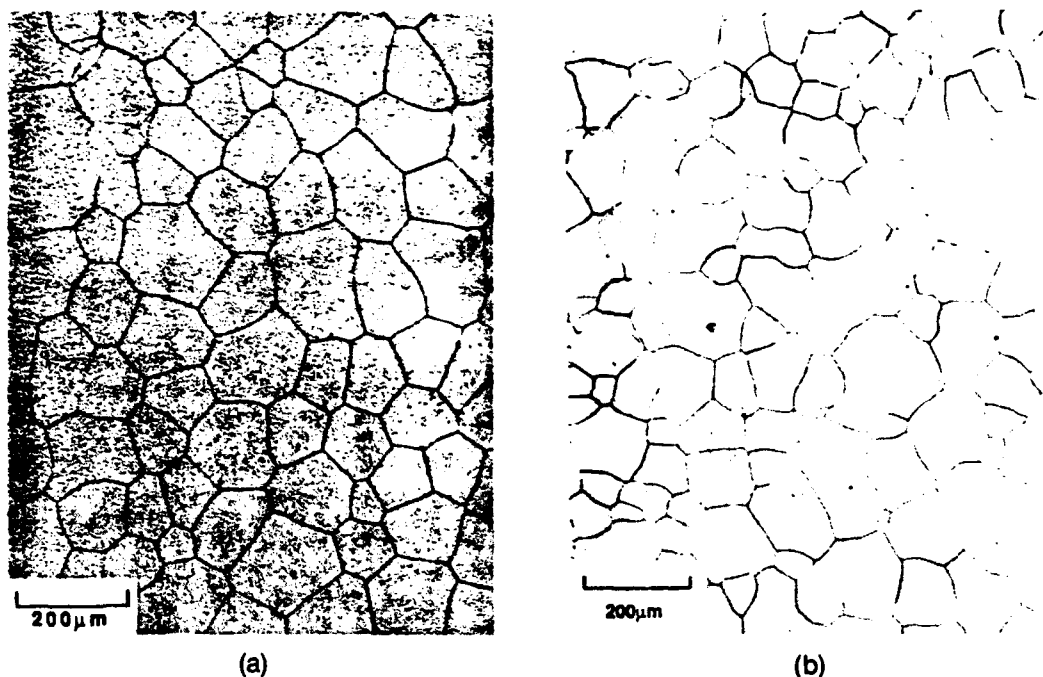


Fig. 1. Optical micrographs of  $Y_2O_3$ - $ZrO_2$  samples sinter/annealed  $\geq 2100^\circ C$ : (a) 3 mol%  $Y_2O_3$ , (b) 8 mol%  $Y_2O_3$ .

polarized light. A similar TOM of a 3 mol%  $Y_2O_3$  single crystal oriented with (100) (on the basis of a pseudocubic symmetry) along the beam direction is shown in Fig. 3(b). On the basis of orientation identified by Laue back reflection, it was determined that the set of lines observed in the figure are along (110) directions. Figure 3(c) shows a TOM of a sample with 8 mol%  $Y_2O_3$  heat-treated at  $\geq 2100^\circ C$ . As seen in the micrograph, no domain structure is observed. XRD of the same sample revealed that it is fully cubic as expected on the basis of the known phase diagram. The TOM method can also be conveniently used to characterize deformation around indents. Figure 3(d) shows an optical micrograph in reflected light of a 3 mol%  $Y_2O_3$  zirconia single crystal ( $t'$ ) which was indented with 0.5-kg load. Figure 3(e) shows the corresponding TOM taken under polarized light revealing the presence of deformation bands.

## (2) Mechanical Properties

Room-temperature fracture toughness,  $K_{Ic}$ , of samples heat-treated at  $\geq 2100^\circ C$  as a function of yttria content is

shown in Fig. 4. The highest  $K_{Ic}$  measured was  $\sim 7.7 \text{ MPa} \cdot \text{m}^{1/2}$  for samples containing 3 mol%  $Y_2O_3$ . The  $K_{Ic}$  decreased with increasing  $Y_2O_3$ , with the lowest value being  $2.4 \text{ MPa} \cdot \text{m}^{1/2}$  for samples containing 8 mol%  $Y_2O_3$ . XRD patterns taken from fracture surfaces failed to reveal the presence of monoclinic phase in any of the samples. By contrast, a 3 mol% sample sintered at  $1450^\circ C/2 \text{ h}$  when fractured exhibits a significant amount of the monoclinic phase. This suggests that in samples heat-treated at  $\geq 2100^\circ C$  the conventional transformation toughening is absent. That is, the toughness cannot be explained on the basis of a wake of a transformed material.

Fracture strength in flexure of samples heat-treated at  $\geq 2100^\circ C$  is shown as a function of the  $Y_2O_3$  content in Fig. 5. For 3 mol%  $Y_2O_3$  samples with a grain size on the order of  $200 \mu\text{m}$ , the strength was about 420 MPa while that for samples with 8 mol%  $Y_2O_3$  (grain size  $\sim 120 \mu\text{m}$ ) was  $\sim 200 \text{ MPa}$ . Scanning electron fractograph of a sample of 4 mol%  $Y_2O_3$  given in Fig. 6 shows that fracture is almost entirely transgranular.

Several samples were tested in compression up to a stress of 1.2 GPa. Prior to compression testing, one of the four lateral surfaces was polished with  $1\text{-}\mu\text{m}$  diamond paste. The actual procedure consisted of subjecting the samples to a predetermined stress, releasing the stress, and then taking XRD traces from the polished surface. Subsequently, the samples were subjected to even greater stress and the same procedure was repeated. Figure 7 shows the XRD traces from a 3 mol%  $Y_2O_3$  ( $t'$ ) sample in the  $2\theta$  range between  $34^\circ$  and  $36^\circ$  subjected to various stresses: (a) 0 MPa, (b) 500 MPa, (c) 650 MPa, (d) 1 GPa, and (e) 1.2 GPa. Note that, with increasing stress, the intensity of the (002) peak ( $I_{(002)}$ ) increases, while that of the (200) peak ( $I_{(200)}$ ) decreases. Also note that a significant increase in  $I_{(002)}$  at the expense of  $I_{(200)}$  occurs at stresses as low as 650 MPa. XRD traces in the  $2\theta$  range between  $26^\circ$  and  $33^\circ$  showed that no monoclinic phase was formed. Samples were examined by Nomarsky microscopy before and after compression testing to 1.2 GPa. Figure 8 shows an optical micrograph of a sample after compression testing. The formation of shear bands, as pointed by arrows, is clearly visible in the micrograph. (The parallel lines traversing the entire field of view are polishing scratches highlighted by Nomarsky interference microscopy.) Similar shear bands have been ob-

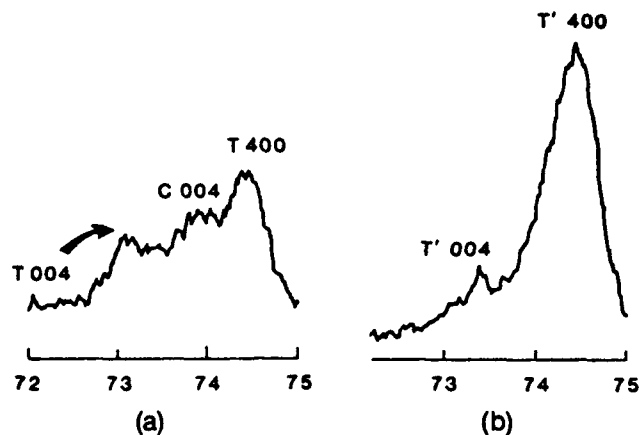


Fig. 2. XRD traces of a 4 mol%  $Y_2O_3$  sample: (a) Sintered at  $1450^\circ C/2 \text{ h}$  showing the presence of tetragonal as well as cubic phases; (b) the same sample after heat-treating  $\geq 2100^\circ C$  showing the presence of only the tetragonal phase.

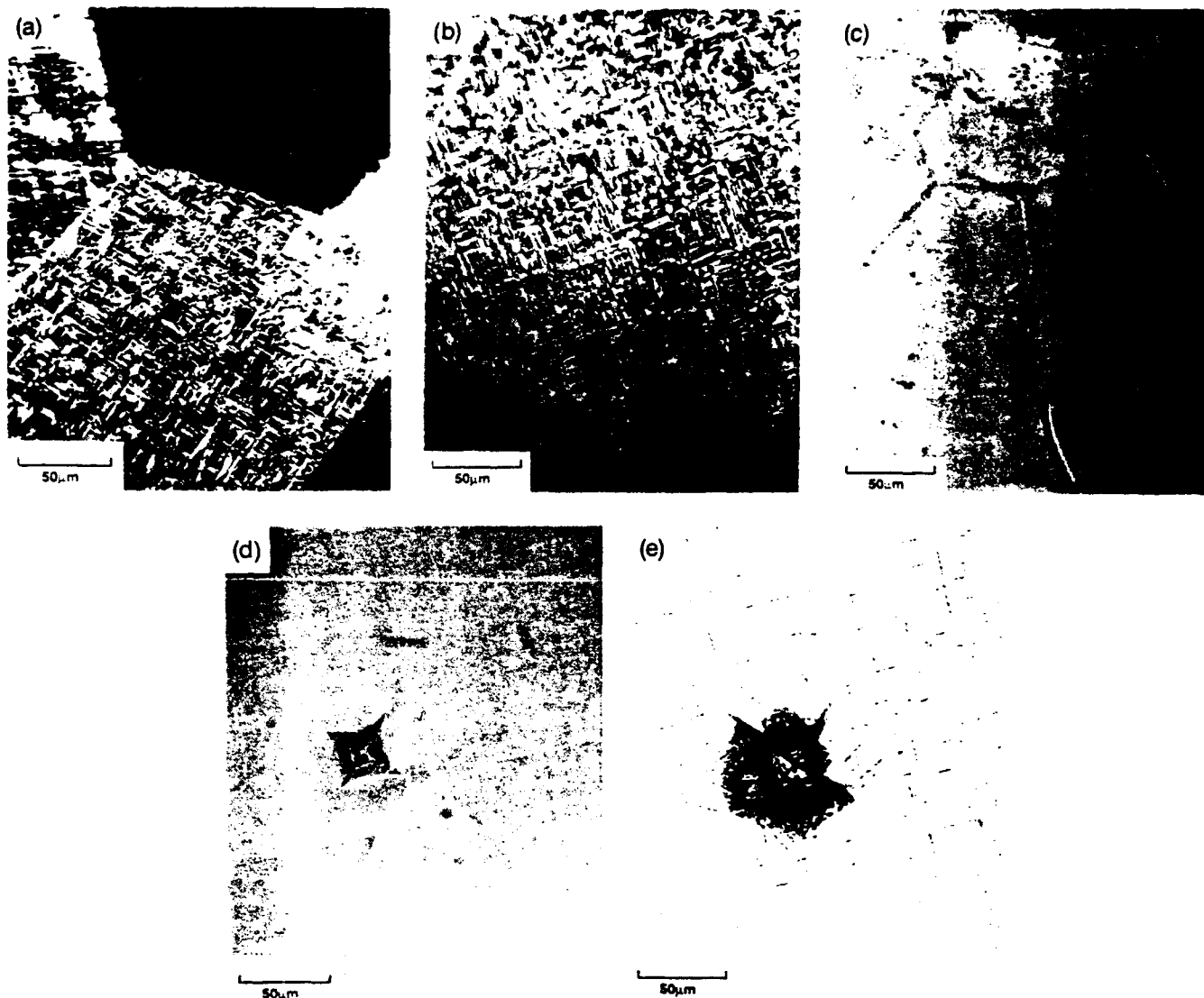


Fig. 3. (a) Transmission optical micrograph (TOM) of a 3 mol%  $Y_2O_3$  polycrystalline sample sinter/annealed  $\geq 2100^\circ C$  showing the characteristic domain structure. (b) TOM of a 2.4 mol%  $Y_2O_3$  single crystal oriented with  $\langle 100 \rangle$  (on the basis of pseudocubic symmetry) along the beam direction. It was determined that the set of lines seen in the figure are along  $\langle 101 \rangle$ . (c) TOM of 8 mol%  $Y_2O_3$  polycrystalline sample (cubic). Note the absence of the domain structure. (d) Optical micrograph (reflected) of a 3 mol%  $Y_2O_3$  single crystal which was indented with 0.5-kg load. (e) TOM of the same sample as in 3(d). The straight line features, away from the indent, are the original domain walls. The indentation is seen to perturb the original domain structure into a star-shaped one. Preliminary work showed that no monoclinic phase was formed by indentation.

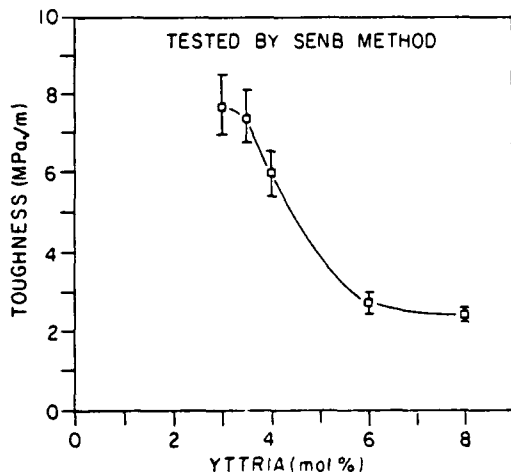


Fig. 4. Fracture toughness,  $K_k$ , vs  $Y_2O_3$  content for samples sinter/annealed  $\geq 2100^\circ C$ .

served by Lankford *et al.*<sup>20</sup> in 3-mol%- $Y_2O_3$ -doped tetragonal single crystals.

After compression testing, the samples were heated to  $1200^\circ C$  in air. XRD patterns taken after this thermal treatment showed a slight decrease in  $I_{(002)}$ . However, the  $I_{(002)}$  was considerably greater than that of the sample prior to compression testing. This shows that the texture developed during the compression test cannot be removed by annealing at  $1200^\circ C$ .

Some of the samples with 3.5 mol%  $Y_2O_3$  heat-treated at  $\geq 2100^\circ C$  were machined in the form of thin beams. They were then polished and placed in a stress fixture for in situ XRD studies. As mentioned previously, the samples were subjected to various stresses by tightening a pair of screws. The strain generated was measured using a strain gage attached on the inner surface. XRD patterns taken from the tensile surface are shown in Fig. 9. Figure 9(a) shows an XRD trace from a polished surface prior to the application of the stress. Figure 9(b) shows a trace from the same surface when the stress was  $\sim 400$  MPa. Note that no monoclinic

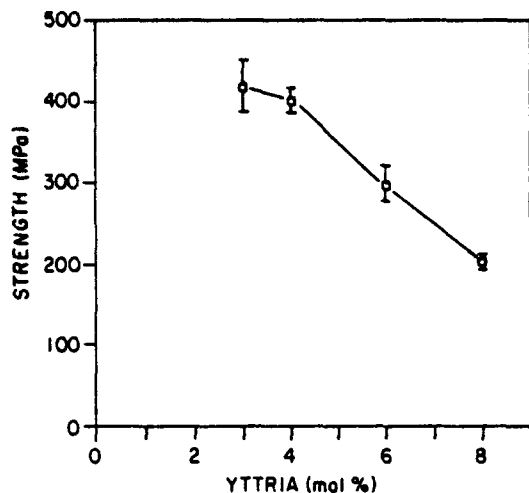


Fig. 5. Flexural strength vs  $Y_2O_3$  content for samples sinter/annealed  $\geq 2100^\circ C$ .

phase was observed in either the pristine or the stressed sample. On the other hand, the  $I_{(200)}$  increased after subjecting to a stress of  $\sim 400$  MPa. Figure 9(c) shows an XRD trace from the same surface after unloading. Note that the texture created did not disappear.

## V. Discussion

### (1) Microstructure and Stability of the $t'$ -Phase

The grain size of the samples after heat treatment at  $\geq 2100^\circ C$  was typically in excess of  $100 \mu m$  and often as large as  $200 \mu m$ . In yttria-doped tetragonal samples sintered in the stability range of the tetragonal phase, the critical grain size above which spontaneous transformation to the monoclinic phase occurs is about  $1$  to  $2 \mu m$ . Despite the very large grain



Fig. 6. SEM fractograph of a 4 mol%  $Y_2O_3$  sample sinter/annealed  $\geq 2100^\circ C$  showing transgranular fracture.

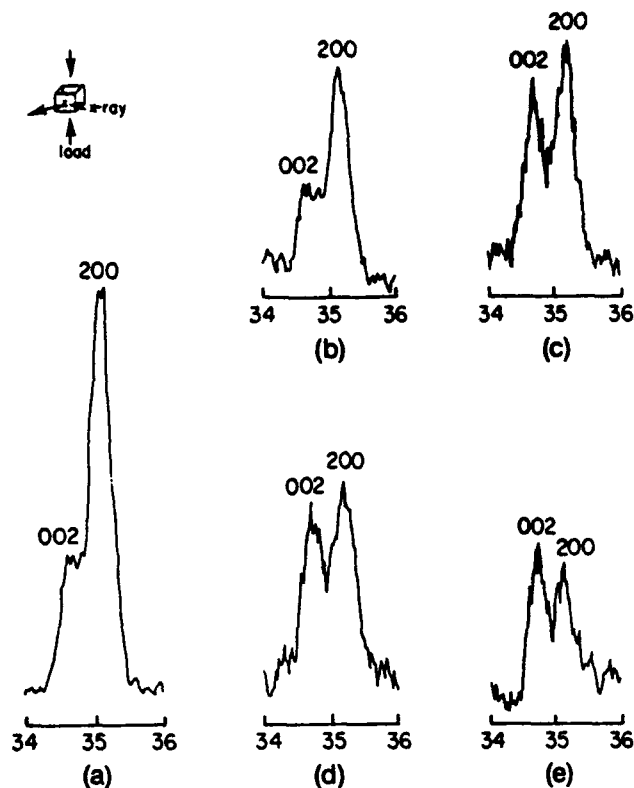


Fig. 7. XRD traces from the lateral surfaces of a 3 mol%  $Y_2O_3$  sample sinter/annealed  $\geq 2100^\circ C$ , subjected to various stresses: (a) unstressed, (b) 500 MPa, (c) 650 MPa, (d) 1 GPa, (e) 1.2 GPa. Note the increase in (002) intensity and a simultaneous decrease in (200) intensity with increasing stress.

size, the  $t'$ -zirconia remains tetragonal because of the coherent nature of the domain or the twin boundaries, as pointed out by Heuer *et al.*<sup>21</sup> Also, for a given domain size, the composition should influence the stability of the tetragonal phase. That is, for a given domain size, the lower the yttria content, the greater must be the tendency of transformation to the monoclinic phase. Transmission optical micrographs clearly show the domain structure. However, transmission electron microscopy shows that the actual domain or the twin size is considerably smaller.<sup>6,15</sup> For a 3 mol%  $Y_2O_3$  sample, the typical domain size is on the order of  $0.5 \mu m$  in length and  $\leq 0.1 \mu m$  in width. The resolution in optical microscopy is not good enough to reveal these. Each rectangular feature seen in Fig. 3(b) contains numerous tiny twins with  $c$  axes in mutually orthogonal (nearly) directions. The contrast observed in transmission optical microscopy under polarized light is due to birefringence as observed in other ferroelastic materials such as 1-2-3 superconductors studied by Schmid *et al.*<sup>19</sup>

The as-heat-treated  $t'$  samples with large grain size also do not exhibit thermal expansion anisotropy cracking such as is often observed in noncubic materials, e.g.,  $Al_2O_3$ . The principal reason for this is again the domain structure or the presence of the three variants. This effectively imparts pseudocubic symmetry to every grain on account of tiny tetragonal domains in three nearly orthogonal directions in approximately equal proportions. Thermal expansion anisotropic cracking can occur provided the domain size exceeds the critical grain size for spontaneous cracking. The actual domain size observed is believed to be smaller than the critical size for spontaneous cracking.

### (2) Ferroelastic Domain Switching and Toughening

Ferroelastic domain switching is synonymous with ferroelastic twin wall motion. Depending upon the state of stress and the orientation, new domains or twins can be nucleated or walls of the existing domains can move under the applied



Fig. 8. Nomarsky interference contrast micrograph of a 3 mol%  $Y_2O_3$  sample sinter/annealed  $\geq 2100^\circ C$  after compression testing. Note the formation of shear bands identified by arrows. Straight lines traversing the entire field of view are polishing scratches. XRD showed that no monoclinic phase was formed.

stress in such a way as to grow one domain at the expense of another. Thus, under the application of stress to a poly-domain material (in which numerous domain walls already exist and domain wall motion is the dominant mechanism of switching), the effective domain size can actually increase.

With reference to tetragonal zirconia, the possible toughening mechanisms include: (i) transformation toughening, (ii) reversible transformation,<sup>22</sup> and (iii) ferroelastic domain switching<sup>15,23,24</sup> or twinning in addition to other conventional mechanisms such as crack deflection and microcracking. The occurrence of either the transformation or the ferroelastic domain switching is dictated by their respective critical stresses. If the critical stress for transformation is less than that for switching, transformation may occur without switching. However, if the critical stress for switching is less than that for transformation, then switching will occur before transformation can occur. Compression tests showed that increase in the intensity of the (002) peak occurred from the lateral surfaces

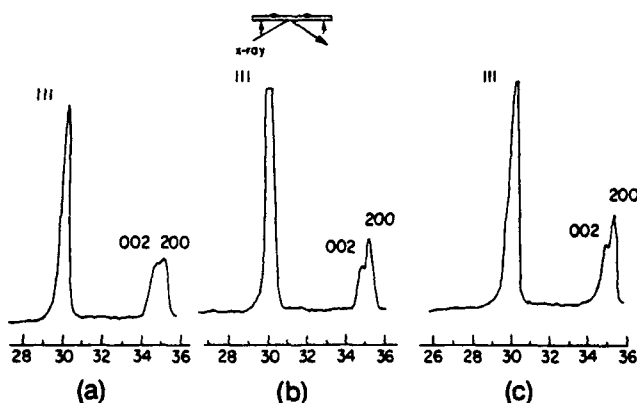


Fig. 9. In situ XRD traces from a sample of 3.5 mol%  $Y_2O_3$  sinter/annealed  $\geq 2100^\circ C$  under various tensile stresses: (a) unstressed, (b) 400 MPa, (c) after unloading. Note that under stress (002) intensity decreases while (200) intensity increases and no monoclinic phase is detected. The texture after unloading is essentially unchanged.

at stresses as low as 650 MPa. Nomarsky micrographs showed the formation of shear bands. At the same time, X-ray diffraction showed that no monoclinic phase was formed. Since dislocation activity is limited at room temperature in these materials and ferroelastic domain switching (twin wall motion) can cause plastic deformation, these results can be explained by the occurrence of domain switching in compression without the formation of any monoclinic phase (similar to the work of Lankford *et al.*<sup>20</sup> on 3-mol%- $Y_2O_3$ -doped tetragonal single crystals). However, the possibility of reverse transformation cannot be ruled out, since in these experiments samples were examined after the stress was released. The in situ experiments were conducted to distinguish between the two possibilities. As shown in Fig. 9, under tensile stress the changes in the intensities of (002) and (200) peaks occur at a stress  $< 400$  MPa without the formation of the monoclinic phase. This experiment shows that no transformation, reversible or otherwise, occurred. On the other hand, the changes in the intensities of (002) and (200) peaks are consistent with domain switching. (In this experiment an in-plane tensile stress is developed which switches domains in such a way that their *c* axes tend to become parallel to the stress axis. Consequently, the intensity of (200) peak is expected to increase and that of (002) peak is expected to decrease, as observed.) This experiment also showed that the critical stress for switching in tension is less than 400 MPa. As the state of stress near a crack tip is tensile, the present results suggest that the occurrence of domain switching in the near crack tip stress field is expected to occur prior to any transformation.

A few samples were also fractured at  $1000^\circ C$ . The reasons for fracturing at  $1000^\circ C$  are twofold. First, no transformation is expected to occur. Second, the critical stress for switching is expected to be lower since it is generally known that  $\sigma_c$  in ferroelastics decreases with increasing temperature. Figure 10(a) shows an XRD trace from a polished surface of a 4 mol%  $Y_2O_3$  (*t'*) sample. Figure 10(b) shows an XRD trace from the fracture surface of the same sample after fracturing at  $1000^\circ C$ . Note that the intensities of (002), (113), and (004) peaks have increased substantially, consistent with the occurrence of domain switching. Fracture tests at  $1000^\circ C$  demonstrate that domain switching does occur during fracture and is a viable toughening mechanism as proposed previously.<sup>23,24</sup>

### (3) Approximate Toughening Contribution by Domain Switching

In plane strain, the state of stress just ahead of the crack tip is that of triaxial tension. Just off the crack plane and near the crack tip (i.e.,  $r \rightarrow 0$  and  $\theta = \pi/2$ ), it can be shown that  $\sigma_{yy} = 3\sigma_{xx}$  where *y* is orthogonal to the crack plane and *x* is in the crack plane orthogonal to the crack front.<sup>25</sup> Assuming the Poisson's ratio,  $\nu = 0.25$ , it can be shown that  $\sigma_{zz} = \nu(\sigma_{xx} + \sigma_{yy}) = \sigma_{xx}$ . This means that the net tensile stress on an element just ahead of the crack tip is along *y* and its magnitude is  $2\sigma_{xx}$  or  $2/3\sigma_{yy}$ . Domain switching will occur provided  $2/3\sigma_{yy} \geq \sigma_c$ , the coercive stress or the critical stress for domain switching. Since the critical stress for domain switching was determined to be  $\sim 400$  MPa in tension, the implication is that domain switching will occur for  $\sigma_{yy} \geq 600$  MPa. The depth to which switching occurs, *h*, can be given by

$$h \approx a \left( \frac{K_I}{\sigma_c} \right)^2 \quad (1)$$

This equation is similar to the one used in the determination of plastic zone size near a crack tip<sup>25</sup> or in the determination of the transformation<sup>26</sup> zone sizes. The value of  $\alpha$  can be determined as follows:

The  $\sigma_{yy}$  near a crack tip is given by<sup>25</sup>

$$\sigma_{yy} = \frac{K_I}{\sqrt{2\pi r}} \cos \left( \frac{\theta}{2} \right) \left[ 1 + \sin \left( \frac{\theta}{2} \right) \sin \left( \frac{3\theta}{2} \right) \right] \quad (2)$$

where  $K_I$  is the mode I stress intensity factor, and (*r*,  $\theta$ ) are

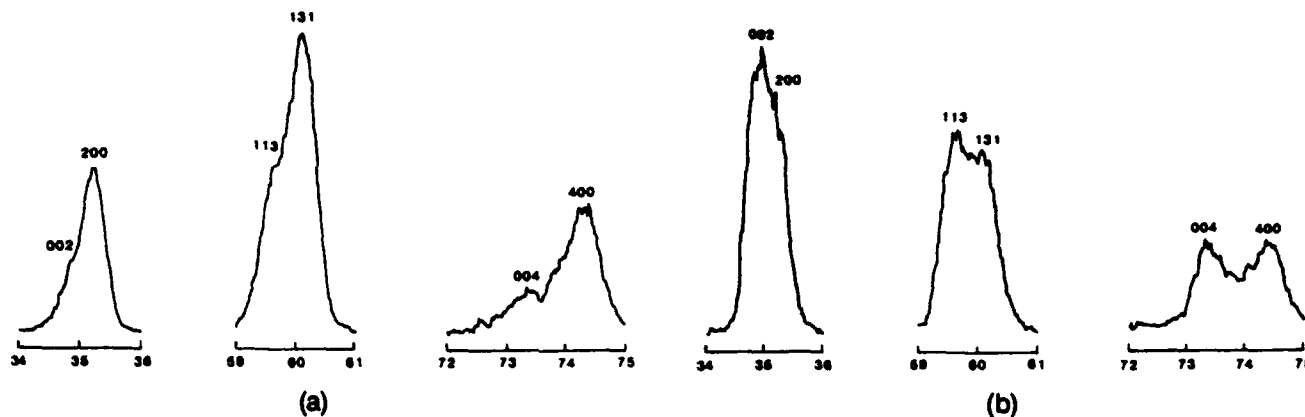


Fig. 10. XRD traces from 4 mol%  $Y_2O_3$  sample sinter/annealed  $\geq 2100^\circ C$ : (a) as-polished surface, (b) fracture surface after testing at  $1000^\circ C$ . Note the relative changes in the intensities.

polar coordinates measured from the crack tip. For  $\theta = \pi/2$ , with  $K_I = K_{Ic}$ , the zone depth,  $h$ , is given by

$$h \approx 0.179 \left( \frac{K_{Ic}}{\sigma_c} \right)^2 = 0.08 \left( \frac{K_{Ic}}{\sigma_c} \right)^2 \quad (3)$$

Thus, the value of  $\alpha$  is about 0.08 in Eq. (1). For a toughness of  $7 \text{ MPa} \cdot \text{m}^{1/2}$  with  $\sigma_c \approx 400 \text{ MPa}$ , the calculated value of the depth of domain switching is about  $24 \mu\text{m}$ .

The elastic energy release rate,  $G_{Ic}$ , is given by

$$G_{Ic} = G_{Ic}^0 + 2h\sigma_c\epsilon_s \quad (4)$$

where  $G_{Ic}^0$  is the critical elastic energy release rate corresponding to the paraelastic state, and  $\epsilon_s$  is the switching strain.

Using Eqs. (3) and (4) and the relation  $G_{Ic} = (1 - \nu^2)K_{Ic}^2/E$  for plane strain where  $E$  is Young's modulus of elasticity, it can be shown that

$$K_{Ic} = \frac{K_{Ic}^0}{\sqrt{1 - \frac{0.17\epsilon_s E}{\sigma_c}}} \quad (5)$$

where  $K_{Ic}^0$  is the fracture toughness corresponding to the paraelastic state.

Assuming  $\sigma_c \approx 350 \text{ MPa}$ ,  $E = 200 \text{ GPa}$ ,  $\epsilon_s \approx 2/3(c/a - 1) \approx 0.0087$ , and  $K_{Ic}^0 \approx 2.4 \text{ MPa} \cdot \text{m}^{1/2}$  (toughness of the cubic phase), the calculated value of  $K_{Ic}$  from Eq. (5) is about  $6.0 \text{ MPa} \cdot \text{m}^{1/2}$  and the zone depth,  $h$ , from Eq. (1) is about  $23 \mu\text{m}$  for 3 mol%  $Y_2O_3$  samples. This approximate calculation shows that in this material (3 mol%  $Y_2O_3$   $t'$ -zirconia) the contribution of ferroelastic domain switching to toughness is 3 to 4  $\text{MPa} \cdot \text{m}^{1/2}$ , assuming no reverse switching.

It is important to realize that domain switching and transformation are not mutually exclusive. In fact, it is quite conceivable that domain switching may serve as a precursor to transformation in some materials or under certain conditions. Alternatively, it is also possible that transformation to the monoclinic phase may occur without the occurrence of switching in the tetragonal phase. However, after transformation, switching may occur in the monoclinic phase. In the materials studied here, no transformation was detected. However, as will be discussed in a separate paper, domain switching followed by transformation can be induced under certain conditions of stress.

## VI. Summary and Conclusions

(1) Large-grained (100- to  $200\text{-}\mu\text{m}$ ), fully tetragonal ( $t'$ ), dense, polycrystalline zirconia samples containing between 3 and 6 mol%  $Y_2O_3$  were fabricated by sintering/annealing in the stability range of the cubic phase ( $\geq 2100^\circ C$ ) followed by rapid cooling.

(2) Polarized light, transmission optical microscopy was used to characterize the domain structure of the tetragonal ( $t'$ ) zirconia samples. This technique has been previously used to characterize the domain structure in other ferroelastics, such as 1-2-3 superconductors. The observation that the tetragonal samples did not exhibit thermal expansion anisotropy-induced cracking nor the presence of any monoclinic phase despite the large grain size is rationalized on the basis of the domain structure, which consists of a random distribution of the three variants. As expected, no domain structure was present in cubic samples (8 mol%  $Y_2O_3$ ).

(3) The formation of shear bands in samples subjected to uniaxial compression, the occurrence of relative changes in the intensities of the (002) and the (200) peaks, and the lack of formation of the monoclinic phase, can all be explained by ferroelastic domain switching. The in situ X-ray diffraction studies on bend samples showed that ferroelastic domain switching (twin wall motion) occurred at stresses  $\leq 400 \text{ MPa}$  without the formation of the monoclinic phase. This shows that the coercive stress for switching is less than that for transformation in the materials tested.

(4) Fracture toughness,  $K_{Ic}$ , of  $t'$  polycrystalline zirconia samples decreases with increasing  $Y_2O_3$  content. The  $K_{Ic}$  of  $t'$ -zirconia with 3 mol%  $Y_2O_3$  is  $\sim 7.7 \text{ MPa} \cdot \text{m}^{1/2}$ , which is about 3 times that of the fully cubic material ( $\sim 2.4 \text{ MPa} \cdot \text{m}^{1/2}$ ). The four-point-bend strength of the 3 mol%  $Y_2O_3$  samples was  $\sim 420 \text{ MPa}$ , while that of the cubic samples was  $\sim 200 \text{ MPa}$ .

(5) The higher  $K_{Ic}$  of the  $t'$ -zirconia samples in comparison to that of the cubic samples can be explained in part on the basis of ferroelastic domain switching. Other mechanisms, such as microcracking and crack deflection, may also be operative.

**Acknowledgments:** Assistance of Mr. Jong Chen, Mr. Karun Mehta, and Mr. Abhijit Abhyankar in some of the experimental work is gratefully acknowledged.

## References

- M. Rühle, N. Clausen, and A. H. Heuer, "Microstructural Studies of  $Y_2O_3$ -Containing Tetragonal  $ZrO_2$  Polycrystals (Y-TZP)", pp. 353-70 in *Advances in Ceramics, Vol. 12, Science and Technology of Zirconia, II*. Edited by N. Clausen, M. Rühle, and A. H. Heuer. American Ceramic Society, Columbus, OH, 1984.
- D. L. Porter and A. H. Heuer, "Microstructural Development in MgO-Partially Stabilized Zirconia (Mg-PSZ)," *J. Am. Ceram. Soc.*, **62** [5-6] 298-305 (1979).
- R. H. J. Hannink and R. C. Garvie, "Sub-Eutectoid Aged Mg-PSZ Alloy with Enhanced Thermal Up-Shock Resistance," *J. Mater. Sci.*, **17**, 2637-43 (1982).
- H. G. Scott, "Phase Relations in the Zirconia-Yttria System," *J. Mater. Sci.*, **10**, 1527-35 (1975).
- R. A. Miller, J. L. Smialek, and R. G. Garlick, "Phase Stability in Plasma-Sprayed Partially Stabilized Zirconia-Yttria", pp. 241-53 in *Advances in Ceramics, Vol. 3, Science and Technology of Zirconia*. Edited by A. H. Heuer and L. W. Hobbs. American Ceramic Society, Columbus, OH, 1981.

<sup>14</sup>A. H. Heuer, R. Chaim, and V. Lanteri, "The Displacive Cubic  $\rightarrow$  Tetragonal Transformation in  $ZrO_2$  Alloys," *Acta Metall.*, **35** [3] 661-66 (1987).

<sup>15</sup>D. J. Kim, "Effect of  $Ta_2O_5$ ,  $Nb_2O_5$ , and  $HfO_2$  Alloying on the Transformability of  $Y_2O_3$ -Stabilized Tetragonal  $ZrO_2$ ," *J. Am. Ceram. Soc.*, **73** [1] 115-20 (1990).

<sup>16</sup>T. Sakuma, Y. A. Yoshizawa, and H. Suto, "The Microstructure and Mechanical Properties of Ytria-Stabilized Zirconia Prepared by Arc-Melting," *J. Mater. Sci.*, **20**, 2399-407 (1985).

<sup>17</sup>V. Lanteri, R. Chaim, and A. H. Heuer, "On the Microstructures Resulting from the Diffusionless Cubic  $\rightarrow$  Tetragonal Transition in  $ZrO_2$ - $Y_2O_3$  Alloys," *J. Am. Ceram. Soc.*, **69** [10] C-258-C-261 (1986).

<sup>18</sup>K. Aizu, "Possible Species of Ferromagnetic, Ferroelectric and Ferroelastic Crystals," *Phys. Rev. B*, **2** [3] 754-72 (1970).

<sup>19</sup>D. Michel, L. Mazerolles, and M. Perez y Jorba, "Fracture of Metastable Tetragonal Zirconia Crystals," *J. Mater. Sci.*, **18**, 2618-28 (1983).

<sup>20</sup>K. Negita, "Lattice Vibrations and Cubic to Tetragonal Phase Transition in  $ZrO_2$ ," *Acta Metall.*, **37** [1] 313-17 (1989).

<sup>21</sup>G. V. Tendeloo and S. Amelinckx, "Group-Theoretical Considerations Concerning Domain Formation in Ordered Alloys," *Acta Crystallogr., Sect. A*, **30**, 431-40 (1974).

<sup>22</sup>V. K. Wadhavan, "Ferroelasticity and Related Properties of Crystals," *Phase Transitions*, **3**, 3-103 (1982).

<sup>23</sup>G. V. Srinivasan, J. F. Jue, S. Y. Kuo, and A. V. Virkar, "Ferroelastic Domain Switching in Polydomain Tetragonal Zirconia Single Crystals," *J. Am. Ceram. Soc.*, **72** [11] 2098-103 (1989).

<sup>24</sup>R. P. Ingel, D. Lewis, B. A. Bender, and R. W. Rice, "Temperature Dependence of Strength and Fracture Toughness of  $ZrO_2$  Single Crystals," *J. Am. Ceram. Soc.*, **65** [9] C-150-C-151 (1982).

<sup>25</sup>R. P. Ingel, D. Lewis, and R. Rice, "Physical, Microstructural and Thermomechanical Properties of  $ZrO_2$  Single Crystals"; pp. 408-14 in Advances in Ceramics, Vol. 12, *Science and Technology of Zirconia II*. Edited by N. Claussen, M. Rühle, and A. H. Heuer. American Ceramic Society, Columbus, OH, 1984.

<sup>26</sup>R. J. Bratton and S. K. Lau, "Zirconia Thermal Barrier Coating"; pp. 226-40 in *Advances in Ceramics, Vol. 3, Science and Technology of Zirconia I*. Edited by A. H. Heuer and L. W. Hobbs. American Ceramic Society, Columbus, OH, 1981.

<sup>27</sup>H. Schmid, E. Eukhardt, E. Walker, W. Brizel, M. Clin, J.-P. Rivera, J.-L. Jorda, M. Francis, and K. Yvon, "Polarized Light and X-ray Precession Study of the Ferroelastic Domains of  $YBa_2Cu_3O_{7-x}$ ," *Z. Phys. B: Condens. Matter*, **72**, 305-22 (1988).

<sup>28</sup>J. Laakford, L. Rabenberg, and P. A. Page, "Deformation Mechanisms in Ytria-Stabilized Zirconia," *J. Mater. Sci.*, **23**, 4144-56 (1988).

<sup>29</sup>A. H. Heuer, V. Lanteri, and A. Dominguez-Rodriguez, "High Temperature Precipitation Hardening of  $Y_2O_3$  Partially-Stabilized  $ZrO_2$  (Y-PSZ) Single Crystals," *Acta Metall.*, **37** [2] 559-67 (1989).

<sup>30</sup>D. B. Marshall and M. R. James, "Reversible Stress-Induced Martensitic Transformation in  $ZrO_2$ ," *J. Am. Ceram. Soc.*, **69** [3] 215-17 (1986).

<sup>31</sup>A. V. Virkar and R. L. K. Matsumoto, "Ferroelastic Domain Switching as a Toughening Mechanism in Tetragonal Zirconia," *J. Am. Ceram. Soc.*, **69** [10] C-224-C-226 (1986).

<sup>32</sup>A. V. Virkar and R. L. K. Matsumoto "Toughening Mechanism in Tetragonal Zirconia Polycrystalline (TZP) Ceramics"; pp. 653-62 in *Advances in Ceramics, Vol. 24, Science and Technology of Zirconia III*. Edited by S. Somiya, N. Yamamoto, and H. Yanagida. American Ceramic Society, Westerville, OH, 1988.

<sup>33</sup>Kare Hellan, *Introduction to Fracture Mechanics*. McGraw-Hill, New York, 1984.

<sup>34</sup>R. McMeeking and A. G. Evans, "Mechanics of Transformation-Toughening in Brittle Materials," *J. Am. Ceram. Soc.*, **65** [5] 242-46 (1982). □

# High-Toughness Ce-TZP/Al<sub>2</sub>O<sub>3</sub> Ceramics with Improved Hardness and Strength

Raymond A. Cutler\* and Robert J. Mayhew

Ceramtec, Inc., Salt Lake City, Utah 84119

Kevin M. Prettyman\* and Anil V. Virkar\*

Department of Materials Science and Engineering, University of Utah, Salt Lake City, Utah 84112

Simultaneous additions of SrO and Al<sub>2</sub>O<sub>3</sub> to ZrO<sub>2</sub> (12 mol% CeO<sub>2</sub>) lead to the in situ formation of strontium aluminate (SrO·6Al<sub>2</sub>O<sub>3</sub>) platelets ( $\approx 0.5 \mu\text{m}$  in width and 5 to 10  $\mu\text{m}$  in length) within the Ce-TZP matrix. These platelet-containing Ce-TZP ceramics have the strength (500 to 700 MPa) and hardness (13 to 14 GPa) of Ce-TZP/Al<sub>2</sub>O<sub>3</sub> while maintaining the high toughness (14 to 15 MPa·m<sup>1/2</sup>) of Ce-TZP. Optimum room-temperature properties are obtained at SrO/Al<sub>2</sub>O<sub>3</sub> molar ratios between 0.025 and 0.1 for ZrO<sub>2</sub> (12 mol% CeO<sub>2</sub>) with starting Al<sub>2</sub>O<sub>3</sub> contents ranging between 15 and 60 vol%. The role of various toughening mechanisms is discussed for these composite ceramics. [Key words: zirconia—tetragonal polycrystals (TZP), strengthening, strontium, alumina, toughening.]

## I. Introduction

AN ENHANCEMENT in fracture toughness and crack growth resistance can be realized for many ceramics through microstructural control.<sup>1</sup> Transformation toughening of zirconia<sup>2-8</sup> is one of the best examples of a toughening process which has resulted in new materials with improved properties. Y-TZP and Ce-TZP, fine-grained tetragonal zirconia polycrystals using yttria or ceria, respectively, to partially stabilize the tetragonal crystal structure, have been investigated in detail.<sup>9-13</sup> The addition of alumina to TZP, which suppresses grain growth of zirconia, increases hardness and strength. Alumina-dispersed zirconia ceramics require higher stress for transformation, and their fracture toughness is significantly decreased compared to monolithic zirconia. Swain and Rose<sup>14</sup> have discussed this strength/toughness trade-off in detail, showing that strength can be transformation-limited or limited by R-curve behavior,<sup>4,5,7,8,15</sup> predominant in tough TZP materials. Methods for strengthening tough TZP ceramics are therefore of interest. Heussner and Claussen<sup>16</sup> recently showed that the strength of Ce-TZP could be increased 200 to 300 MPa by introducing surface compressive stress using a controlled reduction process.

Michel, *et al.*<sup>17</sup> identified domain structure in tetragonal ZrO<sub>2</sub> pseudo-single crystals, a ferroelastic material. Virkar and Matsumoto<sup>18,19</sup> proposed that ferroelastic domain switching can contribute to toughness in tetragonal and monoclinic zirconia. Matsumoto<sup>20</sup> added SrO as a sintering aid to TZP materials, based on the previous work of Drennan and Hannink,<sup>21-23</sup> who showed that small amounts of SrO were effective as a sintering aid to Mg-PSZ. Drennan and

Hannink found that the most beneficial aspect of the SrO addition was its ability to tie up SiO<sub>2</sub> as a glassy phase which migrated to the surface during annealing. In contrast, Matsumoto discovered that the addition of small amounts of strontium-based compounds resulted in enhanced toughness in Ce-TZP/Al<sub>2</sub>O<sub>3</sub> ceramics.<sup>20</sup> The purpose of this paper is to examine the role of strontia on the mechanical properties of Ce-TZP-based ceramics.

## II. Experimental Procedure

### (1) Sample Preparation

Ce-TZP compositions were prepared using either unstabilized ZrO<sub>2</sub>\* to which 12 mol% CeO<sub>2</sub><sup>†</sup> was added or coprecipitated ZrO<sub>2</sub> (12 mol% CeO<sub>2</sub>).<sup>‡</sup> Ce-TZP compositions containing 0, 15, 30, and 60 vol% Al<sub>2</sub>O<sub>3</sub> were prepared with and without SrO additions. Coprecipitated Ce-TZP and Al<sub>2</sub>O<sub>3</sub><sup>§</sup> with high surface area (30 m<sup>2</sup>/g) were used in Ce-TZP/15 vol% Al<sub>2</sub>O<sub>3</sub> compositions. The other three series of compositions were processed using less expensive starting materials by mixing unstabilized ZrO<sub>2</sub>, CeO<sub>2</sub>, and Al<sub>2</sub>O<sub>3</sub>.<sup>¶</sup> SrZrO<sub>3</sub>\*\* was used as the source of strontium. In the 15 and 30 vol% Al<sub>2</sub>O<sub>3</sub> compositions, no extra CeO<sub>2</sub> was added to compensate for the small amount of ZrO<sub>2</sub> in SrZrO<sub>3</sub>. This did not strongly influence the results, however, since CeO<sub>2</sub> content in ZrO<sub>2</sub> ranged from 12.0 mol% for no SrZrO<sub>3</sub> addition to 11.4 mol% at the highest SrZrO<sub>3</sub> concentration. The CeO<sub>2</sub> content in the 60 vol% Al<sub>2</sub>O<sub>3</sub> compositions was kept constant at 12 mol% (on the basis of ZrO<sub>2</sub>) by adding extra CeO<sub>2</sub> to starting compositions.

All powder mixtures were vibratory milled using ZrO<sub>2</sub> media in methanol or *n*-hexane with appropriate dispersants. The powders were passed wet through a 325-mesh screen and through a 170-mesh screen after drying. Bars were formed uniaxially at 35 MPa and subsequently isostatically pressed at 200 MPa. Samples of the various compositions were sintered in air at 1500° to 1600°C for 2 h.

### (2) Sample Characterization

Density was determined by water displacement. Grain size was determined using the linear intercept method on thermally etched surfaces. Sintered bars were X-rayed and subsequently ground using a 220 diamond wheel. The ground and fracture surfaces of selected samples were X-rayed, and percent monoclinic, based on total ZrO<sub>2</sub> content, was determined using the analysis of Toraya.<sup>24</sup> In situ crack extension measurements were made on selected compositions to compare zone widths using Nomarski interference contrast mi-

I-W. Chen—contributing editor

Manuscript No. 197678. Received April 2, 1990; approved August 7, 1990. Supported by AFOSR on DARPA Contract No. F49620-87-C-0077.

\*Member, American Ceramic Society.

\*E-20, Magnesium Elektron, Flemington, NJ.

†Grade 5350, Molycorp, White Plains, NY.

‡Grade TZ-12CE, Tosoh USA, Atlanta, GA.

§Grade CR-30, Baikowski International, Charlotte, NC.

¶Grade HP-DBM, Reynolds International, Bauxite, AK.

\*\*Grade Ticon 160, TAM Ceramics, Niagara Falls, NY.

crosscopy. Polished and fracture surfaces were analyzed in a SEM with energy dispersive spectroscopy (EDS) to determine elemental distributions.

### (3) Mechanical Property Determination

Hardness was determined using a 75-N indent made with a 136° Vickers diamond indenter (at least 10 measurements were made on samples of each composition). Four-point bend strength was measured using a universal testing machine with a crosshead speed of 0.5 cm/min, a support span of 40 mm, and a loading span of 20 mm (between 5 and 13 bars were broken for each composition). Fracture toughness was measured using the double cantilever beam (DCB) technique (typically 3 bars were tested, with 3 to 7 measurements on each specimen). All fracture toughness measurements were made in the long crack regime. Thus, if *R*-curve behavior is exhibited by these materials, one would expect the toughness measured in the present work to correspond to the maximum, plateau region.

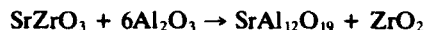
A few samples were ground into cube-shaped specimens, and strain gages were mounted on opposite faces in two orthogonal directions (see Fig. 1). The samples were uniaxially tested in compression. Strain as a function of applied stress was monitored on all three strain gages during loading and unloading. These tests were used to determine Young's modulus, the elastic limit, stress at which transformation occurred, and reversibility of transformation.

## III. Results

### (1) Simultaneous SrO and Al<sub>2</sub>O<sub>3</sub> Additions

(A) *Ce-TZP and Ce-TZP/15 vol% Al<sub>2</sub>O<sub>3</sub>*: The addition of Al<sub>2</sub>O<sub>3</sub> to Ce-TZP increased the hardness and strength but decreased the fracture toughness (see Table I), in agreement with the work of Tsukuma and Takahata.<sup>12</sup> Table I also shows data for Ce-TZP/15 vol% Al<sub>2</sub>O<sub>3</sub> compositions where SrO was added as SrZrO<sub>3</sub>. The density decreased with increasing amounts of SrZrO<sub>3</sub> added above 1 wt%, indicating that SrZrO<sub>3</sub> additions hindered sintering in this system. When the sintering temperature was raised to 1550°C, density greater

than 99% of theoretical was achieved for all compositions. Polished cross sections viewed under an SEM showed an increasing tendency to form plate-shaped grains with increasing SrZrO<sub>3</sub> additions, as shown in Fig. 2. Energy dispersive spectroscopy (EDS) revealed a high concentration of Al and Sr in these grains, with no Sr detected in the matrix. This suggested that strontium hexaluminate (hexagonal SrO·6Al<sub>2</sub>O<sub>3</sub> (density of 3.95 g/cm<sup>3</sup>)) was formed in situ during sintering, as would be expected based on phase equilibria between SrO and Al<sub>2</sub>O<sub>3</sub>,<sup>25</sup> according to the reaction



Fracture surfaces showed that the strontium aluminate grains were platelets (see Fig. 3). The SrAl<sub>12</sub>O<sub>19</sub> platelets which formed in situ were approximately 0.5 μm in thickness and 5 to 10 μm in length and width.

The fracture toughness increased significantly (from 8.3 to 14.0 MPa·m<sup>1/2</sup>) with the addition of SrZrO<sub>3</sub> to Ce-TZP/15 vol% Al<sub>2</sub>O<sub>3</sub> (see Table I). The fracture toughness of Ce-TZP/15 vol% Al<sub>2</sub>O<sub>3</sub> with 1 to 4 wt% SrZrO<sub>3</sub> was comparable to that of Ce-TZP, but the strength and hardness were significantly improved (see Table I). The amount of monoclinic ZrO<sub>2</sub> on ground surfaces was approximately 5%, 12%, 12%, 18%, and 16% for 0.0, 0.5, 1.0, 2.0, and 4.0 wt% SrZrO<sub>3</sub> additions, respectively. The amount of monoclinic ZrO<sub>2</sub> on fracture surfaces increased from 67% for no SrZrO<sub>3</sub> to 73% to 75% for 0.5 to 4.0 wt% SrZrO<sub>3</sub> additions, for fracture toughness values ranging between 8.3 and 14.0 MPa·m<sup>1/2</sup>, respectively, showing only a slight correlation of fracture toughness with the degree of transformation (see Table I).

The grain size of zirconia in Ce-TZP decreases significantly by the addition of 15 vol% Al<sub>2</sub>O<sub>3</sub> (see Table I). The zirconia grain size remains relatively constant near 1.5 μm with SrZrO<sub>3</sub> additions up to 1 wt% and then increases to 2.0 μm with increasing SrO content (see Table I). While the toughness of zirconia ceramics is strongly dependent on grain size,<sup>26</sup> Ce-TZP(15 vol% Al<sub>2</sub>O<sub>3</sub>) and Ce-TZP(15 vol% Al<sub>2</sub>O<sub>3</sub>)–2 wt% SrZrO<sub>3</sub> both had zirconia grain size of ≈1.6 μm, yet differed in fracture toughness by ≈6 MPa·m<sup>1/2</sup>. Neither material had a measurable transformation zone around indentation cracks, based on Normarski interference contrast, despite the large amount of transformation on fracture surfaces of both samples (see Table I). These data suggest that toughening mechanisms in addition to transformation toughening are operative in these materials.

Ce-TZP/15 vol% Al<sub>2</sub>O<sub>3</sub> with 2 wt% SrZrO<sub>3</sub> sintered at 1550° instead of 1500°C had similar strength (519 ± 20 MPa) but much higher toughness (19.2 ± 2.8 MPa·m<sup>1/2</sup>). Acoustic noise and permanent deformation were noted during room-temperature strength testing of this material.

Even though strontium aluminate platelets could clearly be observed bridging crack openings, crack bridging and crack branching tendencies did not appear to differ significantly from Ce-TZP (see Fig. 4). While it is also possible that ferroelastic domain switching was operative, the presence of *m*-ZrO<sub>2</sub>, Al<sub>2</sub>O<sub>3</sub>, and SrAl<sub>12</sub>O<sub>19</sub> made characterization of domain switching by X-ray diffraction<sup>17,18,27</sup> impossible.

Compressive testing was used to determine the transformation stress and to compare the autocatalytic behavior of the various materials. Figure 5 shows the stress–strain curves in compression for Ce-TZP and Ce-TZP/Al<sub>2</sub>O<sub>3</sub>–2 wt% SrZrO<sub>3</sub> sintered at 1500°C. The autocatalytic transformation in Ce-TZP, which is absent in Ce-TZP with SrAl<sub>12</sub>O<sub>19</sub> platelets, has been discussed by Reyes-Morel and Chen.<sup>28</sup> The change in volumes while loading and unloading these high toughness materials is shown in Fig. 6. Both materials show volume expansion due to transformation, with little reverse transformation. Analysis of the initial nonlinear portion of the stress–strain curves in Fig. 6 (as well as more detailed work on Ce-TZP)<sup>29</sup> shows that there is a regime of nonlinear behavior over which there is no volume change prior to the

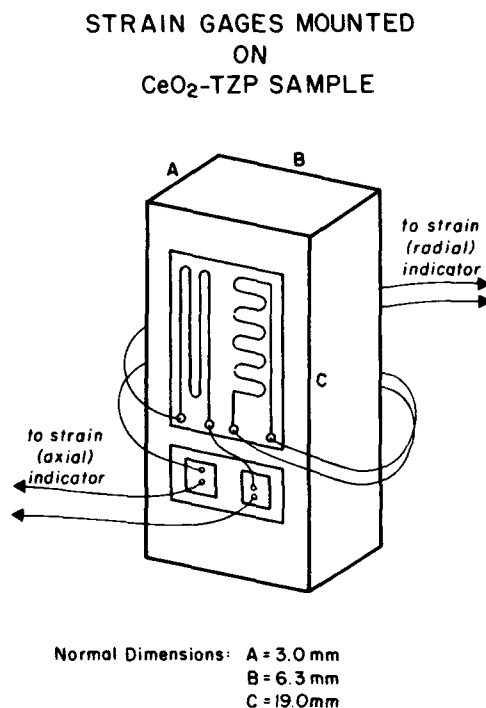


Fig. 1. Strain gage configuration on cube-shaped samples subjected to compressive testing.

**Table I. Room-Temperature Properties of Ceramics Sintered at 1500°C Made Using Coprecipitated ZrO<sub>2</sub> (12 mol% CeO<sub>2</sub>) Powders**

Al <sub>2</sub> O <sub>3</sub> (vol%)	SrZrO <sub>3</sub> (wt%)	Density		$\sigma_f$ (MPa) <sup>a</sup>		$K_{Ic}$ (MPa·m <sup>1/2</sup> ) <sup>b</sup>		$H$ (GPa) <sup>c</sup>		<i>m</i> -ZrO <sub>2</sub> <sup>d</sup> (%)	<i>g</i> s <sup>e</sup> ( $\mu$ m)
		(g/cm <sup>3</sup> )	%TD <sup>**</sup>	$x$ <sup>††</sup>	$s$ <sup>††</sup>	$x$	$s$	$x$	$s$		
0.0	0.0	6.21	99.2	388	17	12.6	1.1	9.5	0.2	83	2.5
15.0	0.0	5.88	99.3	634	19	8.3	0.2	11.5	0.9	67	1.6
15.0	0.5	5.91	99.9	589	17	11.0	0.2	11.5	0.1	73	1.4
15.0	1.0	5.85	99.0	574	46	12.5	0.4	11.5	0.2	73	1.5
15.0	2.0	5.68	96.3	520	53	14.0	0.7	10.3	0.3	75	1.7
15.0	4.0	5.72	96.9	570	38	12.2	0.3	10.2	0.4	75	2.0

<sup>a</sup>Four-point-bend strength. <sup>b</sup>DCB fracture toughness. <sup>c</sup>Vickers hardness. <sup>d</sup>Monoclinic ZrO<sub>2</sub>/total ZrO<sub>2</sub> (%)<sup>24</sup> on fracture surfaces. <sup>e</sup>Grain size measured by linear intercept method. <sup>\*\*</sup>% theoretical density (based on rule of mixtures). <sup>††</sup>Mean value. <sup>†††</sup>Standard deviation.

occurrence of transformation. Mechanisms of deformation, such as ferroelastic switching (twinning) or conventional plastic deformation, are constant volume processes. These data indicate that ferroelastic switching or conventional plastic deformation may trigger transformation in these materials.

Figure 7 shows the elastic limit of Ce-TZP/Al<sub>2</sub>O<sub>3</sub> materials as a function of the amount of SrZrO<sub>3</sub> added to the starting materials. The elastic limit correlated well with the stress required for transformation. The addition of SrO decreased the elastic limit, although separate measurements showed that the formation of strontium aluminate did not decrease the modulus.

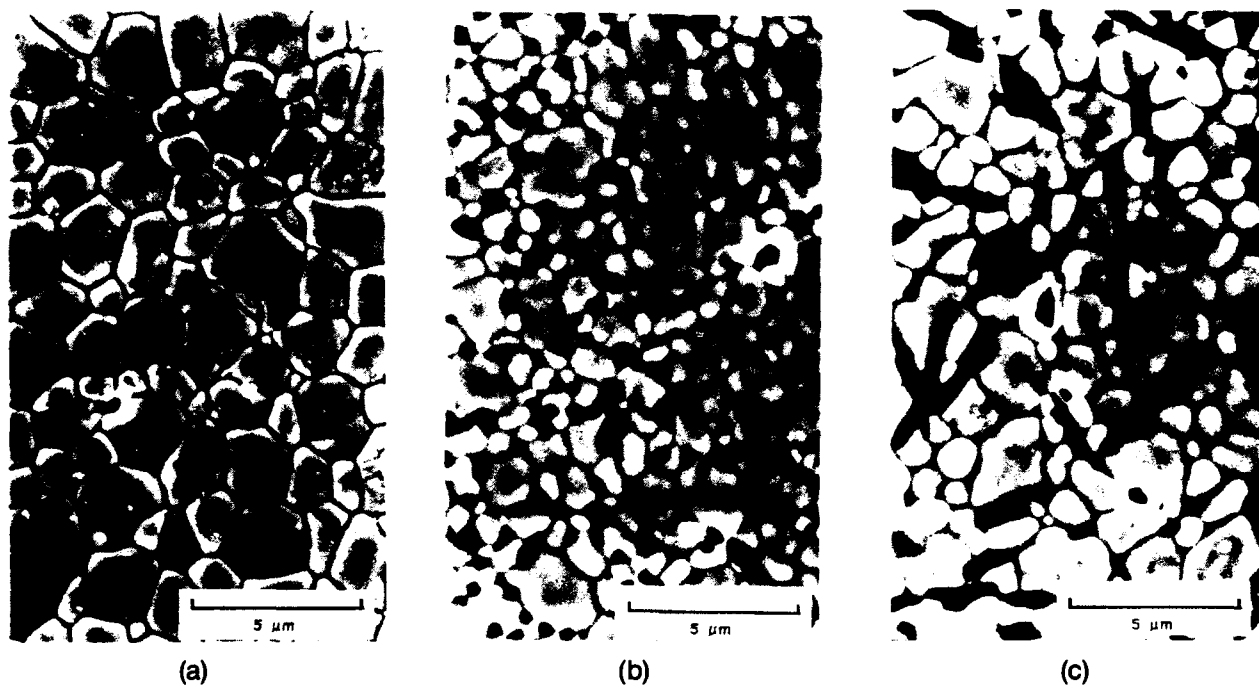
(B) *Higher Platelet Loadings:* Since the aluminates form in situ, higher platelet loadings should be possible by reactive sintering as compared to first synthesizing SrO·6Al<sub>2</sub>O<sub>3</sub> platelets and subsequently sintering the composite. Consequently, both Ce-TZP/30 vol% Al<sub>2</sub>O<sub>3</sub> and Ce-TZP/60 vol% Al<sub>2</sub>O<sub>3</sub> were made with SrZrO<sub>3</sub>, keeping the SrO/Al<sub>2</sub>O<sub>3</sub> molar ratios similar to those used in the Ce-TZP/15 vol% Al<sub>2</sub>O<sub>3</sub> composites discussed above.

Table II shows density, strength, DCB fracture toughness, and hardness values measured on sintered (1500°C for 2 h) samples made from reactants containing Ce-TZP/30 vol% Al<sub>2</sub>O<sub>3</sub> with various amounts of SrZrO<sub>3</sub>. The mechanical property trends for these composites made by mixing inexpensive raw materials were similar to those observed for sintered samples made from coprecipitated Ce-TZP pow-

ders with 15 vol% Al<sub>2</sub>O<sub>3</sub>, and SrZrO<sub>3</sub> additions between 0 and 4 wt%.

The density decreased at high SrO additions, although sintering at 1550°C resulted in densities greater than 97% of theoretical for all compositions. The strength increased with small SrO additions and then decreased at higher strontium aluminate concentrations (see Table II). Strengths were comparable or superior to those measured for the corresponding compositions of Ce-TZP/15 vol% Al<sub>2</sub>O<sub>3</sub> (compare Tables I and II) with the exception of the highest SrZrO<sub>3</sub> content. The main advantage of increased alumina in the starting composition is increased hardness, which was 2 to 3 GPa higher than the corresponding compositions in Table I. Higher alumina content should also result in improved high-temperature properties,<sup>12</sup> although these measurements have not been made on compositions containing strontium aluminate platelets.

Fracture toughness increased with increasing SrZrO<sub>3</sub> content up to 4 wt% and then decreased (see Table II). The fracture toughness of 15.1 MPa·m<sup>1/2</sup> measured for the Ce-TZP/30 vol% Al<sub>2</sub>O<sub>3</sub>-4 wt% SrZrO<sub>3</sub> composition was comparable to that measured for Ce-TZP/15 vol% Al<sub>2</sub>O<sub>3</sub> with 2 wt% SrZrO<sub>3</sub>. Transformation toughening was evident, as the monoclinic ZrO<sub>2</sub> detected on fracture surfaces increased from 42% with no SrZrO<sub>3</sub> to 86% with 4 wt% SrZrO<sub>3</sub>. Nomarski interference contrast optical micrographs, however, showed no measurable transformation zones for any materials containing dispersed second phases despite  $K_{Ic}$  values as high



**Fig. 2.** SEM micrographs of polished and etched cross sections of Ce-TZP and Ce-TZP/15 vol% Al<sub>2</sub>O<sub>3</sub> compositions showing strontium aluminate platelet formation with simultaneous Al<sub>2</sub>O<sub>3</sub> and SrO additions: (a) Ce-TZP, (b) Ce-TZP/15 vol% Al<sub>2</sub>O<sub>3</sub>, (c) Ce-TZP/15 vol% Al<sub>2</sub>O<sub>3</sub>-2.0 wt% SrZrO<sub>3</sub>.

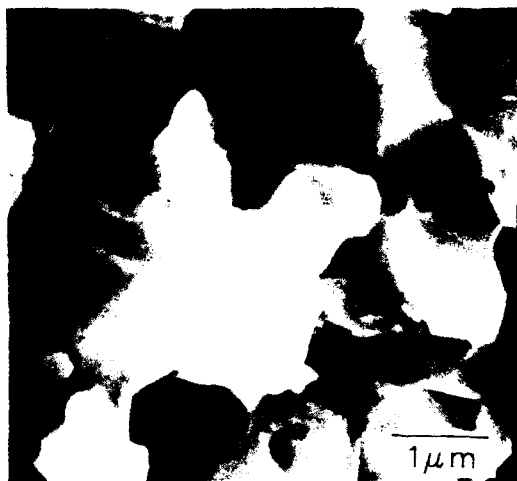


Fig. 3. SEM micrograph of fracture surface of Ce-TZP/15 vol%  $\text{Al}_2\text{O}_3$  with 4.0 wt%  $\text{SrZrO}_3$ . Platelet shape of strontium aluminate is clearly evident.

as  $15 \text{ MPa} \cdot \text{m}^{1/2}$ . By contrast, a significant transformation zone (see Fig. 8) was observed in Ce-TZP (made with  $\text{ZrO}_2$  and  $\text{CeO}_2$  starting powders) containing no second phases with  $K_{IC} \approx 13 \text{ MPa} \cdot \text{m}^{1/2}$ .

SEM micrographs of polished cross sections and fracture surfaces clearly reveal strontium aluminate platelet formation (see Fig. 9(a)). X-ray diffraction showed that the second phase shifted from  $\text{Al}_2\text{O}_3$  to  $\text{SrO} \cdot 6\text{Al}_2\text{O}_3$  with increasing  $\text{SrZrO}_3$  additions to the starting powders.

$\text{ZrO}_2$  (12 mol%  $\text{CeO}_2$ )-60 vol%  $\text{Al}_2\text{O}_3$  samples with  $\text{SrZrO}_3$  ranging between 0 and 16 wt% were made by sintering at  $1600^\circ\text{C}$  with densities greater than 98% of theoretical at  $\text{SrZrO}_3 < 8 \text{ wt}\%$ . Strength (500 to 650 MPa), hardness (13.1 to 14.6 GPa), and toughness (6 to  $14 \text{ MPa} \cdot \text{m}^{1/2}$ ) did not improve as compared to Ce-TZP/30 vol% compositions. The important point, however, is that high toughness ( $14 \text{ MPa} \cdot \text{m}^{1/2}$ ) was achieved in one composition (Ce-TZP/60 vol%  $\text{Al}_2\text{O}_3$ -4 wt%  $\text{SrZrO}_3$ ) containing a high alumina content. Figure 9(b) shows that high platelet loadings were achieved in situ during sintering.

Figure 10 compares the fracture toughness of all of the materials with varying alumina concentrations, based on their  $\text{SrO}/\text{Al}_2\text{O}_3$  molar ratio. Peak toughness occurs at  $\text{SrO}/\text{Al}_2\text{O}_3$  molar ratios between  $\approx 0.03$  and 0.1 for all three alumina contents studied. Further work is needed to determine the reason for the shift in peak toughness to a lower  $\text{SrO}/\text{Al}_2\text{O}_3$  ratio at the higher  $\text{Al}_2\text{O}_3$  content. The data in Fig. 10 also indicate

that the  $\text{SrO}/\text{Al}_2\text{O}_3$  range over which high toughness occurs narrows with increasing alumina content. It is noteworthy that the peak toughness does not change significantly, despite the fact that the amount of  $\text{ZrO}_2$  decreases by a factor of four, again indicating that mechanisms in addition to transformation toughening are operative in these materials.

## (2) $\text{SrZrO}_3$ Additions without $\text{Al}_2\text{O}_3$

In order to determine the effect of  $\text{SrZrO}_3$  additions on the fracture toughness of Ce-TZP, compositions were made as before, except without  $\text{Al}_2\text{O}_3$ . Polished cross sections of sintered samples showed no evidence of second phase formation. This is consistent with aluminate platelet formation in the case of Ce-TZP/ $\text{Al}_2\text{O}_3$  compositions, as discussed above. All of the compositions sintered to high density (see Table III). The strength of Ce-TZP made by mixing inexpensive powders was lower than the strength of Ce-TZP made using commercially available coprecipitated powder (compare Tables I and III). The strength increased significantly with 0.5 and 1.0 wt%  $\text{SrZrO}_3$  additions, as did the hardness (see Table III). Conversely, the DCB fracture toughness decreased from 13.3 to  $5.8 \text{ MPa} \cdot \text{m}^{1/2}$  with increasing  $\text{SrZrO}_3$  content (see Table III). The fracture toughness of the Ce-TZP made by mixing raw materials was similar to the toughness of Ce-TZP made from coprecipitated powders, consistent with their near-identical grain size.

The addition of  $\text{SrZrO}_3$  affects grain size, as grain refinement is obvious with as little as 0.5 wt%  $\text{SrZrO}_3$  (see Table III). Drennan and Hannink<sup>22</sup> found a small decrease in grain size and increase in strength when 0.25 wt% SrO was added to Mg-PSZ. Zirconia grain size has a strong effect on the degree of transformation, with larger grains transforming more readily than smaller grains. The zirconia grain size in the present study did not change appreciably with  $\text{SrZrO}_3$  additions between 1 and 4 wt%.

Without a second phase, transformation in Ce-TZP was unrestrained, and large transformation bands formed under stress (i.e., near indents) and extended beyond the indentation cracks. Increasing  $\text{SrZrO}_3$  additions limited the degree of transformation in Ce-TZP, but transformation bands were still observed near indents in samples of all of the Table III compositions.

## IV. Discussion

SrO additions to Ce-TZP decreased the  $\text{ZrO}_2$  grain size with a corresponding decrease in toughness (from  $\approx 13$  to  $\approx 6 \text{ MPa} \cdot \text{m}^{1/2}$ ). The simultaneous addition of  $\text{Al}_2\text{O}_3$  and SrO to Ce-TZP leads to the formation of strontium hexaluminate platelets within the Ce-TZP matrix. The toughness of Ce-TZP/ $\text{Al}_2\text{O}_3$  compositions increased from  $\approx 8$  to  $\approx 14 \text{ MPa} \cdot \text{m}^{1/2}$

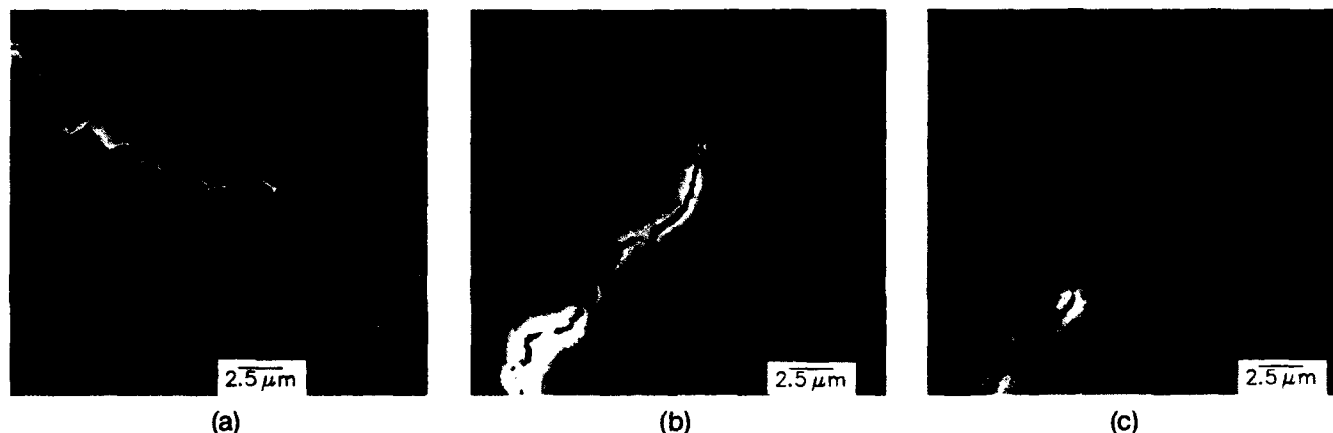


Fig. 4. Polished cross section of (a) Ce-TZP, (b) Ce-TZP/ $\text{Al}_2\text{O}_3$ -2 wt%  $\text{SrZrO}_3$ , and (c) Ce-TZP/ $\text{Al}_2\text{O}_3$ -4 wt%  $\text{SrZrO}_3$ , showing similar tendency for crack branching and crack bridging.

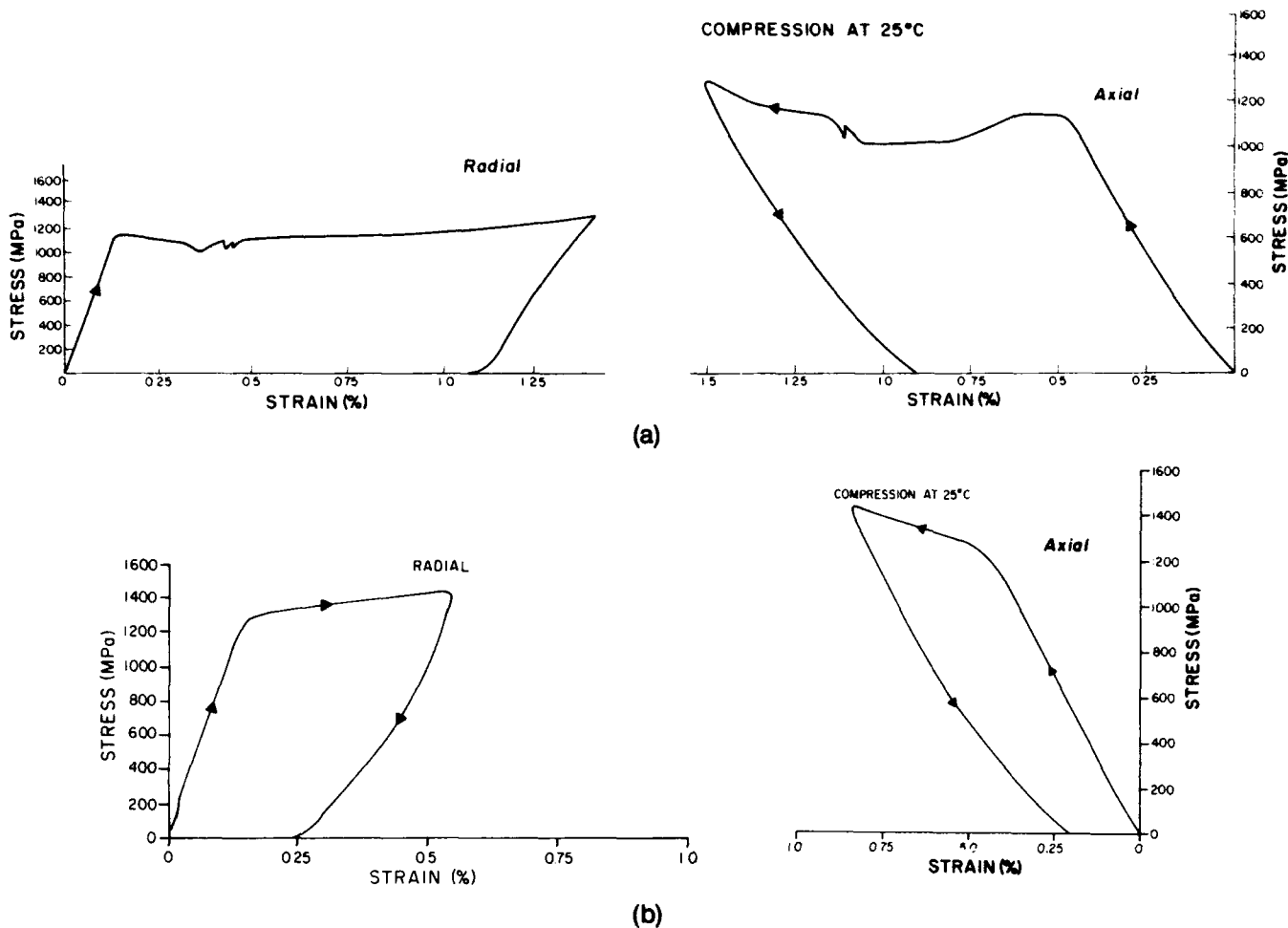


Fig. 5. Stress-strain curves in compression at 25°C for (a) Ce-TZP and (b) Ce-TZP/ $\text{Al}_2\text{O}_3$ -2 wt%  $\text{SrZrO}_3$ . Note autocatalytic transformation in Ce-TZP which is absent in Ce-TZP with  $\text{SrAl}_2\text{O}_9$  platelets.

coincident with the formation of strontium aluminate platelets in the microstructure. The strength and hardness of Ce-TZP/ $\text{Al}_2\text{O}_3$  compositions containing strontium aluminate platelets were also superior to those of Ce-TZP, with or without  $\text{SrZrO}_3$  additions. The fact that strontium aluminate platelets form in situ suggests that SrO, not  $\text{SrZrO}_3$ , is the important constituent and that strontium can be added as an oxide, carbonate, nitrate, etc. and achieve a similar effect.<sup>30</sup> The amount of monoclinic  $\text{ZrO}_2$  on fracture surfaces did not correlate with fracture toughness when comparing Ce-TZP

(SrO doped) with Ce-TZP containing simultaneous additions of  $\text{Al}_2\text{O}_3$  and SrO, since both types of materials have similar amounts of monoclinic  $\text{ZrO}_2$  ( $\approx 75\%$ ) on fracture surfaces, but fracture toughness is lower in Ce-TZP by a factor of 2 (see Tables I and III).

There is also a difficulty in correlating the increase in toughness of Ce-TZP to platelet reinforcement. The highest toughness values observed at each alumina level were at intermediate platelet loadings. Efforts to form strontium aluminate platelets in situ in Y-TZP have been unsuccessful. No toughening has been observed for strontium hexaluminate-reinforced alumina. Furthermore, in a study where CaO, SrO,

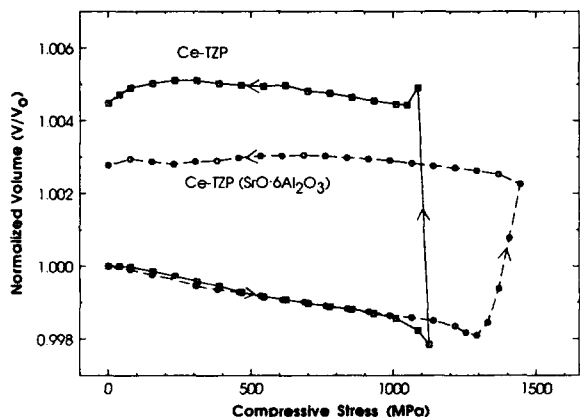


Fig. 6. Normalized volume as a function of compressive stress for Ce-TZP (squares) and Ce-TZP/ $\text{Al}_2\text{O}_3$ -2 wt%  $\text{SrZrO}_3$  (circles).

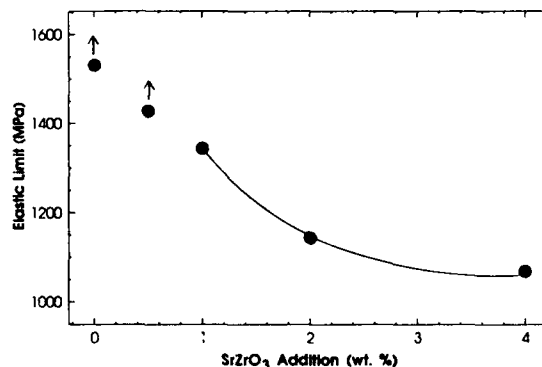


Fig. 7. Elastic limit of Ce-TZP/15 vol%  $\text{Al}_2\text{O}_3$  compositions as a function of  $\text{SrZrO}_3$  content added to the starting powder.

Table II. Ce-TZP/30 vol% Al<sub>2</sub>O<sub>3</sub> Ceramics Sintered at 1500°C Containing Additions of SrO

SrZrO <sub>3</sub> (wt%)	Density		$\sigma_f$ (MPa) <sup>a</sup>		$K_{Ic}$ (MPa·m <sup>1/2</sup> ) <sup>b</sup>		$H$ (GPa) <sup>c</sup>	
	(g/cm <sup>3</sup> )	%TD <sup>d</sup>	$x^*$	$s^{**}$	$x$	$s$	$x$	$s$
0.0	5.53	99.1	632	37	7.8	0.3	14.5	0.2
1.0	5.53	99.1	648	45	9.9	0.1	14.6	0.1
2.0	5.52	99.1	726	29	11.2	0.5	13.7	0.5
4.0	5.47	98.2	530	28	15.1	0.3	12.7	0.2
8.0	5.15	92.5	407	43	11.8	0.3	12.1	1.6

<sup>a</sup>Four-point-bend strength. <sup>b</sup>DCB fracture toughness. <sup>c</sup>Vickers hardness. <sup>d</sup>% theoretical density (based on rule of mixtures). \*Mean value. \*\*Standard deviation.

and BaO were compared as dopants to Ce-TZP/Al<sub>2</sub>O<sub>3</sub>, SrO was the only additive effective in increasing toughness, despite the formation of platelet-shaped aluminates in all three systems.<sup>20</sup> These observations show that the formation of platelets in a microstructure is not a prerequisite for toughening and that further work is needed to understand the mechanism of toughening in Ce-TZP/Al<sub>2</sub>O<sub>3</sub>/SrO·6Al<sub>2</sub>O<sub>3</sub> ceramics.

It is well recognized that large plate-shaped grains reduce strength as they become critical flaws in a microstructure. Elongated  $\alpha$ -SiC and  $\beta''$ -Al<sub>2</sub>O<sub>3</sub> grains, for example, lead to low strength. However, silicon nitride ceramics, with a fibrous microstructure on a finer scale, show simultaneous improvement in strength and toughness coincident with the elongated microstructure.<sup>31</sup> Recent work on high-toughness ( $\approx 11$  MPa·

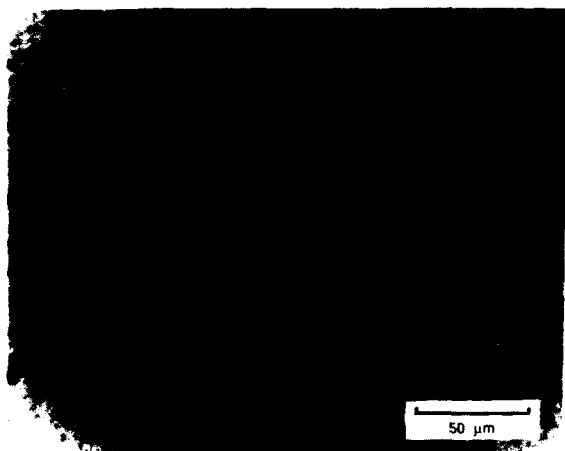
m<sup>1/2</sup>) Si<sub>3</sub>N<sub>4</sub> with coarser grains has shown a trade-off between strength and toughness, consistent with *R*-curve behavior.<sup>32</sup>

Tsukuma and Takahata<sup>12</sup> made Y-TZP with 40 wt% of an elongated La<sub>2</sub>O<sub>3</sub>·11Al<sub>2</sub>O<sub>3</sub> ( $\beta$ -Al<sub>2</sub>O<sub>3</sub> type compound) with similar strength and only slightly reduced toughness in comparison to Y-TZP. The advantage of the platelets was that good strength (600 MPa at 1000°C and 500 MPa at 1300°C) was retained at high temperatures. Y-TZP composites made with elongated La<sub>2</sub>O<sub>3</sub>·11Al<sub>2</sub>O<sub>3</sub> showed better resistance to plastic deformation than their Y-TZP/Al<sub>2</sub>O<sub>3</sub> counterparts.<sup>12</sup> The SrO·6Al<sub>2</sub>O<sub>3</sub> platelets in the present work are similar in dimension to the La<sub>2</sub>O<sub>3</sub>·11Al<sub>2</sub>O<sub>3</sub> platelets formed in Y-TZP.<sup>12</sup>

It is well recognized that Ce-TZP materials exhibit *R*-curve behavior.<sup>14,15</sup> Toughness measurements in the present study were made for long crack lengths, presumably in the plateau region of the *R*-curve. Figure 11 shows the strength-toughness relationship for platelet-containing Ce-TZP in relation to Ce-TZP/Al<sub>2</sub>O<sub>3</sub> and Ce-TZP ceramics. Clearly, the platelet-

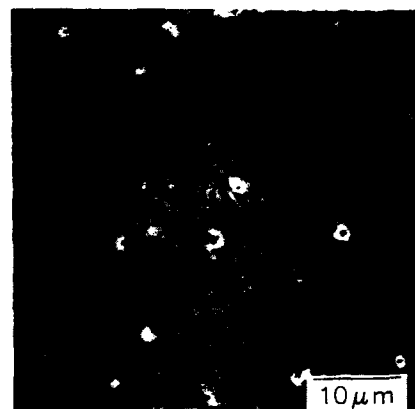


(a)



(b)

Fig. 8. Nomarski interference contrast micrographs of crack surfaces of (a) Ce-TZP and (b) Ce-TZP/15 vol% Al<sub>2</sub>O<sub>3</sub>-2 wt% SrZrO<sub>3</sub> during in situ loading. Note transformation zone in Ce-TZP.



(a)



(b)

Fig. 9. SEM micrographs of polished cross sections showing in situ SrAl<sub>12</sub>O<sub>19</sub> platelet formation: (a) Ce-TZP/30 vol% Al<sub>2</sub>O<sub>3</sub> with 8 wt% SrZrO<sub>3</sub>; (b) Al<sub>2</sub>O<sub>3</sub>/40 vol% Ce-TZP with 8 wt% SrZrO<sub>3</sub>.

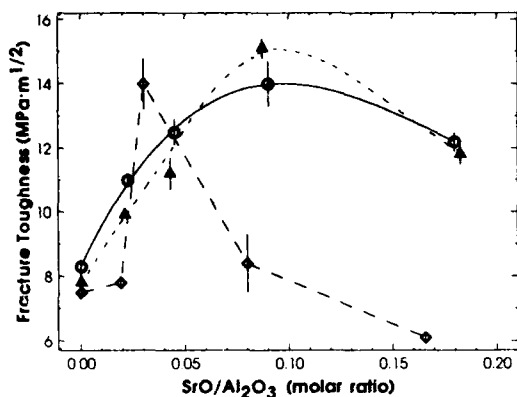


Fig. 10. Fracture toughness of Ce-TZP with 15 (triangles), 30 (circles), and 60 (diamonds) vol% alumina in the starting Ce-TZP composition, as a function of SrO/Al<sub>2</sub>O<sub>3</sub> molar ratio.

reinforced Ce-TZP retains the strength of Ce-TZP/Al<sub>2</sub>O<sub>3</sub> over a wide range of toughness values. The combination of high toughness with moderate strength and hardness, exhibited by the platelet-containing Ce-TZP ceramics, is attractive for low-temperature structural applications.

V. Conclusions

The addition of SrO to Ce-TZP leads to a decrease in zirconia grain size with an increase in hardness. The toughness decreases as the strength increases in accordance with conventional zirconia ceramics. The simultaneous addition of SrO and Al<sub>2</sub>O<sub>3</sub> to Ce-TZP, however, results in the in situ formation of SrO·6Al<sub>2</sub>O<sub>3</sub> platelets. Ce-TZP/Al<sub>2</sub>O<sub>3</sub>/SrO·6Al<sub>2</sub>O<sub>3</sub> ceramics have the strength (500 to 700 MPa) of Ce-TZP/Al<sub>2</sub>O<sub>3</sub>, the hardness (13 to 14 GPa) of Y-TZP/Al<sub>2</sub>O<sub>3</sub>, while maintaining the high toughness (14 to 15 MPa·m<sup>1/2</sup>) of Ce-TZP. Optimum toughness was obtained at a SrO/Al<sub>2</sub>O<sub>3</sub> molar ratio of ≈0.1 for compositions containing 15 and 30 vol% Al<sub>2</sub>O<sub>3</sub>, while the maximum toughness occurred at a SrO/Al<sub>2</sub>O<sub>3</sub> molar ratio of ≈0.03 for compositions with 60 vol% Al<sub>2</sub>O<sub>3</sub>. The in situ formation of platelets allows achievement of high platelet loadings. High toughness was achieved with compositions up to 60 vol% Al<sub>2</sub>O<sub>3</sub>.

The in situ formation of SrAl<sub>12</sub>O<sub>19</sub> platelets (≈0.5 μm in thickness and 5 to 10 μm in width and length) suppressed the autocatalytic transformation of zirconia. While substantial monoclinic ZrO<sub>2</sub> was measured on fracture surfaces of platelet Ce-TZP composites, transformation zones were not observed by optical techniques. Since percent monoclinic ZrO<sub>2</sub> on fracture surfaces did not correlate well with fracture toughness, and high toughness occurred simultaneously with platelet formation, toughening mechanisms in addition to transformation toughening appear to be operative in these materials.

The benefit of simultaneous additions of Al<sub>2</sub>O<sub>3</sub> and SrO to Ce-TZP is that tough ceramics can be produced with good hardness and strength. The retention of strength at high toughness values in these Ce-TZP matrix ceramics suggests that R-curve behavior does not limit strength to the same extent as in Ce-TZP. Further work is needed to explore elevated tem-

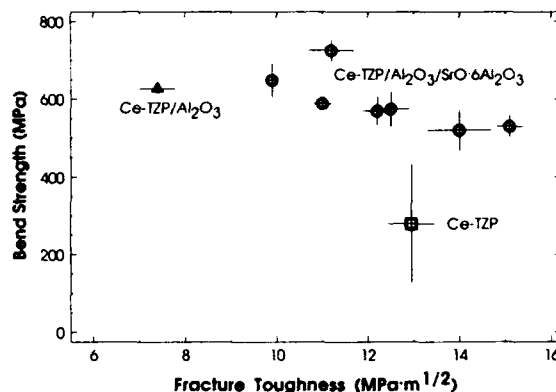


Fig. 11. Strength-toughness relationships for Ce-TZP (squares), Ce-TZP/Al<sub>2</sub>O<sub>3</sub> (triangles), and Ce-TZP/Al<sub>2</sub>O<sub>3</sub>/SrO·6Al<sub>2</sub>O<sub>3</sub> (circles) ceramics with densities greater than 95% of theoretical.

perature properties including strength, toughness, and creep resistance. The role of SrO·6Al<sub>2</sub>O<sub>3</sub> platelets in toughening Ce-TZP deserves further study.

**Acknowledgments:** Discussions with Roger L. K. Matsumoto of Hercules, Inc., and Professor A. G. Evans of University of California (Santa Barbara) are appreciated.

References

- <sup>1</sup>A. G. Evans, "Perspective on the Development of High-Toughness Ceramics," *J. Am. Ceram. Soc.*, **73** [2] 187-206 (1990).
- <sup>2</sup>R. C. Garvie, R. H. Hannink, and R. T. Pascoe, "Ceramic Steel?," *Nature (London)*, **258** [5537] 703-704 (1975).
- <sup>3</sup>Advances in Ceramics, Vol. 3, *Science and Technology of Zirconia I*. Edited by A. H. Heuer and L. W. Hobbs. American Ceramic Society, Columbus, OH, 1981.
- <sup>4</sup>Advances in Ceramics, Vol. 12, *Science and Technology of Zirconia II*. Edited by N. Claussen, M. Rühle, and A. H. Heuer. American Ceramic Society, Columbus, OH, 1984.
- <sup>5</sup>Advances in Ceramics, Vol. 24, *Science and Technology of Zirconia III*. Edited by S. Somiya, N. Yamamoto, and H. Yanagida. American Ceramic Society, Westerville, OH, 1988.
- <sup>6</sup>F. F. Lange, "Transformation Toughening," *J. Mater. Sci.*, **17**, 225-34 (1982).
- <sup>7</sup>*J. Am. Ceram. Soc.*, **69** [3] 169-298 (1986); **69** [7] 511-84 (1986).
- <sup>8</sup>A. H. Heuer, "Transformation Toughening in ZrO<sub>2</sub>-Containing Ceramics," *J. Am. Ceram. Soc.*, **70** [10] 689-98 (1987).
- <sup>9</sup>T. K. Gupta, J. H. Bechtold, R. C. Kuznicki, L. F. Kadoff, and B. R. Rossing, "Stabilization of Tetragonal Phase in Polycrystalline Zirconia," *J. Mater. Sci.*, **13**, 2421-26 (1977).
- <sup>10</sup>K. Tsukuma and K. Ueda, "Strength and Fracture Toughness of Isostatically Hot-Pressed Composites of Al<sub>2</sub>O<sub>3</sub> and Y<sub>2</sub>O<sub>3</sub>-Partially-Stabilized ZrO<sub>2</sub>," *J. Am. Ceram. Soc.*, **68** [1] C-4-C-5 (1985).
- <sup>11</sup>K. Tsukuma, K. Ueda, K. Mashushita, and M. Shimada, "High-Temperature Strength and Fracture Toughness of Y<sub>2</sub>O<sub>3</sub>-Partially-Stabilized ZrO<sub>2</sub>/Al<sub>2</sub>O<sub>3</sub> Composites," *J. Am. Ceram. Soc.*, **68** [2] C-56-C-58 (1985).
- <sup>12</sup>K. Tsukuma and T. Takahata, "Mechanical Property and Microstructure of TZP and TZP/Al<sub>2</sub>O<sub>3</sub> Composites," *Advanced Structural Ceramics*, Vol. 78. Edited by P. F. Becher, M. V. Swain, and S. Somiya. Materials Research Society, Pittsburgh, PA, (1987).
- <sup>13</sup>I. Nettlehip and R. Stevens, "Tetragonal Zirconia Polycrystal (TZP)—A Review," *Int. J. High Technol. Ceram.*, **3**, 1-32 (1987).
- <sup>14</sup>M. V. Swain and L. R. F. Rose, "Strength Limitations of Transformation-Toughened Zirconia Alloys," *J. Am. Ceram. Soc.*, **69** [7] 511-18 (1986).
- <sup>15</sup>C.-S. Yu and D. K. Shetty, "Transformation Zone Shape, Size, and Crack-Growth-Resistance (R-Curve) Behavior of Ceria-Partially-Stabilized Zirconia Polycrystals," *J. Am. Ceram. Soc.*, **72** [6] 921-28 (1989).

Table III. Properties of ZrO<sub>2</sub> (12 mol% CeO<sub>2</sub>) without Al<sub>2</sub>O<sub>3</sub> Additions Sintered at 1500°C

SrZrO <sub>3</sub> (wt%)	Density		σ <sub>f</sub> (MPa) <sup>a</sup>		K <sub>IC</sub> (MPa·m <sup>1/2</sup> ) <sup>b</sup>		H (GPa) <sup>c</sup>		m-ZrO <sub>2</sub> <sup>d</sup> (%)	gs <sup>e</sup> (μm)
	(g/cm <sup>3</sup> )	%TD <sup>**</sup>	x <sup>**</sup>	s <sup>**</sup>	x	s	x	s		
0.0	6.21	99.2	172	7	13.3	0.6	7.7	0.1	90	2.6
0.5	6.21	99.2	264	8	10.1	0.6			89	2.3
1.0	6.21	99.2	388	31	5.8	0.2	9.5	0.2	74	2.0
2.0	6.22	99.4	389	13	5.8	0.2				
4.0	6.20	99.0	392	23	5.8	0.2	9.9	0.2	76	1.9

<sup>a</sup>Four-point-bend strength. <sup>b</sup>DCB fracture toughness. <sup>c</sup>Vickers hardness. <sup>d</sup>Monoclinic ZrO<sub>2</sub>/total ZrO<sub>2</sub> (%)<sup>24</sup> on fracture surfaces. <sup>e</sup>Grain size measured by linear intercept method. <sup>\*\*</sup>% theoretical density (based on rule of mixtures). <sup>\*</sup>Mean value. <sup>\*\*</sup>Standard deviation.

- <sup>16</sup>K.-H. Heussner and N. Claussen, "Strengthening of Ceria-Doped Tetragonal Zirconia Polycrystals by Reduction-Induced Phase Transformations," *J. Am. Ceram. Soc.*, **72** [6] 1044-46 (1989).
- <sup>17</sup>D. Michel, L. Mazerolles, and M. Perez Y Jorba, "Fracture of Metastable Tetragonal Zirconia Crystals," *J. Mater. Sci.*, **18**, 2618-28 (1983).
- <sup>18</sup>A.V. Virkar and R. L. K. Matsumoto, "Ferroelastic Domain Switching as a Toughening Mechanism in Tetragonal Zirconia," *J. Am. Ceram. Soc.*, **69** [10] C-224-C-226 (1986).
- <sup>19</sup>A.V. Virkar and R. L. K. Matsumoto, "Toughening Mechanism in Tetragonal Zirconia Polycrystalline (TZP) Ceramics"; pp. 653-62 in *Advances in Ceramics*, Vol. 24, *Science and Technology of Zirconia III*. Edited by S. Somiya, N. Yamamoto, and H. Yanagida. American Ceramic Society, Westerville, OH, 1988.
- <sup>20</sup>R. L. K. Matsumoto and R. J. Mayhew, "High Temperature Evaluation of New Ferroelastic Toughened Ceramic Materials," Final Report for SBIR Army Contract No. DLAAL04-87-C-0058, 1988.
- <sup>21</sup>J. Drennan and R. H. J. Hannink, "Sintering Aids for Partially Stabilized Zirconia," *J. Aust. Ceram. Soc.*, **20**, 36-37 (1984).
- <sup>22</sup>J. Drennan and R. H. J. Hannink, "Effect of SrO Additions on the Grain-Boundary Microstructure and Mechanical Properties of Magnesia-Partially-Stabilized Zirconia," *J. Am. Ceram. Soc.*, **69** [7] 541-46 (1986).
- <sup>23</sup>R. H. J. Hannink and J. Drennan, "Microstructural and Chemical Aspects of a Strontia Sintering Aid on Mg-PSZ"; pp. 68-78 in *Materials Science Research*, Vol. 20, *Tailoring Multiphase Composite Ceramics*. Plenum Press, New York, 1986.
- <sup>24</sup>H. Toraya, M. Yoshimura and S. Somiya, "Calibration Curve for Quantitative Analysis of the Monoclinic-Tetragonal ZrO<sub>2</sub> System by X-Ray Diffraction," *J. Am. Ceram. Soc.*, **68** [6] C-119-C-121 (1984).
- <sup>25</sup>F. Ganits, T.Y. Chemekova, and Y.P. Udalov, *Russ. J. Inorg. Chem. (Engl. Transl.)*, **24** [2] 260-63 (1979) (see Fig. 6427 in *Phase Diagrams for Ceramists*, Vol. VI, 1987. Edited by R. S. Roth, J. R. Dennis, and H. F. McMurdie. American Ceramic Society, Westerville, OH).
- <sup>26</sup>J.-G. Duh, H.-T. Dai, and B.-H. Chiou, "Sintering, Microstructure, Hardness, and Fracture Toughness Behavior of Y<sub>2</sub>O<sub>3</sub>-CeO<sub>2</sub>-ZrO<sub>2</sub>," *J. Am. Ceram. Soc.*, **71** [10] 813-19 (1988).
- <sup>27</sup>G. Srinivasan, J.-E. Jue, S.-Y. Kuo, and A.V. Virkar, "Ferroelastic Domain Switching in Polydomain Tetragonal Zirconia Single Crystals," *J. Am. Ceram. Soc.*, **72** [11] 2098-103 (1989).
- <sup>28</sup>P. E. Reyes-Morel and I.-W. Chen, "Transformation Plasticity of CeO<sub>2</sub>-Stabilized Tetragonal Zirconia Polycrystals: I, Stress Assistance and Autocatalysis," *J. Am. Ceram. Soc.*, **71** [5] 343-53 (1988).
- <sup>29</sup>K. M. Prettyman and A.V. Virkar; unpublished work.
- <sup>30</sup>R. L. K. Matsumoto, A.V. Virkar, and R. A. Cutler, "Ceramics with High Toughness, Strength and Hardness," U.S. Patent Application, 1989.
- <sup>31</sup>F. F. Lange, "Fabrication and Properties of Dense Polyphase Silicon Nitride," *Am. Ceram. Soc. Bull.*, **62** [12] 1369-74 (1983).
- <sup>32</sup>C. W. Li and J. Yamanis, "Super-Tough Silicon Nitride with R-Curve Behavior," *Ceram. Eng. Sci. Proc.*, **10** [7-8] 632-45 (1989). □

# FERROELASTIC DOMAIN SWITCHING IN TETRAGONAL ZIRCONIA

C. J. Chan<sup>1</sup>, F. F. Lange<sup>1</sup>, M. Rühle<sup>1\*</sup>, J. F. Jue<sup>2</sup> and A. V. Virkar<sup>2</sup>

<sup>1</sup>Materials Department, University of California, Santa Barbara, CA 93106

<sup>2</sup>Department of Materials Science and Engineering, University of Utah, Salt Lake City, Utah 84112

## ABSTRACT

Ferroelastic domain switching is one of the possible toughening mechanisms in ceramic materials. Microstructural evidence of domain reorientation (switching) in polydomain tetragonal zirconia single crystals is observed upon the application of a unidirectional compressive stress. Dark field imaging of the three {112} tetragonal twin variants in a [111] zone indicates that two sets of twin variants grow at the expense of the third set upon application of uniaxial compression. The diminishing variant is the one with its *c* axis parallel to the compression axis. Indentation experiments on uniaxially compressed samples show an anisotropy in crack length. Crack propagates more easily along the loading direction. A construction for the orientation relationship of domains and their twin boundaries is presented.

## INTRODUCTION

Ferroelasticity is the mechanical analogue of ferromagnetism and ferroelectricity. The ferroelastic state is characterized by the existence of a permanent strain and a hysteresis loop between the strain and its applied stress, as shown in Figure 1. According to Michel et al., a metastable tetragonal (*t'*) zirconia is a ferroelastic phase [1]. There are at least two energetically equivalent orientational states existing in the crystal. In principle, crystal orientation may be induced from one state to the other by applying an appropriate external stress [2]. The area within the hysteresis loop is the mechanical energy absorbed in the reorientation process.

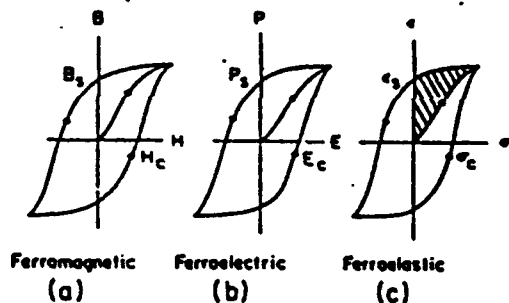


Figure 1. Schematics showing hysteresis loop for (a) ferromagnetic, (b) ferroelectric, and (c) ferroelastic materials. Shaded area is the mechanical energy absorbed in domain reorientations.

Virkar and Matsumoto [3] observed an increase in the (002) peak intensity and a simultaneous decrease in the (200) peak intensity after surface grinding on ceria-stabilized tetragonal zirconia (Ce-TZP) ceramics. The development of crystallographic texture was attributed to the switching of ferroelastic domains by the externally applied stress. They further proposed that domain reorientation may provide a requisite energy absorption mechanism for enhancement of fracture toughness. This mechanism differs from stress-induced transformation toughening in that there is no change in crystal structure, but only reorientation of twin variants within the process zone. Recent work of Srinivasan et al. [4] on polydomain tetragonal zirconia single crystals indicated that ferroelastic domains underwent reorientation under compression at temperatures as high as 1400°C. X-ray diffraction from high temperature fracture surfaces showed that domain reorientation had occurred with no monoclinic phase observed. Work was also done on well-known ferroelectric-ferroelastic materials such as BaTiO<sub>3</sub> and PZT [5]. It was observed that either an applied electrical field or a compressive stress led to domain switching.

The objective of this research is to establish direct microstructural evidence of ferroelastic domain switching in tetragonal zirconia ceramics upon application of stress. Uniaxial compression test on oriented "polydomain" single crystals was first studied. Efforts were then made on studying the microstructural change caused by controlled fracture using indentation, which may have important implications concerning fracture toughness enhancement.

\* Now at IBM Thomas J. Watson Research Center, P.O. Box 218, Yorktown Heights, NY 10598

\*\* Now at Max-Planck-Institut für Metallforschung, Seestr. 92, 7000 Stuttgart 1, Federal Republic of Germany

## EXPERIMENTAL PROCEDURES

Zirconia single crystals with a nominal composition of 3.0 mol%  $Y_2O_3$  produced by skull melting were used in this investigation. The single crystals were oriented and cut into cubes or bars so that the  $\langle 100 \rangle$  pseudo-cubic axes were orthogonal to the surfaces. In order to avoid the possible complication from transformation toughening by the t-to-m transformation, the metastable  $t'$  phase of tetragonal zirconia single crystals were obtained using the following heat treatment procedures. The oriented samples were heated in a gas fired furnace to a temperature  $\geq 2100^\circ C$  in air for 10 minutes, quenched to  $1400^\circ C$ , and subsequently furnace cooled to room temperature.

Uniaxial compression is a mechanical analog of electric poling. Poling in this paper is hereby referred as a material subjected to a uniaxial compression. By applying a unidirectional compression (UCP), it is possible to determine whether the domain orientation can be affected by compressive loading. The oriented specimens were subjected to compressive loading of 200 - 300 MPa at  $1000^\circ C$  and  $1400^\circ C$ . The compressed sample was then x-rayed, and cut into three different crystallographically oriented sections: (111), (100) perpendicular to UCP, and (100) parallel to UCP according to the pseudo-cubic symmetry. The (100) sections were polished to an optical finish, and indentation experiments were performed. Optical microscopy was used to identify microstructural changes before and after the application of uniaxial compression and microindentation. Selected indented specimens were chemically etched using KOH at  $500^\circ C$  in a nickel crucible for SEM observations. TEM thin foils on (111) sections were prepared following the standard grinding, dimpling, and ion milling procedures. Samples of (100) and (111) sections of as-heat-treated polydomain  $t'$  materials were also prepared and studied in the same fashion as UCP samples. The three tetragonal twin variants can be independently imaged by performing dark field imaging using the  $\{112\}$  type reflections present in a  $[111]$  zone axis selected-area diffraction (SAD) pattern [6]. Each variant gives rise to one pair of (112) reflection and corresponds to one of the three possible orientation states of the tetragonal phase. The twin variants are generally referred as ferroelastic domains. It is possible to study the changes of the orientation states upon application of stresses or in the vicinity of a propagating crack by comparing the relative area changes of three  $\{112\}$  tetragonal twin variants.

## RESULTS

### Uniaxial Compression Tests

X-ray diffraction patterns indicated that the diffraction peaks' intensity ratio,  $I(002)_t/I(200)_t$ , on the surface parallel to the compression axis increased after a unidirectional compression. This is the first evidence showing that domain reorientation occurred during compression.

Chemical etching was used to reveal large scale microstructural changes before and after the specimens were subjected to uniaxial compressive loading. Before UCP, an interpenetrated colony structure with its longitudinal axes parallel to pseudo-cubic  $\langle 100 \rangle$  direction was observed as shown in Figure 2(a). The width of each colony is about  $1 \mu m$ . Each colony contains traces of the  $(101)_t$  twins. After UCP the width of the colonies coarsened to 2-3  $\mu m$  in the direction parallel to mechanical loading (Figure 2(b)). The colony boundaries disappeared in the transverse direction.

TEM dark field imaging of  $\{112\}$  type reflections on  $B=[111]$  before UCP revealed that each tetragonal variants (ferroelastic domains) have about same area or intensity (Figure 3(a)). The twin traces are parallel to the  $\langle 110 \rangle$  direction of pseudo-cubic symmetry. A high density of antiphase boundaries can be identified [6,7]. Using the same imaging conditions on the specimens after UCP, one of the  $\{112\}$  twin variants was clearly diminished, as shown in Figure 3(b). After accounting for image rotation in the transmission microscope, the diminishing variant was found to be the one with its c-axis closest to the loading axis. Concurrently, the other two  $\{112\}$  tetragonal variants were observed to increase in size at the expense of the diminishing variant.

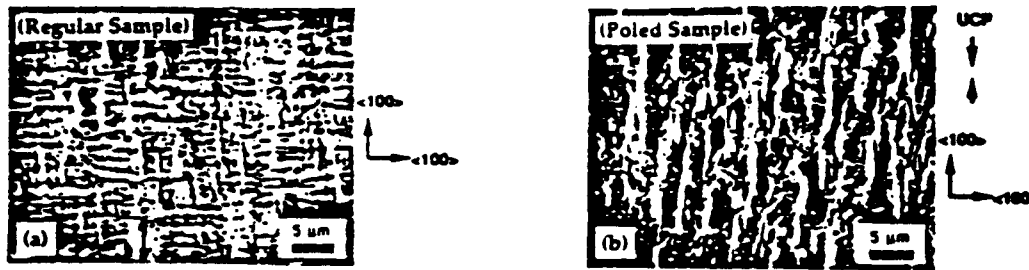


Figure 2. SEM micrograph of (a) (100) section of as-heat-treated sample, (b) (100) section, parallel to the loading direction, of  $t'$  material after high temperature compression test. Both sample were chemically etched using KOH at 500°C for 5 minutes in a nickel crucible.

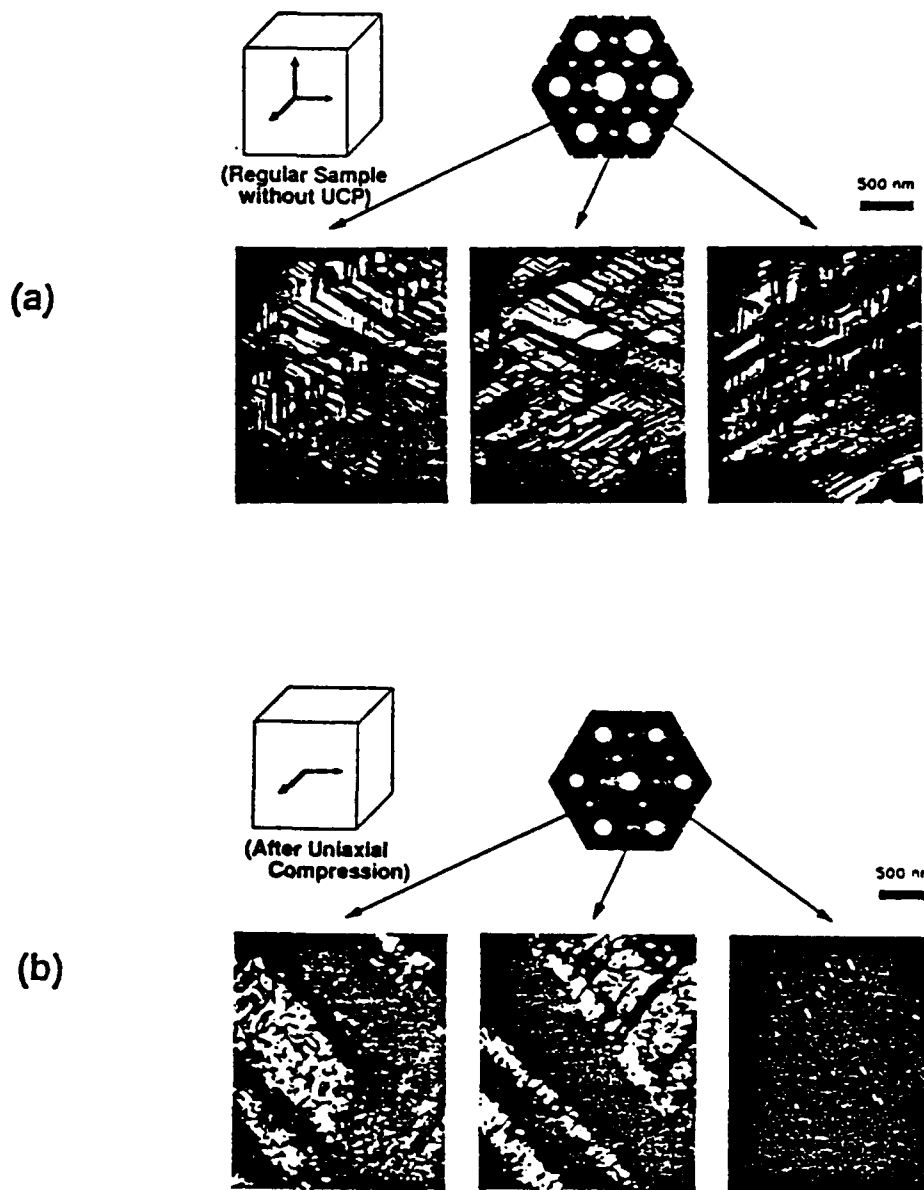


Figure 3. TEM/DF micrograph of three  $\{112\}$  tetragonal twin variants in a  $[111]$  zone axis of (a) an as-heat-treated  $t'$  material, (b) a  $t'$  material after application of a uniaxial compression at high temperature.

## Controlled Fracture by Indentation

Indentation experiments were done on both the mechanically poled (uniaxially compressed) and unpoled specimens. Symmetric traces of slip bands were observed adjacent to the indent together with radial cracks emanating from each corner of the indent for the unpoled sample. Slip traces around the Vickers indent were observed to be  $17^\circ$  away from  $\langle 100 \rangle$  on (100) sections and  $11^\circ$  away from  $\langle 110 \rangle$  on (111) sections. Trace analysis indicated that the slip plane is on  $\{4\ 13\ 14\}$ . Each slip band was found to be nearly a single tetragonal variant. SAD pattern along the  $[111]$  zone axis within each slip band also showed only one pair of  $(112)_t$  diffraction spots present.

Indentations on the (100) section along the loading direction of the poled specimens revealed that the crack length was longer in the compression direction relative to the orthogonal direction, as shown in Figure 4. In addition, under polarized light, some traces parallel to the direction of the ferroelastic twin variants' boundary were observed ahead of the crack in the transverse direction. For the (100) section orthogonal to the loading direction, a higher load was required to initiate radial cracks. Indentations on the (100) section of unpoled specimens indicated no anisotropy in fracture behavior.

### Indentation Fracture on Poled Sample

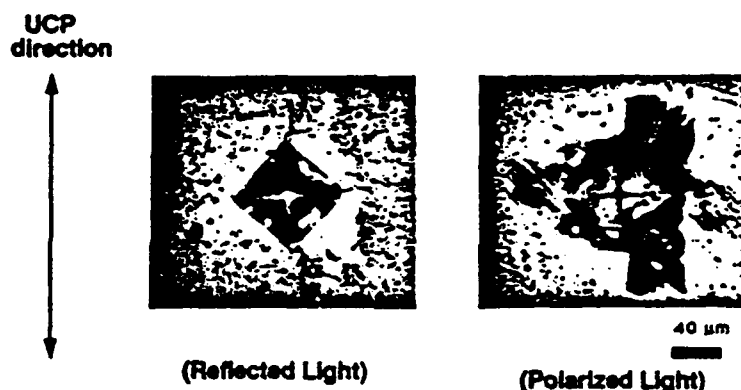


Figure 4. Optical micrograph of a Vickers indent on a poled sample: (a) reflected light, (b) transmitted polarized light. The applied load was 3 kg.

## DISCUSSION

Microstructural observations revealed that  $t'$ - $ZrO_2$  are heavily twinned. The trace of twin planes is parallel to  $\langle 110 \rangle$ . As shown in Figure 5(a), when a basic cell composed of three tetragonal variants is constructed, on a (100) plane the c-axes of two different tetragonal variants must be separated by a  $90^\circ$  twin boundary (Figure 5(b)). Hence, only  $\{101\}_t$  and  $\{011\}_t$  twin planes are allowed due to required symmetry operation considerations.

Theoretically, the diffraction pattern along  $[111]$  of a single variant tetragonal zirconia crystal will only contain the  $(112)_t$  diffractions in the direction of the c-axis. However, a regular unpoled sample is composed of all three tetragonal twin variants. Hence, its SAD pattern along  $[111]$  is the combination of three different single variants  $120^\circ$  apart from each other (Figure 3(a)). When the crystal is subjected to a uniaxial compression, it is apparent that tetragonal variants with their c-axes in the compression direction will try to re-orient perpendicular to the loading axis. Thus the intensity of the  $(112)_t$  diffraction along the UCP axis diminished.

The possibility of detwinning the twinned ferroelastic crystals by applying a uniaxial stress greater than the coercive force has been suggested [2]. It is generally understood that mechanical twinning is accomplished by shear [8]. While applying uniaxial compression, maximum shear stresses occur at  $45^\circ$  to the loading axis, i.e. planes of maximum shear stresses are parallel to  $(101)_t$  twin planes. Growth of two of the three tetragonal variants is favored due to the biaxial shear stresses produced by compression. This, in turn, results in the diminishing of the third tetragonal variant. Figure 5(c) illustrates evolution of a two-variant single crystal from a unpoled three-variant single crystal under a uniaxial compression (bi-axial shear). The maximum uniaxial strain resulting from the ferroelastic domain reorientation is expected to be about 0.5% (i.e.,  $1/3 (1-c/a_t)$ ) for a  $ZrO_2$ -3 mol%  $Y_2O_3$  single crystal [9]. It is possible to predict ferroelastic strains by determining the ratio of the intensity (or area) of the diminishing variant to the other two variants. Furthermore, a biaxial compression (uniaxial tension) will result in the formation of a single variant tetragonal phase. This resembles the condition within a shear band.

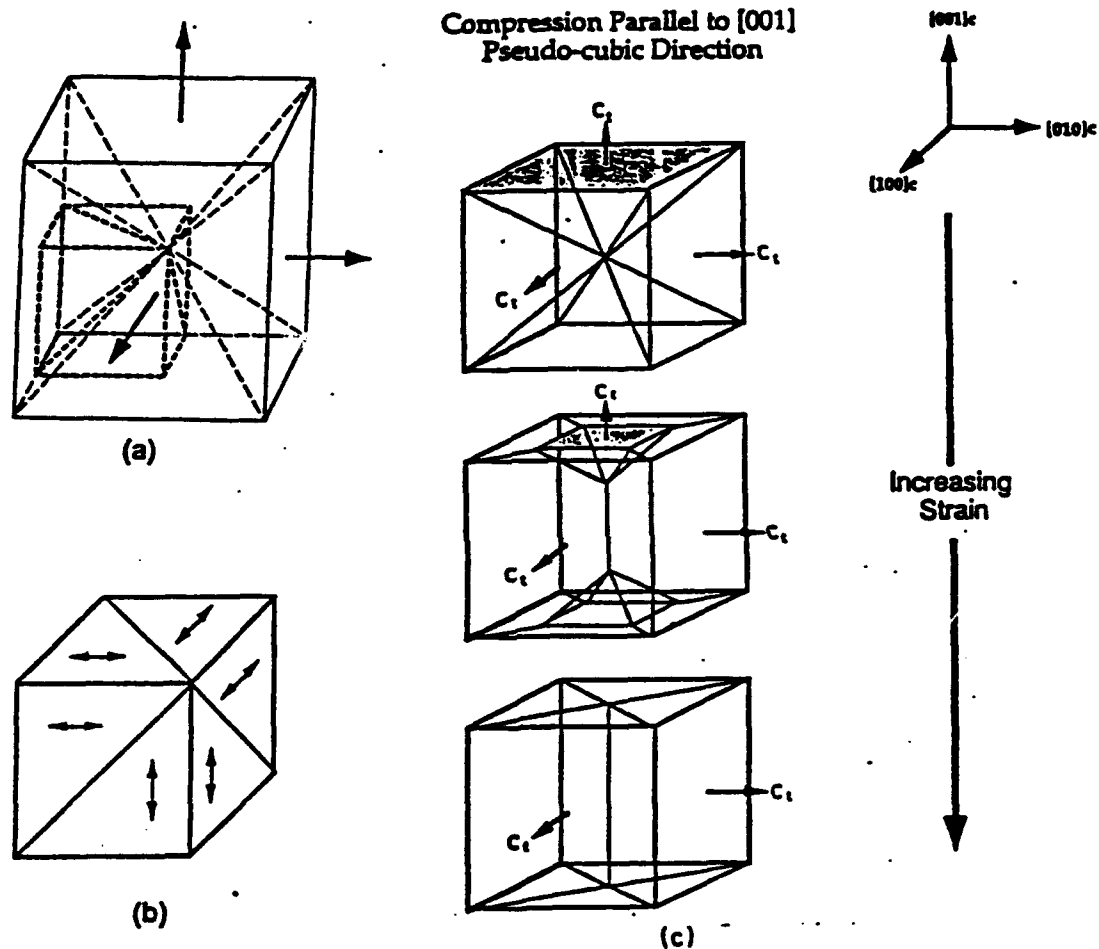


Figure 5. (a) A basic cell consists of all three tetragonal twin variants. Different twin variants are separated by  $(101)$  or  $(011)$  planes. (b) This is a sub-cell of the basic cell outlined in (a). Arrows indicate the directions of  $c$ -axes. (c) Schematic Drawings showing how a three-variant basic cell reduced to two variants under a uniaxial compression. Shaded area indicates the region with tetragonal  $c$ -axis parallel to the loading axis.

Since only two twin variants with their  $c$  axes lying on the same plane are possible on each  $(100)$  section, there are a total of six possible sets of twin planes. A  $(100)$  section of a regular unpoled polydomain sample will contain  $\{011\}$  twin traces as well as the intersecting traces from twins in the other two orientations. The second type of traces is expected to be in the  $\langle 100 \rangle$  directions of the polydomain crystals and they interpenetrate each others. This is believed to be the interpenetrated "colony" structure observed on a chemically etched  $(100)$  section. When an unpoled sample is subjected to uniaxial compression, only twin planes parallel to the loading axis survive. Hence, only intersecting traces parallel to the direction of compressive loading will be observed, as shown in Figure 2(b).

Indentation experiments on mechanically compressed samples are also consistent with the hypothesis of ferroelastic domain switching. Application of a compressive stress (mechanical poling) led to domain realignment. During poling, the *c* axes of several of the domains were oriented perpendicular to the loading axis; consistent with one diminishing {112} variant observed in TEM (Figure 3(b)). The *c*-axes of the remnant two domain variants are now orthogonal to the loading direction (Figure 5(c)). During indentation fracture, domains with *c*-axes parallel to the crack surface are expected to switch so that the domains in the crack tip region orient orthogonal to the crack surface. This process is expected to absorb energy and increase the fracture toughness. In contrast, domains that are already orthogonal to the crack surface should remain unchanged; thus, no toughness increase is expected. Through compressive loading, a large number of domains have their *c*-axes aligned orthogonal to the loading direction. Crack propagation is then expected to be easier along the loading axis, as observed in Figure 4.

## CONCLUSIONS

Ferroelastic domain switching in  $t'$ -ZrO<sub>2</sub> was successfully observed through TEM dark field imaging technique using (112)<sub>1</sub> diffraction spots in a [111] zone. For a uniaxially compressed specimen, two of the three ferroelastic twin variants were found to grow in size while the third set diminished. Indentation experiments on mechanically compressed specimens showed an anisotropy in crack length. Cracks propagated more easily along the loading direction. Evidences suggest that domain reorientation may occur around the fracture surface. Since domain reorientation is an energy absorbing process, their occurrence around the crack surface may absorb work from the loading system and therefore enhance the fracture toughness of the material.

## ACKNOWLEDGEMENTS

This work was sponsored by DARPA through AFOSR Contract No. F49620-89-C-0054. The authors also thank Professor A. G. Evans for valuable discussions.

## REFERENCES

1. D. Michel, L. Mazerolles, and M. Perez y Jorba, in Science and Technology of Zirconia II, edited by N. Claussen, M. Rühle and A. H. Heuer (Advances in Ceramics, Vol. 12, American Ceramic Society, Columbus, OH, 1984), pp. 131-138
2. V. K. Wadhawan, Phase Transitions, 3, 3-103, (1982).
3. A. V. Virkar and R. L. K. Matsumoto, in Science and Technology of Zirconia III, edited by S. Somiya, N. Yamamoto, and H. Yanagida (Advances in Ceramics, Vol. 24, part A, American Ceramic Society, Columbus, OH, 1988), pp. 653-662
4. G. V. Srinivasan, J. F. Jue, S. Y. Kuo and A. V. Virkar, J. Am. Ceram. Soc., 72[11], 2098-2103, (1989).
5. K. Mehta and A. V. Virkar, J. Am. Ceram. Soc., 73[3], 567-574, (1990).
6. V. Lanteri, A. H. Heuer, and T. E. Mitchell, in Science and Technology of Zirconia II, edited by N. Claussen, M. Rühle and A. H. Heuer (Advances in Ceramics, Vol. 12, American Ceramic Society, Columbus, OH, 1984), pp. 118-130
7. A. H. Heuer, V. Lanteri, and A. Dominguez-Rodriguez, Acta Metall., 32 [2], 559-567, (1989).
8. M. V. Klassen-Neklyudova, Mechanical Twinning of Crystals, Consultants Bureau, New York, (1964).
9. R. P. Ingel and D. Lewis III, J. Am. Ceram. Soc., 69[4], 325-332, (1986).

# Ferroelastic Domain Switching in Tetragonal Zirconia Single Crystals—Microstructural Aspects

Chin-Jong Chan,\*<sup>†</sup> Fred F. Lange,\* and Manfred Rühle\*<sup>‡</sup>

Materials Department, University of California, Santa Barbara, California 93106

Jan-Fong Jue\* and Anil V. Virkar\*

Department of Materials Science and Engineering, University of Utah, Salt Lake City, Utah 84112

Ferroelastic domain switching is one of the possible toughening mechanisms in ceramic materials. Microstructural evidence of domain reorientation (switching) in polydomain tetragonal zirconia single crystals is observed upon the application of a unidirectional compressive stress at 1000° and 1400°C. Dark-field imaging of the three {112} tetragonal twin variants in a [111] zone indicates that two sets of twin variants grow at the expense of the third set upon application of uniaxial compression. The diminishing variant is the one with its *c* axis parallel to the compression axis. Inducing cracks into polydomain tetragonal zirconia single crystals provides further evidence of domain reorientation near the crack surface. It is noted again that two sets of twin variants grow at the expense of the third set. A construction for the orientation relationship of domains and their twin boundaries is presented, and a relation between shear stress and reorientation is proposed. [Key words: ferroelastic materials, domains, zirconia, switching, twinning.]

## I. Introduction

TRANSFORMATION toughening has been established as the dominant toughening mechanism in many zirconia-based ceramic materials.<sup>1,2</sup> However, this phenomenon appears not to fully account for all of the toughening observed in some zirconia materials. For example, Ingel *et al.*<sup>3,4</sup> observed that partially stabilized zirconia single crystals doped with 3.4 mol% yttria exhibited twice the strength and fracture toughness of fully stabilized crystals (with 12 mol% yttria) at 1100°C. Normally, the stress-induced tetragonal-to-monoclinic transformation is expected to decrease with increasing temperature and disappear altogether above ~900°C.<sup>2</sup> Specifically, at a temperature >900°C, tetragonal zirconia is the stable phase for the composition tested. Hence, transformation toughening cannot adequately explain the high toughness observed at temperatures >900°C as seen by Ingel *et al.* Furthermore, Michel *et al.*<sup>5,6</sup> also found that the fracture toughness of tetragonal (3 mol% Y<sub>2</sub>O<sub>3</sub>) and cubic (9 mol% Y<sub>2</sub>O<sub>3</sub>) single crystals were ~6 and ~1.8 MPa·m<sup>1/2</sup>, respectively; yet, X-ray diffraction of the fracture surfaces failed to reveal the existence of the stress-induced monoclinic phase.

As a result of Ingel *et al.* and Michel *et al.* observations, there is possibly another mechanism contributing to the

toughening in zirconia materials. Virkar and Matsumoto<sup>7,8</sup> suggested that stress-induced reorientation (switching) of ferroelastic domains in tetragonal zirconia is responsible for the increase of fracture toughness. They observed an increase in the (002) peak intensity and a simultaneous decrease in the (200) peak intensity after surface grinding on ceria-stabilized tetragonal zirconia (Ce-TZP) ceramics. The development of crystallographic texture was attributed to the switching of ferroelastic domains by the externally applied stress. They proposed that domain reorientation near the stress field of the crack tip provides a requisite energy absorption mechanism for enhancement of fracture toughness. This mechanism differs from stress-induced transformation toughening in that there is no change in crystal structure, but only reorientation of twin variants within the process zone. Lankford *et al.*<sup>9</sup> observed a two-stage yielding in the stress-strain behavior of 2.8-mol%-Y<sub>2</sub>O<sub>3</sub>-stabilized zirconia single crystals when the crystals were oriented along (100) and tested at 23° and 700°C. An instantaneous yielding with a plastic strain of 0.0049 was observed for both testing temperatures. However, no monoclinic phase was present immediately following this preyielding "step." They indicated that this instantaneous plasticity was caused by possible ferroelastic domain reorientation, as proposed by Virkar and Matsumoto.<sup>7,8</sup>

According to Michel *et al.*,<sup>5</sup> the cubic-to-tetragonal transformation in zirconia is a ferroelastic transition represented by *m3mF4/mmm* using Aizu's notations.<sup>10</sup> Based on group theory considerations, the tetragonal phase is expected to be a ferroelastic phase. There are at least two energetically equivalent orientational states existing in the crystal. In principle, crystal orientation may be induced from one state to the other by applying an appropriate external stress.<sup>11</sup> Therefore, the development of texture upon grinding is consistent with the existence of ferroelasticity in tetragonal zirconia. Recent work of Srinivasan *et al.*<sup>12</sup> on polydomain tetragonal zirconia single crystals indicated that ferroelastic domains underwent reorientation under compression at temperatures as high as 1400°C. X-ray diffraction from high-temperature fracture surfaces showed that domain reorientation had occurred with no monoclinic phase observed. Work was also done on well-known ferroelectric-ferroelastic materials, such as BaTiO<sub>3</sub> and PZT.<sup>13</sup> It was observed that either an applied electrical field or a compressive stress led to domain switching.

The objective of this research was to establish direct microstructural evidence of ferroelastic domain switching in tetragonal zirconia ceramics upon application of stress. A uniaxial compression test on oriented "polydomain" single crystals was first studied. Efforts were then made on studying the microstructural change near a crack surface on the same type of single crystals. Optical microscopy, scanning electron microscopy (SEM), transmission electron microscopy (TEM), and related microanalytical techniques were used to identify microstructural changes which may have important implications concerning fracture toughness enhancement.

I-W. Chen—contributing editor

Manuscript No. 197411. Received July 27, 1990; approved January 3, 1991. Supported by DARPA through AFOSR Contract No. F49620-89-C-0054.

\*Member, American Ceramic Society.

<sup>†</sup>Now at IBM Thomas J. Watson Research Center, Yorktown Heights, NY 10598.

<sup>‡</sup>Now at Max-Planck-Institut für Metallforschung, Institute für Werkstoffwissenschaft, Stuttgart 1, FRG.

## II. Experimental Procedures

Zirconia single crystals with a nominal composition of 3.0 mol%  $Y_2O_3$  produced by skull melting<sup>2</sup> were used in this investigation. The single crystals were oriented and cut into cubes or bars so that the  $\langle 100 \rangle$  pseudocubic axes were orthogonal to the surfaces. In order to avoid the possible complication from transformation toughening by the tetragonal-to-monoclinic transformation, the  $t'$  phase of tetragonal zirconia single crystals were obtained using the following heat treatment procedures. The oriented samples were heated in a gas-fired furnace to a temperature  $\geq 2100^\circ C$  in air for 10 min, quenched to  $1400^\circ C$ , and subsequently furnace-cooled to room temperature. This heat treatment formed the polydomain  $t'$  phase used in both high-temperature uniaxial compression tests (mechanical poling) and controlled cracking experiments using microindentation at room temperature.

Uniaxial compression is a mechanical analogue of electric poling. Poling in this paper hereby refers to a material subjected to a uniaxial compression. Twinned ferroelastic crystals can be detwinned by applying a uniaxial stress greater than the coercive force.<sup>11</sup> By applying a unidirectional compression (UCP), it is possible to determine whether the domain orientation can be affected by compressive loading. The oriented specimens were subject to compressive loading up to 300 MPa at  $1400^\circ C$  and 700 MPa at  $1000^\circ C$  with a strain rate of  $4.6 \times 10^{-4}$ /s. The compressed sample was then X-rayed and cut into three different crystallographically oriented sections: (111), (100) perpendicular to UCP, and (100) parallel to UCP according to the pseudocubic symmetry. The (100) sections were polished to an optical finish, and indentation experiments were performed. Optical microscopy was used to identify microstructural changes before and after the application of uniaxial compression and microindentation. Selected indented specimens were chemically etched using KOH at  $500^\circ C$  in a nickel crucible for SEM observations. TEM thin foils on (111) sections after UCP were prepared following the standard grinding, dimpling, and ion milling procedures.

The three tetragonal twin variants can be independently imaged by performing dark-field imaging using the  $\{112\}$  type reflections present in a  $[111]$  zone axis selected area diffraction (SAD) pattern.<sup>14</sup> Each variant gives rise to one pair of  $\{112\}$  reflections and corresponds to one of the three possible orientation states of the tetragonal phase. The twin variants are generally referred as ferroelastic domains. Since ferroelasticity is actually a type of mechanical twinning,<sup>15,16</sup> it is thus possible to study the changes of the orientation states upon application of stresses or in the vicinity of a propagating crack by comparing the relative area changes of three  $\{112\}$  tetragonal twin variants.

Samples of (100) and (111) sections of as-heat-treated polydomain  $t'$  materials were also prepared and studied in the same fashion as UCP samples. Microindentations using a Vickers indenter with loads up to 10 kg were used to create radial cracks on a relatively thick ( $\sim 500\text{-}\mu\text{m}$ ) optically finished (111) section. The indent-cracked section was then mechanically dimpled from the indented side so that plastically deformed regions around the indent were removed to ensure no further crack propagation during ion thinning. The specimens were then carefully ion thinned to electron transparency.

## III. Results

### (1) Uniaxial Compression Tests

X-ray diffraction patterns indicated that the diffraction peaks' intensity ratio,  $I(002)/I(200)$ , on the surface parallel to the compression axis increased after a unidirectional compression. This is the first evidence to show that domain reori-

entation occurred during compression. As shown in Fig. 1, a crystal about 2 mm thick was opaque before the compression test and became optically transparent after the test. From TEM observations, the  $\{112\}$  type tetragonal variants (ferroelastic domains) have a size of about  $0.1\ \mu\text{m} \times 0.4\ \mu\text{m}$  before the compression test, as shown in Fig. 2. The twin traces are parallel to the  $\langle 110 \rangle$  direction of pseudocubic symmetry. A high density of antiphase boundaries can be identified.<sup>14,18</sup>

Chemical etching was used to reveal large-scale microstructural changes before and after the specimens were subjected to uniaxial compressive loading. Before UCP, an interpenetrated columnar structure with its longitudinal axes parallel to pseudocubic  $\langle 100 \rangle$  direction was observed, as shown in Fig. 3(A). The width of each column is about  $1\ \mu\text{m}$ . Each columnar structure contains traces of the  $\{101\}$  twins. After UCP the width of the columns coarsened to  $2\text{--}3\ \mu\text{m}$  in the direction parallel to mechanical loading, as shown in Fig. 3(B). The columnar boundaries disappeared in the transverse direction.

TEM dark-field imaging of  $\{112\}$  type reflections on  $\bar{B} = [111]$  before UCP revealed that each of the three  $\{112\}$  tetragonal variants have about same area or intensity as shown in Fig. 2. Using the same imaging conditions on the specimens after high-temperature uniaxial compression, one of the  $\{112\}$  twin variants was clearly diminished, as shown in Fig. 4. After accounting for image rotation in the transmission microscope, the diminishing variant was found to be the one with its  $c$  axis closest to the loading axis. Concurrently, the other two  $\{112\}$  tetragonal variants increased in size at the expense of the diminishing variant. Generally, one of the two remaining variants has higher intensity (greater volume) than the other.

### (2) Controlled Fracture by Indentation

Indentation experiments were done on both the mechanically poled (uniaxially compressed) and unpoled specimens. Symmetric traces of shear bands were observed adjacent to the indent, together with radial cracks emanating from each corner of the indent on both poled and unpoled samples. Traces of shear bands around the Vickers indent were observed to be  $17^\circ$  away from  $\langle 100 \rangle$  on (100) sections and  $11^\circ$  away from  $\langle 110 \rangle$  on (111) sections. Trace analysis indicated that the shear plane is on  $\{4\ 13\ 14\}$ . As shown in Fig. 5, each shear band was found to be nearly a single tetragonal variant.

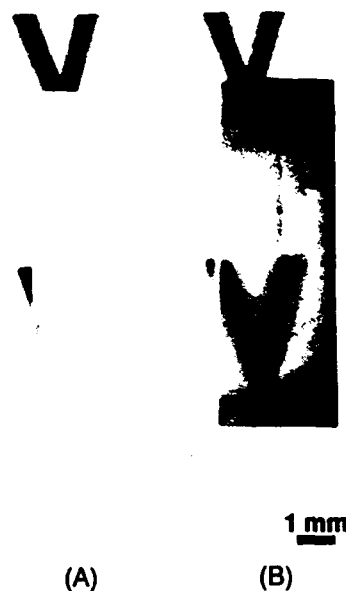


Fig. 1. Optical photograph of  $t'$ - $ZrO_2$  samples subjected to high-temperature compression testing along  $[001]$ : (A) Before test, the sample appeared to be opaque. (B) It became more transparent after the test.

<sup>2</sup>Ceres Corp., N. Billerica, MA.

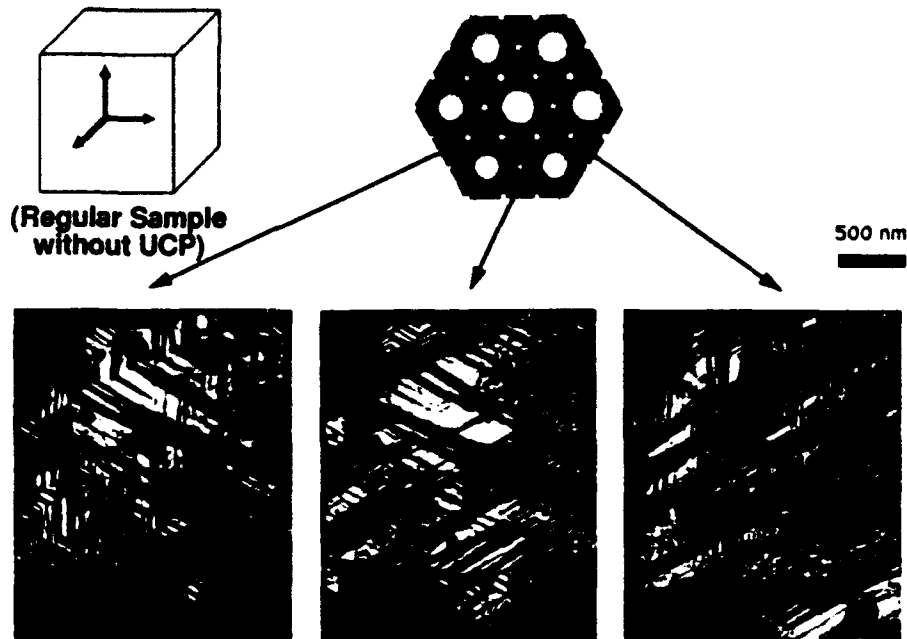


Fig. 2. TEM/DF micrograph of three  $\{112\}$  tetragonal twin variants in a  $[111]$  zone axis of an as-heat-treated  $t'$  material.

SADP along the  $[111]$  zone axis within each slip band also showed only one  $(112)$ , diffraction spot present.

Indentations on the  $(100)$  section along the loading direction of the poled specimens revealed that the crack length was longer in the compression direction relative to the orthogonal direction, as shown in Fig. 6. In addition, under transmitted polarized light, some traces parallel to the direction of the ferroelastic twin variants' boundary were observed ahead of the crack. For the  $(100)$  section orthogonal to the loading direction, a higher load was required to initiate radial cracks.

Indentations on the  $(100)$  section of unpoled specimens indicated no anisotropy in fracture behavior. Dark-field imaging around the crack surface using  $(112)$ , type diffraction spots revealed the following two phenomena for the unpoled specimen: First, one of the  $\{112\}$  tetragonal twin variants almost disappeared. The width of the twins decreased and became needle shaped. Second, large "columnlike" plates consisting of many twins with identical orientation were separated by small diminishing needle-shaped twins, as shown in Fig. 7. Areas far from the crack surface had a microstructure similar to the bulk; i.e., the three variants had similar volume fractions.

#### IV. Discussion

Microstructural observations revealed that  $t'$ - $ZrO_2$  specimens are heavily twinned. The trace of twin planes is parallel to  $\langle 110 \rangle$  on the  $(100)$  section of the polydomain tetragonal single crystals. As shown in Fig. 8, when a basic cell composed of three tetragonal variants is constructed, the  $c$  axes of each tetragonal variant must be separated by a  $90^\circ$  twin boundary and must lie on the same  $(100)$  plane. Hence, only  $\{101\}$ , and  $\{011\}$ , twin planes are allowed, because of required symmetry operation considerations.

The possibility of detwinning the twinned ferroelastic crystals by applying a uniaxial stress greater than the coercive force has been suggested.<sup>12</sup> From TEM observations, the  $(112)$ , ferroelastic twin variants have a size of about  $0.1 \mu\text{m} \times 0.4 \mu\text{m}$  (Fig. 2) before uniaxial compression. Since this twin size is close to the wavelength of visible light, light scattering can be significant. The light scattering is consistent with the observation of unpoled  $t'$ - $ZrO_2$  being opaque, as shown in Fig. 1. After high-temperature uniaxial compression, two of the three twin variants grew at the expense of the third. As shown in Fig. 4, the new twin size of the two growing vari-

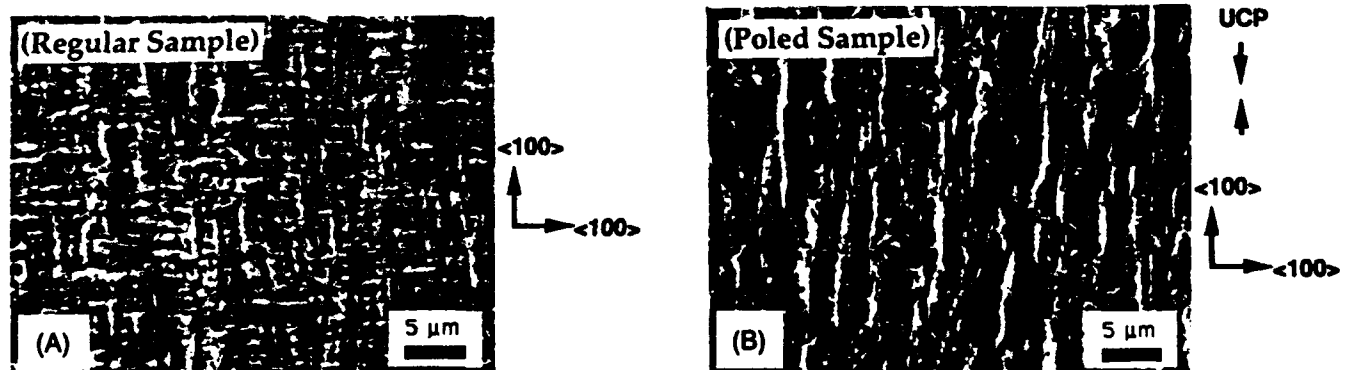


Fig. 3. SEM micrograph of (A)  $(100)$  section of as-heat-treated  $t'$  material, (B)  $(100)$  section, parallel to the loading direction, of  $t'$  material after high-temperature compression test. Both samples were chemically etched using KOH at  $500^\circ\text{C}$  for 5 min in a nickel crucible.

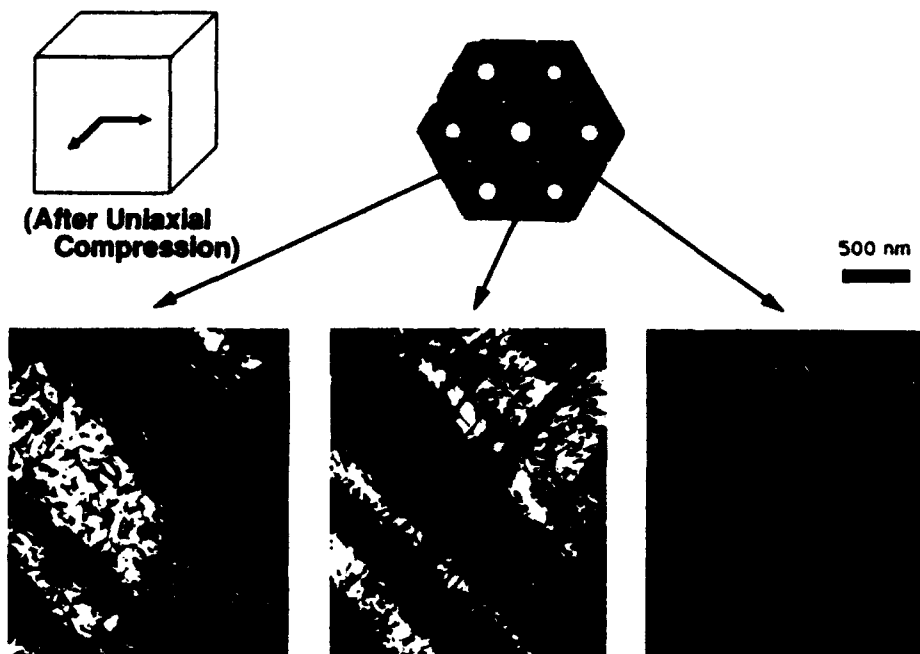


Fig. 4. TEM/DF micrograph of three  $\{112\}$  tetragonal twin variants in a  $[111]$  zone axis of a  $t'$  material after application of a uniaxial compression at high temperature.

ants is about  $0.5 \mu\text{m} \times 2.0 \mu\text{m}$ , whereas the third diminishing variant has a size of  $0.015 \mu\text{m} \times 0.1 \mu\text{m}$ . The twin variants grew either larger or smaller than the wavelength of visible light, and therefore the specimen became more transparent, as shown in Fig. 1.

Theoretically, the diffraction pattern along  $[111]$  of a single variant tetragonal zirconia crystal will contain only one pair of  $(112)_h$  diffractions in the direction of the  $c$  axis. However, a regular unpoled sample is composed of all three of the tetragonal twin variants. Hence, its selected area diffraction pattern along  $[111]$  is the combination of three different single vari-

ants  $120^\circ$  apart from each other, as observed in Fig. 2. According to electron microscopy observations, uniaxial compression causes the intensity of one of  $(112)_h$  twin variants to diminish. This diminishing variant was the one with its  $c$  axis parallel to the loading axis. It is apparent that tetragonal variants with their  $c$  axes in the compression direction will try to reorient perpendicular to the loading axis when subjected to a compressive loading. Thus, the intensity of the  $(112)_h$  diffractions along the compression axis is diminished.

While applying uniaxial compression, maximum shear stresses occur at  $45^\circ$  to the loading axis; i.e., planes of maxi-

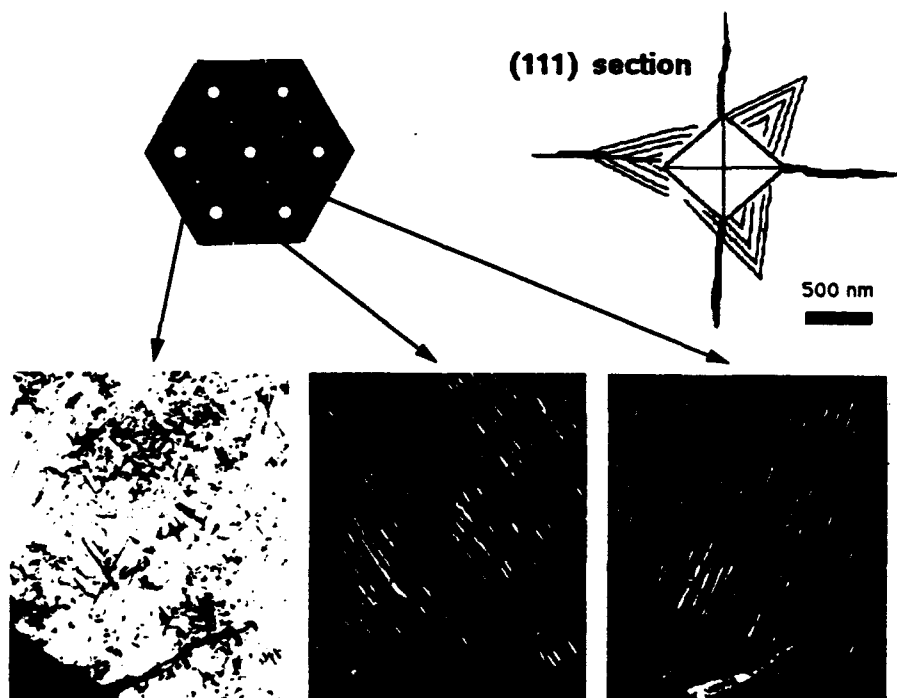


Fig. 5. TEM/DF micrograph of three  $\{112\}$  tetragonal twin variants in a  $[111]$  zone axis within a shear band near an indent on an as-heat-treated  $t'$  material.

UCP  
direction



(A)

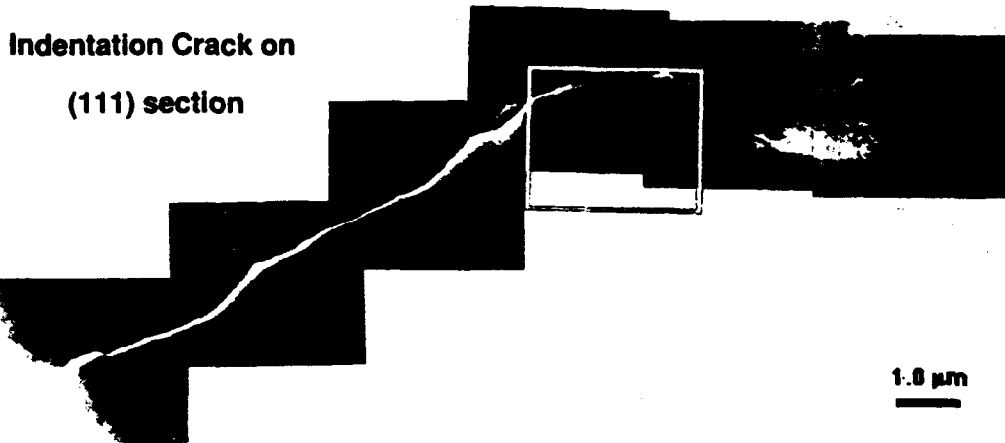


(B)

40  $\mu$ m



Fig. 6. Optical micrograph of a Vickers indent on a poled sample: (A) reflected light, (B) transmitted polarized light. The applied load was 3 kg.

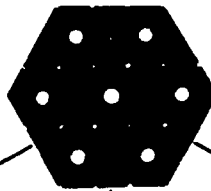


(A)

1.0  $\mu$ m



(Indentation Crack  
on (111) TEM Section)



500 nm



Fig. 7. (A) TEM montage micrographs of a crack on (111) section of as-heat-treated  $t'$  material. Boxed area is the area for (112), DF imaging in (B). (B) TEM/DF micrograph of three {112} tetragonal twin variants in a [111] zone axis near a crack surface.

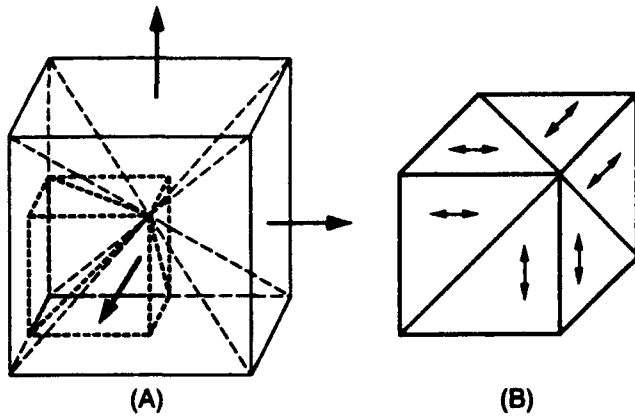


Fig. 8. (A) A basic cell consists of all three tetragonal twin variants. Different twin variants are separated by  $\{101\}$  or  $\{011\}$  planes. (B) This is a sub-cell of the basic cell outlined in (A). Arrows indicate the directions of  $c$  axes.

imum shear stresses are parallel to  $\{101\}$ , twin planes. Growth of two of the three tetragonal variants is favored because of the lateral shear stresses produced by compression. This, in turn, results in the diminishing of the third tetragonal variant. Figure 9 illustrates evolution of a two-variant single crystal from an unpoled three-variant single crystal under a uniaxial compression (biaxial shear). The maximum uniaxial strain resulting from the ferroelastic domain reorientation is about 0.5% (i.e.,  $(1/3)(1 - c_t/a_t)$ ) for a  $ZrO_2$ -3 mol%  $Y_2O_3$  single crystal.<sup>16</sup> The value of this predicted ferroelastic strain matches the instantaneous strain observed by Lankford *et al.*<sup>9</sup>

#### Compression Parallel to $[001]$ Pseudo-cubic Direction

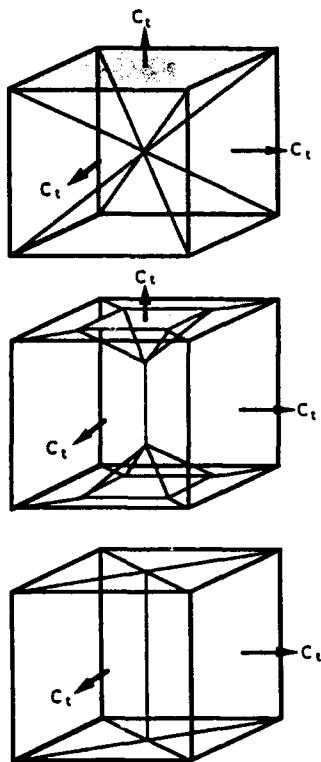


Fig. 9. Schematic drawings showing how a three-variant basic cell reduced to two variants under a uniaxial compression. Shaded area indicates the region with tetragonal  $c$  axis parallel to the loading axis.

It is also possible to predict ferroelastic strains by determining the ratio of the intensity (or area) of the diminishing variant to the other two variants. Furthermore, a biaxial compression (uniaxial tension) will result in the formation of a single variant tetragonal phase, as shown in Fig. 10. This resembles the condition within a shear band, as shown in Fig. 5.

Since only two twin variants with their  $c$  axes lying on the same plane are possible on each  $\{100\}$  section, there are a total of six possible sets of twin planes. A  $\{100\}$  section of a regular unpoled polydomain sample will contain  $\{101\}$  twin traces as well as the traces from intersections of twins in the other two orientations. The second type of traces is expected to be in the  $\{100\}$  directions of the polydomain crystals and they interpenetrate each other. It is believed that this is the interpenetrated "columnar" structure observed on a chemically etched  $\{100\}$  section. When an unpoled sample is subjected to uniaxial compression, the twin planes in the transverse directions will eventually disappear. Hence, only traces parallel to the direction of compressive loading will be observed, as shown in Fig. 3(B).

Indentation experiments on mechanically compressed samples are also consistent with the hypothesis of ferroelastic domain switching. Application of a compressive stress (mechanical poling) led to domain realignment. During poling, the  $c$  axes of several of the domains were oriented perpendicular to the loading axis, consistent with one diminishing  $\{112\}$  variant observed in TEM (Fig. 4). The  $c$  axes of the remanent two domain variants are now orthogonal to the loading direction (Fig. 9). During indentation fracture, domains with  $c$  axes parallel to the crack surface are expected to switch so that the domains in the crack tip region orient orthogonal to the crack surface. This process is expected to absorb energy

#### Compression Parallel to $[010]$ and $[001]$ Pseudo-cubic Direction

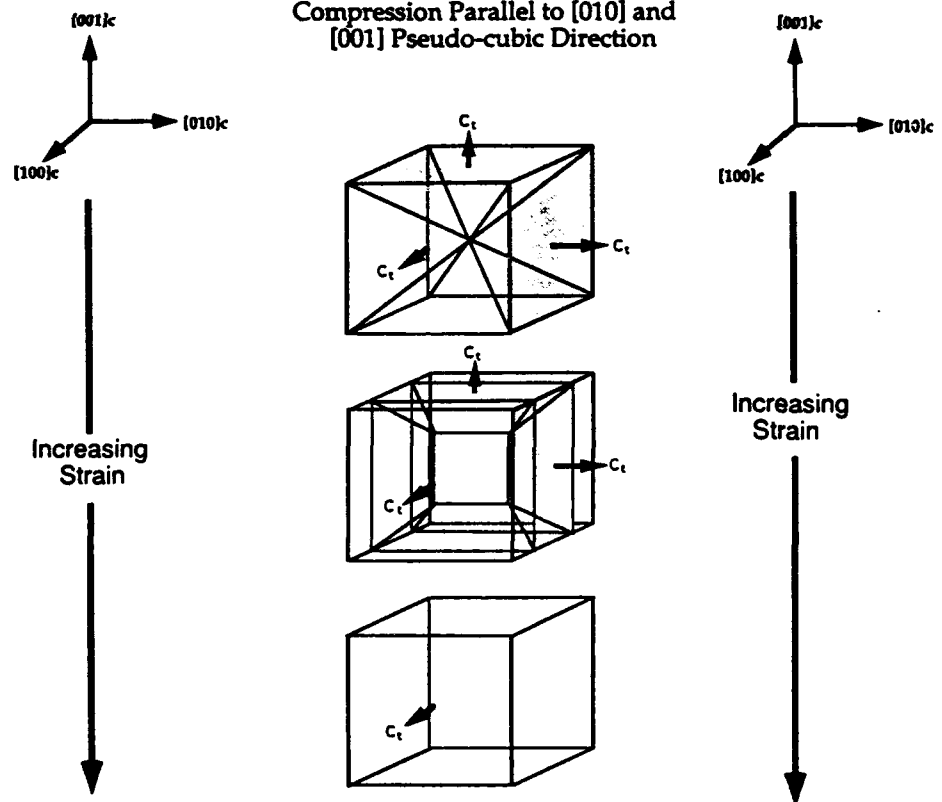


Fig. 10. Schematic drawings showing how a three-variant basic cell reduced to a single variant within a shear band. The stress state within a shear band can be decomposed into a superposition of a tension and a compression in the transverse direction. Shaded area indicates the region with tetragonal  $c$  axis parallel to the loading axis.

and increase the fracture toughness. In contrast, domains that are already orthogonal to the crack surface should remain unchanged; thus, no toughness increase is expected. Through compressive loading, a large number of domains have their  $c$  axes aligned orthogonal to the loading direction. Crack propagation is then easier along the loading axis, as observed in Fig. 5.

As stated previously, variants with their  $c$  axes parallel to the crack surface are expected to switch so that the twin variant in the crack tip region orients orthogonal to the crack surface during fracture. If the stress field around a crack tip were considered under plane strain condition, the area near a crack tip is subjected to an in-plane biaxial tension. This is similar to applying a uniaxial compression in the out-of-plane direction. Transmission electron microscopy observations did indeed reveal the diminishing of one of the three tetragonal twin variants, as shown in Fig. 7. However, the stress state near a crack tip is complicated. A more rigorous analysis is needed to fully explain these results.

### V. Conclusions

Ferroelastic domain switching was successfully observed through TEM dark-field imaging technique using (112), diffraction spots in a [111] zone. For a high-temperature uniaxially compressed specimen, two of the three ferroelastic twin variants grew in size while the third set diminished. Indentation experiments on mechanically compressed specimens showed an anisotropy in crack length. Cracks propagated more easily along the loading direction of poled samples. Dark-field imaging of (112), reflections around the crack surface revealed microstructural changes as in the uniaxial compressed specimens. These observations clearly indicated that domain reorientation occurred around the fracture surface. Since domain reorientation is an energy-absorbing process, their occurrence around the crack surface may absorb work from the loading system and therefore enhance the fracture toughness of the material.

**Acknowledgment:** The authors thank Professor A. G. Evans for valuable discussions.

### References

- <sup>1</sup>A. G. Evans and R. M. Cannon, "Toughening of Brittle Solids by Martensitic Transformations," *Acta Metall.*, **34** [5] 761–800 (1986).
- <sup>2</sup>F. F. Lange, "Transformation Toughening: Part 5: Effect of Temperature and Alloy on Fracture Toughness," *J. Mater. Sci.*, **17**, 255–62 (1982).
- <sup>3</sup>R. P. Ingel, D. Lewis, B. A. Bender, and R. W. Rice, "Physical, Microstructural, and Thermomechanical Properties of ZrO<sub>2</sub> Single Crystals"; pp. 408–14 in *Advances in Ceramics*, Vol. 12, *Science and Technology of Zirconia II*. Edited by N. Claussen, M. Rühle, and A. H. Heuer. American Ceramic Society, Columbus, OH, 1984.
- <sup>4</sup>R. P. Ingel, D. Lewis, B. A. Bender, and R. W. Rice, "Temperature Dependence of Strength and Fracture Toughness of ZrO<sub>2</sub> Single Crystals," *J. Am. Ceram. Soc.*, **65** [9] C-150–C-152 (1982).
- <sup>5</sup>D. Michel, L. Mazerolles, and M. Perez y Jorba, "Fracture of Metastable Tetragonal Zirconia Crystals," *J. Mater. Sci.*, **18**, 2618–28 (1983).
- <sup>6</sup>D. Michel, L. Mazerolles, and M. Perez y Jorba, "Polydomain Crystals of Single Phase Tetragonal ZrO<sub>2</sub>: Structure, Microstructure and Fracture Toughness"; pp. 131–38 in *Advances in Ceramics*, Vol. 12, *Science and Technology of Zirconia II*. Edited by N. Claussen, M. Rühle, and A. H. Heuer. American Ceramic Society, Columbus, OH, 1984.
- <sup>7</sup>A. V. Virkar and R. L. K. Matsumoto, "Ferroelastic Domain Switching as a Toughening Mechanism in Tetragonal Zirconia," *J. Am. Ceram. Soc.*, **69** [10] C-224–C-226 (1986).
- <sup>8</sup>A. V. Virkar and R. L. K. Matsumoto, "Toughening Mechanism in Tetragonal Zirconia Polycrystalline (TZP) Ceramics"; pp. 653–62 in *Advances in Ceramics*, Vol. 24, *Science and Technology of Zirconia III*. Edited by S. Somiya, N. Yamamoto, and H. Yanagida. American Ceramic Society, Westerville, OH, 1988.
- <sup>9</sup>J. Lankford, R. A. Page, and L. Rabenberg, "Deformation Mechanisms in Yttria-Stabilized Zirconia," *J. Mater. Sci.*, **23**, 4144–56 (1988).
- <sup>10</sup>K. Aizu, "Possible Species of Ferromagnetic, Ferroelectric, and Ferroelastic Crystals," *Phys. Rev. B*, **2** [3] 754–72 (1970).
- <sup>11</sup>V. K. Wadhawan, "Ferroelasticity and Related Properties of Crystals," *Phase Transitions*, **3**, 3–103 (1982).
- <sup>12</sup>G. V. Srinivasan, J. F. Jue, S. Y. Kuo and A. V. Virkar, "Ferroelastic Domain Switching in Polydomain Tetragonal Zirconia Single Crystals," *J. Am. Ceram. Soc.*, **72** [11] 2098–103 (1989).
- <sup>13</sup>K. Mehta and A. V. Virkar, "Fracture Mechanisms in Ferroelectric-Ferroelastic Lead Zirconate Titanate (Zr:Ti = 0.54:0.46) Ceramics," *J. Am. Ceram. Soc.*, **73** [3] 567–74 (1990).
- <sup>14</sup>V. Lanteri, A. H. Heuer, and T. E. Mitchell, "Tetragonal Phase in the System ZrO<sub>2</sub>-Y<sub>2</sub>O<sub>3</sub>"; pp. 118–30 in *Advances in Ceramics*, Vol. 12, *Science and Technology of Zirconia II*. Edited by N. Claussen, M. Rühle, and A. H. Heuer. American Ceramic Society, Columbus, OH, 1984.
- <sup>15</sup>R. W. Cahn, "Twinned Crystals," *Adv. Phys.*, **3**, 363–445 (1954).
- <sup>16</sup>M. V. Klassen-Neklyudova, *Mechanical Twinning of Crystals*. Consultants Bureau, New York, 1964.
- <sup>17</sup>R. P. Ingel and D. Lewis III, "Lattice Parameters and Density for Y<sub>2</sub>O<sub>3</sub>-Stabilized ZrO<sub>2</sub>," *J. Am. Ceram. Soc.*, **69** [4] 325–32 (1986).
- <sup>18</sup>A. H. Heuer, V. Lanteri, and A. Dominguez-Rodriguez, "High-Temperature Precipitation Hardening of Y<sub>2</sub>O<sub>3</sub> Partially-Stabilized ZrO<sub>2</sub> (Y-PSZ) Single Crystals," *Acta Metall.*, **32** [2] 559–67 (1989). □

# Highly asymmetric electric-field gradients at the Nb sites in ferroelastic $GdNbO_4$ and $NdNbO_4$

Gary L. Catchen

*Department of Nuclear Engineering and Center for Electronic Materials and Processing, The Pennsylvania State University, University Park, Pennsylvania 16802*

Ian D. Williams

*Materials Research Laboratory, The Pennsylvania State University, University Park, Pennsylvania 16802*

David M. Spaar, Stephen J. Wukitch, and James M. Adams

*Department of Nuclear Engineering and Center for Electronic Materials and Processing, The Pennsylvania State University, University Park, Pennsylvania 16802*

(Received 12 June 1990; revised manuscript received 9 July 1990)

Perturbed-angular-correlation (PAC) measurements were performed on two members of the isostructural family of ferroelastic rare-earth niobates,  $GdNbO_4$  and  $NdNbO_4$ . These compounds were prepared as ceramics doped with 0.1 at. % of Hf that carried the  $^{181}\text{Hf} \rightarrow ^{181}\text{Ta}$  PAC probes. Nuclear-electric-quadrupole interactions were measured from 77 K through the ferroelastic-to-paraelastic transition temperatures  $T_c$  (1085 and 1007 K). Both materials exhibited electric-field gradient parameters  $V_{zz}$  and  $\eta$  that changed anomalously with temperature. At lower temperatures the asymmetry parameters  $\eta$  increased with temperature and passed through distinct, unusually high maxima ( $\eta > 0.9$ ). At higher temperatures, the asymmetries decreased until they showed near-axial symmetry slightly above  $T_c$ . The values of  $V_{zz}$  changed slowly and passed through minima at temperatures well below  $T_c$ . Over the temperature range from several hundred degrees below the transition to  $T_c$ , the temperature dependences of  $\eta$  for the two compounds were similar. These temperature dependences indicate that the PAC technique is extremely sensitive to slight changes in the coordination geometry of the Nb site.

Ferroelastic materials, which are the mechanical analogs of ferroelectric materials, have domain structures and exhibit spontaneous strains. These materials are of potential technological importance because the ferroelastic phenomenon may contribute to increasing the fracture toughness of certain types of ceramic materials such as stabilized zirconia.<sup>1</sup> Generally, ferroelasticity is manifest in low-temperature, low-symmetry phases, and these phases undergo either first-order or second-order transitions to high-temperature higher-symmetry paraelastic phases at a temperature  $T_c$ . These transitions are often at least in part displacive, and they usually involve softening of vibrational modes.<sup>2-4</sup> Because the ferroelastic-to-paraelastic transitions are not well understood in terms of chemical effects, we decided to use a technique that is very sensitive to local chemical effects in crystal lattices, namely, perturbed-angular-correlation (PAC) spectroscopy, to study the rare-earth niobates.

The rare-earth niobates have the composition  $LNbO_4$ , in which  $L$  can stand for La, Ce, Pr, . . . , Lu. These compounds have fergusonite structures at temperatures below  $T_c$ , and they have monoclinic symmetry in the space group  $I2/a$ . These compounds have scheelite structures at temperatures above  $T_c$ , and they have tetragonal symmetry in the space group  $I4_1/a$ . Figure 1 presents a diagram of the Nb coordination in the ferroelastic phase. In terms of their cell parameters, these compounds are essentially isostructural.<sup>5</sup> Since the fergusonite structure is centrosymmetric, the associated ferroelasticity is not

accompanied by ferroelectricity. Also, the relative stabilities of the low- and high-temperature phases are sensitive to the sizes of the corresponding rare-earth sites in the monoclinic and in the tetragonal structures.<sup>6,7</sup>

The (zero-external-field) PAC experiment uses the nuclear-electric-quadrupole moments of  $^{181}\text{Hf} \rightarrow ^{181}\text{Ta}$  radioactive probe atoms, which are substituted into specific lattice sites, to measure extranuclear electric-field gradients (efg) at the probe sites. The scope of this initial study includes two members of this rare-earth niobate family,  $GdNbO_4$  and  $NdNbO_4$ . The specific questions addressed are (1) Can the  $^{181}\text{Hf}$  and  $^{181}\text{Ta}$  probe be substituted into the Nb site and can associated effects such as oxygen defects be mitigated? (2) Can well-defined static interactions be measured that yield unique efg parameters? (3) If so, do these parameters give new information about the influence of the rare-earth on the phase transition?

Samples of Hf-doped  $NdNbO_4$  and  $GdNbO_4$  were prepared using a resin-intermediate method.<sup>8</sup> The x-ray powder-diffraction patterns indicated that the radioactive sintered-pellet samples were phase pure.

The PAC measurements were made using a four-CsF-detector apparatus.<sup>9</sup> The perturbation functions  $A_{22}G_{22}(t)$  were derived from eight concurrently measured time distributions (four at  $90^\circ$  and four at  $180^\circ$ ). To analyze the measured perturbation functions, a one-site model for nuclear-electric-quadrupole interactions in a polycrystalline source was used:

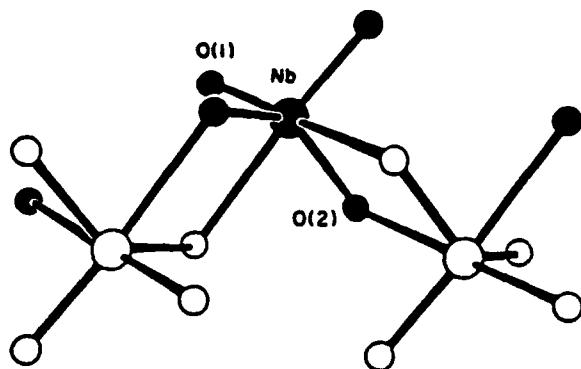


FIG. 1. Structural diagram of the Nb coordination in the low-temperature, monoclinic fergusonite structure. The O(1) ions are three coordinate, and the O(2) ions are four coordinate. The O ions that form the NbO<sub>4</sub> tetrahedra in the paraelastic phase are indicated by the shading.

$$A_{22}G_{22}(t) = A_1 \left[ S_0(\eta) + \sum_{k=1}^3 S_k(\eta) \exp(-\frac{1}{2}\delta\omega_k t) \times \cos(\omega_k t) \right] + A_2. \quad (1)$$

Here,  $A_1$  is the normalization factor,  $\delta$  is the line-shape parameter, and  $A_2$  takes into account the fraction of probe atoms that are not in a well-defined chemical environment. The frequencies  $\omega_k$  and the  $S_i(\eta)$  coefficients describe a static interaction in a polycrystalline source. The free parameters  $\omega_1$ ,  $\omega_2$ ,  $A_1$ ,  $A_2$ , and  $\delta$  were derived from each data set, and the ratio  $\omega_2/\omega_1$  was used to determine the quadrupole frequency  $\omega_Q$  and the asymmetry parameter  $\eta$ .<sup>10</sup> The nonvanishing electric-field gradient (efg) components  $V_{ii}$  in the principal axis system where the probe nucleus is at the origin are related to these parameters by  $\omega_Q = [eQV_{zz}/4I(2I-1)\hbar]$  and  $\eta = (V_{xx} - V_{yy})/V_{zz}$ , in which  $Q$  is the nuclear quadrupole moment (2.51 b) and  $I$  is the nuclear spin ( $\frac{5}{2}$ ).

Figure 2 presents the perturbation functions measured on a 0.1 at. % Hf-doped GdNbO<sub>4</sub> ceramic sample and the fitted curves. On a NdNbO<sub>4</sub> sample, we obtained qualitatively similar data and fitted curves in which the efg parameters had a somewhat different temperature dependence. Figure 3 summarizes the derived parameters  $V_{zz}$ ,  $\eta$ ,  $\delta$ , and  $f_1$  for both compounds. These parameter values indicate that primarily a single static interaction occurred in a well-defined chemical environment.

Crystal chemical considerations such as the similarity in ionic radii between Hf<sup>4+</sup> and Nb<sup>5+</sup> ions suggest strongly that the <sup>181</sup>Hf and <sup>181</sup>Ta probe substituted into the Nb sites in GdNbO<sub>4</sub> and NdNbO<sub>4</sub>. We performed some similar measurements on samples of GdNbO<sub>4</sub>, NdNbO<sub>4</sub>, and several other rare-earth niobates, in which the Hf concentrations were approximately 1 at. %. Using Eq. (1), we could not obtain satisfactory fits to the laboratory-temperature perturbation functions. A two-site version provided better fits but the derived frequencies were not unique. Thus reducing the probe concentration from approximately 1 to 0.1 at. % diminished the

effects of multiple interactions so that the analysis of the measured perturbation functions yielded unambiguous parameters. Reducing the probe concentration also reduced the concentration of oxygen vacancies that the Hf substitution caused. As Fig. 3 shows, the site-occupancy fraction  $f_1$  increased with temperature. Some of the oxygen vacancies could have been trapped near Hf<sup>4+</sup> ions at low temperatures; and at higher temperatures, the vacancies could have randomized. This scenario is consistent with the oxygen vacancies having caused the multiple interactions, whereas the other possibility, namely, that a significant fraction of the probes substituted into the rare-earth sites, is not consistent with the observed increase in  $f_1$  with temperature.

At low temperatures, the asymmetry parameter is large, which is consistent with the low symmetry of the Nb site in the monoclinic structure, and it increases with temperature from 77 K until it passes through a maximum. Then the asymmetry parameter decreases as the transition temperature is approached. Above  $T_c$ ,  $\eta \approx 0$ , which is consistent with the fourfold rotational symmetry of the tetragonal structure. These features confirm the probe substitution into the Nb sites. The values of the line-shape parameter  $\delta$  remain relatively small and essentially constant over the entire temperature range. These results indicate that the frequencies that correspond to the large values of the asymmetry parameters,  $\eta \approx 1$ , are unique. The 695- and 540-K perturbation functions show asymmetry values that are close to unity. These functions show marked attenuation with time; whereas, the lower- $\eta$  functions show much less attenuation. The attenuation associated with the large- $\eta$  perturbation functions results because  $\omega_1$  is very close to  $\omega_2$  in magnitude.

The temperature dependences of the efg's at the Nb sites in GdNbO<sub>4</sub> and NdNbO<sub>4</sub> are anomalous, because the largest efg component  $V_{zz}$  goes through a minimum at a temperature that is several hundred degrees below  $T_c$ . Similarly, the temperature dependence of the asymmetry parameter  $\eta$  is anomalous because it goes through a maximum at a temperature well below  $T_c$ . In the case of GdNbO<sub>4</sub>, the minimum in  $V_{zz}$  occurs in the same temperature region as the maximum occurs in  $\eta$ , whereas in the case of NdNbO<sub>4</sub>, the minimum on  $V_{zz}$  occurs at a higher temperature. Both of these compounds undergo reconstructive second-order phase transitions. The Nb coordination changes from six-coordinate distorted octahedra in the monoclinic phase to four-coordinate distorted tetrahedra in the tetragonal phase.<sup>11</sup> In addition the values of  $V_{zz}$  are approximately the same for both phases at temperatures close to  $T_c$ .

In the case of the PAC studies on nonstabilized zirconia, the efg parameters  $V_{zz}$  and  $\eta$  exhibit the conventional temperature dependence<sup>12</sup> through a range that includes the monoclinic-to-tetragonal martensitic transition.<sup>13</sup> Here  $V_{zz}$  slowly decreases as temperature increases and  $\eta$  correspondingly increases slowly until a discontinuity occurs at the transition temperature,<sup>14</sup> which is expected for a first-order transition.

Generally PAC measurements on solids provide information about the local probe environments. Sometime

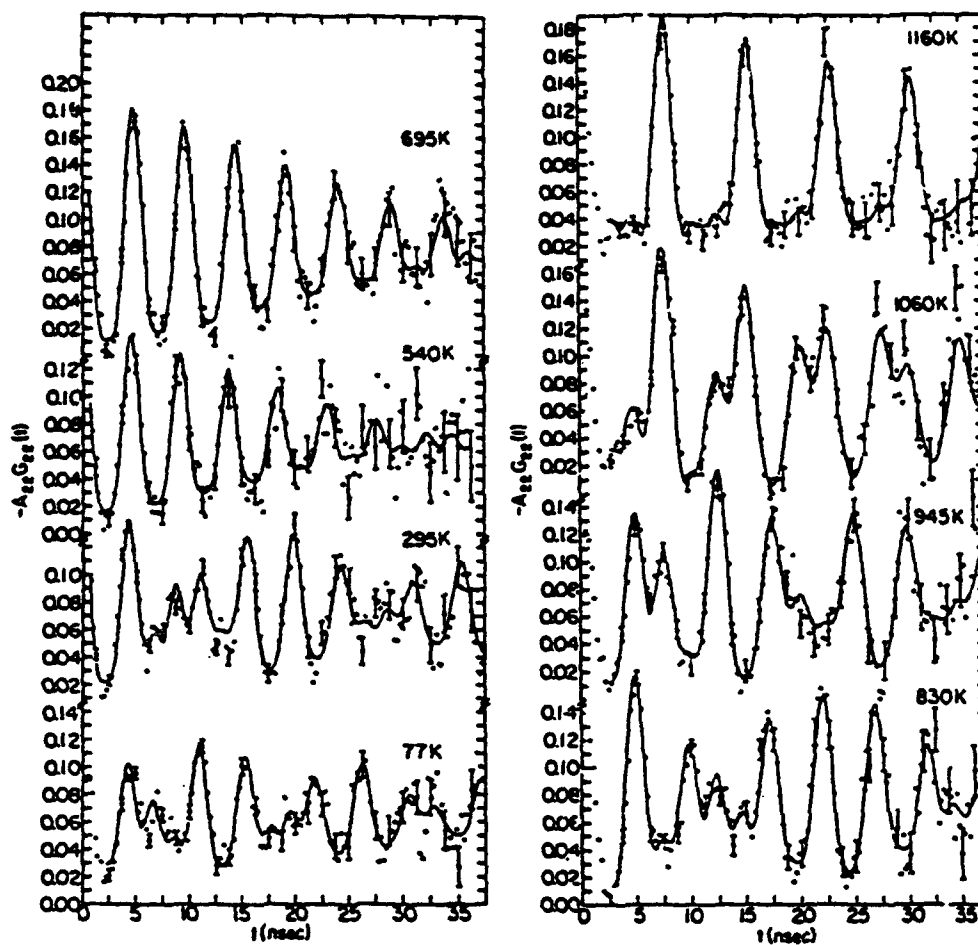


FIG. 2. Perturbation functions for a  $\text{GdNbO}_4$  ceramic sample that was measured at the indicated temperatures. The solid lines represent fits of Eq. (1) to the data. The 77- and 295-K perturbation functions show qualitatively more deviations from the fitted curves than the higher-temperature functions show. We attribute these additional interactions to the effects of oxygen vacancies that resulted from the substitution of tetravalent  $\text{Hf}^{4+}$  ions for pentavalent  $\text{Nb}^{5+}$  ions.

but not always this information correlates with the effects of long-range structural phase transitions. Specifically the PAC measurements on  $\text{GdNbO}_4$  and  $\text{NdNbO}_4$  provide information about the local rearrangement of metal-oxygen bonds. Since the ferroelastic-to-paraelastic phase transition involves breaking two of the six Nb—O bonds, we explore the possibility that the local interactions measured by PAC correlate with the phase-transition phenomenon. Since the asymmetry parameter exhibits maxima at temperatures well below  $T_c$ , we discuss the high-temperature and low-temperature regimes separately.

For these two compounds,  $T_c$  differs by only about 80 K. In Fig. 3, the three  $\eta$  values measured below  $T_c$  for  $\text{NdNbO}_4$  would coincide with those values corresponding to  $\text{GdNbO}_4$  if the  $\text{NdNbO}_4$  points were shifted 80 K to higher temperature. Thus the change in  $\eta$  at temperatures above the maximum is essentially the same for both compounds. At temperatures above the asymmetry maxima, the gradual change from almost complete asymmetry  $\eta \approx 1$  to near-axial symmetry  $\eta \approx 0$  over a temperature range of several hundred degrees indicates that the change in Nb—O bonding is not abrupt. Over this particular temperature range, the values of the asymmetry

parameter, which change rapidly, indicate that corresponding major changes in the Nb—O bonding occur. In the monoclinic structure, the Nb ions are coordinated by six O ions that are of two types.<sup>14</sup> Four of the six O ions are four coordinate and are bonded to the central Nb ion, to one other Nb ion, and to two rare-earth ions. Two of the six O ions are three coordinate and are bonded to the central Nb ion and to two rare-earth ions. In the tetragonal structure in which the Nb ions are four coordinate, the four O ions are chemically equivalent and three coordinate. During the phase transition, two Nb O bonds are broken, which Fig. 1 indicates. This change in bonding involves a rearrangement in electronic charge density in the vicinity of the probe ion at the Nb site, and the efg asymmetry is very sensitive to these gradual, subtle changes in the probe-oxygen bonding. Moreover the asymmetry temperature dependence and the associated gradual change in Nb coordination indicate that the phase transition is also a slow, gradual process, which is unlike the aforementioned case of zirconia. This correlation suggests that the asymmetry parameter is strongly coupled to the order parameter for the transition.

The  $\eta$  dependence in the temperature range below the maximum is different for  $\text{GdNbO}_4$  and  $\text{NdNbO}_4$ . The  $\eta$

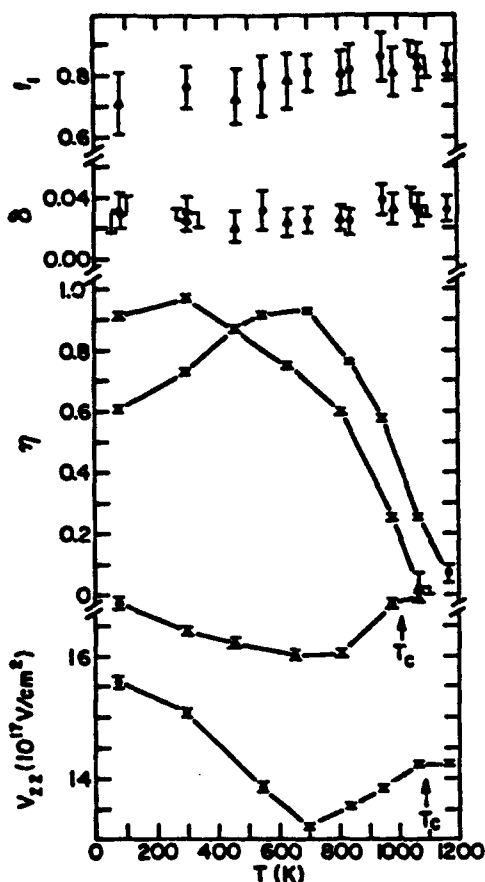


FIG. 3. The electric-field-gradient parameters  $V_{zz}$  and  $\eta$ , the line-shape parameter  $\delta$ , and the primary site-occupancy fraction  $f_1 = A_1/(A_1 + A_2)$ . The circles indicate values for  $\text{GdNbO}_4$  ( $T_c = 1085$  K), and the triangles indicate values for  $\text{NdNbO}_4$  ( $T_c = 1007$  K). The lines are shown to guide the eye.

values for both compounds decrease from their respective maxima, but the decrease toward low temperatures is more rapid in the case of  $\text{GdNbO}_4$ . Overall the  $\eta$  dependences for the two compounds show the same general features. This effect suggests that the same Nb-coordination geometries can be found in the two compounds when  $\text{GdNbO}_4$  is at a higher temperature than  $\text{NdNbO}_4$ .

The laboratory temperature x-ray-diffraction-determined structures of  $\text{GdNbO}_4$  and  $\text{NdNbO}_4$  indicate that the two longer Nb—O bonds are of different length for the two compounds, 2.44 Å for  $\text{GdNbO}_4$  (Ref. 15) and

2.49 Å for  $\text{NdNbO}_4$ ,<sup>11</sup> since the size of the Nd ion is larger than the size of the Gd ion. The larger Nd ion causes the spacing of the corresponding adjacent Nb ions to be further apart in the structure. The associated Nb—O—Nb bridging bond angles and bond lengths are larger. At laboratory temperature, the measured asymmetry parameter for  $\text{NdNbO}_4$  is significantly higher ( $\eta = 0.97$ ) than that for  $\text{GdNbO}_4$  ( $\eta = 0.73$ ), and  $\eta$  for  $\text{NdNbO}_4$  is essentially at its maximum value. As a result, at laboratory temperature, the ions that form the  $\text{NdNbO}_4$  structure are closer to the high-temperature configuration than are the corresponding ions in the  $\text{GdNbO}_4$  structure. The lower transition temperature of  $\text{NdNbO}_4$  arises because the structure is closer to the highly asymmetric, i.e., high- $\eta$ , form at lower temperature than in the case of  $\text{GdNbO}_4$ .

In conclusion, the temperature dependences of  $V_{zz}$  and  $\eta$  for both of the rare-earth niobates are anomalous. The asymmetry-parameter temperature dependences show maxima at temperatures well below  $T_c$ . At temperatures within several hundred degrees of  $T_c$ , the asymmetry parameters change slowly at about the same rate for both compounds. This behavior correlates with the ferroelastic-to-paraelastic transition, and it reflects subtle changes in the local electronic charge density that result in part from differences in chemical bonding between the three-coordinate and the four-coordinate O ions in the probe-ion coordination sphere. At lower temperatures, differences in the measured values of  $V_{zz}$  and  $\eta$  for  $\text{GdNbO}_4$  and  $\text{NdNbO}_4$  result at least in part from differences in the chemical bonding of the O ions that bridge between the rare-earth ions and the probe ions. These bonding differences result from the differences in relative size between the Gd and the Nd ions. Although the analysis of the macroscopic x-ray-diffraction data indicates that  $\text{GdNbO}_4$  and  $\text{NdNbO}_4$  are virtually isostructural, the PAC technique is sensitive to small differences in chemical bonding between the two compounds.

We thank Professor Stewart K. Kurtz for much encouragement, and we thank Professor Robert L. Rasera of the University of Maryland, Baltimore County for many helpful comments and suggestions. We gratefully acknowledge support from the Department of Nuclear Engineering and from the U.S. Defense Advanced Research Projects Agency (DARPA) (Contract No. F49620-89-C-0054).

<sup>1</sup>A. L. Virkar and R. L. Matsumoto, *J. Am. Ceram. Soc.* 69, C224 (1986).

<sup>2</sup>M. Wada *et al.*, *J. Phys. Soc. Jpn.* 47, 1575 (1979).

<sup>3</sup>G. V. Anan'eva *et al.*, *Fiz. Tverd. Tela (Leningrad)* 23, 1079 (1981) [*Sov. Phys. Solid State* 23, 625 (1981)].

<sup>4</sup>Y. Ishibashi *et al.*, *Physica B* 150, 258 (1988).

<sup>5</sup>G. J. McCarthy, *Acta Crystallogr.* B27, 2285 (1971).

<sup>6</sup>K. A. Gingerich and H. E. Bair, *Adv. X-Ray Anal.* 7, 22 (1964).

<sup>7</sup>L. L. Kukueva *et al.*, *Ferroelectrics* 55, 129 (1984).

<sup>8</sup>For more details, see, G. L. Catchen *et al.*, *Phys. Rev. B* 42,

1885 (1990).

<sup>9</sup>G. L. Catchen *et al.*, *Phys. Rev. B* 39, 3826 (1989), and references therein.

<sup>10</sup>G. L. Catchen, *Hyperfine Interact.* 52, 65 (1989).

<sup>11</sup>W. I. F. David, *Mater. Res. Bull.* 18, 809 (1983).

<sup>12</sup>G. L. Catchen *et al.*, *Phys. Rev. B* 37, 4839 (1988).

<sup>13</sup>H. Jaeger *et al.*, *J. Am. Ceram. Soc.* 69, 458 (1986); *Mater. Res. Soc. Symp. Prod.* 73, 599 (1986).

<sup>14</sup>A. Santoro *et al.*, *J. Solid State Chem.* 35, 167 (1980).

<sup>15</sup>L. N. Kinzhibalo *et al.*, *Kristallografiya* 27, 43 (1982) [*Sov. Phys. Crystallogr.* 27, 22 (1981)].

## THE ROLE OF FERROELASTICITY IN TOUGHENING OF BRITTLE MATERIALS

ANIL V. VIRKAR, JAN FONG JUE, PAUL SMITH, KARUN MEHTA and  
KEVIN PRETTYMAN

*Department of Materials Science & Engineering, 304 EMRO, University of Utah,  
Salt Lake City, Utah 84112, USA.*

*(Received 30 October 1990)*

Ferroelastic materials, which are characterized by the existence of a hysteresis between strain and stress, can exhibit enhanced toughness relative to the paraelastic, prototypic phase. Domain switching in the near crack tip stress field provides the requisite energy absorption mechanism and thus a toughening mechanism. Experimental evidence (X-ray diffraction) is presented on three different types of ferroelastics: namely, tetragonal (*t'*) zirconia, gadolinium molybdate (GMO) and its terbium (TMO) and dysprosium (DMO) analogs, and lead zirconate titanate (PZT). It is shown that ferroelastic domain switching occurs in these materials in the vicinity of a crack tip. The fracture toughness of the ferroic phase is shown to be two to three times that of the nonferroic phase in all three materials. The results of the present study demonstrate that ferroelastic domain switching is viable toughening mechanism.

### 1 INTRODUCTION

In analogy with ferroelectrics and ferromagnetics, Aizu (1969, 1970) was the first to coin the term ferroelasticity. The collective term ferroics was also coined by him in this context. The onset of ferroelectricity or ferromagnetism is characterized by the development of spontaneous polarization or magnetization in the absence of an externally applied electric or magnetic field, respectively. Further, the ferroic state is characterized by the existence of at least two orientation states which are energetically equivalent; it must be possible, at least in principle, to switch between the two states by a suitably applied external field. It is this property which is the basis of the hysteresis between the externally applied field and the requisite response function. In ferroelectrics the response function is the polarization, **P**, and the applied field is **E**, the electric field. In ferromagnetics the response function is magnetization, **M**, and the applied field is **H**, the magnetic field. In either case the unit of the area enclosed by the hysteresis loop is the energy absorbed in a single cycle. This energy is unavailable to do useful work as is simply degraded as heat.

Ferroelastic materials are characterized by the existence of a spontaneous strain. Further, there are at least two orientation states which are energetically equivalent and it must be possible, at least in principle, to switch from one to the other by a suitably applied external stress. Thus, in proper ferroelastics strain is the response

function and stress is the applied field. Again, the area enclosed by the hysteresis is the mechanical energy absorbed and dissipated as heat. The structural and crystallographic aspects of ferroelasticity based on group theoretic considerations have since been examined by several authors (Abrahams and Keve, 1971; Tendeloo and Amelinckx, 1974; Janovec, 1976). Aizu (1970) has shown that there are 94 crystallographic species which would permit the occurrence of ferroelasticity. Based on point groups of the prototype phase and symmetry reduction upon the occurrence of paraelastic  $\rightarrow$  ferroelastic transition, the crystallography of the resulting ferroelastic domains, domain walls and the formation of anti-phase domain boundaries has been discussed by Sapriel (1975) and by Tendeloo and Amelinckx (1974). Apart from the crystallographic considerations, the occurrence of ferroelasticity in specific materials has been generally documented by demonstrating the movement of domain walls under the application of an external stress. Many perovskite-type materials, rare earth molybdates, boracites (Sapriel, 1975),  $\text{KH}_3(\text{SeO}_3)_2$  (Rudyak, 1983) etc. are some of the materials in which experimental evidence for the existence of ferroelasticity has been documented.

The toughness of most materials is due to some dissipative mechanism operative for the absorption of mechanical energy and its eventual dissipation as heat in the material. In metallic materials, for example, the motion of dislocations under the application of an external stress is the dominant dissipative mechanism. In polymeric materials, viscous deformation is the dissipative mechanism. In fiber-reinforced composites, frictional losses at the fiber/matrix interfaces lead to the absorption of mechanical energy and thus effectively an increase in the toughness. In ferroelastic materials, the hysteresis loop between the applied stress and the strain provides a natural mechanism for the absorption of mechanical energy and thus a mechanism for toughening. The physical process for the hysteretic behavior is primarily due to the domain wall motion or domain formation which occurs by twinning (Cahn, 1954). It should, however, be recognized that ferroelastic domain switching can not occur in the prototypic phase. For example, no ferroelastic switching can occur in a cubic material. By contrast, conventional deformation twinning can occur in a cubic material. A classification of the various twin types has been recently given by Wadhawan (1987).

The origin of the toughening effect in ferroelastics, associated with the ferroelastic behavior, is expected to be primarily related to the occurrence of domain switching (ferroelastic twinning) in the near stress field of a crack tip. As the hysteresis loop is a manifestation of the dissipation of mechanical energy, its occurrence in regions near a crack tip means that some of the work done by the applied loads or tractions is simply dissipated as heat and is unavailable to advance the crack tip. As a result, more work must be put in to advance the crack than would have been necessary in the absence of ferroelasticity. The excess work needed to cause domain switching manifests as increased toughness.

While the details of the actual toughening that can be realized will depend upon a number of material-related parameters such as the Curie temperature, the magnitude of the spontaneous strain, and the coercive stress, it is to be expected that the phenomenon of ferroelastic toughening must be operative in numerous materials.

Perhaps a better understanding of ferroelasticity and its dependence on materials chemistry, microstructure and other parameters, will provide a greater insight into the phenomenon. This knowledge may then form the basis of designing structural materials exhibiting ferroelasticity.

The purpose of the present work was to examine the phenomenon of ferroelastic toughening in a variety of brittle materials. The materials chosen for the work included tetragonal zirconia, gadolinium molybdate and other rare earth molybdates, and lead-zirconate-titanate. Experimental work consisted of specimen fabrication, mechanical testing, microstructural characterization and the characterization of crystallographic texture.

## 2 EXPERIMENTAL PROCEDURE, RESULTS AND DISCUSSION

In the following paragraphs, some of the results on these three types of materials are presented followed by a brief discussion of the results. A separate section on the experimental procedure is not given although the necessary information is provided as a part of the results. The details of the experimental procedure are described in the relevant references cited here.

### 2(A) *Tetragonal zirconia*

Over the past decade or so, zirconium oxide or zirconia has been studied extensively as a structural ceramic because of its unusually high strength and toughness (Garvie, Hannink, and Pascoe, 1975). Unstabilized, pure zirconium oxide exhibits three crystallographic polymorphs: cubic above 2370°C, tetragonal between ~1000°C and 2370°C, and monoclinic below 1000°C (Subbarao, Maiti, and Srivastava, 1974). The tetragonal → monoclinic phase transition is known to be martensitic with a substantial volume increase associated with the transition. A variety of alloying oxides lower the tetragonal → monoclinic transition temperature, often below room temperature (Yoshimura, 1988). The grain size or the particle size is known to have a major influence on the tetragonal → monoclinic transition temperature (Garvie and Goss, 1986); the finer the grain size the greater the tendency to metastably retain the tetragonal phase below the equilibrium transition temperature. In such materials, the tetragonal → monoclinic transformation is known to occur in the near stress field of a crack tip. Theoretical models have been proposed which adequately explain the enhanced toughness in some of the zirconias (McMeeking and Evans, 1982). This phenomenon is known as transformation toughening (Heuer, Swain, Lange, and Evans, 1986).

While the phenomenon of transformation toughening has been well documented and studied, there are some zirconias which exhibit high toughness and strength without the apparent occurrence of transformation. For example, work on tetragonal zirconia single crystals shows that high toughness can be realized despite the nonoccurrence of transformation to the monoclinic phase (Ingel, Lewis, Bender, and

Rice, 1982; Michel, Mazerolles, and Jorba, 1983). Similarly, the toughness of tetragonal single crystals is substantially higher than that of the cubic single crystals well above the tetragonal  $\rightarrow$  monoclinic phase transition temperature where no transformation toughening is possible. In addition to the above discrepancies, there also are some transformation-toughened zirconias in which a one-to-one correspondence between the toughness and the transformed zone size can not be documented.

The probable reason for this discrepancy lies in the nature of both the cubic  $\rightarrow$  tetragonal and tetragonal  $\rightarrow$  monoclinic transitions. Michel *et al.* (1983) were the first to recognize that the cubic  $\rightarrow$  tetragonal transition in zirconia is of the paraelastic  $\rightarrow$  ferroelastic type with the associated Aizu species  $m3mF4/mmm$ . Based on this, Virkar and Matsumoto (1986) proposed ferroelastic domain switching as a possible toughening mechanism in tetragonal zirconia. Further, the tetragonal  $\rightarrow$  monoclinic transition is of the ferroelastic  $\rightarrow$  ferroelastic type with the monoclinic phase also being ferroelastic. The potential for toughening by domain switching in the monoclinic phase has been discussed by Wadhawan (1982). In light of the ferroic nature of both the tetragonal and the monoclinic phases in addition to the tetragonal  $\rightarrow$  monoclinic transformation toughening, Virkar and Matsumoto (1987) suggested that in a material thought to exhibit only transformation toughening, there may be *two* ferroelastic contributions relating to the switching in the tetragonal and the monoclinic phases. Subsequent works by Srinivasan, Jue, Kuo, and Virkar (1989) and Chan, Lange, Rühle, Jue, and Virkar (1990) have demonstrated the occurrence of ferroelastic domain switching in tetragonal zirconia pseudo single crystals. Jue and Virkar (1990) have also shown ferroelastic domain switching and the associated toughening in polycrystalline tetragonal zirconia formed by the cubic  $\rightarrow$  tetragonal displacive transformation (which is known to yield the so-called  $t'$ -morphology, Scott, 1975; Miller, Smialek, and Garlick, 1981).

Various rare earth oxides can be used to partially stabilize the tetragonal polymorph of zirconia to lower temperatures (Yoshimura, 1988).  $Y_2O_3$  as a stabilizer has been extensively investigated. The tetragonal polymorph can be formed either by precipitation (diffusional process) (Porter and Heuer, 1979) or by a displacive transformation (the  $t'$ -morphology). Single crystals of tetragonal polymorph, which are actually polydomain pseudo single crystals, are of the  $t'$ -morphology containing three variants with the c-axes of the individual domains in three nearly mutually orthogonal directions. This is consistent with Aizu's prediction for the  $m3mF4/mmm$  transition (Aizu, 1970). In the present work, experiments were conducted on polydomain single crystals of tetragonal zirconia with 2.4 and 3 mol.%  $Y_2O_3$  as well as on polycrystalline zirconia containing between 3 and 8 mol.%  $Y_2O_3$ . Polycrystalline samples were initially sintered at 1450°C for 2 hours, heat treated at  $\sim 2100^\circ\text{C}$  for 15 minutes in a gas-fired furnace followed by rapid cooling to  $\sim 1200^\circ\text{C}$  in order to prevent diffusional decomposition. Thereafter, the samples were cooled slowly to room temperature. The high temperature treatment was necessary to ensure that the samples are fully cubic so that the cubic  $\rightarrow$  tetragonal diffusionless transition can be effected. Thin sections of the samples were prepared for microstructural characterization by transmission optical and electron microscopy. A few samples were subjected to bending stresses in order to determine the coercive stress. Some of the samples

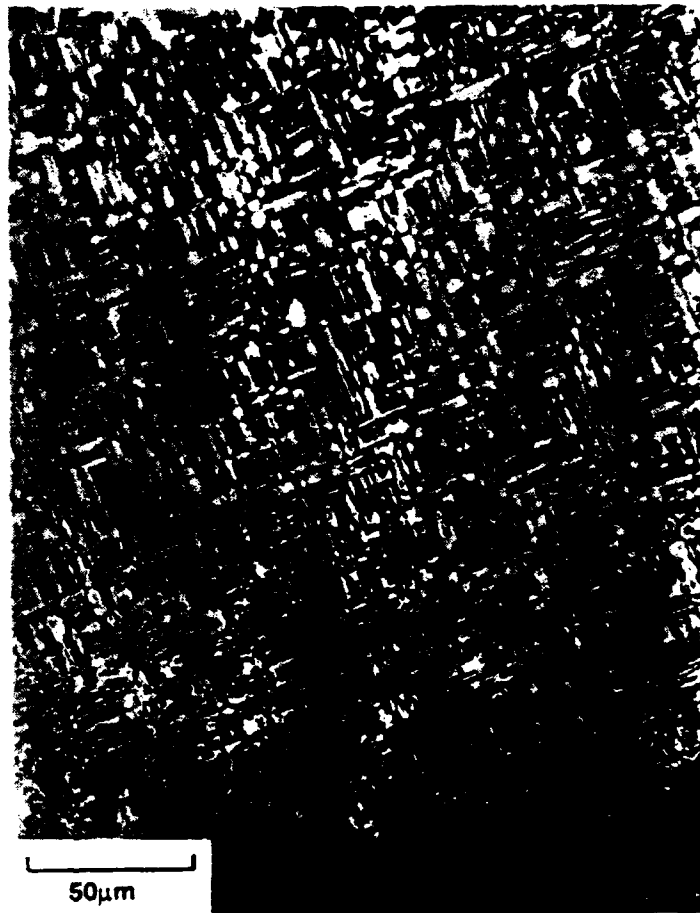
were notched and fractured to determine the fracture toughness. The fracture surfaces were examined by X-ray diffraction.

Figure 1(a) shows a transmission optical micrograph (TOM) of a polycrystalline sample containing 3 mol.%  $Y_2O_3$  under cross-polarized light. The domain structure is clearly visible in the microstructure. The domains are typically on the order of  $1 \mu m$  in size. The grain size, however, is on the order of  $100 \mu m$ . X-ray diffraction revealed that the structure is tetragonal with no monoclinic or cubic phases present. In zirconia ceramics that have been prepared by sintering in the tetragonal phase field, it is well known that the critical grain size for the spontaneous transformation of the tetragonal phase into the monoclinic phase is on the order of 1 to  $2 \mu m$  (Garvie and Goss, 1986). By contrast, samples in the present work which were heated into the cubic phase field ( $\sim 2100^\circ C$ ) and which underwent the cubic  $\rightarrow$  tetragonal displacive transition were fully tetragonal and stable even when the grain size was in excess of  $100 \mu m$ . The excellent stability of tetragonal zirconia formed by displacive transformation ( $t'$ -zirconia) can be attributed to the presence of the domains which are on the order of  $0.5 \mu m$  or less in size (Jue and Virkar, 1990). Figure 1(b) shows a TOM under cross-polarized light of a polydomain single crystal with  $\langle 100 \rangle$ , on the basis of the pseudo-cubic symmetry, along the beam direction. Similar domain structure is seen in this micrograph also. Finally, Figure 1(c) shows a TOM under cross-polarized light of a sample containing 8 mol.%  $Y_2O_3$ . No domains are seen as this composition corresponds to a single phase cubic polymorph. The domain structure observed in Figures 1(a) and (b) is typical of other ferroelastics, most notably that of  $YBa_2Cu_3O_{7-\delta}$  superconductors (Schmid, Eurkhardt, Walker, Brixel, Clin, Rivera, Jorda, Francis, and Yvon, 1988). Schmid *et al.* (1988) have examined the domain structure of  $YBa_2Cu_3O_{7-\delta}$  materials by polarized light microscopy. In the present system, however, TOM is not adequate to resolve fine details of the domain structure as the domain size is very small compared to  $YBa_2Cu_3O_{7-\delta}$  in which it can be on the order or several tens of microns. Such can not be the case in zirconia because if the domain size becomes too large, spontaneous transformation to the monoclinic phase would occur. Electron microscopy, however, can be conveniently used to delineate the microstructure. Figure 2 shows a bright field, transmission electron micrograph (TEM) of the tetragonal ( $t'$ ) phase. The domain boundaries are clearly visible in the micrograph. Note that the individual domains are submicron in size and thus can not be delineated by optical microscopy. Optical microscopy under polarized light, nonetheless, serves as a very powerful tool for the identification of the domain structure and other associated features.

The occurrence of domain switching under the action of an externally applied stress can be demonstrated using X-ray diffraction techniques. A sample of a polycrystalline  $t'$ -zirconia was subjected to a four point bending load and X-ray diffraction (XRD) pattern was obtained while the sample was still under load. It was observed that intensity of the (200) peak,  $I_{(200)}$ , increased and that of the (002) peak,  $I_{(002)}$ , decreased from the tensile surface while no monoclinic phase was seen to form. Figure 3 shows the corresponding XRD peaks: (a) before the application of stress, (b) while under stress, and (c) after removal of the stress. The decrease in the intensity of the (002) peak is consistent with the alignment of domains with their c-axes along



(a)



(b)



**Figure 1** (a): Transmission optical micrograph (TOM) of a 3 mol.%  $Y_2O_3$  (Tetragonal) sinter/annealed  $\geq 2100^\circ C$  showing the characteristic domain structure. (b) A TOM of a 2.4 mol.%  $Y_2O_3$  single crystal with  $\langle 100 \rangle$  (on the basis of pseudocubic symmetry) along the beam direction. (c) A TOM of 8 mol.%  $Y_2O_3$  (cubic) sinter/annealed  $\geq 2100^\circ C$ . Note the absence of domain structure.

the direction of the tensile stress. The stress above which crystallographic texture developed was about 350 MPa suggesting that the coercive stress is on the order of 350 MPa. The occurrence of ferroelastic domain switching at stresses as low as 350 MPa suggests that domain reorientation in the near stress field of a crack tip is possible and thus should contribute to toughness. Figure 4 compares the XRD traces from a polished surface and a fracture surface of a 4 mol.%  $Y_2O_3$ -doped polycrystalline zirconia sample fractured at 1000 C. The polished surface is representative of a random orientation of the domains in which case it is expected that the  $I_{(200)}$  will be about twice  $I_{(002)}$ . On the other hand, if domain switching does occur within the stress field of a crack tip, one would expect an increase in  $I_{(002)}$  with a simultaneous decrease in  $I_{(200)}$ . As seen in the figure, the ratio  $I_{(002)}/I_{(200)}$  is greater from fracture surfaces confirming the occurrence of domain switching during fracture. This implies that this toughening mechanism is operative in zirconia at high temperatures. Crystallographic texture may not always be observed on fracture surfaces. It should be emphasized, however, that the nonobservance of texture on fracture surfaces does



Figure 2 A bright field transmission electron micrograph (TEM) of 3 mol.% Y<sub>2</sub>O<sub>3</sub> (tetragonal) sinter/annealed  $\geq 2100$  C showing the characteristic domain structure.

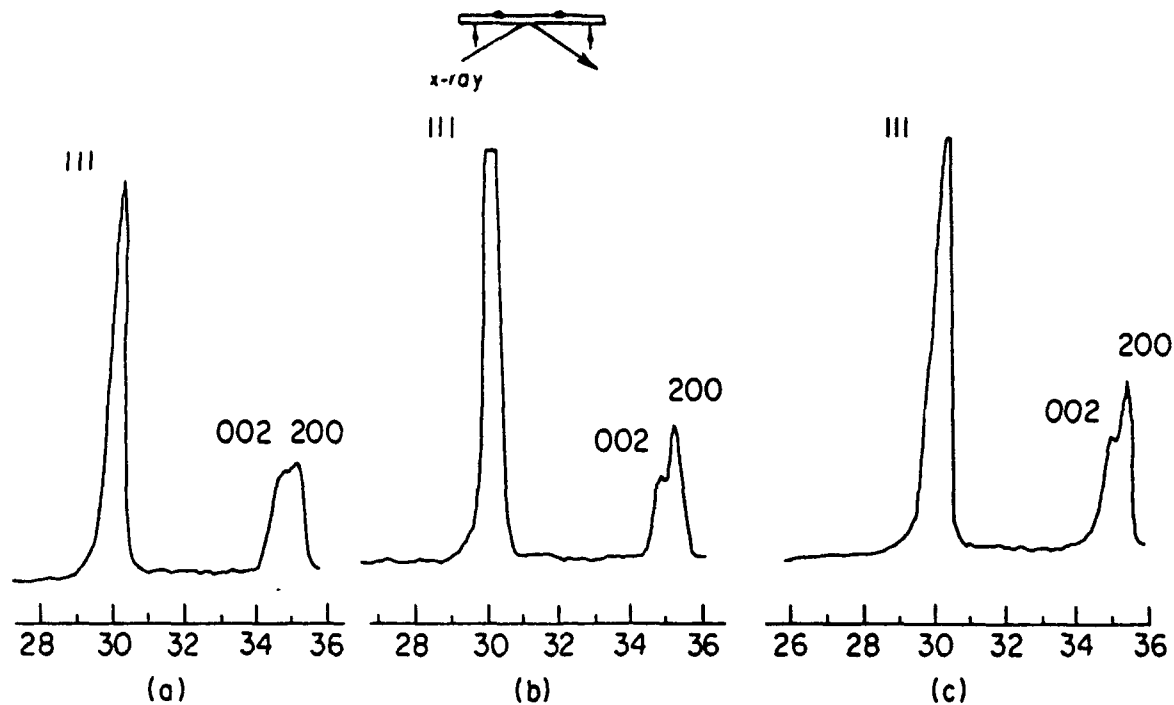


**Figure 3** In-situ XRD traces from a sample of 3.5 mol.%  $Y_2O_3$  sinter/annealed  $\geq 2100^\circ C$  under various stresses: (a) Unstressed, (b) 400 MPa, and (c) after unloading.

not necessarily imply the nonoccurrence of domain switching. It is well known that domain switching is a relaxative process with some relaxation time associated with it (Rudyak, 1983). If the crack growth is fast relative to the relaxation time of the domain switching process, no texture will be developed on the fracture surface. However, texture will still develop in the near tip region of the crack during quasi-static loading. Also, reversible switching may occur in which case no permanent texture will be developed. Tsunekawa and Takei (1976) have observed reverse switching in  $LaNbO_4$  and  $NdNbO_4$ .

The fracture toughness,  $K_c$ , of fully tetragonal samples of composition 3 mol.%  $Y_2O_3$  was  $\sim 7.7 \text{ MPa}\sqrt{\text{m}}$ . By contrast,  $K_c$  of samples with 8 mol.%  $Y_2O_3$ , which is fully cubic, was  $\sim 2.4 \text{ MPa}\sqrt{\text{m}}$ . The variation of  $K_c$  with  $Y_2O_3$  % is shown in Figure 5. The substantially higher toughness of the fully tetragonal zirconia in the present  $t'$  samples is thus attributed to the ferroelastic character of the tetragonal phase. Approximate contribution of ferroelasticity to toughness can be given as (Mehta and Virkar, 1990; Jue and Virkar, 1990)

$$K_c \approx \frac{K_c^0}{\sqrt{1 - \frac{0.17\epsilon_s E}{\sigma_c}}} \quad (1)$$

where  $K_c^0$  is the fracture toughness in the absence of ferroelasticity,  $\epsilon_s$  is the switching strain,  $\sigma_c$  is the coercive stress and  $E$  is the Young's modulus of elasticity. In the preceding equation, Poisson's ratio,  $\nu$ , was assumed to be 0.25. The calculated

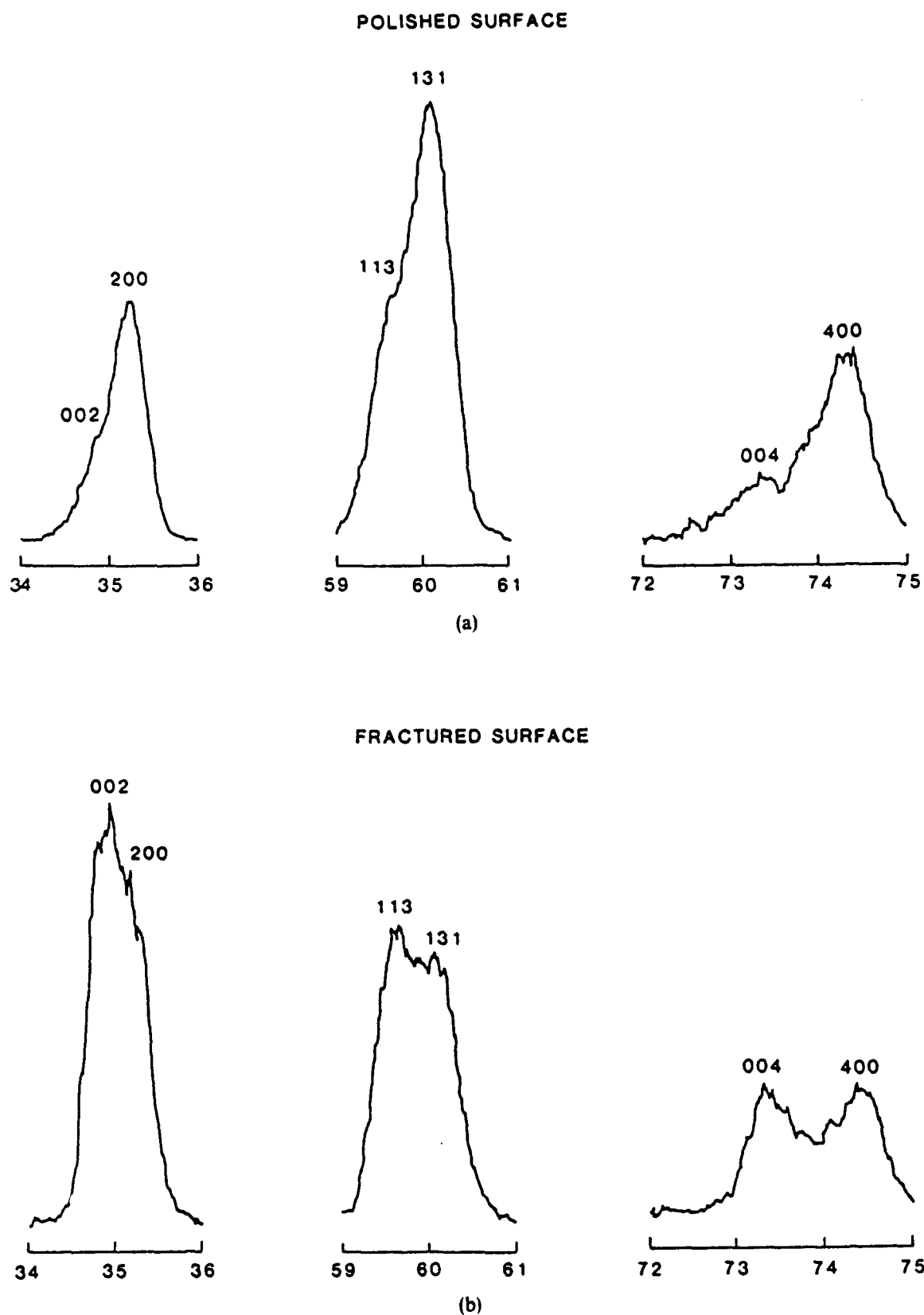


**Figure 4** XRD traces from a 4 mol.%  $Y_2O_3$  sample sinter/annealed  $\geq 2100^\circ C$ : (a) As-polished surface, (b) Fracture surface after testing at  $1000^\circ C$ . Note the relative change in the intensities.

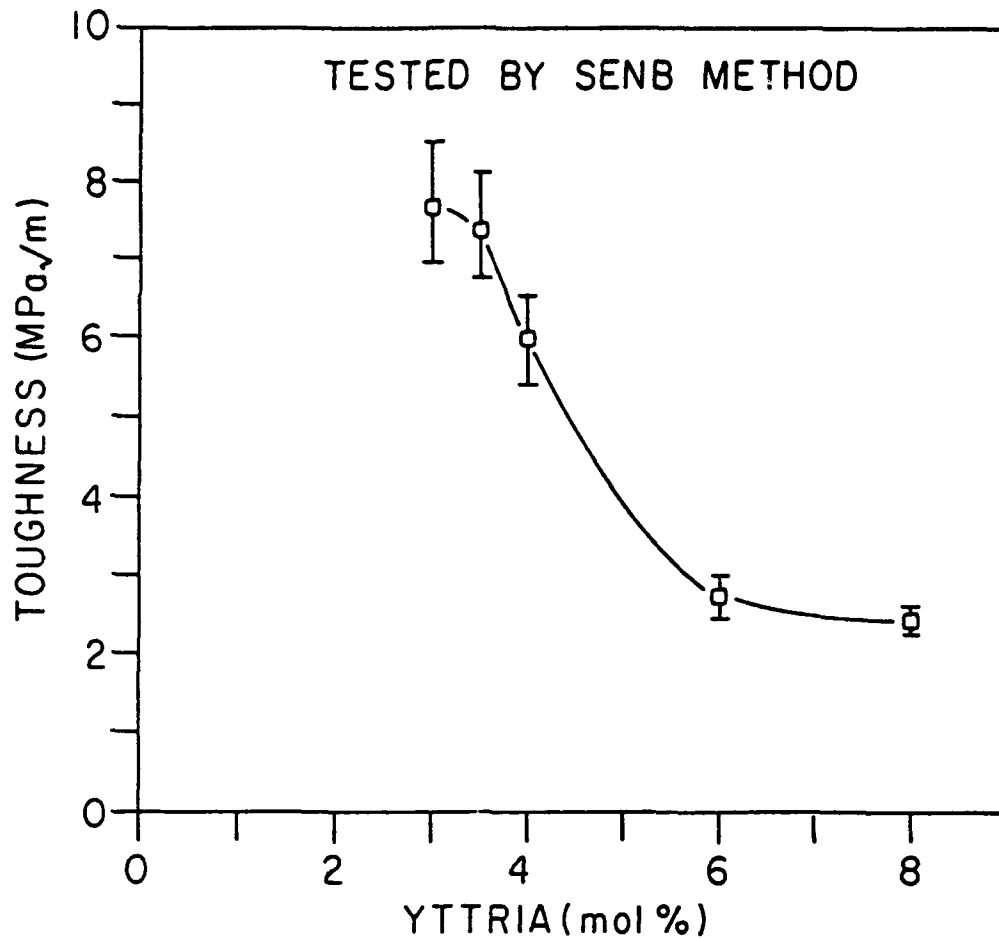


Figure 5 Toughness,  $K_c$ , vs.  $Y_2O_3$  content for samples sinter/annealed  $\geq 2100^\circ C$ .

value of  $K_c$  for 3 mol.%  $Y_2O_3$ -stabilized polycrystalline material using  $\epsilon_s \approx 0.0087$ ,  $\sigma_c \approx 350$  MPa and  $E \approx 200$  GPa, and  $K_c^0 \approx 2.4$  MPa√m is 6.1 MPa√m, showing a substantial contribution of ferroelastic domain switching to toughness in the  $t'$ -zirconia polycrystalline ceramics.

The Curie temperature in zirconia is the cubic  $\rightarrow$  tetragonal displacive transition temperature which, depending upon the type of stabilizer and its concentration, can be as high as  $\sim 2370^\circ C$ . This suggests that it may be possible to develop zirconia-based materials with high toughness at elevated temperatures. Recent work on high temperature testing of polycrystalline  $t'$ -zirconia shows that deformation strain on the order of 0.5% is possible (Prettyman, Jue, Virkar, Hubbard, Cavin, and Ferber, 1990).

#### 2(B) Gadolinium, terbium, and dysprosium molybdates (GMO, TMO, and DMO)

Gadolinium molybdate,  $Gd_2(MoO_4)_3$ , (GMO) is a fully coupled ferroelectric/ferroelastic and belongs to the Aizu species  $\bar{4}2mFmm2$  with the ferroic phase being of

orthorhombic symmetry (Aizu, Kumada, Yumoto, and Ashida, 1969). The polarization vector is directed along the *c*-axis [001]. Polarization reversal is accomplished by an interchange between the 'a' [100] and 'b' [010] axes which results in a 90° rotation of the strain tensor. The *b*-axis is slightly longer than the *a*-axis. The spontaneous strain tensor is always orthogonal to the spontaneous polarization. The low temperature  $\beta'$ -GMO ferroic phase (mm2) transforms into the high temperature prototypic  $\beta$ -GMO phase ( $\bar{4}2m$ ) at  $\sim 159^\circ\text{C}$ . Many isotopes of GMO with other rare earth ions substituted for Gd exist with similar properties. In the present study, experiments were done on single crystals of GMO as well as polycrystalline materials of TMO ( $\text{Tb}_2(\text{MoO}_4)_3$ ) and DMO ( $\text{Dy}_2(\text{MoO}_4)_3$ ). Single crystals were supplied by Dr. L. H. Brixner of E. I. DuPont Co. The as-received crystals were oriented using Laue X-ray back reflection. Specimens of typical dimensions 15 mm  $\times$  10 mm  $\times$  2 mm were cut such that the rectangular faces were of the (100), (010), and (001) type with the largest face being the (001) face. All faces were polished in a 0.3  $\mu\text{m}$  alumina slurry. Domain walls could be easily delineated in transmission optical microscopy under cross-polarized light. The domain walls are of {110} type in GMO.

The occurrence of domain switching in GMO is consistent with an interchange between the 'a' and 'b' axes. Since 'b' is slightly longer than 'a' ( $a = 10.38582 \text{ \AA}$ ,  $b = 10.41861 \text{ \AA}$ , Keve, Abrahams, Nassau, and Glass, 1970), a tensile stress along 'a' or a compressive stress along 'b' will be expected to cause domain switching. On the other hand, a tensile stress along 'b' or a compressive stress along 'a' will cause no domain switching as the domains are already oriented in the low energy direction in relation to the stress applied. The process of domain switching may alternatively be viewed as being effected by a shear stress of the requisite sign. With respect to the present interest in toughening, domain reorientation (or nucleation) in the near stress field of a crack tip may occur if the normal to the crack plane is along the [100] direction since a tensile stress will change it into a 'b' axis [010]. On the other hand, if the normal to the crack plane is along the [010] direction, no domain switching is expected as the domains are already in the correct direction. This scenario implies that if cracks are introduced in these two orientations in a single crystal, switching will occur in one of the orientations. In the event that switching occurs, the crack length will be shorter reflecting the fact that some of the energy was used up in domain reorientation and unavailable for crack extension. In other words, this energy absorption is reflected as increased toughness.

Cracks in specific orientations may conveniently be introduced by using diamond pyramidal indenters. In order to examine the effect of ferroelastic switching in GMO single crystals, Vicker's indentations were introduced under a 200 gm. load in such a way that the prospective cracks would be along the [100] and [010] directions. Figure 6 shows a photomicrograph of such an indent. As seen in the figure, the crack lengths in the two directions are very different; the crack along the [100] direction (such that normal to the crack plane is along the [010] direction) is much longer than that along the [010] direction (such that the normal to the crack plane is along the [100] direction) in agreement with the above prediction. Indentation cracks were also introduced such that they are along the [110] and  $[\bar{1}10]$  directions. No switching is expected by the crack tip stress field for this orientation. Figure 7 confirms this in

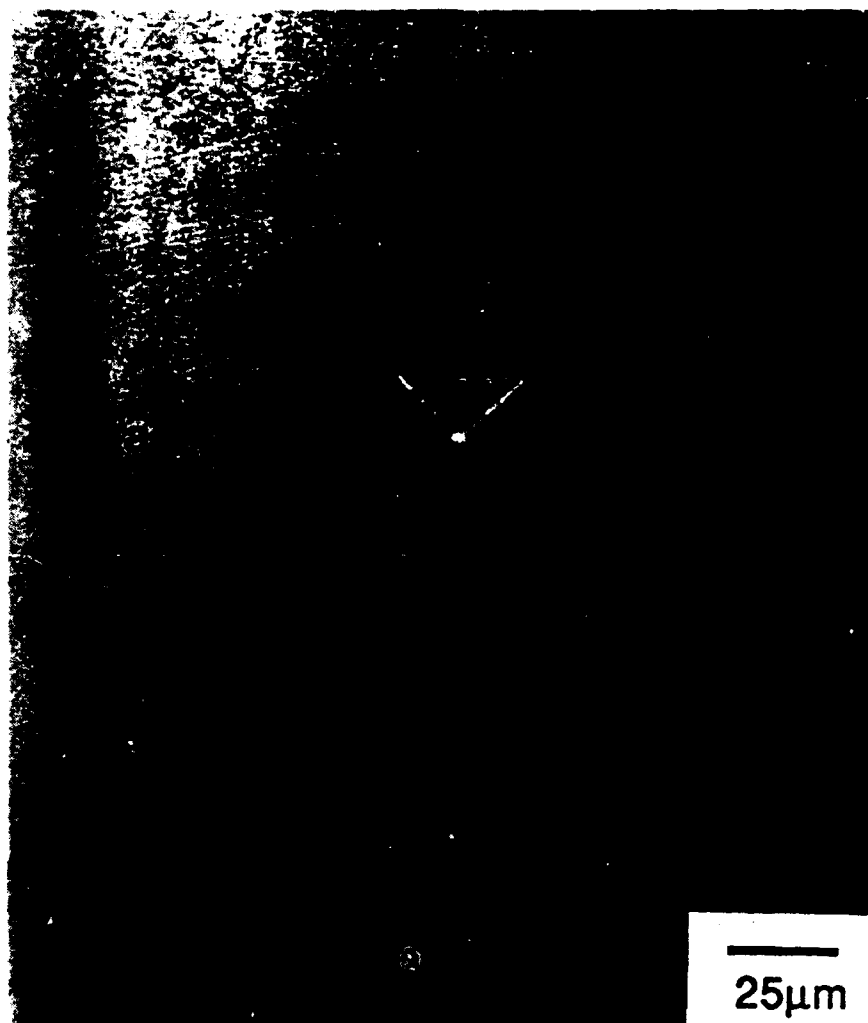


**Figure 6** A Vicker's indent in a GMO single crystal with cracks along [100] and [010]. Note that the lengths of the cracks are different in the two direction.

that the two cracks are of equal lengths. These experiments conclusively show the occurrence of domain switching during fracture, an important requirement for the ferroelastic toughening effect. Using the indentation technique of Evans and Charles (1976), the orientation dependent toughness,  $K_{Ic}$ , was estimated. For cracks along the [010] axis, the  $K_{Ic} \approx 1.2 \text{ MPa}\sqrt{\text{m}}$  while for cracks along the [100] axis,  $K_{Ic} \approx 0.42 \text{ MPa}\sqrt{\text{m}}$ . That is  $K_{Ic}$  for the crack direction in which ferroelastic domain switching does occur is nearly three times that of the other crack direction in which no switching can occur. This shows that ferroelastic domain switching can significantly contribute to toughness. The  $K_{Ic}$  for cracks along  $\langle 110 \rangle$  was measured to be  $\sim 0.55 \text{ MPa}\sqrt{\text{m}}$ . As mentioned above, no ferroelastic domain switching is expected in this orientation. Details of twin formation are described elsewhere (Smith, 1990).

Fabrication of polycrystalline GMO proved to be difficult due to phase instabilities. Therefore, experimental work on polycrystalline materials was done on TMO and DMO. Samples were fabricated to high densities by hot pressing under 35 MPa at  $\sim 900^\circ\text{C}$  in air. The grain size of the samples was typically on the order of  $\sim 6$

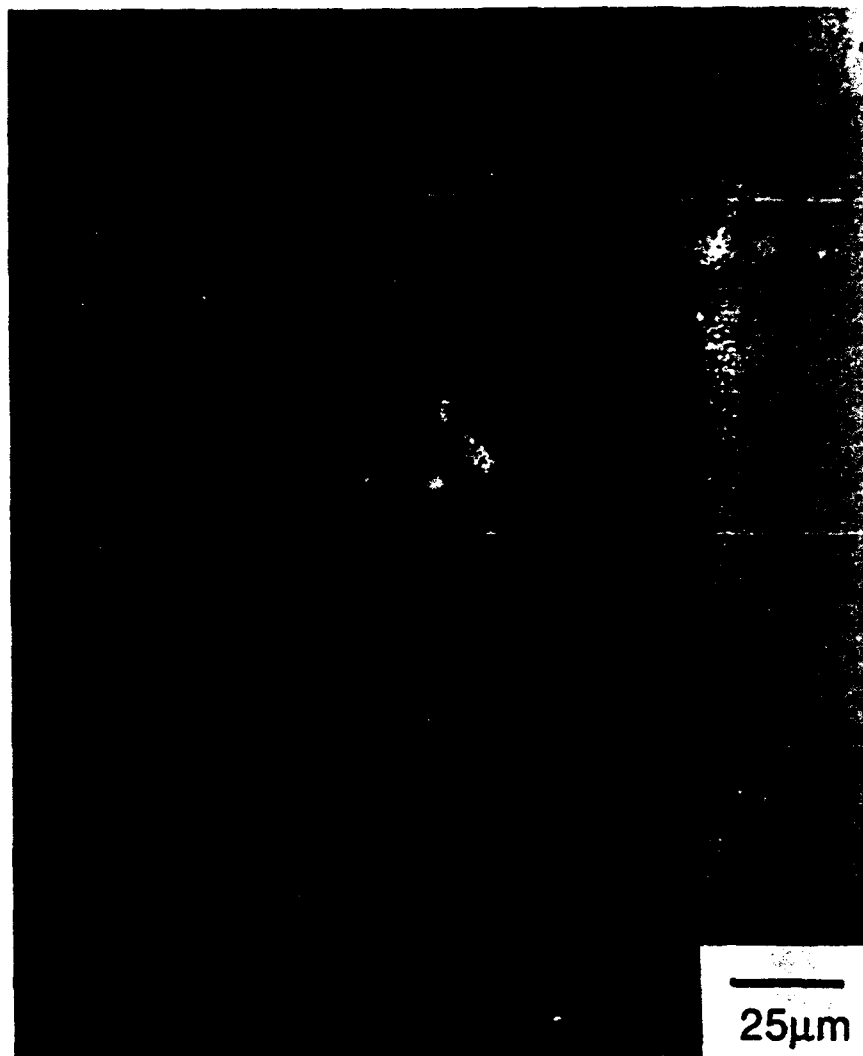


**Figure 7** A Vicker's indent in a GMO single crystal with cracks along  $[110]$  and  $[\bar{1}10]$ . Note that the cracks are of essentially identical length.

$\mu\text{m}$ . Fracture toughness of some of the polycrystalline samples was determined as a function of temperature using the indentation technique (Evans and Charles, 1976). Figure 8 shows the measured toughness as a function of temperature. Note that the toughness,  $K_c$ , decreases with increasing temperature up to about  $160^\circ\text{C}$  and remains nearly constant thereafter. Since the Curie temperature is  $\sim 160^\circ\text{C}$  for GMO, TMO, and DMO, no ferroelastic domain switching is expected above this temperature. At room temperature, the toughness is as high as twice that above the Curie temperature, indicating a substantial contribution of ferroelastic domain switching to  $K_c$  in both TMO and DMO.

### 2(C) Lead-zirconate-titanate (PZT)

Lead zirconate ( $\text{PbZr}_x\text{Ti}_{(1-x)}\text{O}_3$ ) or PZT are simultaneously ferroelectric-ferroelastic ceramics. Depending upon the relative amounts of Zr and Ti, various ferroic

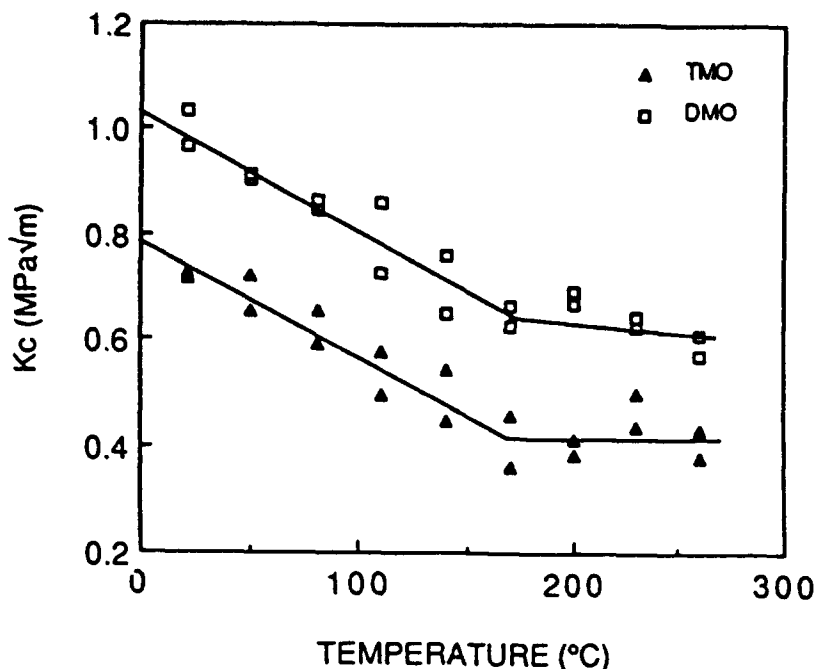


Figure 8 Toughness,  $K_c$ , as a function of temperature for polycrystalline TMO and DMO.

transitions are possible in this system. Mechanical properties of PZT and  $\text{BaTiO}_3$  have been examined by Pohanka, Freiman, and Bender (1978); Pohanka, Freiman, and Rice (1980); and Pohanka, Freiman, Okazaki, and Tashiro (1986). The ferroic phase was shown to exhibit higher fracture energy compared to the para phase. Microcracking, ferroelastic twin formation and twin wall motion were proposed as toughening mechanisms. Mechanics of toughening by domain switching in PZT was examined by Pisarenko, Chushko, and Kovalev (1985). Experimental evidence of domain switching during fracture has been recently presented by Mehta and Virkar (1990).

For the present work, the composition  $x = 0.54$  was chosen. Materials of this composition are tetragonal at room temperature and transform into the prototypic cubic phase at  $\sim 350^\circ\text{C}$ . The Aizu species which describes the transition is  $m3mF4mm$ . Dense, polycrystalline samples of this composition were supplied by Ms. Angela Richardson of Edo Western Co., Salt Lake City, Utah. The as-received, unpoled PZT samples were machined in the shape of single edge notched beam (SENB) specimens for the measurement of  $K_c$  (Hellan, 1984). The typical dimensions were:  $35 \text{ mm} \times 6.5 \text{ mm} \times 3 \text{ mm}$ . After introducing a notch of  $0.25 \text{ mm}$  width and  $3 \text{ mm}$  depth, the samples were annealed at  $500^\circ\text{C}$  in order to remove the texture caused by the machining operations. The samples were subsequently fractured in four point bending for the determination of  $K_c$ . A few samples were also tested in the double cantilever beam (DCB) geometry (Hellan, 1984). The objective was to investigate the switching phenomenon in the fast as well as slow regimes of crack growth. XRD traces were obtained from slow and fast regimes. Some of the bar-shaped samples were poled mechanically and electrically. These samples were then indented with a Vicker's indenter to examine the crack pattern.

Figure 9 shows the toughness,  $K_c$ , as a function of temperature (Mehta and Virkar, 1990). The  $K_c$  decreases with increasing temperature and becomes nearly constant above the Curie temperature which is  $\sim 350^\circ\text{C}$ . The room temperature  $K_c$  is  $\sim 1.85 \text{ MPa}\sqrt{\text{m}}$  while that above the Curie temperature is  $\sim 1.00 \text{ MPa}\sqrt{\text{m}}$ . This behavior is very similar to that observed in TMO and DMO. In the DCB tests, the crack was initially allowed to propagate very slowly followed by rapid fracture. In the slow crack regime, the crack velocity was  $\sim 100 \mu\text{m}/\text{sec}$ . In the fast regime the crack velocity was at least several m/sec. XRD traces of fracture surfaces from the two regimes are shown in Figure 10. The  $I_{(002)}/I_{(200)}$  is greater from the slow regime compared to that from the fast regime. The implication is that domain switching occurred in the slow regime of crack growth. This effect can be explained on the basis of relaxation time for the switching process (Rudyak, 1983) and the crack velocity (Mehta and Virkar, 1990). This experiment shows that domain switching can occur during quasi-static loading of a crack and thus contribute to toughness. In general, the relaxation time is expected to decrease with increasing temperature. Thus, switching may be observed from fracture surfaces of typical samples fractured at

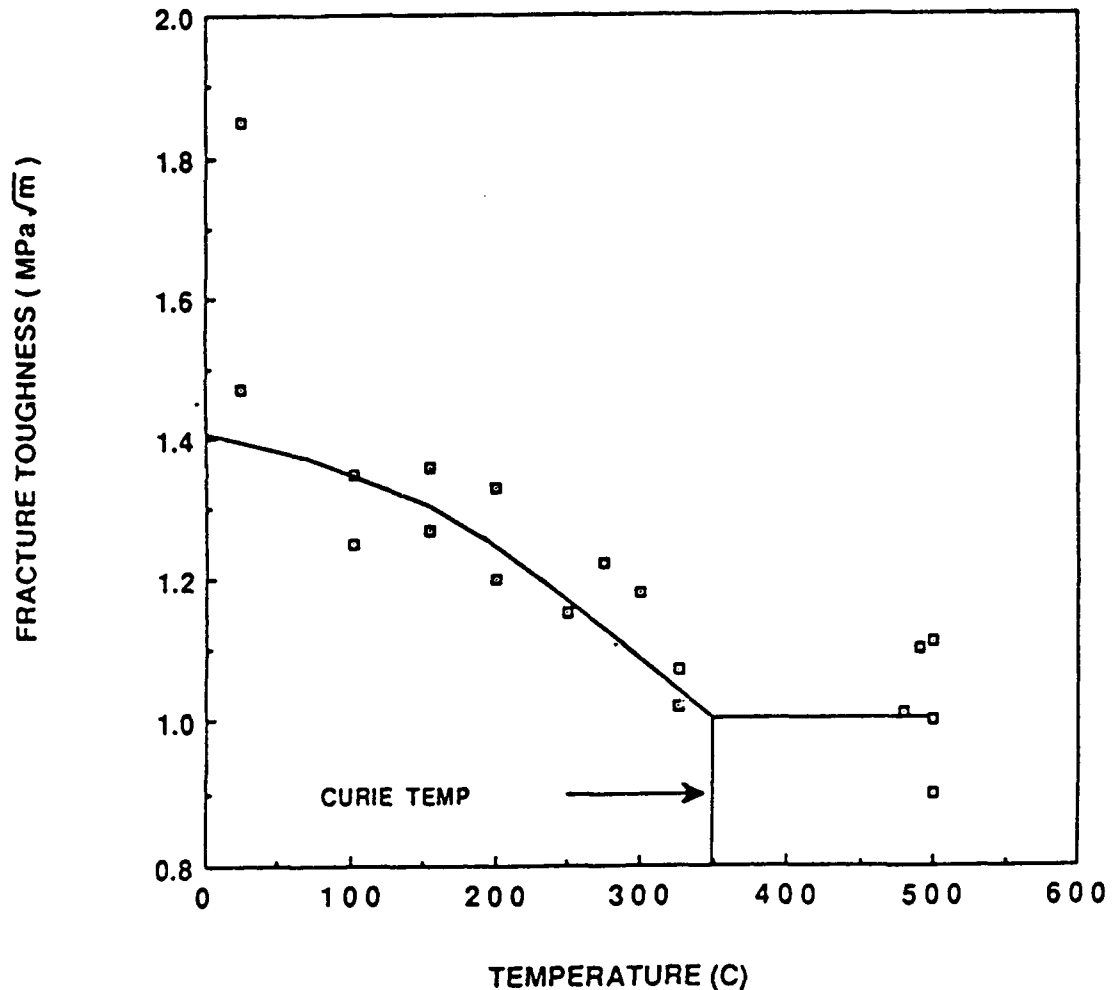
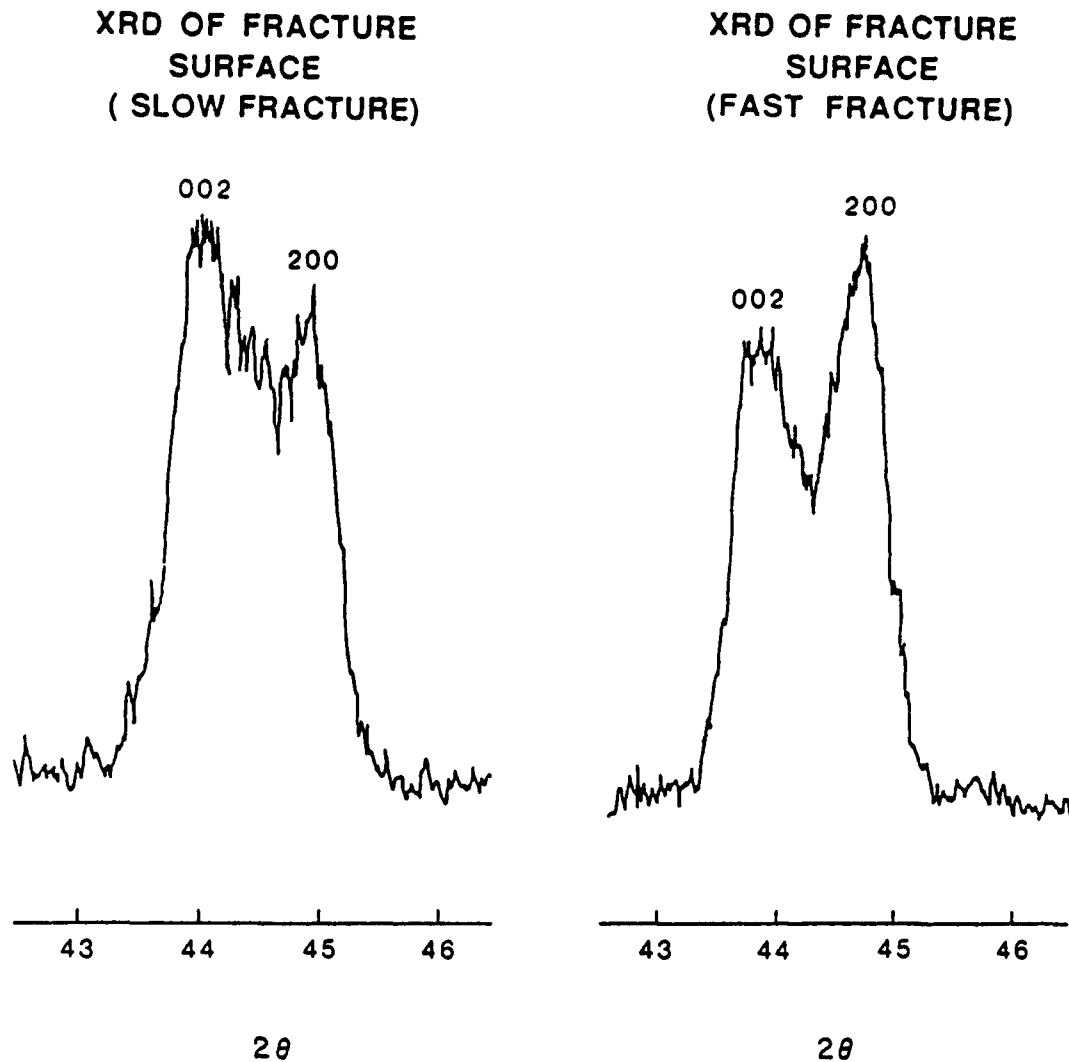


Figure 9 Fracture toughness,  $K_c$ , of unpoled PZT samples as a function of temperature.



**Figure 10** (a) XRD trace of fracture surface from the stable crack region of DCB sample; crack velocity  $\sim 100 \mu\text{m}/\text{sec}$ . Note that  $I_{(002)} > I_{(200)}$ , showing clearly that domain switching occurred during fracture. (b) XRD trace of fracture surface from the rapid crack growth region of the same DCB sample. Note that  $I_{(002)} < I_{(200)}$  with  $I_{(002)}/I_{(200)} \sim 0.5$ , indicating that very little domain switching occurred during fast crack growth.

elevated temperatures (but still in the ferroic state) but not from those fractured at room temperature. In tetragonal (*t'*) zirconia, this effect has been observed.

Indentation tests were performed on mechanically poled samples. Poling tends to align the domains in such a manner that the *c*-axes of the domains are perpendicular to the compressive load applied. During indentation fracture, domains in the crack tip region with *c*-axes parallel to the crack surface should reorient perpendicular to the crack plane. By contrast, domains that are already perpendicular to the crack surface should remain unaffected. Consequently, the crack lengths in the two directions should be different. Figure 11 shows that indeed the cracks in the two directions are of different lengths. The reasoning is very similar to that for GMO single crystals.

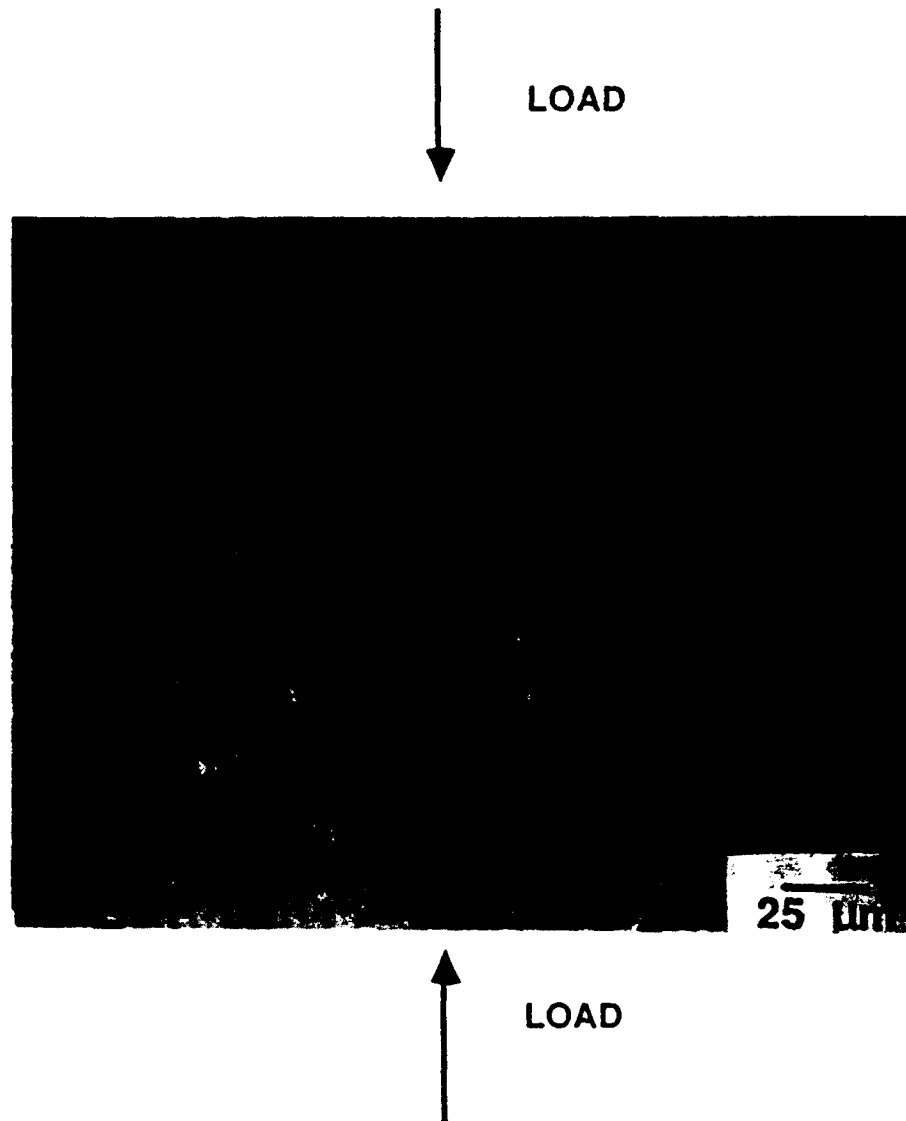


**Figure 11** Photomicrograph showing a microindent (500 gm. for 10 sec.) introduced in a mechanically poled PZT sample. Note the anisotropy in crack lengths. The arrow indicates the direction of compression (poling).

### 3 SUMMARY

The present results demonstrate that ferroelastic domain switching occurs in three different ferroelastics studied: namely, tetragonal zirconia, GMO and its isotypes, and PZT. Domain switching can be effected by the application of an external uniform stress as well as in the near stress field of a crack tip. Its occurrence in the near stress field of a crack tip implies that domain switching in a natural manner provides a mechanism for toughening. If all of the excess toughness of the ferroic phase in relation to the nonferroic phase can be attributed to ferroelasticity, the present results indicate that toughness enhancement on the order of two to three times is possible.

In brittle materials, this contribution may be significant. The vast information and background literature on ferroelastic materials in addition to the nature of hysteretic behavior in other ferroic materials such as ferroelectrics and ferromagnetics suggests that it may be possible to engineer mechanical properties of materials through the understanding of the crystallography and the characteristics of the phase transition. For example, the application of the Landau order parameter theory may allow some day to design materials with the desired properties. In this sense, the design of materials for structural applications based on their ferroelastic behavior will offer a new approach for the development of materials. This is a radical departure from the conventional micromechanical approach which tends to ignore the basic physical and chemical aspects of materials.

#### Acknowledgements

This work was supported by the Defense Advanced Research Projects Agency (DARPA) through AFOSR: Contract No. F49620-89-C-0054 at the University of Utah through a subcontract from Ceramtec, Inc.

#### References

- Abrahams, S. C. and E. T. Keve (1971). Structural Basis of Ferroelectricity and Ferroelasticity, *Ferroelectrics*, **2**, 129-154.
- Aizu, K. (1969). Possible Species of Ferroelastic Crystals and Simultaneously Ferroelectric and Ferroelastic Crystals, *J. Phys. Soc. Japan*, **27**, 387-396.
- Aizu, K. (1970). Possible Species of Ferromagnetic, Ferroelectric and Ferroelastic Crystals, *Phys. Rev.*, **B**, **2**, 754-772.
- Aizu, K., A. Kumada, H. Yumoto and S. Ashida (1969). Simultaneous Ferroelectricity and Ferroelasticity of  $Gd_2(MoO_4)_3$ , *J. Phys. Soc. Japan*, **27**, 511.
- Cahn, R. W. (1954). Twinned Crystals, *Adv. Phys.*, **3**, 363-445.
- Chan, C. J., F. F. Lange, M. Rühle, J. F. Jue and A. V. Virkar (1990). Domain Switching in Tetragonal Zirconia Single Crystal-Microstructure Aspects, submitted to the *J. Am. Ceram. Soc.*
- Evans, A. G. and E. A. Charles (1976). Fracture Toughness Determinations by Indentation, *J. Am. Ceram. Soc.*, **59**, 371-372.
- Garvie, R. C., R. H. J. Nannink and R. T. Pascoe (1975). Ceramic Steel?, *Nature (London)*, **258**, 703-705.
- Garvie, R. C. and M. F. Goss (1986). Intrinsic Size Dependence of the Phase Transformation Temperature in Zirconia Microcrystals, *J. Mat. Sci.*, **21**, 1253-1257.
- Hellan, K. (1984). 'Introduction to Fracture Mechanics', McGraw-Hill, New York.
- Heuer, A. H., F. F. Lange, M. V. Swan and A. G. Evans, eds. (1986). Transformation Toughening, *J. Am. Ceram. Soc.*, **69**, 169-298.
- Ingel, R. P., D. L. Lewis, B. A. Bender and R. W. Rice (1982). Temperature Dependence of Strength and Fracture Toughness of  $ZrO_2$  Single Crystals, *J. Am. Ceram. Soc.*, **65**, C150-C151.
- Janovec, V. (1976). Symmetry Approach to Domain Structures, *Ferroelectrics*, **12**, 43-53.
- Jue, J. F. and A. V. Virkar (1990). Fabrication, Microstructural Characterization and Mechanical Properties of Polycrystalline, *t'*-Zirconia, *J. Am. Ceram. Soc.*, **73**, 3650-3657.
- Keve, E. T., S. C. Abrahams, K. Nassau and A. M. Glass (1970). Ferroelectric Ferroelastic Paramagnetic Terbium Molybdate  $\beta$ - $Tb_2(MoO_4)_3$ , *Solid State Comm.*, **8**, 1517-1520.
- McMeeking, R. M. and A. G. Evans (1982). Toughening of Brittle Solids by Martensitic Transformation, *J. Am. Ceram. Soc.*, **65**, 242-247.
- Mehta, K. and A. V. Virkar (1990). Fracture Mechanisms in Ferroelectric-Ferroelastic Lead Zirconate Titanate (Zr:Ti = 0.54:0.46) Ceramics, *J. Am. Ceram. Soc.*, **73**, 567-574.
- Michel, D., L. Maerolles and M. Perez y Jorba (1983). Fracture of Metastable Tetragonal Zirconia Crystals, *J. Mater. Sci.*, **18**, 2618-2628.
- Miller, R. A., J. L. Smialek, and R. G. Garlick (1981). Phase Stability in Plasma-Sprayed Partially Stabilized Zirconia-Yttria, A. H. Heuer and L. W. Hobbs, eds., 'Advances in Ceramics. Science and technology of Zirconia, Vol. 3, American Ceramic Society, Columbus, OH. 241-253.

- Pisarenko, G. G., V. M. Chushko and S. P. Kovalev (1985). Anisotropy of Fracture Toughness of Piezoelectric Ceramics. *J. Am. Ceram. Soc.*, **68**, 259-65.
- Pohanka, R. C., S. W. Freiman and B. A. Bender (1978). Effect of Phase Transformation on the Fracture Behavior of BaTiO<sub>3</sub>. *J. Am. Ceram. Soc.*, **61**, 72-75.
- Pohanka, R. C., S. W. Freiman and R. W. Rice (1980). Fracture processes in Ferroic Materials, *Ferroelectrics*, **28**, 337.
- Pohanka, R. C., S. W. Freiman, K. Okazaki and S. Tashiro (1983). Fracture of Piezoelectric Materials, in 'Fracture Mechanics of Ceramics', edited by R. C. Bradt, A. G. Evans, D. P. H. Hasselman and F. F. Lange, Vol. 5, Plenum Press, 353-364.
- Prettyman, K. M., J. F. Jue, A. V. Virkar, C. R. Hubbard, O. B. Cavin and M. K. Ferber (1990). Unpublished work.
- Porter, D. L. and A. H. Heuer (1979). Microstructural Development in MgO-Partially Stabilized Zirconia (Mg-PSZ). *J. Am. Ceram. Soc.*, **62**, 298-305.
- Rudiyak, V. M. (1983). Viscosity Phenomenon and Switching Processes in Ferroelastics, *Ferroelectrics*, **48**, 131-141.
- Sapriel, J. (1975). Domain Wall Orientations in Ferroelastics. *Phys. Rev., B*, **12**, 5128-5140.
- Schmid, H., E. Eurkhardt, E. Walker, W. Brixel, M. Clin, J-P Rivera, J-L Jorda, M. Francis and K. Yvon (1988). Polarized Light and X-Ray Precession Study of the Ferroelastic Domains of YBa<sub>2</sub>Cu<sub>3</sub>O<sub>7- $\delta$</sub> . *Z. Phys. B-Condensed Matter*, **72**, 305-322.
- Scott, H. G. (1975). Phase Relations in Zirconia-Yttria System, *J. Mater. Sci.*, **10**, 1527-1535.
- Smith, P. (1990). Ferroelastic Fracture Properties of Gadolinium Molybdate and Related Isotypic Compounds, M. S. Thesis, University of Utah.
- Srinivasan, G. V., J. F. Jue, S. Y. Kuo and A. V. Virkar (1989). Ferroelastic Domain Switching in Polydomain Tetragonal Zirconia Single Crystals, *J. Am. Ceram. Soc.*, **72**, 2098-2103.
- Subbarao, E. C., H. S. Maiti and K. K. Srivastava (1974). Martensitic Transformation in Zirconia, *Phys. Stat. Solidi (a)*, **21**, 9-40.
- Tendeloo, G. V. and S. Amelinckx (1974). Group-Theoretical Considerations Concerning Domain Formation in Order Alloys, *Acta Cryst.*, **A30**, 431-440.
- Tsunekawa, S. and H. Takei (1976). Domain Switching Behavior of Ferroelastic LaNbO<sub>4</sub> and NdNbO<sub>4</sub>. *J. Phys. Soc.*, **40**, 1523-1524.
- Virkar, A. V. and R. L. K. Matsumoto (1986). Ferroelastic Domain Switching as a Toughening Mechanism in tetragonal Zirconia, *J. Am. Ceram. Soc.*, **69**, C224-C226.
- Virkar, A. V. and R. L. K. Matsumoto (1988). Toughening Mechanism in Tetragonal Zirconia (TZP) Ceramics, S. Somiya, N. Yamamoto and H. Yanagida, eds. 'Advances in Ceramics, Science and Technology of Zirconia, III, Vol. 24, American Ceramic Society, Westerville, OH, 653-662.
- Wadhawan, V. K. (1982). Ferroelasticity and Related Properties of Crystals, *Phase Transitions*, **3**, 3-103.
- Wadhawan, V. K. (1987). A New Classification of Twinning in Crystals, *Phase Transitions*, **9**, 297-316.
- Yoshimura, M. (1988). Phase Stability of Zirconia, *Bull. Am. Ceram. Soc.*, **67**, 1950-1955.

## Low-Temperature Aging of $t'$ -Zirconia: The Role of Microstructure on Phase Stability

Jan Fong Jue,\* Jong Chen,\* and Anil V. Virkar\*

Department of Materials Science and Engineering, University of Utah, Salt Lake City, Utah 84112

Polycrystalline, tetragonal ( $t'$ ) zirconia samples containing 3 and 4 mol% yttria were fabricated by annealing pressureless-sintered samples in air at  $\sim 2100^\circ\text{C}$  for 15 min. The grain size of these fully tetragonal samples was on the order of 100 to 200  $\mu\text{m}$ . Domain structure of the samples and of a 3-mol%-yttria-doped tetragonal zirconia single crystal was examined by transmission optical microscopy under polarized light and by transmission electron microscopy. The orientations of the domain/colony boundaries were in accord with the predictions of group theory. As-polished surfaces of polycrystalline  $t'$  materials showed no monoclinic phase even after 1000 h at  $275^\circ\text{C}$  in air. By contrast, conventionally yttria-doped tetragonal zirconia polycrystalline (Y-TZP) ceramics of grain size  $>0.5 \mu\text{m}$  showed substantial transformation. Surface grinding enhanced the resistance to degradation of Y-TZP but decreased that of  $t'$  materials. Even then, the  $t'$  materials exhibited better resistance to degradation than the Y-TZP ceramics. Excellent resistance of the  $t'$  materials to low-temperature aging despite a very large grain size and the opposite effect of grinding on phase stability are all explained on the basis of ferroelastic domain structure of these materials. [Key words: zirconia; yttria stabilized tetragonal polycrystals, aging, low temperature, microstructure, domains.]

### I. Introduction

ZIRCONIA-BASED materials, in particular yttria-doped tetragonal zirconia polycrystalline (Y-TZP) ceramics, exhibit very high strength and high toughness at room temperature. Strengths as high as 1.5 GPa are routinely achieved.<sup>1,2</sup> Many of these ceramics are typically very fine grained with a grain size less than 1  $\mu\text{m}$ . These materials are currently used in several applications including grinding media, die inserts for pharmaceuticals, scissors, knives, chemical pumps, roller guides, tweezers, adjusters, diesel engine parts, etc.<sup>2</sup> The high strength of these ceramics decreases with increasing temperature, typical of all transformation-toughened ceramics.<sup>3</sup> Despite this, the strength is higher than that of fully stabilized cubic phase and higher than many other oxides. As a result, there has been a considerable interest in Y-TZP for applications at higher temperatures. Because of the superior mechanical properties of Y-TZP ceramics compared with fully stabilized cubic zirconia, these materials also offer an obvious alternative to cubic zirconia as an electrolyte material. During an investigation of Y-TZP materials as

electrolytes, Kobayashi *et al.*<sup>4</sup> observed that these materials are sensitive to low-temperature aging, during which tetragonal  $\rightarrow$  monoclinic transformation occurs.

Over the past decade, several studies have documented the phenomenon of low-temperature aging in Y-TZP ceramics.<sup>1-4,30</sup> The general observations of these studies are summarized as follows:

(1) The strength of Y-TZP ceramics degrades when heated in a moist environment over a range of temperatures between  $100^\circ$  and  $500^\circ\text{C}$ .<sup>13</sup>

(2) The degradation is time dependent.<sup>4</sup>

(3) The extent of damage depends upon the composition and the grain size; materials with higher yttria content and smaller grain size are more resistant to degradation.<sup>1,4,6,15,17,18,20,21,53</sup>

(4) The rate of degradation is maximum at some intermediate temperature between  $100^\circ$  and  $500^\circ\text{C}$ , which depends upon the yttria content and the grain size.<sup>13,16,19</sup>

(5) The rate of degradation is much slower in dry, inert atmospheres.<sup>22</sup>

(6) Texture develops in both the monoclinic phase and the residual tetragonal phase.<sup>26-28</sup>

The degradation is associated with tetragonal  $\rightarrow$  monoclinic transition. Various hypotheses have been forwarded to explain this behavior, in particular the role of moisture.<sup>5,15,24,25</sup>

Most Y-TZP ceramics are fabricated by sintering at  $\leq 1600^\circ\text{C}$  in air. Under these sintering conditions for yttria content of interest, which is typically between 2.5 and 4 mol%, the equilibrium phase diagram shows the existence of a cubic plus tetragonal two-phase field.<sup>31</sup> Structurally identical but morphologically different tetragonal material can be produced by first heating the samples into the cubic single-phase field followed by rapid cooling to prevent diffusional processes. Under these conditions, the cubic phase undergoes a composition-invariant, displacive transition to the tetragonal phase.<sup>31-52</sup> This phase, which in principle is crystallographically identical with the regular tetragonal material, is commonly referred to as the  $t'$  phase. The  $t'$  phase is characterized by the existence of three variants<sup>33,36,38,40,41,45,47,48,50-52</sup> and the presence of antiphase boundaries (APBs).<sup>33,36,40,43,45-47,49-53</sup>

This  $t'$  phase is highly resistant to stress-induced transformation to the monoclinic phase.<sup>5,32,33,36,37,45,46,51,53-56</sup> Tetragonal single crystals studied by Ingel *et al.*<sup>54-56</sup> and Michel *et al.*<sup>46,51,52</sup> contained the  $t'$  phase. Recently, practical applications of the  $t'$  phase have emerged because it is this phase which is formed in plasma spray coatings used in engine interiors.<sup>32,57,58</sup> In such applications, the presence of moisture is unavoidable. It is thus of interest to know the aging behavior of  $t'$  zirconia. To the authors' knowledge, with the exception of some work on arc-melted Y-TZP ceramics by Noma *et al.*,<sup>25</sup> no information is available on the aging behavior of  $t'$ -zirconia ceramics. The objective of the present work was to investigate the low-temperature aging behavior of polycrystalline  $t'$ -zirconia and relate the properties to microstructure. Experiments were also done on Y-TZP ceramics for comparison and on polydomain single crystals to elucidate the role of morphology of the variants on aging.

F. F. Lange—contributing editor

Manuscript No. 197075. Received December 11, 1990; approved April 15, 1991.

Supported by DARPA through AFOSR under Contract No. F49620-89-C-0054; subcontract from Ceramtec, Inc., to the University of Utah.

\*Member, American Ceramic Society.

## II. Experimental Procedure

### (1) Sample Fabrication

Experimental work was performed on both polydomain single crystals as well as polycrystalline ceramics. Work on single crystals was confined to samples containing 3 mol% yttria which were purchased from a commercial vendor.\* The as-received crystals were oriented using a Laue back-reflection camera and cut such that the cut surfaces were orthogonal to  $\langle 111 \rangle$ ,  $\langle 110 \rangle$ , and  $\langle 100 \rangle$  on the basis of the pseudocubic symmetry. X-ray diffraction (XRD) revealed that the as-received samples contained some monoclinic phase. Apparently, the crystals must have cooled slowly during the growth process, thereby affecting the diffusion-controlled precipitation of the tetragonal phase ( $t$  phase). This  $t$  phase presumably transformed into the monoclinic phase during the cutting operation. To obtain homogeneous, single-phase  $t'$  phase, the cut samples were heated in a gas-fired furnace to  $\geq 2100^\circ\text{C}$  in air. After holding the samples at temperature for 15 min, the platen of the furnace was lowered to a region where the temperature was  $\leq 1100^\circ\text{C}$ . In this manner, the samples were cooled sufficiently rapidly to minimize diffusional precipitation of the  $t$  phase. Subsequently, the samples were furnace-cooled to room temperature. The samples were then ground, polished to remove the surface damage and/or texture caused by grinding, and core drilled to form disk-shaped samples for transmission optical and electron microscopic examination. The disk-shaped samples were further dimple ground to a thickness of  $\sim 30 \mu\text{m}$ . Samples were then examined using an optical microscope under polarized light in a transmission mode. Subsequently, the samples were ion milled to perforation for examination by scanning transmission electron microscopy (STEM).†

Polycrystalline samples were made of two compositions: 3 and 4 mol% yttria, using powders from a commercial source.‡ Bar-shaped samples were green formed by die pressing followed by isostatic pressing. Samples were then sintered in air over a range of temperatures between  $1450^\circ$  and  $1600^\circ\text{C}$  for 2 h. This sintering schedule was expected to yield two-phase samples containing the cubic and the tetragonal ( $t$ ) phases. To obtain a single-phase  $t'$  material, it was necessary to heat the samples in the stability region of the cubic phase. Therefore, the as-sintered samples were heated in a gas-fired furnace to  $\geq 2100^\circ\text{C}$  in air. The samples were maintained at temperature for 15 min followed by a cooling procedure similar to that used for the single crystals.

### (2) Low-Temperature Aging

Polycrystalline  $t'$  and  $t$  samples were prepared for aging studies after three surface treatments: (1) as-polished, (2) as-ground, and (3) ground and annealed at  $1200^\circ\text{C}$  for 1 h or ground and annealed at  $1450^\circ\text{C}$  for 30 min. After these treatments, the samples were placed in a furnace at  $275^\circ\text{C}$  in air for up to 1000 h. In the case of  $t'$ -zirconia, some of the samples were subjected to unidirectional compression testing prior to aging.

### (3) Mechanical Testing

Some of the  $t'$ -zirconia samples were polished and then subjected to a uniaxial compression up to a stress of 1.2 GPa with the stress axis parallel to the polished surface. These samples were then subjected to aging. Also, transmission electron microscopy (TEM) foils were prepared from the sample before and after compression testing. The objective was to determine the change in the domain structure, if any, caused by the compression testing.

### (4) X-ray Diffraction

XRD was primarily used for determining single-crystal orientation (Laue back reflection) and the type and the amount of phases present (diffractometer traces).§ Laue back-reflection patterns were obtained of single crystals oriented in the three orientations,  $\langle 111 \rangle$ ,  $\langle 110 \rangle$ , and  $\langle 100 \rangle$ . XRD traces were obtained on polycrystalline samples in the as-sintered, as-heat-treated, and as-aged states. The objective was to determine the types and the amounts of the various possible phases, namely, cubic, tetragonal, and monoclinic. The procedure given by Garvie and Nicholson¶ was used to determine the amount of the monoclinic phase.

### (5) Microstructural Examination

Dimple-ground single crystals were examined using transmission optical microscopy (TOM) with polarized light. The objective was to determine the crystallographic features of the twin/domain boundaries. TOM micrographs were also obtained of selected polycrystalline samples ( $t'$ ) after dimple grinding. After TOM, the samples were ion milled to perforation and were examined by STEM. The objective was to examine the domain structure in addition to exploring the relation between the TOM micrographs and TEM micrographs. Scanning electron microscopy (SEM)§§ was used to examine the microstructure of 4 mol% yttria samples sintered at  $1500^\circ$  and  $1600^\circ\text{C}$ . The samples, after heat treatment at  $2100^\circ\text{C}$ , were examined under an optical microscope. Aged samples were also examined in an optical microscope with Nomarsky interference contrast to determine the presence of the monoclinic phase.

## III. Results

### (1) Microstructure

Figures 1(a), (b), and (c) show TOM micrographs under polarized light of polydomain single crystals in  $\langle 100 \rangle$ ,  $\langle 110 \rangle$ , and  $\langle 111 \rangle$  orientations, respectively. The domain structure typical of ferroelastic materials is shown in these micrographs.

Based on group theoretic considerations, the domain or twin boundaries are expected to be of the  $\{101\}$  type in  $m3mF4/mmm$  species. The intersections of the domain or twin boundaries with the plane of observation are expected to make angles of  $90^\circ$  and  $45^\circ$  for  $\langle 100 \rangle$  orientation;  $70.5^\circ$  and  $54.7^\circ$  for  $\langle 110 \rangle$  orientation; and  $30^\circ$ ,  $60^\circ$ , and  $90^\circ$  for  $\langle 111 \rangle$  orientation. The domain width, as revealed by TEM, is less than  $0.1 \mu\text{m}$ , which cannot be delineated in optical microscopy. The traces observed in Fig. 1 are actually those of the intersections of colony boundaries with the plane of observation. As shown in Fig. 1, the angles between the traces are  $90^\circ$  for  $\langle 100 \rangle$ ,  $\sim 70^\circ$  for  $\langle 110 \rangle$ , and  $60^\circ$  for  $\langle 111 \rangle$ , in agreement with geometric predictions. Finally, Fig. 1(d) shows a TOM micrograph of a polycrystalline sample of 3 mol% yttria that was annealed at  $\sim 2100^\circ\text{C}$  for 15 min. Fig. 1(d) shows that the domain structure is similar to that in single crystals. The grain size is on the order of  $100 \mu\text{m}$ . The grain marked by an arrow appears to be in  $\langle 100 \rangle$  orientation. XRD indicates that the sample is fully tetragonal (no monoclinic) with  $c/a \approx 1.013$ .

Figures 2(a) to (c) show bright-field TEM micrographs for the three orientations. For the  $\langle 100 \rangle$  orientation (Fig. 2(a)), the  $45^\circ$  and  $90^\circ$  angles are shown in the micrograph. Also note that the domain width is typically less than  $0.1 \mu\text{m}$ . The distinction between domain and colony boundaries is shown in the micrograph (Fig. 2(a)). For the  $\langle 110 \rangle$  orientation (Fig. 2(b)), the morphology of the domain structure is quite different from that in the  $\langle 100 \rangle$  orientation. The characteristic angle between the domain/colony boundaries is  $\sim 70^\circ$ . For the  $\langle 111 \rangle$

\*Ceres Corp., Waltham, MA.

†Model JEM 200CX, JEOL, USA, Peabody, MA.

‡Tosoh Corp., Atlanta, GA.

§Model XRD-8000, Diano Corp., Woburn, MA.

¶Model S-450, Hitachi, Danbury, CT.

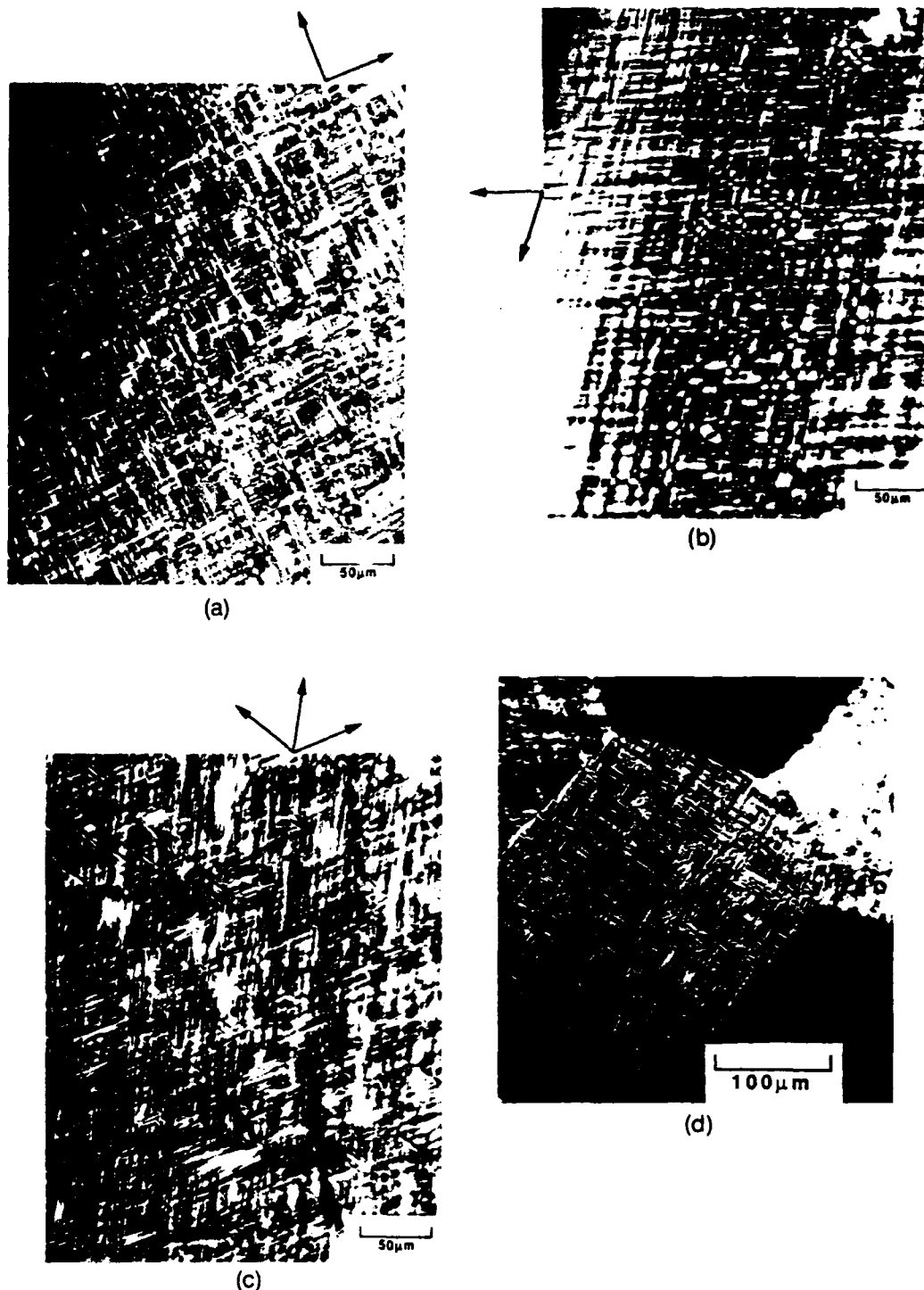


**Fig. 1.** TOM micrographs of a 3-mol%  $Y_2O_3$ -doped polydomain tetragonal zirconia single crystal after annealing at  $2100^\circ C$  for various orientations: (a) (100) (on the basis of pseudocubic) along the beam direction, (b) (110) along the beam direction, and (c) (111) along the beam direction. (d) TOM micrograph of a polycrystalline sample containing 3 mol%  $Y_2O_3$ , annealed at  $\sim 2100^\circ C$ , showing the presence of domains within each grain.

orientation (Fig. 2(c)), all three angles between the traces, namely  $30^\circ$ ,  $60^\circ$ , and  $90^\circ$ , are visible.

Figures 3(a) and (b) show SEM micrographs of samples containing 4 mol% yttria sintered in air for 2 h at  $1500^\circ C$  and  $1600^\circ C$ , respectively. At the sintering temperature, the 4 mol% yttria composition is in the cubic plus tetragonal two-phase field. The average grain size (which includes that for both cubic and tetragonal phases) is  $\sim 0.8$  and  $\sim 1.8$   $\mu m$  for samples sintered at  $1500^\circ C$  and  $1600^\circ C$ , respectively. Figure 3(c) shows an optical micrograph of a sample of 4 mol% yttria after annealing for 15 min at  $\sim 2100^\circ C$ . The average grain

size of this sample is  $\sim 100$   $\mu m$ . Despite the very large grain size, the sample is fully tetragonal with  $c/a \approx 1.01$  (with no monoclinic phase present) on the basis of XRD.

## (2) Low-Temperature Aging

Figure 4 shows the aging behavior (percent monoclinic phase formed) of samples of 4 mol% yttria composition as a function of time at  $275^\circ C$  in air for (a) samples sintered at  $1500^\circ C$  for 2 h, (b) samples sintered at  $1600^\circ C$  for 2 h, and (c) samples annealed at  $\sim 2100^\circ C$  for 15 min. All samples were polished prior to the aging treatment. After aging at  $275^\circ C$  for

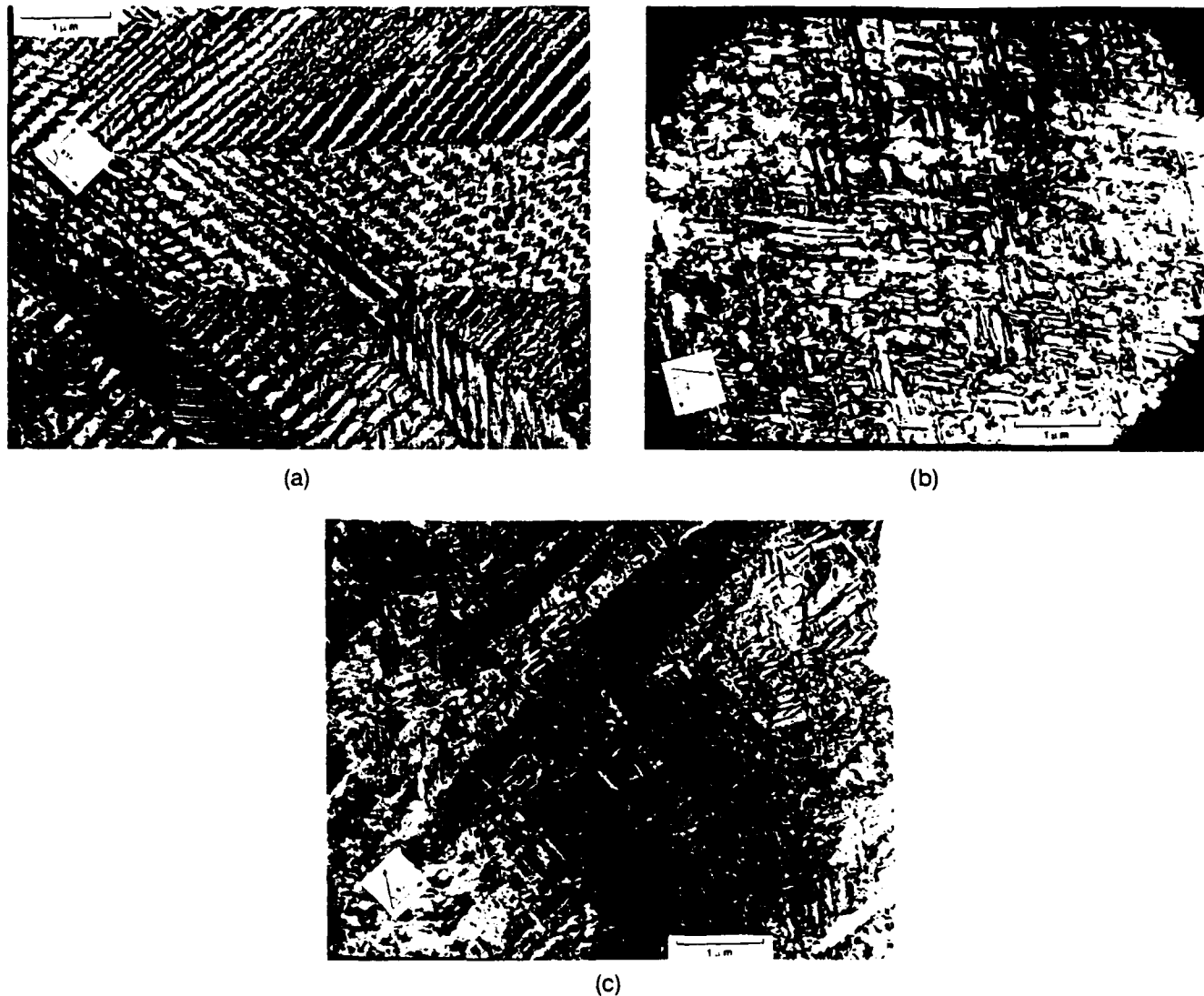


Fig. 2. Bright-field TEM micrographs of a 3-mol%  $Y_2O_3$ -doped polydomain tetragonal zirconia single crystal after annealing at  $2100^\circ C$  for various orientations: (a)  $\langle 100 \rangle$  along the beam direction, (b)  $\langle 110 \rangle$  along the beam direction, and (c)  $\langle 111 \rangle$  along the beam direction.

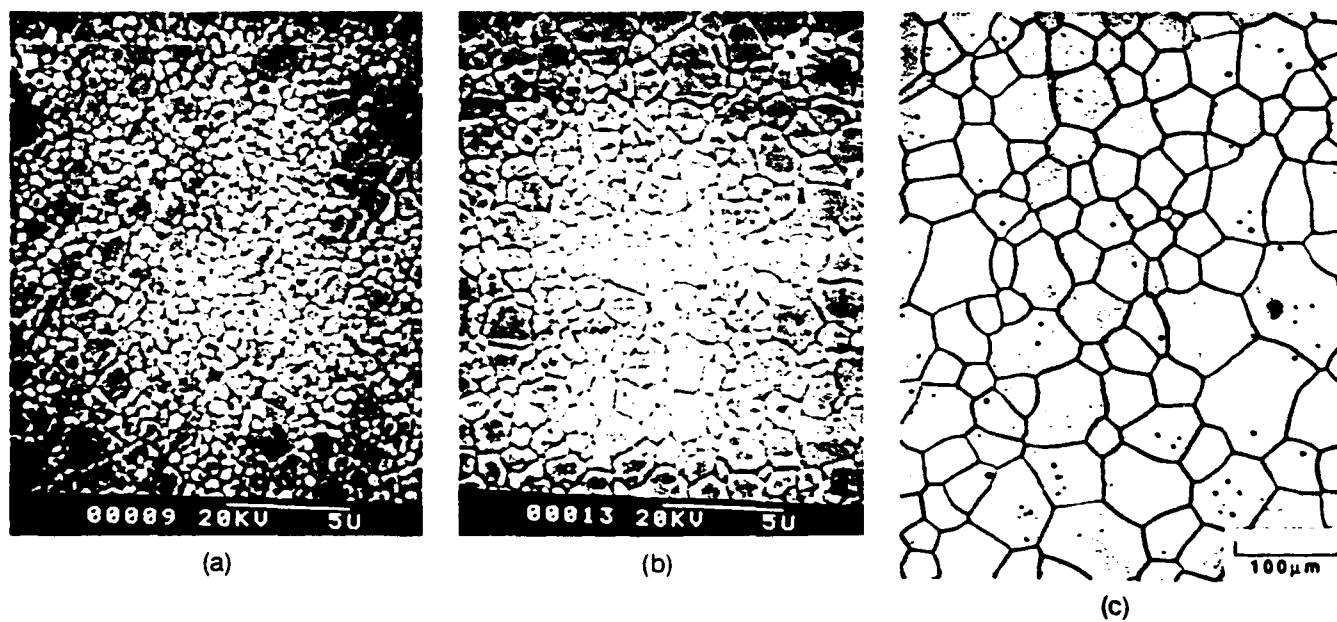


Fig. 3. SEM micrographs of 4-mol%  $Y_2O_3$ -doped polycrystalline samples: (a) sintered at  $1500^\circ C$  for 2 h and (b) sintered at  $1600^\circ C$  for 2 h. (c) Optical micrograph of a 4-mol%  $Y_2O_3$ -doped polycrystalline sample sintered at  $1450^\circ C$  followed by annealing at  $2100^\circ C$  for 15 min.

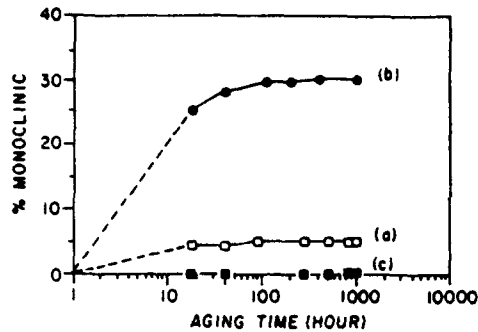


Fig. 4. Percent monoclinic phase versus aging time at 275°C in air of polycrystalline samples containing 4 mol%  $Y_2O_3$ : (a) polished surface of a sample sintered at 1500°C, (b) polished surface of a sample sintered at 1600°C, and (c) polished surface of a sample sintered at 1450°C followed by annealing at 2100°C for 15 min.

1000 h, samples sintered at 1600°C show more degradation (~30% monoclinic) compared with samples sintered at 1500°C (~5% monoclinic). The amount of monoclinic phase appears to reach an asymptotic value after about 100 h. The samples annealed at 2100°C, by contrast, show no evidence of the monoclinic phase even after aging for 1000 h, despite a very large grain size (~100  $\mu m$ ).

Figure 5 shows the effect of grinding on the aging behavior of the as-sintered samples containing 3 mol% yttria. The as-sintered (1450°C for 2 h) and polished samples exhibit a monoclinic phase content >60% after 40 h. The higher monoclinic phase content in these samples compared with the 4 mol% yttria samples (Fig. 4) is primarily due to the lower yttria content (i.e., higher tetragonal/cubic ratio in the as-sintered samples). Trace (b) shows the aging behavior of samples that were surface ground prior to the aging treatment. The maximum monoclinic phase content is ~45%, suggesting that the grinding treatment suppresses the aging phenomenon, in agreement with the work of Whalen *et al.*<sup>30</sup>

Figure 6 shows the aging behavior of polycrystalline  $t'$ -zirconia ceramics containing 3 mol% yttria subjected to three treatments: (a) as-polished, (b) polished and uniaxially compressed, and (c) surface ground. Note that, in the case of  $t'$ -zirconia, the polished surfaces show no monoclinic, even after 1000 h at 275°C in both 3- and 4-mol% yttria-containing samples. However, after surface grinding, the propensity to transformation actually increases (curve (c) in Fig. 6) even though the amount (~7%) of transformation after 1000 h at 275°C is considerably lower than that in Y-TZP ( $t$ ) ceramics. This behavior (the effect of surface grinding) is exactly opposite to that exhibited by Y-TZP ( $t$ ) ceramics shown in Fig. 5. A few polished  $t'$  samples were subjected to a uniaxial compressive stress of ~1.2 GPa. Prior work has shown that substantial domain switching occurs in compression beyond a stress of ~650 MPa.<sup>31</sup> After the compression testing, the

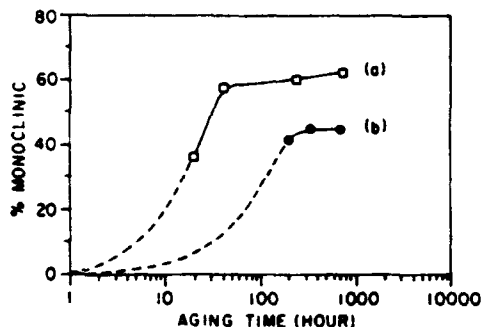


Fig. 5. Percent monoclinic phase versus aging time at 275°C in air of polycrystalline samples containing 3 mol%  $Y_2O_3$ : (a) polished surface and (b) machine-ground surface.

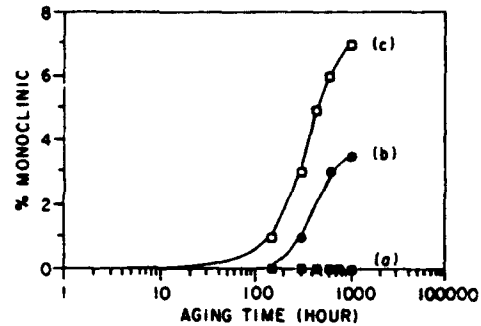


Fig. 6. Percent monoclinic phase versus aging time at 275°C in air of polycrystalline samples containing 3 mol%  $Y_2O_3$ , sintered at 1450°C followed by annealing at 2100°C for 15 min: (a) polished surface, (b) polished surface after compression test up to 1.2 GPa of stress parallel to the polished surface, and (c) machine-ground surface.

samples were aged. Figure 6 (curve (b)) shows that some monoclinic phase formed after ~200 h. Figure 7 shows Nomarsky interference contrast micrographs of as-polished, pristine sample after aging for 1000 h (Fig. 7(a)) and as-polished and compressed (1.2 GPa) samples after aging for 1000 h (Fig. 7(b)). A substantial amount of surface uplift exists in the compressed sample indicative of tetragonal  $\rightarrow$  monoclinic transformation. By contrast, no surface uplift seems to exist in the pristine, polished samples.

Figure 8 shows the effect of an annealing treatment on aging behavior of ground and compressed samples. Specifically, a few of the  $t'$ -zirconia samples were first surface ground and compressed at 1.2 GPa. Of these, some of the samples were annealed at 1200°C for 1 h. Both sets of samples were aged at 275°C for up to 1000 h. Curve (a) in Fig. 8 for the ground and compressed samples exhibits up to 17% monoclinic phase. This shows that the effects of grinding and compression testing are cumulative. No monoclinic phase is observed in samples that had been annealed at 1200°C after grinding and compression testing. This behavior is similar to that reported by Whalen *et al.*<sup>30</sup> in Y-TZP ( $t$ ) ceramics.

#### IV. Discussion

##### (1) Domain Structure

Michel *et al.*<sup>51</sup> were the first to note that the cubic  $\rightarrow$  tetragonal transition in zirconia is of the *paraelastic*  $\rightarrow$  ferroelastic type belonging to the Aizu species  $m3mF4/mmm$ .<sup>61,62</sup> The transition temperature for the cubic  $\rightarrow$  tetragonal displacive phase transformation is identified with the Curie temperature. According to the calculation by Sapriel,<sup>63</sup> the  $m3mF4/mmm$  species is characterized by domain boundaries of the  $\{110\}$  type on the basis of the pseudo-cubic symmetry and the presence of three variants which are mutually orthogonal (nearly) to each other. Heuer *et al.*<sup>33,36</sup> and Shibata *et al.*<sup>41,48</sup> have shown that the twin boundaries are of  $\{101\}$  type on the basis of tetragonal symmetry. Domain structure of a ferroelastic can be identified using TOM as has been recently shown in 123 superconductors.<sup>64</sup> The present results also show the applicability of this technique in zirconia.

For a foil with  $\langle 100 \rangle$  orientation, the twin or colony boundaries ( $\{110\}$ -type) intersect with the foil surface in such a way that the included angle between traces can be 45° or 90°. For  $\langle 101 \rangle$  orientation of the foil, the included angle between the traces is 54.7° and 70.5°. Finally, for  $\langle 111 \rangle$  orientation, the expected angles between traces are 30°, 60°, and 90°. These angles are given on the basis of a cubic symmetry but for the tetragonal structure, and thus are applicable for a  $c/a$  ratio approximately unity. Examination of Figs. 1(a) to 1(c) shows good agreement with predictions although traces with some included angles are not clearly visible, probably because

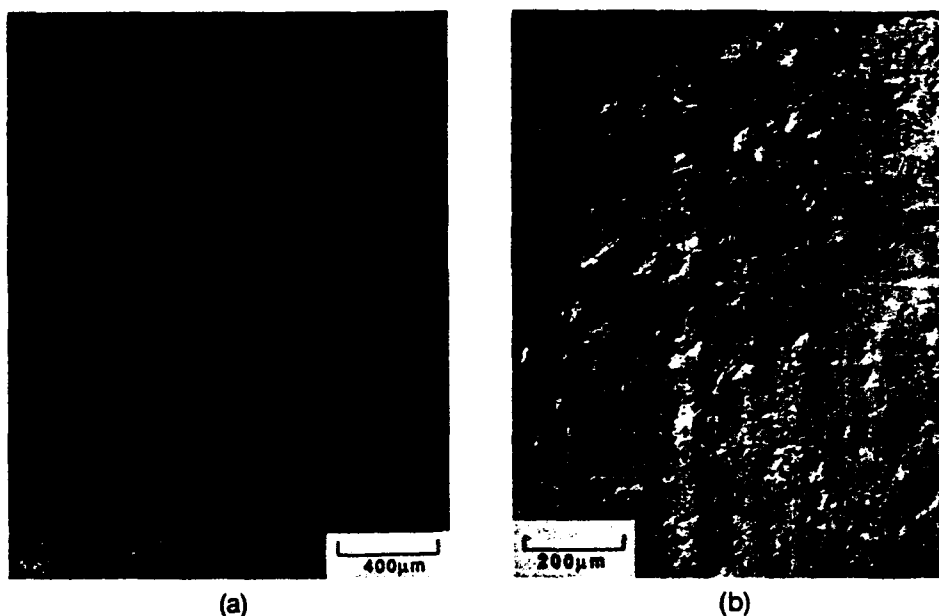


Fig. 7. (a) Nomarsky interference contrast micrograph of a polished surface of a polycrystalline sample containing 3 mol%  $Y_2O_3$  sintered at  $1450^\circ C$  followed by annealing at  $2100^\circ C$  for 15 min. (b) Nomarsky interference contrast micrograph of a polished surface after compression testing up to 1.2 GPa of stress of a polycrystalline sample containing 3 mol%  $Y_2O_3$  sintered at  $1450^\circ C$  and annealed at  $2100^\circ C$  for 15 min.

of a lack of contrast. Most importantly, all angles observed are in accord with expectation. Electron micrographs for the same orientations given in Figs. 2(a) to (c) also show the expected angular relationships.

Typical domain size in the present material is on the order of  $0.1 \mu m$  (width) although the grain size of the polycrystalline  $t'$ -zirconia containing 3 mol% yttria is about  $100 \mu m$ . The extreme stability of the  $t'$  material despite the large grain size must be related to the domain size. The domain boundaries are coherent, which makes the nucleation of the monoclinic phase difficult.<sup>45,45</sup> Because of this, the propensity to transformation may be dictated by domain size. This also suggests that processes which tend to increase the domain size would promote transformation. Noma *et al.*<sup>25</sup> and Heuer *et al.*<sup>45</sup> have shown that domain growth can be affected by annealing at elevated temperatures. Note, however, that annealing conditions are typically such that they correspond to the cubic plus tetragonal two-phase field suggesting the possibility of the occurrence of phase separation. Indeed, greater variation in composition has been noted by Noma *et al.*<sup>25</sup> in annealed samples. Also, Heuer *et al.*<sup>45</sup> have shown that phase separation does occur upon annealing. Domain growth in ferroelastic materials can also be caused by an externally applied stress of a magnitude greater than the coercive stress. In

$t'$ -zirconia, the work of Srinivasan *et al.*<sup>66</sup> and Jue and Virkar<sup>60</sup> clearly shows that domain switching can be caused by an applied stress. The occurrence of domain switching is concomitant with the enlargement of some of the domains at the expense of the others. Thus, it is expected that externally applied stress causes some of the domains to grow, and their stability is affected. Figure 9(a) shows a typical domain structure of a 3-mol%-yttria-doped polycrystalline  $t'$ -zirconia ceramic used in the present study. The domain width is  $\sim 70$  nm. The grain orientation is along (110). Figure 9(b) shows the domain structure of the same sample after the sample was subjected to a compressive stress greater than 1.2 GPa. XRD shows the occurrence of domain switching. The domain structure in Fig. 9(b) shows that alternate domains have grown at the expense of the neighboring ones. Note that the light ones (which presumably have the same orientation) have grown at the expense of the dark ones. The widths of the domains in Fig. 9(b) after compression testing are  $\sim 120$  and  $\sim 20$  nm, respectively. Figure 9(c) shows a schematic of a probable process in which the domains with  $c$  axes along the direction of the compressive stress decrease in width and those with  $c$  axes perpendicular to the compressive stress increase in width. As discussed in the following paragraphs, the domain size has a direct effect on the aging behavior and the stability of the tetragonal phase.

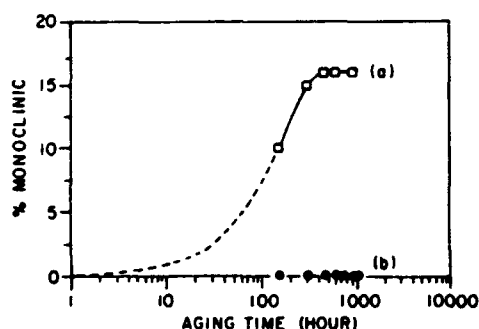


Fig. 8. Percent monoclinic phase versus aging time at  $275^\circ C$  in air of polycrystalline samples containing 3 mol%  $Y_2O_3$  sintered at  $1450^\circ C$  followed by annealing at  $2100^\circ C/15$  min: (a) machine-ground surface after compression testing up to 1.2 GPa of stress and (b) machine-ground surface after compression testing up to 1.2 GPa of stress followed by annealing at  $1200^\circ C$  for 1 h.

## (2) Low-Temperature Aging

Several studies have focused on the mechanisms of degradation by low-temperature aging in Y-TZP ceramics.<sup>5,6,11,25</sup> With the exception of some work by Noma *et al.*<sup>25</sup> on arc-melted samples, however, no work has been reported on  $t'$ -zirconia. The greater amount of transformation in Y-TZP ceramics (Fig. 4) sintered at  $1600^\circ C$  compared with those sintered at  $1500^\circ C$  is primarily related to differences in grain size (1.8 versus  $0.8 \mu m$ ). In  $t'$ -zirconia, which shows no monoclinic phase although the grain size is  $\sim 100 \mu m$ , the domain width is less than  $0.1 \mu m$ . The excellent stability of the  $t'$  zirconia must thus be related to the domain size.

Figures 5 and 6 show that the effect of grinding, as far as the propensity to transformation is concerned, is opposite in Y-TZP ceramics and  $t'$ -zirconia ceramics. This effect can be explained in terms of the domain size. In Y-TZP materials sintered in the stability range of the tetragonal plus cubic two-phase field, the entire tetragonal grain is a single domain.

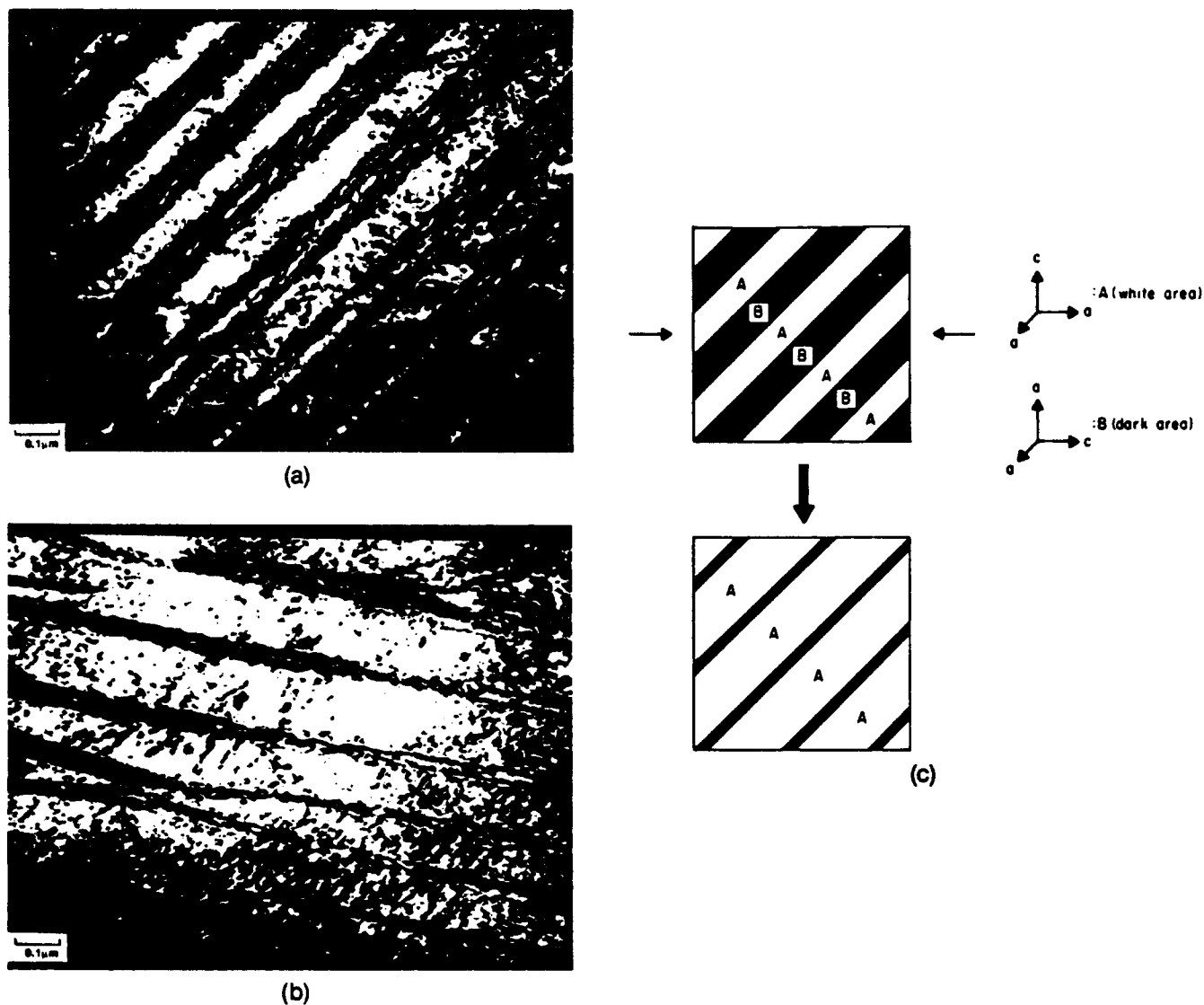


Fig. 9. Bright-field TEM micrographs of a 3-mol%- $\text{Y}_2\text{O}_3$ -doped polycrystalline sample oriented with (110) along the beam direction: (a) after annealing at 2100°C. (b) after annealing at 2100°C followed by compression test up to 1.2 GPa of stress, and (c) schematic showing thickening of some domains at the expense of the others. Domains with  $c$  axes along the compression stress axis decrease in width while those with  $c$  axes perpendicular to the compressive stress axis increase in width.

When the surface is ground, previous work shows that a substantial amount of switching can be induced by the grinding.<sup>6,7</sup> However, to switch an entire grain of 0.5  $\mu\text{m}$  or larger is expected to be energetically difficult. Based on XRD line-broadening work, it has been suggested that part of the grains may switch.<sup>8</sup> Recent work by Swain and Hannink<sup>9</sup> shows that tetragonal variants are formed by grinding in previously monodomain grains (in ceria-doped TZP). The net effect of the grinding process in Y-TZP ceramics must then be such as to decrease the domain size. Figure 10 shows a schematic of a probable domain formation process. The enhanced resistance to low-temperature aging in ground materials can be rationalized in terms of a reduction in the domain size. By contrast, in  $t'$  materials which already contain domains of width less than 0.1  $\mu\text{m}$ , the process of grinding would switch some of the domains at the expense of others, thereby in effect increasing the size of some of the domains. Since the stress required to move an already existent domain wall is known to be lower than that required to form a new domain, the process of stress accommodation during grinding is expected to occur by domain wall motion and not by domain nucleation. Recent work by Chan *et al.*<sup>71</sup> shows the occurrence of domain growth near an indent. The net effect is that there would be some domains of size larger than the original ones. These

larger domains would be more prone to transformation in the subsequent aging process. Figure 9(c) shows a schematic of the probable domain growth process. The experimental results given in Figs. 5 and 6 are in accord with this analysis. Note that the extent of degradation in ground  $t'$  samples is still much less than that in ground Y-TZP materials. Application of uniaxial tension or compression to a  $t'$  material also causes domain switching and thus growth in some of the domains. The fact that samples subjected to a uniaxial compression prior to an aging treatment exhibit a greater amount of the monoclinic phase during low-temperature aging in comparison to the as-polished samples is also in accord with the preceding analysis.

Whalen *et al.*<sup>30</sup> were the first to report recrystallization behavior in surface-ground Y-TZP ceramics subjected to an annealing treatment. These surface-recrystallized ceramics were also shown to exhibit a greater resistance to low-temperature degradation. Gasdaska *et al.*<sup>71</sup> further showed that grinding followed by annealing of monoclinic hafnia also caused recrystallization. Since no phase transformation occurred in monoclinic hafnia over the range of temperatures in their experiments, it appeared that the recrystallization was related to deformation induced during grinding and not to transformation. In the present work, it was observed that samples sur-

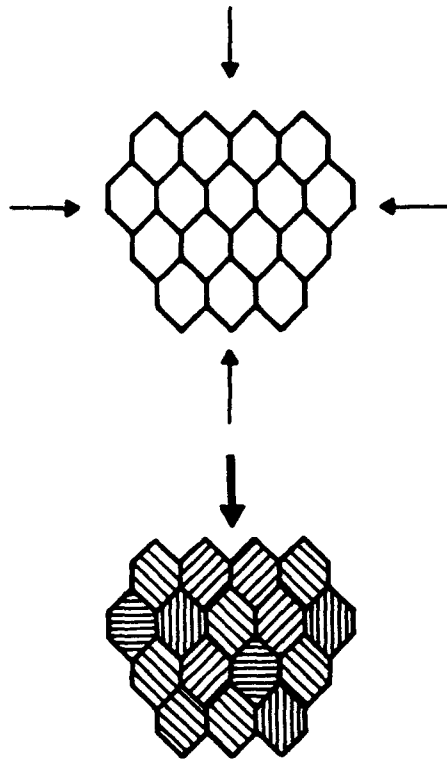


Fig. 10. Schematic showing domain formation process under stress. Note that a grain can be subdivided into several small domains.

face ground, compressed, and annealed at 1200°C for 1 h were immune to low-temperature degradation. Samples were examined by SEM. However, the resolution was not adequate enough to determine if recrystallization had occurred. To explain this behavior, *t'*-zirconia samples containing 3 mol% yttria with a grain size of  $\sim 100 \mu\text{m}$  were surface ground, followed by annealing at 1450°C for 30 min. SEM examination showed that very fine grains ( $\sim 0.3 \mu\text{m}$ ) had formed by



Fig. 11. SEM micrograph of a sample containing 3 mol%  $\text{Y}_2\text{O}_3$  subjected to the following treatments: (1) sample sintered at 1450°C followed by annealing at 2100°C for 15 min and (2) surface ground and heated at 1450°C for 30 min. Note that the original grain size is  $\sim 100 \mu\text{m}$  (Fig. 3(c)), while the recrystallized grains have a size less than  $0.5 \mu\text{m}$ .

recrystallization as shown in Fig. 11. Several samples, after this treatment, were subjected to a low-temperature degradation test at 275°C for up to 1000 h. No monoclinic phase formed. This suggests that the enhanced stability of the ground and annealed *t'*-zirconia can be explained by recrystallization, in agreement with the work of Whalen *et al.*<sup>30</sup> in regular, tetragonal zirconia (Y-TZP). On the basis of these observations, it appears that the increased resistance to low-temperature degradation of materials annealed at 1200°C after surface grinding is probably due to recrystallization. Presumably, the recrystallized grain size is too small to be resolved by SEM in samples annealed at 1200°C.

## V. Conclusions

Based on the present work, the following conclusions are drawn:

(1) Ferroelastic domain structure of polycrystalline *t'*-zirconia ceramics and of tetragonal zirconia polydomain single crystals can be characterized by transmission optical microscopy (TOM) and by transmission electron microscopy (TEM). The orientation relationships between domain/colony boundaries are in agreement with the predictions of group theory.

(2) *t'*-zirconia ceramics exhibit exceptional resistance to low-temperature degradation despite a very large grain size. By contrast, conventional, fine-grained Y-TZP ceramics of grain size  $>0.5 \mu\text{m}$  readily degrade. These results demonstrate that the critical parameter which determines phase stability in *t'*-zirconia ceramics is the domain size and not the grain size.

(3) Surface grinding enhances the resistance to degradation of Y-TZP ceramics but decreases that of *t'*-zirconia ceramics. This behavior can be explained on the basis of ferroelastic domain structure. Specifically, in *t'*-zirconia, surface grinding can enhance the domain size of some of the domains, thus decreasing phase stability. On the other hand, surface grinding of Y-TZP ceramics creates domains of a size smaller than the original grain size, thereby enhancing phase stability. Even after surface grinding, however, the *t'*-zirconia ceramics still exhibit greater resistance to degradation in comparison to Y-TZP ceramics.

(4) Annealing of surface-ground *t'*-zirconia ceramics at high temperatures ( $\sim 1450^\circ\text{C}$ ) leads to recrystallization similar to that observed in Y-TZP ceramics.

**Acknowledgment:** Experimental assistance of Mr. Karun Mehta and Mr. Abhijit Abhyankar is acknowledged.

## References

- <sup>1</sup>K. Tsukuma, Y. Kubota, and T. Tsukidate, "Thermal and Mechanical Properties of  $\text{Y}_2\text{O}_3$ -Stabilized Tetragonal Zirconia Polycrystals", pp. 382-90 in *Advances in Ceramics*, Vol. 12. *Science and Technology of Zirconia II*. Edited by N. Claussen, M. Rühle, and A. H. Heuer. American Ceramic Society, Columbus, OH, 1984.
- <sup>2</sup>T. Masaki and K. Sinjo, "Mechanical Properties of Highly Toughened  $\text{ZrO}_2\text{-Y}_2\text{O}_3$ ," *Ceram. Int.*, **13**, 109-12 (1987).
- <sup>3</sup>F. F. Lange, "Transformation Toughening—Effect of Temperature and Alloy on Fracture Toughness," *J. Mater. Sci.*, **17**, 255-62 (1982).
- <sup>4</sup>K. Kobayashi, H. Kuwajima, and T. Masaki, "Phase Change and Mechanical Properties of  $\text{ZrO}_2\text{-Y}_2\text{O}_3$  Solid Electrolyte After Ageing," *Solid State Ionics*, **34**, 489-95 (1981).
- <sup>5</sup>M. Yoshimura, "Phase Stability of Zirconia," *Am. Ceram. Soc. Bull.*, **67** [12] 1950-55 (1988).
- <sup>6</sup>F. F. Lange, G. L. Dunlop, and B. I. Davis, "Degradation During Aging of Transformation-Toughened  $\text{ZrO}_2\text{-Y}_2\text{O}_3$  Material at 250°C," *J. Am. Ceram. Soc.*, **69** [3] 237-40 (1986).
- <sup>7</sup>M. Yoshimura, T. Noma, K. Kawabata, and S. Sōmiya, "Role of  $\text{H}_2\text{O}$  on the Degradation Process of Y-TZP," *J. Mater. Sci. Lett.*, **6** [4] 465-67 (1987).
- <sup>8</sup>T. Sato and M. Shimada, "Transformation of Yttria-Doped Tetragonal  $\text{ZrO}_2$  Polycrystals by Annealing in Water," *J. Am. Ceram. Soc.*, **68** [6] 356-59 (1985).
- <sup>9</sup>Y. Murase and E. Kato, "Role of Water Vapor in Crystallite Growth and Tetragonal-Monoclinic Phase Transformation of  $\text{ZrO}_2$ ," *J. Am. Ceram. Soc.*, **66** [3] 196-200 (1983).
- <sup>10</sup>T. Sato, S. Ohtaki, T. Endo, and M. Shimada, "Transformation of Yttria-

- Doped Tetragonal  $ZrO_2$  Polycrystals by Annealing under Controlled Humidity Conditions." *J. Am. Ceram. Soc.*, **68** [12] C-320-C-322 (1985).
- <sup>11</sup>M. Yoshimura, T. Noma, K. Kawabata, and S. Sōmiya. "The Effects of High-Temperature and High-Pressure Water on the Low-Temperature Degradation Behavior of Y-TZP." *J. Ceram. Soc. Jpn. Int. Ed.*, **96**, 263-68 (1989).
- <sup>12</sup>S.-Y. Chen and H.-Y. Lu. "Sintering of 3 mol%  $Y_2O_3$ -TZP and Its Fracture after Ageing Treatment." *J. Mater. Sci.*, **23**, 1195-200 (1988).
- <sup>13</sup>S.-Y. Chen and H.-Y. Lu. "Low-Temperature Ageing Map for 3 mol%  $Y_2O_3$ - $ZrO_2$ ." *J. Mater. Sci.*, **24**, 453-56 (1989).
- <sup>14</sup>K. Nakajima, K. Kobayashi, and Y. Murata. "Phase Stability of Y-PSZ in Aqueous Solutions"; pp. 399-407 in *Advances in Ceramics*, Vol. 12, *Science and Technology of Zirconia II*, Edited by N. Claussen, M. Rühle, and A. H. Heuer. American Ceramic Society, Columbus, OH, 1984.
- <sup>15</sup>A. J. A. Winnubst and A. J. Burggraaf. "The Aging Behavior of Ultrafine-Grained Y-TZP in Hot Water"; pp. 39-47 in *Advances in Ceramics*, Vol. 24, *Science and Technology of Zirconia III*, Edited by S. Sōmiya, N. Yamamoto, and H. Yanagida. American Ceramic Society, Westerville, OH, 1988.
- <sup>16</sup>T. Sato, S. Ohtaki, and M. Shimada. "Transformation of Ytria Partially Stabilized Zirconia by Low-Temperature Annealing in Air." *J. Mater. Sci.*, **20**, 1466-70 (1985).
- <sup>17</sup>W. Watanabe, S. Iio, and I. Fukuura. "Aging Behavior of Y-TZP"; pp. 391-98 in *Advances in Ceramics*, Vol. 12, *Science and Technology of Zirconia II*, Edited by N. Claussen, M. Rühle, and A. H. Heuer. American Ceramic Society, Columbus, OH, 1984.
- <sup>18</sup>M. Matsui, T. Soma, and I. Oda. "Effect of Microstructure on the Strength of Y-TZP Component"; pp. 371-78 in *Advances in Ceramics*, Vol. 12, *Science and Technology of Zirconia II*, Edited by N. Claussen, M. Rühle, and A. H. Heuer. American Ceramic Society, Columbus, OH, 1984.
- <sup>19</sup>T. Sato and M. Shimada. "Crystalline Phase Change in Ytria-Partially Stabilized Zirconia by Low-Temperature Annealing." *J. Am. Ceram. Soc.*, **67** [10] C-212-C-213 (1984).
- <sup>20</sup>H. Schubert and G. Petzow. "Microstructural Investigations on the Stability of Ytria-Stabilized Tetragonal Zirconia"; pp. 21-27 in *Advances in Ceramics*, Vol. 24, *Science and Technology of Zirconia III*, Edited by S. Sōmiya, N. Yamamoto, and H. Yanagida. American Ceramic Society, Westerville, OH, 1988.
- <sup>21</sup>T. Sato, S. Ohtaki, T. Endo, and M. Shimada. "Improvement of the Thermal Stability of Ytria-Doped Tetragonal Zirconia Polycrystals by Alloying with Various Oxides"; pp. 29-37 in *Advances in Ceramics*, Vol. 24, *Science and Technology of Zirconia III*, Edited by S. Sōmiya, N. Yamamoto, and H. Yanagida. American Ceramic Society, Westerville, OH, 1988.
- <sup>22</sup>S. Iio, W. Watanabe, K. Kuroda, H. Saka, and I. Imura. "Tetragonal-to-Monoclinic Transformation in Y-TZP During Low-Temperature Aging and its Restraint by Coating"; pp. 49-54 in *Advances in Ceramics*, Vol. 24, *Science and Technology of Zirconia III*, Edited by S. Sōmiya, N. Yamamoto, and H. Yanagida. American Ceramic Society, Westerville, OH, 1988.
- <sup>23</sup>T. Arai, T. Yamamoto, and T. Tsuji. "Transition-Free Zirconia Ceramics"; pp. 517-22 in *Advances in Ceramics*, Vol. 24, *Science and Technology of Zirconia III*, Edited by S. Sōmiya, N. Yamamoto, and H. Yanagida. American Ceramic Society, Westerville, OH, 1988.
- <sup>24</sup>T. Sato, S. Ohtaki, T. Endo, and M. Shimada. "Changes in Crystalline Phase and Microstructure on the Surface of Ytria-Doped Tetragonal Zirconia Polycrystals 'Y-TZP' by Annealing in Humid Conditions"; pp. 501-508 in *Advances in Ceramics*, Vol. 24, *Science and Technology of Zirconia III*, Edited by S. Sōmiya, N. Yamamoto, and H. Yanagida. American Ceramic Society, Westerville, OH, 1988.
- <sup>25</sup>T. Noma, M. Yoshimura, and S. Sōmiya. "Effect of Cooling Rate on the Properties and the Nanostructures of Y-TZP." Report of the Research Laboratory of Engineering Materials, Tokyo Institute of Technology, Tokyo, Japan, No. 13, pp. 47-58, 1988.
- <sup>26</sup>M. Matsui, T. Soma, and I. Oda. "Stress-Induced Transformation and Plastic Deformation for  $Y_2O_3$ -Containing Tetragonal Zirconia Polycrystals." *J. Am. Ceram. Soc.*, **69** [3] 198-202 (1986).
- <sup>27</sup>F. Reidinger and P. J. Whalen. "Texture on Ground, Fractured, and Aged Y-TZP Surfaces." *Mater. Res. Soc. Symp. Proc.*, **78**, 25-33 (1987).
- <sup>28</sup>J. Wang and R. Stevens. "Preferred  $ZrO_2(l) \rightarrow ZrO_2(m)$  Transformation on the Aged Surface of TZP Ceramics." *J. Mater. Sci. Lett.*, **8**, 1195-98 (1989).
- <sup>29</sup>J. Wang and R. Stevens. "Surface Toughening of TZP Ceramics by Low-Temperature Ageing." *Ceram. Int.*, **15**, 15-21 (1989).
- <sup>30</sup>P. J. Whalen, F. Reidinger, and P. F. Antrim. "Prevention of Low-Temperature Surface Transformation by Surface Recrystallization in Ytria-Doped Tetragonal Zirconia." *J. Am. Ceram. Soc.*, **72** [2] 319-21 (1989).
- <sup>31</sup>H. G. Scott. "Phase Relationships in the Zirconia-Ytria System." *J. Mater. Sci.*, **10**, 1527-35 (1975).
- <sup>32</sup>R. A. Miller, J. L. Smialek, and R. G. Garlick. "Phase Stability in Plasma-Sprayed Partially Stabilized Zirconia-Ytria"; pp. 241-53 in *Advances in Ceramics*, Vol. 3, *Science and Technology of Zirconia*, Edited by A. H. Heuer and L. W. Hobbs. American Ceramic Society, Columbus, OH, 1981.
- <sup>33</sup>A. H. Heuer, R. Chaim, and V. Lanteri. "The Displacive Cubic  $\rightarrow$  Tetragonal Transformation in  $ZrO_2$  Alloys." *Acta Metall.*, **35** [3] 661-66 (1987).
- <sup>34</sup>M. Yoshimura, M. Yashima, T. Noma, and S. Sōmiya. "Formation of Diffusionlessly Transformed Tetragonal Phases by Rapid Quenching of Melts in  $ZrO_2$ - $RO_2$  Systems (R = Rare Earths)." *J. Mater. Sci.*, **25**, 2011-16 (1990).
- <sup>35</sup>M. Yoshimura, M. Yashima, T. Noma, and S. Sōmiya. "Formation and Phase Stability of Tetragonal Phase in Rapidly Quenched  $ZrO_2$ - $ErO_{1.5}$ ." *Jpn. J. Appl. Phys.*, **27** [9] L1757-L1760 (1988).
- <sup>36</sup>R. Chaim, M. Rühle, and A. H. Heuer. "Microstructural Evolution in a  $ZrO_2$ -12 wt%  $Y_2O_3$  Ceramic." *J. Am. Ceram. Soc.*, **68** [8] 427-31 (1985).
- <sup>37</sup>T. Sakuma, Y. Yoshizawa, and H. Suto. "The Microstructure and Mechanical Properties of Ytria-Stabilized Zirconia Prepared by Arc-Melting." *J. Mater. Sci.*, **20**, 2399-407 (1985).
- <sup>38</sup>M. Shibata, M. Kato, H. Seto, T. Noma, M. Yoshimura, and S. Sōmiya. "The Effects of External Stress on the Cubic-Tetragonal Transformation in Rapidly Quenched  $ZrO_2$ - $Y_2O_3$ ." *J. Mater. Sci.*, **22**, 1432-36 (1987).
- <sup>39</sup>T. Noma, M. Yoshimura, S. Sōmiya, S. Kato, M. Yanagisawa, and H. Seto. "Formation of Diffusionlessly Transformed Tetragonal Phases in Rapid Quenching of  $ZrO_2$ - $Y_2O_3$  Melts." *J. Mater. Sci.*, **23**, 2689-92 (1988).
- <sup>40</sup>T. Sakuma. "Development of Domain Structure Associated with the Diffusionless Cubic-to-Tetragonal Transition in  $ZrO_2$ - $Y_2O_3$  Alloys." *J. Mater. Sci.*, **22**, 4470-75 (1987).
- <sup>41</sup>M. Shibata-Yanagisawa, M. Kato, H. Seto, N. Ishizawa, N. Mizutani, and M. Kato. "Crystallographic Analysis of the Cubic-to-Tetragonal Phase Transformation in the  $ZrO_2$ - $Y_2O_3$  System." *J. Am. Ceram. Soc.*, **70** [7] 503-509 (1987).
- <sup>42</sup>K. Negita. "Lattice Vibrations and Cubic-to-Tetragonal Phase Transition in  $ZrO_2$ ." *Acta Metall.*, **37** [1] 313-17 (1989).
- <sup>43</sup>A. H. Heuer and M. Rühle. "Phase Transformations in  $ZrO_2$ -Containing Ceramics: The Instability of c- $ZrO_2$  and the Resulting Diffusion-Controlled Reactions"; pp. 1-13 in *Advances in Ceramics*, Vol. 12, *Science and Technology of Zirconia II*, Edited by N. Claussen, M. Rühle, and A. H. Heuer. American Ceramic Society, Columbus, OH, 1984.
- <sup>44</sup>C. A. Andersson, J. Gregg, Jr., and T. K. Gupta. "Diffusionless Transformations in Zirconia Alloys"; pp. 78-85 in *Advances in Ceramics*, Vol. 12, *Science and Technology of Zirconia II*, Edited by N. Claussen, M. Rühle, and A. H. Heuer. American Ceramic Society, Columbus, OH, 1984.
- <sup>45</sup>V. Lanteri, A. H. Heuer, and T. E. Mitchell. "Tetragonal Phase in the System  $ZrO_2$ - $Y_2O_3$ "; pp. 118-30 in *Advances in Ceramics*, Vol. 12, *Science and Technology of Zirconia II*, Edited by N. Claussen, M. Rühle, and A. H. Heuer. American Ceramic Society, Columbus, OH, 1984.
- <sup>46</sup>D. Michel, L. Mazerolles, and M. Perez y Jorba. "Polydomain Crystals of Single-Phase Tetragonal  $ZrO_2$ : Structure, Microstructure, and Fracture Toughness"; pp. 131-38 in *Advances in Ceramics*, Vol. 12, *Science and Technology of Zirconia II*, Edited by N. Claussen, M. Rühle, and A. H. Heuer. American Ceramic Society, Columbus, OH, 1984.
- <sup>47</sup>A. H. Heuer, R. Chaim, and V. Lanteri. "Review Article: Phase Transformations and Microstructural Characterization of Alloys in the System  $Y_2O_3$ - $ZrO_2$ "; pp. 3-20 in *Advances in Ceramics*, Vol. 24, *Science and Technology of Zirconia III*, Edited by S. Sōmiya, N. Yamamoto, and H. Yanagida. American Ceramic Society, Westerville, OH, 1988.
- <sup>48</sup>M. Shibata, H. Seto, M. Kato, T. Noma, M. Yoshimura, S. Sōmiya, N. Ishizawa, M. Mizutani, and M. Kato. "The Morphology and Crystallography of Cubic-to-Tetragonal Phase Transformations in  $ZrO_2$ - $Y_2O_3$ "; pp. 523-30 in *Advances in Ceramics*, Vol. 24, *Science and Technology of Zirconia III*, Edited by S. Sōmiya, N. Yamamoto, and H. Yanagida. American Ceramic Society, Westerville, OH, 1988.
- <sup>49</sup>T. Sakuma and H. Suto. "Cubic-Tetragonal Phase Separations in Y-PSZ"; pp. 531-35 in *Advances in Ceramics*, Vol. 24, *Science and Technology of Zirconia III*, Edited by S. Sōmiya, N. Yamamoto, and H. Yanagida. American Ceramic Society, Westerville, OH, 1988.
- <sup>50</sup>M. Sugiyama and H. Kubo. "Microstructure of the Cubic and Tetragonal Phases in a  $ZrO_2$ - $Y_2O_3$  Ceramic System"; pp. 965-73 in *Advances in Ceramics*, Vol. 24, *Science and Technology of Zirconia III*, Edited by S. Sōmiya, N. Yamamoto, and H. Yanagida. American Ceramic Society, Westerville, OH, 1988.
- <sup>51</sup>D. Michel, L. Mazerolles, and M. Perez y Jorba. "Fracture of Metastable Tetragonal Zirconia Crystals." *J. Mater. Sci.*, **18**, 2618-28 (1983).
- <sup>52</sup>D. Michel, L. Mazerolles, and R. Portier. "Electron Microscopy Observation of the Domain Boundaries Generated by the Cubic  $\rightarrow$  Tetragonal Transition of Stabilized Zirconia." *Sud. Inorg. Chem.*, **3**, 809-12 (1982).
- <sup>53</sup>B. A. Bender, R. W. Rice, and J. R. Spann. "Precipitate Character in Laser-Melted PSZ." *J. Mater. Sci. Lett.*, **4**, 1331-36 (1985).
- <sup>54</sup>R. P. Ingel, R. W. Rice, and D. Lewis. "Room-Temperature Strength and Fracture of  $ZrO_2$ - $Y_2O_3$  Single Crystals." *J. Am. Ceram. Soc.*, **65** [7] C-108-C-109 (1982).
- <sup>55</sup>R. P. Ingel, D. Lewis, B. A. Bender, and R. W. Rice. "Temperature Dependence of Strength and Fracture Toughness of  $ZrO_2$  Single Crystals." *J. Am. Ceram. Soc.*, **65** [9] C-150-C-152 (1982).
- <sup>56</sup>R. P. Ingel, D. Lewis, B. A. Bender, and R. W. Rice. "Physical, Microstructural, and Thermomechanical Properties of  $ZrO_2$  Single Crystals"; pp. 408-14 in *Advances in Ceramics*, Vol. 12, *Science and Technology of Zirconia II*, Edited by N. Claussen, M. Rühle, and A. H. Heuer. American Ceramic Society, Columbus, OH, 1984.
- <sup>57</sup>P. Boch, P. Fauchais, D. Lombard, B. Rogeaux, and M. Vardelle. "Plasma-Sprayed Zirconia Coating"; pp. 488-502 in *Advances in Ceramics*, Vol. 12, *Science and Technology of Zirconia II*, Edited by N. Claussen, M. Rühle, and A. H. Heuer. American Ceramic Society, Columbus, OH, 1984.
- <sup>58</sup>D. S. Suhr, T. E. Mitchell, and R. J. Keller. "Microstructure and Durability of Zirconia Thermal Barrier Coating"; pp. 503-17 in *Advances in Ceramics*, Vol. 12, *Science and Technology of Zirconia II*, Edited by N. Claussen, M. Rühle, and A. H. Heuer. American Ceramic Society, Columbus, OH, 1984.
- <sup>59</sup>R. C. Garvie and P. S. Nicholson. "Phase Analysis in Zirconia Systems." *J. Am. Ceram. Soc.*, **55** [6] 303-305 (1972).

- <sup>40</sup>J. F. Jue and A. V. Virkar, "Fabrication Microstructural Characterization and Mechanical Properties of Polycrystalline  $t'$ -Zirconia," *J. Am. Ceram. Soc.*, **73** [12] 3650-57 (1990).
- <sup>41</sup>K. Aizu, "Possible Species of 'Ferroelastic' Crystals and of Simultaneously Ferroelectric and Ferroelastic Crystals," *J. Phys. Soc. Jpn.*, **27**, 387-96 (1969).
- <sup>42</sup>K. Aizu, "Possible Species of Ferromagnetic, Ferroelectric, and Ferroelastic Crystals," *Phys. Rev. B: Solid State*, **2** [3] 754-72 (1970).
- <sup>43</sup>J. Sapriel, "Domain-Wall Orientations in Ferroelastics," *Phys. Rev. B: Solid State*, **12** [11] 5128-40 (1975).
- <sup>44</sup>H. Schmid, E. Eukhardt, E. Walker, W. Brixel, M. Clin, J.-P. Rivera, J.-L. Jorba, M. Francis, and K. Yvon, "Polarized Light and X-ray Precession Study of the Ferroelastic Domain of  $\text{YBa}_2\text{Cu}_3\text{O}_{7-x}$ ," *Z. Phys. B: Condens. Matter*, **72**, 305-22 (1988).
- <sup>45</sup>A. H. Heuer, S. Kraus-Lanteri, P. A. Labun, V. Lanteri, and T. E. Mitchell, "HREM Studies of Coherent and Incoherent Interfaces in  $\text{ZrO}_2$ -Containing Ceramics: A Preliminary Account," *Ultramicroscopy*, **18**, 335-48 (1985).
- <sup>46</sup>G. V. Srinivasan, J. F. Jue, S. Y. Kuo, and A. B. Virkar, "Ferroelastic Domain Switching in Polydomain Tetragonal Zirconia Single Crystals," *J. Am. Ceram. Soc.*, **72** [11] 2098-103 (1989).
- <sup>47</sup>A. V. Virkar and R. L. K. Matsumoto, "Ferroelastic Domain Switching as a Toughening Mechanism in Tetragonal Zirconia," *J. Am. Ceram. Soc.*, **69** [10] C-224-C-226 (1986).
- <sup>48</sup>A. V. Virkar and R. L. Matsumoto, "Toughening Mechanism in Tetragonal Zirconia Polycrystalline (TZP) Ceramics"; pp. 653-62 in *Advances in Ceramics, Vol. 24, Science and Technology of Zirconia III*. Edited by S. Sömiya, N. Yamamoto, and H. Yanagida. American Ceramic Society, Westerville, OH, 1988.
- <sup>49</sup>M. V. Swain and R. H. J. Hannink, "Metastability of the Martensitic Transformation in a 12 mol% Ceria-Zirconia Alloy: II, Grinding Studies," *J. Am. Ceram. Soc.*, **72** [8] 1358-64 (1989).
- <sup>50</sup>C. J. Chan, F. F. Lange, M. Rühle, J. F. Jue, and A. V. Virkar, "Ferroelastic Domain Switching in Tetragonal Zirconia Single Crystals—Microstructural Aspects," *J. Am. Ceram. Soc.*, **74** [4] 807-13 (1991).
- <sup>51</sup>C. J. Gasdaska, P. J. Whalen, J. Marti, and F. Reidinger, "Texture and Recrystallization on Ground Surfaces of Hafnia," *J. Am. Ceram. Soc.*, **73** [7] 1941-46 (1990). □

# Hysteresity Effects in Three Mole Percent Yttria-Doped Zirconia (t' phase)

Kevin M. Prettyman, Jan-Fong Jue, and Anil V. Virkar

Department of Materials Science and Engineering, University of  
Utah, 304 EMRO, Salt Lake City, Utah 84112 USA

Camden R. Hubbard, O. Burl Cavin, and Mattison K. Ferber

Oak Ridge National Laboratory, Oak Ridge, Tennessee 37831 USA

## **ABSTRACT:**

Single crystal and polycrystal samples of 3 m/o  $Y_2O_3$ -doped zirconia (t' phase) were subjected to uniaxial compression tests at  $1000^{\circ}C$  in order to separate the effects of phase transformation (t to m) from ferroelastic domain switching. Plastic deformation was observed after an elastic regime, with attributes characteristic of domain switching. X-ray diffraction traces at room and high temperatures before and after the compression test verified that there was indeed a variant reorientation within each sample. Deformation bands were observed on single crystals and Raman spectroscopy revealed that no monoclinic phase was present. These results verify the existence of ferroelastic domain switching phenomenon in this material. [Keywords: hysteresis, ferroelasticity, zirconia.]

## I. Introduction

The concept of ferroelastic behavior being involved in phase transitions has been well defined and its study has been ongoing for over twenty years [1]. It was proposed as a potential toughening mechanism in zirconia in 1986 [2]. From TEM (transmission electron microscopy) and TOM (transmission optical microscopy) techniques, it is known that ferroelastic domains exist in three mole percent yttria doped zirconia in the  $t'$  phase, with typical dimensions of  $0.05\ \mu\text{m}$  by  $1.0\ \mu\text{m}$  [3-7]. This previous work had been done at room temperature. Figure 1 illustrates the "herringbone" domain structure typical in these materials.

Heretofore, it had been assumed by many that the  $t'$  phase was a "non-transformable phase", since no monoclinic phase had been observed when the sample was stressed [8]. It has been shown however that this is not the case, but that transformation is possible and is a function of domain size [5,9,10]. The purpose here is to clearly demonstrate the ferroelastic domain switching phenomenon in these materials by eliminating the possibility of both the reversible and irreversible tetragonal to monoclinic phase transformation. This was done by eliminating the driving force for this transformation by conducting uniaxial compression tests at

temperatures well above the equilibrium transition temperature between the tetragonal and monoclinic phases. For 3 m/o  $Y_2O_3$ -doped TZP (tetragonal zirconia polycrystal), this phase transition occurs at 750 °C or below, based on the available diagram [11-15]. Ferroelastic domain switching is easier at high temperatures since coercive stress ( $\sigma_{coer}$ ) is an inverse function of temperature [16]. It is important however not to exceed the Curie temperature ( $T_c$ ) of the material since at that temperature, the material no longer exists in a ferroelastic phase, but instead becomes paraelastic. In 3 m/o  $Y_2O_3$ -doped TZP, this occurs when the tetragonal ferroic phase transforms into the cubic prototype phase at around 2000°C [17,18]. It is also necessary to choose a temperature low enough to prevent, or at least minimize, softening and plastic deformation of all test set-up materials. A temperature of 1000 °C was used in this study, since it met the above criteria.

## II. Experimental Procedure

Single crystal and polycrystal samples were prepared in the  $t'$  phase. The tetragonal single crystal was purchased commercially\* and had been prepared using a skull melt technique. The sample was not actually a true single crystal but a "pseudo-single crystal", having three variants in mutually orthogonal directions. The irregularly shaped samples were oriented using back reflection Laue x-ray diffraction and cut in the shape of parallelepipeds (3 x 3 x 9 mm) such that the faces were perpendicular to  $\langle 100 \rangle$  directions, based on pseudocubic symmetry, as depicted in Figure 2. They were then heated in air at 2100 °C for fifteen minutes in a gas fired furnace, quenched to 1200 °C, and furnace cooled to room temperature.

The polycrystalline samples were prepared using a premixed commercial powder\*\*. The powder was die pressed at 28 MPa, isostatically pressed at 207 MPa, and sintered in air at 1450 °C for two hours. The sintered samples were then heated to 2100 °C for 15 minutes in a gas fired furnace, quenched to 1200 °C, furnace cooled to room

\* Ceres Corporation, Waltham, Massachusetts, USA.

\*\* TZ-3Y from TOSOH USA Inc., Atlanta, Georgia, USA.

temperature, and cut to size (3 x 3 x 9 mm).

A rocking curve x-ray analysis was done on representative samples to insure that crystallite size and preferred orientation due to processing would not significantly affect the quantitative XRD results. This was deemed particularly important for the polycrystalline samples after the high temperature (2100 °C) heat treatment due to their large average grain size (greater than 100 μm). A rocking curve XRD analysis is performed by making multiple XRD traces on a flat sample surface oriented at various angles to the incoming x-ray beam. This involves "rocking" the sample between plus or minus fifteen degrees in both the x and y directions in order to observe whether or not there is a significant shift in the 2θ peak positions. Multiple x-ray diffraction traces\* were obtained from various faces of all samples at room temperature and at 1000 °C before and after high temperature testing. They were stressed in uniaxial compression at a rate of 0.01 mm/min between two silicon carbide push-rods at 1000 °C on a universal testing machine\*\*. Load verses displacement was monitored during the loading/unloading cycle and a stress/strain plot was

\* Scintag Pad X XRD, Germany

\*\* INSTRON Model 6027, Boston, Massachussetts, USA

constructed afterward. A silicon-carbide "core sample" (6.35 mm diameter x 12.7 mm length) was first run under the same conditions in order to determine compliance of the loading assembly. All samples were aligned pre-loaded to 35 N at room temperature, and heated to 1000 °C under constant load conditions before any data were recorded.

Additional single crystals were prepared having the same <100> orientation. The lateral faces were polished to a one micron finish, and stressed in compression to 2.2 GPa at room temperature. Each face was studied before and after compression using Nomarski interference microscopy\*, X-ray Diffraction\*\*, and Laser Induced Raman Spectroscopy. A triple spectrometer\*\*\* and an argon ion laser\*\*\*\*, operating at 488 nm, with a beam size of five microns in diameter, were used in the Raman study. Irradiance at the sample was  $1 \times 10^9$  watts/m<sup>2</sup>. A more complete discussion of the Raman technique used will be published in a separate paper [19].

\* Model BH2, Olympus Optical Co., LTD, Tokyo, Japan

\*\* Model XRD-8000, Diano Corp., Woburn, Massachusetts, USA

\*\*\* Model 1877C-AG, 0.6 m, Triple Spectrometer, Spex Industries Inc.,  
Edison, New Jersey, USA

\*\*\*\* Model 2045, Spectra Physics, Mountain View, California, USA

### III. Results and Discussion

#### (1) Single Crystal

Density was measured using the Archimedean displacement technique and was determined to be  $6.10 \text{ g/cm}^3$  (100 % of the theoretical value). Compressive strength was found to be greater than 2.2 GPa at room temperature and greater than 400 MPa at  $1000 \text{ }^\circ\text{C}$ . Greater stresses could not be applied for fear of damaging the test apparatus. A stress versus strain plot for this single crystal can be seen in Figure 3. The sample behaved elastically to around 750 MPa, where it began to deform plastically. Not all of the observed plastic deformation can be due to ferroelastic domain switching. Deformation due to switching is a function of the "c/a ratio" of the individual unit cells and of the relative percentage of cells with variants in each of the three directions. From XRD data before stressing, we know that about one-third of the total number of cells exist in each of the three variant directions and that the "c/a ratio" is about 1.013 at room temperature and at  $1000 \text{ }^\circ\text{C}$ . We would therefore expect around 0.43% deformation due to ferroelastic domain switching. Here, we see 1.4 % plastic strain. Dislocation movement may also be

occurring simultaneously at this high temperature and is discussed later in this paper.

Young's modulus is slightly different when loading and unloading the sample. This may be due to the anisotropy in the [100] and [001] directions before and after the domain switching has occurred. After removing the effects of apparatus compliance and plasticity, the actual modulus, upon loading, at 1000°C is around 127 GPa, in accordance with values obtained using the free floating beam method (138 GPa for 3.5 m/0 Y-TZP at 1000°C) [20]. From the figure, it is seen that some of the plastic deformation is reversible. In this case, roughly half of the plastic strain produced in loading was recovered upon unloading. Part of this recovered strain can possibly be explained by data reported by Takei and Tsunekawa [21,22]. When studying ferroelastic single crystals of neodymium niobate and lanthanum niobate, they found that the domain orientations could be switched irreversibly, or partially or completely reversibly, depending upon the strain rate while loading. The strain rate was not varied in this study.

It is clear that the material exhibits quite a bit of plastic deformation, but it is not obvious that part of this deformation is due to ferroelastic domain switching, despite the occurrence of characteristics

expected in switching, as previously described. XRD data however, verify this conclusion. An average overall cell orientation can be determined by observing the (002)/(200) relative peak heights and integrated intensities [14]. Table I summarizes the averages of XRD data obtained from multiple runs on the front face of the sample at room temperature. It is seen that from either the relative heights or integrated intensities, the (002) peak grows at the expense of the (200) peak, in accordance with the switching phenomenon. Figure 4 shows some actual XRD traces from this face. Deconvolutions were done using software provided by the manufacturer of the diffractometer. XRD traces obtained from this face at 1000 °C and on other faces at both room and high temperatures confirm these results.

Samples whose lateral faces had been polished to a one micron surface finish were stressed in compression at room temperature to 2.2 GPa. The faces were observed using Nomarski Interference Microscopy. One such face after stress is shown in Figure 5. A definite deformation zone has appeared due to the applied stress and can clearly be seen. XRD on the entire face showed no evidence of monoclinic phase being present. Laser Induced Raman Spectroscopy was used to examine the deformation zone. The beam size was about five microns. Multiple spectra were obtained in various areas within and outside the zone. One such spectrum is shown in

Figure 6. Peaks corresponding to the monoclinic phase are conspicuously absent [19,23-25]. In fact, no monoclinic phase could be detected anywhere in the zone or on the sample surface. This finding indicates that deformation zones produced during crack propagation in zirconia, as identified by Nomarski microscopy, may not be entirely due to the t to m phase transformation. When trying to correlate material toughness with transformation zone size (eg., crack shielding effects), it is important to realize that there is not necessarily a one to one correspondence between the deformation zone and the phase transformation zone.

These data also demonstrate that ferroelastic domain switching is a deformation process. Since deformation processes expend energy, some of the mechanical energy that might normally be channeled into crack formation and extension will instead be expended in the formation and/or switching of ferroelastic domains [2]. Hence, ferroelasticity is a potential toughening mechanism.

## (2) Polycrystalline $t'$ ZrO<sub>2</sub>

Density was measured to be 6.06 g/cm<sup>3</sup>. The samples were translucent and no porosity was observed under an optical microscope. Due to the 2100 °C heat treatment, the grain size in the TZP material had grown from 0.6 μm to around 200 μm (Figure 7). A number of the polycrystalline  $t'$  ZrO<sub>2</sub> samples were first loaded in compression to failure at 1000 °C to determine fracture stress, as well as to insure that the material exhibited a significant amount of plastic deformation. The compressive strength at room temperature was greater than 1200 MPa. Again, the applied stress was not greater than 1200 MPa for fear of damaging the fixtures in the test apparatus. A typical stress-strain curve to failure at 1000 °C is shown in Figure 8. The material exhibits quite a bit of plasticity beginning at 450 MPa, with the sample fracturing catastrophically at 620 MPa. After removing strain contributions from the test apparatus, about 0.96 % strain was due to plastic deformation of the sample. A Young's modulus of around 125 GPa was a little lower than the value obtained for the single crystal and is consistent with data published and referred to earlier [20].

Two consecutive stress runs were made on a different sample (cut

from the same "parent bar" as the sample taken to failure). Temperature was again 1000°C. Multiple XRD traces were obtained from various faces at room and high temperature before and after each run. The samples were unloaded before failure occurred, but after plastic deformation had begun. Figure 9 shows typical stress-strain plots from both runs. Again, a permanent strain is observed in the material. During the first run, plastic deformation began at around 450 MPa as it did in the samples taken to failure. The sample was unloaded once a stress of 500 MPa had been reached. It was cooled, x-rayed, and loaded in run #2 at 1000 °C to a stress of about 600 MPa. In run #2, the sample behaved elastically up to 500 MPa, where we had stopped loading on the first run. This behavior is typical in many strain hardened materials. It also indicates that domains which had switched between 450 and 500 MPa in the first run, appear to have done so irreversibly, and did not switch again in run #2. In this second run, 0.68 % strain was produced through plastic deformation. Since the "c/a" ratio for this specimen was again about 1.013, a maximum of around 0.43% total plastic strain would be expected if ferroelastic domain switching was the only plastic deformation mechanism in operation. Dislocation motion may again be a possible mechanism contributing to the observed plasticity. Dislocation movement has been shown to occur in

yttria doped TZP at elevated temperatures due to grain boundary sliding and creep cavitation within a thin (less than ten microns) glassy phase present at the grain boundaries [26,27]. This glassy phase is due to impurities such as  $\text{SiO}_2$  and  $\text{Al}_2\text{O}_3$  existing in the material [28]. XRD traces indicate that no monoclinic phase existed on any of the sample surfaces, as expected. Upon loading, the Young's moduli were identical in each of the two runs. The difference in moduli observed during loading and unloading is smaller than that observed for the single crystal. These observations are consistent with the fact that in polycrystalline materials, fewer grains are of a favorable orientation for switching to occur. Hence, any anisotropy caused by ferroelastic behavior would be more subdued. This is evidenced by the data shown in Table II which summarizes average values of XRD data, again indicating an increasing degree of reorientation of some of the variants in the sample with increasing stress, in agreement with the ferroelastic domain switching mechanism. Some average values for XRD data obtained at  $1000^\circ\text{C}$  are also included in the table. Figures 10 and 11 demonstrate this switching phenomenon through some actual XRD traces along with their deconvoluted peaks. From these traces, it is clear that some switching had occurred prior to loading due to the compressive stresses involved in surface

grinding [14]. Here again,  $I_{(002)}$  increased at the expense of  $I_{(200)}$  in accordance with ferroelastic theory.

Partial hysteresis loops under compressive stress at room temperature have also been observed in this material, as seen in Figure 12. XRD data again support the ferroelastic domain switching mechanism as being partially responsible for the plastic deformation.

#### IV. Summary and Conclusions

From this study, it is possible to draw a number of conclusions. The first is that ferroelastic domains are indeed present in three mole percent yttria-doped zirconia existing in single crystalline and polycrystalline forms (t' phase).

Secondly, three mole percent yttria-doped zirconia existing in single crystalline and polycrystalline forms (t' phase) undergoes ferroelastic domain switching when loaded in uniaxial compression at 1000 °C. This contributes to the partial hysteresis loops observed in the stress versus strain curves.

The third and perhaps most significant conclusion is that ferroelastic domain formation and/or switching is a deformation process and can expend mechanical energy which might otherwise be used for crack formation and propagation. It is therefore a potential toughening mechanism in ferroelastic materials. This also implies that care must be exercised when attributing deformation zone size to phase transformation alone when dealing with such theories as the "crack shielding effect".

**Acknowledgment:** Jong Chen of the University of Utah is gratefully acknowledged for his help with the TEM micrographs used in this paper.

This research was supported by DARPA (through AFOSR Contract Number F49620-89-C-0054) and subcontracted through Ceramatec Inc., to the University of Utah.

## References

1. K. AIZU, *J. Phys. Soc. Jap.* **27** (1969) 387.
2. A. VIRKAR and R. MATSUMOTO, *J. Amer. Ceram. Soc.* **69** (1986) C224.
3. G. SRINIVASAN, J. JUE, and A. VIRKAR, *J. Amer. Ceram. Soc.* **72** (1989) 2098.
4. J. JUE and A. VIRKAR, *J. Amer. Ceram. Soc.* **73** (1990) 3650.
5. J. JUE, J. CHEN, and A. VIRKAR, *J. Amer. Ceram. Soc.* (in press).
6. A. HEUER, R. CHAIM, and V. LANTERI, *Acta. metall.* **35** (1987) 661.
7. T. SAKUMA, *J. Mater. Sci.* **22** (1987) 4470.
8. R. MILLER, J. SMIALEK, and R. GARLICK, in "Advances in Ceramics", Vol. 3, edited by A. Heuer and L. Hobbs (American Ceramic Society, Columbus, Ohio, 1981) p. 241.
9. M. HAYAKAWA, N. KUNTANI, and M. OKA, *Acta metall.* **37** (1989) 2223.
10. M. HAYAKAWA and M. OKA, *Acta metall.* **37** (1989) 2229.
11. H. SCOTT, *J. Mater. Sci.*, **10** (1975) 1527.
12. E. LEVIN, C. ROBBINS, and H. MCMURDIE, in "Phase Diagrams for Ceramists", edited by M. Reser (American Ceramic Society, Columbus, Ohio, 1964) p. 140.
13. M. JAYARATNA, M. YOSHIMURA, and S. SOMIYA, *J. Amer. Ceram. Soc.* **67** (1984) C240.

14. V. STUBICAN and J. HELLMANN, in "Advances in Ceramics", Vol. 3, edited by A. Heuer and L. Hobbs (American Ceramic Society, Columbus, Ohio, 1981) p. 25.
15. V. STUBICAN, R. HINK, and S. RAY, *J. Amer. Ceram. Soc.* **61** (1978) 17.
16. V. WADHAVAN, *Phase Transitions*, **3** (1982) 3.
17. D. MICHEL, L. MAZEROLLES, and M. PEREZ Y JORBA, *J. Mater. Sci.* **18** (1983) 2618.
18. D. MICHEL, L. MAZEROLLES, and M. PEREZ Y JORBA, in "Advances in Ceramics", Vol. 12, edited by N. Claussen, M. Ruhle, and A. Heuer (American Ceramic Society, Columbus, Ohio, 1984) p.131.
19. K. PRETTYMAN and A. VIRKAR, unpublished work.
20. J. BUCKLEY and D. BRASKI, *J. Amer. Ceram. Soc.* **50** (1967) 220.
21. S. TSUNEKAWA and H. TAKEI, *J. Phys. Soc. Jap.* **40** (1976) 1523.
22. H. TAKEI and S. TSUNEKAWA, *J. Crys. Growth* **38** (1977) 55.
23. R. DAUSKARDT, D. VEIRS, and R. RITCHIE, *J. Amer. Ceram. Soc.* **72** (1989) 1124.
24. D. CLARKE and F. ADAR, *J. Amer. Ceram. Soc.* **65** (1982) 284.
25. D. MARSHALL, M. SHAW, R. DAUSKARDT, R. RITCHIE, M. READEY, and A. HEUER, *J. Amer. Ceram. Soc.* **73** (1990) 2659.
26. A. DOMINGUEZ-RODRIGUEZ, K. LAGERLOF, and A. HEUER, *J. Amer. Ceram. Soc.* **69** (1986) 281.

27. A HEUER, V. LANTERI, and A. DOMINGUEZ-RODGIGUEZ, *Acta. metall.* 37  
(1989) 559.

28. J. LANKFORD and R. PAGE, *J. Mater. Sci.* 23 (1988) 4144.

**Table I.**

**Average Values of XRD Data for  
3 m/0 Y<sub>2</sub>O<sub>3</sub> - ZrO<sub>2</sub> (t') Single Crystal  
(Front Lateral Face at 25 °C)**

	<b><u>I<sub>002</sub> / I<sub>200</sub></u> (Peak Height)</b>	<b><u>I<sub>002</sub> / I<sub>200</sub></u> (Integ. Int.)</b>
<b>Before Stress</b>	<b>0.4</b>	<b>0.5</b>
<b>After Stress</b>	<b>0.8</b>	<b>1.3</b>

**Table II.**

**Average Values of XRD Data for  
3 m/0 Y<sub>2</sub>O<sub>3</sub> - ZrO<sub>2</sub> (t') Polycrystal**

	<b><u>I<sub>002</sub> / I<sub>200</sub></u></b> <b><u>(Peak Height)</u></b>	<b><u>I<sub>002</sub> / I<sub>200</sub></u></b> <b><u>(Integ. Int.)</u></b>
<b><u>Front Lateral Face</u></b> <b><u>at 25 Deg. C</u></b>		
Before Stress	1.8	1.8
After Stress Run #1	2.4	2.2
After Stress Run #2	3.1	2.6
<b><u>Rear Lateral Face</u></b> <b><u>at 25 Deg. C</u></b>		
Before Stress	1.7	1.6
After Stress Run #1	2.7	2.5
After Stress Run #2	3.1	3.0
<b><u>Right Lateral Face</u></b> <b><u>at 25 Deg. C</u></b>		
Before Stress	0.9	1.0
After Stress Run #2	1.5	1.5
<b><u>Front Lateral Face</u></b> <b><u>at 1000 Deg. C</u></b>		
Before Stress	1.3	1.7
After Stress Run #1	2.1	1.9
After Stress Run #2	3.4	2.2



Fig. 1

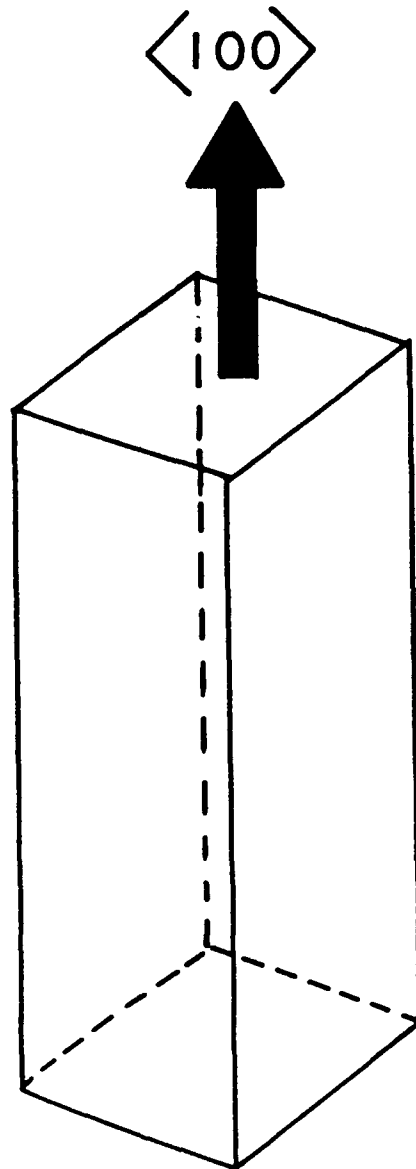


Fig. 2

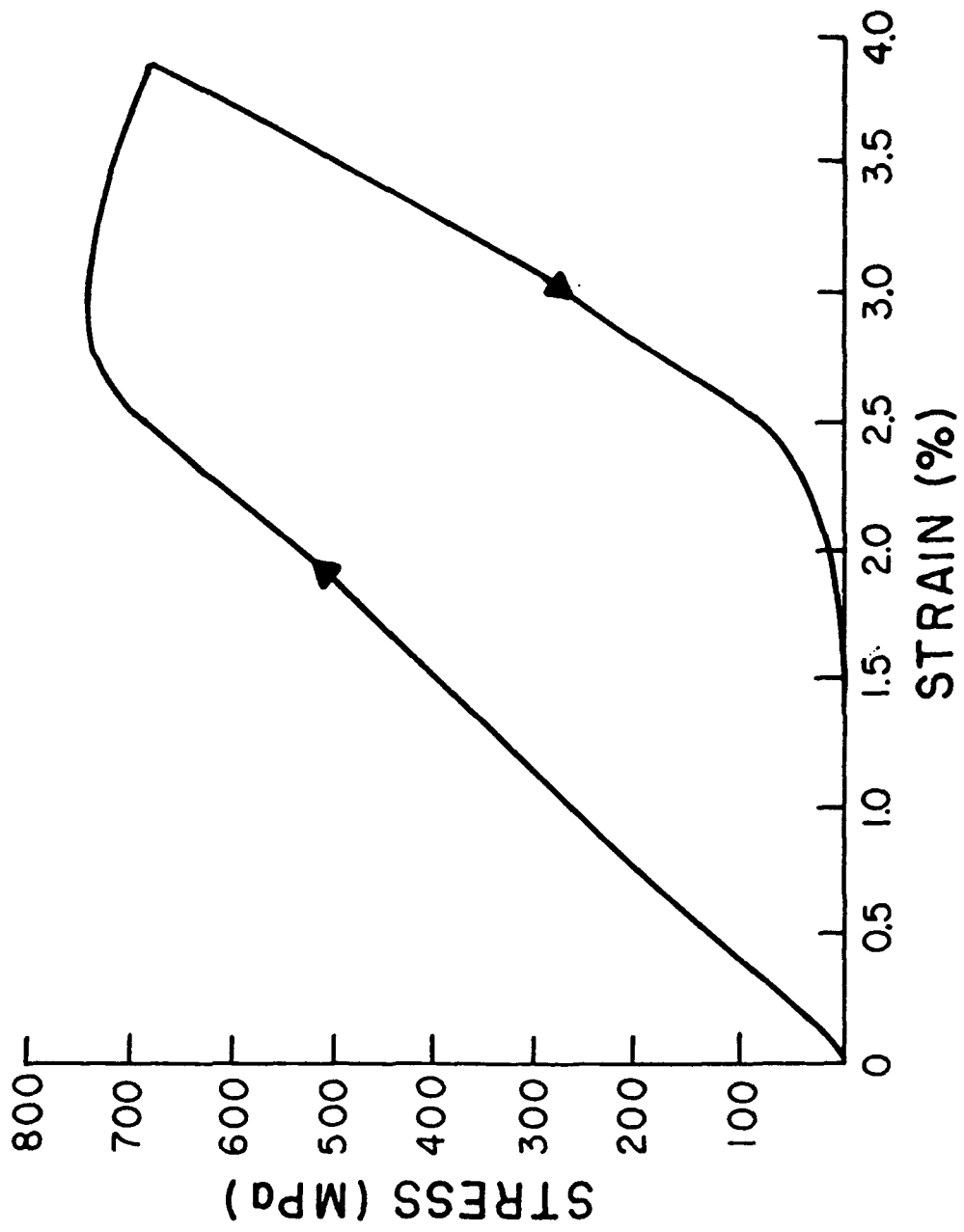
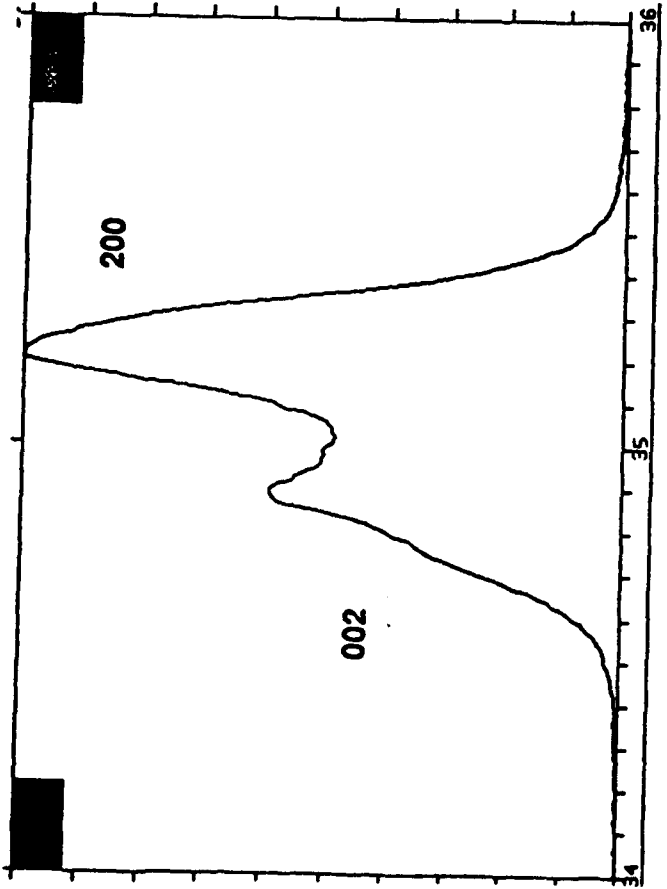
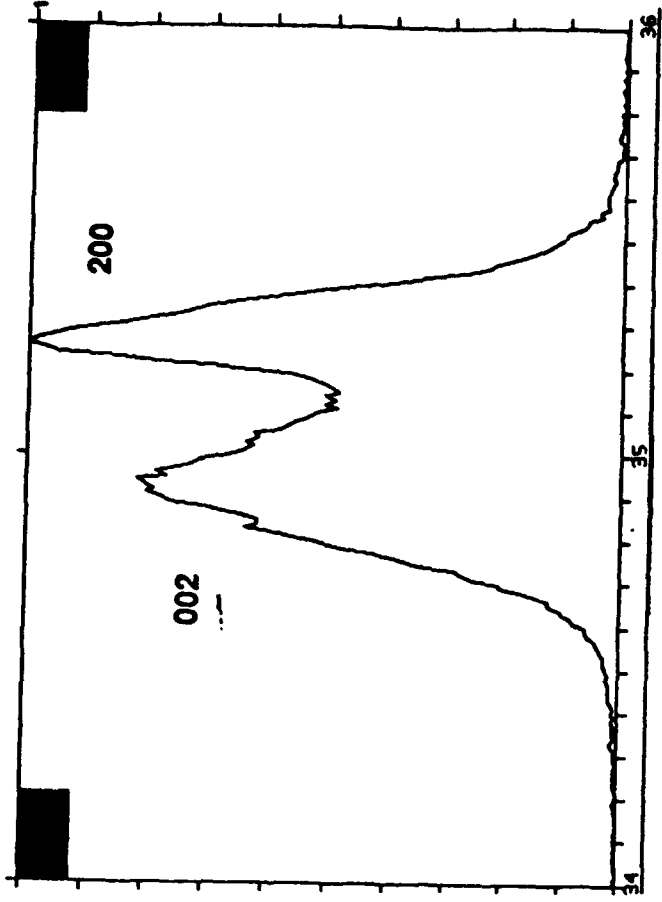


Fig. 3



Before Stress



After Stress

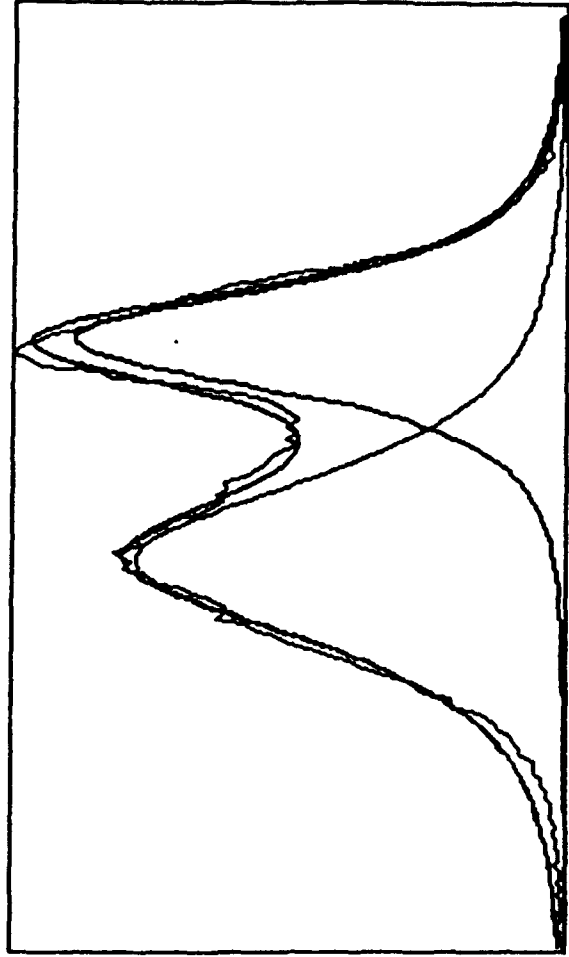
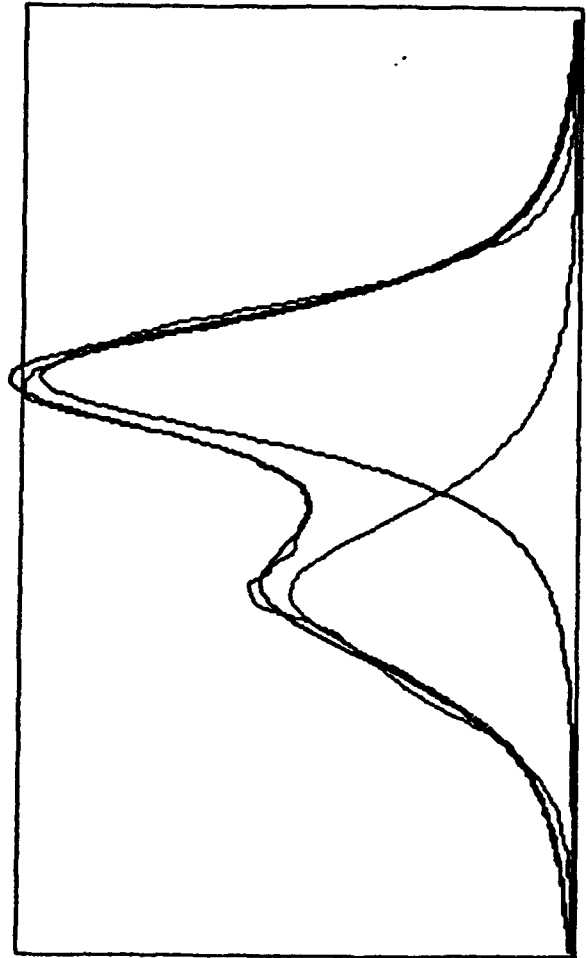


Fig. 4



Fig. 5

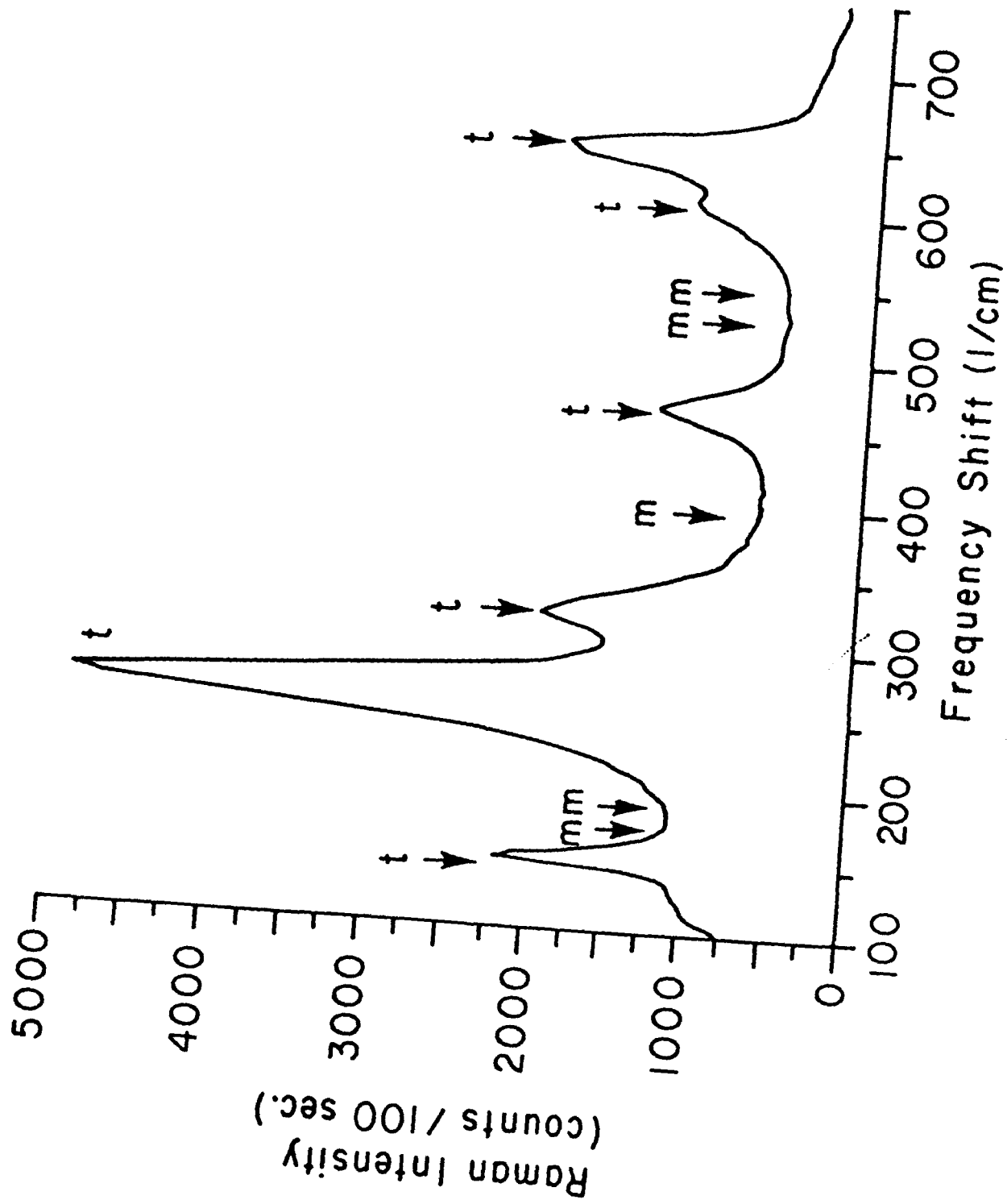


Fig. 6

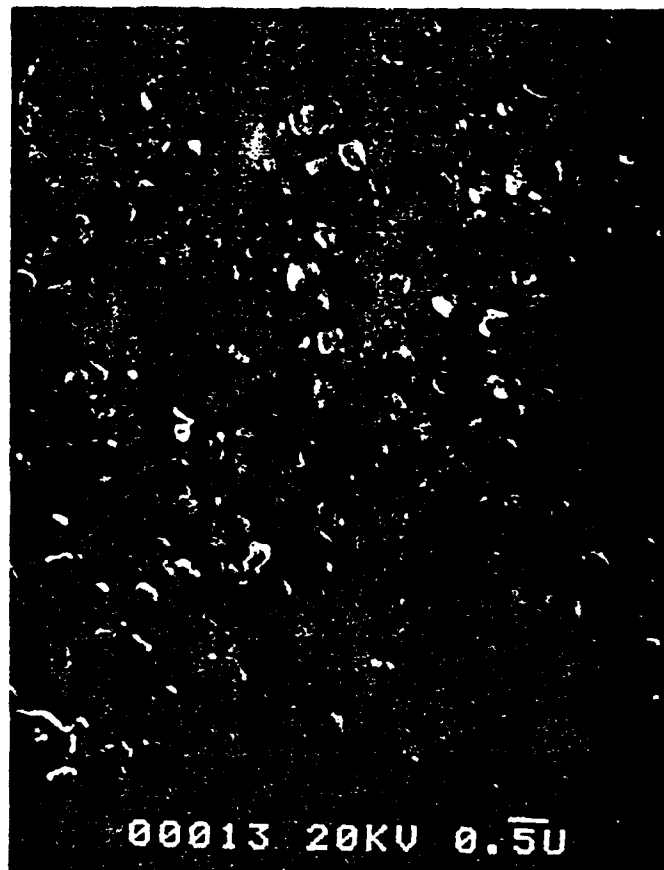


Fig. 7a

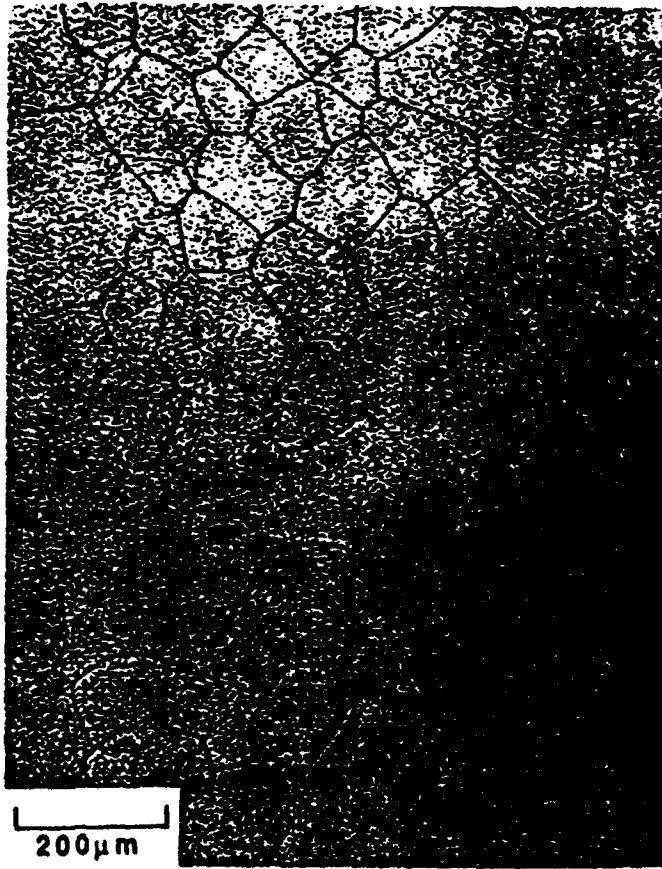


Fig. 7b

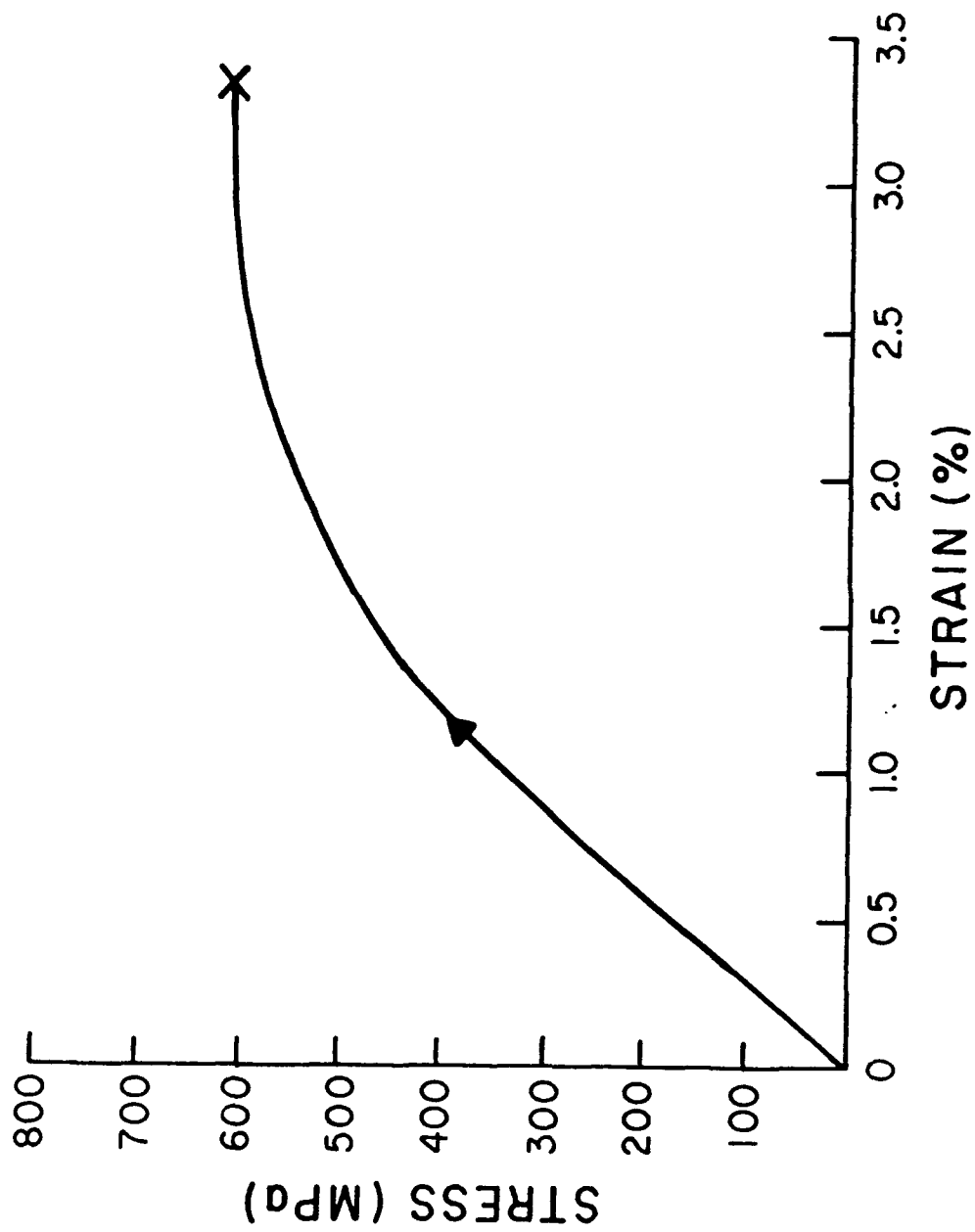


Fig. 8

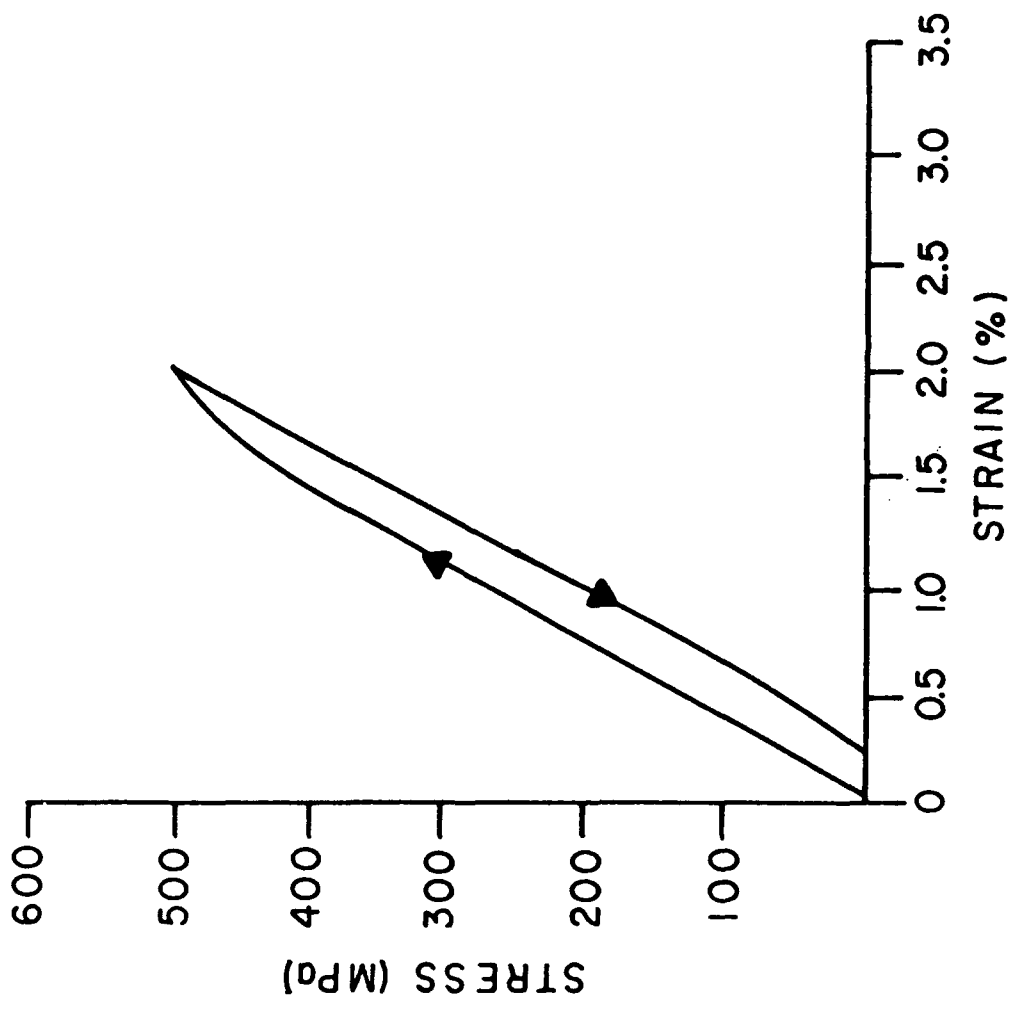


Fig. 9a

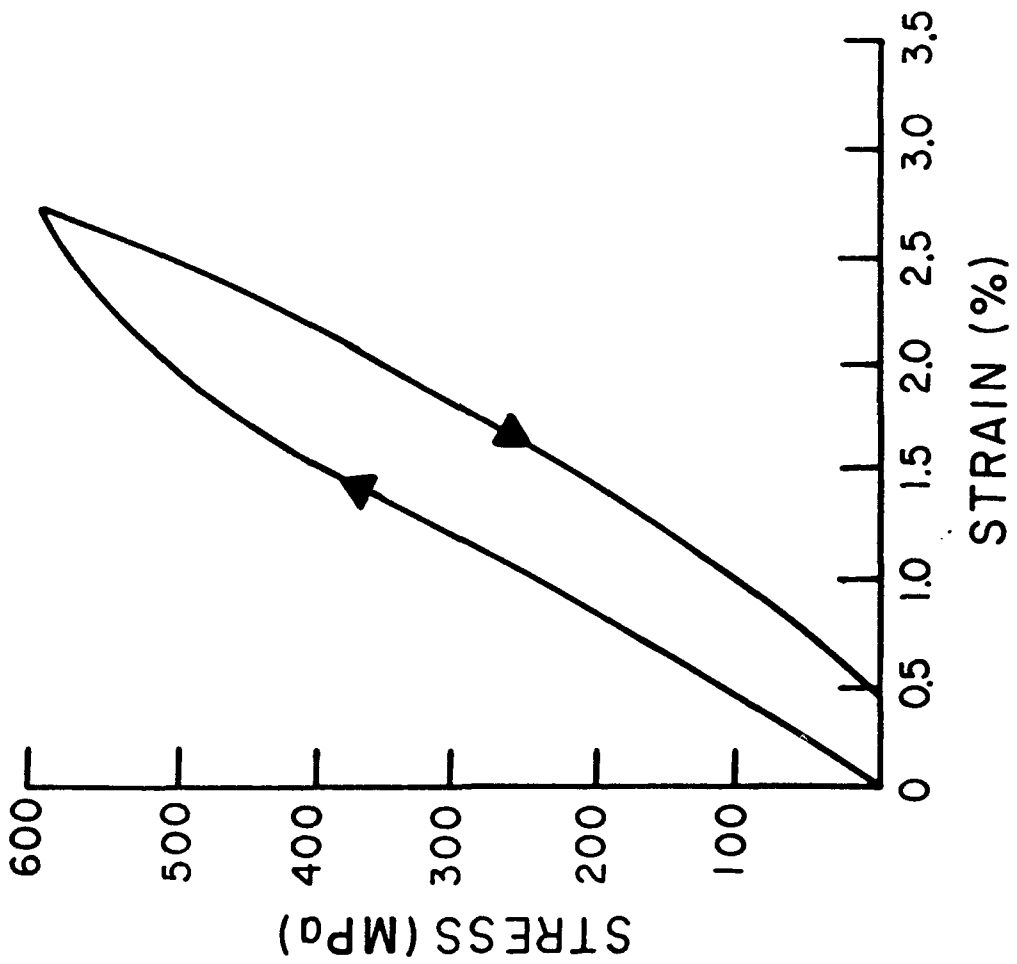
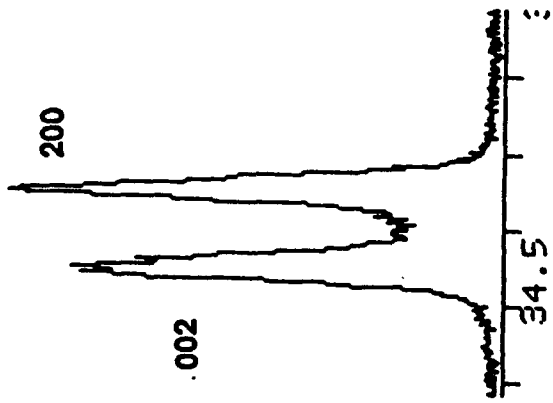
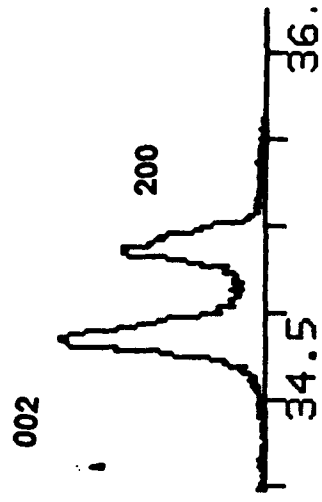


Fig. 9b



Before Stress



After Stress Run #2

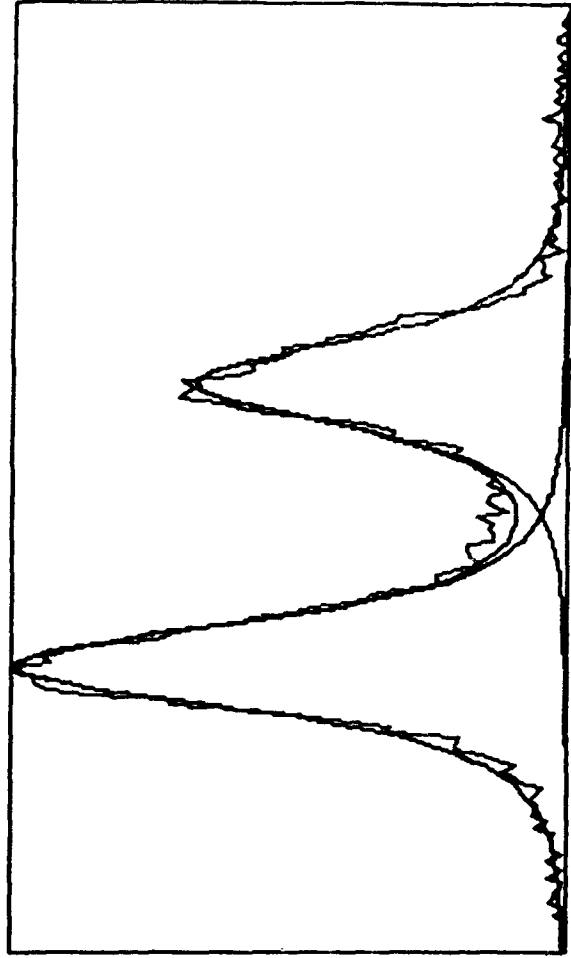
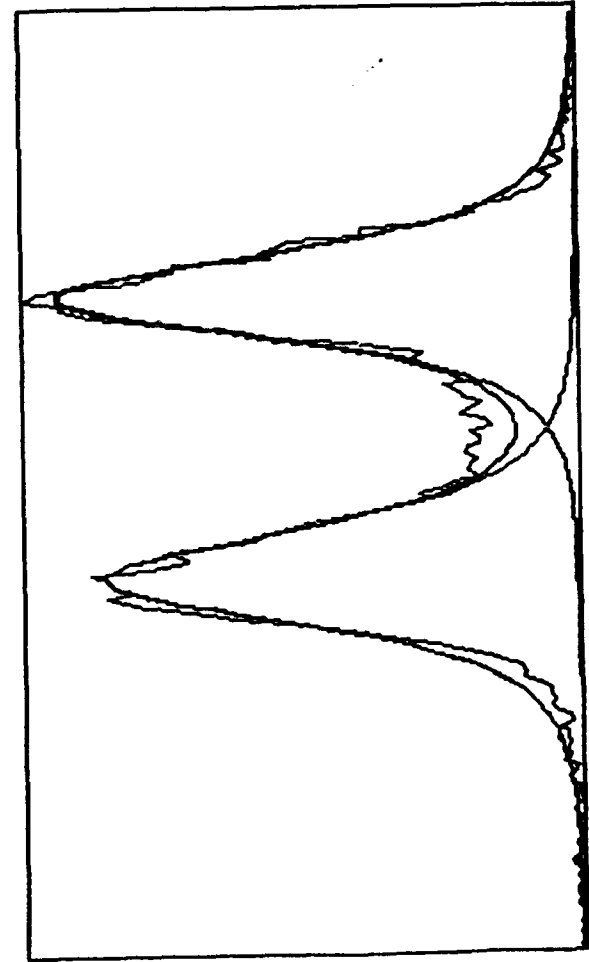
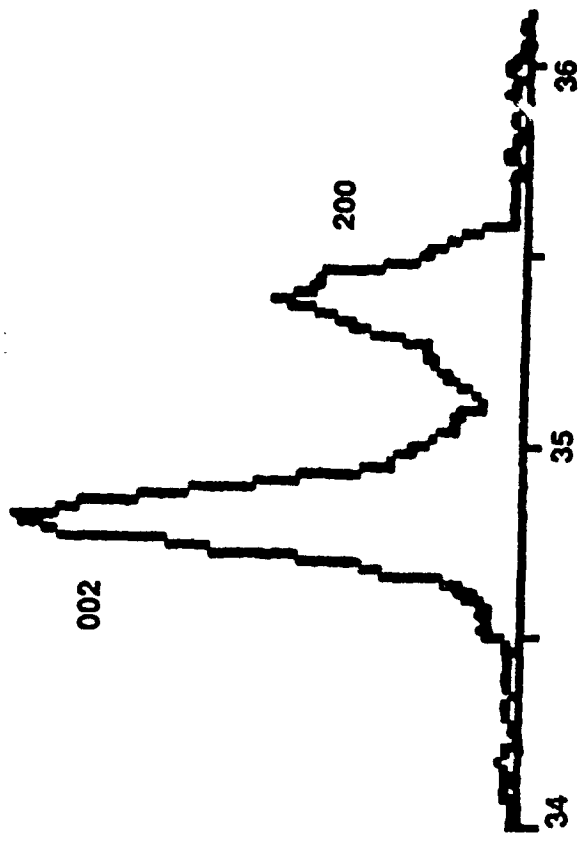
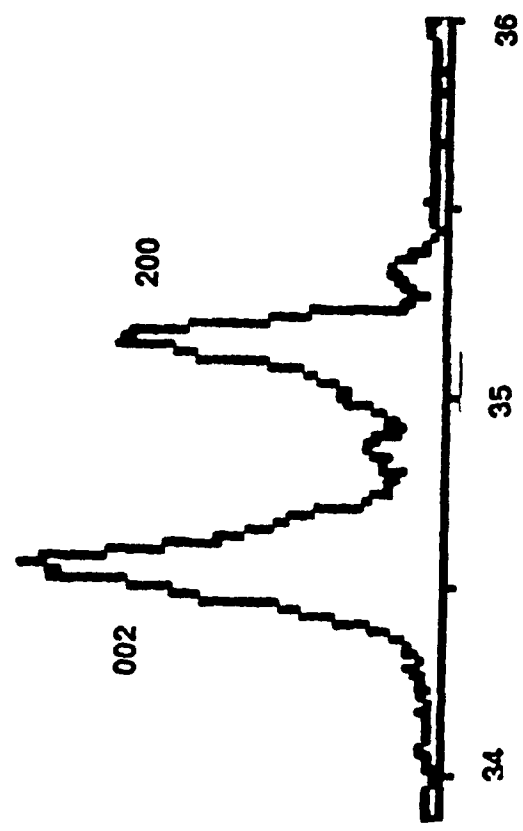


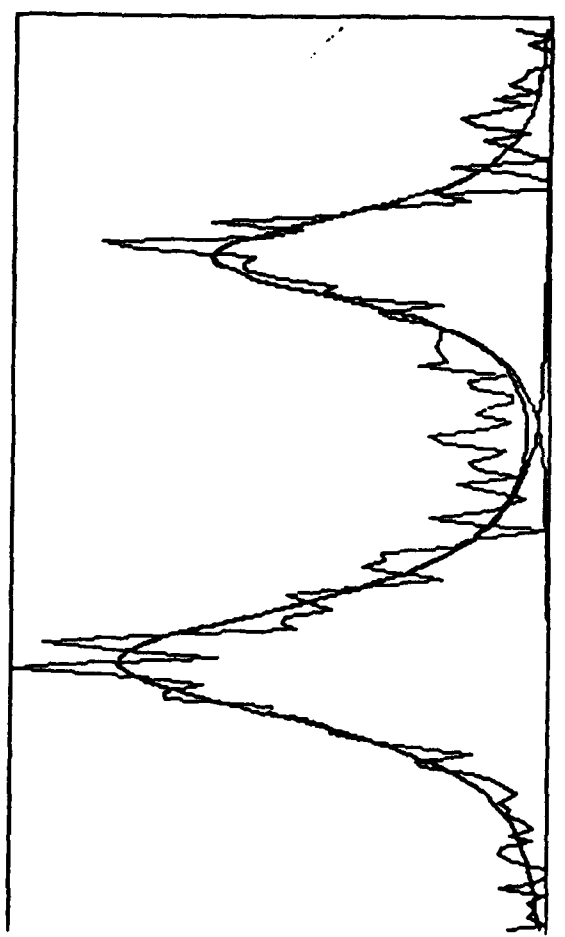
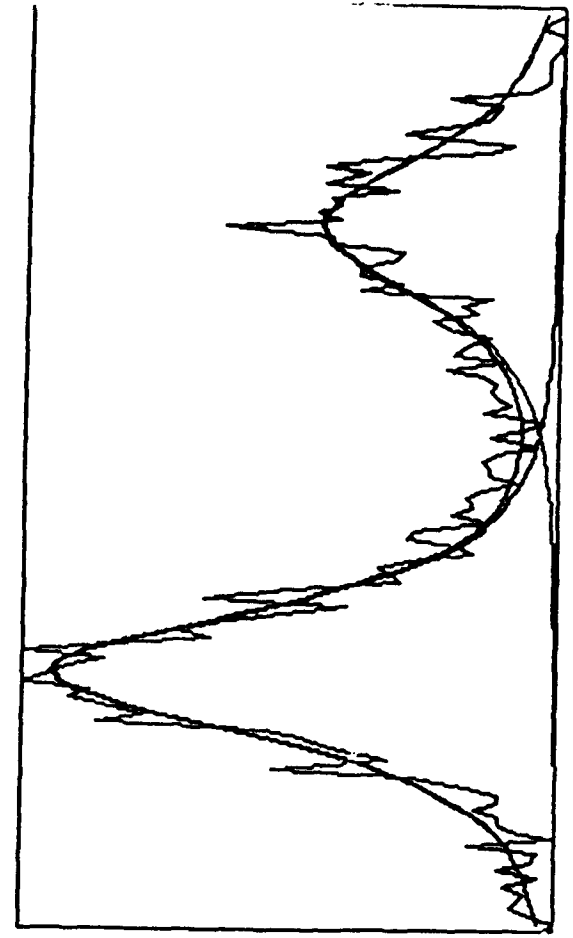
Fig. 10



After Stress Run #1



Before Stress



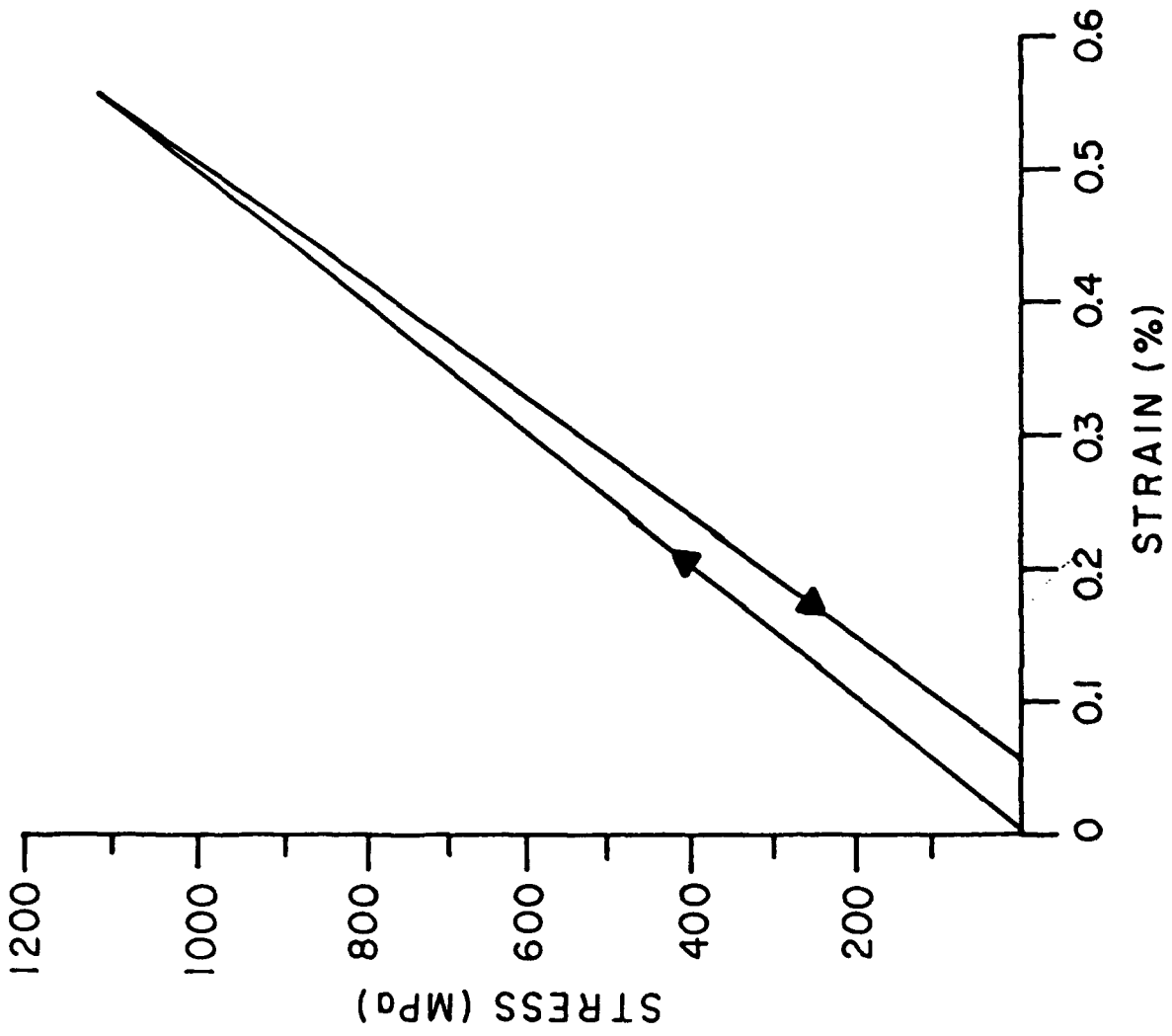


Fig. 12

## List of Figures

- Figure 1      TEM micrograph of 3 m/o  $Y_2O_3$  doped zirconia ( $t'$  phase) showing existing domain structure.
- Figure 2      Orientation and dimensions of single crystal samples.
- Figure 3      Stress versus strain curve for 3 m/o  $Y_2O_3$  doped  $ZrO_2$  single crystal ( $t'$  phase) in compression at 1000 °C. (Longitudinal Direction)
- Figure 4      Room temperature x-ray diffraction traces and deconvolutions before and after stress in 3 m/o  $Y_2O_3$  - $ZrO_2$  ( $t'$ ) single crystal. (Front Lateral face)
- Figure 5      Nomarski interference contrast micrograph of the deformation zone produced on a lateral face during compression of a 3 m/o  $Y_2O_3$  -  $ZrO_2$  ( $t'$ ) single crystal.

**Figure 6** A typical Raman spectra produced from inside the deformation band shown in Figure 5. Note that no monoclinic phase is observed.

**Figure 7** A scanning electron micrograph and an optical micrograph of the microstructure of 3 m/o  $Y_2O_3 - ZrO_2$  (t') polycrystal before (grain size of around 1 micron) and after (grain size greater than 100 microns) the 2100°C heat treatment.

**Figure 8** Stress versus strain curve to failure for 3 m/o  $Y_2O_3 - ZrO_2$  (t') polycrystal in uniaxial compression at 1000 °C.  
(Longitudinal Direction)

**Figure 9** Stress/strain curves for two consecutive runs of a 3 m/o  $Y_2O_3 - ZrO_2$  (t') polycrystal stressed in uniaxial compression at 1000 °C. (Longitudinal Direction). Note that the yield stress increases from Run 1 to Run 2.

**Figure 10** Room temperature x-ray diffraction traces and deconvolutions before and after stress in 3 m/o  $Y_2O_3 - ZrO_2$  (t' phase) polycrystal. (Right Lateral Face)

**Figure 11** High temperature (1000 °C) x-ray diffraction traces and deconvolutions before and after stress in 3 m/0 Y<sub>2</sub>O<sub>3</sub> - ZrO<sub>2</sub> (t' phase) polycrystal. (Front Lateral Face)

**Figure 12** Partial hysteresis loop for a 3 m/0 Y<sub>2</sub>O<sub>3</sub> - ZrO<sub>2</sub> (t') polycrystal stressed in uniaxial compression at room temperature.

## Sintering and Characterization of Polycrystalline Monoclinic, Tetragonal, and Cubic Zirconia

Raymond A. Cutler,\* James R. Reynolds,\* and Aaron Jones\*

Ceramatec, Inc., Salt Lake City, Utah 84119

**Polycrystalline monoclinic (*m*), tetragonal (*t*), and cubic (*c*) ZrO<sub>2</sub>, sintered at 1500°C, were annealed in the cubic stability field and rapidly cooled to permit the displacive *c* → *t'* transformation to occur in compositions containing 0–6 mol% Y<sub>2</sub>O<sub>3</sub>. The bulk fracture toughness of coarse-grained (>25 μm) *m*, *t'*, and *c* zirconias were compared with conventionally sintered, fine-grained (typically less than 1 μm) materials. The ferroelastic monoclinic and tetragonal zirconias were more than twice as tough as paraelastic cubic zirconia. [Key words: zirconia, fracture toughness, ferroelastic materials, microcracking, polycrystalline materials.]**

### I. Introduction

WADHAWAN<sup>1</sup> was the first to recognize that the tetragonal-to-monoclinic martensitic transformation in zirconia ceramics, which leads to transformation toughening in many ceramics, is also a ferroelastic phase transition. He suggested that during transformation, ferroelastic twinning and slip absorb the shear stress associated with the *m* → *t* transition.<sup>1</sup> Michel *et al.*<sup>2</sup> identified domain structure in *t'*-ZrO<sub>2</sub><sup>3</sup> materials and suggested that crack deflection, due to the domain structure, may be responsible for the high toughness of the nontransformable tetragonal phase relative to cubic ZrO<sub>2</sub>. Virkar and Matsumoto<sup>4,5</sup> suggested that ferroelastic switching, which was observed on the ground surfaces of tetragonal zirconia polycrystalline (TZP) ceramics, could contribute to the high toughness measured for zirconia ceramics. Lanteri *et al.*,<sup>6,7</sup> Sakuma *et al.*,<sup>8,9</sup> Noma *et al.*,<sup>10</sup> Ingel *et al.*,<sup>11</sup> and Srinivasan *et al.*<sup>12</sup> showed domain structure in *t'*-ZrO<sub>2</sub> single crystals rapidly cooled from the cubic stability field. In addition, Srinivasan *et al.*<sup>12</sup> demonstrated that domain switching can occur in these materials, which have considerably higher toughness than cubic ZrO<sub>2</sub>, which is not ferroelastic. Mehta and Virkar<sup>13</sup> showed that ferroelastic toughening is not exclusive to ZrO<sub>2</sub>, by showing toughening due to domain switching in ferroelectric-ferroelastic PZT ceramics.

Jue and Virkar<sup>14</sup> have recently observed domain structure and domain switching in polycrystalline *t'*-ZrO<sub>2</sub> ceramics. Large-grained *t'*-ZrO<sub>2</sub> ceramics, which were fabricated by rapidly cooling ZrO<sub>2</sub> (3 mol% Y<sub>2</sub>O<sub>3</sub>) from sintering temperatures near ≈2100°C in air, had at least twice the toughness and strength of cubic ZrO<sub>2</sub>. The implication of this work on *t'*-ZrO<sub>2</sub>, which does not show transformation toughening, yet has considerable toughness, is that part of the toughness typically associated with the *t* → *m* transformation is due to ferroelastic switching, or that ferroelastic switching may precede transformation.

Adams *et al.*<sup>15</sup> and Ingel *et al.*<sup>16</sup> showed that skull-melted single crystals of polydomain *m*-ZrO<sub>2</sub> could be cycled through the *m* ↔ *t* transitions without catastrophic fracture. The mono-

clinic single crystals were heavily twinned and showed transformation toughening upon cycling through the *m* ↔ *t* transitions.

Buljan *et al.*<sup>17</sup> showed twinning (i.e., domain formation) in tetragonal ZrO<sub>2</sub> upon heating flux-grown monoclinic ZrO<sub>2</sub> single crystals into the tetragonal stability field. They used optical transmission microscopy with polarized light at high temperatures to see the domain colonies which formed because of the stress of the *m* ↔ *t* transformation at temperatures of ≈1200°C. Bulk flux-grown single crystals generally microcrack upon cycling through the *m* ↔ *t* transitions. One possible reason for the ability to cycle skull-melted single crystals and the difficulty in cycling flux-grown crystals is related to twin orientation. As recognized by Smith and Newkirk,<sup>18</sup> the cubic-to-tetragonal transition in ZrO<sub>2</sub> is displacive, and three variants form upon cooling. The three *t'* variants form because of stress accommodation. Chan<sup>19</sup> has shown that in monovariant *t*-ZrO<sub>2</sub> there are four possible monoclinic variants. Muddle and Hannink<sup>20</sup> showed that 12 monoclinic variants (i.e., four from each *t'* variant) are observed for monoclinic ZrO<sub>2</sub> in MgO-PSZ heat-treated in the cubic stability field and rapidly cooled.

It is well-recognized that dense polycrystalline unstabilized ZrO<sub>2</sub> components are difficult to fabricate without severe cracking, because of the volume expansion (≈4.5%) and shape change (≈7%) which occur upon cooling monoclinic ZrO<sub>2</sub> through the *t* → *m* transformation. However, Sense<sup>21</sup> found that it was possible to fabricate polycrystalline monoclinic ZrO<sub>2</sub> with a density of 5.77 g/cm<sup>3</sup> which was nearly crack-free by hot-pressing below 1000°C to a density of 4.22 g/cm<sup>3</sup> and then heating to temperatures above at least 2250°C in a reducing environment. At temperatures below 2250°C, Sense found severe cracking. Carniglia *et al.*<sup>22</sup> always found a thin Zr film along grain boundaries in oxygen-deficient ZrO<sub>1.946</sub> when vacuum sintering unstabilized ZrO<sub>2</sub> at 2100°C. Garrett and Ruh<sup>23</sup> were able to achieve bulk densities of monoclinic ZrO<sub>2</sub> between 5.43 and 5.52 g/cm<sup>3</sup> by vacuum sintering at 2300°C for 3 h followed by reoxidation at 1000°C for 18 h. Since they did not heat into the tetragonal stability field upon reoxidation, it is not possible to conclude whether the reoxidized parts would avoid microcracking.

The purpose of this paper is to compare the fracture toughness of polycrystalline monoclinic, tetragonal, and cubic ZrO<sub>2</sub>. Based on the above discussion, it was hypothesized that domain orientation would minimize microcracking in *m*-ZrO<sub>2</sub> processed in the cubic stability range and allow a comparison of ferroelastic monoclinic and tetragonal ZrO<sub>2</sub> with paraelastic (i.e., nonferroelastic) cubic ZrO<sub>2</sub>.

### II. Experimental Procedure

ZrO<sub>2</sub> powders (grades TZ-0, TZ-2Y, TZ-3Y, TZ-4Y, TZ-6Y, TZ-8Y, Tosoh USA, Atlanta, GA; grade HSY-8.0, Daiichi Kigenso Kagaku, Co., Ltd., Osaka, Japan) containing 0, 2, 3, 4, 6, or 8 mol% Y<sub>2</sub>O<sub>3</sub> were used in the as-received condition. Bars (≈4 mm × 5 mm × 60 mm) and short rods (≈16-mm diameter × 25 mm long) were formed uniaxially at 35 MPa and subsequently isostatically pressed at 200 MPa. The pressed samples were sintered in air at either 1500°C (0–6 mol% Y<sub>2</sub>O<sub>3</sub>) or 1600°C (8 mol% Y<sub>2</sub>O<sub>3</sub>) for 2 h. Sintered parts

R. Ruh—contributing editor

Manuscript No. 197006. Received January 14, 1991; approved March 18, 1992.

Supported by DARPA through AFOSR under Contract No. F49620-89-C-0054.

\*Member, American Ceramic Society.

of 2–8 mol%  $Y_2O_3$  were cladless-HIPed at 1550°C with 200 MPa in Ar for 30 min.

Sintered and HIPed samples of 2–8 mol%  $Y_2O_3$  were annealed along with unsintered samples of unstabilized  $ZrO_2$ . Heat treatments were performed in a  $ZrO_2$ (3 mol%  $Y_2O_3$ ) crucible inside of a graphite resistance-heated furnace by rapidly heating ( $\approx 100^\circ C/min$  above 1500°C) to temperature in either He or Ar gas. The hold time at temperature was generally 5 min or less. The cooling rate was  $\approx 100^\circ C/min$  to 1500°C. Samples were reoxidized (by heating to 1000°C in air at a rate of 80°C/h and held at temperature for 2 h). Selected samples were aged at 1700°C for 72 h in air.

Density was determined by water displacement. Four-point bend strength of ground (220-grit) bars was measured using a universal testing machine with a crosshead speed of 0.5 cm/min, a support span of 40 mm, and a loading span of 20 mm. Fracture toughness was measured using the short-rod technique<sup>24</sup> on 12.5-mm-diameter samples. Ground, polished, and fractured surfaces were X-rayed to determine phases present<sup>25</sup> and to examine switching.<sup>26</sup> Hardness was determined using a 75-N indent made with a Vickers diamond indenter on polished surfaces. Young's modulus was determined by strain-gaging flexural bars.

### III. Results

#### (1) Sintering and Characterization of *m*-, *t*-, and *c*- $ZrO_2$

The HIPed  $ZrO_2$ , 2, 3, 4, 6, and 8 mol%  $Y_2O_3$  were generally fine-grained and near theoretical density (see Fig. 1), with densities of 6.12, 6.10, 6.05, 6.04, and 5.95 g/cm<sup>3</sup>, respectively. Ground surfaces of the 2 and 3 mol%  $Y_2O_3$  samples contained 4.3% and 0.2 mol% monoclinic  $ZrO_2$  (with the balance tetragonal), respectively. The 4 and 6 mol% samples consisted of tetragonal and cubic  $ZrO_2$ , and the 8 mol%  $Y_2O_3$  composition was fully cubic. None of the samples had any open porosity. Room-temperature mechanical properties, given in Table I, show that cubic  $ZrO_2$  has significantly lower strength and toughness than *t*- $ZrO_2$ , in agreement with expectation. The similar bulk fracture toughness of 2, 3, and 4 mol%  $Y_2O_3$  is in contrast to the indentation data of Sakuma *et al.*<sup>27</sup> which showed peak toughness at 2 mol%  $Y_2O_3$ , with the 2 mol% composition having three times the toughness of the 4 mol% composition. Although it is well-known that the toughness of TZP materials is very dependent on grain size, indentation data, such as those reported by Tsukuma and Takahata,<sup>28</sup> generally give much higher toughness values than bulk toughness measurements. The hardness increased with increasing cubic content, although spalling occurred at loads as low as 10 N for the 8 mol%  $Y_2O_3$  (fully cubic) sample, because of its low toughness. The hardness data are consistent with those of a Sakuma *et al.*<sup>8</sup> for arc-melted samples.

Dilatometric measurements showed that bars made from the unstabilized  $ZrO_2$  were densified by 1400°C. The *t* → *m* temperature was observed at 1060°C using polycrystalline  $ZrO_2$  cooled from 1600°C, in good agreement with the work of Adams *et al.*<sup>15</sup> who observed *t* → *m* transformation starting at  $\approx 1050^\circ C$  for polydomain single-crystal *m*- $ZrO_2$ . Linear shrinkage of  $\approx 18.5\%$  was measured on samples sintered in air at 1500°C for 2 h. The sintered bars were extensively cracked and were easily pulverized because of the volume expansion upon cooling through the *t* → *m* transformation. Extended (72-h) annealing in air at 1700°C resulted in unstabilized  $ZrO_2$  with similar shrinkage. The sintered parts could be handled but turned to powder when put into water to measure density. Sintering of unstabilized  $ZrO_2$  in Ar at 1700°C resulted in a material microcracked similarly to that observed in air at the same temperature. Hot-pressing at 1900°C and 28 MPa in Ar produced similar results. These experiments confirm the well-known fact that commercially available monoclinic powders can be densified by conventional means but cannot survive

the large volume and shape change upon cooling below the *t* → *m* transformation.

#### (2) High-Temperature Annealing

Upon heat treatment, the grain size increased for all of the compositions, as shown in Fig. 2. The grain size increased more for the 4 and 6 mol%  $Y_2O_3$  compositions which contained both cubic and tetragonal phases, as compared to the cubic 8 mol%  $Y_2O_3$  or the primarily tetragonal 2 and 3 mol%  $Y_2O_3$  compositions.

The fracture toughness of the  $ZrO_2$ (3 mol%  $Y_2O_3$ ) increased with increasing sintering temperature, with room temperature fracture toughness of  $5.16 \pm 0.11$  MPa · m<sup>1/2</sup> for samples annealed at 2150°C for 5 min. Figure 3 shows fracture surfaces of samples annealed at 1800°C for 5 min in Ar (Fig. 3(A)) and at 2150°C (Fig. 3(B)), revealing an increase in grain size from  $\approx 1$  μm to greater than 25 μm because of rapid grain growth. The fracture mode changed from intergranular for samples annealed at 1800°C to transgranular for the same  $ZrO_2$ (3 mol%  $Y_2O_3$ ) annealed at 2150°C. Despite the nearly two orders of magnitude increase in grain size, the hardness ( $12.8 \pm 0.6$  GPa) of the coarse-grained *t'*- $ZrO_2$  was similar to the hardness ( $13.3 \pm 0.1$  GPa) of the fine-grained *t*- $ZrO_2$ , while the strength decreased dramatically from  $1457 \pm 143$  MPa to  $216 \pm 24$  MPa.

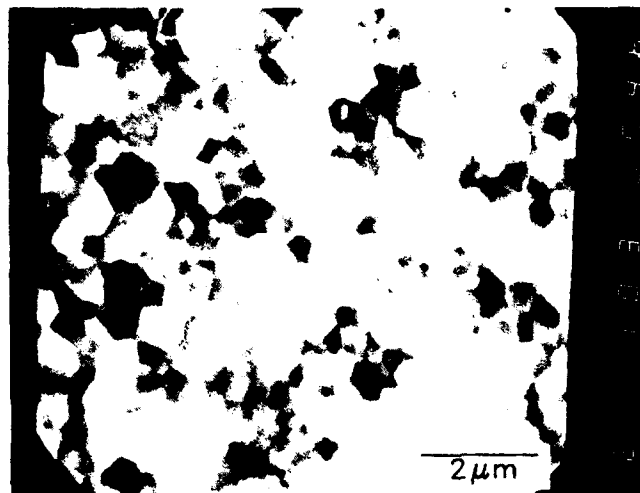
$ZrO_2$ (3 mol%  $Y_2O_3$ ) fracture surfaces analyzed after annealing above  $\approx 2100^\circ C$  and rapid cooling were fully tetragonal, as expected.<sup>3</sup> In addition, the Curie temperature upon heating was monitored by switching studies as shown in Table II.

The density of  $ZrO_2$ (3 mol%  $Y_2O_3$ ) decreased from 6.10 g/cm<sup>3</sup> (HIPed) to 5.88 g/cm<sup>3</sup> (2200°C), whereas 4, 6, and 8 mol%  $Y_2O_3$  samples showed essentially no change in density. The density of unstabilized  $ZrO_2$  samples sintered/annealed at 2200°C was 5.39 g/cm<sup>3</sup> ( $\approx 92.5\%$  TD) and the samples were heavily microcracked, as evidenced by crack closure during loading-unloading cycles of the short-rod fracture toughness tests. At temperatures greater than  $\approx 2350^\circ C$ , unstabilized  $ZrO_2$  of slightly higher density (5.51 g/cm<sup>3</sup> ( $\approx 94.5\%$  TD)) displayed conventional load-displacement behavior,<sup>24</sup> with fracture toughness of 4.8 MPa · m<sup>1/2</sup>.

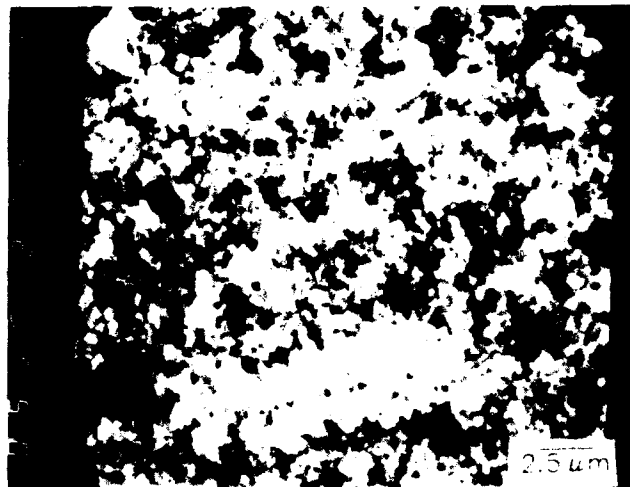
Densities of 5.55–5.75 g/cm<sup>3</sup> were typical of unstabilized  $ZrO_2$  fired at temperatures between 2350° and 2500°C. As shown in Fig. 4, the sintered unstabilized  $ZrO_2$  typically had 2%–5% closed porosity, with fracture surfaces showing significantly rougher texture than the tetragonal or cubic compositions sintered under similar conditions. The surface texture (see Fig. 4(B)) of the monoclinic  $ZrO_2$  was similar to that reported by Ingel *et al.*<sup>16</sup> for monoclinic single crystals tested at 1300°–1400°C. While there is no doubt that the unstabilized  $ZrO_2$  samples are microcracked, as evidenced by their low strength and modulus (see Table III), they retain their structural integrity after oxidation and can be cycled through the *m* ↔ *t* phase transitions, as opposed to  $ZrO_2$ , which microcracks catastrophically when sintered below the cubic temperature (see Fig. 5).

Figure 6 shows the outward appearance of samples sintered/annealed in the cubic stability range. The unstabilized  $ZrO_2$  could be reoxidized and cycled through the *m* → *t* and *t* → *m* phase transition temperatures (see Fig. 7) despite the large (25–100 μm) monoclinic  $ZrO_2$  grains (see Fig. 8). Figure 9 shows the reoxidized sample from Fig. 8 after thermal etching at 1400°C for 15 min. Monoclinic twin colonies of different orientations are readily apparent on the as-polished surface.

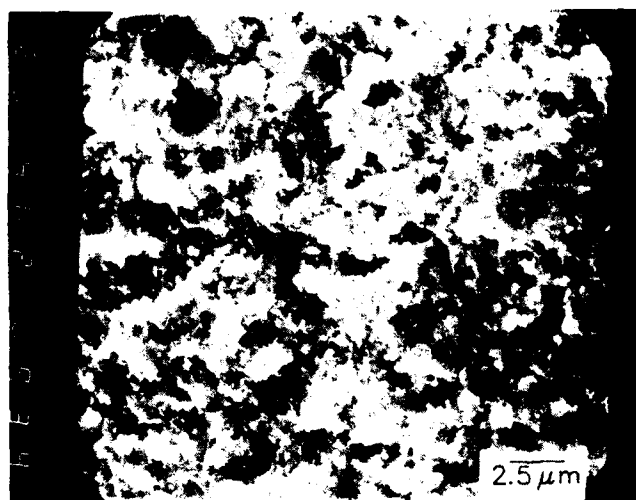
Jagged grain boundaries were observed in polished cross sections of thermally etched polycrystalline monoclinic  $ZrO_2$  (see Fig. 9). The grain boundaries are cracked because of oxidation of Zr or ZrC at grain boundaries (compare Figs. 8 and 9). Jagged grain boundaries may have occurred because of exaggerated grain growth. These jagged boundaries helped



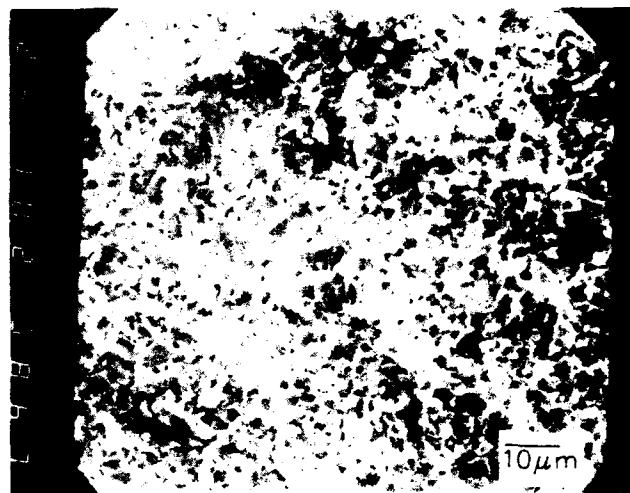
HIPed  $ZrO_2$ (2 mol. %  $Y_2O_3$ )  
(A)



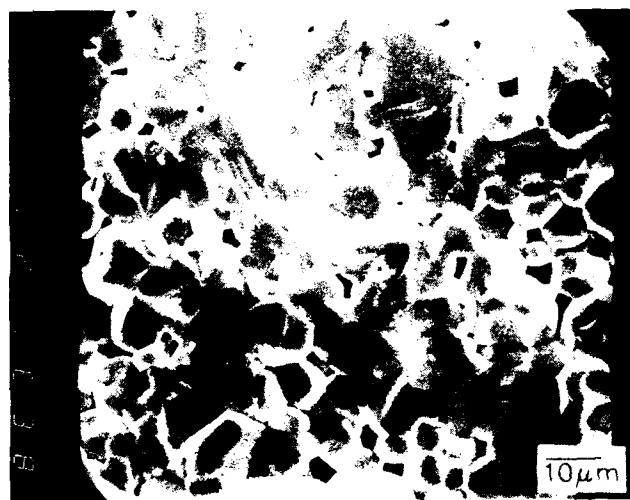
HIPed  $ZrO_2$ (3 mol. %  $Y_2O_3$ )  
(B)



HIPed  $ZrO_2$ (4.0 mol. %  $Y_2O_3$ )  
(C)



HIPed  $ZrO_2$ (6.0 mol. %  $Y_2O_3$ )  
(D)



HIPed  $ZrO_2$ (8.0 mol. %  $Y_2O_3$ )  
(E)

Fig. 1. Fracture surfaces of HIPed  $ZrO_2$ : (A)  $ZrO_2$ (2 mol%  $Y_2O_3$ ), (B)  $ZrO_2$ (3 mol%  $Y_2O_3$ ), (C)  $ZrO_2$ (4 mol%  $Y_2O_3$ ), (D)  $ZrO_2$ (6 mol%  $Y_2O_3$ ), (E)  $ZrO_2$ (8 mol%  $Y_2O_3$ ).

Table I. Room-Temperature Properties of HIPed ZrO<sub>2</sub> Samples

Y <sub>2</sub> O <sub>3</sub> (mol%)	Phases present*	GS <sup>†</sup> (μm)	σ <sub>4</sub> <sup>‡</sup> (MPa)	K <sub>IC</sub> <sup>§</sup> (MPa · m <sup>1/2</sup> )	H <sup>v</sup> (GPa)	Fracture mode**
0	100% <i>m</i>	††	††	††	††	††
2	4.3% <i>m</i> ground 20.4% <i>m</i> fracture	0.8	1404 ± 76	4.07 ± 0.13	12.9 ± 0.1	I
3	0.2% <i>m</i> ground 3.8% <i>m</i> fracture	0.5	1457 ± 134	3.54 ± 0.12	13.3 ± 0.1	I
4	<i>t</i> > <i>c</i>	2.3	1077 ± 115	3.64	13.8 ± 0.1	T
6	<i>c</i> > <i>t</i>	2.6	326 ± 55	2.18 ± 0.17	13.7 ± 0.1	T
8	<i>c</i>	11.2 <sup>‡‡</sup>	211 ± 21	1.54 ± 0.05	14.1 ± 0.9	T > I

\*Monoclinic (*m*), tetragonal (*t*), and cubic (*c*) by XRD. <sup>†</sup>Grain size. <sup>‡</sup>Four-point bend strength. <sup>§</sup>Short-rod fracture toughness. <sup>v</sup>Vickers hardness. \*\*Intergranular (I), transgranular (T). <sup>‡‡</sup>Microcracked after sintering at 1500°C. <sup>‡‡</sup>Larger grain size due to higher sintering temperature.

hold the grains together and resulted in noncatastrophic fracture during strength testing.

### (3) High-Temperature Stability of *m*-, *t*-, and *t'*-ZrO<sub>2</sub>

A comparison between ZrO<sub>2</sub> processed above and below the cubic stability field was made by heating unstabilized monoclinic ZrO<sub>2</sub> in air at 1700°C and comparing it to the same composition heat-treated first at 2440°C for 5 min in Ar and subsequently reoxidized at 1000°C for 2 h. Both samples were held at 1700°C for 72 h. The sample which had never been heated above 1700°C showed shrinkage similar to that of the samples sintered/annealed in the cubic stability field. Upon placing in water to determine percent open porosity, however, the sample which had never been heated above 1700°C turned into powder. In direct comparison, the sample which had been previously annealed in the cubic stability field could be readily handled (see Fig. 10). The excellent high-temperature stability of *m*-ZrO<sub>2</sub> processed in the cubic stability regime is shown by only a slight increase in open porosity (from 0.8% to 1.6%) and decrease in density (from 5.56 g/cm<sup>3</sup> to 5.53 g/cm<sup>3</sup>) after 72 h at 1700°C. The sample had additionally been cycled three times through the *m* ↔ *t* transitions with dimensional changes as shown in Fig. 7.

For a direct comparison to the monoclinic polycrystalline samples studied above, *t*-ZrO<sub>2</sub> (sintered at 1500°C) with 4% monoclinic and *t'*-ZrO<sub>2</sub> (same as *t*-ZrO<sub>2</sub> except heat-treated at 2000°C for 5 min in Ar and subsequently reoxidized) were held at 1700°C in a manner identical to that of the two monoclinic materials. The *t'*- and *t*-ZrO<sub>2</sub> samples contained 56 and 71% monoclinic ZrO<sub>2</sub>, respectively, after the 72-h age. Severe microcracking occurred in both materials, in comparison to the monoclinic material, which showed no change in outward appearance.

### (4) Fracture Toughness Comparison between *m*-, *t*-, *t'*-, and *c*-ZrO<sub>2</sub>

The comparison between the fracture toughness of monoclinic, tetragonal, and cubic ZrO<sub>2</sub> is given in Table IV for

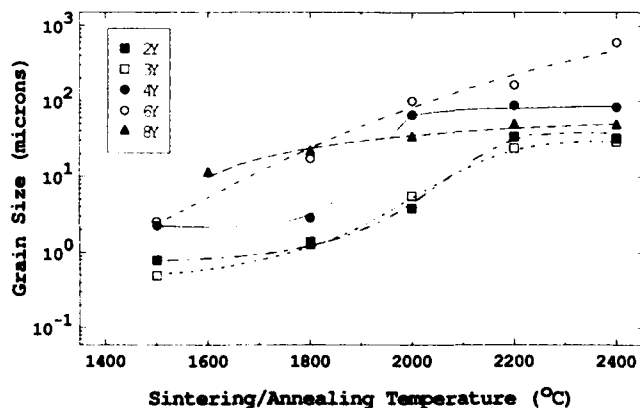
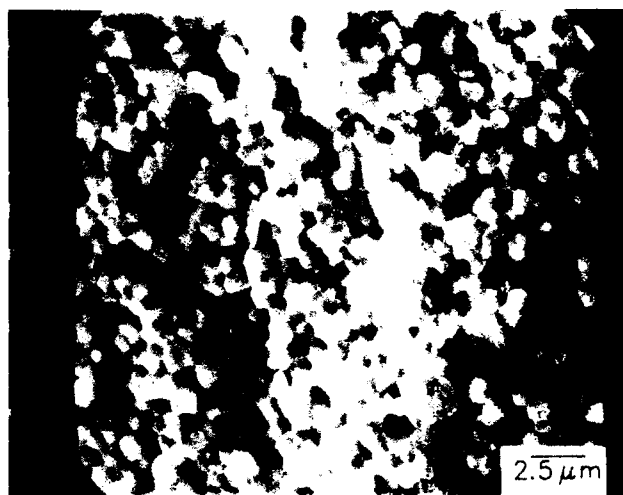


Fig. 2. Grain size as a function of annealing temperature for ZrO<sub>2</sub> containing either 2, 3, 4, 6, or 8 mol% Y<sub>2</sub>O<sub>3</sub>.

samples annealed at 2450°C for 5 min in He and Table V for samples annealed under various conditions in Ar. The fracture toughness of monoclinic ZrO<sub>2</sub> varied significantly, depending upon the processing parameters, ranging between 3.7 and 6.0 MPa · m<sup>1/2</sup>. Sintering in Ar produced K<sub>IC</sub> values between 4.8 and 6.0 MPa · m<sup>1/2</sup>, whereas sintering in He resulted in values as low as 3.7 MPa · m<sup>1/2</sup>. Fracture toughness measurements



1800°C ZrO<sub>2</sub>(3 mol% Y<sub>2</sub>O<sub>3</sub>)  
(A)

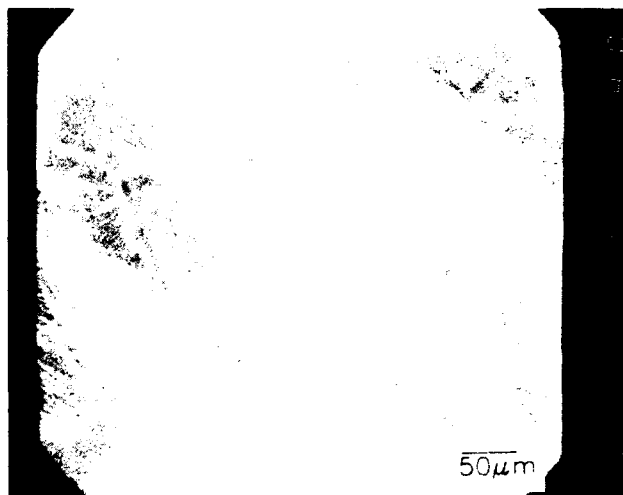


Fig. 3. ZrO<sub>2</sub>(3 mol% Y<sub>2</sub>O<sub>3</sub>) annealed at (A) 1800°C and (B) 2150°C for 5 min in Ar. Note change in grain size and fracture mode.

**Table II. Switching Tendency of  $ZrO_2(3 \text{ mol}\% Y_2O_3)$  as a Function of Annealing Temperature**

Annealing temp. ( $^{\circ}C$ )	As-sintered surface ((002):(200))	Ground surface ((002):(200))
22	0.77	1.90
1550	0.61	2.14
2050	0.30	0.67
2150	0.40	0.41

<sup>a</sup>Ratio of integrated tetragonal (002), (200) peaks. The higher the value, the more domain switching has occurred. After sintering at 1500 $^{\circ}C$  for 2 h.

could not be made on monoclinic  $ZrO_2$  processed below the Curie temperature, because of excessive microcracking.

#### IV. Discussion

##### (I) High-Temperature Annealing

The reducing environment of the graphite furnace used in the present study was not ideal for the high-temperature

annealing studies, since zirconia became oxygen-deficient and  $ZrO_2-Zr$  or  $ZrO_2-ZrC$  composites were formed (see Fig. 8). Virkar<sup>17</sup> found that there is always oxygen dissolved in  $Zr$  in  $ZrO_2-Zr$  mixtures and that the dissolved oxygen embrittles the zirconium. In addition, the large volume increase associated with the reoxidation of  $Zr$  and/or  $ZrC$  located along grain boundaries caused microcracking (see Fig. 9). The  $Zr$  or  $ZrC$  formed was below detection limits for XRD because of the short annealing times used. A far better approach would be to use an oxidizing atmosphere, but inadequate high-temperature insulation and temperature control in the 2100 $^{\circ}$ -2500 $^{\circ}C$  range limited this approach.

A problem related to processing in a reducing environment is knowing the Curie temperature (i.e., the  $t \rightarrow c$  transition temperature). While  $t \rightarrow c$  temperature for  $ZrO_2$  is well-defined at  $\approx 2370^{\circ}C$  in air,<sup>18</sup> this temperature is not established for the reducing conditions within the graphite furnace ( $P_{O_2} \approx 1 \times 10^{-14}$  atm). The work of Ruh and Garrett<sup>14</sup> and Rauh and Garg<sup>15</sup> shows that the  $t \rightarrow c$  temperature for  $ZrO_2$

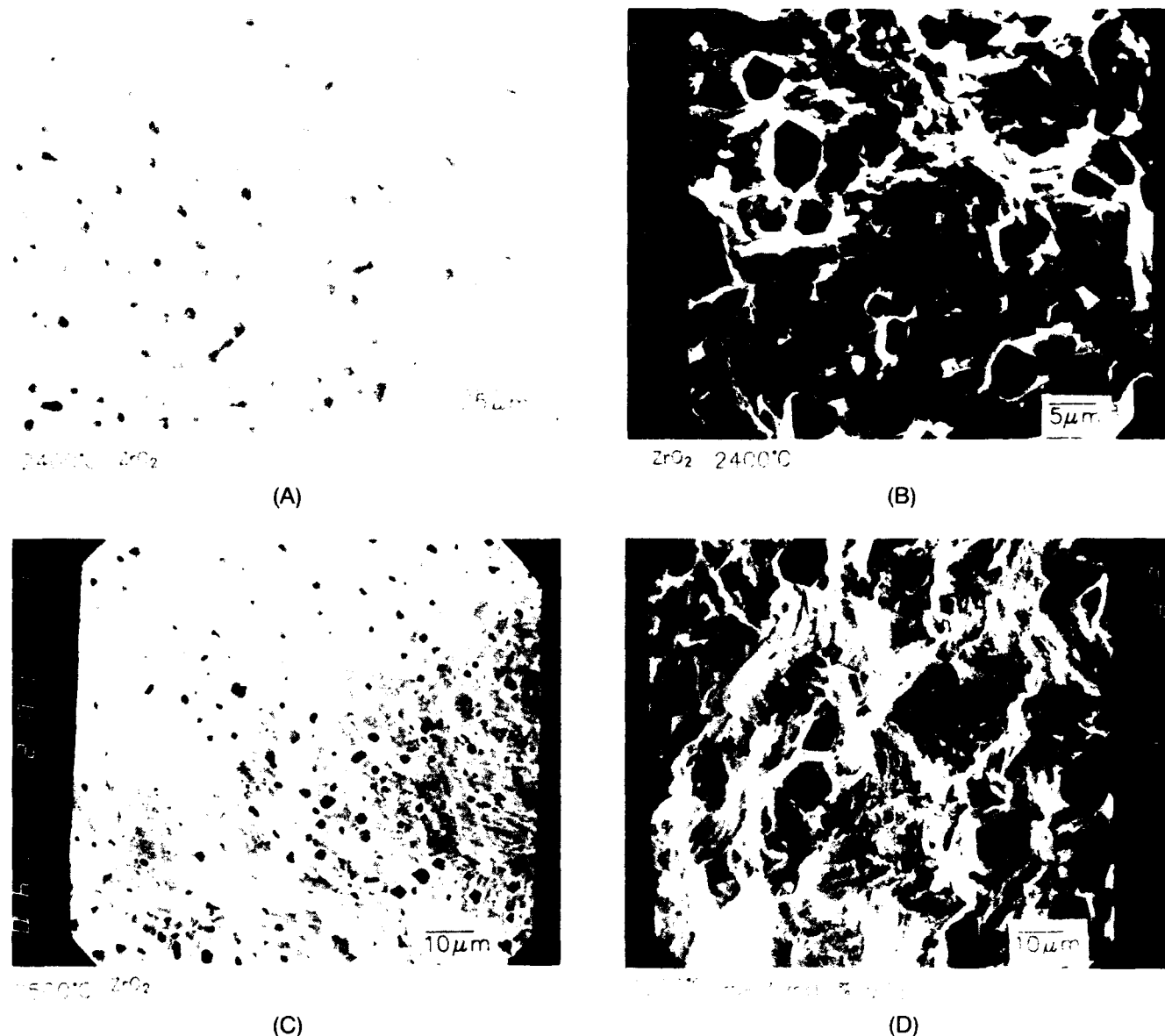


**Fig. 4.** Comparison of monoclinic, tetragonal, and cubic  $ZrO_2$  sintered/annealed at various temperatures. (A) Polished cross section and (B) fracture surface of unstabilized  $ZrO_2$  annealed at 2400 $^{\circ}C$ . (C) Fracture surface of unstabilized  $ZrO_2$  annealed at 2500 $^{\circ}C$ .  $ZrO_2(3 \text{ mol}\% Y_2O_3)$  heat-treated at (D) 2000 $^{\circ}C$  and (E) 2400 $^{\circ}C$ . Note increase in porosity at 2400 $^{\circ}C$ .  $ZrO_2(4 \text{ mol}\% Y_2O_3)$  heat-treated at (F) 2000 $^{\circ}C$  and (G) 2400 $^{\circ}C$ . Note change in fracture mode with heat treatment.  $ZrO_2(8 \text{ mol}\% Y_2O_3)$  heat-treated at (H) 2000 $^{\circ}C$  and (I) 2400 $^{\circ}C$ .



24% Cr<sub>2</sub>O<sub>3</sub>/ZrO<sub>2</sub>(3.3 mol % Y<sub>2</sub>O<sub>3</sub>)

(E)



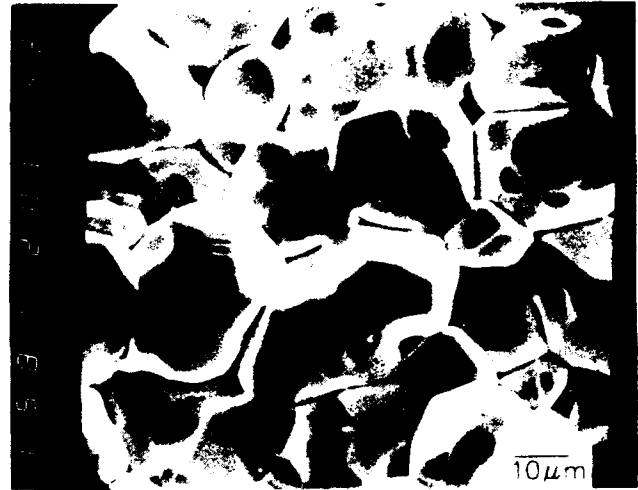
24% Cr<sub>2</sub>O<sub>3</sub>/ZrO<sub>2</sub>(4.4 mol % Y<sub>2</sub>O<sub>3</sub>)

(F)



24% Cr<sub>2</sub>O<sub>3</sub>/ZrO<sub>2</sub>(4.4 mol % Y<sub>2</sub>O<sub>3</sub>)

(G)



24% Cr<sub>2</sub>O<sub>3</sub>/ZrO<sub>2</sub>(5.0 mol % Y<sub>2</sub>O<sub>3</sub>)

(H)



24% Cr<sub>2</sub>O<sub>3</sub>/ZrO<sub>2</sub>(5.3 mol % Y<sub>2</sub>O<sub>3</sub>)

(I)

Fig. 4. (Continued)

**Table III. Properties of Polycrystalline Monoclinic ZrO<sub>2</sub>**

Sintered at 1500°C	
Linear shrinkage:	18.5%
Heavily microcracked (easily pulverized)	
Sintered/annealed above ≈2350°C	
Linear shrinkage:	18.7%
Density:	5.55–5.75 g/cm <sup>3</sup> (>95% of theoretical)
Open porosity:	≈0.7%
Lattice parameters:	$a = 5.14 \text{ \AA}$ , $b = 5.21 \text{ \AA}$ , $c = 5.31 \text{ \AA}$ , and $\beta = 99.2^\circ$
Thermal expansion (25°–1175°C):	$8.7 \times 10^{-6}/^\circ\text{C}$
Hardness:	4.1–5.2 GPa
Strength:	75–150 MPa
Fracture toughness:	3.7–6.0 MPa · m <sup>1/2</sup>
Young's modulus:	175 GPa
Easily reoxidized and cycled through $m \leftrightarrow t$ transition	
Good high-temperature stability with density only decreasing from 5.56 to 5.53 g/cm <sup>3</sup> upon cycling three times through $m \leftrightarrow t$ transition and aging 72 h at 1700°C in air	

in reducing atmospheres decreases rapidly with increasing oxygen vacancies. The wide variation in temperature which different investigators have used to sinter polycrystalline ZrO<sub>2</sub><sup>21, 23</sup> is likely due to this variation in  $t \rightarrow c$  transformation temperature.

Table II data for ZrO<sub>2</sub>(3 mol% Y<sub>2</sub>O<sub>3</sub>) are consistent with a Curie temperature of ≈2100°C,<sup>3</sup> since the ground surface retains a high degree of texture, relative to the unground surface, at high temperatures (i.e., 1500°C) and does not have similar (002)/(200) tetragonal ratios until temperatures above 2100°C. Once the ground surface is reheated into the cubic stability field, it has the same intensity as the as-sintered surface. As expected, grinding of the annealed samples creates new texture. Unfortunately, ground surfaces recrystallize<sup>33,34</sup> at elevated temperatures, complicating this approach for determining Curie temperatures.

Ferroelastic switching was observed on ground surfaces of polycrystalline  $m$ -ZrO<sub>2</sub> surfaces, as shown in comparison to polished surfaces in Fig. 11. Gasdaska *et al.*<sup>33</sup> showed texture due to ferroelastic domain switching (i.e., twinning) in monoclinic HfO<sub>2</sub>. They predicted, based on calculated maximum resolved shear stress under uniaxial tension, that (111), (113), and (022) peaks should decrease in intensity upon grinding, while (201), (202) and (312) should increase in

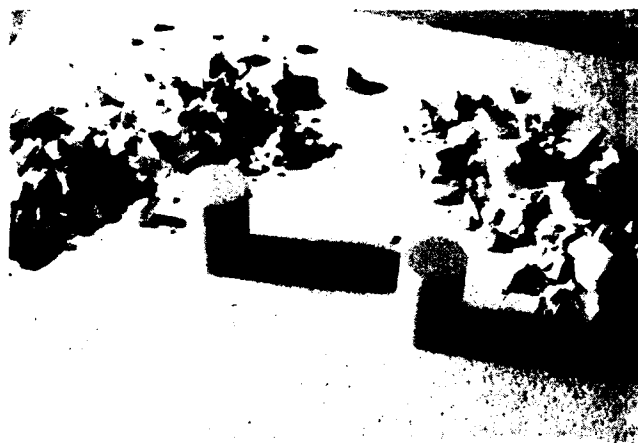


**Fig. 5.** Comparison of monoclinic ZrO<sub>2</sub> sintered/annealed at ≈2450°C for 5 min (short-rod samples with structural integrity in foreground) and at 1500°C for 2 h (crumbled short rods in background). Dilatometric studies show that both materials experienced similar shrinkage prior to cooling through the  $t \rightarrow m$  transformation.

## POLYCRYSTALLINE MONOCLINIC ZIRCONIA

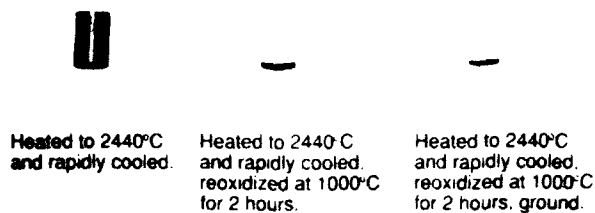


**Fig. 6.** Outward appearance of polycrystalline monoclinic ZrO<sub>2</sub>.

intensity upon grinding.<sup>33</sup> This is clearly the case of the (111) monoclinic peak in Fig. 11. Further work, however, is needed to evaluate switching in monoclinic ZrO<sub>2</sub>.

### (2) Polycrystalline Monoclinic ZrO<sub>2</sub>

It is interesting to compare the data for polycrystalline  $m$ -ZrO<sub>2</sub> with polydomain ZrO<sub>2</sub> single crystals, since both were processed in the cubic regime and rapidly cooled. A comparison of thermal expansion (see Fig. 7) of polycrystalline ZrO<sub>2</sub> is in good agreement with the work of Adams *et al.*<sup>15</sup> for single-crystal ZrO<sub>2</sub>, which could also be cycled through the  $t \leftrightarrow m$  transitions without catastrophic failure. Adams *et al.* found that the  $m \rightarrow t$  transformation initiated at ≈1180°C was completed at ≈1190°C. The  $t \rightarrow m$  transformation during cooling began at ≈1050°C and was completed by approximately ≈920°C.<sup>15</sup> The monoclinic single crystals had densities of 5.75 g/cm<sup>3</sup> (Ref. 16), or 98.6% of theoretical,<sup>17</sup> which is similar to the highest densities achieved for the polycrystalline materials. Both the hardness (6.6 GPa) and strength (as high as 246 MPa at room temperature on polished bars) were higher for the single crystals, but the fracture toughness of ≈2.5 MPa · m<sup>1/2</sup> at room temperature was lower.<sup>16</sup> The lower strength and hardness are likely related to greater microcracking and porosity in the polycrystalline samples fabricated in the present study. The higher toughness in the present study may be related to enhanced microcrack toughening,  $R$ -curve effects, or differences in techniques. Ingel *et al.*<sup>16</sup> observed that the fracture toughness increased to 4.0 MPa · m<sup>1/2</sup> at 1225°C and

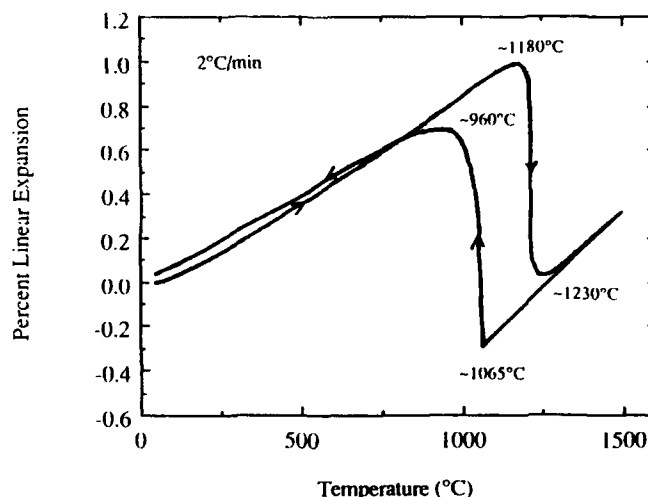


**Fig. 7.** Linear expansion as a function of temperature for monoclinic ZrO<sub>2</sub> previously heated to 2440°C and rapidly cooled, reoxidized at 1000°C for 2 h, and aged at 1700°C for 72 h.

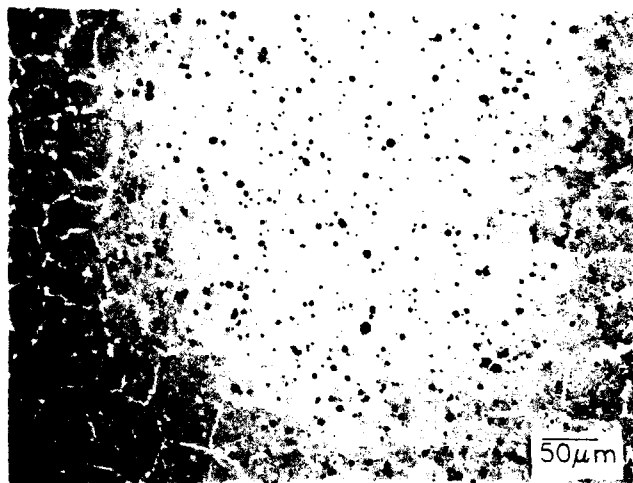


Fig. 8. Optical micrograph of polished cross section of monoclinic  $ZrO_2$  sintered/annealed at  $2470^\circ C$  in He for 5 min. Gray phase is monoclinic  $ZrO_2$ , light phase is free Zr or  $ZrC$ , and dark spots are pores.

then decreased to  $2.6 \text{ MPa} \cdot \text{m}^{1/2}$  at  $1400^\circ C$  for single crystals. A similar increase in toughness occurred near the  $t \rightarrow m$  transformation temperature upon cooling. The increase in fracture toughness was explained based on transformation toughening.<sup>16</sup> High-temperature toughness was not explored for the polycrystalline samples fabricated in the present study.

The ability to make monoclinic  $ZrO_2$  with significant mechanical strength (see Table III) by annealing in the cubic stability field, as opposed to the low strength of monoclinic  $ZrO_2$  sintered in the tetragonal stability field, is believed to be due to the formation of the same three variants upon rapid cooling into the tetragonal stability field which occur for  $t'$ - $ZrO_2$ . It is well-documented that domain size, not grain size, controls transformation in  $ZrO_2(Y_2O_3)$  ceramics cooled rapidly from the cubic temperature.<sup>34</sup> The stress accommodation due to the submicrometer tetragonal variants allows large-grained ( $> 100\text{-}\mu\text{m}$ ) polycrystalline tetragonal  $ZrO_2$  to be studied.<sup>12,14,34</sup>

Muddle and Hannink<sup>20</sup> and Hayakawa *et al.*<sup>35</sup> both observed 12 variants for  $m$ - $ZrO_2$  formed from partially stabilized  $ZrO_2$  materials heated into the cubic regime, rapidly quenched, and

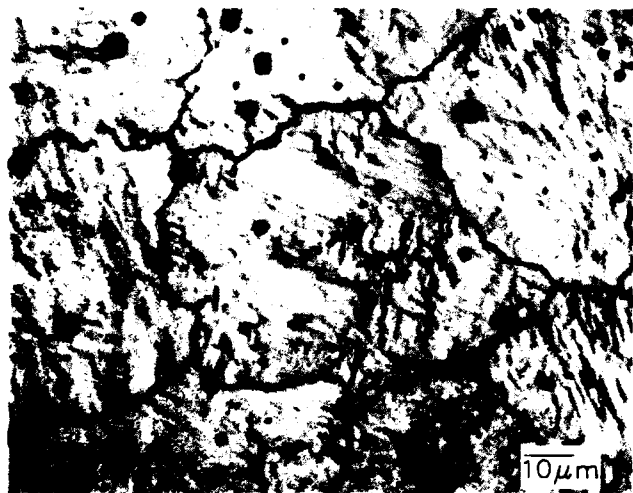


Fig. 9. Nomarski interference contrast micrograph of monoclinic  $ZrO_2$  sintered/annealed at  $2470^\circ C$  in He for 5 min, reoxidized at  $1000^\circ C$ , and polished prior to being thermally etched in air at  $1400^\circ C$  for 15 min. Note twin colonies with different orientations within single grains.

## POLYCRYSTALLINE MONOCLINIC ZIRCONIA

Heated to  $2440^\circ C$   
and rapidly cooled,  
reoxidized at  $1000^\circ C$   
for 2 hours, aged at  
 $1700^\circ C$  for 72 hours.

Sintered/annealed at  
 $1700^\circ C$  for 72 hours.

Fig. 10. Monoclinic  $ZrO_2$  heat-treated above the Curie temperature (right) compared with  $m$ - $ZrO_2$  sintered in the tetragonal stability regime (left). Both materials have been heated at  $1700^\circ C$  for 72 h. Note structural integrity of  $m$ - $ZrO_2$  processed at high temperatures compared to severe microcracking resulting in pulverization of the material processed at normal sintering temperatures.

then annealed at low temperatures to form  $m$ - $ZrO_2$  from the three tetragonal variants in  $t'$ - $ZrO_2$ .

Muddle and Hannink<sup>20</sup> explained the 12 variants, given three variants of the parent tetragonal lattice, two possible orientation relationships between tetragonal and monoclinic lattices, and two possible variants of each orientation relationship (plus their twin relationships). This is consistent with only four variants for monoclinic  $ZrO_2$  formed from single-domain  $t$ - $ZrO_2$ .<sup>19</sup> There is disagreement, however, on the number of monoclinic variants possible from a single tetragonal grain, since at least 12 variants are possible based on six variants of correspondence and two variants of orientation (plus their twin relationships).<sup>36</sup> TEM studies comparing  $m$ - $ZrO_2$  twins formed from  $t'$ -grains (i.e., rapidly cooled from the cubic stability regime) with  $m$ - $ZrO_2$  formed from  $t$ - $ZrO_2$  (cooled from the tetragonal stability regime) are required to see if more (or smaller) variants are formed for stress accommodation in the monoclinic  $ZrO_2$  cooled from the cubic phase.

If all the  $t'$  variants transformed into monoclinic variants at the same time, the volume expansion ( $\approx 4.5\%$ ) would result in no net stress. As shown in Fig. 7, the polycrystalline monoclinic  $ZrO_2$  has thermal expansion behavior similar to the polydomain skull-melted single crystals,<sup>15</sup> where different domains transform at different temperatures. The temperature range for transformation in polycrystalline monoclinic  $ZrO_2$  is similar to that for single-crystal monoclinic  $ZrO_2$ . Assuming similar or smaller (due to more rapid cooling) domain size in the polycrystalline monoclinic  $ZrO_2$  as in the polydomain single crystals, polycrystalline monoclinic  $ZrO_2$  can survive the  $t' \rightarrow m$  transformation, since the variants are oriented so as to minimize stress within a single grain. It is the domain size, not the grain size, which is critical when considering transformation in polydomain materials.<sup>14,34</sup> The size of the three mutually orthogonal domains in polycrystalline  $t'$   $ZrO_2$  was found to be on the order of  $0.5 \mu\text{m}$  in length and less than  $0.1 \mu\text{m}$  in width.<sup>14</sup> It is expected that domain size will increase with increasing  $c/a$  ratio as the stability of the tetragonal phase decreases.<sup>37</sup> TEM of skull-melted monoclinic  $ZrO_2$  single crystals, however, showed that the twin width was about  $100\text{--}300 \text{ nm}$ .<sup>38</sup>

Even if all of the  $t'$  domains transformed simultaneously, there would still be stresses due to the shape change ( $\approx 7\%$ ) as monoclinic twins are formed. The twinning process accommodates some of the stress associated with the transformation.

**Table IV. Short-Rod Fracture Toughness Comparison of Polycrystalline Zirconias Annealed at 2450°C for 5 min in Helium**

Material	Polymorph	Fracture toughness (MPa · m <sup>1/2</sup> )
ZrO <sub>2</sub>	Monoclinic	3.7 ± 0.3
ZrO <sub>2</sub> (3 mol% Y <sub>2</sub> O <sub>3</sub> )	Tetragonal ( <i>t'</i> )	4.5 ± 0.2
ZrO <sub>2</sub> (8 mol% Y <sub>2</sub> O <sub>3</sub> )	Cubic	1.7 ± 0.2

Green *et al.*<sup>39</sup> has recently reviewed much of the work on transformation processes, including the thermodynamics of crack propagation with chemical, dilatational, and shear energy contributions. As discussed by Evans and Heuer,<sup>40</sup> the change in strain energy,  $\Delta U$ , due to the transformation of precipitates in an infinite matrix is given as

$$\Delta U = -V_p e_{ij}^T \left( \sigma_{ij}^A + \left( \frac{1}{2} \right) \sigma_{ij}^I \right)$$

where  $V_p$  is the volume of the precipitate particle,  $e_{ij}^T$  are the unconstrained transformation strains, and  $\sigma_{ij}^A$  and  $\sigma_{ij}^I$  are the applied and hydrostatic stresses, respectively, on the precipitate. Twin/variant configurations will occur so as to minimize microcracking. Wunderlich and Rühle<sup>38</sup> experimentally determined maximum tensile strains of 0.14 for monoclinic twins in single crystals and calculated a critical tensile stress of 29 GPa for microcracking. This calculation indicates that small domains (twins) can withstand large strains.

### (3) Aging Experiments

Noma *et al.*<sup>37</sup> studied the stability at 1700°C of *t'*-zirconias formed by arc-melting and rapid quenching. The ZrO<sub>2</sub>(3 mol% Y<sub>2</sub>O<sub>3</sub>) *t'*-ZrO<sub>2</sub> materials with fine domain structure showed no change in (004) and (400) peaks after aging at 1700°C for 48 h. These results suggest that diffusion and the subsequent formation of *t*- and *c*-ZrO<sub>2</sub> from *t'*-ZrO<sub>2</sub> is sluggish for the rapidly quenched samples because of their fine domain size.

The high amount of monoclinic observed after aging the *t'*-ZrO<sub>2</sub>(4 mol% Y<sub>2</sub>O<sub>3</sub>) of the present study at 1700°C for 72 h is consistent with the slower quenching compared to Noma *et al.*<sup>37</sup> One advantage of the reoxidized monoclinic ZrO<sub>2</sub> is that high-temperature aging cannot occur via diffusion to the cubic phase, since temperatures up to 2300°C are in the tetragonal stability field. Hence, the excellent stability of these materials at very high temperatures. A potential problem, however, may be repeated cycling through the *m* ↔ *t* transitions where stress can induce domain growth.

### (4) Fracture Toughness

The high-temperature heat treatments which allow the displacive *c* → *t'* transformation to occur were performed in order to eliminate the influence of transformation toughening in the tetragonal materials studied. In materials which undergo stress-induced transformations, it is difficult to isolate the magnitude of ferroelastic toughening for samples which show significant transformation toughening. This is because switching can occur preceding transformation.<sup>5</sup> The samples processed at high temperatures have large grain size, which may be desirable for creep resistance but is not desirable for high strength.

The bright phase (i.e., Zr or ZrC below detection limits of XRD) observed in polished cross sections of the oxygen-deficient zirconia, resulting from the annealing in the graphite

resistance-heated furnace, did not likely affect the fracture toughness measurements, since ZrO<sub>2</sub>(3 mol% Y<sub>2</sub>O<sub>3</sub>) annealed at 2000°C for 5 min in Ar had a fracture toughness of 5.26 ± 0.15 MPa · m<sup>1/2</sup>, while identical (except white instead of black) samples annealed at 1000°C for 2 h in air had a fracture toughness of 5.37 ± 0.04 MPa · m<sup>1/2</sup>. This is consistent with the work of Virkar<sup>39</sup> on ZrO<sub>2</sub>-Zr composites and the low concentration of the metallic phase (below XRD detection levels). There were no significant differences between the toughness of tetragonal ZrO<sub>2</sub> processed above and below the Curie temperature (see Fig. 12). High-temperature processing of cubic ZrO<sub>2</sub> did not affect its toughness, as shown in Fig. 12.

Monoclinic ZrO<sub>2</sub> reoxidized at 1000°C showed significant anelastic effects (load-displacement traces with positive displacement from the origin) in short-rod tests.<sup>24</sup> This is likely due to microcracking which occurred during reoxidation and associated problems with crack closure. Obviously, high-temperature sintering/annealing in air would be preferred in order to avoid problems with reoxidation. Despite the problems of reoxidation, similar crack patterns were found around indents for monoclinic ZrO<sub>2</sub> in the "as-annealed" and "reoxidized" states (see Fig. 13).

The fracture toughness comparison of polycrystalline *m*-, and *t*- and *c*-ZrO<sub>2</sub> materials shows that the ferroelastic *m*-, and *t*- materials are at least twice as tough as paraelastic *c*-ZrO<sub>2</sub> under all conditions evaluated. While microcrack toughening may be significant in *m*-ZrO<sub>2</sub>, the fact that cooling from the cubic stability regime allows *m*-ZrO<sub>2</sub> to avoid catastrophic microcracking suggests that ferroelastic domain switching is contributing to toughening.

There may be a number of practical applications for polycrystalline monoclinic ZrO<sub>2</sub> because of its relatively good toughness. One such application was investigated by slip casting and sintering exhaust port liners. The high thermal expansion of ZrO<sub>2</sub> is a better match for metals than low expansion ceramics. Reoxidized samples could withstand high thermal shock, presumably because of their high toughness and microcracked structure. Although there are other methods for making polycrystalline monoclinic ZrO<sub>2</sub> at low temperatures, such as superplastic forming<sup>41,42</sup> or low-temperature sintering of fine powders,<sup>43,44</sup> it is doubtful that these materials have the toughness to survive such severe thermal shock.

## V. Conclusions

The room-temperature fracture toughness of polycrystalline monoclinic, tetragonal, and cubic ZrO<sub>2</sub> was compared for materials sintered/annealed at temperatures between 1500° and 2500°C. The fracture toughness of ferroelastic *m*-ZrO<sub>2</sub> was comparable to that of ferroelastic *t* and *t'* zirconias, which were 2–3 times higher than paraelastic cubic ZrO<sub>2</sub>.

Monoclinic ZrO<sub>2</sub> sintered in the cubic stability range had densities greater than 95% of theoretical. Open porosities

**Table V. Short-Rod Toughness Comparison of Monoclinic, Tetragonal, and Cubic ZrO<sub>2</sub> Annealed in Ar Under Various Conditions**

Y <sub>2</sub> O <sub>3</sub> (mol%)	Polymorph	Annealing conditions	Fracture toughness (MPa · m <sup>1/2</sup> )
0	Monoclinic	2440°C/30 min	6.0 ± 0.1
3	Tetragonal	2000°C/5 min	5.3 ± 0.2
8	Cubic	2400°C/5 min	1.8 ± 0.2

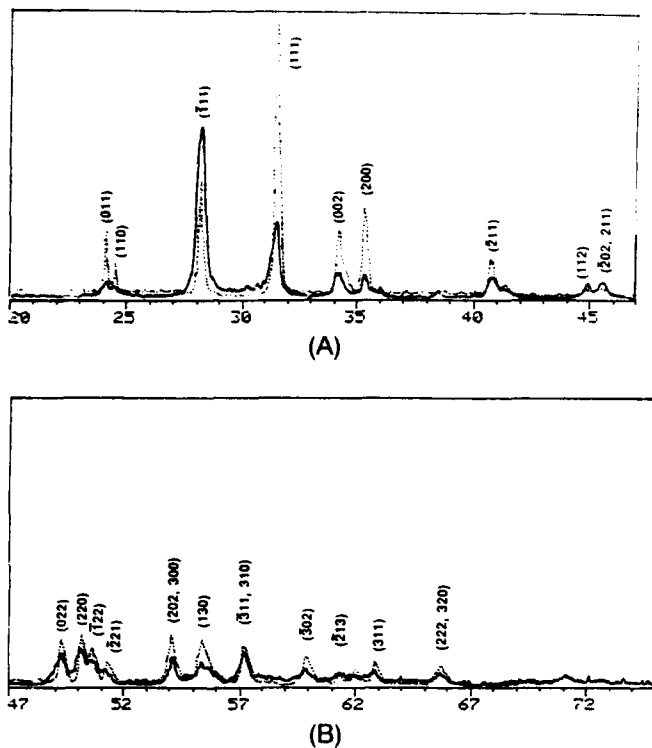


Fig. 11. X-ray diffraction ( $\text{CuK}\alpha$ ) pattern of polycrystalline  $\text{ZrO}_2$  as polished (dotted line) and after grinding (solid line). (A)  $20^\circ$ – $47^\circ$   $2\theta$ . (B)  $47^\circ$ – $70^\circ$   $2\theta$ .

were  $\approx 0.7\%$ , indicating that some microcracking may have occurred while cooling through the  $t \rightarrow m$  transition. The  $m$ - $\text{ZrO}_2$  could be cycled through the  $m \leftrightarrow t$  transitions with only a slight decrease in density and slight increase in open porosity. This is in stark contrast to  $m$ - $\text{ZrO}_2$  sintered in the tetragonal stability range, which undergoes severe microcracking upon cooling through the  $m \leftrightarrow t$  transition. Enhanced domain structure in  $m$ - $\text{ZrO}_2$  cooled from the cubic stability range is

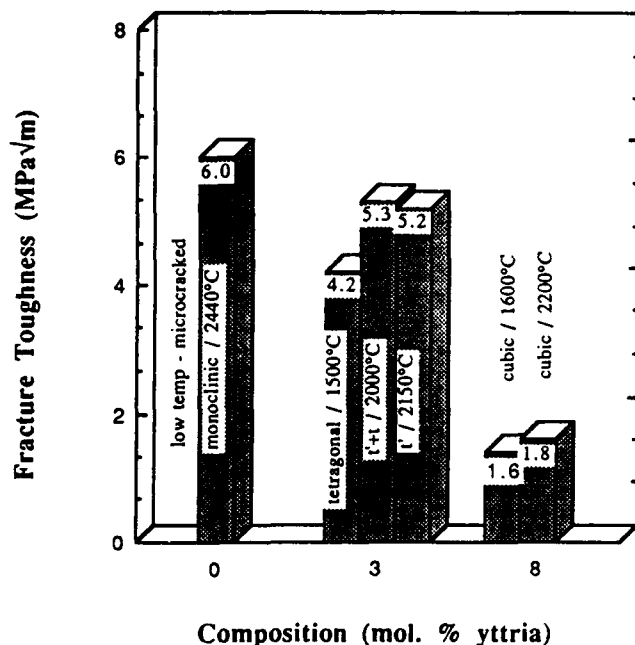
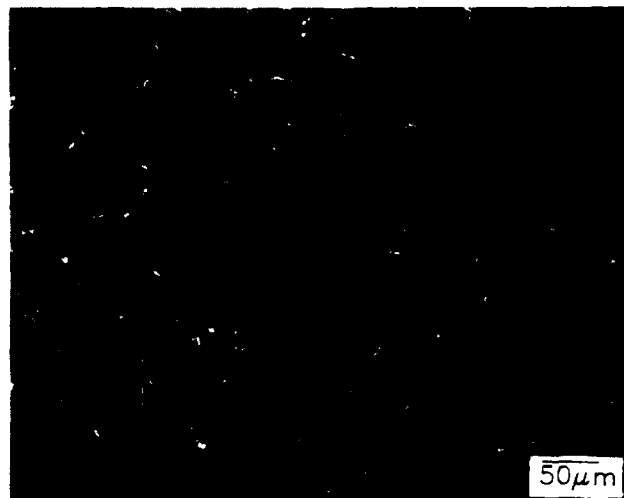
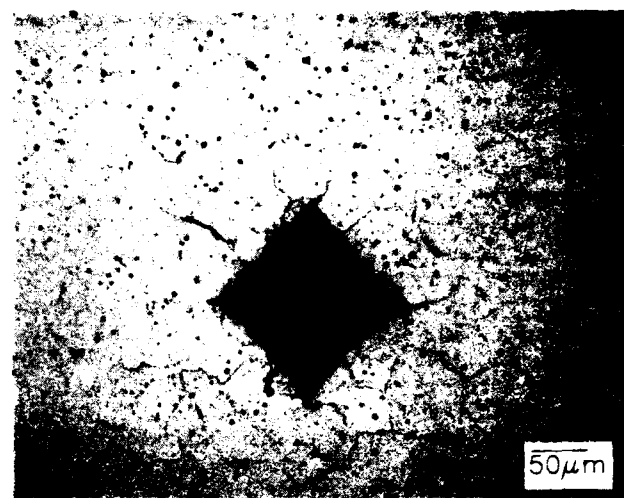


Fig. 12. Fracture toughness comparison of conventionally sintered and high-temperature-processed monoclinic, tetragonal, and cubic  $\text{ZrO}_2$ .



(A)



(B)

Fig. 13. Crack propagation around 75-N Vickers indents in monoclinic  $\text{ZrO}_2$  sintered at  $2470^\circ\text{C}$  in He for 5 min and rapidly cooled. (A) As-sintered. (B) reoxidized at  $1000^\circ\text{C}$  for 2 h. Note similar crack patterns around indents.

believed to be the primary reason for the ability of the high-temperature-processed  $m$ - $\text{ZrO}_2$  to survive  $t \leftrightarrow m$  transitions. Aging at  $1700^\circ\text{C}$  for 72 h did not affect the ability of the monoclinic zirconia to survive the  $t \leftrightarrow m$  transitions.

Work is needed to compare the domain structure and toughness of monoclinic  $\text{ZrO}_2$  annealed in the cubic stability regime with  $m$ - $\text{ZrO}_2$  fabricated below the monoclinic-tetragonal transformation temperature. The higher toughness of polycrystalline  $m$ - $\text{ZrO}_2$  as compared to single-crystal  $m$ - $\text{ZrO}_2$  deserves further investigation to determine the role of crack bridging and microcracking on toughening.

**Acknowledgment:** Discussions with Professor Anil V. Virkar of the University of Utah are gratefully acknowledged.

#### References

- V. K. Wadhawan, "Ferroelasticity and Related Properties of Crystals," *Phase Transitions*, **3**, 3-103 (1982).
- D. Michel, L. Mazerolles, and M. Perez Y Jorba, "Fracture of Metastable Tetragonal Zirconia Crystals," *J. Mater. Sci.*, **18**, 2618-28 (1983).
- H. G. Scott, "Phase Relationships in the Zirconia-Yttria System," *J. Mater. Sci.*, **10** [9] 1527-35 (1975).
- A. V. Virkar and R. L. K. Matsumoto, "Ferroelastic Domain Switching as a Toughening Mechanism in Tetragonal Zirconia," *J. Am. Ceram. Soc.*, **69** [10] C-224-C-226 (1986).

- <sup>9</sup>A. V. Virkar and R. L. K. Matsumoto, "Toughening Mechanism in Tetragonal Polycrystalline (TZP) Ceramics"; pp. 653-62 in *Advances in Ceramics*, Vol. 24, *Science and Technology of Zirconia III*. Edited by S. Somiya, N. Yamamoto, and H. Yanagida. American Ceramic Society, Westerville, OH, 1988.
- <sup>10</sup>V. Lanteri, R. Chaim, and A. H. Heuer, "On the Microstructures Resulting from the Diffusionless Cubic  $\rightarrow$  Tetragonal Transformation in  $ZrO_2$ - $Y_2O_3$  Alloys," *J. Am. Ceram. Soc.*, **69** [10] C-258-C-261 (1986).
- <sup>11</sup>V. Lanteri, A. H. Heuer, and T. E. Mitchell, "Tetragonal Phase in the System  $ZrO_2$ - $Y_2O_3$ "; pp. 118-30 in *Advances in Ceramics*, Vol. 12, *Science and Technology of Zirconia II*. Edited by N. Claussen, M. Rühle, and A. H. Heuer. American Ceramic Society, Westerville, OH, 1983.
- <sup>12</sup>T. Sakuma, Y. Yoshizawa, and H. Suto, "The Microstructure and Mechanical Properties of Yttria-Stabilized Zirconia Prepared by Arc-Melting," *J. Mater. Sci.*, **20**, 1399-2407 (1985).
- <sup>13</sup>T. Sakuma, "Development of Domain Structure Associated with the Diffusionless Cubic-to-Tetragonal Transition in  $ZrO_2$ - $Y_2O_3$  Alloys," *J. Mater. Sci.*, **22**, 4470-75 (1987).
- <sup>14</sup>T. Noma, M. Yoshimura, S. Somiya, M. Kato, M. Yanagisawa, and H. Seto, "Formation of Diffusionlessly Transformed Tetragonal Phases in Rapid Quenching of  $ZrO_2$ - $Y_2O_3$  Melts," *J. Mater. Sci.*, **23**, 2689-92 (1988).
- <sup>15</sup>R. P. Ingel, D. Lewis, B. A. Bender, and S. C. Semken, "Properties and Microstructures of Rapidly Solidified Zirconia-Based Ceramic Alloys"; see Ref. 5, pp. 385-96.
- <sup>16</sup>G. V. Srinivasan, J. F. Jue, S. Y. Kuo, and A. V. Virkar, "Ferroelastic Domain Switching in Polydomain Tetragonal Zirconia Single Crystals," *J. Am. Ceram. Soc.*, **72** [11] 2098-103 (1989).
- <sup>17</sup>K. Mehta and A. V. Virkar, "Fracture Mechanisms in Ferroelastic-Ferroelastic Lead Zirconate Titanate Ceramics," *J. Am. Ceram. Soc.*, **73** [3] 567-74 (1990).
- <sup>18</sup>J. F. Jue and A. V. Virkar, "Fabrication, Microstructural Characterization and Mechanical Properties of Polycrystalline *t'*-Zirconia," *J. Am. Ceram. Soc.*, **73** [12] 3650-57 (1990).
- <sup>19</sup>J. W. Adams, H. H. Nakamura, R. P. Ingel, and R. W. Rice, "Thermal Expansion Behavior of Single-Crystal Zirconia," *J. Am. Ceram. Soc.*, **68** [9] C-228-C-231 (1985).
- <sup>20</sup>R. P. Ingel, P. A. Willging, B. A. Bender and T. W. Coyle, "The Physical and Thermomechanical Properties of Monoclinic Single Crystals"; see Ref. 5, pp. 459-69.
- <sup>21</sup>S. T. Buljan, H. A. McKinstry, and V. S. Stubican, "Optical and X-ray Single Crystal Studies of the Monoclinic  $\leftrightarrow$  Tetragonal Transition of  $ZrO_2$ ," *J. Am. Ceram. Soc.*, **59** [7-8] 351-54 (1976).
- <sup>22</sup>D. K. Smith and H. W. Newkirk, "The Crystal Structure of Baddeleyite (Monoclinic  $ZrO_2$ ) and Its Relation to the Polymorphism of  $ZrO_2$ ," *Acta Crystall.*, **18**, 983-91 (1965).
- <sup>23</sup>S.-K. Chan, "Theory of the Energetics and Nonclassical Nucleation for the Tetragonal-Monoclinic Transformation of Zirconia"; see Ref. 5, pp. 983-95.
- <sup>24</sup>B. C. Muddle and R. H. J. Hannink, "Crystallography of the Tetragonal to Monoclinic Transformation in MgO-Partially-Stabilized Zirconia," *J. Am. Ceram. Soc.*, **69** [7] 547-55 (1986).
- <sup>25</sup>K. A. Sasse, "A Method of Producing Very Dense  $ZrO_2$ ," *J. Am. Ceram. Soc.*, **44** [9] 465 (1961).
- <sup>26</sup>S. C. Carniglia, S. D. Brown, and T. F. Schroeder, "Phase Equilibria and Physical Properties of Oxygen-Deficient Zirconia and Thoria," *J. Am. Ceram. Soc.*, **54** [1] 13-17 (1971).
- <sup>27</sup>H. J. Garrett and R. Ruh, "Fabrication of Specimens from Pure Dense Oxidized Zirconia," *Am. Ceram. Soc. Bull.*, **47** [6] 578-79 (1968).
- <sup>28</sup>L. M. Barker, "Specimen Size Effects in Short-Rod Fracture Toughness Measurements"; pp. 117-33 in *Chevron-Notched Specimens: Testing and Stress Analysis*, ASTM STP 855. Edited by J. H. Underwood, S. W. Freiman, and F. I. Baratta. ASTM, Philadelphia, PA, 1984.
- <sup>29</sup>H. Toraya, M. Yoshimura, and S. Somiya, "Calibration Curve for Quantitative Analysis of the Monoclinic-Tetragonal  $ZrO_2$  System by X-ray Diffraction," *J. Am. Ceram. Soc.*, **68** [6] C-119-C-121 (1984).
- <sup>30</sup>K. Mehta, J. F. Jue, and A. V. Virkar, "Grinding-Induced Texture in Ferroelastic Tetragonal Zirconia," *J. Am. Ceram. Soc.*, **73** [6] 1777-79 (1990).
- <sup>31</sup>T. Sakuma, H. Edo, and H. Suto, "Compositional Optimization of  $ZrO_2$ - $Y_2O_3$  Alloys to Improve the Fracture Toughness"; see Ref. 5, pp. 357-63.
- <sup>32</sup>K. Tsukuma and T. Takahata, "Mechanical Property and Microstructure of TZP and TZP/ $Al_2O_3$  Composites"; pp. 123-35 in *Advanced Structural Ceramics*, Vol. 78. Edited by P. F. Becher, M. V. Swain, and S. Somiya. Materials Research Society, Pittsburgh, PA, 1987.
- <sup>33</sup>A. V. Virkar, "Fracture Behavior of  $ZrO_2$ - $Zr$  Composites"; Ph.D. Dissertation. Northwestern University, Evanston, IL, 1973.
- <sup>34</sup>M. Yoshimura, "Phase Stability of Zirconia," *Am. Ceram. Soc. Bull.*, **67** [12] 1950-55 (1988).
- <sup>35</sup>R. Ruh and H. J. Garrett, "Nonstoichiometry of  $ZrO_2$  and Its Relation to Tetragonal-Cubic Inversion in  $ZrO_2$ ," *J. Am. Ceram. Soc.*, **50** [5] 257-61 (1967).
- <sup>36</sup>E. G. Rauh and S. P. Garg, "The  $ZrO_2$ -(Cubic)- $ZrO_2$ -(Cubic + Tetragonal) Phase Boundary," *J. Am. Ceram. Soc.*, **63** [3-4] 239-40 (1980).
- <sup>37</sup>C. J. Gasdaska, P. J. Whalan, J. Marti, and F. Reindinger, "Texture and Recrystallization of Ground Surfaces of  $HfO_2$ ," *J. Am. Ceram. Soc.*, **73** [7] 1941-46 (1990).
- <sup>38</sup>J. F. Jue, J. Chen, and A. V. Virkar, "Low-Temperature Aging of *t'*-Zirconia: The Role of Microstructure on Phase Stability," *J. Am. Ceram. Soc.*, **74** [8] 1811-20 (1991).
- <sup>39</sup>M. Hayawawa, N. Knutani, and M. Oka, "Structural Study on the Tetragonal to Monoclinic Transformations in Arc-Melted  $ZrO_2$ -2 mol%  $Y_2O_3$ -I. Experimental Observations," *Acta Metall.*, **37** [8] 2223-28 (1989).
- <sup>40</sup>P. M. Kelley, private communication with R. A. Cutler, 1991.
- <sup>41</sup>T. Noma, M. Yoshimura, and S. Somiya, "Stability of Diffusionlessly Transformed Tetragonal Phases in Rapidly Quenched  $ZrO_2$ - $Y_2O_3$ "; see Ref. 5, pp. 377-84.
- <sup>42</sup>W. Wunderlich and M. Rühle, "Critical Stresses for Microcracking in Monoclinic Zirconia"; see Ref. 5, pp. 509-15.
- <sup>43</sup>D. J. Green, R. H. J. Hannink, and M. V. Swain, *Transformation Toughening of Ceramics*. CRC Press, Boca Raton, FL, 1989.
- <sup>44</sup>A. G. Evans and A. H. Heuer, "Review—Transformation Toughening in Ceramics: Martensitic Transformations in Crack-Tip Stress Fields," *J. Am. Ceram. Soc.*, **63** [5-6] 241-48 (1980).
- <sup>45</sup>A. C. D. Chaklader and V. T. Baker, "Reactive Hot-Pressing: Fabrication and Densification of Non-stabilized  $ZrO_2$ ," *Am. Ceram. Soc. Bull.*, **44** [3] 258-59 (1965).
- <sup>46</sup>J. L. Hart and A. C. D. Chaklader, "Superplasticity in Pure  $ZrO_2$ ," *Mater. Res. Bull.*, **2**, 521-26 (1967).
- <sup>47</sup>M. Yoshimura and S. Somiya, "Fabrication of Dense, Nonstabilized  $ZrO_2$  Ceramics by Hydrothermal Reaction Sintering," *Am. Ceram. Soc. Bull.*, **59** [2] 246 (1980).
- <sup>48</sup>M. Yoshimura and S. Somiya, "Hydrothermal Reaction Sintering of Monoclinic Zirconia"; pp. 455-63 in *Advances in Ceramics*, Vol. 3, *Science and Technology of Zirconia*. Edited by A. H. Heuer and L. W. Hobbs. American Ceramic Society, Westerville, OH, 1981. □

# Liquid Precursor Route for Hetero-epitaxy of $Zr(Y)O_2$ Thin Films on (001) Cubic Zirconia

Andreas Seifert, Fred F. Lange,\* and J. S. Speck

Materials Department, College of Engineering, University of California, Santa Barbara, California 93106

$ZrO_2$ -3 mol%  $Y_2O_3$  "single-crystal" thin films with multiple variants were epitaxially formed on (100) cubic zirconia substrates. The films were prepared by spin-coating an aqueous zirconium acetate/yttrium nitrate solution onto the cubic zirconia substrates and subsequently heat-treated at temperatures between 1100° and 1400°C. Electron diffraction and dark-field TEM observations showed that the film has tetragonal symmetry and consists of 50-100 nm variants with their  $c$ -axes aligned with one of the three substrate cube axes. Unrelaxed strain energy estimates indicate that the two variants with their  $c_1$ -axis parallel to the substrate/thin film interface are energetically favorable.

## I. Introduction

MANY different liquid precursor chemistries (soluble inorganic salts, metal organics, etc.) exist to produce different and interesting inorganic materials upon heat treatment. Liquid precursors can be used to coat substrates by either spin-on<sup>1</sup> or dip-coating<sup>2</sup> techniques. Once coated and the liquid phase is removed, the precursor film decomposes at modest temperatures to produce a low-density network of nanometer crystallites of the desired compound. It is well known<sup>3</sup> that dense, polycrystalline films can be formed upon further heat treatment; also it has been demonstrated that liquid precursors can produce either single-crystal<sup>4-9</sup> or multivariant<sup>10</sup> thin films on single-crystal substrates. When the film and substrate structures are very similar, single-crystal thin films can form despite different film and substrate chemistries; e.g., single-crystal thin films of  $LiNbO_3$  can be formed on sapphire ( $Al_2O_3$ ) substrates.<sup>6-8</sup>

Studies by Miller *et al.*<sup>5,9</sup> for  $Zr(Y)O_2$  solid-solution film compositions ranging from 0 to 4 mol%  $Y_2O_3$  produced on 9.5 mol% cubic, {100}  $Zr(Y)O_2$  substrates, have shown that the growth of the single-crystal thin film initiates when the  $Zr(Y)O_2$  crystallizes from the precursor during heat treatment. Namely, the nanometer crystallites at the film/substrate interface are observed to have the same orientation as the substrate, whereas the remainder of the film is a low-density network of unoriented, nanometer crystallites. As the low-density network densifies during further heat treatment, the oriented grains at the interface are observed to consume the unoriented grains via grain growth to produce a single-crystal thin film. This process has been termed "epitaxial grain growth." For film compositions containing  $\geq 6$  mol%  $Y_2O_3$ , both the film and substrate have cubic, fluorite structures. TEM observations and XRD results show that, as expected, a dislocation network at the

film/substrate interface accommodates  $\approx 90\%$  of the unrelaxed strain energy associated with the different lattice parameters due to the difference in the solid-solution chemistry of the film relative to the substrate.

The same study<sup>5</sup> indicated that single-crystal thin films are apparently produced when the composition of the film is in a range where the tetragonal structure is usually observed for solid solutions containing  $\leq \approx 4$  mol%  $Y_2O_3$ . Although XRD analysis and electron backscattering patterns of these films suggested a highly oriented thin film, neither technique could unambiguously identify their symmetry. Thus, an additional study was initiated. As shown below, thin films formed with a  $ZrO_2$  solid solution containing 3 mol%  $Y_2O_3$  are tetragonal and contain three structurally related variants that have a defined orientation relative to the cubic substrate.

## II. Experimental Procedure

As described elsewhere,<sup>5,10</sup> the liquid precursor used to synthesize the 3 mol%  $ZrO_2$ - $Y_2O_3$  thin films was prepared by dissolving previously assayed yttrium nitrate (Aesar, Johnson Matthey Inc., Seabrook, NH) powder in an aqueous zirconium acetate solution (Magnesium Electron Inc., Flemington, NJ) containing 0.0023 mol of Zr per gram of solution. To ensure a homogeneous distribution of the constituents, the solution was mixed for  $\approx 2$  h with a shake table. Cubic single-crystal {001}<sub>c</sub> zirconia substrates, containing 9.5 mol%  $Y_2O_3$  in solid solution, were used for this study (Ceres Corp., North Bellerica, MA). The substrates were cleaned with an aqueous ammonium hydroxide/sodium hydroxide solution, rinsed in deionized water, and subsequently dried with compressed air. The aqueous precursor was deposited on the substrates by spin-coating at 5500 rpm for 30 s. During this process the precursor dried to an amorphous gel-like solid film. As described by others<sup>9,11</sup> the subsequent heating in air decomposes the acetate and nitrate into a solid-solution oxide ( $Zr(Y)O_2$ ) which crystallizes at temperatures between 350° and 450°C. The crystallization appears to be concurrent with pyrolysis.<sup>12</sup> For this study the films were heated at 5°C/min to temperatures between 1100° and 1400°C, held for 1 to 3 h, and cooled at 15°C/min.

After heat treatment, the films were studied by XRD (XDS 2000, Scintag Inc., Sunnyvale, CA) and TEM (2000FX, JEOL Ltd., Tokyo, Japan). For XRD analysis, the thin films were aligned by maximizing the intensity of the {400}<sub>c</sub> substrate peak using the two degrees of angular freedom available on the diffractometer. For comparison, the same 3 mol%  $Y_2O_3$ - $ZrO_2$  liquid precursor used for spinning the thin films was dried at room temperature in a petri dish for about 2 days. The resulting powders were heat-treated to 1400°C in the same manner as the thin films. The lattice parameters of these powders were determined by XRD with an internal silicon standard.

The microstructure and crystalline structure of films prepared at 1300°C (1 h) and 1400°C (1 and 3 h) were determined by TEM using both plan-view and cross-section specimens. Plan-view specimens were prepared by conventional techniques; these specimens were dimpled and ion-milled from the substrate side to maximize film observations. Cross-section

C. J. Brinker—contributing editor

Manuscript No. 195754. Received April 27, 1992; approved September 24, 1992.

Supported by DARPA and monitored by AFOSR under Contract No. F49620-87-C-0077, with the prime contract at Ceramatec, Inc., under the guidance of Dr. Raymond A. Cutler.

\*Member, American Ceramic Society.

specimens were prepared by a sandwiched-ring method described elsewhere.<sup>13</sup>

### III. Results

#### (1) X-ray Diffraction Analysis

XRD analysis showed the heat-treated powders derived from the 3 mol%  $Y_2O_3$  zirconia precursor to be tetragonal as reported by others,<sup>14,15</sup> with lattice parameters  $a_c = 0.5097$  nm and  $c_c = 0.5169$  nm.<sup>†</sup> It should be noted that the 3 mol%  $Y_2O_3$  composition lies within a two-phase field, tetragonal + cubic, in the  $ZrO_2$ - $Y_2O_3$  binary system at temperatures within our processing range. Others<sup>16</sup> have shown that tetragonal structure is always produced from well-mixed precursors for compositions <4 to 5 mol%  $Y_2O_3$ ; these phases are metastable. A single phase with tetragonal symmetry is observed, instead of the equilibrium tetragonal and cubic phases, because long-range diffusion is limited at the crystallization temperature. In addition, the same studies<sup>16</sup> have shown that complete partitioning into the equilibrium tetragonal ( $\approx 1.0$  to 1.25 mol%  $Y_2O_3$ ) and cubic ( $\approx 7.0$  mol%  $Y_2O_3$ ) phases at 1400°C requires  $\approx 200$  h. Nearly identical behavior is observed for similar compositions within the  $ZrO_2$ - $Gd_2O_3$  system.<sup>17</sup>

For all films examined, XRD analysis only showed film reflections on the high  $2\theta$  side of the  $(200)_c$ ,  $(400)_c$ , and  $(600)_c$  single-crystal substrate peaks that could correspond to diffraction from either  $\{00l\}$  if the film were tetragonal or  $\{h00\}_c$  in the case of a cubic film. Using the substrate diffraction peaks as an internal standard, the observed film peaks gave  $a_{film} = 0.5096$  nm, which is very similar to the tetragonal  $a$  parameter of the powder. If the thin film were tetragonal with a  $c$  parameter close to the value determined for the powder, the  $(002)_t$ ,  $(004)_t$ , and  $(006)_t$  diffraction peaks would not be observable due to the proximity to the cubic substrate parameter of  $a_c = 0.5144$  nm<sup>†</sup> and the excessive substrate/film signal ratio. Thus, XRD did reveal that the films were highly oriented with respect to the substrate, but could not distinguish whether they were of cubic or tetragonal symmetry.

#### (2) Transmission Electron Microscopy

Only films processed at 1300° and 1400°C were examined with TEM. All had a single-crystal character and were crystallographically related to the substrate as demonstrated by selected area diffraction (SAD) and Kikuchi line patterns. In all cases, a given zone axis remained invariant during translation of the TEM specimen, suggesting that the films were single crystals. Additionally, the diffraction patterns of the thin films had the same orientation as the substrate, showing that they are epitaxially related as  $\{100\}_{substrate} \parallel \{100\}_{film}$ .

Figure 1 illustrates a bright-field (BF) TEM micrograph of a cross-section specimen processed at 1300°C for 1 h with a film thickness of  $\sim 150$  nm. As seen, although the SAD indicated single-crystal character, the films have a mottled appearance. In addition, pores were observed in the films processed at this temperature. To determine the thin film symmetry and the source of the microstructure, plan-view and cross-section specimens were tilted to the  $\langle 111 \rangle_{c,t}$  zone axis.<sup>†</sup> For this zone axis, additional reflections of the type  $\{odd, odd, even\}$  appear for the tetragonal phase which are forbidden for the cubic structure and thus allow the two phases to be distinguished.<sup>18</sup> As expected, SAD patterns along  $\langle 111 \rangle_c$  of substrate regions free of the film showed only evidence of cubic symmetry, as shown in Fig. 2(a) for the 1300°C/1 h cross-section specimen. The  $\langle 111 \rangle_{c,t}$  diffraction pattern in Fig. 2(b) of the same specimen includes diffraction information from both the film and the substrate and displays extra reflections of the type  $\{112\}$ , associated with the

thin film. These extra reflections are consistent with tetragonal symmetry. Figure 2(c) shows the area used to obtain the SAD pattern in Fig. 2(b). A calculated diffraction pattern for a tetragonal single crystal with a  $\langle 111 \rangle_c$  zone axis is illustrated in Fig. 3. It shows that only one third of the observed reflections associated with the tetragonal film in Fig. 2(b) should be present if the structure within the film had only one orientation relative to the substrate. A comparison of Fig. 3 with Fig. 2(b) shows that all the additional reflections with mixed indices, e.g.,  $\{112\}$ , in Fig. 2(b) are symmetrically related by a 60° rotation about  $\langle 111 \rangle_c$ . Thus, the thin film is a multivariant "single crystal" with the tetragonal variants related to one another by a 60° rotation about  $\langle 111 \rangle_c$  of the substrate. The  $c$ -axis of the tetragonal variants can be aligned parallel to any one of the cube-axes of the substrate. Thus the three possible tetragonal variants give rise to  $\{odd, odd, even\}$  reflections and combine to form the SAD pattern shown in Fig. 2(b).

To further verify the multivariant nature of the tetragonal thin films and to obtain a better understanding of their microstructure, the three different variants were imaged in dark field (DF) using  $\langle 112 \rangle_c$  reflections in a  $\langle 111 \rangle_c$  zone axis orientation. This is shown in Fig. 4 for a series of DF micrographs taken of the 1400°C/3 h plan-view specimen. The corresponding SAD patterns close to the  $\langle 111 \rangle_{c,t}$  zone axes display  $\langle 112 \rangle_c$  reflections for each variant. By following the  $\{220\}_c$  Kikuchi band during tilting from the  $(100)_c$  pole to the  $(111)_c$  pole and with the information of the specimen position in the holder, it is possible to identify the variants in Fig. 4(c) as the ones with the  $c$ -axis normal to the substrate/thin film interface. Figure 5 shows an SAD pattern parallel to the  $\langle 111 \rangle_c$  zone axis for an area approximately 2  $\mu$ m in diameter of the 1400°C/3 h plan-view specimen. The intensity of the reflections corresponding to the reciprocal cell of the variant with  $c_c \parallel [001]_c$  (i.e., normal to the interface) is smaller than the intensity of reflections associated with the other variants with their  $c$ -axes lying in the plane of the film (i.e., parallel to  $[100]_c$  and  $[010]_c$  of the cubic substrate). This indicates that the volume of variants with  $c_c \parallel [001]_c$  is less than the volume of the variants with  $c_c$  lying in the substrate/thin film interfacial plane. The three different tetragonal variants show an even lateral distribution across the film and their size varies from  $\approx 50$  to 100 nm, as demonstrated by DF imaging in Fig. 4.

The tetragonal variants in the thin film form a blocky structure as shown in the  $[001]_c$  zone axis of BF micrographs of Figs. 6(a) and (b). Increasing the processing periods at 1400°C causes the average variant size to increase from  $\approx 50$  nm for 1 h to  $\approx 100$  nm for 3 h. The SAD patterns, shown as insets in Figs. 6(a) and (b), indicate that the variant boundaries (or 90° twin boundaries) are planes of the type  $\{101\}_t$  or  $\{011\}_t$ . However,  $\{110\}_t$  twin boundaries cannot occur since they are mirror planes in the tetragonal structure.<sup>18</sup>



Fig. 1. Bright-field electron micrograph parallel to  $[100]_c$  of the thin film heat-treated at 1300°C for 1 h. The cross-section specimen shows porosity (arrows) and a film thickness of  $\sim 150$  nm. Note complex microstructure of this apparent "single-crystal" thin film.

<sup>†</sup>For convenience we hereby refer not to the standard primitive tetragonal unit cell, but to a C-centered tetragonal cell with approximately  $a_c = 0.51$  nm and  $c_c = 0.517$  nm,<sup>18</sup> which is in fact a slightly distorted side-centered cell of the cubic phase with  $a_c = 0.5144$  nm,<sup>†</sup> containing 9.5 mol%  $Y_2O_3$ . All indexing reported here is referred to these two nonprimitive cells.

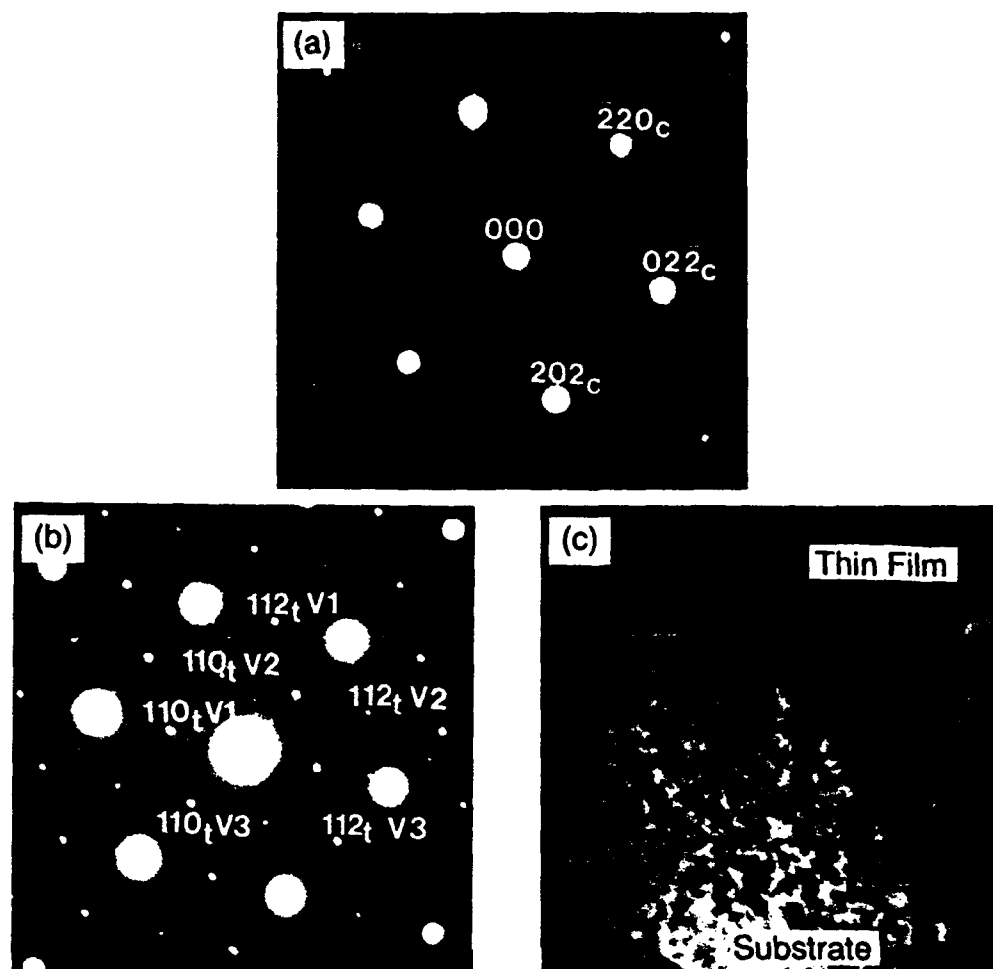


Fig. 2. Selected area diffraction pattern (SADP) parallel to a  $\langle 111 \rangle_c$  zone axis, taken on the cross-section specimen of the  $1300^\circ\text{C}$  (1 h) thin film shown in Fig. 1: (a) shows a SADP of the substrate only, whereas (b) shows the SADP for both thin film and substrate. The additional  $\{\text{odd, odd, even}\}$  reflections are associated with the thin film. Indexed are the three occurring tetragonal variants  $v_1$ ,  $v_2$ , and  $v_3$ . (c) shows the area used to obtain the SADP in (b).

#### IV. Discussion

The observations reported above clearly show that the  $ZrO_2$  precursor containing 3 mol%  $Y_2O_3$  produces a multivariant, "single-crystal" tetragonal film on a cubic  $\{100\}_c$  solid-solution  $ZrO_2$  (9.5 mol%  $Y_2O_3$ ) substrate surface. The tetragonal variants in the film are crystallographically related to the cubic substrate by  $[001]_t \parallel [100]_c$ ,  $[001]_t \parallel [010]_c$ , and  $[001]_t \parallel [001]_c$ , where  $\langle 100 \rangle_t \parallel \langle 100 \rangle_c$  for all variants. Within the film, variant boundaries are of either the  $\{101\}_t$  or  $\{011\}_t$  type. Figure 8 of Ref. 19 illustrates the crystallographic relation between the three distinguishable variants.

As reported by Michel *et al.*,<sup>15</sup> large  $ZrO_2$  single crystals with the same composition (3 mol%  $Y_2O_3$ ), produced by skull-melting, first crystallize with the cubic structure and then undergo a diffusionless cubic-to-tetragonal phase transformation during cooling into the two-phase ( $t + c$ ) field. Because of insufficient diffusion to allow partitioning into their equilibrium tetragonal + cubic phases, these crystals retain their tetragonal structure during cooling and have a polyvariant domain structure that is identical<sup>1</sup> to that shown in Fig. 4 for the films examined in the current study. Lanteri *et al.*<sup>18</sup> find the same polyvariant microstructure for skull-melt, tetragonal crystals formulated with 4.5 mol% of  $Y_2O_3$ . As suggested by both

Michel *et al.*,<sup>20</sup> and Heuer *et al.*,<sup>21</sup> the three crystallographically related variants arise during the cubic-to-tetragonal phase transformation to minimize the strain energy associated with the transformation. This implies<sup>22</sup> that the material is ferroelastic; that is, the volume fraction of one or two of the three variants can diminish as others grow by domain (twin) boundary motion

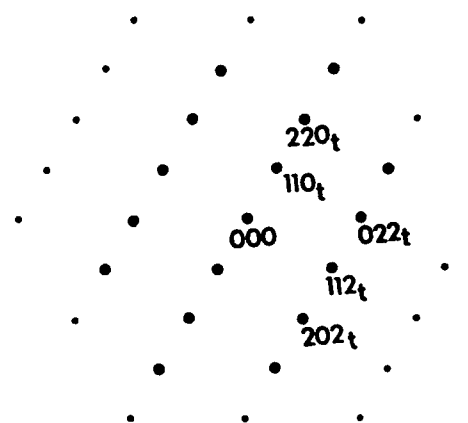


Fig. 3. Calculated SAD pattern with a  $\langle 111 \rangle_t$  zone axis for a tetragonal single crystal (C-centered cell). This gives a diffraction pattern for a thin film microstructure with only one of the three orientations relative to the substrate.

<sup>1</sup>Michel *et al.*<sup>15</sup> determined the lattice parameters of the multivariant single crystals as  $a_t = 0.5105$  nm and  $c_t = 0.5168$  nm, which are nearly identical to that obtained here for the powders produced from the precursors with the same composition, viz.,  $a_t = 0.5097$  nm and  $c_t = 0.5169$  nm.

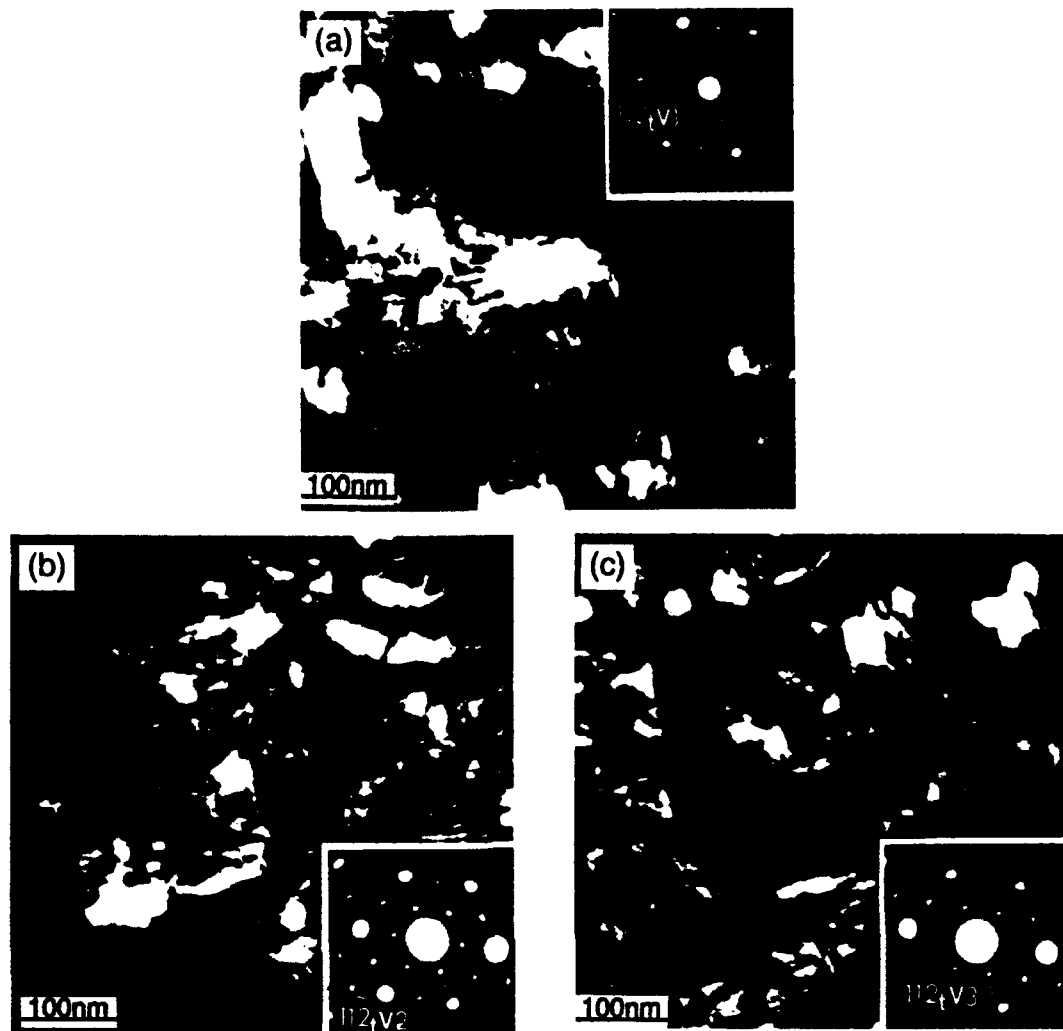


Fig. 4. Series of DF micrographs close to a  $\langle 111 \rangle$ , zone axis taken on the plan-view sample of the 1400°C (3 h) thin film. The three different tetragonal variants were imaged with their corresponding  $\{112\}$ , reflections. This is shown in (a) for variant 1, in (b) for variant 2, and in (c) for variant 3. For variant 3 the tetragonal  $c$ -axis is normal to the substrate film interface plane.

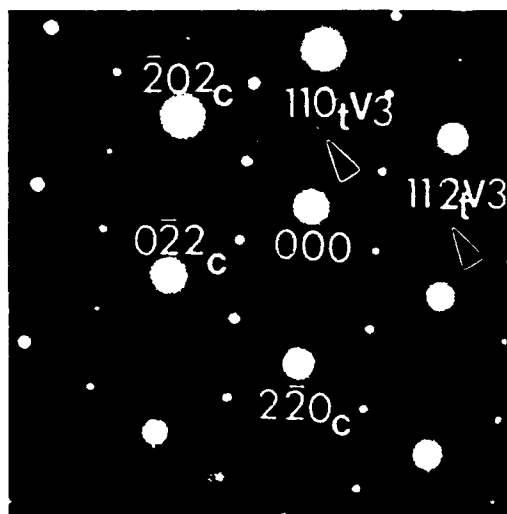


Fig. 5. SAD pattern along  $\langle 111 \rangle$ , over an area of  $\sim 2 \mu\text{m}$  in diameter of the 1400°C plan-view specimen, including both thin film and substrate material. The  $\{\text{odd, odd, even}\}$  reflections of variant 3 are less intense than the reflections associated with the other two variants.

to minimize strain energy during the application of stress.<sup>19</sup> By analogy to ferroelectric materials, this phenomenon is called domain switching (tetragonal  $\text{ZrO}_2$  is ferroelastic, but not ferroelectric, because it has a center of symmetry ( $P4_2/nmc$ )). Virkar *et al.*<sup>23</sup> have suggested that ferroelastic domain switching can be a toughening mechanism for polyvariant, tetragonal  $\text{ZrO}_2$ , an idea consistent with observations by Michel *et al.*<sup>15</sup>

Although it is well established that  $\text{Zr(Y)O}_2$  solid solutions, cooled from the cubic phase field into the two-phase ( $c + t$ ) field, will develop a three-variant tetragonal microstructure during the cubic-to-tetragonal transformation, this phenomenon cannot be responsible for the multivariant, thin film microstructures. Work on precursors in both the  $\text{ZrO}_2\text{-Y}_2\text{O}_3$ <sup>16</sup> and  $\text{ZrO}_2\text{-Gd}_2\text{O}_3$ <sup>17</sup> systems show that for  $\text{ZrO}_2$ -rare-earth compositions well within the range studied here, the tetragonal structure directly crystallizes during precursor pyrolysis and the cubic structure is not observed until the metastable, tetragonal composition partitions after long times at high temperatures (e.g., 1400°C). TEM observations<sup>16,17</sup> of tetragonal grains prior to their partitioning do not show a polyvariant microstructure. In addition, the equilibrium single phase field for cubic  $\text{Zr(Y)O}_2$  resides at much higher temperatures ( $\approx 1700^\circ\text{C}$ )<sup>14</sup> for the 3 mol%  $\text{Y}_2\text{O}_3$  composition, relative to the thin film processing temperatures ( $\leq 1400^\circ\text{C}$ ). Thus, the cubic-to-tetragonal transformation cannot be responsible for the multivariant microstructure of the oriented, tetragonal thin films.

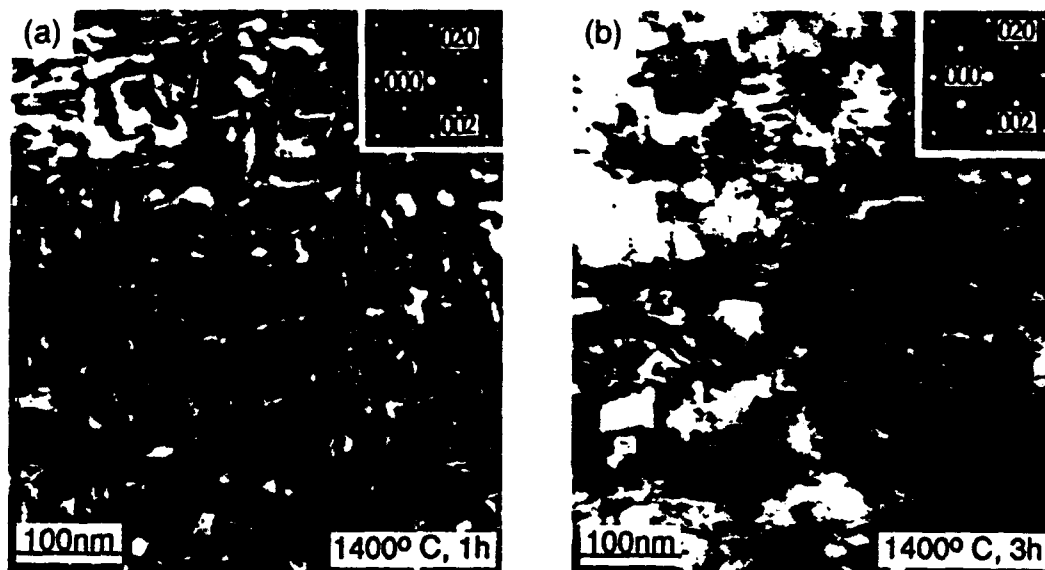


Fig. 6. Bright-field micrographs of two plan-view specimens, both parallel to the [100] zone axis (normal view onto the specimen). The SAD patterns show that the variant boundary planes are of the type {101} and {011}. Comparing the image of the 1400°C (1 h) specimen in (a) with the 1400°C (3 h) specimen in (b) shows that the domain size increases significantly with heat-treatment period.

The multivariant microstructure of the tetragonal thin films might initiate at low temperatures, during crystallization of the precursor. Namely, similar to the direct observation of cubic compositions<sup>9</sup> ( $\geq 6$  mol% Y<sub>2</sub>O<sub>3</sub>) on cubic substrates, the nanometer tetragonal crystallites are expected to crystallize, during precursor pyrolysis, at the film/substrate interface with preferred orientations relative to the cubic substrate. To examine which variant might be preferred, we need to determine the unrelaxed strain energy associated with the different variant orientations.

The unrelaxed strain energy per unit volume ( $E_v$ ) can be estimated for each variant ( $v = 1, 2, 3$ ) by (in reduced notation)

$$E_v = \frac{1}{2} c_{ij} \epsilon_i^v \epsilon_j^v \quad (1)$$

assuming that (a) the elastic properties of the tetragonal phase can be represented by three elastic constants— $c_{11}$ ,  $c_{12}$ ,  $c_{44}$ —as suggested by Ingel and Lewis<sup>24</sup> and (b) the substrate is rigid,

i.e., does not relax the strains within the variant. The strains,  $\epsilon^v$ , are associated with the lattice mismatch between the different tetragonal structure ( $a_t = 0.5097$  nm and  $c_t = 0.5169$  nm, determined from the powder produced from the precursor) and the cubic substrate ( $a_c = 0.5144$  nm). Strain energy density calculations are possible because Ingel and Lewis<sup>24</sup> have reported the elastic constants of Zr(Y)O<sub>2</sub> single crystals for compositions ranging between 1.7 to 20 mol% Y<sub>2</sub>O<sub>3</sub>. In the range of composition needed for our calculations (3 mol% Y<sub>2</sub>O<sub>3</sub>), they assumed that their single crystal consisted of a cubic matrix containing tetragonal precipitates. They represented the elastic constants of this "mixed" crystal with three constants:  $c_{11} = 410$  GPa,  $c_{12} = 125$  GPa, and  $c_{44} = 52$  GPa, consistent with our first assumption.<sup>8</sup>

<sup>8</sup>The change of the three elastic constants over the complete range of composition determined by Ingel and Lewis<sup>24</sup> is small.

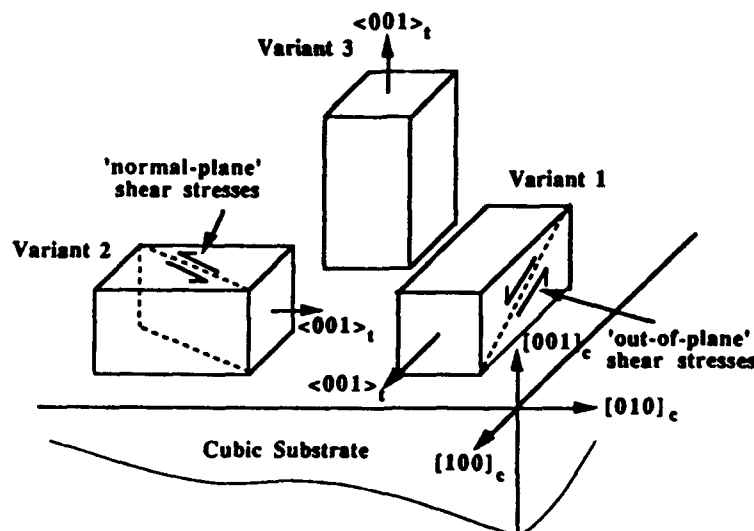


Fig. 7. Schematic of the three tetragonal variants as related to the cubic substrate with  $a_c = 0.5144$  nm. For the tetragonal cell  $a_t = 0.5097$  nm and  $c_t = 0.5169$  nm. Both "normal-plane" and "out-of-plane" shear stresses exist within variants 1 and 2 because  $\sigma_1 \neq \sigma_2$  and  $\sigma_3 = 0$ , whereas only "out-of-plane" shear stress exists within variant 3 because  $\sigma_1 = \sigma_2$  and  $\sigma_3 = 0$ .

As schematically shown in Fig. 7, the two variants with the  $c$ -axis lying in the substrate/thin film interface plane are symmetrically equivalent (one orientation with  $c_i \parallel [100]$ , and the other one with  $c_i \parallel [010]$ ). Also shown is the third variant, where the tetragonal  $c$ -axis is normal to the interface ( $c_i \parallel [001]$ ). For the first two equivalent variants,  $a_i$  and  $c_i$  are parallel to the interface plane and parallel to  $\langle 100 \rangle$ , of the cubic substrate. The in-plane strains for these two equivalent variants are

$$\varepsilon_1^{1,2} = \frac{a_c - a_i}{a_c}, \quad \varepsilon_2^{1,2} = \frac{a_c - c_i}{a_c} \quad (2a)$$

Likewise, the in-plane strains for the third variant are

$$\varepsilon_1^3 = \varepsilon_2^3 = \frac{a_c - a_i}{a_c} \quad (2b)$$

Because of plane stress conditions, the stress normal to the film  $\sigma_3 = 0$ , and it can be shown that

$$\varepsilon_3 = -\frac{c_{12}}{c_{11}}(\varepsilon_1 + \varepsilon_2) \quad (2c)$$

For all three variants. Because of the choice of coordinate axes,  $\sigma_6 = 0$ . Equation (1) reduces to

$$E_v = \frac{1}{2}c_{11}[(\varepsilon_1)^2 + (\varepsilon_2)^2] - \frac{1}{2}\frac{c_{12}^2}{c_{11}}(\varepsilon_1 + \varepsilon_2)^2 + c_{12}(\varepsilon_1)(\varepsilon_2) \quad (3)$$

Recalling that  $\sigma_3 = 0$ , it can be shown that the in-plane stresses are

$$\sigma_1 = \left(c_{11} - \frac{c_{12}^2}{c_{11}}\right)\varepsilon_1 + \left[c_{12}\left(1 - \frac{c_{12}}{c_{11}}\right)\right]\varepsilon_2 \quad (4a)$$

$$\sigma_2 = \left[c_{12}\left(1 - \frac{c_{12}}{c_{11}}\right)\right]\varepsilon_1 + \left(c_{11} - \frac{c_{12}^2}{c_{11}}\right)\varepsilon_2 \quad (4b)$$

Table I lists the strains, stresses, and unrelaxed strain energy density for different nucleating variants. For comparison, Table I also lists these values for the case of the cubic  $Zr(Y)O_2$  (+40 mol%  $Y_2O_3$ ) film grown on the cubic  $Zr(Y)O_2$  (+9.5 mol%  $Y_2O_3$ ) substrate (listed as cubic/cubic) representing the largest mismatch strain studied by Miller *et al.*<sup>9</sup>

Table I shows that the estimated unrelaxed strain energy density for the two equivalent variants (both  $a_i$  and  $c_i$  in plane) is  $\approx 40\%$  of the third variant ( $c_i$  normal to the plane). Although the equivalent variants would be most energetically favorable, it is also known that cubic crystallites can nucleate on the same substrates as demonstrated by Miller *et al.*<sup>9</sup> despite their very high strain energy density (see Table I). It might therefore be concluded that all three variants could concurrently nucleate at different surface sites on the substrate during pyrolysis of the precursor.

The unrelaxed strain energy densities shown in Table I do not necessarily describe the strain energy density within the thin

film. Shear stresses present within the growing variants can activate phenomena to reduce the strain energy. For the cubic thin films examined by Miller *et al.*,<sup>9</sup> out-of-plane shear stresses ( $\sigma_1 = \sigma_2$  and  $\sigma_3 = 0$ , see Table I and Fig. 7) cause dislocations to move to the interface to decrease the unrelaxed strain energy by  $\approx 90\%$ . For the equivalent tetragonal variants (1 and 2), both have normal-plane and out-of-plane shear stresses ( $\sigma_1 \neq \sigma_2$  and  $\sigma_3 = 0$ , see Table I and Fig. 7). Current experimental and theoretical efforts are under way to ascertain whether the multiple-variant thin film microstructure results from nucleation phenomena during pyrolysis or twinning phenomena during epitaxial grain growth.

## References

- C. J. Brinker and G. W. Scherer, *Sol-Gel Science*. Academic Press, New York, 1990.
- W. J. Daughton and S. L. Givens, "Investigation of the Thickness Variation of Spun-on Thin Films Commonly Associated with the Semi-Conductor Industry," *J. Electrochem. Soc.*, **129** [1] 173-179 (1982).
- J. V. Mantese, A. L. Micheli, A. H. Hamdi, and R. W. West, "Metalorganic Deposition (MOD): A Nonvacuum, Spin-on, Liquid-Based, Thin Film Method," *MRS Bull.*, **14** [10] 48-53 (1989).
- D. P. Parlow and J. Gregg, "Properties and Microstructure of Thin LiNbO<sub>3</sub> Films Prepared by a Sol-Gel Process," *J. Mater. Res.*, **2** [5] 595-605 (1987).
- K. T. Miller and F. F. Lange, "Single Crystal Zirconia Thin Films from Liquid Precursors," pp. 191-98 in *Processing Science of Advanced Ceramics*, Vol. 155, Edited by I. A. Aksay, G. L. McVay, and D. R. Ulrich. Materials Research Society, Pittsburgh, PA, 1989.
- S. Hirano and K. Kato, "Processing of Crystalline Li(Nb,Ta)O<sub>3</sub> Films with Preferred Orientation Through Metal Alkoxides," pp. 181-90 in *Processing Science of Advanced Ceramics*, Vol. 155, Edited by I. A. Aksay, G. L. McVay, and D. R. Ulrich. Materials Research Society, Pittsburgh, PA, 1989.
- D. S. Hagberg and D. A. Payne, "Grain-Oriented Lithium Niobate Thin-Layers Prepared by Sol-Gel Methods"; unpublished work.
- K. Nashimoto and M. J. Cima, "Epitaxial LiNbO<sub>3</sub> Thin Films Prepared by a Sol-Gel Process," *Mater. Lett.*, **10** [7,8] 348-54 (1991).
- K. T. Miller, C.-J. Chan, M. Cain, and F. F. Lange, "Homo-Epitaxy of Cubic ZrO<sub>2</sub> Solid-Solutions (6 to 40 mol% Y<sub>2</sub>O<sub>3</sub>) on Single Crystal Thin Films on (100) ZrO<sub>2</sub> (9.5 mol% Y<sub>2</sub>O<sub>3</sub>) Substrates via Liquid Precursor Route," *J. Mater. Res.*, in press.
- K. T. Miller and F. F. Lange, "Highly Oriented Thin Films of Cubic Zirconia on Sapphire Through Grain Growth Seeding," *J. Mater. Res.*, **6** [11] 2387-92 (1991).
- E. Leroy, C. Robin-Brosse, and J. P. Torre, "Fabrication of Zirconia Fibers from Sol-Gels," pp. 219-31 in *Ultrastructure Processing of Ceramics, Glasses and Composites*, Edited by L. L. Hench and D. R. Ulrich. Wiley, New York, 1984.
- M. L. Balmer, F. F. Lange, and C. G. Levi, "Metastable Phase Selection and Partitioning in ZrO<sub>2</sub>-MgO Processed from Liquid Precursors," *J. Am. Ceram. Soc.*, **75** [4] 946-52 (1992).
- M. Lanham, J. Mayer, S. J. Golden, F. F. Lange, and M. Rühle, "Cation Interdiffusion at YBCO/MgO Interfaces," *Mater. Res. Soc. Symp. Proc.*, **169**, 1173 (1989).
- H. G. Scott, "Phase Relationships in the Zirconia-Yttria System," *J. Mater. Sci.*, **10**, 1527-35 (1975).
- D. Michel, L. Mazerolles, and M. Perez y Jorba, "Polydomain Crystals of Single-Phase Tetragonal ZrO<sub>2</sub>: Structure, Microstructure, and Fracture Toughness," pp. 131-138 in *Advances in Ceramics*, Vol. 12, *Science and Technology of Zirconia II*, Edited by N. Claussen, M. Rühle, and A. H. Heuer. American Ceramic Society, Columbus, OH, 1984.
- F. F. Lange, D. B. Marshall, and J. R. Porter, "Controlling Microstructures Through Phase Partitioning from Metastable Precursors: The ZrO<sub>2</sub>/Y<sub>2</sub>O<sub>3</sub> System," pp. 519-32 in *Ultrastructure Processing of Advanced Ceramics*, Edited by J. D. MacKenzie and D. R. Ulrich. Wiley, New York, 1988.
- D. K. Leung, C.-J. Chan, M. Rühle, and F. F. Lange, "Metastable Crystallization, Phase Partitioning, and Grain Growth of ZrO<sub>2</sub>-Gd<sub>2</sub>O<sub>3</sub> Materials Processed from Liquid Precursors," *J. Am. Ceram. Soc.*, **74** [11] 2786-92 (1991).
- V. Lanteri, A. H. Heuer, and T. E. Mitchell, "Tetragonal Phase in the System ZrO<sub>2</sub>-Y<sub>2</sub>O<sub>3</sub>," pp. 118-30 in *Advances in Ceramics*, Vol. 12, *Science and Technology of Zirconia II*, Edited by N. Claussen, M. Rühle, and A. H. Heuer. American Ceramic Society, Columbus, OH, 1984.
- C. J. Chan, F. F. Lange, M. Rühle, J. F. Jue, and A. V. Virkar, "Ferroelastic Domain Switching in Tetragonal Zirconia Single Crystals—Microstructural Aspects," *J. Am. Ceram. Soc.*, **74** [4] 807-13 (1991).
- D. Michel, L. Mazerolles, and R. Portier, "Electron Microscopy Observation of the Domain Boundaries Generated by the Cubic to Tetragonal Transition of Stabilized Zirconia," pp. 809-12 in *Studies in Inorganic Chemistry*, Vol. 3, *Solid State Chemistry 1982*, Edited by R. Metselaar, H. J. M. Heijligers, and J. Schoorman. Elsevier, New York, 1983.
- A. H. Heuer, R. Chaim, and V. Lanteri, "The Displacive Cubic to Tetragonal Transformation in ZrO<sub>2</sub> Alloys," *Acta Metall.*, **35** [3] 661-66 (1987).
- K. Aizu, "Possible Species of Ferromagnetic, Ferroelectric and Ferroelastic Crystals," *Phys. Rev. B*, **2** [3] 754-72 (1970).
- A. V. Virkar and R. L. K. Matsumoto, "Ferroelastic Domain Switching as a Toughening Mechanism in Tetragonal Zirconia," *J. Am. Ceram. Soc.*, **69** [10] C-224-C-226 (1986).
- R. P. Ingel and D. Lewis III, "Elastic Anisotropy in Zirconia Single Crystals," *J. Am. Ceram. Soc.*, **71** [4] 265-71 (1988). □

**Table I. Strains, Stresses, and Unrelaxed Strain Energy Density for Different Tetragonal Variants on Cubic Single-Crystal Substrates**

Parameter*	Variant 1,2 <sup>b</sup>	Variant 3 <sup>c</sup>	Cubic/Cubic**
$\varepsilon_1$	0.0093	0.0093	-0.0160
$\varepsilon_2$	-0.0048	0.0093	-0.0160
$\varepsilon_3$	-0.0014	-0.0057	0.0118
$\sigma_1$	3.04 GPa	4.27 GPa	-6.1 GPa
$\sigma_2$	-0.98 GPa	4.27 GPa	-6.1 GPa
$E_v$	16.6 MPa	39.9 MPa	90 MPa <sup>d</sup>
	341 J/mol ZrO <sub>2</sub>	819 J/mol ZrO <sub>2</sub>	1848 J/mol ZrO <sub>2</sub>

\*Positive values represent tensile strains and stresses within a given variant.  $c_{11} = 410$  GPa,  $c_{12} = 125$  GPa.<sup>24</sup> <sup>b</sup>Zr(Y)O<sub>2</sub> (+40 mol% Y<sub>2</sub>O<sub>3</sub>) on cubic substrate (9.5 mol% Y<sub>2</sub>O<sub>3</sub>). Elastic parameters extrapolated from data of Ingel and Lewis.<sup>24</sup> <sup>c</sup>Dislocation network at interface reduces unrelaxed strain energy.<sup>9</sup>

LITERATURE

# Polycrystalline $t'$ -ZrO<sub>2</sub>(Ln<sub>2</sub>O<sub>3</sub>) formed by displacive transformations

T. LOG\*

*Elkem Keramer, P.O. Box 126, Kristiansand, Norway*

R. A. CUTLER

*Ceramatec, Inc., 2425 S. 900W., Salt Lake City, Utah 84119, USA*

J. F. JUE, A. V. VIRKAR

*Department of Materials Science and Engineering, University of Utah, Salt Lake City, Utah 84112, USA*

ZrO<sub>2</sub> (3 mol% Y<sub>2</sub>O<sub>3</sub>) tetragonal and  $t'$ -ceramics (displacively formed ceramics) were compared with ZrO<sub>2</sub> ceramics (3 mol% Ln<sub>2</sub>O<sub>3</sub>, where Ln = La, Pr, Nd, Sm, Gd, Tb, Dy, Er, or Yb) processed in an identical manner. Sintering at 1500 °C for 2 h produced mainly tetragonal polytypes for the dopants with smaller ionic radii than Dy (i.e., Er, Y and Yb) but when ZrO<sub>2</sub> was reaction sintered with dopants with larger ionic radii excessive monoclinic phase transformation and associated microcracking resulted. High-temperature annealing in the cubic stability regime and rapid cooling through the tetragonal stability regime was used to fabricate  $t'$ -composites of ZrO<sub>2</sub> doped with Y, Yb, Er or Dy. Room-temperature fracture toughness and strength values are explained on the basis of a ferroelastic-cubic-to-tetragonal transformation. The domain structure was viewed by transmission optical microscopy (TOM) or transmission electron microscopy (TEM).

## 1. Introduction

Wadhawan [1] in a review article on ferroelasticity suggested that ferroelastic switching during the monoclinic-to-tetragonal transformation in zirconia ceramics may contribute to their toughness in addition to the well-documented transformation toughening [2] in these materials. Michel *et al.* [3] studied skull-melted polydomain ZrO<sub>2</sub> single crystals doped with Y, Gd or Yb and found that these  $t'$  (displacively formed) crystals had higher toughnesses than cubic ZrO<sub>2</sub> (9 mol% Y<sub>2</sub>O<sub>3</sub>) crystals. They attributed the higher toughnesses to ferroelastic domains giving rise to textures due to crack deflection. Virkar and Matsumoto [4, 5] suggested that toughening in fine-grained, tetragonal-zirconia-polycrystalline (TZP) ceramics was due in part to ferroelastic domain switching, based on textures observed by X-ray diffraction (XRD). They suggested that this energy-absorbing mechanism was not limited to TZP materials but was a feature of a wide variety of ferroelastics. Subsequent studies [6-13] have verified that ferroelastic toughening is a viable toughening mechanism in a variety of materials.

One of the most interesting results of this recent research is the study of displacively formed  $t'$ -zirconia materials. Large-grained (50-150  $\mu\text{m}$ ) polycrystalline  $t'$ -ZrO<sub>2</sub> can be formed by annealing polycrystalline zirconia in the cubic stability regime ( $\geq 2050$  °C for

ZrO<sub>2</sub> (3 mol% Y<sub>2</sub>O<sub>3</sub>)) and rapidly cooling through the cubic-to-tetragonal-transition temperature. Jue and Virkar [8] showed that these large-grained materials have toughnesses similar to fine-grained-transformation-toughened Y-TZP materials, despite the fact that the  $t'$ -high-temperature-processed materials did not transform to monoclinic ZrO<sub>2</sub>. Both the tetragonal materials ( $t$ -materials) and  $t'$ -materials had toughness two to three times greater than cubic zirconia ( $c$ -zirconia), which is neither transformation nor ferroelastic toughened. Switching of submicrometre domains was identified as the reason for toughening in the polycrystalline  $t'$ -materials; and domain size, not grain size, controls whether the ZrO<sub>2</sub> remains tetragonal upon cooling into the monoclinic stability regime. A subsequent study by Jue *et al.* [11] showed that domain growth can occur upon switching and that a critical domain size can be achieved so that switching triggers transformation.

While the polycrystalline  $t'$ -materials display high toughness and good resistance to low-temperature ageing (i.e., transformation), their large grain size limits their strength, as expected. Sintering at temperatures above 2100 °C in an oxidizing environment is not practical for many applications. The purpose of this paper is to report on an effort which explored the feasibility of lowering the annealing temperature for  $t'$ -zirconia polycrystalline ceramics by substituting

\* Now with Statens Sikkerhetshøgskole, N-5500 Haugesund, Norway.

lanthanide oxides for  $Y_2O_3$ , as well as investigating the feasibility of annealing these materials for short times in a graphite furnace.

## 2. Experimental procedure

Compositions were prepared by the vibratory milling of  $ZrO_2$  (Daiichi DK-1) in methanol (using  $ZrO_2(MgO)$  media) with either 3 mol %  $Y_2O_3$  (Molycorp 5600) or 3 mol %  $Ln_2O_3$ , where  $Ln = La, Pr, Nd, Sm, Gd, Dy, Er, \text{ or } Yb$ . The lanthanide oxides (Molycorp) were generally purer than 99.9%. The powders were vibratory milled for 16 h, followed by wet screening through a 45  $\mu m$  screen and dry screening through a 80  $\mu m$  screen. The powders were uniaxially dry pressed at 35 MPa into bar-shaped and rod-shaped samples and then isostatically pressed at 200 MPa.

The pressed bars were sintered at 1500 °C for 2 h in air. Compositions were subsequently cladless hot isostatically pressed (cladless HIPed) at 1550 °C for 30 min in 200 MPa Ar. High-temperature annealings were performed in a  $ZrO_2$  (3 mol %  $Y_2O_3$ ) crucible inside a graphite-resistance-heated furnace, by rapidly heating ( $\sim 75\text{--}100^\circ C \text{ min}^{-1}$ ) above 1000 °C to the desired annealing temperature in Ar. The hold time at temperature was 5 min or less. The cooling rate was  $\sim 100^\circ C \text{ min}^{-1}$  to 1500 °C. Samples were reoxidized by heating to 1000 °C in air at a rate of 80 °C  $h^{-1}$  and held at temperature for 2 h before examination using transmission optical microscopy (TOM) and transmission electron microscopy (TEM). TOM specimens were viewed under cross-polarized light after dimpling and polishing to a thickness of 10–15  $\mu m$ . TOM samples were subsequently ion-beam milled for TEM analysis.

The density was measured by water displacement. Sintered bars were X-rayed and subsequently ground using a 220 grit diamond wheel. Four-point bend strength was measured using a universal testing machine with a cross-head speed of 0.05 mm  $min^{-1}$ , a support span of 40 mm and a loading span of 20 mm. The fracture toughness was measured using the short-rod technique [14] on 12.5 mm diameter samples. Ground, polished and fractured samples were X-rayed to determine the  $ZrO_2$  polytypes present [15] and to examine switching. The hardness was determined using a 75 N indent made with a Vickers 136° diamond indenter on polished surfaces.

## 3. Results and discussion

### 3.1. Sintering and hot isostatic pressing

The green densities of the pressed samples were only 46–48% of the theoretical values. These low values were the result of the high surface area and poor packing of the powder. Sintered densities ranged between 90% of theoretical ( $ZrO_2(La_2O_3)$ ) to 99% of theoretical ( $ZrO_2(Dy_2O_3)$ ) as shown in Table I.  $ZrO_2$  sintered with  $Y_2O_3$ ,  $Dy_2O_3$ ,  $Er_2O_3$  or  $Yb_2O_3$  had closed porosity after sintering. Open porosity, mainly due to microcracking, resulted in a decrease, rather than an increase in density after hot isostatic pressing

TABLE I Sintering behaviour of  $ZrO_2$  (3 mol %  $Ln_2O_3$ ) in air at 1500 °C

Dopant	Density sintered	(% TD*) HIPed	t (%)	Comments
$La_2O_3$	90.0	86.5	0.0	Severely cracked
$Pr_2O_3$	92.2	90.0	0.0	Several cracks
$Nd_2O_3$	92.1	89.7	24.9	Some cracks
$Sm_2O_3$	92.3	92.3	21.3	Several cracks
$Gd_2O_3$	93.8	98.2	70.6	Cracks
$Dy_2O_3$	98.7	100.0	88.1	No cracks
$Y_2O_3$	97.1	99.2	93.3	No cracks
$Er_2O_3$	98.2	100.0	92.5	No cracks
$Yb_2O_3$	95.4	100.0	86.9	No cracks

\* Percentage of the theoretical density.

(HIPing) for  $ZrO_2$  sintered with La, Pr, Nd and Sm.  $ZrO_2$  (3 mol %  $Gd_2O_3$ ) had mainly closed porosity after sintering, as evidenced by the increase in density upon HIPing, but visual cracks were observed after sintering due to the large amount of monoclinic zirconia (m-zirconia) (see Table I). Dy, Y, Er, and Yb-TZP samples had densities greater than 99% of the theoretical value after HIPing. These samples had no visual cracks despite relatively high amounts of m- $ZrO_2$  (7–13%) and were therefore used for the high-temperature heat treatments.

It is widely recognized that the ionic size of the dopant affects the stabilization of  $ZrO_2$  [16, 17]. The closer the ionic size is to  $Zr^{+4}$ , the easier the stabilization. In the case of lanthanide-series dopants, the lower the ionic size, the closer the mismatch in size between Zr and Ln. The fact that large ions can go into solution with Zr is evidenced by effective stabilization of zirconia with Ca or La [2]. The present results, however, show the difficulty of stabilizing t- $ZrO_2$  by doping with large ions using reaction sintering.

A problem with reaction sintering (as opposed to calcining, milling, and sintering the tetragonally stabilized powder) is the volume change associated with transformation of the c-lanthanides to either m-polymorphs or hexagonal polymorphs (h-polymorphs) [18] prior to reaching temperatures where solid-state diffusion can occur. Reaction sintering was effective for dopants with c-structures stable up to the sintering temperature (i.e., Y, Yb, Er or Dy), whereas dopants which transformed from cubic to monoclinic (i.e., Sm or Gd) or from cubic to hexagonal (i.e., La, Pr or Nd) showed visual cracks after sintering. It is possible that some of these cracks occurred during heating due to phase transformation of the dopants.

The use of coprecipitated powders, improved dispersion of the dopant, a more reactive  $ZrO_2$ , or the addition of a calcination step would probably overcome the sintering problems observed in the present study. However, the  $ZrO_2$  compositions which sintered well were those with the lowest Curie temperatures (see Table II) and those which were most desired. Rouanet [19] showed that the cubic-to-tetragonal transformation temperature was lowered with decreasing ionic radius of the lanthanide-oxide

**TABLE II** Tetragonal-to-cubic transformation temperature for  $ZrO_2$  (3 mol %  $Ln_2O_3$ ) [19, 20]

Dopant	Approximate Curie temperature (°C)
$La_2O_3$	2140
$Pr_2O_3$	2095
$Nd_2O_3$	2095
$Sm_2O_3$	2070
$Gd_2O_3$	2045
$Tb_2O_3$	2030
$Dy_2O_3$	2030
$Y_2O_3$	2000
$Er_2O_3$	2000
$Yb_2O_3$	1950

additive in solution with  $ZrO_2$ . The equilibrium temperature between the c-polymorphs and t-polymorphs of 3 mol %  $ZrO_2$  compositions [19, 20] is given in Table II. In order to form t'-materials, it is necessary to heat above this temperature and then rapidly cool to retain the displacively formed t'-domain structure.

### 3.2. High-temperature heat treatments

Upon annealing  $ZrO_2$  (3 mol %  $Dy_2O_3$ ,  $Y_2O_3$ ,  $Er_2O_3$ , or  $Yb_2O_3$ ) at 2000 °C for 5 min, only the  $ZrO_2$ -( $Yb_2O_3$ ) composition avoided microcracking. This is consistent with the lower tetragonal-to-cubic transformation temperature for this composition, as compared to the compositions partially stabilized with  $Dy_2O_3$ ,  $Y_2O_3$  or  $Er_2O_3$ . If the sample does not reach the cubic stability range, the rapid grain growth which occurs upon heating results in transformation from tetragonal to monoclinic (and associated microcracking) upon cooling. As expected, by heating to 2200 °C it was possible to obtain crack-free  $Dy_2O_3$ ,  $Y_2O_3$  or  $Er_2O_3$  partially stabilized  $ZrO_2$  short-rod samples.

A comparison between the sintered compositions and the samples 2200 °C annealed in Ar and then reoxidized is given in Table III. The density was essentially unaffected by the high-temperature annealing but the grain size increased dramatically and the samples were t' rather than t + m (see Tables III and IV). The formation of t'-grains, despite the large grain size, is in accord with the work of Jue and co-workers [8, 11] for  $ZrO_2(Y_2O_3)$  annealed for much longer times in air at 2100 °C. The hardness of the t'-materials was similar to that of t- $ZrO_2$ , despite the increase in grain size of approximately two orders of magnitude (see Table IV). Grinding caused switching in all four t'-materials with no substantial differences between the four materials after surface grinding with a downfeed of  $5 \mu\text{m pass}^{-1}$ . The  $ZrO_2$  (3 mol %  $Yb_2O_3$ ) showed a greater tendency to switch than the other materials when only hand pressure was applied (see Table IV), but quantitative experiments are required to see if the onset of switching occurs more readily with this material.

TOM showed domain structure in all four materials, as expected. The resolution using TOM, as shown in Fig. 1, is not adequate to distinguish differences in domain size between the four materials. A cursory

**TABLE III** Comparison of HIPed (t + m) and annealed (t')  $ZrO_2$  (3 mol %  $Ln_2O_3$ ) compositions

Dopant	Density (% TD) <sup>a</sup>		t or t' (%)		Grain size ( $\mu\text{m}$ )	
	1500 °C	2200 °C	1500 °C	2200 °C	1500 °C	2200 °C
$Dy_2O_3$	100	99.7	88.1	100	0.7	50
$Y_2O_3$	99.2	99.0	93.3	100	0.7	50
$Er_2O_3$	100	99.7	92.5	100	0.7	45
$Yb_2O_3$	100	99.7	86.9	100	0.7	60

<sup>a</sup> Percentage of the theoretical density.

**TABLE IV** Comparison of hardness and switching in HIPed (t + m) and annealed (t')  $ZrO_2$  (3 mol %  $Ln_2O_3$ )

Dopant	$T_c$ (°C)	Hardness (GPa)		XRD [(002)/(200)] <sup>a</sup>	
		1500 °C	2200 °C	Hand <sup>b</sup>	Machine <sup>c</sup>
$Dy_2O_3$	~ 2030	9.0	11.1	1.4	4.4
$Y_2O_3$	~ 2000	11.5	11.3	1.4	2.6
$Er_2O_3$	~ 2000	11.6	11.7	1.5	4.9
$Yb_2O_3$	~ 1950	11.1	11.3	2.1	3.8

<sup>a</sup> XRD of samples annealed at 2200 °C. The values represent the ratio of (002)/(200) peak integrated intensities on ground/polished surfaces (the higher the values, the more switching has occurred).

<sup>b</sup> Moderate pressure via hand grinding.

<sup>c</sup> Surface grinding under typical finish-grinding conditions.

attempt to do so was made using TEM. Bright-field TEM micrographs delineating twins in grains oriented along the [110] zone axis are shown in Fig. 2. Selected-area diffraction showed no monoclinic  $ZrO_2$ , as expected on the basis of the XRD data. The domain size (twin spacing) was ~ 0.1  $\mu\text{m}$  for the  $ZrO_2$  containing  $Dy_2O_3$ ,  $Y_2O_3$ , or  $Er_2O_3$ , but appeared less (~0.06  $\mu\text{m}$ ) for the  $ZrO_2$  (3 mol %  $Yb_2O_3$ ) samples. Further TEM work is required to verify the differences, if any, in domain size.

The microstructural differences between the four materials were minimal. Yoshimura [21] has shown that partially stabilized  $ZrO_2$  ( $Ln_2O_3$ ) materials have similar tetragonality at a given concentration of  $Ln_2O_3$ . It is, therefore, not surprising that all four t'- $ZrO_2$  compositions result in similar microstructures.

### 3.3. Strength and fracture toughness

The strength of t'-composites was significantly decreased in relation to the as-HIPed strengths, as shown in Fig. 3, due to the larger grains acting as stress concentrators. The strength of the HIPed  $ZrO_2$  (3 mol %  $Y_2O_3$ ), however, was low in comparison to commercially available  $ZrO_2$  (3 mol %  $Y_2O_3$ ) (TOSOH TZ-3Y), which when sintered, HIPed and tested in a similar manner, resulted in a strength of  $1457 \pm 134 \text{ MPa}$  [13]. It is well recognized that the processing of ceramics plays a key role in determining their strength and that typical defects (agglomerates, pores, surface cracks, inclusions, etc.) limit the strength

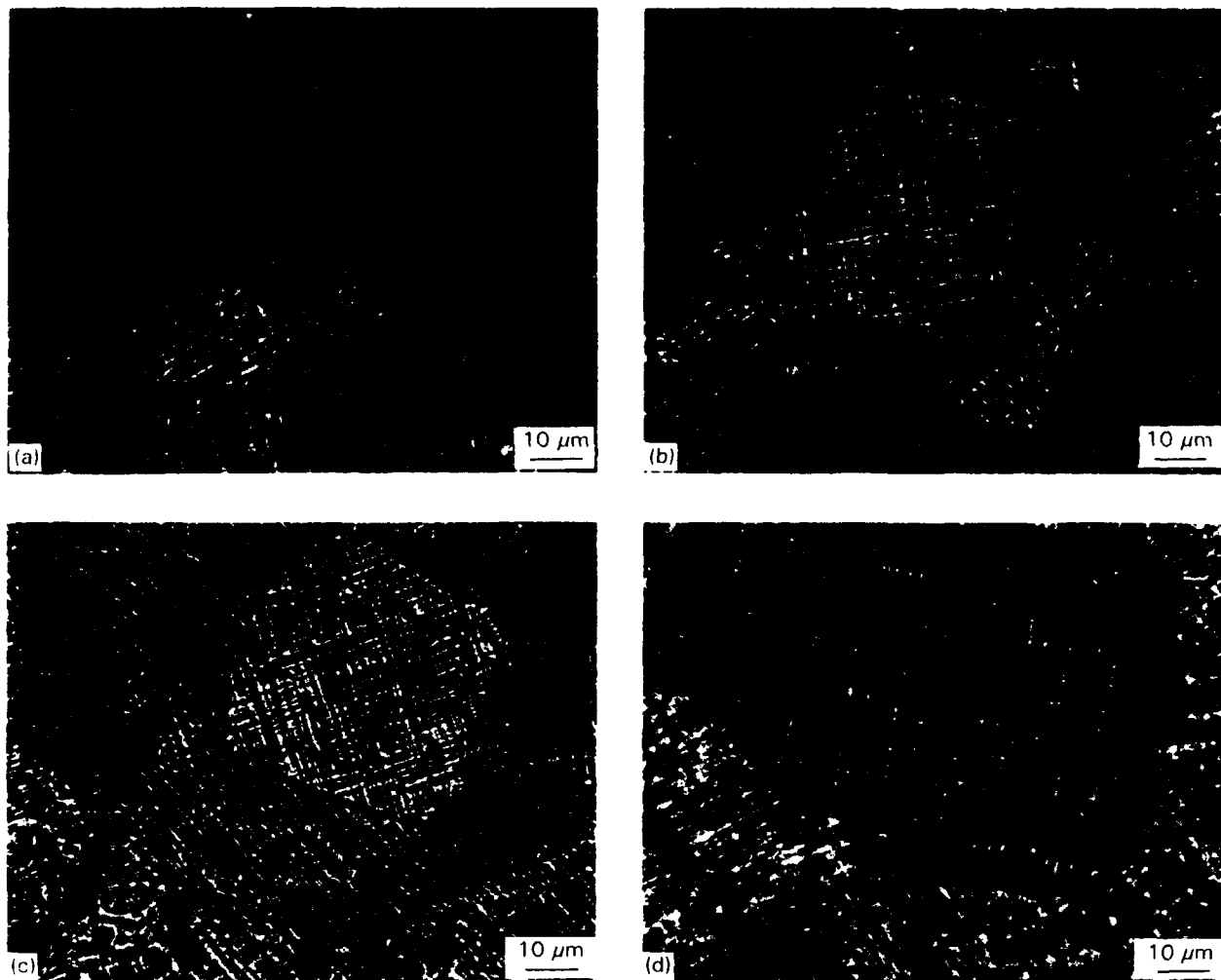


Figure 1 TOM micrographs of  $t'$ -ZrO<sub>2</sub> (3 mol% Ln<sub>2</sub>O<sub>3</sub>) annealed at 2200 °C in Ar and reoxidized at 1000 °C. Note the domain structure visible in cross-polarized light. (a) Ln = Dy, (b) Ln = Y, (c) Ln = Er, and (d) Ln = Yb.

in fine-grained ceramics [22, 23]. The reason for the lower strength of HIPed ZrO<sub>2</sub> (3 mol% Yb<sub>2</sub>O<sub>3</sub>) was not obvious by fractography but it is probably related to agglomerate size and shape, and their packing during pressing.

Despite the lower strength of the  $t'$ -materials relative to the HIPed compositions, it is interesting to observe that the strength values are still considerably higher than for  $c$ -ZrO<sub>2</sub>. A commercially available ZrO<sub>2</sub> (8 mol% Y<sub>2</sub>O<sub>3</sub>) (TOSOH TZ-8Y) sintered, HIPed and tested in a similar manner to the above bars resulted in a strength of  $211 \pm 21$  MPa [13] despite a grain size five times smaller than the  $t'$ -materials. X-ray analysis of fractured  $t'$ -ZrO<sub>2</sub> bars showed no monoclinic formation and therefore transformation toughening could only have been operative if reverse transformation occurred. The higher strength of  $t'$ -bars in comparison to  $c$ -ZrO<sub>2</sub> is believed to be related to the higher toughness of  $t'$ -ZrO<sub>2</sub> relative to  $c$ -ZrO<sub>2</sub>.

The toughness of sintered (1500 °C) or HIPed (1550 °C) transformation-toughened materials was compared with nontransformation-toughened  $t'$ -materials annealed either at 2000 °C (Yb doped in Fig. 4a) or 2200 °C (Dy, Y, or Er doped in Fig. 4b). As

mentioned above, the cracking associated with the 2000 °C annealing of Dy-, Y-, or Er-doped zirconias was related to grain growth causing the tetragonal-to-monoclinic transformation and associated microcracking, whereas the Yb-doped at 2000 °C and all of the 2200 °C materials consisted entirely of  $t'$ -ZrO<sub>2</sub> since they had been heated into the cubic stability regime. Dy-doped ZrO<sub>2</sub> had the highest toughness, and Yb-doped ZrO<sub>2</sub> the lowest toughness, although the differences were not substantial.

The short-rod bulk toughness of the  $t'$ -materials is very similar to the transformation-toughened materials. However,  $c$ -ZrO<sub>2</sub> (8 mol% Y<sub>2</sub>O<sub>3</sub>) had a toughness of  $1.5-1.8$  MPa m<sup>1/2</sup> when compared by the same technique [13]. No  $m$ -ZrO<sub>2</sub> was detected by XRD in the  $t'$ -ZrO<sub>2</sub>(Ln<sub>2</sub>O<sub>3</sub>) ceramics, consistent with the earlier work of Jue and Virkar which showed that ZrO<sub>2</sub> (3 mol% Y<sub>2</sub>O<sub>3</sub>) annealed in air at >2100 °C showed no signs of a reversible transformation [8]. Jue and Virkar found that the toughnesses of  $t'$ -ZrO<sub>2</sub> (3 mol% Y<sub>2</sub>O<sub>3</sub>) samples were about three times greater than  $c$ -ZrO<sub>2</sub> (8 mol% Y<sub>2</sub>O<sub>3</sub>) using the single-edge-notch-bend (SENB) technique for fracture toughness. The short-rod measurements resulted in values for the  $t'$ -materials which were two to three times higher than

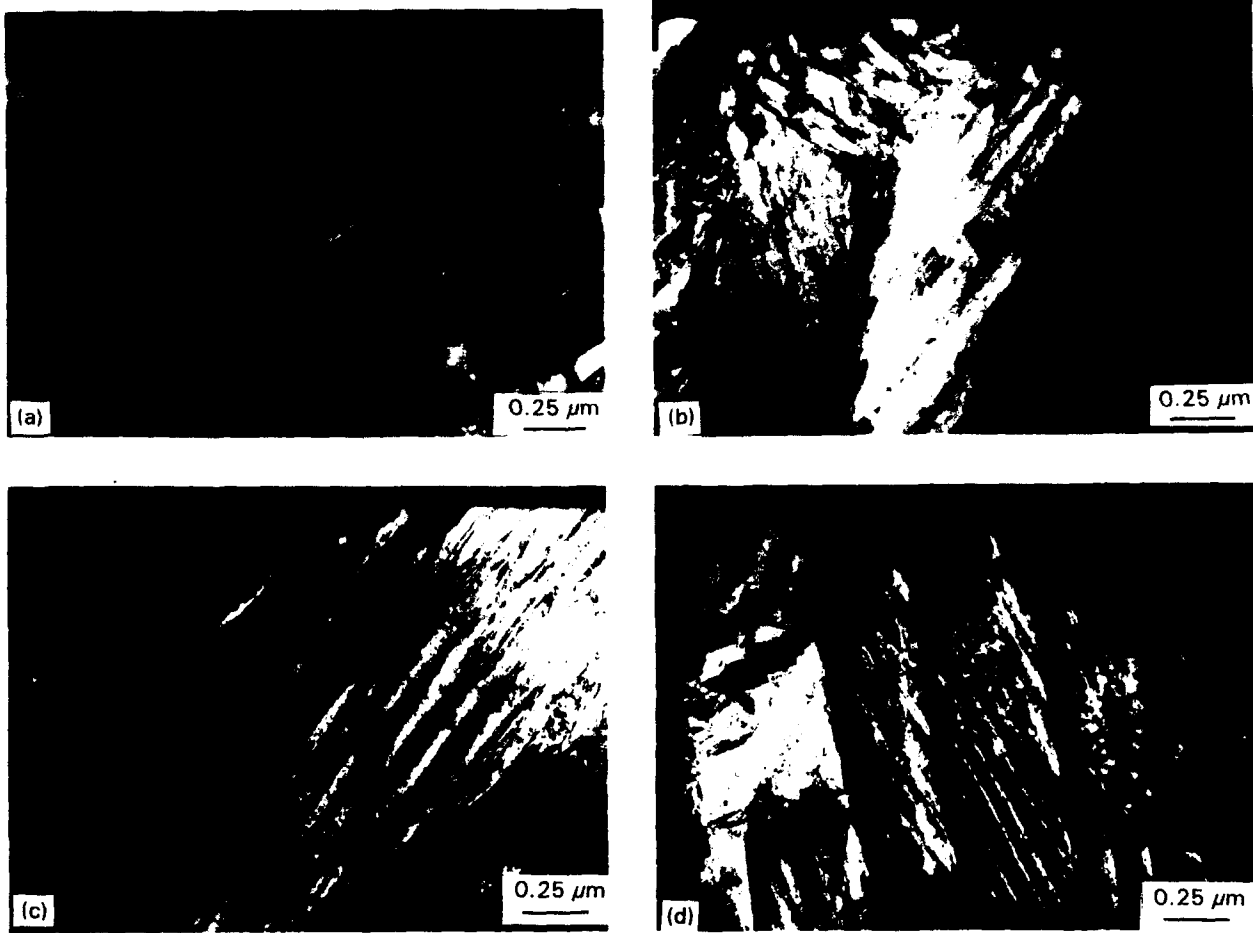


Figure 2 TEM micrographs of  $t'$ -ZrO<sub>2</sub> (3 mol % Ln<sub>2</sub>O<sub>3</sub>) annealed at 2200 °C in Ar and reoxidized at 1000 °C. Note the domains in grains oriented along the [110] zone axis. (a) Ln = Dy, (b) Ln = Y, (c) Ln = Er, and (d) Ln = Yb.

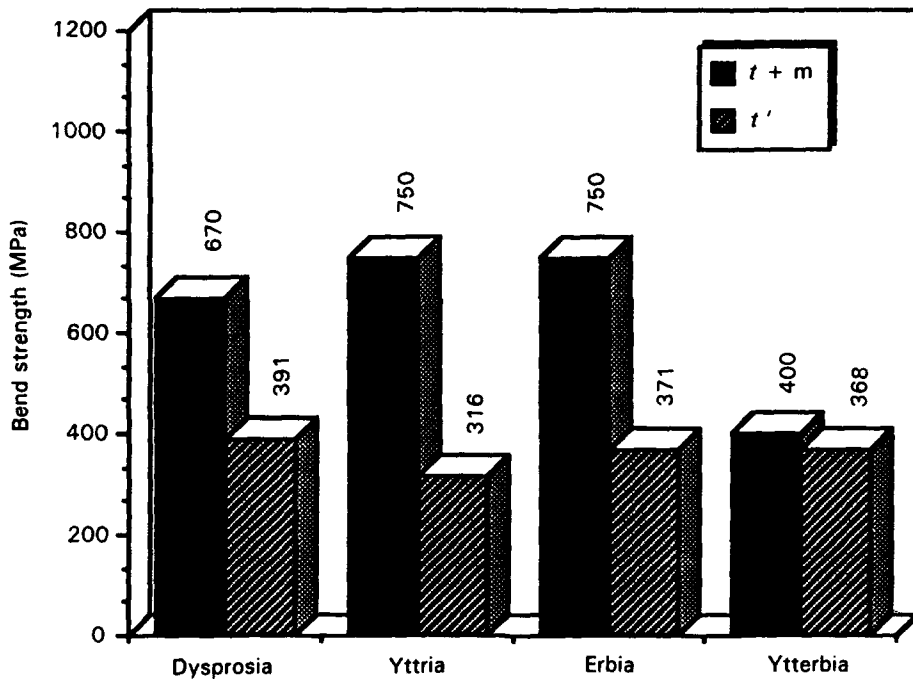


Figure 3 Strength comparison of sintered ( $t + m$ , HIPed at 1550 °C) and annealed ( $t'$ , heat treated at 2200 °C) ZrO<sub>2</sub> (3 mol % Ln<sub>2</sub>O<sub>3</sub>).

for  $c$ -ZrO<sub>2</sub> [13] and only slightly lower in toughness than transformation-toughened ZrO<sub>2</sub>. This is consistent with the conclusions of Virkar *et al.* [12] that ferroelastic switching can play a significant role in toughening ceramics.

#### 4. Conclusion

Polycrystalline  $t'$ -ZrO<sub>2</sub> (3 mol % Dy<sub>2</sub>O<sub>3</sub>), ZrO<sub>2</sub> (3 mol % Er<sub>2</sub>O<sub>3</sub>), and ZrO<sub>2</sub> (3 mol % Yb<sub>2</sub>O<sub>3</sub>) were all successfully fabricated by heating them into the cubic stability range (>2000 °C) and cooling at rates of

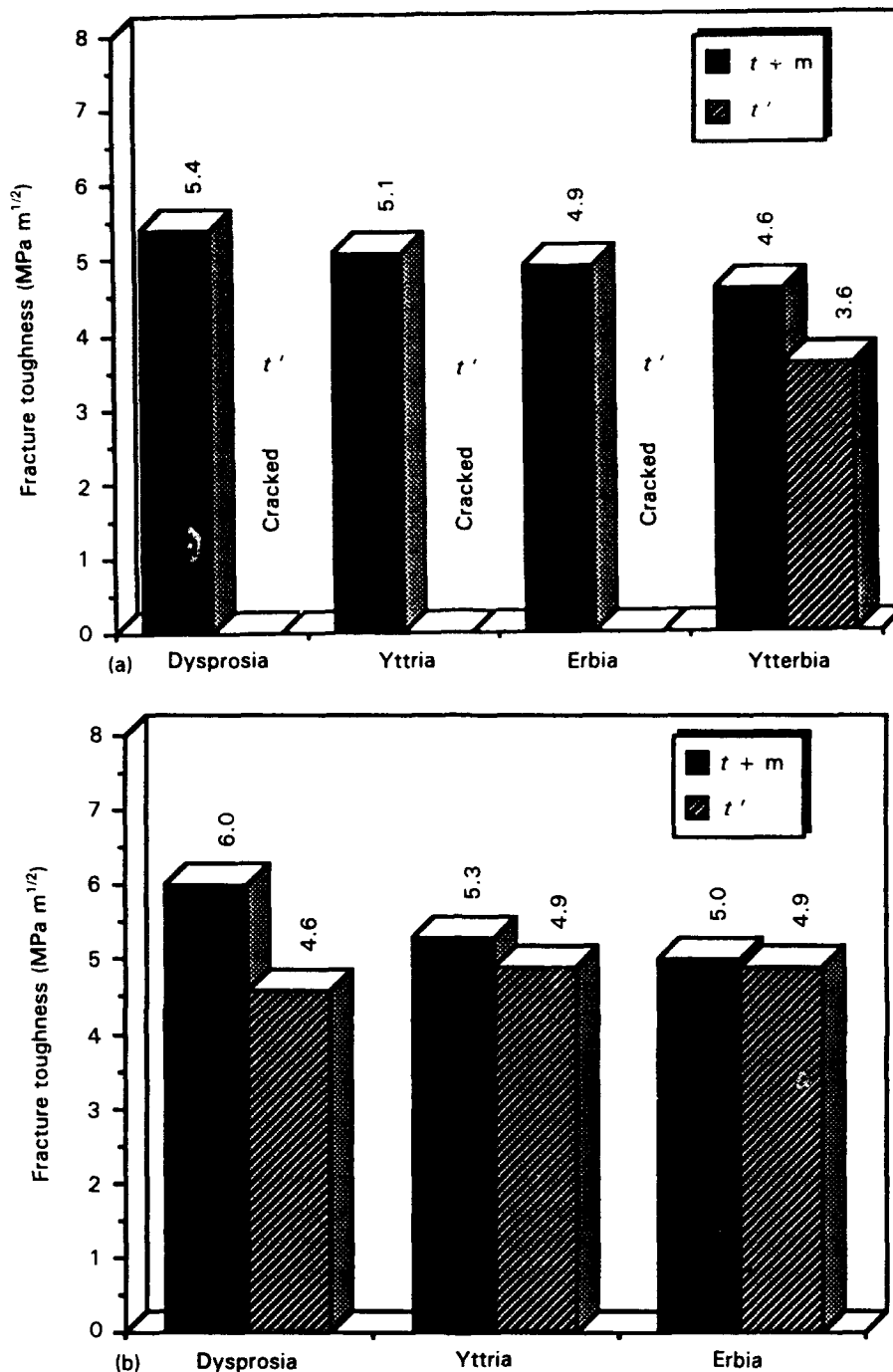


Figure 4 Short-rod-fracture-toughness comparison of sintered (t + m) and annealed (t') ZrO<sub>2</sub>. (a) Sintered in air at 1500°C (t + m) and sintered samples annealed at 2000°C for 5 minutes (t'). (b) samples HIPed at 1550°C (t + m) and HIPed samples annealed at 2200°C for 5 min (t').

~100°C min<sup>-1</sup>. These materials have domain structures similar to t'-ZrO<sub>2</sub> (3 mol% Y<sub>2</sub>O<sub>3</sub>) based on TOM and TEM. Domain switching after surface grinding was also similar for all four materials.

High-temperature-annealed t'-zirconias have similar toughnesses to their transformation-toughened counterparts and are two to three times tougher than c-ZrO<sub>2</sub>. The high toughness in t'-materials, relative to c-ZrO<sub>2</sub>, was attributed to ferroelastic switching since transformation toughening is not operative in these materials.

The hardness of the 45–60 μm grain size t'-zirconias was similar to that of the 0.7 μm grain size HIPed materials. The strength of t'-materials decreased dramatically in comparison to the sintered and HIPed

materials due to the increase in grain size. However, strengths on the order of 300–400 MPa are still significantly higher than those measured for c-zirconia with a finer grain size. The higher strength is believed to be due to the increased toughness of these materials.

No significant advantage was observed when substituting lanthanide oxides for Y<sub>2</sub>O<sub>3</sub> in t'-zirconias. The lower tetragonal-to-cubic transition temperature did not result in a dramatically improved strength since rapid grain growth occurs at temperatures of 2000°C. Short-term exposures to the reducing environment of graphite furnaces did nothing more than change the colour of the ceramic from white to black and can be used to form t'-ceramics. Rapid sintering (e.g. by microwave) in air, however, should be investig-

ated as an alternative route for synthesizing finer-grained t'-Y-ZrO<sub>2</sub> in an effort to achieve better strengths.

### Acknowledgement

This work was supported by the Defense Advanced Research Projects Agency (DARPA) through AFOSR under Contract No. F49620-89-C-0054.

### References

1. V. K. WADHAWAN, *Phase Transitions* 3 (1982) 3.
2. D. J. GREEN, R. H. J. HANNINK and M. V. SWAIN, "Transformation toughening of ceramics" (CRC, Boca Raton, FL, 1989).
3. D. MICHEL, L. MAZEROLLES, M. PEREZ, Y. JORBA, *J. Mater. Sci.* 18 (1983) 2618.
4. A. V. VIRKAR and R. L. K. MATSUMOTO, *J. Amer. Ceram. Soc.* 69 (1986) C224.
5. A. V. VIRKAR and R. L. K. MATSUMOTO in "Advances in ceramics", Vol. 24, edited by S. Somiya, N. Yamamoto and H. Yanagida (American Ceramic Society, Westerville, OH, 1988) p. 653.
6. G. V. SRINIVASEN, J. F. JUE, S. Y. KUO and A. V. VIRKAR, *J. Amer. Ceram. Soc.* 72 (1989) 2098.
7. K. MEHTA and A. V. VIRKAR, *J. Amer. Ceram. Soc.* 73 (1990) 567.
8. J. F. JUE and A. V. VIRKAR, *J. Amer. Ceram. Soc.* 73 (1990) 3650.
9. C. J. CHAN, F. F. LANGE, M. RÜHLE, J. F. JUE and A. V. VIRKAR, *J. Amer. Ceram. Soc.* 74 (1991) 807.
10. T. L. BAKER, K. T. FABER and D. W. READY, *J. Amer. Ceram. Soc.* 74 (1991) 1619.
11. J. F. JUE, J. CHEN and A. V. VIRKAR, *J. Amer. Ceram. Soc.* 74 (1991) 1811.
12. A. V. VIRKAR, J. F. JUE, P. SMITH, K. MEHTA and K. PRETTYMAN, *Phase Transitions* 35 (1991) 27.
13. R. A. CUTLER, J. R. REYNOLDS and A. JONES, *J. Amer. Ceram. Soc.* 75 (1992) 2173.
14. L. M. BARKER in "Chevron-notched specimens: Testing and stress analysis" (American Society for Testing and Materials, Philadelphia, PA, 1984) p. 117.
15. H. TORAYA, M. YOSHIMURA and S. SOMIYA, *J. Amer. Ceram. Soc.* 68 (1984) C-119.
16. W. W. BARKER and L. S. WILLIAMS, *J. Australian Ceram. Soc.* 4 (1968) 1.
17. S. L. HWANG and I. W. CHEN, *J. Amer. Ceram. Soc.* 73 (1990) 3269.
18. W. M. KRIVEN, *J. Amer. Ceram. Soc.* 71 (1988) 1021.
19. A. ROUANET, *Rev. Int. Hautes Temp. Refract.* 8 (1971) 161.
20. D. MICHEL, L. MAZEROLLES, and M. PEREZ Y JORBA in "Advances in ceramics", Vol. 12, edited by N. Claussen, M. Rühle and A. H. Heuer (American Ceramic Society, Westerville, OH, 1984) 131.
21. M. YOSHIMURA, *Bull. Amer. Ceram. Soc.* 67 (1988) 1950.
22. F. F. LANGE, *J. Amer. Ceram. Soc.* 72 (1989) 3.
23. G. D. QUINN and R. MORRELL, *J. Amer. Ceram. Soc.* 74 (1991) 2037.

Received 2 June 1992  
and accepted 11 January 1993

# Damage-Resistant SrO-Doped Ce-TZP/Al<sub>2</sub>O<sub>3</sub> Composites

R. A. Cutler<sup>1</sup>, J. M. Lindemann<sup>2</sup>, J. H. Ulvensøen<sup>3</sup> and H. I. Lange<sup>3</sup>

**Abstract** - Simultaneous additions of SrO and Al<sub>2</sub>O<sub>3</sub> to ZrO<sub>2</sub> (12 mol. % CeO<sub>2</sub>) lead to the in situ formation of SrO·6Al<sub>2</sub>O<sub>3</sub> platelets in the Al<sub>2</sub>O<sub>3</sub>/Ce-TZP matrix. These composites have superior damage resistance compared to Al<sub>2</sub>O<sub>3</sub>/Y-TZP ceramics despite their lower strength. The increased damage resistance appears to be primarily related to the higher residual stress due to grinding with smaller contributions due to micromechanical toughening. High damage resistance was also obtained by introduction of temperature-induced surface compressive stresses. Damage resistance is only obtained at low temperatures (<500°C). The applicability of conventional powder processing (slip casting or spray drying) to these tailored microstructures is demonstrated.

## Introduction

Zirconia-based ceramics have established themselves as useful materials for low-temperature applications due to their high toughness relative to most other ceramics. The increased toughness in these polycrystalline materials is primarily due to transformation toughening[1-3] which is grain size and temperature dependent[4]. Toughening contributions can also occur due to stress-induced microcracking[5], ferroelastic switching[6], residual stress[7], crack deflection[8], crack bridging[9], transformation-zone control[10], and microstructural engineering[11]. In most ceramic systems, more than one toughening mechanism is occurring simultaneously[2]. Some of these toughening mechanisms lead to R-curve behavior such that toughness increases with crack length which can limit strength[12]. The advantage of R-curve behavior is that damage tolerant ceramics can be produced in this manner[13-15]. Since crack instability (i.e., fracture) in most ceramics does not occur in the long crack plateau region, natural (sharp) short cracks are most useful for obtaining design data[16].

The ability to grow elongated rods or platelets in-situ is one of the most desired means of obtaining damage-resistant microstructures due primarily to crack-bridging mechanisms[17, 18]. In-situ formed platelets in tetragonal zirconia polycrystals (TZP) have generally resulted in improved mechanical properties[19-23]. These platelets, which generally have hexaluminate structures similar to β-Al<sub>2</sub>O<sub>3</sub> or magnetoplumbite, result in only a modest contribution to toughening due to crack bridging because of their low cohesive strength[24]. The higher toughness achieved in Ce-TZP ceramics with platelets is likely due to control of the transformation-zone morphology[10-24,25] concentrating transformation to the region around the crack tip.

1. Ceramtec, Inc., 2425 S. 900 W., Salt Lake City, Utah 84119, USA

2. Elkem Keramer, P. O. Box 126, N-4602, Kristiansand, Norway. FAX 47 380 14970

3. Univ. of Trondheim, Dept. of Metallurgy, N-7034, Trondheim, Norway

Ce-TZP with a combination of SrO·6Al<sub>2</sub>O<sub>3</sub> platelets and Al<sub>2</sub>O<sub>3</sub> equiaxed grains results in a favorable combination of toughness, hardness, and strength. A polycrystalline material containing 30 vol. % second phases (aluminate platelets and alumina particles) resulted in a strength of 725 MPa, a fracture toughness of 11 MPa√m, and a hardness of 13.5 GPa. The properties are attractive since Ce-TZP in the absence of Al<sub>2</sub>O<sub>3</sub> has high toughness (12.5 MPa√m) but has low strength (400 MPa) and low hardness (9.5 GPa). The addition of 30 vol. % Al<sub>2</sub>O<sub>3</sub> as a second phase increases the strength (630 MPa) and hardness (14.5 GPa) but lowers the toughness (8 MPa√m)[22]. By adding SrO and allowing the in situ platelet formation, one obtains both high strength and high toughness, with a small drop in hardness.

The purpose of this paper is to discuss processing and design considerations which can be applied to such ceramics. Additionally, the damage tolerance of these ceramics will be assessed. A simple method for increasing the damage resistance by the incorporation of residual compressive stresses to a sufficient depth to give high damage tolerance will be discussed.

### Experimental Procedure

Co-precipitated powders with binder in aqueous slips were either spray dried using conventional equipment or slip cast using conventional plaster molds at solids contents of 35-40 vol. %. Pressing or casting of layered composites was performed using techniques formerly applied to Al<sub>2</sub>O<sub>3</sub>-ZrO<sub>2</sub> ceramics[26,27]. Sample characterization was performed as described previously[22]. Biaxial strength testing was similar to that described by Lindemann and Nissen[28]. Residual stress was assessed using a strain gage technique developed by Virkar[29, 30]. Damage response was assessed by indentation/ strength measurements, as previously applied to Al<sub>2</sub>O<sub>3</sub>-ZrO<sub>2</sub> ceramics with transformation-induced stresses[31].

### Toughening With SrO Additions

Figure 1 shows that additions of SrO to Ce-TZP (i.e., ZrO<sub>2</sub>(12 mol. % CeO<sub>2</sub>)) lower the toughness since it reduces the ZrO<sub>2</sub> grain size while additions of SrO to Ce-TZP containing Al<sub>2</sub>O<sub>3</sub> results in an increase in toughness despite its constant grain size[22]. The main role of SrO additions is a change in the shape and properties of the second phase. Increasing additions of SrO up to a SrO/Al<sub>2</sub>O<sub>3</sub> molar ratio of ≈0.1 lead to an increase in toughness as SrO·6Al<sub>2</sub>O<sub>3</sub> platelets are formed in the microstructure[22]. Using electron dispersive spectroscopy (EDS) Schmid has shown that the aluminates contain less Sr than predicted and have Ce in solution. The atomic ratio of Al: Sr: Ce: Zr measured by EDS using analytical transmission electron microscopy was 94.8:3.5:1.3:0.4, which gives a ration Al:(Sr+Ce+Zr) of 18.2 as compared to expected ratio of 12 for SrO·6Al<sub>2</sub>O<sub>3</sub>[32]. Ce and Zr diffusion into the aluminate lattice is similar to the previous results reported for Al-rich lanthanum hexaluminates[23]. An important point for the Al-rich strontium hexaluminates is that the lattice parameter for the mixed oxide matches SrO·6Al<sub>2</sub>O<sub>3</sub>[32].

Typical properties for Ce-TZP/30 vol. % Al<sub>2</sub>O<sub>3</sub>+SrO·6Al<sub>2</sub>O<sub>3</sub> prepared by slip casting are given in Table 1. The strength is similar to that reported by Cutler, et al[22] but the hardness and toughness are lower. Since both the

hexaluminate and zirconia matrix are soft phases, relative to alumina, increased hardness in these composites is very dependent on the size and distribution of alumina. The extensive vibratory milling of reactants by Cutler, et al[22] compared to the less aggressive milling used in the present study may explain the lower hardness. Toughness is very dependent on measurement technique due to R-curve effects as well as the microstructure of the material. The fracture toughness listed in Table 1 is from chevron-notched beam specimens.

Figure 2 shows the microstructure of polished and fractured surfaces of slip cast Ce-TZP/30 vol. %  $\text{Al}_2\text{O}_3$ +SrO-6 $\text{Al}_2\text{O}_3$  compared to the same composition prepared by dry pressing coprecipitated spray dried powders. As shown in Figure 2(a), both materials consist of a 1-3  $\mu\text{m}$  Ce-TZP matrix with equiaxed  $\text{Al}_2\text{O}_3$  grains (0.1-1  $\mu\text{m}$ ) and SrO-6 $\text{Al}_2\text{O}_3$  platelets 1-3  $\mu\text{m}$  in length. The faceted platelets may provide easy nucleation sites for transformation as suggested by Shetty[25]. Both processing routes (i.e., slip casting and dry pressing of spray dried coprecipitated powders) result in similar microstructures, as expected. Fracture in this material occurs intergranularly, revealing the plate-shaped morphology of the SrO-6 $\text{Al}_2\text{O}_3$  (see Figure 2(b)). Figure 2(c) shows cracks from a diamond indenter which is to the left of the microphotographs. The cracks propagate along grain boundaries with crack branching, crack bridging, and crack deflection all evident. The primary mode of toughening in these composites is believed to be alteration of the transformation zone ahead of the crack tip due to hexaluminate formation. Marshall has taught that microstructural modifications which decrease the elongation of the zone ahead of the crack could increase the toughness by a factor of two[33]. Platelets aligned orthogonal to the crack tip would cause the transformation zone to spread out in an analogous manner to that observed by Marshall et al[10] in layered composites or by Shetty and co-workers[21,25,34] for Ce-TZP/ $\text{Al}_2\text{O}_3$  containing MnO (which results in an elongated  $\text{CeMnAl}_{11}\text{O}_{19}$  grains with similar structure to strontium hexaluminate).

For many wear applications, higher  $\text{Al}_2\text{O}_3$  composites are desired since they lead to an increase in hardness and thermal conductivity with a decrease in thermal expansion and specific gravity. The strength of these materials is excellent but the fracture toughness is decreased relative to high zirconia compositions. In order to show that SrO additions could be beneficially used to toughen these systems, a series of five compositions (see Table 2) was prepared by mixing oxides ( $\text{Al}_2\text{O}_3$ ,  $\text{ZrO}_2$ ,  $\text{CeO}_2$  and/or  $\text{Y}_2\text{O}_3$  with and without  $\text{SrZrO}_3$ ), slip casting, and sintering at 1600°C for 3 hours. Fracture toughness was measured by the double cantilever beam technique and is compared in Table 2.

Taking values of 3  $\text{MPa}\sqrt{\text{m}}$  for the toughness of  $\text{Al}_2\text{O}_3$ [24], 4-5  $\text{MPa}\sqrt{\text{m}}$  as the toughness of Y-TZP[35,36], and 8  $\text{MPa}\sqrt{\text{m}}$  as the toughness of Ce-TZP/ $\text{Al}_2\text{O}_3$ [22], the toughness predicted by a simple rule-of-mixtures calculation would be 3.3-3.6  $\text{MPa}\sqrt{\text{m}}$  for  $\text{Al}_2\text{O}_3$ /30 vol. % Y-TZP and 4.5  $\text{MPa}\sqrt{\text{m}}$  for  $\text{Al}_2\text{O}_3$ /30 vol. % Ce-TZP, in fair agreement with the measured values. The toughness of  $\text{Al}_2\text{O}_3$ +SrO-6 $\text{Al}_2\text{O}_3$ /30 vol. % TZP composites were  $\approx$ 14% higher than the  $\text{Al}_2\text{O}_3$ /30 vol. % TZP baseline materials.

The 4.2-5.7  $\text{MPa}\sqrt{\text{m}}$  toughness values for  $\text{Al}_2\text{O}_3$ +SrO-6 $\text{Al}_2\text{O}_3$ /30 vol. % TZP composites are only slightly higher than the results of Chen[24] where toughness values up to 4.5  $\text{MPa}\sqrt{\text{m}}$  (50% higher than baseline alumina) were

achieved for alumina/aluminate composites. While the toughness is dependent on the SrO/Al<sub>2</sub>O<sub>3</sub> ratio, as discussed by Cutler et al[22], and optimization of particle size and morphology may enhance toughness, the toughness values measured for the Al<sub>2</sub>O<sub>3</sub>+SrO·6Al<sub>2</sub>O<sub>3</sub>/30 vol. % TZP composites indicate that these materials show only a modest improvement over conventional Al<sub>2</sub>O<sub>3</sub>/ZrO<sub>2</sub> composites.

### Reliability and Damage Resistance

One desirable feature of Al<sub>2</sub>O<sub>3</sub>+SrO·6Al<sub>2</sub>O<sub>3</sub>/30 vol. % TZP composites is that they can be made with good strength and high reliability. This is demonstrated for the Al<sub>2</sub>O<sub>3</sub>+SrO·6Al<sub>2</sub>O<sub>3</sub>/30 vol. % Ce-TZP composites in Figure 3 where a mean flexural strength of 607±37 MPa with a Weibull modulus of 17 was obtained on 35 slip cast bars. The same material had a mean biaxial strength of 635±30 MPa and a Weibull modulus of 25 as measured by the linear regression and 33 as determined by the maximum likelihood method on 21 plate-shaped samples (see Figure 4). This high reliability is a desirable feature for ceramics but it should be remembered that this is processing controlled and is not a material property.

Al<sub>2</sub>O<sub>3</sub>/Y-TZP composites can also be made with high reliability and have the added advantage that their strength can be increased by decreasing the critical flaw size by hot isostatic pressing (HIPing). Figure 5 compares the strength of "as-sintered" Al<sub>2</sub>O<sub>3</sub>/30 vol. %Y-TZP made by dry pressing spray dried coprecipitated powders with the same material sintered and cladless HIPed. The Weibull modulus was high (m=25-28) in the sintered state when the strength was moderate (σ<sub>f</sub>=652±30 MPa), but the reliability decreased (m=8-13) upon hot isostatic pressing (HIPing) when the strength increased dramatically (σ<sub>f</sub>=1395±176 MPa). These data are similar to that observed for Y-TZP without Al<sub>2</sub>O<sub>3</sub>[35]. Ce-TZP composites must be HIPed in high P<sub>O2</sub> environments to keep CeO<sub>2</sub> from converting to Ce<sub>2</sub>O<sub>3</sub> with the accompanying volume change which can induce catastrophic failure.

While Y-TZP and Al<sub>2</sub>O<sub>3</sub>/Y-TZP composites have found increasing use in wear parts at low temperatures, due to their high strength, they are susceptible to surface damage and their strength falls off precipitously with even small flaws. Recent interest in duplex microstructures result in damage resistant materials but strength is compromised[37,38].

An advantage of Ce-TZP/30 vol. % Al<sub>2</sub>O<sub>3</sub>+SrO·6Al<sub>2</sub>O<sub>3</sub> ceramics is their improved damage resistance (see Figure 6) in comparison to high strength Al<sub>2</sub>O<sub>3</sub>/30 vol. % Y-TZP and moderate strength Si<sub>3</sub>N<sub>4</sub> sintered without N<sub>2</sub> overpressure with 13 wt. % Y<sub>2</sub>O<sub>3</sub> and 4 wt. % Al<sub>2</sub>O<sub>3</sub>[39]. When the fracture strength (σ<sub>f</sub>) data are plotted as a function of the inverse cube root of the indenter load, as shown in Figure 7, a linear relationship is expected with the slope related to the fracture toughness, K<sub>IC</sub>, and the intercept giving the residual stress, σ<sub>r</sub>, as[40]:

$$\sigma_f = \left\{ \frac{CK_{IC}^{4/3}}{(E/H)^{1/6}P^{1/3}} \right\} + \sigma_r \quad (1)$$

where C is a constant, E is Young's modulus, H is hardness, and P is the indentation load. Taking C as 2.02[41], and values of E and H given in Table 1, the K<sub>IC</sub> calculated from the slope of the data for Ce-TZP/30 vol. % Al<sub>2</sub>O<sub>3</sub> +

$\text{SrO}\cdot 6\text{Al}_2\text{O}_3$  (see Figure 7) is  $4.9 \text{ MPa}\sqrt{\text{m}}$  and the residual compressive stress is  $-443 \text{ MPa}$ . The fracture toughness values calculated for  $\text{Al}_2\text{O}_3/\text{Y-TZP}$  and  $\text{Si}_3\text{N}_4$  were  $5.1 \text{ MPa}\sqrt{\text{m}}$  and  $5.8 \text{ MPa}\sqrt{\text{m}}$ , respectively. These materials showed residual stress values near zero, as expected. HIPing had no effect on the damage resistance of the  $\text{Al}_2\text{O}_3/\text{Y-TZP}$  material. The linear fit of the Ce-TZP/ $\text{Al}_2\text{O}_3$  data is poor ( $r^2=0.64$ ) in comparison to the  $\text{Al}_2\text{O}_3/\text{Y-TZP}$  ( $r^2=0.98$ ) and  $\text{Si}_3\text{N}_4$  ( $r^2=0.99$ ). Due to the poor fit of the data for Ce-TZP/ $\text{Al}_2\text{O}_3$ , neither the fracture toughness nor the residual stress is reliable. However, the damage resistance of the Ce-TZP/ $\text{Al}_2\text{O}_3$  material is excellent compared to the other two materials.

The strain gage technique[29,30] showed no residual stresses for any of the three materials, although the smallest material removed was  $\approx 25\mu\text{m}$ . It is well known that grinding can introduce significant compressive stresses but the stress is limited to the transformation zone which is small in both materials containing TZP[22]. A small zone of high compression, however, can still influence crack initiation, as evidenced by data on ion-exchanged glass where the zone of compression is  $\approx 10 \mu\text{m}$  but the peak compressive stress is high ( $\approx 500 \text{ MPa}$ )[42,43]. To test out the hypothesis that a small zone of residual compression is leading to the excellent damage resistance of the Ce-TZP/ $\text{Al}_2\text{O}_3$  samples, ground samples were annealed at  $1500^\circ\text{C}$  for 3 hours in air. The annealing relaxed the residual stresses as shown in Figure 8. The data fits the expected linear relationship and yields a fracture toughness of  $10.0 \text{ MPa}\sqrt{\text{m}}$  and an intercept showing a tensile stress of  $68 \text{ MPa}$ . These data show that the damage resistance of the Ce-TZP/ $\text{Al}_2\text{O}_3$  is due to transformation-induced shallow ( $<25 \mu\text{m}$ ) compressive stresses which can be relieved by high-temperature annealing.

### Surface Compression

An extremely effective method of increasing damage resistance is to put the surface under compression to a sufficient depth that the surface cracks are contained within the outer region of high compressive stress[3]. The method of controlling the depth of transformation-induced stresses in the green state, as proposed by Virkar[44], is one of the most effective means of obtaining both high strength[27] and excellent damage resistance[31]. The main value of the technique is that the residual stresses are temperature-independent up to the monoclinic-tetragonal transformation temperature. Conversely, when residual stresses are created due to thermal expansion mismatch between phases, the stresses decrease nearly linearly as the materials approach the temperature where creep allows stress-relaxation.

Layered composites were made either by dry pressing or slip casting. Dry pressed composites had  $\approx 300 \mu\text{m}$  thick  $\text{Al}_2\text{O}_3/30 \text{ vol. } \% \text{ Y-TZP}$  outer layers. Slip cast composites were made with  $\approx 750 \mu\text{m}$  thick  $\text{Al}_2\text{O}_3+\text{SrO}\cdot 6\text{Al}_2\text{O}_3/30 \text{ vol. } \% \text{ Ce-TZP}$  outer layers. The inner layer in both types of composites was Ce-TZP/30 vol.  $\% \text{ Al}_2\text{O}_3+\text{SrO}\cdot 6\text{Al}_2\text{O}_3$  such that outer layer thicknesses were in the range of  $1/7$  to  $1/17$  the total thickness of the bars. Using simple beam theory, the expected stresses are given by[26]:

$$\sigma_c = (\alpha_1 - \alpha_2) \Delta T d_2 E_1 E_2 / [(2E_1 d_1)(1 - \nu_1) + (E_2 d_2)(1 - \nu_2)] \quad (2)$$

and

$$\sigma_t = -\sigma_c 2d_1/d_2 \quad (3)$$

where  $\sigma_c$  is compressive residual stress,  $\alpha$  is the coefficient of thermal expansion,  $\Delta T$  is the differential between the creep and test temperatures,  $d$  is thickness,  $\nu$  is Poisson's ratio,  $\sigma_t$  is tensile residual stress, and the subscripts 1 and 2 refer to the outer and inner layers, respectively. Taking  $\Delta\alpha$  as  $-8 \times 10^{-7}/^\circ\text{C}$ ,  $\Delta T$  as  $1000^\circ\text{C}$ ,  $E_1$  as 315 GPa,  $E_2$  as 250 GPa,  $\nu$  as 0.25, and measured values of  $d$ ,  $\sigma_c$  in the 310  $\mu\text{m}$  dry pressed outer layers was calculated to be -288 MPa ( $\sigma_t = 38$  MPa) in excellent agreement with the strength increase of 298 MPa measured by flexural tests. The Weibull modulus was 42 for the three-layer bars as compared to 25 for the monolithic outer-layer specimens. The increase in both Weibull modulus and strength is a highly desired feature and is consistent with superposition of stress. If one were to increase the strength of each bar of the monolithic outer-layer material by 298 MPa, the difference in mean strength between three-layer and outer-layer samples, the Weibull modulus would increase from 25 to 36. The fact that the measured Weibull modulus is higher than 36 suggests that the compressive stress is higher than 298 MPa.

Virkar[30] has shown that a simple strain gage technique can be used to calculate the residual stress profile of the sample by determining  $\Delta\epsilon_0$ , the free strain in the outer layer in relation to the inner layer. The measurement consists of measuring strain,  $\epsilon_M$ , from a strain gage attached to the opposite side from which material is ground off to a depth,  $\delta$ , so that for  $0 \leq \delta \leq d_1$

$$\epsilon_M(0, \delta) = \{\Delta\epsilon_0 d_2 \delta (2d + \delta) / (d - \delta)^2 d\} \quad (4)$$

so that the residual stress can be calculated as

$$\sigma_c = -\Delta\epsilon_0 d_2 E_1 E_2 / \{(2E_1 d_1)(1 - \nu_1) + (E_2 d_2)(1 - \nu_2)\} \quad (5)$$

Using the data in Figure 9 to determine  $\Delta\epsilon_0$  (by curve fitting the data to Equation (4)), a residual compressive stress of -520 MPa was calculated for the dry pressed samples. Superimposing this stress on the monolithic strength data, the Weibull modulus increases from 25 to 45, in agreement with the measured change in Weibull modulus to 42. There is no sharp change in strain (see Figure 9) for the dry pressed samples at the interface ( $\approx 310 \mu\text{m}$ ). This is explained by the diffuse interface of the dry pressed samples compared to the sharp interface which occurs during slip casting, as shown in Figure 10. Strain gage measurements for three-layer slip cast composites showed a distinct change of slope at the interface ( $\approx 760 \mu\text{m}$ ) between outer and inner layers (see Figure 9), as predicted by Virkar [29,30]. The expected tensile strain in the inner layer, for

$d_1 \leq \delta \leq d_1 + d_2$ , is given by[30]

$$\epsilon_M(0, \delta) = \Delta\epsilon_0 \{ [(d_1^2 - (d_2 - \delta)^2) / (d - \delta)^2] + (d_2/d) \} \quad (6)$$

The solid line in through the data points measured for the three-layer slip cast composites (see Fig. 9) show the excellent agreement between experimental data and the predicted fit of the data using Equations (4) and (6) when  $\Delta\epsilon_0$  is taken as  $1.55 \times 10^{-3}$ . This strain translates to a residual compressive stress of

-421 MPa in the outer layers and a residual tensile stress of 183 MPa in the inner layer.

Table 3 gives hardness and indentation toughness data for the layered composites in comparison to the monolithic materials from which they were made. The outer layers of three-layered composites show increased hardness relative to their respective outer layers. This is not the result of the surface compressive stresses since the stress needed to cause plastic deformation is on the order of the hardness while the compressive stresses are at least an order of magnitude lower. Micrographs (Figure 11(a)) showed that the grain sizes of the layered composites were similar to those of the monolithic outer-layer materials.

The apparent toughness, however, is expected to increase as shown in Table 3. Smaller crack length/indenter diagonal length ( $c/a$ ) values were obtained for materials with higher toughness. Figure 11(b) shows that the outer layers of three-layer composites show only minor microstructural toughening features (crack branching, crack deflection, crack bridging) compared to the tougher inner layer.

The most significant advantage of the layered composites is their remarkable damage resistance as shown in Figure 12. The residual stress calculated from the intercepts was -596 MPa for the dry pressed composites where a poor linear fit from Equation (1) was obtained, and -571 MPa for the slip cast materials where the linear fit was excellent. The shallower slopes for the layered composites compared to the monolithics (see dry pressed  $\text{Al}_2\text{O}_3$ -30 vol. % Y-TZP in Figures 6 and 12) is not in accord with prediction[31] but demonstrates the excellent resistance to contact damage which can be expected for these materials. The advantage of putting the surface under compression to a significant depth is that surface cracks are wholly contained in the outer layer. Furthermore, since the stresses are related to thermal expansion mismatch and not transformation-induced by grinding, these composites can be cycled above the monoclinic to tetragonal transformation temperature and still retain their high damage resistance when returned to low temperatures. The limitation of this method of introducing compressive stresses, of course, is that the stresses decrease with increasing temperature and therefore only low temperature (<500°C) applications will exhibit high damage tolerance.

### **Design Considerations and Potential Applications**

Elkem Keramer is currently making  $\text{Al}_2\text{O}_3/\text{Y-TZP}$  ceramics for large gate valves for the North Sea, briquetting plates, rock crushing wear plates, and other applications requiring high corrosion and/or wear resistance. Experience with tough TZP-based ceramics is limited and there is little experience for the materials discussed in this article. The high toughness of TZP/30 vol. %  $\text{Al}_2\text{O}_3+\text{SrO}\cdot 6\text{Al}_2\text{O}_3$  material has been demonstrated by making and testing rock chisels made from the material. Knife blades have also been produced. Wear plates attached to steel to see if they could withstand the shock experienced by plowing rocky ground in Denmark and Germany. There were several ceramics and hardmetals (WC-Co) involved in the test and the Ce-TZP material was the only ceramic which could withstand the high stresses, but it did not wear as well as the best hardmetal tested.

TZP ceramics are replacing hardmetals in the can drawing industry where Y-TZP can usually take the stresses imposed by high drawing rates. Ce-TZP is usually substituted for Y-TZP materials in applications requiring higher toughness. Layered composites are only now being considered for applications due to the increased difficulty of processing these materials. Since glazes on pottery date back to antiquity and dinnerware using this technique in glass ceramics are well developed[45], it is only natural that damage resistant structural ceramics will find applications in the near future.

Designers must realize that even tough ceramics are brittle as compared to most metals and care must be exercised when using strength data in design[46]. It is now well recognized that design changes are often necessary when replacing metallic components with metals and that complex components require finite element analysis and proof testing[47]. Designers are often frustrated by the fact that comparable data required for design are not available which allow material selection without prototype testing for recently developed candidate ceramic materials.

### Conclusions

Ce-TZP/ $\text{Al}_2\text{O}_3$ +SrO-6 $\text{Al}_2\text{O}_3$  belong to a family of zirconia-based ceramics which have in-situ platelet formation[19,21-23,25,34]. The platelets do not have high modulus or strength[4] but appear to give high toughness due to control of the transformation zone ahead of the crack tip. These materials can be engineered to have high toughness while retaining good strength and hardness[22]. The materials can be processed by any method used for conventional ceramic processing as seen by the present work on spray drying and slip casting. Materials with high reliability and excellent damage resistance have been demonstrated. The high damage resistance in monolithic materials is due to transformation-induced compressive stresses due to grinding and can be removed by annealing.

The introduction of substantial compressive stresses was demonstrated by slip casting and dry pressing layered composites. The layered composites were designed with hard, wear-resistant outer layers and tough inner layers. The resulting composites had excellent damage resistance to contact stresses and showed a simultaneous increase in flexural strength and reliability, as expected based on superposition of stresses. Residual stresses were quantified by strength, indentation/strength, and strain gage measurements.

These materials should be used for low temperature (<500°C) applications since both the driving force for transformation and compressive stress decrease with increasing temperature. A variety of low temperature applications are being discovered for  $\text{Al}_2\text{O}_3$ /TZP ceramics.

### Acknowledgment

This work was supported in part by AFOSR on ARPA Contract No. F49620-87-C-0077. R. Lakshminarayanan made strain gage measurements. Appreciation is expressed to Dr. K. H. Johanssen of Elkem Keramer for making facilities available for this work.

## References

1. **Garvie, R C, Hannink, R H and Pascoe, R T.** Ceramic Steel? *Nature*, Vol 258, 1975, pp 703-704
2. **Evans, A G.** Perspective on the Development of High-Toughness Ceramics, *J. Am. Ceram. Soc.*, Vol 73, 1990, pp. 187-206
3. **Green, D J, Hannink, R H J, and Swain, M V.** Transformation Toughening of Ceramics, CRC Press (Boca Raton, FL) 1989
4. **Becher, P F and Swain, M V.** Grain-Size-Dependent Transformation Behavior in Polycrystalline Tetragonal Zirconia, *J. Am. Ceram. Soc.*, Vol. 75, 1992, pp. 493-502
5. **Bischoff, E and Ruhle, M.** Microcrack and Transformation Toughening of Zirconia-Containing Alumina, *Advances in Ceramics*, Vol. 24, Science and Technology of Zirconia III. Edited by S. Somiya, N. Yamamoto, and H. Yanagida, *Am. Ceram. Soc.*, Westerville, OH, 1988, pp. 635-643.
6. **Virkar, A V, Fong, J, Smith, P, Mehta, K and Prettyman, K.** The Role of Ferroelasticity in Toughening of Brittle Materials, *Phase Transitions*, Vol. 35, 1991, pp. 27-46
7. **Claussen, N and Ruhle, M.** Design of Transformation-Toughened Ceramics, *Advances in Ceramics*, Vol. 3, Science and Technology of Zirconia. Edited by A. H. Heuer and L. W. Hobbs, *Am. Ceram. Soc.*, Westerville, OH, 1981, pp. 137-163.
8. **Becher, P F.** Microstructural Design of Toughened Ceramics, *J. Am. Ceram. Soc.*, Vol. 74, 1991, pp. 255-269.
9. **Claussen, N, Weisskopf, K L and Ruhle, M.** Tetragonal Zirconia Polycrystals Reinforced with SiC Whiskers, *J. Am. Ceram. Soc.*, Vol. 69, 1986, pp. 288-92
10. **Marshall, D B, Ratto, J J and Lange, F F.** Enhanced Fracture Toughness in Layered Microcomposites of Ce-ZrO<sub>2</sub> and Al<sub>2</sub>O<sub>3</sub>, *J. Am. Ceram. Soc.*, Vol. 74, 1991, pp. 2979-2987.
11. **Harmer, M P, Chan, H M and Miller, G A.** Unique Opportunities for Microstructural Engineering with Duplex and Laminar Ceramic Composites, *J. Am. Ceram. Soc.*, Vol. 75, 1992, pp. 1715-1728
12. **Swain, M V and Rose, L R F.** Strength Limitations of Transformation-Toughened Zirconia Alloys, *J. Am. Ceram. Soc.*, Vol. 69, 1986, pp. 511-518
13. **Li, C W and Yamanis, J.** Super-Tough Silicon Nitride with R-Curve Behavior, *Ceram. Eng. and Sci. Proc.*, 10, 1989, pp. 632-45
14. **Yu, C S and Shetty, D K.** Transformation Zone Shape, Size and Crack Growth Resistance (R-Curve) of Ceria Partially Stabilized Zirconia Polycrystals, *J. Am. Ceram. Soc.*, Vol. 72, 1989, pp. 921-928
15. **Janssen, R and Heussner, K H.** Platelet-Reinforced Ceramic Composite Materials, *Pow. Met. Int.*, Vol. 23, 1991, pp. 241-245
16. **Steinbrech, R W.** Toughening Mechanisms for Ceramic Materials, *J. Europ. Ceram. Soc.*, Vol. 10, 1992, pp. 131-142
17. **Pyzik, A J and Beaman, D R.** "Microstructure and Properties of Self-Reinforced Silicon Nitride, *J. Am. Ceram. Soc.*, Vol. 76, 1993, pp. 2737-2744
18. **Claar, T D, Johnson, W B and Anderson, C A.** Microstructure and Properties of Platelet Reinforced Ceramics Formed by the Directed Reaction of Zirconium with Boron Carbide, *Ceram. Eng. Sci. Proc.*, Vol. 10, 1989, pp. 599-609

19. **Tsukuma, K and Takahata, T.** Mechanical Property and Microstructure of TZP and TZP/Al<sub>2</sub>O<sub>3</sub> Composites, *Advanced Structural Ceramics*, Vol. 78. Ed. by P. F. Becher, M. V. Swain, and S. Somiya. Materials Research Society, Pittsburgh, PA, 1987, pp. 123-135.
20. **Yang, S G and Chen, K.** Preparation of Ce-TZP and Its Mechanical Behavior, *Ceramic Materials and Components for Engines*, Ed. by V. J. Tennery. Am. Ceram. Soc., Westerville, OH. 1989, pp. 904-918.
21. **Wang, J S, Tsai, J F, Shetty, D K, and Virkar, A V.** Effect of MnO and the Microstructures, Phase Stability, and Mechanical Properties of Ceria-Partially Stabilized Zirconia (Ce-TZP) and Ce-TZP-Al<sub>2</sub>O<sub>3</sub> Composites, *J. Mater. Res.*, Vol. 5, 1990, pp. 1948-1957
22. **Cutler, R A, Mayhew, R J, Prettyman, K M and Virkar, A V.** High-Toughness Ce-TZP/Al<sub>2</sub>O<sub>3</sub> Ceramics with Improved Hardness and Strength, *J. Am. Ceram. Soc.*, Vol. 74, 1991, pp. 179-186.
23. **Schmid, H K, Pennefather, R, Meriani, S and Schmid, C.** Redistribution of Ce and La During Processing of Ce(La)-TZP/Al<sub>2</sub>O<sub>3</sub> Composites, *J. Europ. Ceram. Soc.*, Vol. 10, 1993, pp. 381-392
24. **Chen, P L and Chen, I W.** In-Situ Alumina/Aluminate Platelet Composites, *J. Am. Ceram. Soc.*, Vol. 75, 1992, pp. 2610-2612
25. **Tsai, J F, Chon, U, Ramachandran, N and Shetty, D K.** Transformation Plasticity and Toughening in CeO<sub>2</sub>-Partially-Stabilized Zirconia-Alumina (Ce-TZP/Al<sub>2</sub>O<sub>3</sub>) Composites Doped with MnO, *J. Am. Ceram. Soc.*, Vol. 75, 1992, pp. 1229-1238
26. **Virkar, A V, Huang, J L and Cutler, R A.** Strengthening of Oxide Ceramics by Transformation Induced Stresses, *J. Am. Ceram. Soc.*, Vol. 70, 1987, pp. 164-170
27. **Cutler, R A, Brinkpeter, C B, Virkar, A V and Shetty, D K.** Fabrication and Characterization of Slip-Cast Layered Al<sub>2</sub>O<sub>3</sub>-ZrO<sub>2</sub> Composites, 4th Int. Sym. on Ceramic Materials and Components for Engines, Ed. by R. Carlsson, T. Johansson, and L. Kahlman. Elsevier, London, 1992, pp. 397-408.
28. **Lindemann, J M and Nissen, A.** Effect of Testing Methods and Surface Grinding Conditions on Strength Values of Ceramics, 4th Int. Sym. on Ceramic Materials and Components for Engines, Ed. by R. Carlsson, T. Johansson, and L. Kahlman. Elsevier, London, 1992, pp. 846-855.
29. **Virkar, A V, Jue, J F, Hansen, J J and Cutler, R A.** Measurement of Residual Stresses in Oxide-ZrO<sub>2</sub> Three-layer Composites, *J. Am. Ceram. Soc.*, Vol. 71, 1988, pp. C-148-C-151
30. **Virkar, A V.** Determination of Residual Stress Profile Using a Strain Gage Technique, *J. Am. Ceram. Soc.*, Vol. 73, 1990, pp. 2100-2102
31. **Hansen, J J, Cutler, R A, Shetty, D K and Virkar, A V.** Indentation Fracture Response and Damage Resistance of Al<sub>2</sub>O<sub>3</sub>-ZrO<sub>2</sub> Composites Strengthened by Transformation-Induced Residual Stresses, *J. Am. Ceram. Soc.*, Vol. 71, 1988, C-501-C-505
32. **Schmid, H K.** private communication with R A Cutler, 1992
33. **Marshall, D B.** Crack Shielding in Ceria-Partially-Stabilized Zirconia, *J. Am. Ceram. Soc.*, Vol. 73, 1990, pp. 3119-3121.
34. **Tsai, J F, Belnap, J D and Shetty, D K.** Crack Shielding in Ce-TZP/Al<sub>2</sub>O<sub>3</sub> Composites: Comparison of Fatigue and Sustained Load Crack Growth Specimens, *J. Am. Ceram. Soc.*, Vol. 77, 1994, pp. 105-117

35. **Cutler, R A, Reynolds, J R and Jones, A.** Sintering and Characterization of Polycrystalline Monoclinic, Tetragonal, and Cubic Zirconia, *J. Am. Ceram. Soc.*, Vol. 75, 1992, pp 2173-2183
36. **Log, T, Cutler, R A, Jue, J F and Virkar A V.** Polycrystalline  $t'$ - $ZrO_2(Ln_2O_3)$  formed by displacive transformations, *J. Mater. Sci.*, Vol. 28, 1993, pp. 4503-4509
37. **Lutz, H E and Claussen, N.** Duplex Ceramics, *J. Europ. Ceram. Soc.*, Vol. 7, 1991, pp. 209-226
38. **Padture, N P, Bennison, S and Chan H M.** Flaw-Tolerance and Crack-Resistance Properties of Alumina-Aluminum Titanate Composites with Tailored Microstructures, *J. Am. Ceram. Soc.*, Vol. 76, 1993, 2312-2320
39. **Miller, C W and Wittmer, D E.** Continuous Sintering of  $Si_3N_4$  in a Controlled Atmosphere Belt Furnace, Presented at AUSTCERAM 90, August 26-31, 1990, Perth, Australia.
40. **Marshall, D B, Lawn B R and Chantikul, P.** Residual Stress Effects in Sharp Contact Cracking, Part 2, Strength Degradation, *J. Mater. Sci.*, Vol. 14, 1979, pp. 2225-2235
41. **Chantikul, P, Anstis, G R, Lawn, B R and Marshal D B.** A Critical Evaluation of Indentation Techniques for Measuring Fracture Toughness: II, Strength Method, *J. Am. Ceram. Soc.*, Vol. 64, 1981, pp. 539-543.
42. **Tandon, R, Green D J and Cook, R F.** Surface Stress Effects on Indentation Fracture Sequences, *J. Am. Ceram. Soc.*, Vol. 73, 1990, pp. 2619-2627
43. **Tandon, R and Cook R F.** Indentation Crack Initiation and Propagation in Tempered Glass, *J. Am. Ceram. Soc.*, Vol. 76, 1993, pp. 885-889.
44. **Virkar, A V.** Ceramic Bodies Having a Plurality of Stress Zones, U.S. Patent 4,656,071 (April 7, 1987).
45. **Duke, D A, Megles, J E, MacDowell, J F and Bopp H F.** Strengthening Glass-Ceramics by Application of Compressive Glazes, *J. Am. Ceram. Soc.*, Vol. 51, 1968, pp. 98-102.
46. **Quinn, G D and Morrell, R.** Design Data for Engineering Ceramics: A Review of the Flexural Test, *J. Am. Ceram. Soc.*, Vol. 74, 1991, pp. 2037-2066
47. **McLean, A F and Hartsock, D L.** An Overview of the Ceramic Design Process, *Engineered Materials Handbook. Vol. 4, Ceramics and Glasses*, American Society for Metals, ASM Int. Metals Park, PA, 1991, pp. 676-689

**Table 1**  
**Properties of Ce-TZP/30 vol. %  $Al_2O_3+SrO \cdot 6Al_2O_3$**   
**Prepared by Slip Casting\***

Density: 5.5 g/cc  
 Thermal expansion (20-1200°C):  $10 \times 10^{-6}/^{\circ}C$   
 Thermal conductivity: 5 W/mK  
 Young's modulus: 240 GPa  
 Poisson's ratio: 0.3  
 Hardness: 11 GPa  
 Four-point flexural strength: 750 MPa with a Weibull modulus of 12  
Fracture toughness: 7.5 MPa $\sqrt{m}$   
 \*Elkem Keramer Grade EZ CS30

**Table 2**  
**DCB Fracture Toughness of Al<sub>2</sub>O<sub>3</sub>/ZrO<sub>2</sub> Composites**  
**With and Without SrO Additions**

Code	Composition (wt. %)					Fracture Toughness (MPa√m)
	Al <sub>2</sub> O <sub>3</sub>	ZrO <sub>2</sub>	CeO <sub>2</sub>	Y <sub>2</sub> O <sub>3</sub>	SrZrO <sub>3</sub>	
Al <sub>2</sub> O <sub>3</sub> /30 vol. % Y-TZP	60.0	37.9	0.0	2.1	0.0	3.7±0.2
Al <sub>2</sub> O <sub>3</sub> +SrO·6Al <sub>2</sub> O <sub>3</sub> / 30 vol. % Y-TZP	58.0	36.0	0.0	2.0	4.0	4.2±0.1
Al <sub>2</sub> O <sub>3</sub> /30 vol. % Ce-TZP	60.0	33.6	6.4	0.0	0.0	5.0±0.1
Al <sub>2</sub> O <sub>3</sub> +SrO·6Al <sub>2</sub> O <sub>3</sub> / 30 vol. % Ce-TZP	58.0	31.2	6.8	0.0	4.0	5.7±0.1
Al <sub>2</sub> O <sub>3</sub> +SrO·6Al <sub>2</sub> O <sub>3</sub> / 30 vol. % Y,Ce-TZP	58.0	33.5	3.4	1.1	4.0	4.4±0.1

**Table 3**  
**Hardness and Indentation Toughness Data**

Code	Hardness (GPa)	Fracture Toughness	
		(MPa√m)	(c/a)*
Al <sub>2</sub> O <sub>3</sub> /30 vol. % Y-TZP (dry pressed outer-layer)	15.3±0.3	2.7	3.1
Ce-TZP/Al <sub>2</sub> O <sub>3</sub> +SrO·6Al <sub>2</sub> O <sub>3</sub> (dry pressed inner-layer)	11.2±0.1	9.4	1.2
Dry pressed three-layer	16.5±0.4	4.3	2.4
Al <sub>2</sub> O <sub>3</sub> +SrO·6Al <sub>2</sub> O <sub>3</sub> /30 vol. % Ce-TZP (slip cast outer-layer)	13.2±0.2	5.9	2.3
Ce-TZP/Al <sub>2</sub> O <sub>3</sub> +SrO·6Al <sub>2</sub> O <sub>3</sub> (slip cast inner-layer)	11.0±0.2	10.4	1.3
Slip cast three-layer	13.9±0.4	6.2	1.8

\*Ratio of crack length to indent diagonal length

## Figure Captions

1. Fracture toughness of Ce-TZP with and without Al<sub>2</sub>O<sub>3</sub> additions as a function of SrZrO<sub>3</sub> additions[22]. SrO additions to Ce-TZP lower the toughness due to a refinement in grain size while SrO additions to Ce-TZP/Al<sub>2</sub>O<sub>3</sub> increase the toughness most likely due to modification of the transformation zone around the crack tip caused by in situ SrO·6Al<sub>2</sub>O<sub>3</sub> formation.

2. SEM micrographs of Ce-TZP/30 vol. % Al<sub>2</sub>O<sub>3</sub>+SrO·6Al<sub>2</sub>O<sub>3</sub> prepared either by slip casting ZrO<sub>2</sub>(12 mol. % CeO<sub>2</sub>) mixed with Al<sub>2</sub>O<sub>3</sub> and SrZrO<sub>3</sub> or by pressing spray dried agglomerates of the same composition prepared by coprecipitating ZrO<sub>2</sub>, CeO<sub>2</sub>, Al<sub>2</sub>O<sub>3</sub> and SrO. (a) Polished and etched surfaces (bars are 1 μm), (b) Fracture surfaces (bars are 10 μm), and (c) Polished and etched surfaces (bars are 1 μm) near crack tip created by diamond indent to left of photographs. Note that crack branching, crack bridging and crack deflection mechanisms are operative in addition to transformation toughening.

Figure 3. Flexural strength of slip cast Al<sub>2</sub>O<sub>3</sub>+SrO·6Al<sub>2</sub>O<sub>3</sub>/30 vol. % Ce-TZP tested at room temperature in 4-point loading. The mean flexural strength was 607±37 MPa with a Weibull modulus of 17 by either linear regression or maximum likelihood methods.

Figure 4. Biaxial strength of slip cast Al<sub>2</sub>O<sub>3</sub>+SrO·6Al<sub>2</sub>O<sub>3</sub>/30 vol. % Ce-TZP tested at room temperature in ring-on-ring loading. The mean strength was 635±30 MPa with a Weibull modulus of 25 (dotted line=linear regression) or 33 (solid line=maximum likelihood).

Figure 5. Flexural strength of dry pressed Al<sub>2</sub>O<sub>3</sub>/30 vol. % Ce-TZP tested at room temperature in 4-point loading. (a) The mean flexural strength "as-sintered" was 652±30 MPa with a Weibull modulus of 25 by linear regression (dotted line) or 28 by the maximum likelihood method (solid line). (b) The mean flexural strength "as-HIPed" was 1395±176 MPa with a Weibull modulus of 8 by linear regression (dotted line) or 13 by the maximum likelihood method (solid line).

Figure 6. Indentation load dependence of fracture stress for Ce-TZP/30 vol. % Al<sub>2</sub>O<sub>3</sub>+SrO·6Al<sub>2</sub>O<sub>3</sub> (triangles), Al<sub>2</sub>O<sub>3</sub>/30 vol. % Y-TZP (circles), and Si<sub>3</sub>N<sub>4</sub>/Y<sub>2</sub>O<sub>3</sub>-Al<sub>2</sub>O<sub>3</sub> (squares). Note high strength of Ce-TZP/Al<sub>2</sub>O<sub>3</sub> even with surface flaws made with Vicker's diamond pyramid indenter at loads up to 1000 N.

Figure 7. Fracture stress ( $\sigma_f$ ) versus inverse cube root load ( $P^{-1/3}$ ) plots for the three ceramics shown in Figure 6.

Figure 8. Damage resistance of Ce-TZP/Al<sub>2</sub>O<sub>3</sub> before (solid triangles) and after (open triangles) annealing at 1500°C for 3 hours. Annealing eliminated residual compressive stress which was reason for high damage resistance.

Figure 9. Measured strain as a function of outer layer depth removed for monolithic and three-layer bar-shaped samples. Note that the three-layer samples have high surface compression while the monolithic materials show no residual stresses by the strain gage technique. Solid line is predicted behavior of slip cast three-layer samples based on analysis by Virkar[30].

Figure 10. Cross-sections of polished three-layer strength bars showing (a) sharp interface obtained by slip casting compared to (b) diffuse interface which results from dry pressing. White error bars are 100  $\mu\text{m}$ .

Figure 11. SEM micrographs of outer layers of slip cast ( $\text{Al}_2\text{O}_3+\text{SrO}\cdot 6\text{Al}_2\text{O}_3/30$  vol. % Ce-TZP) and dry pressed ( $\text{Al}_2\text{O}_3/30$  vol. % Y-TZP) three-layer composites (error bars are 1  $\mu\text{m}$ ). (a) Polished and etched surfaces, and (b) Polished and etched surfaces near crack tip created by diamond indent to left of photographs. Compare with Figure 2.

Figure 12. Strength as a function of indenter load plots for three-layer dry pressed and slip cast composites. Note that exceptional damage resistance of layered composites is due to high compressive surface stresses which are much deeper than stresses introduced by grinding.

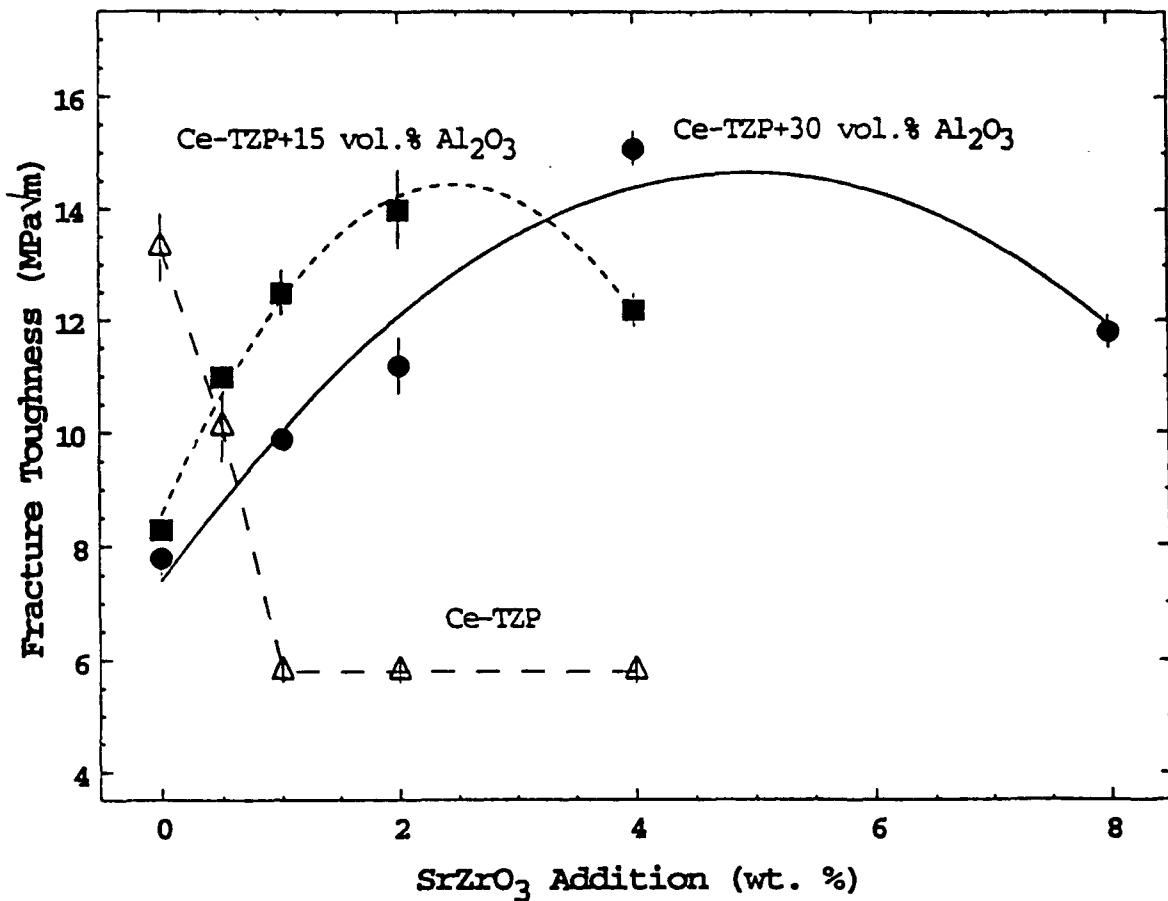


Figure 1

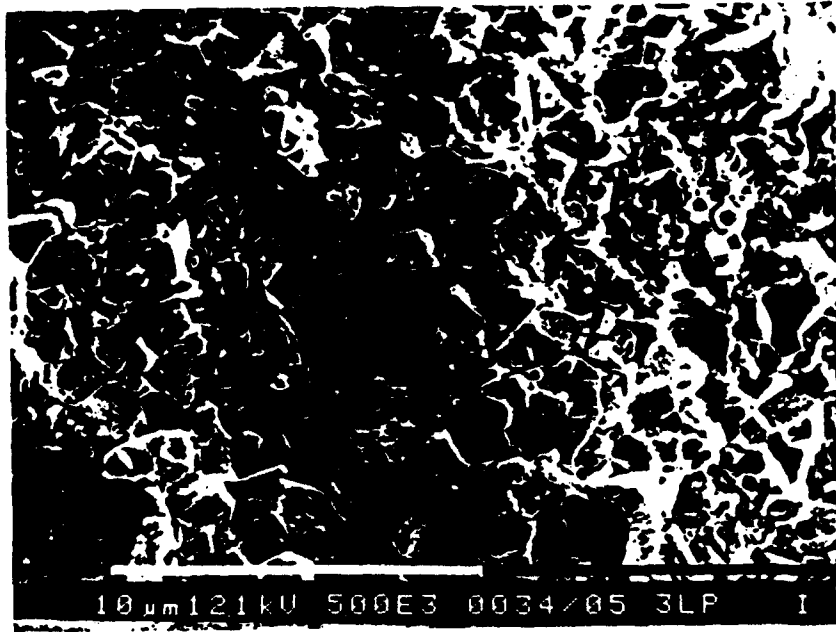


Slip Cast

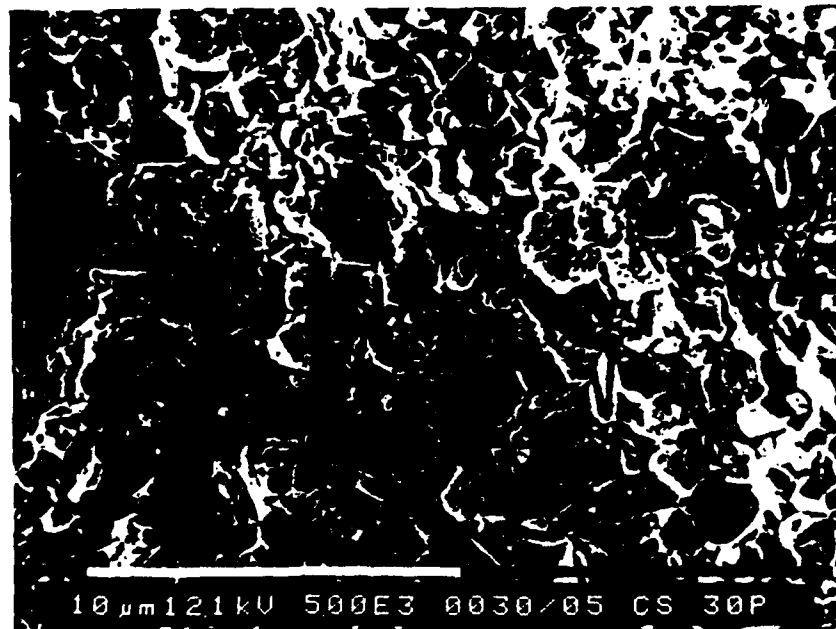


Dry Pressed

Figure 2(a)



Slip Cast

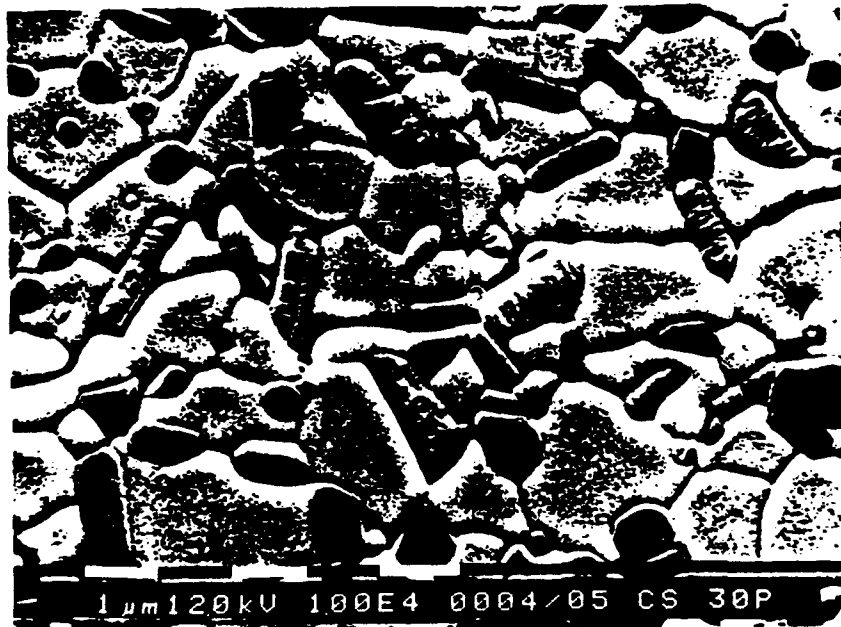


Dry Pressed

Figure 2(b)



Slip Cast



Dry Pressed

Figure 2(c)

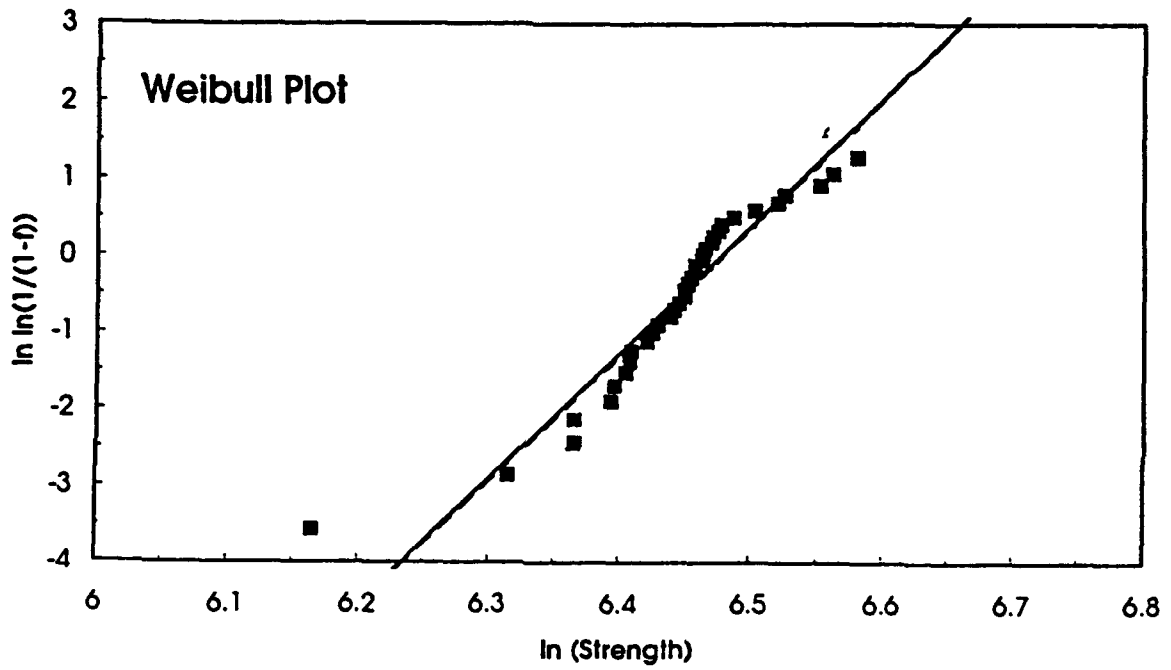
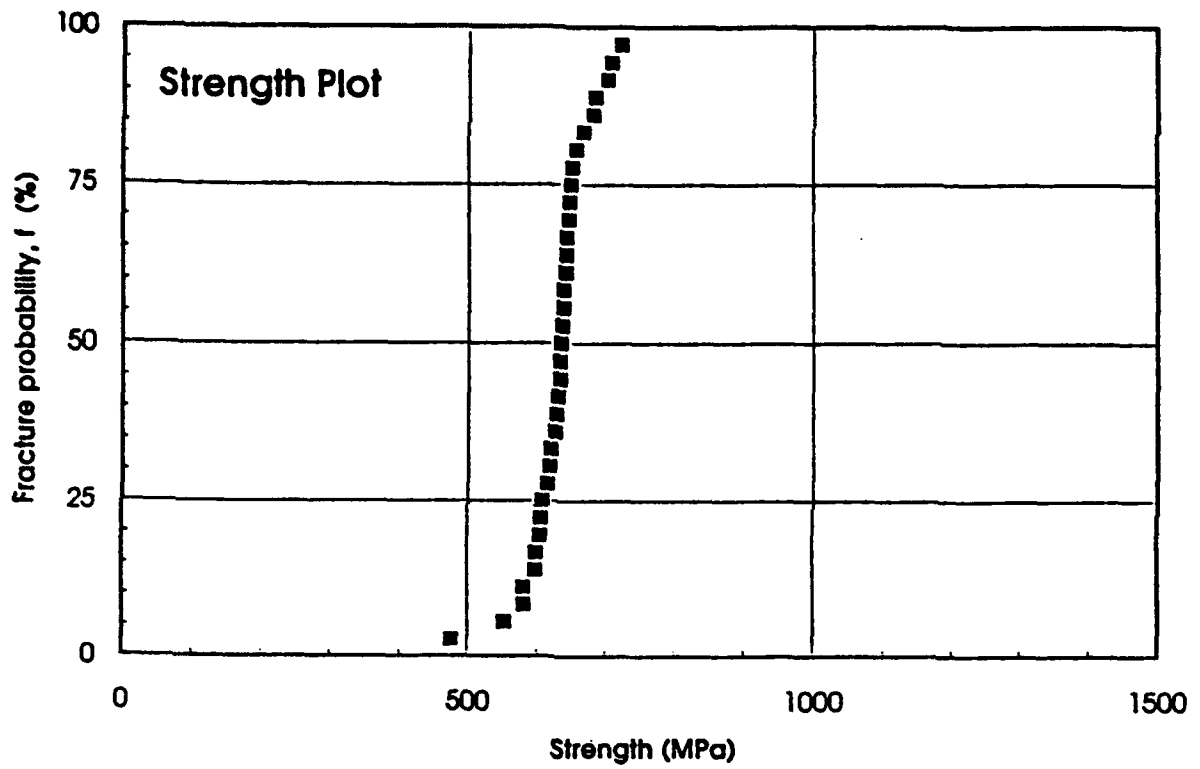


Figure 3

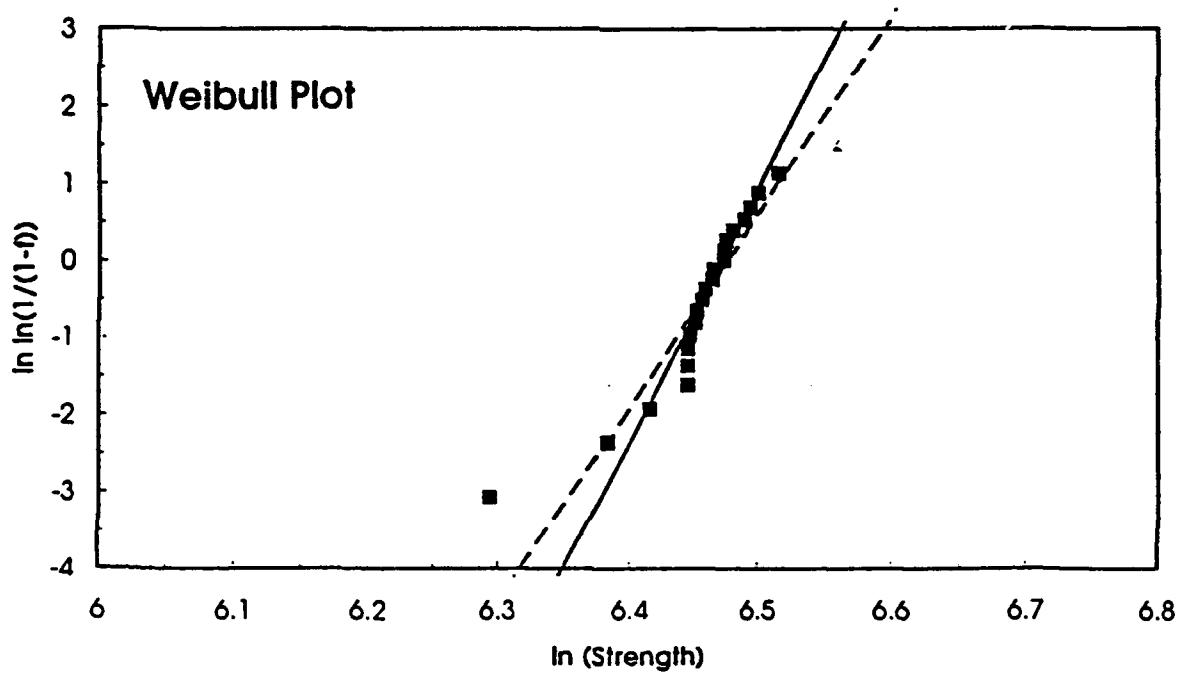
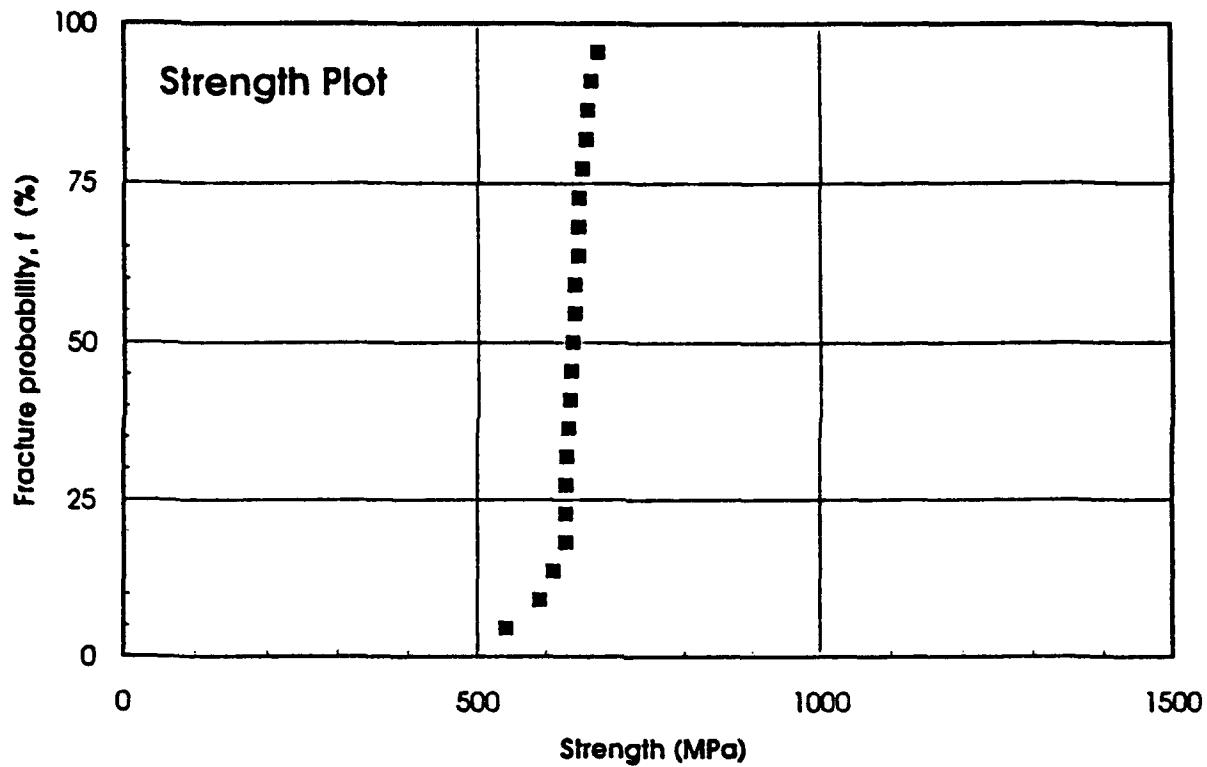


Figure 4

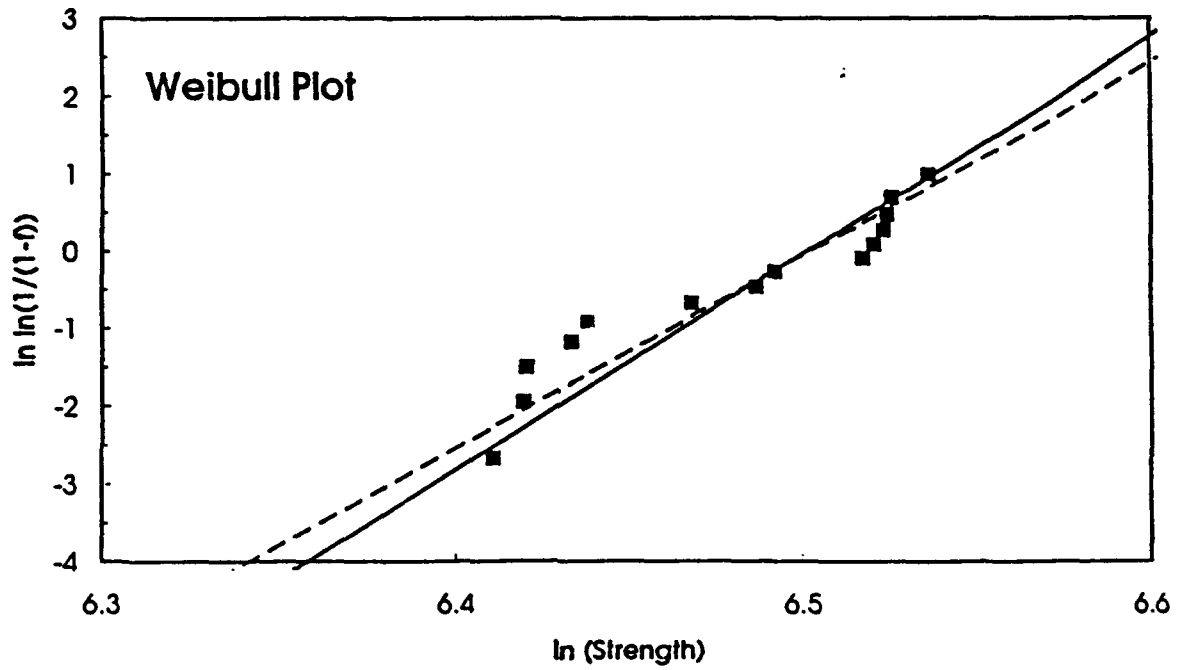
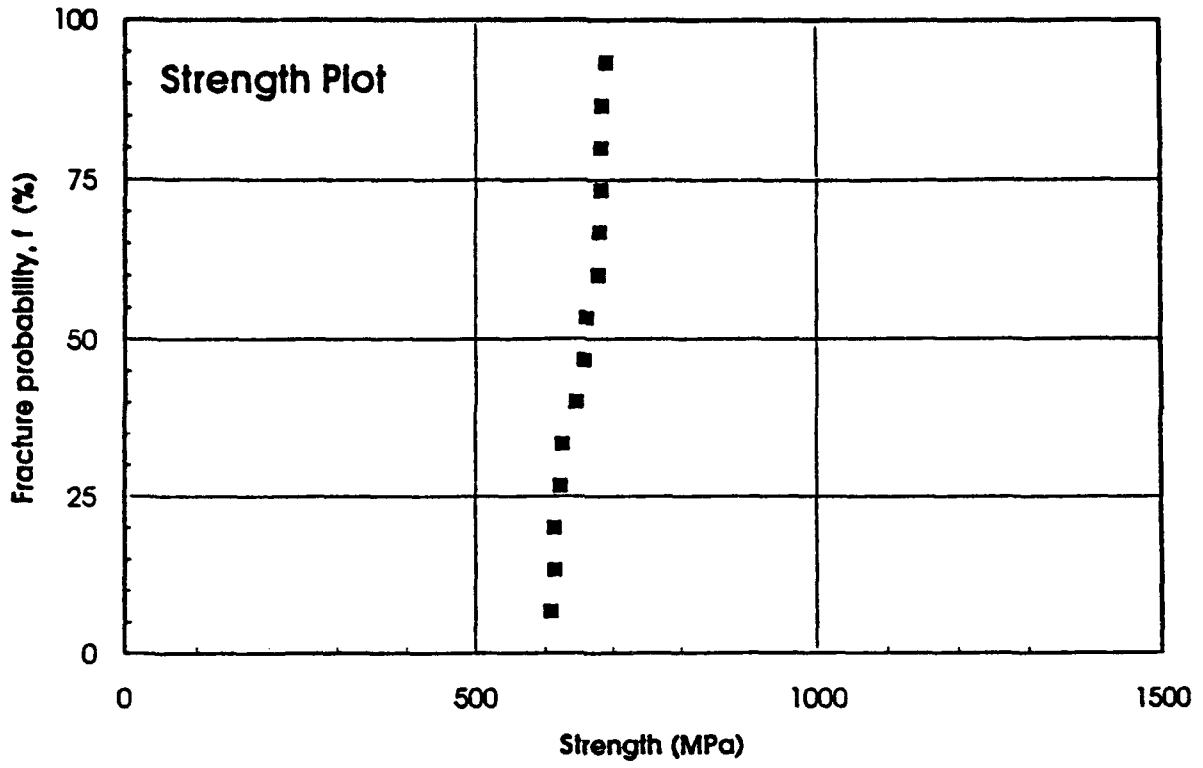


Figure 5(a)

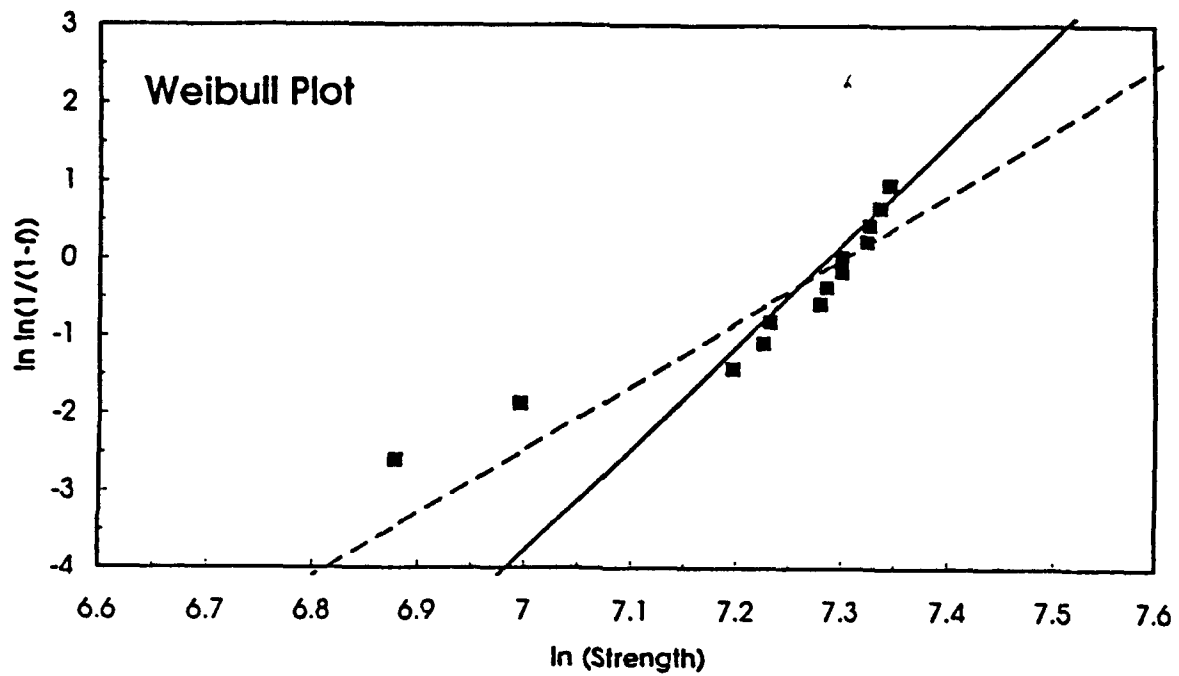
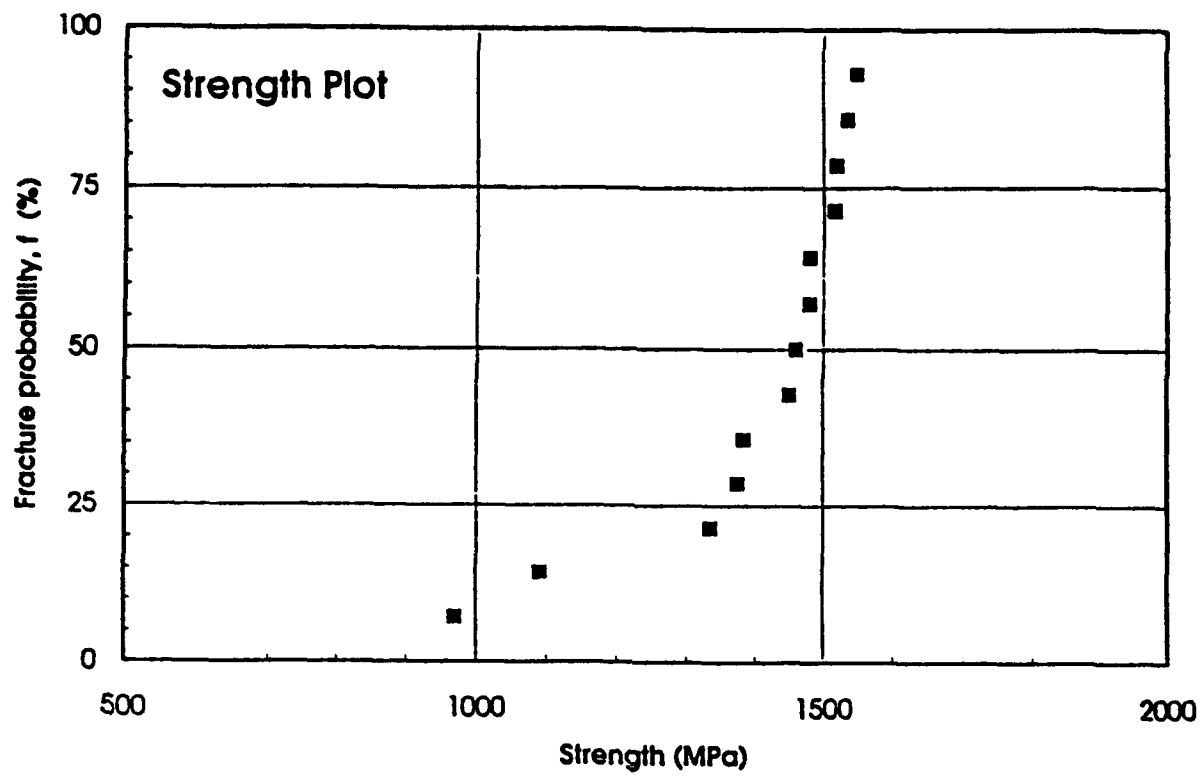


Figure 5(b)

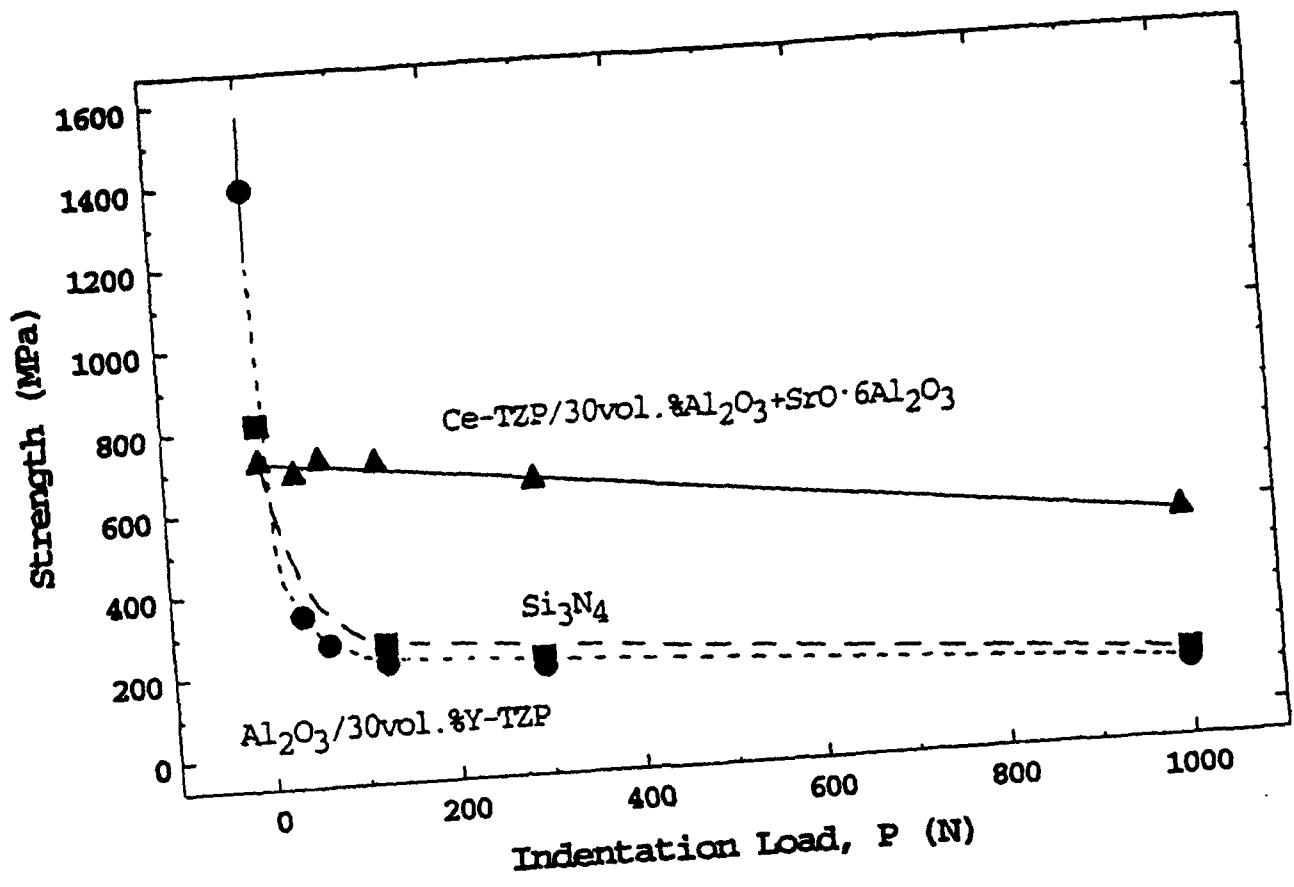


Figure 6

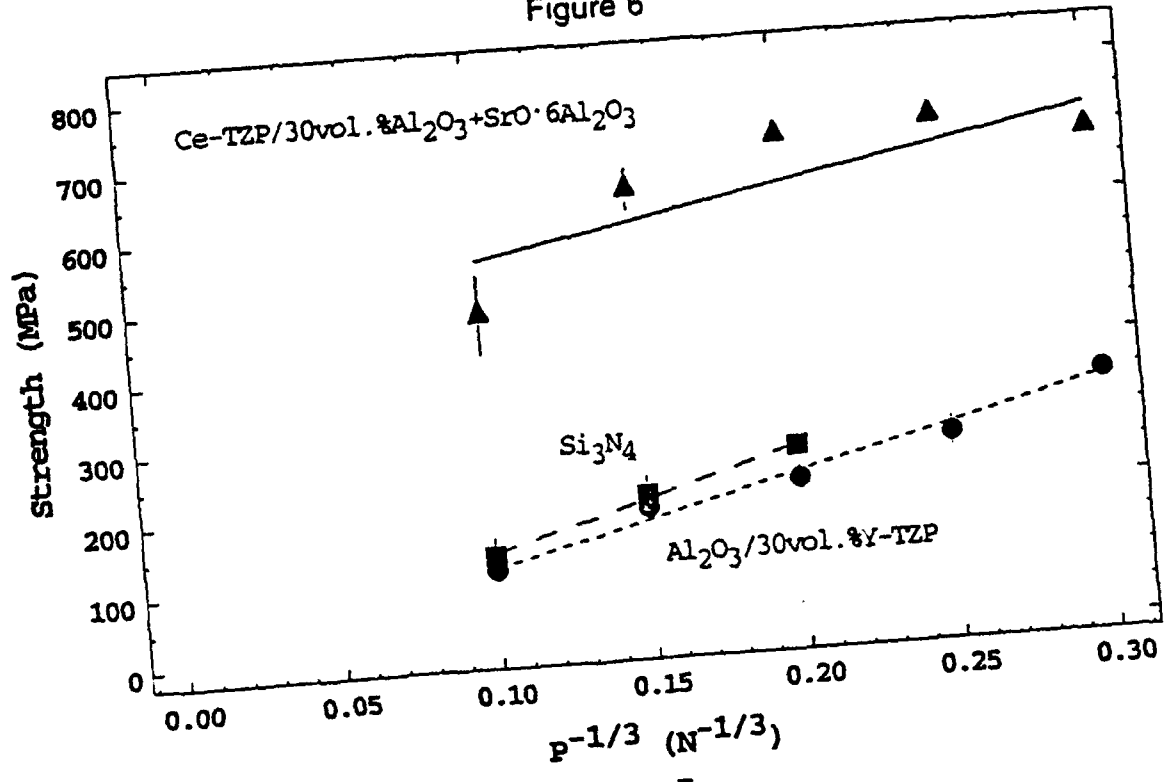


Figure 7

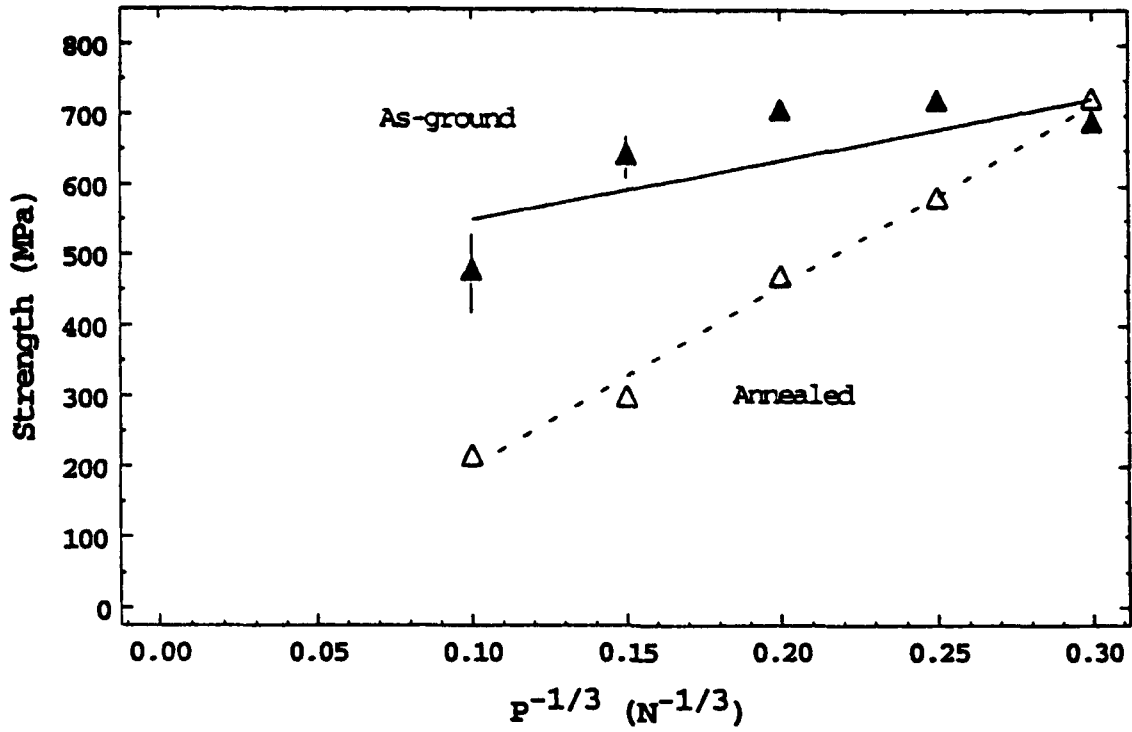


Figure 8

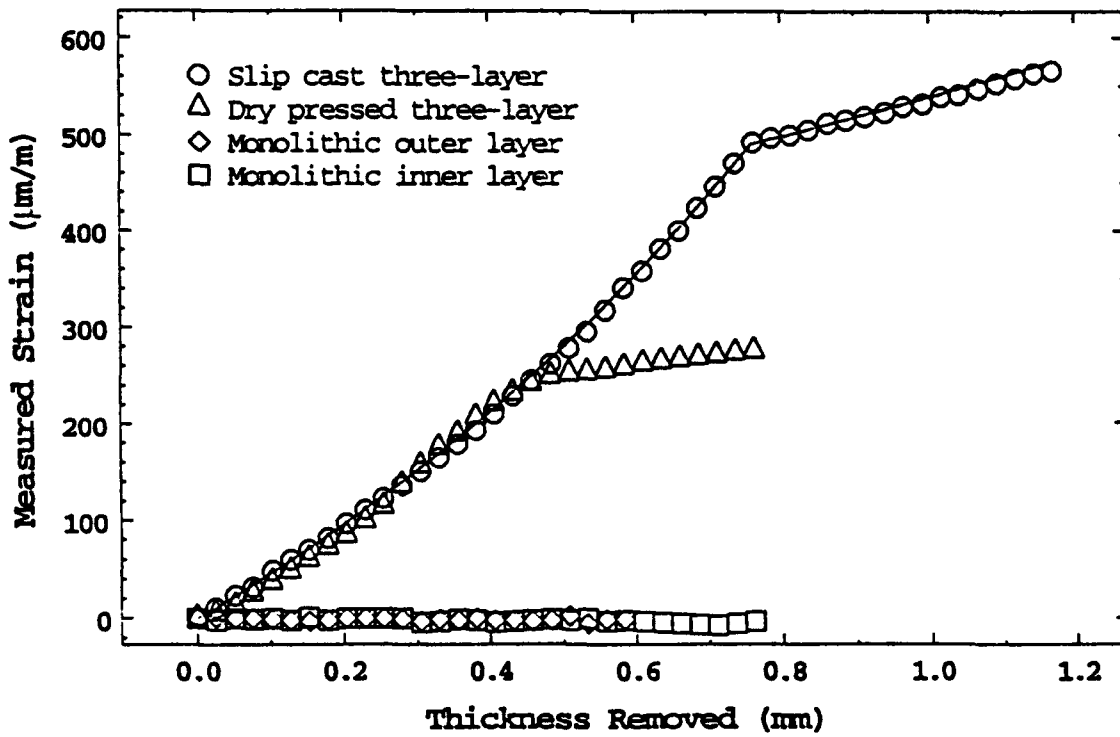


Figure 9

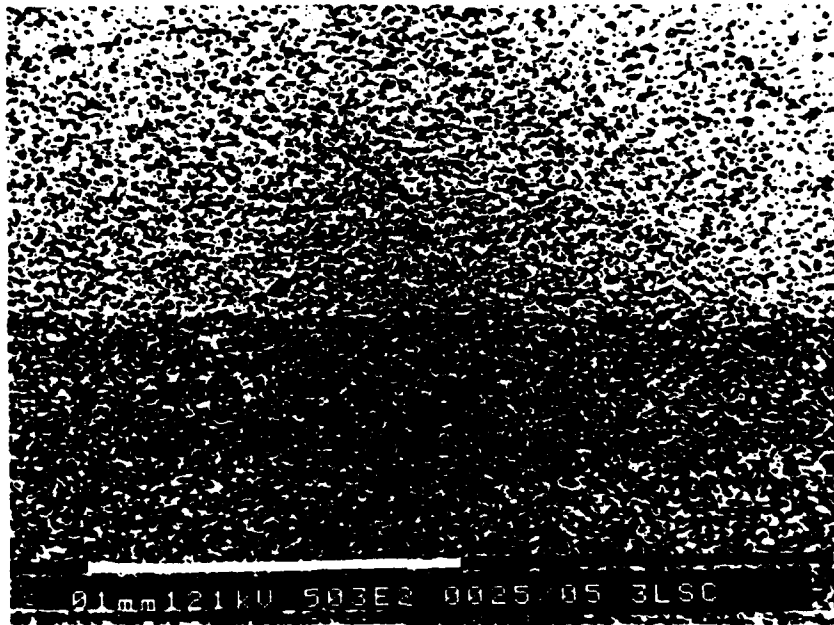


Figure 10(a)

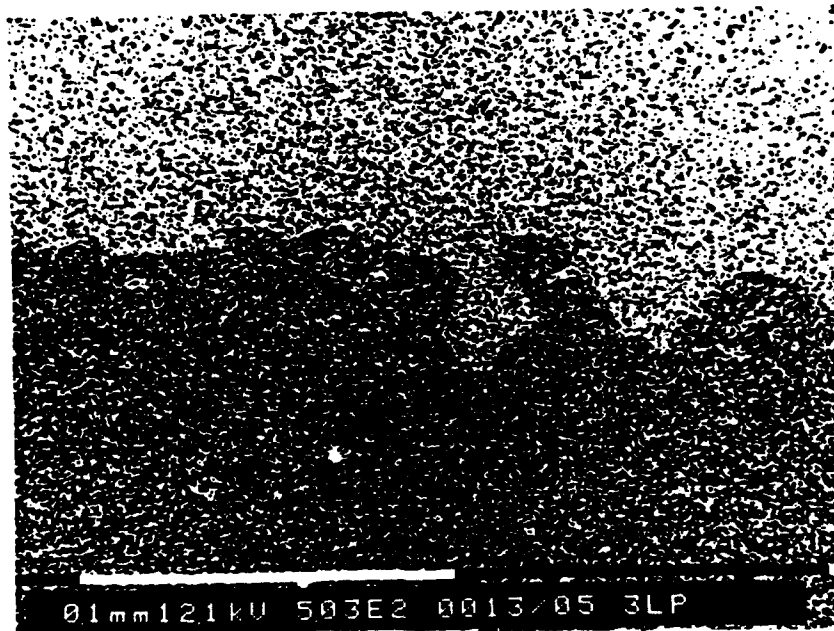
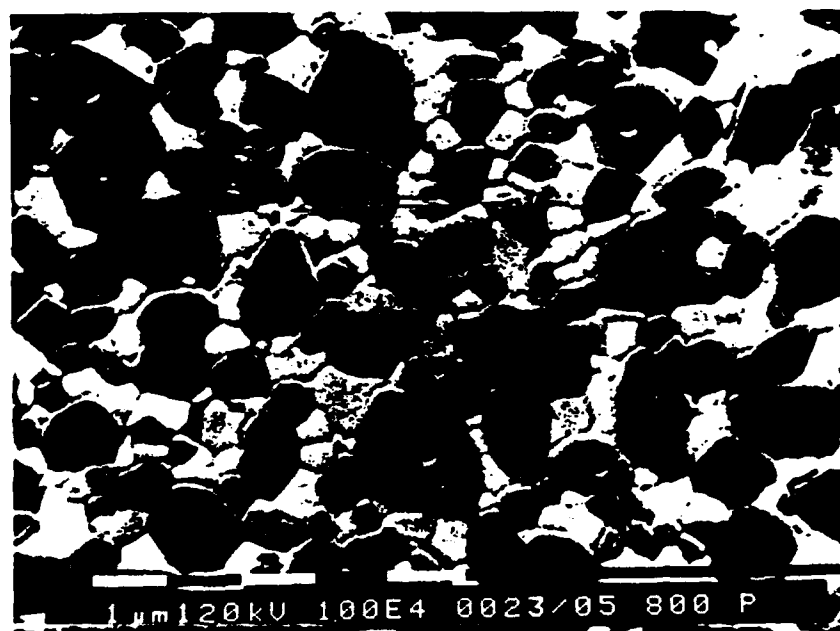


Figure 10(b)



Slip Cast

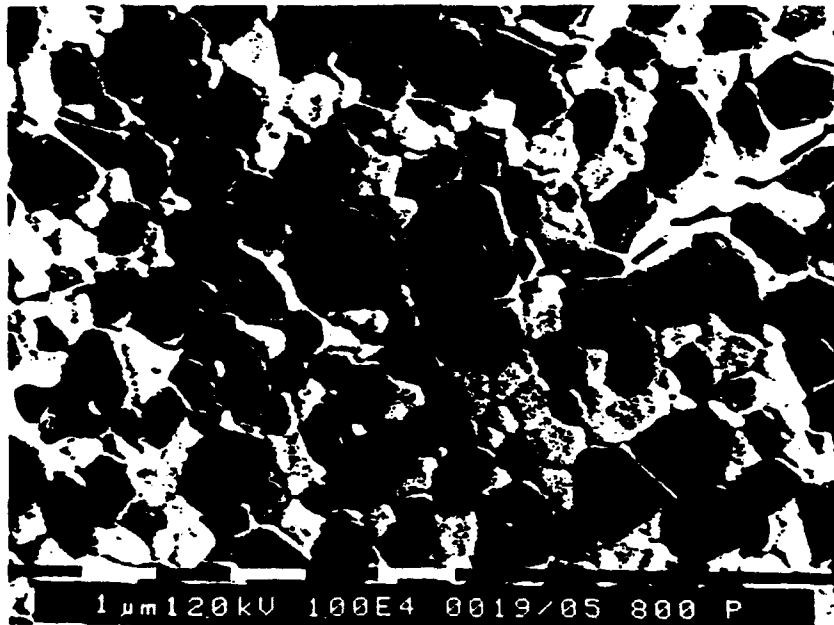


Dry Pressed

Figure 11(a)



Slip Cast



Dry Pressed

Figure 11(b)

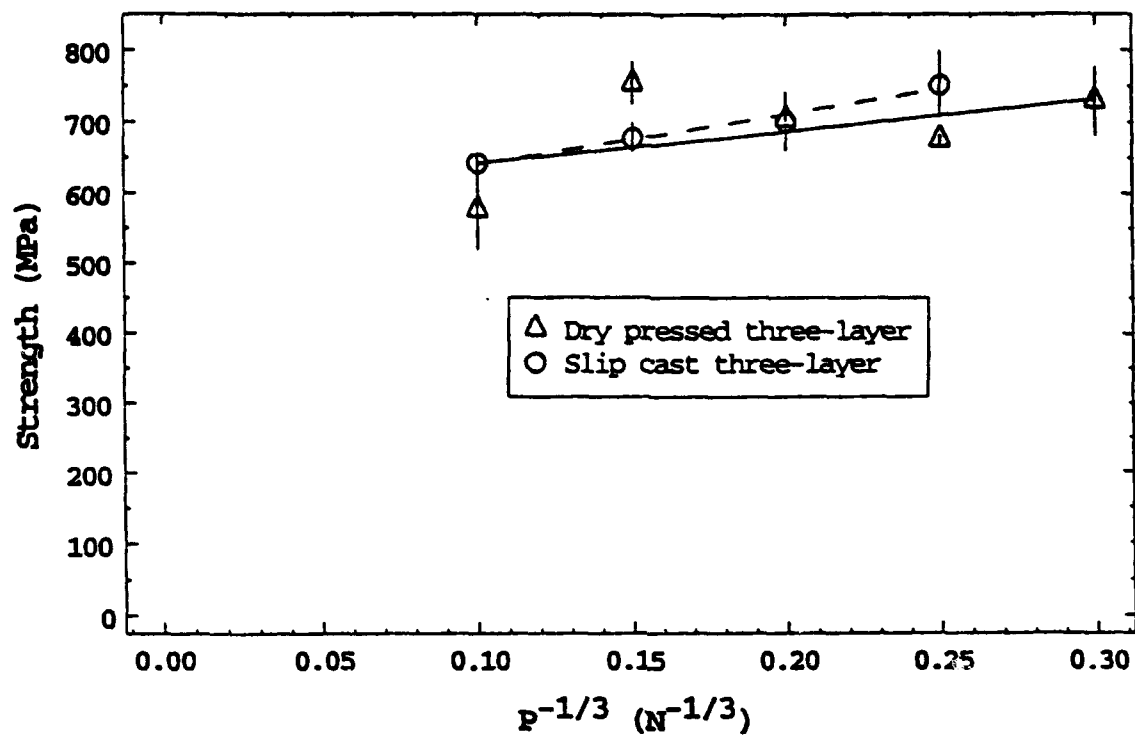


Figure 12

# FERROELASTIC FRACTURE PROPERTIES OF GADOLINIUM MOLYBDATE AND ISOTYPIC COMPOUNDS

by

Paul C. Smith and Anil V. Virkar

Department of Materials Science & Engineering, 304 EMRO  
University of Utah  
Salt Lake City, Utah 84112

## Abstract

Single crystal specimens of the simultaneously ferroelastic and ferroelectric material gadolinium molybdate (GMO) were indented to determine orientational fracture toughness in the  $\langle 100 \rangle$ ,  $\langle 010 \rangle$  and  $\langle 110 \rangle$  directions. Significantly higher fracture toughness in the  $\langle 010 \rangle$  over the  $\langle 100 \rangle$  direction was attributed to ferroelastic domain switching. Polycrystalline samples of ferroelastic rare earth molybdate compounds isostructural with GMO were fabricated by hot pressing. Hot pressed samples exhibited higher toughness below the Curie temperature (in the ferroelastic phase) over that above the Curie temperature (in the paraelastic phase.) Although the results were consistent with ferroelastic toughening, microcracking and thermal expansion anisotropy effects may also have contributed to toughness increases in the polycrystalline samples.

## 1. Introduction

In analogy to the hysteresis loop that a ferroelectric displays between an applied electric field ( $E$ ) and the observed electric polarization ( $P$ ), the ferroelastic state (Fig. 1) displays a hysteresis loop between an applied stress ( $\sigma$ ) and the observed strain ( $\epsilon$ .) The similarity between these two types of materials is more than accidental, as both ferroelectricity and ferroelasticity owe their peculiar properties to the same origins: the occurrence of two or more structurally identical 'orientation states', which can be interchanged by the application of an applied external field. For ferroelectric materials, the applied field is electric, and for ferroelastic materials the applied field is mechanical. Hysteretic behavior in ferroelastics is indicative of the existence of a reorientable spontaneous strain ( $\epsilon_s$ ), existing in the absence of an

applied force. Regions of common spontaneous strain tensor orientation are referred to as domains. The spontaneous strain can be identified from the hysteresis loop, and is given by the intercept between the loop and the strain axis. The intercept between the loop and the stress axis is termed the coercive stress ( $\sigma_c$ .) Upon heating, ferroelastics generally display a phase transition in which the spontaneous strain disappears, either abruptly or gradually, thereby resulting in a crystallographic form of higher symmetry. The temperature that this transition occurs at is labeled the Curie temperature ( $T_c$ ), and the higher temperature and symmetry structure is called the paraelastic phase.

"Ferroelastic toughening" refers to increasing the plane strain fracture toughness ( $K_{IC}$ ) of a ferroelastic material by taking advantage of its intrinsic ferroelastic properties, specifically via spontaneous strain tensor reorientation. The two principal toughening processes available are crack energy absorption and crack shielding. Crack energy absorption toughening arises as a consequence of the energy dissipation that occurs when ferroelastic domains switch in the vicinity of a crack tip. Hysteresis energy losses always accompany domain switching, and thereby make less energy available for crack tip propagation. Crack shielding arises from (1) stress field reductions (at the crack tip) due to the redistribution of the stress field made possible by domain switching, and (2) crack closure accompanying spontaneous strain reorientation. Although several good papers exist relating to ferroelasticity as a general topic (in particular the reader is referred to the papers by Wadhavan(1) and Aizu(2,3)), the amount of research effort directed into the topic of ferroelastic toughening is somewhat limited to date. Virkar and Matsumoto(4) examined orientation effects on ground surfaces of tetragonal zirconia using X-ray diffraction (XRD) methods. Mehta and Virkar(5) examined orientation and viscoelastic relaxation in lead zirconate titanate using XRD, indentation, and stress strain testing methods. Subsequent work by Srinivasan et. al (6) and Jue and Virkar(7) demonstrated the occurrence of ferroelastic domain switching in t'-zirconia, both polydomain single crystals and polycrystals.

The compound  $Gd_2(MoO_4)_3$  (gadolinium molybdate or GMO) is simultaneously both ferroelectric and ferroelastic; in fact it is one of the few crystals known where the two properties are fully coupled. The occurrence of these coupled ferroic properties in GMO has previously lead to interest in the material for electrooptic applications(8,9,10,11,12), but it is the ferroelastic properties that are of interest in this paper. Single crystal GMO is transparent in the

visible light range, presenting an opportune prospect for directly observing the interaction between cracks and domains. By introducing cracks of known orientation in monodomain single crystals, fracture behavior in both switchable and nonswitchable orientations can be observed and compared. By using a Vickers diamond indenter, the same indentation can be used to simultaneously generate cracks in both orientations of interest.

At room temperature, GMO is orthorhombic, with  $a=10.3858 \text{ \AA}$ ,  $b=10.4186 \text{ \AA}$ , and  $c=10.7004 \text{ \AA}$ , and with the polarization vector directed along the  $\langle 001 \rangle$  (c) axis(13). Polarization reversal produces  $180^\circ$  reversal of the c axis and is accompanied by an interchange of the  $\langle 100 \rangle$  (a) and  $\langle 010 \rangle$  (b) axes of the crystal(14). This produces a spontaneous strain of  $\epsilon_s=1.576 \times 10^{-3}$ . Similarly, switching of the spontaneous strain tensor (a $\rightarrow$ b axis interchange) is always accompanied by polarization vector (c axis) reversal. The spontaneous strain tensor is at right angles to the spontaneous polarization vector. GMO is isostructural(15) with other rare earth molybdates of the general structure  $L_2(\text{MoO}_4)_3$ , where L represents one of the rare earth ions, Pr through Ho, as well as some mixtures with trivalent ions that give an average ionic radius within the same range. For the case of mixed ions at the L site, the average ionic radii can generally be interchanged with the equivalent sized rare earth cation for the prediction of phase stability. Crystals have been grown using the Czochralski method for many of the rare earth molybdates, and especially the compound GMO(16).

Ideally, comparison of the fracture properties of (the available) GMO single crystal samples and polycrystalline material would best be accomplished by fabricating polycrystalline GMO samples. Unfortunately, problems associated with the phase stability of polycrystalline GMO make this approach difficult. It is possible to fabricate the rare earth molybdate compounds  $\text{Tb}_2(\text{MoO}_4)_3$  (TMO),  $\text{Dy}_2(\text{MoO}_4)_3$  (DMO), and  $\text{GdY}(\text{MoO}_4)_3$  (GYMO), and these compounds are all isotypic with GMO. Further, the material properties for these molybdates are closely matched with GMO. Consequently, these compounds were fabricated by hot pressing, and their fracture properties characterized to compare with the data from the single crystal GMO samples.

There are three known phases of GMO that exist between room temperature and its melting temperature(15,17,18). The high temperature  $\beta$ -GMO phase is stable from the melting temperature ( $1165^\circ\text{C}$ ) down to  $850^\circ\text{C}$ . Below  $850^\circ\text{C}$   $\alpha$ -GMO is the stable phase. However, the kinetics of the  $850^\circ\text{C}$   $\beta \rightarrow \alpha$  transition are extremely

sluggish(17), and for single crystals and large grained powders  $\beta$ -GMO is the metastable phase that is usually found at lower temperatures, down to 159°C. Below 159°C, metastable  $\beta$ -GMO converts to another metastable phase,  $\beta'$ -GMO.

$\beta'$ -GMO is the orthorhombic and a simultaneously ferroelectric-ferroelastic phase of interest in this study.  $\beta$ -GMO is tetragonal and forms the paraelectric-paraelastic prototype structure for the ferroic  $\beta'$ -GMO phase. The  $\beta \rightarrow \beta'$  transition temperature (159°C) is the Curie temperature. Details of the crystal structure of both the  $\beta$  and  $\beta'$  phases and the exact atomic displacements involved in the transition can be found elsewhere(13,19).  $\alpha$ -GMO is monoclinic and displays a considerably higher density ( $\approx 4.75 \text{ g/cm}^2$ ) than either  $\beta$ -GMO ( $4.52 \text{ g/cm}^2$ ) or  $\beta'$  GMO ( $4.56 \text{ g/cm}^2$ .) The situation for TMO, DMO, and GYMO is generally the same as for GMO, with slightly different Curie temperatures, and with lower  $\beta \rightarrow \alpha$  transition temperatures (750°C to 800°C.) TMO, DMO, and expectedly GYMO also display an additional high temperature phase, appearing over a narrow temperature range between the melting temperature and the  $\beta$  phase, termed the  $\gamma$  phase(15). The Curie temperatures of the entire series of isostructural rare earth molybdates are expected to be roughly within 10°C of one another, due to small differences of the ionic radii of the members of the lanthanide group. Unless otherwise specified, GMO in this paper always refers to the  $\beta'$  phase of GMO, with the same convention adopted for TMO, DMO, and GYMO.

The present work was undertaken to examine the phenomenon of ferroelastic toughening in both single crystal and polycrystalline GMO-type compounds. Procedures for the fabrication of hot pressed polycrystalline GMO-type compounds were developed to accomplish this, and particulars of the procedures, microstructural characterization, and phase transition anomalies for hot pressed TMO, DMO, and GYMO are discussed as well. Mechanical testing of both single and polycrystalline specimens was done using indentation fracture techniques.

## 2. Experimental Procedure

Single crystals of GMO, which were grown via the Czochralski process\*, were oriented using Laue X-ray back reflection, then cut into small rectangular pieces (roughly 15 mm x 10 mm x 2 mm) with cuts along the {100}, {010}, and {001} planes. The large face was oriented to be the {001} plane. All sides of each cut piece were then polished progressively down with a final polish using a 0.3  $\mu\text{m}$

alumina slurry. Domain walls in polished samples are easily visible using an optical microscope with transmitted cross polarized light. Stress free walls always form along the {110} planes(20). When required, domain walls were removed completely from samples by manipulating their orientation during polishing. Individual domain walls within a piece were manipulated by applying a compressive pressure to opposing {010} faces.

\*[Supplied by Dr. L. H. Brixner, E. I. Dupont Co.]

Diamond indentations were made on the {001} face of polished samples using a Vickers diamond point mounted in a microhardness testing machine, using various test loads and time periods. Fracture toughness ( $K_{IC}$ ) was calculated from the resultant indentation cracks using an equation derived by Evans and Charles(21). The values for the elastic modulus  $E$  and the hardness  $H$  required by this equation were determined from measurements made on polycrystalline TMO samples above  $T_c$  (paraelastic phase.) The  $K_{IC}$  equation was derived for isotropic materials in which indentation resulted in median crack formation. Application of this equation to single crystals, or non-median crack formation, is therefore limited to the determination of trends in fracture toughness, and for qualitative relative toughness comparisons.

Powders of GMO were prepared for hot pressing samples from precursor powders of  $Gd_2O_3$  and  $MoO_3$ . Stoichiometric quantities of  $Gd_2O_3$  and  $MoO_3$  were mixed with  $C_6H_{12}$ , zirconia grinding media, and a small amount of a deflocculent. The mixture was then milled in a polyethylene jar, dried, calcined in a Pt lined crucible, and pestled to break up agglomerates formed during calcination. A second milling and calcining was subsequently required to completely convert the powders to GMO. After a final milling and drying, the powder was heated to  $600^\circ C$  for 2 h to burn out the residual carbon attributable to remnant cyclohexane and polyethylene jar wear. The powder was then screened (-100 mesh) and stored in a sealed container. Lots of powder produced of (TMO), (DMO), and (GYMO) were made using exactly the same procedure.

Powders were hot pressed in a mullite and alumina die at 35 MPa pressure at a temperature between  $800^\circ C$  and  $900^\circ C$ . The inside of the die was lined with mica to prevent the sample from sticking to and for facilitating its removal from the die. All mica was ground off of the sample after hot pressing, leaving the dense bulk sample for characterization. Hot pressed samples were roughly 25 mm in diameter and weighed 6 to 8 g.

Sample densities were determined using Archimedes principle in deionized water. For microstructural examination, sample surfaces

were progressively polished down to 1  $\mu\text{m}$  diamond abrasive, then etched thermally (825°C for 2 h). Examinations were performed using both optical and scanning electron microscopes (SEM.) All of the optical micrographs were taken under crosspolarized light to observe any possible domain formations.

Phase verification for all of the compounds was accomplished using X-ray diffraction (XRD) with nickel filtered  $\text{Cu } k_{\alpha}$  radiation. A rough lattice parameter fit for the GYMO compound (used for theoretical densities) was obtained from the XRD data, with an internal KCl standard incorporated into the powder. The cell parameters for GYMO were determined from the {400/040} and {008} reflections, resulting in a theoretical density for this material of 4.20  $\text{g/cm}^3$ . Transition characteristics of the  $\text{B} \rightarrow \text{B}'$  phase transition (at around 160°C for all of these rare earth molybdates) were examined using differential scanning calorimetry (DSC.)

Indentations were introduced into polished polycrystalline sample surfaces using an Instron testing machine. The Vickers diamond point was mounted on the crosshead. Samples were indented at various temperatures to obtain  $K_{\text{IC}}$  versus temperature data. The temperature was measured using a thermocouple mounted close to the diamond point. The  $K_{\text{IC}}$  calculations were done using the same equation used for single crystal specimens.

Stress-strain curves for polycrystalline samples were generated by mounting a strain gage directly to a ground surface of a rectangularly cut sample and applying compressive stress along the gage axis on an Instron testing machine.

### 3. Results

Fig. 2 shows a micrograph of two indentations (200 g for 10 sec) introduced into the {001} surface and on opposite sides of a domain wall. Both indentations are oriented to place their diagonals in the  $\langle 100 \rangle$  and  $\langle 010 \rangle$  directions. The domain wall separates regions of the single crystal with the  $\langle 100 \rangle$  and  $\langle 010 \rangle$  axes switched, providing an explicit demonstration of the relationship between specific crack orientation and crack length. Cracks oriented in the  $\langle 100 \rangle$  directions are consistently much larger than cracks oriented in the  $\langle 010 \rangle$  directions. The  $\langle 110 \rangle$  domain wall between the two indentations provides a ready reference of the relative orientation of the indentations, as well as clear visual confirmation that the differences in crack lengths are in fact due to specific crack orientation and not experimental misalignment errors. At higher

magnification (Fig 3) it becomes apparent that domains have formed close to the indentation in the  $\langle 010 \rangle$  directions. The constraints imposed by coexisting within the bulk crystal always cause domains to form in the sliver shaped geometries observed, with domain walls close to the required  $\langle 110 \rangle$  orientations. Fig. 4 demonstrates the geometry involved in domain switching about the indentation schematically. Micrographs (not shown) taken of these domains with the microscope focused at and then slightly below the surface of the same indentation indicate that the sliver shaped domains are relatively shallow. A thin slice ( $\approx 0.25$  mm) of single crystal GMO was cut, polished and mounted on a glass plate prior to indentation. Indentation of this slice introduced domains that interacted with the polarized light much more strongly (Fig. 5) than those of Fig. 3. Referenced to the indentation center, domain formation is clearly evident in the  $\langle 010 \rangle$  directions, and clearly inhibited in the  $\langle 100 \rangle$  directions.

Fig. 6 presents a micrograph of two indentations (200 g for 10 sec) introduced into the  $\{001\}$  surface and on opposite sides of a domain wall, but this time with the indentation diagonals oriented in the  $\langle 110 \rangle$  directions. There is almost no difference in the crack lengths, either for a specific indentation or between the two indentations. Higher magnification (Fig. 7) reveals the existence of domains in the  $\langle 010 \rangle$  directions, implying that domains are formed by the compressive stress field associated with the indenter.

A total of 30 indentations were introduced into the  $\{001\}$  surface of a sample, with the indentation pattern separated into two symmetric regions separated by a domain wall (Fig. 8.) Indentation fracture toughness values were calculated for each of the cracks in the array, and the results of this experiment are presented in Table 1. Twelve of the indentations were oriented with the indentation diagonal in the  $\langle 100 \rangle$  and  $\langle 010 \rangle$  directions at loads of 200 g for 10 s, 12 were in the  $\langle 110 \rangle$  directions at the same load, and 6 were in the  $\langle 100 \rangle$  and  $\langle 010 \rangle$  directions at loads of 200 g for 45 s. Four of the 200 g for 10 s  $\langle 010 \rangle$  indentations and one 200 g for 45 s indentation produced no cracking in the  $\langle 010 \rangle$  direction, and as this made the calculated toughness for these cracks smaller than three standard deviations from the mean, they were not incorporated into the final statistics. In Table 1, N refers to the number of cracks included in the data,  $\langle K_{IC} \rangle$  are the average of the calculated fracture toughness values, and  $\sigma$  the standard deviations. The 45 s loading was done to determine if significant stress assisted-corrosion cracking was occurring. Most of the difference that exists between the short and long duration indentations is attributed to experimental scatter. The

differences in fracture toughness between the  $\langle 100 \rangle$  and the  $\langle 010 \rangle$  orientations is clearly evident, with the  $\langle 010 \rangle$  (switchable) fracture toughness roughly 2.8 times the  $\langle 100 \rangle$  (nonswitchable) value. Fracture calculations done using a published Palmqvist crack equation(22) produced a similar 2.1 fold value for the increase. The  $\langle 110 \rangle$  fracture toughness values are consistently slightly larger than the  $\langle 100 \rangle$  values.

Figs. 9 (a) and (b) show micrographs of domain formation that occurred at the tip of a preexisting  $\langle 110 \rangle$  oriented crack. The crack formed in the center of a single crystal and extended completely through the sample, from the face displayed to the face on the opposite side of the sample. The crack formed at the location where a small perpendicular domain wall was trapped between parallel domain walls, roughly in the center of the sample. This trapped wall became the short length crack observed after heating the sample through the Curie temperature, and is located in the center of the figures. Domains formed spontaneously at both crack tips, with domain walls at  $90^\circ$  relatively to the orientation of the crack. An external stress was applied to the sample by mounting it in a small vice and mechanically compressing opposing  $\{010\}$  faces, resulting in a  $\langle 100 \rangle$  oriented compressive stress acting on both the crack and domains. The micrographs show this crack and the domain formations interacting with the crack tips under the conditions of 9(a) the externally applied compressive stress applied in the  $\langle 100 \rangle$  direction and 9(b) with the applied compressive stress subsequently released (no stress applied.) The domains size after release of the applied compression state (Fig. 9(a) is close to the domain size that was observed before any stress was applied initially. GMO is a fully coupled ferroelectric-ferroelastic, and the measured coercive stress is a strong function of the electrical resistance between the opposing  $\langle 001 \rangle$  polarization faces. The bubbles on the surface are from a soap solution used to effectively short these faces together and thereby reduce the coercive stress of the crystal during the test.

Fig. 10 presents densities of polycrystalline GYMO and TMO compositions hot pressed for 15 min at temperatures ranging from  $800^\circ\text{C}$  to  $900^\circ\text{C}$ . TMO samples hot pressed at  $800^\circ\text{C}$  were in the stability field of the  $\alpha$  phase. This accounts for the apparent anomaly in the density for that temperature. Microstructures of TMO, GYMO, and DMO hot pressed at  $900^\circ\text{C}$  are shown in Figs. 11, 12, and 13 respectively. The average grain size in these samples is  $7.1\ \mu\text{m}$ ,  $7.2\ \mu\text{m}$ , and  $4.6\ \mu\text{m}$  respectively. The duplex microstructure evident in the GYMO composition is clearly evident even in samples pressed at

much lower temperatures where grain growth was limited, and is probably related to powder milling problems. Extensive microcracking was observed in all of the hot pressed samples. When heated from room temperature to slightly above the Curie temperature, the c axis of single crystal GMO exhibits a positive strain of  $\approx .006$ , whereas the a axis exhibits a negative strain of  $\approx .002$ , due to the combined effects of thermal expansion and the ferroic phase transition at  $159^\circ\text{C}$ (9). Given the close relation assumed between GMO and the polycrystalline sample compositions of GYMO, TMO, and DMO, and considering the large anisotropy of cell parameters with temperature noted for GMO, it is reasonable to conclude that the microcracking observed in the polycrystalline samples can be attributed to the combined effects of thermal expansion anisotropies and cell parameter changes that result from the  $\beta \rightarrow \beta'$  phase transition, which both occur as the hot pressed samples are cooled. It was not possible to reduce the average grain size sufficient(23) to eliminate these microcracks. No domain structure was observed in any of the hot pressed samples using optical microscopy. Domain structure was only observed in pressureless sintered samples exhibiting extremely large grains ( $>100 \mu\text{m}$ .)

All of the hot pressed GMO samples displayed significant  $\alpha$  phase, even when rapid quenching rates were used ( $>100^\circ\text{C}/\text{min}$ .) The lower  $\beta \rightarrow \alpha$  transition temperatures of TMO and DMO made producing the required metastable  $\beta$  phase in these materials much easier. Hot pressed TMO continued to show slight  $\alpha$  phase, while hot pressed DMO and GYMO appeared to be completely free of it. The mixture of Gd and Y ions in the GYMO compound results in an average ionic radius of  $0.9155 \text{ \AA}$ , midway between the other two successfully hot pressed compounds of Tb ( $0.923 \text{ \AA}$ ) and Dy ( $0.908 \text{ \AA}$ ), and may account for its comparable stability.

To determine if there was any preferred orientation induced by hot pressing, XRD traces of hot pressed GYMO ( $900^\circ\text{C}$  for 1 h) were obtained in planes perpendicular and parallel to the hot pressing direction (Figs. 14 (a) and (b) respectively.) Preferred orientation was indicated, with the  $\langle 001 \rangle$  axis of the grains aligning parallel to the hot pressing direction. Visual inspection of micrographs (not shown) taken in each the two planes indicated that the grains preferred to grow in a direction perpendicular to the hot pressing direction, but this morphological texture may or may not be related to the crystallographic texture. It should be noted that the samples fracture and stress-strain tested were hot pressed at  $900^\circ\text{C}$  for 15

min. The XRD traces for the samples held at temperature for these shorter durations (always taken in the plane perpendicular to the hot pressing direction) were a closer match to the powder traces than either of the traces shown for the sample hot pressed at 900°C for 1 h, implying less orientational effects were present.

Some attempts were made to use differential scanning calorimetry (DSC) data as a source of verification for the first order  $\beta \rightarrow \beta'$  transition. It was soon found that significant alumina contamination (1 to 2 weight percent) introduced by the milling operations completely altered the  $\beta \rightarrow \beta'$  phase transition character from first order to diffuse. A change was made to zirconia grinding media and reduced milling times to preserve the first order transitional character of the powders. DSC scans of a lot of TMO powder and a hot pressed sample from that lot (Figs. 15 (a) and (b) respectively) show that the 154°C transitional heat peak in the lot powder scan is completely suppressed in the hot pressed sample. The suppression of this peak is probably related to the influence of microstructure related stresses acting to inhibit or promote the transition at the individual grain sites, depending on the sign of the stress. Hydrostatic tension will increase the  $T_c$  and hydrostatic compression will lower the  $T_c$ . The transition temperature (154°C) for the powder is also about 9°C lower than that reported (18) for single crystals (163°C.) The slight exothermic peak at 126.8°C and endothermic peak at 167.4°C are attributable to the calorimeter itself, and are probably related to slight contamination of the sample chambers by previous users. Curve (c) is of a high purity GYMO powder standard, showing the transition for this material to be clearly diffuse. As is often the case for such substitutions(24), incorporation of dissimilar trivalent anions into the Gd type site on the lattice apparently results in shifting the transitional character from first order to diffuse.

Hot pressed samples of TMO and DMO were indented (1 kg for 10 s) at temperatures spanning from 25°C (well below  $T_c$ ) to 260°C (well above  $T_c$ ) at 30°C increments. Fig. 16 presents a graph of  $K_{IC}$  determined from the indentation crack lengths as a function of the indentation temperature, for these samples. Fig. 17 presents a SEM micrograph of one such indentation for inspection. Both materials display a relatively constant toughness for temperatures above  $T_c$  ( $\approx 160^\circ\text{C}$ ) and a monotonically decreasing toughness with increasing  $T$  for temperatures below  $T_c$ . The increase in toughness, from 160°C to 25°C, for TMO is  $\approx 80\%$  and for DMO is  $\approx 55\%$ .

Stress-strain curves for hot pressed TMO generated at sample

temperatures of 25°C and 170°C are presented in Fig. 18 (a) and (b) respectively, using a loading/unloading rate of 0.05 mm/min. The low temperature curve (generated in the ferroelastic region) exhibits the expected hysteresis behavior (i.e., an open loop trace.) This hysteresis, however, has almost completely disappeared by the end of the unloading portion of the cycle. The high temperature trace (generated in the paraelastic region) exhibits no hysteresis at all. The apparent elastic modulus is considerably different between the two curves, displaying about 125  $\mu$  strain difference at maximum load (73 MPa.) If the assumption is made that the sample initially was composed of a completely random grain orientation, then this value corresponds to state of roughly 45% of full theoretical poling.

#### 4. Discussion

The occurrence of a toughness anomaly between the  $\langle 100 \rangle$  and  $\langle 010 \rangle$  oriented cracks in the single crystal GMO, as displayed quite graphically in Fig. 3, and verified in statistically in Table 1, was the expected and sought after result. For ferroelastic materials, the occurrence of large stress field components in the vicinity of a crack tip (this will be discussed later in this section) means that switching is likely to occur that in vicinity, if the orientation is appropriate to allow such. The switching process is expected to result in hysteretic losses, thereby reducing the energy available for further crack tip growth (relative to a material exhibiting similar mechanical properties but excepting the possibility of ferroelastic switching.) As the  $\langle 100 \rangle$  and  $\langle 010 \rangle$  orientations in GMO are structurally almost interchangeable, and it seems logical to infer that these two orientations will exhibit similar properties in most respects except for those involving ferroelastic switching (or other ferroic properties.) It follows that differences in the observed fracture toughness between the  $\langle 100 \rangle$  and  $\langle 010 \rangle$  orientations would indicate a toughness anomaly almost wholly attributable to the occurrence of ferroelastic switching. The fact that the orientation where switching proceeded (i.e.,  $\langle 010 \rangle$ ) resulted in significantly higher toughness values than the orientation where switching did not proceed ( $\langle 100 \rangle$ ) is both consistent with and predicted from this viewpoint.

Possibly even more significant than hysteretic losses at the crack tip is the possibility of crack shielding in that vicinity. The act of switching favorably oriented domains in the vicinity of a  $\langle 010 \rangle$  crack tip in single crystal GMO will tend to reduce (or limit) the stress in the  $\langle 100 \rangle$  orientation and increase the stress in the  $\langle 010 \rangle$

orientation. This action effectively shunts the stress away from an orientation that acts perpendicular to the crack plane surface towards an orientation that acts parallel to that surface. It is the stress acting perpendicular to the crack plane surface that is most responsible for crack propagation, and the reduction or limiting of this stress is highly desirable if crack propagation is to be avoided. As further stress is applied, the domains must grow in size and/or new domains must be formed. Consequently, the domain boundaries where the stress shunting action is proceeding will shift further away from the immediate crack tip vicinity. To some extent, this provides a buffering capability which allows the material to shunt more energy, but as the switching zone progresses to far away from the crack tip, the influence that further switching has in the region close to the crack tip is substantially reduced.

An analysis of the stress field expected in the immediate vicinity of these crack tips may help in understanding the impetus for domain growth. The stress field for a mode I crack tip for the geometry shown in Fig 19 is well known and given by(25):

$$\sigma_y = \frac{K}{\sqrt{2\pi r}} \cos \frac{\theta}{2} \left[ 1 + \sin \frac{\theta}{2} \sin \frac{3\theta}{2} \right]$$

$$\sigma_x = \frac{K}{\sqrt{2\pi r}} \cos \frac{\theta}{2} \left[ 1 - \sin \frac{\theta}{2} \sin \frac{3\theta}{2} \right]$$

$$\tau_{xy} = \frac{K}{\sqrt{2\pi r}} \left[ \sin \frac{\theta}{2} \cos \frac{\theta}{2} \cos \frac{3\theta}{2} \right]$$

Note that the relative magnitudes of the stress field components  $\sigma_y$  and  $\sigma_x$  vary between being of equal magnitude at  $\theta=0$  (directly in front of the crack tip) to the extreme case of  $\sigma_y=3\sigma_x$  at  $\theta=90^\circ$  (just off the crack tip in the y direction.) Consider the case of the indentation introduced into the {001} surface of the single crystal GMO sample and oriented to align the indentation diagonals in the  $\langle 100 \rangle$  and  $\langle 010 \rangle$  directions (Fig. 20). For a crack propagating in the  $\langle 100 \rangle$  direction, the x axis of Fig 19 will correspond to the  $\langle 100 \rangle$  crack orientation, and the y axis to the  $\langle 010 \rangle$  orientation. As such, the mode I conditions that are expected just off the tip of this crack, in the  $\theta=90^\circ$  direction, of  $\sigma_y=3\sigma_x$ , will result in a larger tensile stress in the  $\langle 010 \rangle$  direction (perpendicular to the plane of the crack) than in the  $\langle 100 \rangle$  direction (the crack propagation direction) in that vicinity. During indentation, the indenter may drive this stress field

differential between  $\sigma_y$  and  $\sigma_x$  even further apart (possibly even driving the radially oriented  $\langle 100 \rangle$  stress compressive far away from the crack tip.) Ferroelastic switching of domains requires the stress to be more tensile in the  $\langle 100 \rangle$  direction than in the  $\langle 010 \rangle$  direction. As such, this combination of stresses in the vicinity of the  $\langle 100 \rangle$  oriented crack tip is opposite to that which is required to induce domain switching and no switching (or domain formation) is expected to occur. The crack should behave similar to that expected for a paraelastic material.

By contrast, for a crack propagating in the  $\langle 010 \rangle$  direction, the x axis of Fig 19 will correspond to the  $\langle 010 \rangle$  crack orientation, and the y axis to the  $\langle 100 \rangle$  orientation. The mode I conditions that are expected just off the tip of this crack, in the  $\theta=90^\circ$  direction, of  $\sigma_y=3\sigma_x$  will now result in a smaller tensile stress in the  $\langle 010 \rangle$  direction (perpendicular to the plane of the crack) than in the  $\langle 100 \rangle$  direction (the crack propagation direction) in that vicinity. This is exactly the loading required to induce switching of these axes. As such, for this orientation, switching is expected to occur and thereby result in new domain formation. If domain formation does occur then the toughness should be higher for this orientation compared to that of the nonswitchable  $\langle 100 \rangle$  orientation. As the actual changes in interatomic distances involved after switching are relatively small for GMO (the largest being 0.043 Å), it is reasonable to conclude that any toughness differences observed between the  $\langle 100 \rangle$  and  $\langle 010 \rangle$  orientations must be almost wholly due to ferroelastic effects alone and not related to intrinsic surface effects. Toughness anomalies between the  $\langle 100 \rangle$  (nonswitchable) and the  $\langle 010 \rangle$  (switchable) oriented cracks will immediately be apparent in the single indentation, as the higher toughness  $\langle 010 \rangle$  orientation should resist cracking to a greater extent than the lower toughness  $\langle 100 \rangle$  orientation, and result in a shorter observed crack length for the  $\langle 010 \rangle$  crack. This is precisely the behavior observed in Figs. 2, 3, and 5, with domain structure evident only in the vicinity surrounding the  $\langle 010 \rangle$  oriented crack, again in good agreement with the discussion.

Now consider the indentation introduced into the  $\{001\}$  surface and oriented to align the indentation diagonals in the  $\langle 110 \rangle$  directions (Fig. 21.) The specific cracks of interest in this case are those oriented to propagate in the  $[110]$  and  $[\bar{1}10]$  directions. For both of these orientations, the differences in the stress field components in the vicinity of the tip of the crack, acting in the  $\langle 100 \rangle$  and  $\langle 010 \rangle$  directions, for any value of  $\theta$ , are always shear stresses,

and will not induce domain switching. Between the two cracks, in the  $\langle 010 \rangle$  direction (w.r.t the indentation center) a stress field differential between the radial and circumferential components may be introduced at the sample surface, during indentation, by the indenter itself (unrelated to any crack tip stresses), resulting in a larger compressive stress in the  $\langle 010 \rangle$  direction than in the  $\langle 100 \rangle$  direction. This difference in stress components again can induce domain switching, however, any stress reductions due to switching in that region would be shared equally by both cracks. The observed lengths of the two crack are therefore expected to be the same, regardless of whether switching occurs or not. This leads quickly to the prediction that all four corner cracks introduced during indentation should be of the same length, with any possible domain formation occurring only in the  $\langle 010 \rangle$  orientations. This is precisely the behavior observed Figs 6 and 7. Crack lengths for all four corners are very close to the same length, and domain formation is indeed observed in the  $\langle 010 \rangle$  orientations about the indentation center, leading to the conclusion that the indenter stress field differential is large enough to induce switching.

For the polycrystalline samples, it is reasonable to speculate that the widening of the  $b$  to  $a$  ratio that occurs in the unit cell as the temperature is reduced below the Curie temperature results in increasing the energy absorption capability of those grains (or domains) that switch, resulting in the observed toughness increases. In a similar manner, it is also possible that increases in the  $b$  to  $a$  ratio further favor the stress shunting action produced by switching, thereby enhancing the crack shielding mechanism. The larger spontaneous strain produced by an increase in the  $b$  to  $a$  ratio means that the material surrounding the domain must absorb (elastically) a larger strain upon switching to achieve the same ultimate domain size. Larger strain in the material surrounding the domain means a larger elastic stress there as well, and the energy shunted from one orientation to the other (for a given domain size) must therefore also increase. This is advantageous, as the growth of domains into regions farther away from the crack tip produces progressively diminishing returns in stress shunting at the crack tip, as switching becomes too far away from the tip to significantly effect the stresses in the immediate crack tip region.

There are other mechanisms which may also produce the obtained results, and which cannot be overlooked. One such mechanism is microcracking of ceramics during the fracture process, which has been proposed to be a toughening mechanism(26). The increasing  $b$  to  $a$  ratio may lower the additional stress required to

induce microcracking, and thereby enhance the toughness. If induced microcrack toughening is active, an increased microcrack density must occur near the crack tips during fracture. Inspection of one of the cracks formed during the 25°C DMO indentation test (Fig. 17), however, does not support this contention, but it is difficult to separate out the various microcracks in samples exhibiting such widespread microcracking initially.

Another plausible explanation involves the intergrain strain anisotropies produced by the increasing  $b$  to  $a$  ratio. In polycrystalline materials, expansion anisotropies tend to produce a stress distribution that is cyclic with distance, alternating between tensile and compressive values on a scale periodic with (and attributable to) the microstructure. Periodic stress distribution (tensile-compressive) has been shown to enhance  $K_C$  (27,28) according to the relation:

$$K_I^R = -A \sigma_1 \lambda^{\frac{1}{2}}$$

where  $K_I$ =toughness gains attributable to a periodic microstructure,  $\sigma_1$ =residual stress due to microstructural forces,  $\lambda$ =periodic wavelength for a given microstructure, and  $A$ =constant that depends on the ratio of the grain sizes for a two phase material (determined numerically.) It is interesting to estimate the approximate contribution of this type of toughness enhancement for the particular case of TMO, using appropriate estimations. Using a value of  $2.016 \times 10^{-6}$  for  $\epsilon_s$ , and the measured value of  $E=62$  GPa for polycrystalline material, and approximating the quenched in microstructural stress induced by the  $\beta \rightarrow \alpha$  phase transition by  $\sigma_1 = \epsilon_s E$  gives  $\sigma_1 \sim 125$  MPa. The periodic wavelength is taken as twice the average grain diameter (with  $\langle d \rangle = 7.1 \mu\text{m}$ .) The value of  $A$  is calculated in the paper by Cutler and Virkar(29) for the case of a two phase material with both phases possessing the same average grain size, and is  $A = 1.215$ . This leads to an estimated toughness enhancement of  $K_I = .405 \text{ MPa}\sqrt{\text{m}}$ , accounting roughly for all of the toughness enhancement observed in the TMO samples. This may mean that much of the  $K_C$  in the polycrystalline material is due to the internal stress related to the microstructure, however, that in the single crystals must still be due to switching.

## 5. Summary and Conclusions

1) Indentation experiments done on single crystal specimens of GMO showed a large anisotropy in fracture toughness values between the  $\langle 010 \rangle$  and  $\langle 100 \rangle$  orientations. Domains were observed to form in the higher toughness  $\langle 010 \rangle$  orientation, and were not observed to form in the lower toughness  $\langle 100 \rangle$  orientation. A 2.8 fold increase in toughness between orientations was indicated.

2) No anisotropy difference was observed for indentation cracks formed in the  $\langle 110 \rangle$  and  $\langle \bar{1}10 \rangle$  orientations. Domains were not observed to form in either of these orientations, but did form in the  $\langle 010 \rangle$  direction. Both of these results are in accordance with prediction.

3) The application of a compressive mechanical stress in the stressing of crack tips was observed to result in domain growth in the immediate vicinity of the crack tip in single crystal GMO.

3) The  $K_{IC}$  of hot pressed polycrystalline DMO and TMO ceramics tested decreased with increasing temperature up to  $T_c$  ( $\approx 160^\circ\text{C}$ ), beyond which it remained close to constant up to the maximum test temperature of  $260^\circ\text{C}$ . The increase in  $K_{IC}$  going from  $T_c$  to room temperature was 55% and 80 % respectively for these two materials.

4) On the basis of these observations, it is proposed that ferroelastic domain switching is active in enhancing the toughness in single crystal GMO. Ferroelastic switching may also be responsible for enhancing the toughness of the polycrystalline rare earth molybdates, however, internal stresses resulting from the microstructure may also be responsible for much or all of the  $K_C$  increases for these materials.

5) DMO and GYMO were hot pressed to produce close to 100%  $\beta'$  phase samples, and TMO was hot pressed to produce sufficient  $\beta'$  phase samples to maintain mechanical integrity. Hot pressed GMO samples exhibited large scale  $\beta \rightarrow \alpha$  phase conversion when cooled, resulting in mechanical failure.

6) Additions of significant quantities ( $>1\%$ ) of dissimilar trivalent anions at the Gd type site in GMO type compounds was observed to change the  $\beta \rightarrow \beta'$  transitional character of the from first order to diffuse.

#### Acknowledgements

This work was supported in part by DARPA through AFOSR (subcontract from Ceramtec to the University of Utah) under contract No. F49620-89-C0054. It is also a pleasure to acknowledge

the assistance of Dr. L. H. Brixner of E. I. DuPont Co., who graciously supplied the single crystal specimens used in this work.

## REFERENCES

1. V. K. Wadavan, "Ferroelasticity and Related Properties of Crystals," *Phase Transitions*, 3, 3-103 (1982).
2. K. Aizu, "Possible species of "Ferroelastic" Crystals and of Simultaneously Ferroelectric and Ferroelastic Crystals," *J. Phys. Soc. Jap.*, 27 [2] 387-396 (1969).
3. K. Aizu, "Possible species of Ferromagnetic, Ferroelectric, and Ferroelastic Crystals," *Phys. Rev.*, B2 [3] 754-772 (1970).
4. A. V. Virkar and R. L. K. Matsumoto, "Ferroelastic Domain Switching as a Toughening Mechanism in Tetragonal Zirconia," *J. Am. Cer. Soc.*, 69 [10] C224-C226 (1986).
5. K. Mehta and A. V. Virkar, "Fracture Mechanisms in Ferroelectric-Ferroelastic Lead Zirconate Titanate (Zr:Ti=0.54:0.46) Ceramics," *J. Am. Cer. Soc.*, 73 [3] 567-574 (1990).
6. G. V. Srinivasan, J. F. Jue, S. Y. Kuo, and A. V. Virkar, "Ferroelastic Domain Switching in Polydomain Tetragonal Zirconia Single Crystals," *J. Am. Cer. Soc.*, 72 [11] 2098-2103 (1989).
7. J. F. Jue and A. V. Virkar, "Fabrication, Microstructural Characterization and Mechanical Properties of Polycrystalline t'-Zirconia," *J. Am. Cer. Soc.* (Accepted).
8. A. W. Smith and G. Burns, "Optical Properties and Switching in  $Gd_2(MoO_4)_3$ ," *Phys. Lett.*, 28A [7] 501-502 (1969).
9. S. E. Cummins, "Electrical, Optical, and Mechanical Behavior of Ferroelectric  $Gd_2(MoO_4)_3$ ," *Ferroelectrics*, 1, 11-17 (1970).
10. J. A. Rajchman, "Promise of Optical Memories," *J. Appl. Phys.*, 41 [3] 1376-1383 (1970).
11. J. R. Barkley, L. H. Brixner, E. M. Hogan, and R. K. Waring, "Control and Application of Domain Wall Motion in Gadolinium Molybdate," *Ferroelectrics*, 3, 191-197 (1972).

12. A. Kumada, "Optical Properties of Gadolinium Molybdate and Their Device Applications," *Ferroelectrics*, **3**, 114-123 (1972).
13. E. T. Keve, S. C. Abrahams, and J. L. Bernstein, "Ferroelectric Ferroelastic Paramagnetic Beta-Gd<sub>2</sub>(MoO<sub>4</sub>)<sub>3</sub> Crystal Structure of the Transition-Metal Molybdates and Tungstates. VI," *J. Chem. Phys.*, **54** [7] 3185-3194 (1971).
14. K. Aizu, A. Kumada, H. Yumoto, and S. Ashida, "Simultaneous Ferroelectricity and Ferroelasticity of Gd<sub>2</sub>(MoO<sub>4</sub>)<sub>3</sub>," *J. Phys. Soc. Jap.*, **27**, 511 (1969).
15. K. Nassau, J. W. Shiever, and E. T. Keve, "Structural and Phase Relationships among Trivalent Tungstates and Molybdates," *J. Sol. St. Chem.*, **3**, 411-419 (1971).
16. L. H. Brixner,, "Single Crystal Growth of the Ln<sub>2</sub>(MoO<sub>4</sub>)<sub>3</sub>-Type Rare Earth Molybdates," *J. Crys. Growth*, **18**, 297-302 (1973).
17. K. Nassau, H. J. Levinstein, and G. M. Loicono, "A Comprehensive Study of Trivalent Tungstates and Molybdates of the Type L<sub>2</sub>(MO<sub>4</sub>)<sub>3</sub>," *J. Phys. Chem. Sol.*, **26**, 1805-1816 (1965).
18. E. T. Keve, S. C. Abrahams, N. Nassau, and A. M. Glass, "Ferroelectric Ferroelastic Paramagnetic Terbium Molybdate B-Tb<sub>2</sub>(MoO<sub>4</sub>)<sub>3</sub>," *Sol. State Commun.*, **8**, 1517-1520 (1970).
19. Wolfgang Jeitschko, "A Comprehensive X-ray Study of the Ferroelectric-Ferroelastic and Paraelectric-Paraelastic Phases of Gd<sub>2</sub>(MoO<sub>4</sub>)<sub>3</sub>," *Acta Crys.*, **B28**, 60-76 (1972).
20. J. Sapriel, "Domain-wall Orientations in Ferroelastics," *Phys. Rev.*, **B12** [11] 5128-5140 (1975).
21. A. G. Evans and E. A. Charles, "Fracture Toughness Determinations by Indentation," *J. Am. Cer. Soc.*, **59** [7-8] 371-372 (1976).
22. D. K. Shetty, I. G. Wright, P. N. Mincer, and A. H. Clauer, "Indentation Fracture of WC-Co Cermets," *J. Mat. Sc.*, **20**, 1873-1882 (1985).
23. A. G. Evans, "Microfracture from Thermal Expansion Anisotropy-

1. Single Phase Systems," *Acta. Metall.*, 26, 1845-1853 (1978).
24. M. E. Lines and A. M. Glass, Principles and Applications of Ferroelectrics and Related Materials; pp. 285-292. Oxford University Press, Oxford, 1977.
25. R. W. Hertzberg, Deformation and Fracture Mechanics of Engineering Materials; pp. 275-287. John Wiley and Sons, New York, 1983.
26. M. Ruhle, A. G. Evans, R. M. McMeeking, and P. G. Charalambides, "Microcrack Toughening in Alumina/Zirconia," *Acta. Metall.*, 35 [11] 2701-2710 (1987).
27. A. V. Virkar and D. L. Johnson, "
28. R. A. Cutler and A. V. Virkar, "The Effect of Binder Thickness and Residual Stresses on the Fracture Toughness of Cemented Carbides", *J. Mat. Sc.*, 20, 3557-3573 (1985).

## Figure Captions

- Fig. 1. Ferroelastic Hysteresis Curve
- Fig. 2.  $\langle 100/010 \rangle$  Indentations with Domain Wall in Single Crystal GMO
- Fig. 3. Close Up of  $\langle 100/010 \rangle$  Indentation in Single Crystal GMO
- Fig. 4. Schematic of Domain Formation in bulk Single Crystal
- Fig. 5. High Contrast  $\langle 100/010 \rangle$  Indentation in Thin Sliced Single Crystal GMO
- Fig. 6.  $\langle 110 \rangle$  Indentations with Domain Wall in Single Crystal GMO
- Fig. 7. Close Up of  $\langle 110 \rangle$  Indentation in Single Crystal GMO
- Fig. 8. Indentation Pattern
- Fig. 9. Crack Interacting with Domains which Formed at the Crack Tip (a) Under no Stress and (b) Under Compressive Stress in the  $\langle 100 \rangle$  Direction
- Fig. 10. Hot Pressed GMO and TMO Densities versus Pressing Temperature
- Fig. 11. TMO Microstructures Hot Pressed at 900°C
- Fig. 12. GYMO Microstructures Hot Pressed at 900°C
- Fig. 13. DMO Microstructure Hot Pressed at 900°C
- Fig. 14. XRD Powder Diffraction Pattern of Hot Pressed GYMO Sample: (a) in Plane Parallel to Pressing Direction and (b) in Plane Perpendicular to Pressing Direction
- Fig. 15. DSC Scans of (a) Lot TMO Powder, (b) Hot Pressed TMO Sample from that Lot, and (c) GYMO Powder Standard
- Fig. 16. Polycrystalline TMO and DMO Indentation Fracture Toughness versus Indentation Temperature

Fig. 17. SEM Indentation Crack Close Up in TMO at 25°C Indentation Temperature

Fig. 18. Stress Strain Curves for Hot Pressed TMO Tested at (a) 25°C and (b) 170°C

Fig. 19. Geometry of Mode I Crack

Fig. 20. Stresses for Indentation Crack Oriented in the  $\langle 100/010 \rangle$  Direction

Fig. 21. Stresses for Indentation Crack Oriented in the  $\langle 110 \rangle$  Direction

#### TABLE CAPTIONS

Table 1.  $\langle 100 \rangle$ ,  $\langle 010 \rangle$ , and  $\langle 110 \rangle$  Single Crystal GMO Indentation Data

Table 1. <100>, <010>, and <110> Single  
Crystal GMO Indentation Data.

<u>Indentation</u>	<u>N</u> <u>(Indents)</u>	<u><math>\langle K_{IC} \rangle</math></u> <u>(MPa)</u>	<u><math>\sigma</math></u> <u>(MPa)</u>
<100> (All)	18	.427	.026
<010> (All)	12	1.1774	.234
<110>	23	.559	.032
<100> (200g/10s)	14	.431	.027
<100> (200g/45s)	4	.403	.009
<010> (200g/10s)	9	1.111	.196
<010> (200g/45s)	3	1.377	.258

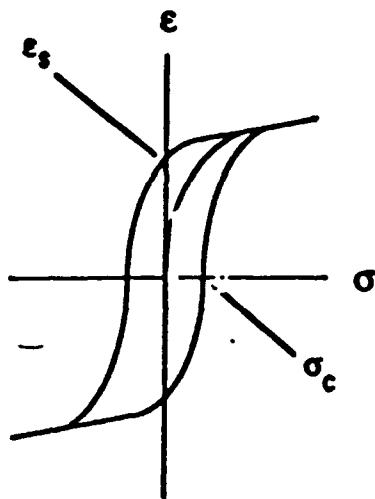


FIG. 1

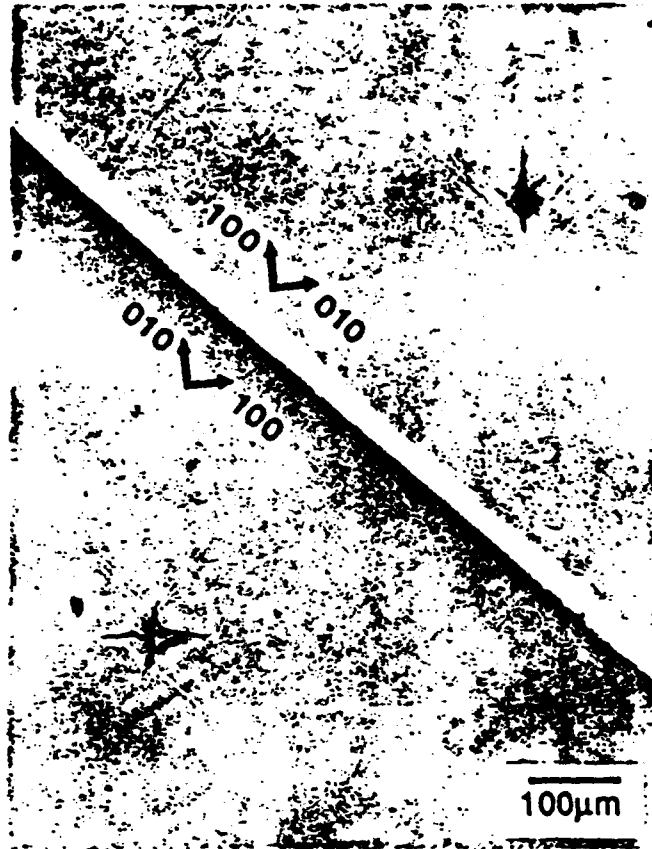


FIG. 2

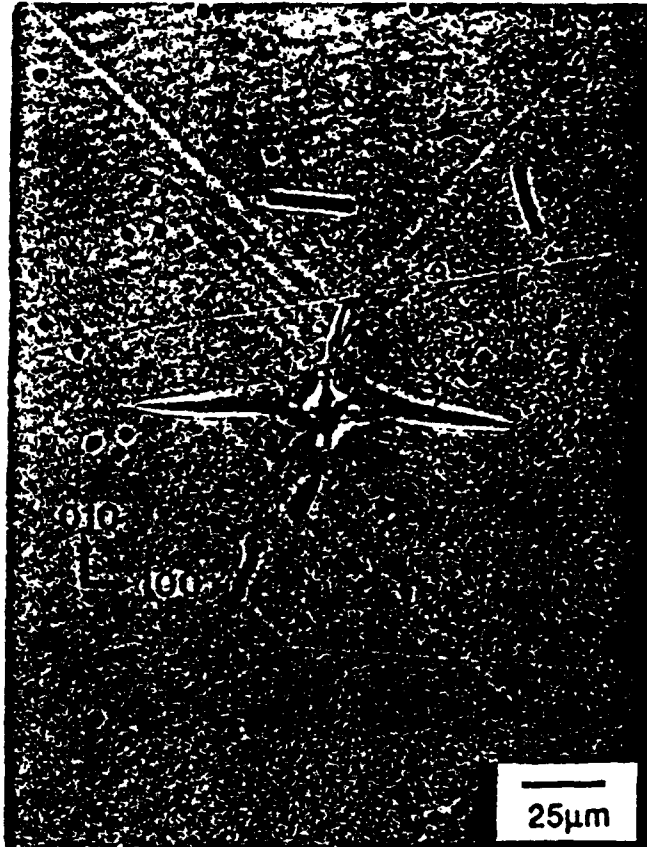


FIG. 3

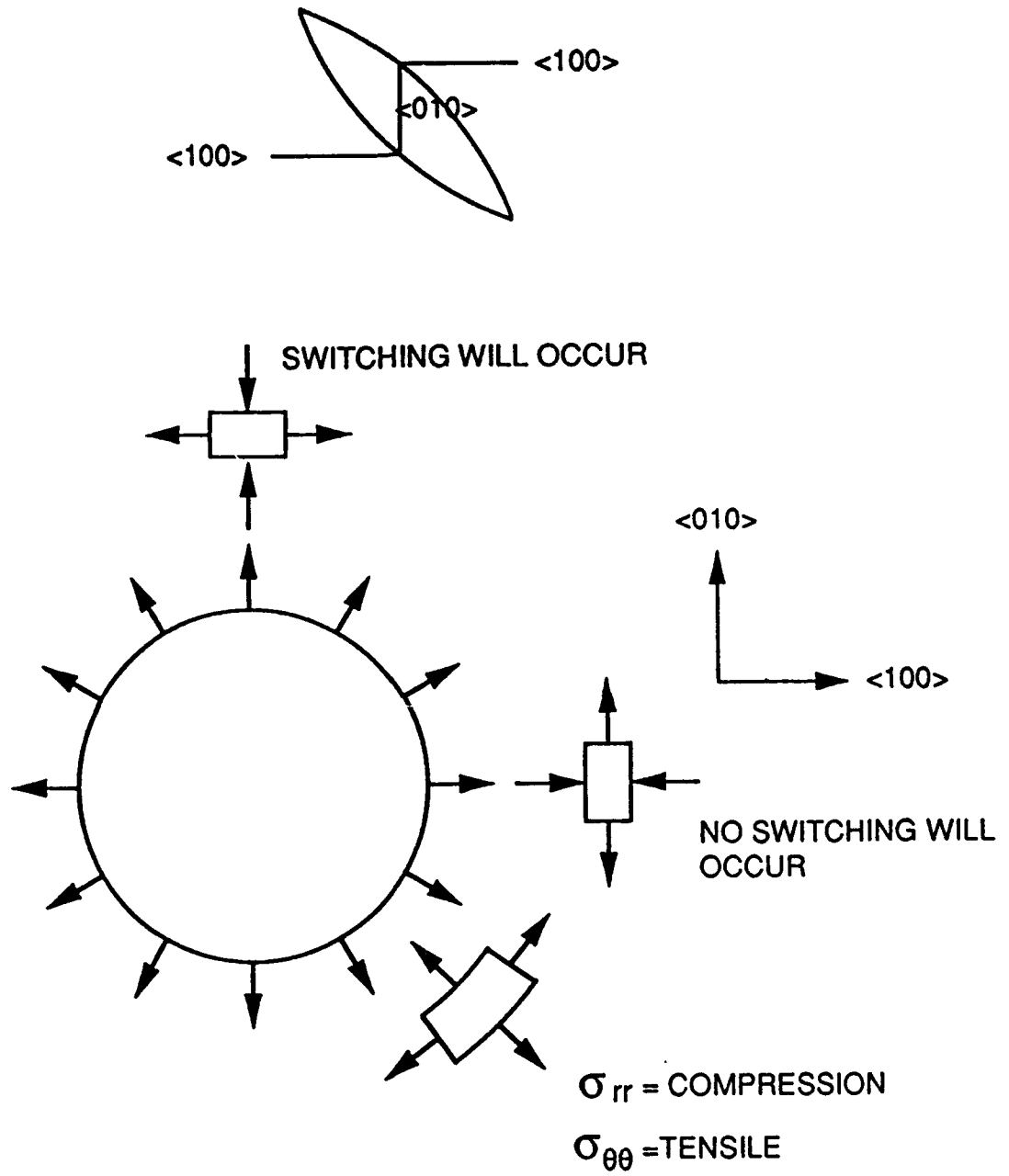


Fig. 4

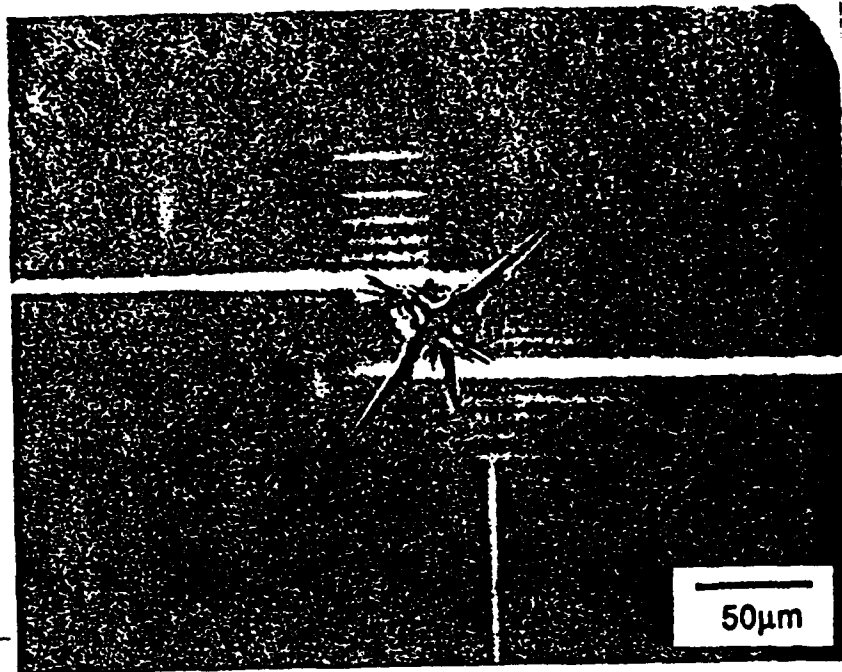


FIG. 5

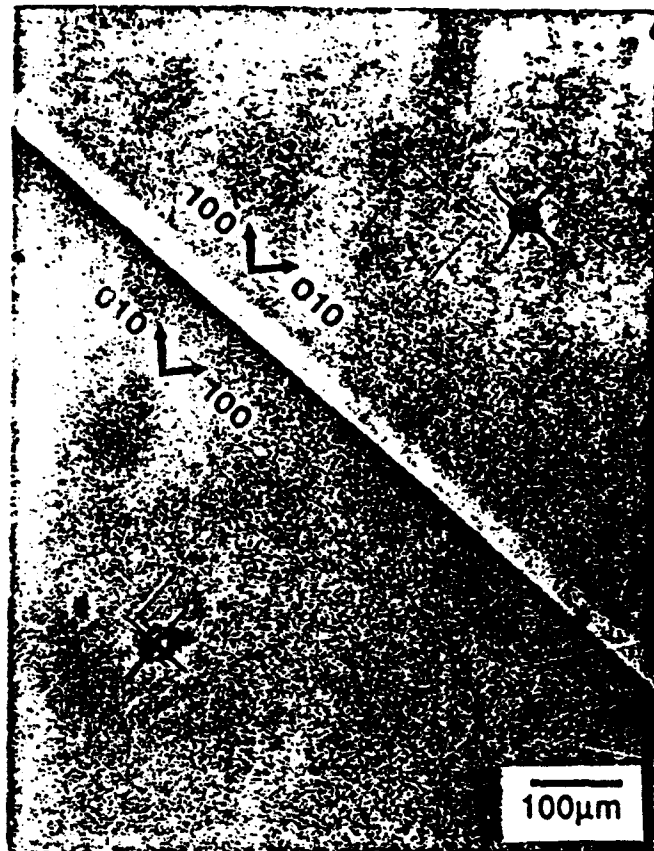


FIG. 6

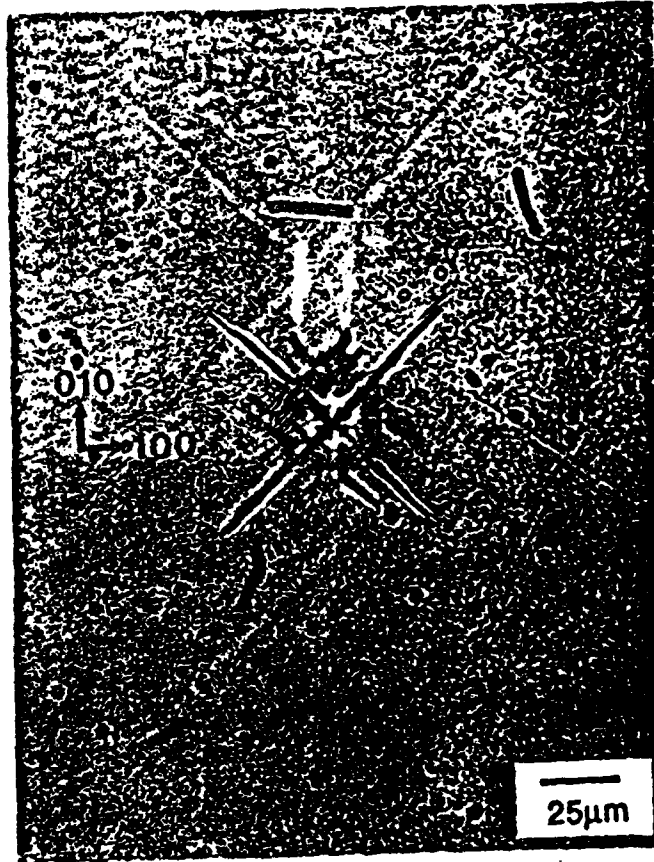


FIG. 7

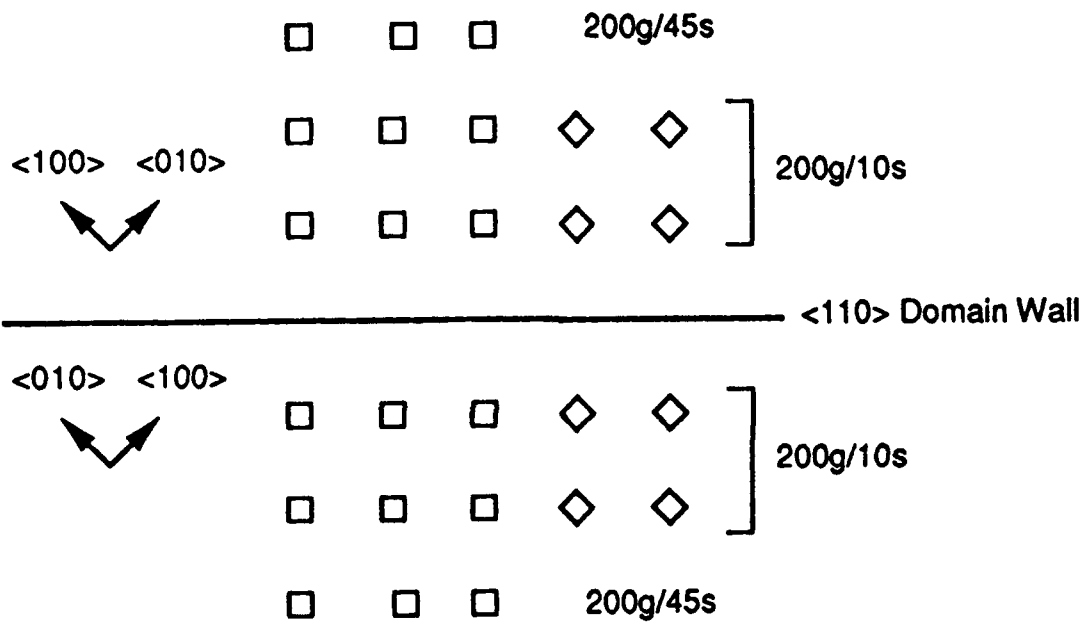


FIG. 8



Fig. 7(a)

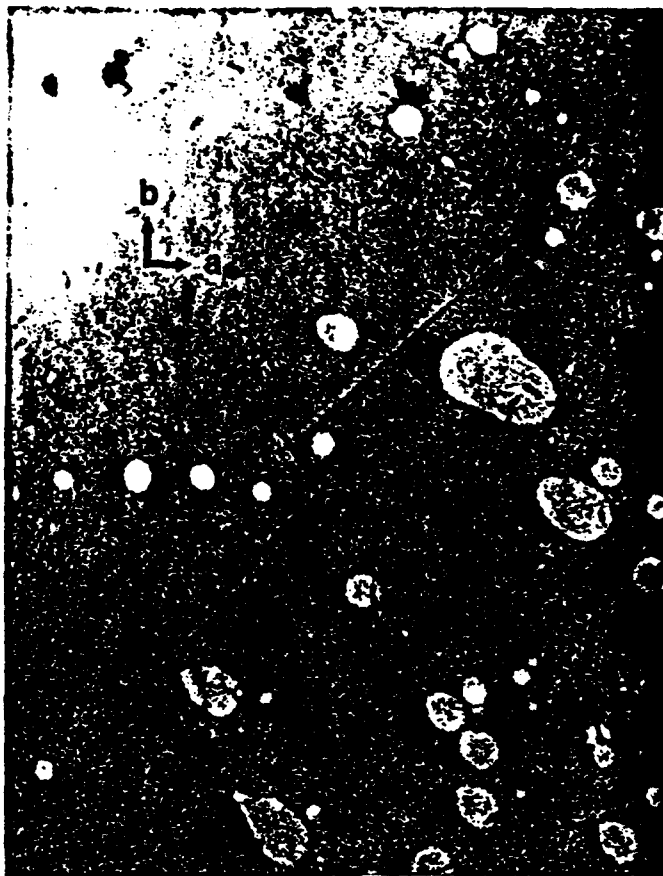


FIG. 9(b)

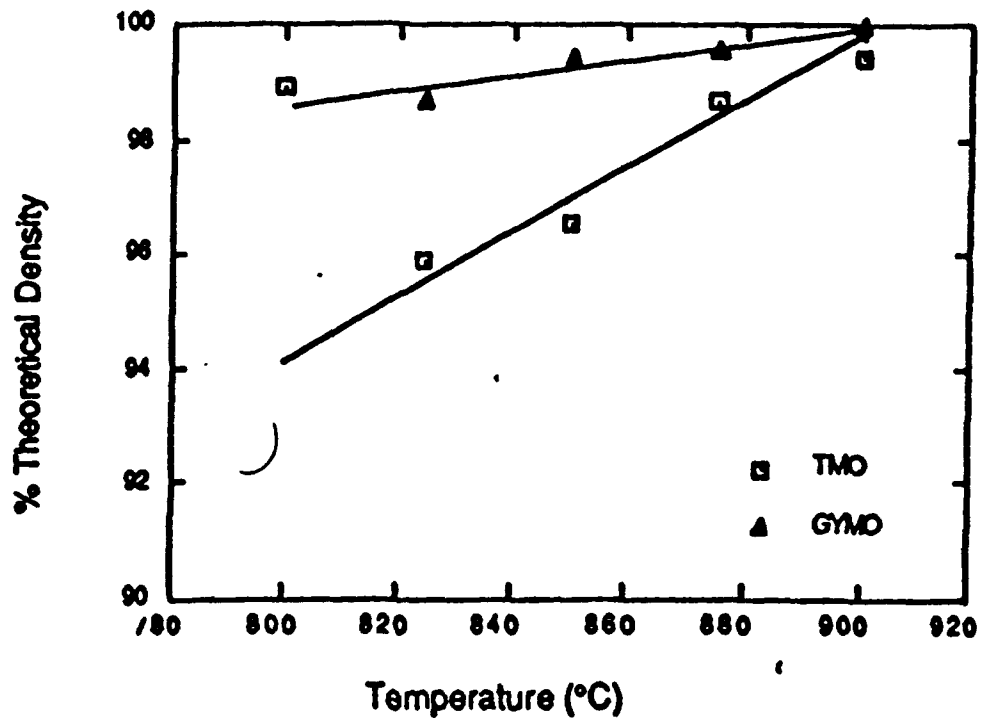


FIG. 10

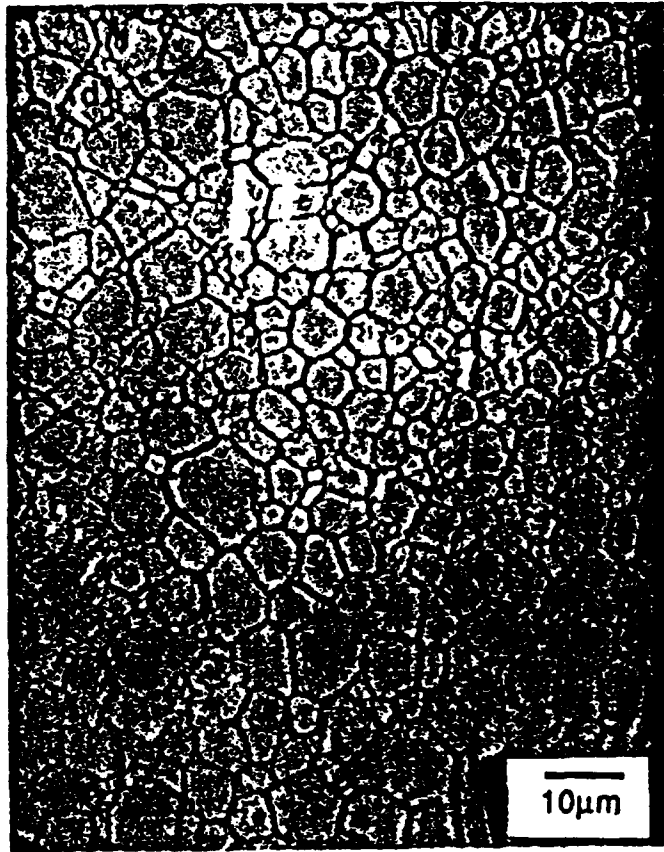


FIG. 11

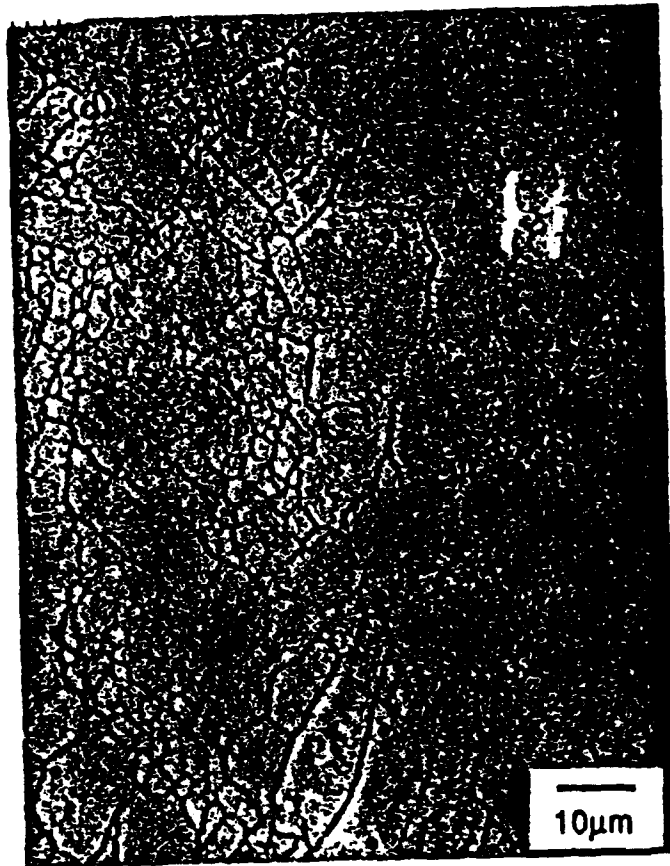


FIG. 12

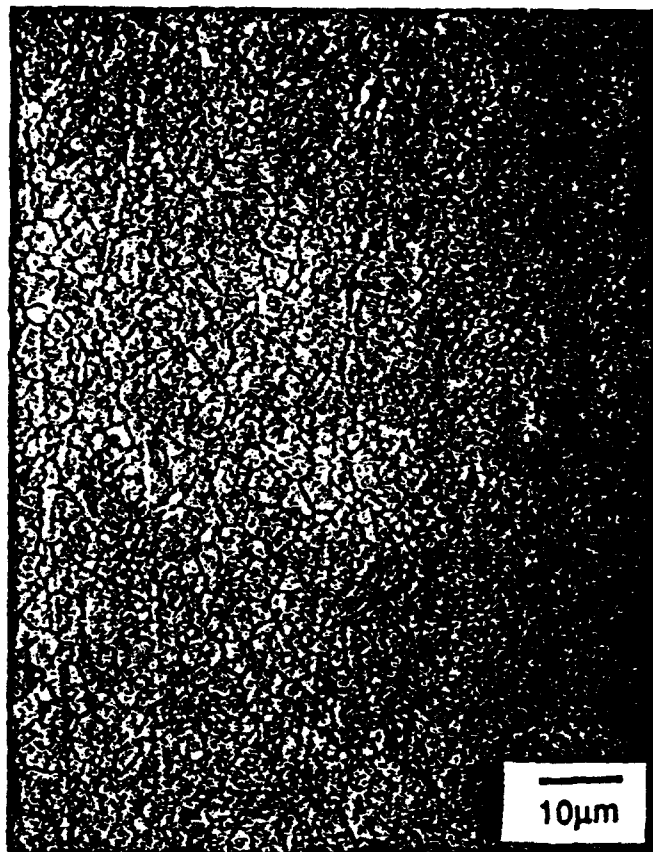


FIG. 13

X-RAY INTENSITY (ARB. UNITS)

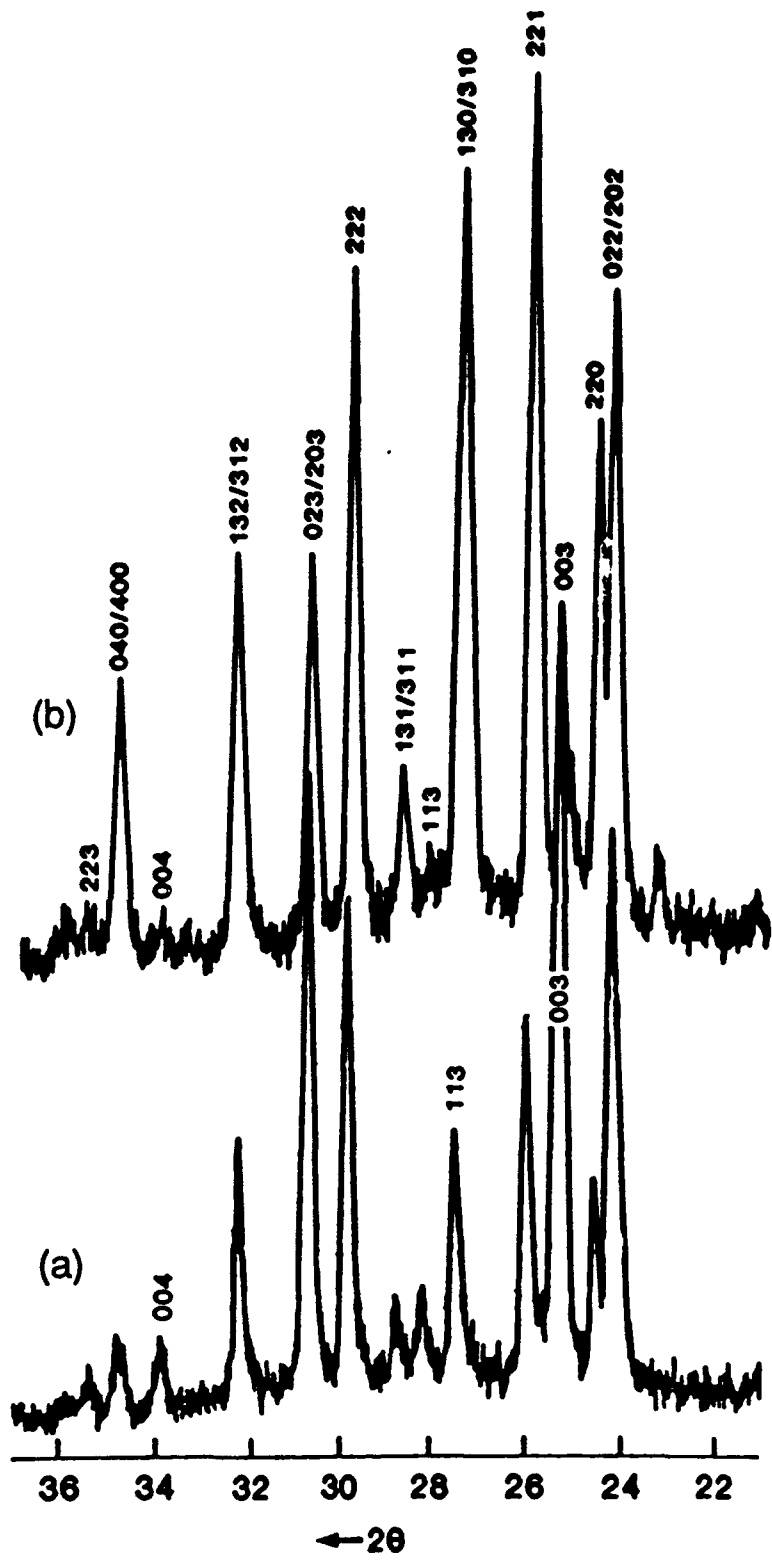


FIG. 14

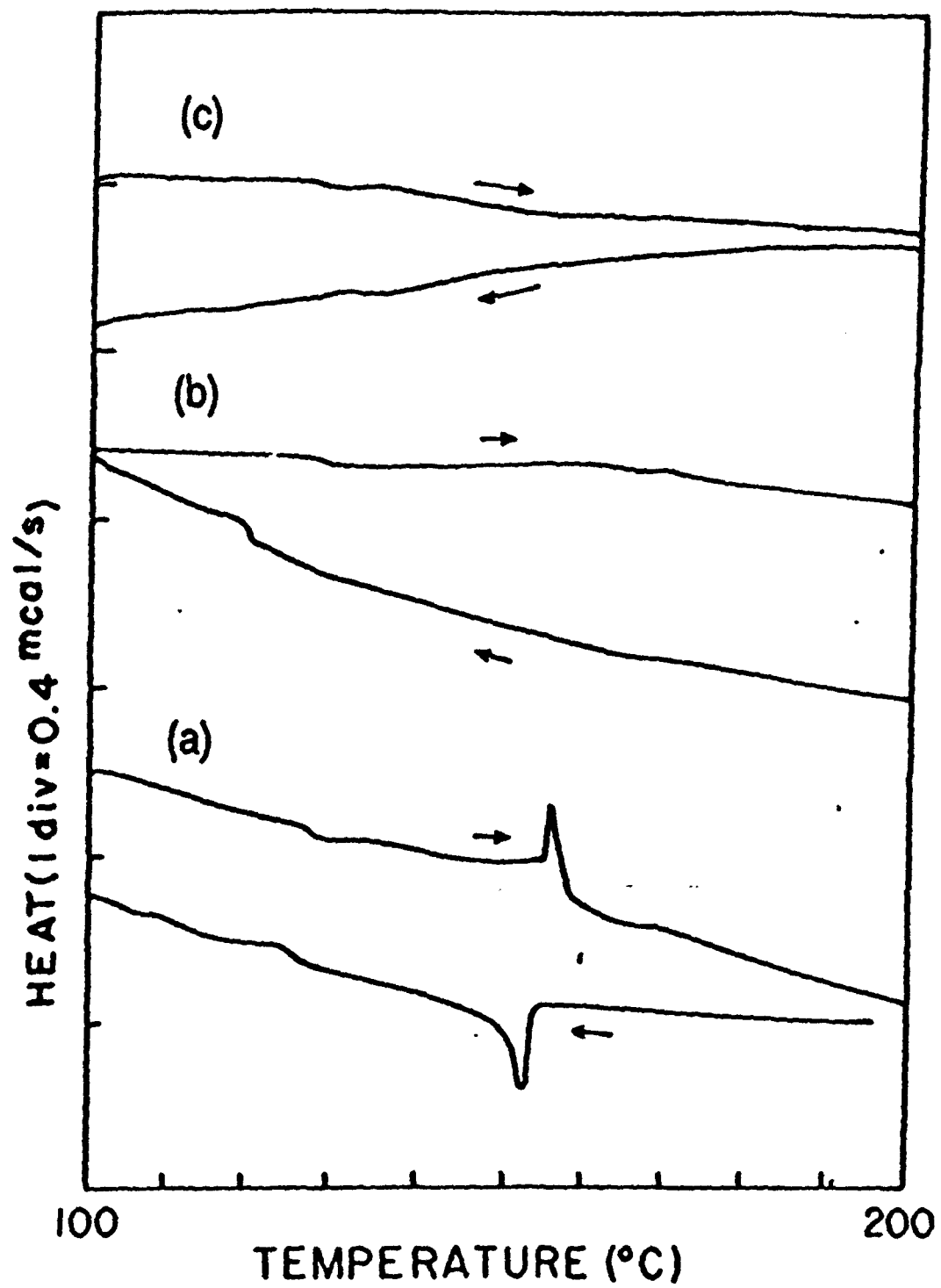


FIG. 15

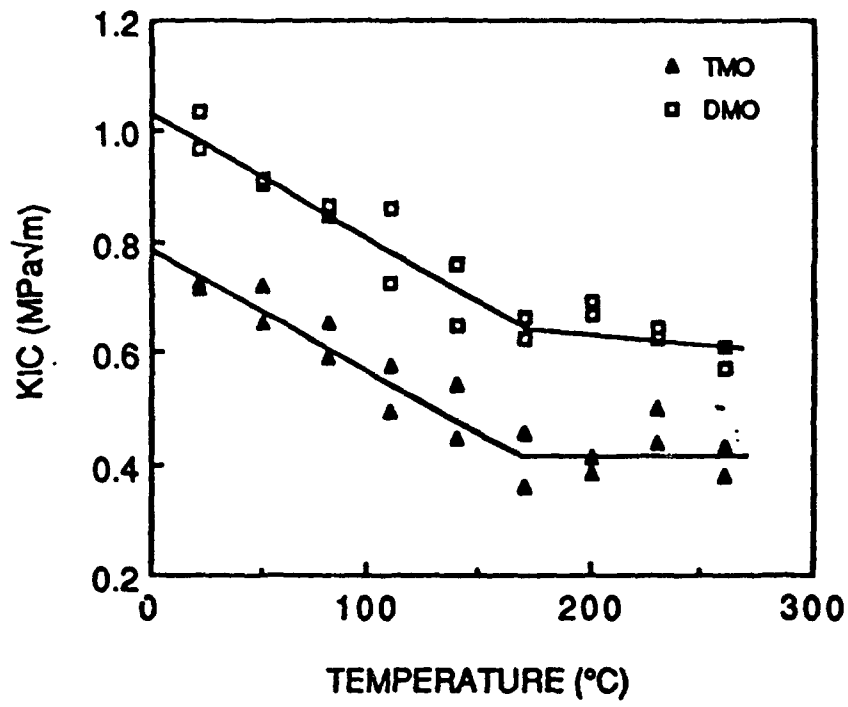


Fig. 16

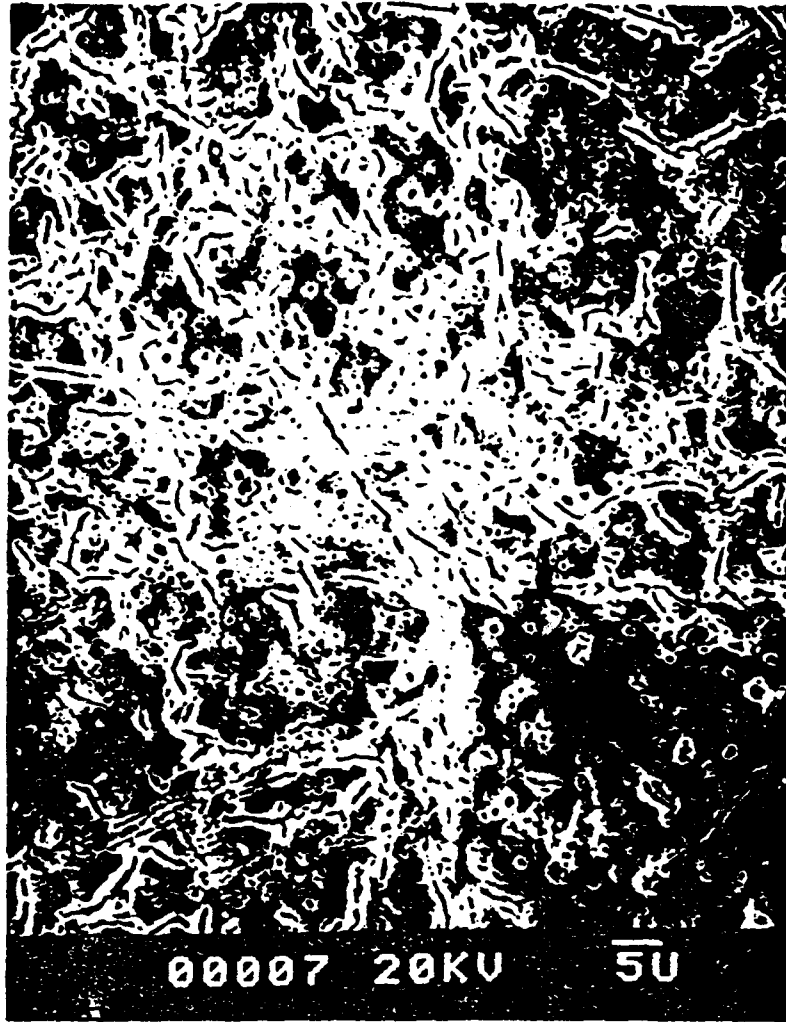


FIG. 17

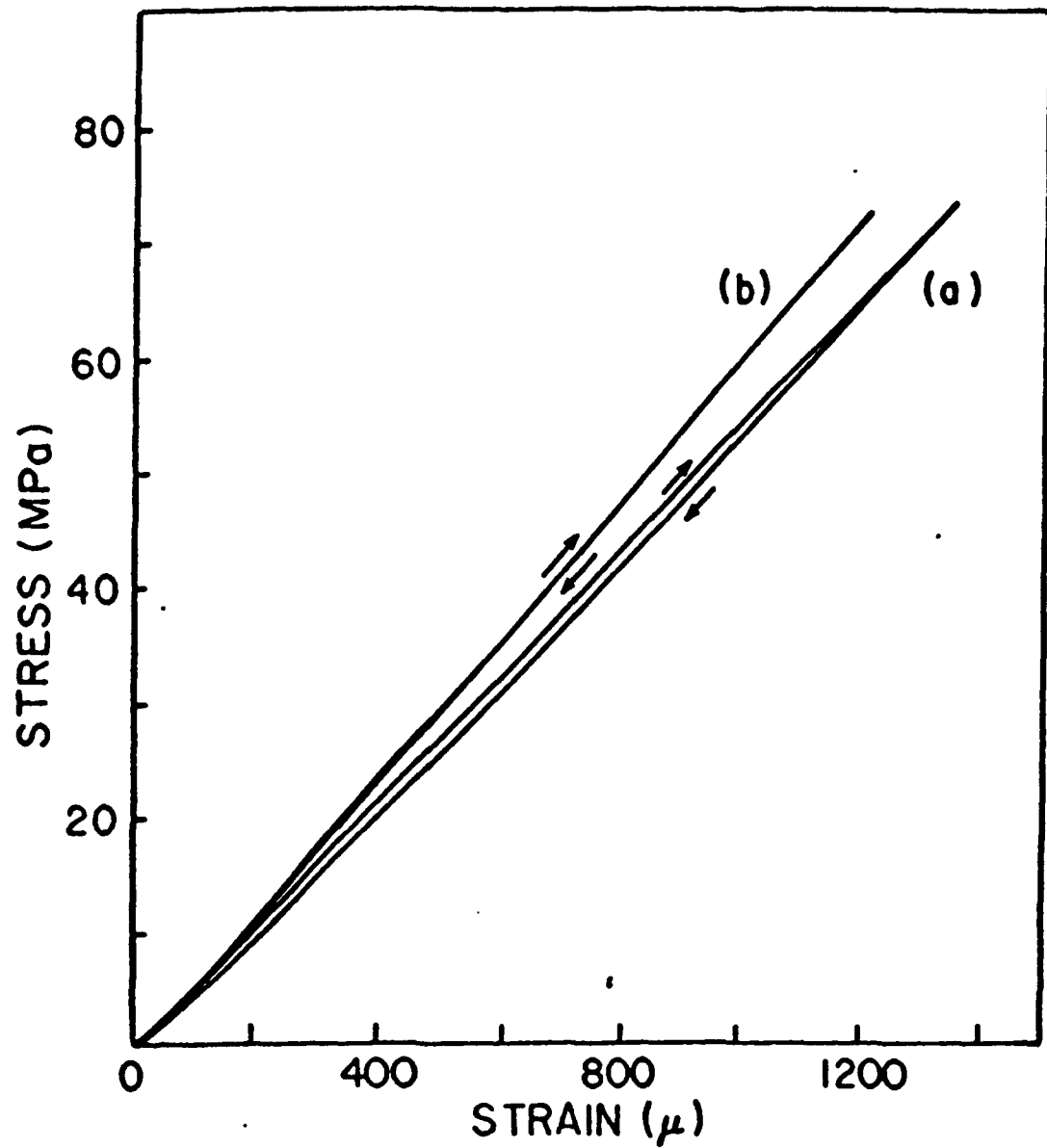


FIG. 18

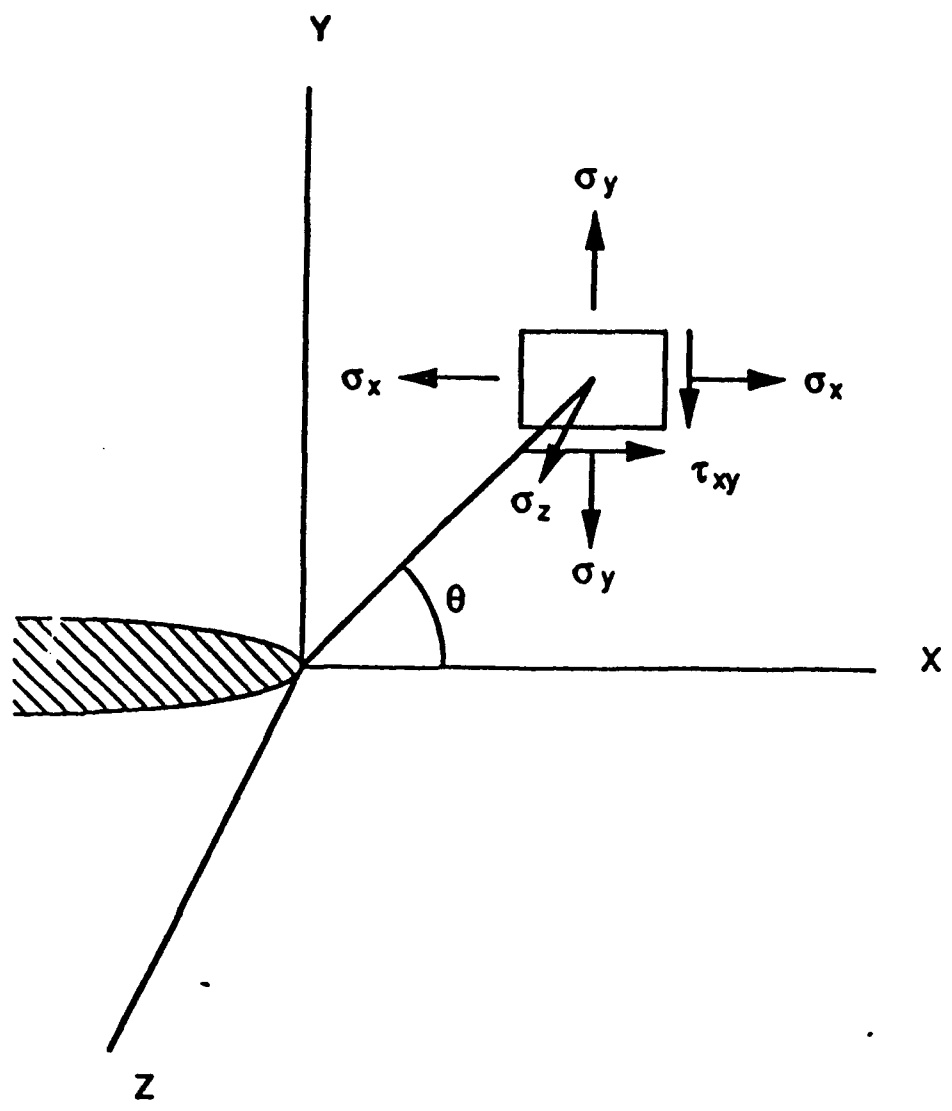


FIG. 19

# CHARACTERIZATION OF t' PHASE IN Ce-TZP MATERIALS.

by

Jan Fong Jue, Jong Chen, and A. V. Virkar

Department of Materials Science & Engineering

University of Utah

Salt Lake City, Utah 84112

## ABSTRACT

Polycrystalline, tetragonal (t') zirconia samples containing 12-20 mol% CeO<sub>2</sub> were fabricated by annealing pressureless sintered samples in air at 2050°C for 15 minutes. The existence of herringbone structure, three tetragonal variants, and antiphase boundaries, all representative of the t' phase, was confirmed using electron microscopy. The fracture toughness of these materials decreased with increasing CeO<sub>2</sub> content, from 13.88 MPa√m for 12 mol% CeO<sub>2</sub> materials to 8.4 MPa√m for 14 mol% CeO<sub>2</sub> materials. Polished t' samples exhibited extensive surface uplift after unidirectional compression tests, while no change was detected in monoclinic phase content on these surfaces. In-situ XRD revealed that domain reorientation took place before the tetragonal to monoclinic phase transformation during four point bending tests. The mechanical properties of t' phase Ce-TZP materials could thus be attributed to ferroelastic and subsequent transformation-based toughening.

## **I. Introduction:**

Ceria stabilized-tetragonal zirconia polycrystal (Ce-TZP) materials exhibit moderate strengths and high toughnesses [1-6]. A significant amount of phase transformation occurs during the fracture process and this contributes to the high toughness of Ce-TZP materials. The transformation zone formation prior to fracture in Ce-TZP materials has been studied extensively [2-6]. Ce-TZP materials, unlike yttria partially stabilized zirconia, do not experience degradation of their mechanical properties at low temperature by spontaneous tetragonal to monoclinic phase transformation on the surface [7]. However, their properties are very sensitive to process parameters like sintering temperature, because the transformability of Ce-TZP is reported to be very sensitive to grain size [6].

In order to enhance transformability and thereby improve the fracture toughness and the mechanical properties of Ce-TZPs, traditionally, only the as-sintered tetragonal phase has been considered desirable. Miller et al., however, reported the existence of another useful tetragonal phase called  $t'$  zirconia in the yttria-stabilized zirconia system [8]. This zirconia phase is the major phase in plasma sprayed protection coatings in engine applications. With such a zirconia coating, the operation temperature of engines could be raised 150°C above normal operating temperatures. The mechanical properties of yttria stabilized  $t'$  zirconia have been studied by Jue et al. [9]. The  $t'$  phase has good phase stability under mechanical stress and is not susceptible to low temperature aging degradation [9,10]. The existence of  $t'$  phase in ceria-stabilized zirconia systems also has been reported, but only limited amount of information exists in the literature [11-14]. Also, most of these works are on high CeO<sub>2</sub> content materials (20-60 mol% CeO<sub>2</sub>) sintered or heat treated at ~1700°C and thus, a direct comparison of these data with the well studied Ce-TZP (12-16 mol% CeO<sub>2</sub>) materials is difficult to make. Ingel et al. fabricated samples of  $t'$  phase by the rapid solidification process using lower (~15 mol%) CeO<sub>2</sub> content. But evaluation of these materials was limited only to microstructural studies [13].

The cubic-phase range temperatures of the pure zirconia system is different in air as compared to reducing atmospheres [15]. Accordingly, the phase diagram of ceria-zirconia system has been revised recently [16,17]. However, some inconsistencies still exist. The exact tetragonal to cubic transformation temperatures were not properly determined. For materials with less than 20 mol% CeO<sub>2</sub>, the single phase cubic stability temperature is expected to be higher than 2000°C according to the existing phase diagram [15]. The high vapor pressure of CeO<sub>2</sub> at high temperatures (>1800°C) causes evaporation of ceria during heat treatment in the cubic-phase range at a temperature higher than 2100°C. On the other hand, heat treatment in an inert atmosphere would require lower temperatures but creates the problem of ceria getting reduced. Thus, in this work, to obtain the t' phase, heat treatment was conducted in air at a temperature of about 2050°C.

The formation of the t' phase is characterized by the following: (1) the existence of herring bone structure in the grain, (2) the presence of antiphase boundaries, and (3) the existence of three variants in the as heat treated samples. Typically, Ce-TZP materials sintered in the single phase tetragonal region will lack these features which are unique to the t' phase formed by the cubic to tetragonal phase transformation during cooling. Since this tetragonal phase is expected to exhibit ferroelastic properties based on group theory [18,19], the variants would tend to rearrange themselves when a mechanical stress is applied.

In this study, the t' phase of zirconia stabilized with low ceria content (less than 20 mol%) was fabricated by heat treating presintered Ce-TZP samples at 2050°C in air followed by rapid cooling. The microstructure and fracture toughness of these t' materials were characterized. Properties of these t' materials were compared to those of a regular Ce-TZP material that was only sintered at 1550°C for 2 hours.

## **II. Experimental Procedure**

### **(i) Sample fabrication**

Commercial zirconia and ceria powders were mixed in required proportions (containing 12 to 50 mol% CeO<sub>2</sub>) in cyclohexane, ball milled for 24 hours, pan dried, sieved through a -200mesh screen and then pressed into bars by die pressing at 5000psi and cold isostatic pressing at 30000psi. The green formed samples were sintered at 1550°C for 2 hours. Some of the as sintered samples (containing 12-20 mol% CeO<sub>2</sub>) were heated at 2050°C in air in a gas-fired furnace. After holding the samples at temperature for 15 minutes, the platform of the furnace was lowered to a cooler portion of the furnace (~ 1200°C) and then allowed to cool further by furnace cooling. The fast cooling was done to prevent phase separation by a diffusion mechanism at high temperatures. The samples fabricated in this manner did not crack even though the grains were as large as 100µm, or larger. A high temperature treatment of compositions with even lower CeO<sub>2</sub> content was not conducted because of the possible depletion of ceria due to evaporation at temperatures of about 2100°C. To obtain samples with more than 30 mol% CeO<sub>2</sub>, bar specimens were directly sintered at 1700°C for two hours, since the single phase cubic temperatures of stability in CeO<sub>2</sub>- ZrO<sub>2</sub> system is less than 1700°C for materials with more than 30 mol% CeO<sub>2</sub> content.

### **(ii) Sample characterization:**

**X-ray Diffraction:** X-ray diffraction (with Cu K $\alpha$ ) was conducted to identify the phases present on polished, ground, and fractured surfaces of selected samples, and surfaces of samples subjected to compressive tests. The accelerating voltage was 30 KV and the tube current was 30 mA.

**Optical and Scanning Electron Microscopy:** The heat treated samples were examined using optical microscopy for grain size and microstructure. SEM was used to reveal finer details

of the microstructure inside the grains. Prior to microstructure analysis samples were thermally-etched at 1400°C for 1 hour. This temperature corresponds to the stability of the tetragonal single-phase region, so no phase separation was expected during this treatment. Some of the samples were mechanically thinned down to less than 100µm thickness, then ion-beam thinned down to 30µm and examined under cross-polarized, transmitted light to reveal the fine microstructure within the grain. Some samples after mechanical testing (i.e. compression tests) were examined under a microscope equipped with Nomarski interference contrast capabilities in order to characterize the deformation bands formed as a result of transformation or other mechanisms.

Transmission Electron Microscopy: A few representative samples were dimpled and ion-milled to perforation and examined under a transmission electron microscope. The objectives were to determine the existence of the three variants and antiphase boundaries in heat treated samples (as predicted by the group theory), and observe the domain structures change before and after mechanical stressing.

Mechanical Testing: Several parallelepipeds of both t and t' Ce-TZP materials of dimension 3mm x 4mm x 8mm were subjected to unidirectional-compression loading along their long direction. The samples were subjected to a stress of 800MPa. XRD and OM with Nomarski interference contrast were used to determine the deformation mechanisms in the t and t' materials. Fracture toughnesses of some of these materials were determined by an SENB method. Some samples were subjected to in - situ XRD experiments in bending to determine the stress required for t to m phase transformation and the stress required for domain reorientation.

### **III. Results:**

The optical micrograph of Figure 1 shows that samples after heat treatment at 2050°C exhibit no cracking due to tetragonal to monoclinic phase transformation. Samples after heat treatment at 2050°C and etching at 1400°C revealed grains of size about 100µm. In regular Ce-TZP materials, above a critical grain size - which is typically less than 5 µm, spontaneous t to m transformation occurs upon cooling and causes significant cracking of the specimens. However, in contrast to the regular Ce-TZP t phase materials, the heat treated Ce-TZP samples did not crack despite their much larger grain sizes. XRD of the polished surfaces showed evidence of trace amount of (if any) monoclinic phase in these large grained materials. The low transformability of these samples after heat treatment suggested that this material should be the t' phase which has been well studied in the yttria - zirconia systems and reported for ceria-zirconia systems when cooling from the melt [13]. The c/a ratio of these materials are shown in Figure 2. The c/a ratios for t' materials are similar to those reported for regular Ce-TZP materials [1].

A few heat treated samples were dimpled to a thickness of about 30µm and examined using transmission optical microscopy (TOM). The domain-like structure as seen in Figure 3 is similar to that observed in the yttria - zirconia system. Since the size of these regions is larger than 1 µm, these features most likely represent colonies (assembly of domains) instead of individual domains. Some of the heat treated, polished, and thermally etched samples were examined under scanning electron microscopy in order to reveal the fine structure inside the grains. An SEM micrograph of one such sample containing 12 mol% CeO<sub>2</sub> is shown in Figure 4. Previous research has shown that this kind of fine structure exists in the Ce-TZP samples (containing more than 20 mol% CeO<sub>2</sub>) heat treated in the cubic phase temperature range [14].

The group theory predicts the existence of three different variants and antiphase boundaries because of the symmetry reduction from the high temperature cubic phase (Fm3m) to the

low temperature tetragonal phase (4/mmm)[18,19]. The occurrence of this phenomenon in going from the cubic to tetragonal phase could be verified by TEM examination. Samples after high temperature heat treatment were dimpled and then ion beam thinned. The bright field TEM image of Figure 5 shows the existence of the herringbone structure - a characteristic morphology of the t' phase. Whereas, the TEM bright field image of the t phase Ce-TZP regular materials shows featureless grains. This is consistent with the prediction that the samples that have not been heat-treated in the cubic phase temperature range would have single domain structure within grains. Figure 6 represents a selected area diffraction (SAD) of the  $\langle 111 \rangle$  zone axis. It reveals the existence of three sets of the 112 fluoride forbidden spots. In contrast, an SAD from a sample without heat treatment (as depicted by Figure 7), shows only one set of such forbidden spots. Finally, the dark field image from one of the 112 fluoride forbidden spots in Figure 6 showing the existence of the antiphase boundaries is indicated by arrows in Figure 8. Thus, from the TEM micrographs, it is established that the tetragonal phase found in the heat treated samples is the t' phase which formed through a ferroic cubic to tetragonal phase transformation. On the other hand, in the regular Ce-TZP materials (with less than 20 mol% CeO<sub>2</sub>) sintered at 1550-1600°C only one variant (single domain) exists in a grain after sintering.

Some of the heat treated samples were subjected to uni-directional compression tests at room temperature. The samples were stressed to 800MPa, and the stress released shortly. These stressed samples were then subjected to OM and XRD examinations. The polished surface of samples after the compression test revealed some surface uplift (or deformation bands). This can be seen in the micrograph of Figure 9. Such features would normally be interpreted as t to m transformation in regular Ce-TZP materials. However, the XRD revealed no change in the monoclinic phase content on the surface before and after stressing. It has to be noted here that the cubic to tetragonal phase transformation is known to be ferroelastic in nature. The surface uplifts due to mechanical stress can thus be

explained to be a result of the ferroelastic domain reorientation. This is justified by the TEM analysis also. The SAD micrograph of Figure 10 suggests that one set of the three sets of 112 fluorite forbidden spots became very weak and the area corresponding to this variant became very small in the dark field mode image of these spots obtained after stressing the sample. The possibility of reverse transformation that could occur during the unloading process should be considered. Reverse transformation occurs when the tetragonal phase that transformed to monoclinic phase during loading, transforms back to tetragonal symmetry after unloading. Arguably, this is consistent with no change in monoclinic phase contents as detected by XRD. However, the constancy of monoclinic phase contents before and after stressing could be due to no transformation also. In order to examine this issue, thin bar samples were polished on one side and subjected to in-situ XRD examination under bending, as done previously for yttria-zirconia t' materials [9]. The stress applied in bending was 500MPa. The ratio of XRD peak intensities  $I_{002}/I_{200}$  and  $I_{113}/I_{311}$  decreased from 0.94 to 0.7 and 1.36 to 0.31, respectively, under the application of stress. However, the percentage of monoclinic phase remained unchanged after stressing. This experiment demonstrates that the stress required for tetragonal to monoclinic phase transformation is higher than that for domain reorientation in the ceria-zirconia system. This is similar to the observations made on the yttria-zirconia system [9]. Accordingly, it can be inferred that at stresses such as those in our experiments, domain reorientation occurred regardless of any tetragonal to monoclinic phase transformation or subsequent reverse transformation.

The fracture toughness values of the tetragonal (t') phase obtain by high temperature heat treatment are 13.88, 12.45, and 8.4 MPa $\sqrt{m}$  for materials containing 12, 13 and 14 mol% CeO<sub>2</sub>, respectively. Unlike the regular Ce-TZP materials which typically have 80 or more vol% monoclinic phase on the fracture surface, the XRD from the fracture surface of t' materials revealed only about 30 % monoclinic phase. This implies that some tetragonal to monoclinic transformation occurs prior to fracture in the t' phase materials also, but only

after domain reorientation. However, it is interesting to note that the fracture toughness is similar for samples with or without heat treatment. This could be explained to be due to the increased relative contribution of ferroelastic toughening as compared to tetragonal to monoclinic transformation toughening in the t' materials.

#### **IV. Discussion:**

According to the group theory both the t and t' materials should exhibit ferroelastic behavior. Thus, when a stress is applied to tetragonal materials, the domains tend to rearrange themselves in order to accommodate the stress. The t materials sintered in the tetragonal region have a single domain structure within a grain, whereas, t' materials exhibit a multi-domain structure due to the cubic to tetragonal phase transformation. The experimental results of this study confirm the ferroelastic nature of t' materials as predicted by the group theory. In an earlier study, the stress required to activate the transformation toughening mechanism was found to be higher than the stress required to cause domain reorientation in yttria-zirconia systems [9]. The same is the case with the ceria-zirconia system of this study. However, it is likely that the stresses required to activate the transformation toughening mechanisms are not very much higher than that for domain reorientation in the ceria t' materials, because monoclinic phase could be detected by XRD method on the fracture surfaces.

Numerous studies in the past have attempted to relate the ability of transformation to grain size. This work clearly shows that microstructural features other than grain size could, in fact, be the dominant factor in governing transformation effects. The grain size of t' materials of this study were as large as 100 $\mu\text{m}$  while that of regular Ce-TZP materials is usually less than 10 $\mu\text{m}$ . However, it is of great significance to note that the former has better resistance to the tetragonal to monoclinic phase transformation upon stressing, despite its much larger grain size. It can, thus, be stated that in the yttria - zirconia and ceria

- zirconia systems. the ability of transformation in t' materials should actually relate to the domain size, geometry, and compositions instead of grain size .

The fracture toughnesses measured for the ceria-zirconia t' phase materials of this study are higher than that for the yttria - zirconia t' materials. This may be explained by the additional contribution to toughness arising from the tetragonal to monoclinic phase transformation during fracture occurring in ceria - zirconia systems, unlike the yttria-stabilized zirconias where no monoclinic phase could be detected on the fracture surface of stressed samples. However, the amount of monoclinic phase detected on the fracture surface are about the same for 12 and 14 mol% CeO<sub>2</sub> stabilized zirconia materials even though their fracture toughness are very different (13.88 and 8.4 MPa√m, respectively).

It was earlier noted that the t-phase materials should also be expected to exhibit ferroelasticity. Accordingly, a mechanical stress should generate extra variants in t materials also, if the stresses required for tetragonal to monoclinic phase transformation are higher than that for creation of domains with different orientation within grains. In one previous study, SAD along the <111> zone axis did reveal the existence of an extra variant after compression tests. TEM bright field image also showed twin like structure in a regular TZP grain [2]. Thus, it is possible that in regular Ce-TZP t phase materials also, domain reorientation occurred before the tetragonal to monoclinic phase transformation process but was overshadowed by the transformation effects. Future research is, therefore, required to investigate ferroelasticity and its effects in regular Ce-TZP materials.

### **Conclusions:**

1) t' phase materials in the ceria-zirconia systems, containing less than 20 mol% ceria stabilizer have been fabricated by heat treating presintered Ce-TZP materials at 2050°C in air. The existence of t' phase was confirmed by TOM, SEM, and TEM examinations.

2) The toughness of ceria-zirconia t' phase materials decreases with increasing ceria content. The toughness values are 13.88 MPa√m for t' materials containing 12 mol% CeO<sub>2</sub> and 8.4 MPa√m for those with 14 mol% CeO<sub>2</sub>. The fracture toughnesses of the t' materials are comparable to that of the regular Ce-TZP materials despite significantly lower tetragonal to monoclinic phase transformation during fracture. The tetragonal to monoclinic phase transformation toughening mechanism is not the only toughening mechanism in t' phase Ce-TZPs.

3) The ferroelastic characteristics of t' materials in the ceria-zirconia system which are similar to that in the yttria-zirconia system have been identified. Under mechanical stress, both t and t' materials can create or annihilate tetragonal variants in order to accommodate the mechanical stresses. The surface uplift after compression tests could be explained based on the ferroelastic nature of the tetragonal phase. This agrees well with the fact that stress required for tetragonal to monoclinic phase transformation is higher than that required to activate the domain reorientation process in 12-14 mol% Ce-t' zirconia systems.

**Acknowledgements:** This work is supported by DARPA through AFOSR under Contract Number F49620-89-C-0054; subcontract from Ceramtec, Inc. to the University of Utah.

**References:**

- 1) K. Tsukuma and M. Shimada, "Strength, Fracture Toughness and Vickers Hardness of CeO<sub>2</sub>-Stabilized Tetragonal ZrO<sub>2</sub> Polycrystals (Ce-TZP)," *J. Mater. Sci.*, **20** 1178-1184, (1985).
- 2) K. M. Prettyman, "Ferroelastic Domain Formation and Switching as A Toughening Mechanism in Ceria-Doped Zirconia," Ph.D Thesis, University of Utah, (1992).

- 3) C. S. Yu and D. K. Shetty, "Transformation Zone Shape, Size, and Crack-Growth-Resistance (R-Curve) Behavior of Ceria-Partially-Stabilized Zirconia Polycrystals," *J. Am Ceram. Soc.*, **72** [6] 921-928 (1989).
- 4) P. E. Reyes-Moral and I. W. Chen, "Transformation Plasticity of CeO<sub>2</sub>-Stabilized Tetragonal Zirconia Polycrystals: I, Stress Assistance and Autocatalysis," *J. Am Ceram. Soc.*, **71** [5] 343-353 (1988).
- 5) L. R. F. Rose and M. V. Swain, "Transformation Zone Shape in Ceria-Partially-Stabilized Zirconia," *Acta Metall.*, **36** [4] 955-962, (1988).
- 6) C. S. Yu, "Stress-State Effect on Transformation Yield Stress and Fracture Toughness on Zirconia Ceramics" Ph.D. Thesis, University of Utah, (1991).
- 7) R. L. K. Matsumoto, "Aging Behavior of Ceria-Stabilized Tetragonal Zirconia Polycrystals" *J. Am Ceram. Soc.*, **71** [3] 125-127 (1988).
- 8) R. A. Miller, J. L. Smialek, and R. G. Garlick, "Phase Stability in Plasma-Sprayed, Partially Stabilized Zirconia-Yttria," pp241-253 in *Advances in Ceramics*, vol.3. Edited by A. H. Heuer and L. W. Hobbs. American Ceramic Society, Columbus, OH, 1981.
- 9) J. F. Jue and A. V. Virkar, "Fabrication, Microstructural Characterization, and Mechanical properties of Polycrystalline t'-Zirconia," *J. Am. Ceram. Soc.*, **73** [12] 3650-3657, (1990).
- 10) J. F. Jue, J. Chen, and A. V. Virkar, "Low Temperature Phase Stability of t' zirconia," *J. Am. Ceram. Soc.*, **74** [7] 1745-1750, (1991).
- 11) M. Yashima, K. Morimoto, N. Ishizawa, and M. Yoshimura, "Zirconia-Ceria Solid Solution Synthesis and the Temperature-Time-Transformation Diagram for the 1 : 1 Composition," *J. Am. Ceram. Soc.*, **76** [7] 1745-1750, (1993).
- 12) Y. Zhou, "Microstructural Development of Sintered ZrO<sub>2</sub>-CeO<sub>2</sub> Ceramics," *Ceram. Int.*, **17**, 343-346 (1991).
- 13) R. P. Ingel, D. Lewis III, B. A. Bender, and S. C. Semken, "Properties and Microstructures of Rapidly Solidified Zirconia-Based Ceramic Alloys," pp385-396 in *Advances in Ceramics*, vol.24. Edited by S. Somiya, N. Yamamoto, and H. Yanagita. American Ceramic Society, Westerville, OH, 1988.
- 14) S. Meriani, "Feature of the Caeria-Zirconia Systems," *Materials Science and Engineering*, **A109** 121-130, (1989).
- 15) R. Ruth and H. J. Garrett, "Nonstoichiometry of ZrO<sub>2</sub> and Its Relation to Tetragonal-Cubic Inversion in ZrO<sub>2</sub>," *J. Am. Ceram. Soc.*, **50** [5] 257-261, (1967)..
- 16) M. Yoshimura, "Phase Stability of Zirconia," *Am. Ceram. Soc. Bull.*, **67** [12] 1950-1955, (1989).
- 17) P. Duran, M. Gonzalez, C. Moure, J. R. Jurado, and C. Pascual, "A New Tentative Phase Equilibrium Diagram for the ZrO<sub>2</sub>-CeO<sub>2</sub> system in air," *J. Mater. Sci.*, **25** 5001-5006, (1990).

18) K. Aizu, "Possible Species of Ferromagnetic, Ferroelectric, and Ferroelastic Crystals," *Phys. Rev. B*, **2** [3], 754-772, (1970).

19) D. Michel, L. Mazerolles, and M. Perez y Jorba, "Fracture of Metastable Tetragonal Zirconia Crystals," *J. Mater. Sci.*, **18**, 2618-2628, (1983).

### Figure Caption

- Figure 1.** Optical micrograph showing the grain size of a 12 mol% Ce-TZP sample after heat treatment at 2050°C.
- Figure 2.**  $c/a$  ratio vs. compositions in  $t'$  phase Ce-TZP materials
- Figure 3.** Transmission optical micrograph (TOM) under cross polarized light shows the domain structure of a 12 mol% Ce-TZP sample after heat treatment at 2050°C.
- Figure 4.** Scanning electron micrograph showing the domain structure within the grain of a 12 mol% Ce-TZP samples after heat treated at 2050°C.
- Figure 5.** Bright-field electron micrograph shows the herringbone structure of a 12 mol% Ce-TZP samples after heat treated at 2050°C.
- Figure 6.** A  $\langle 111 \rangle$  zone axis selected area diffraction (SAD) pattern of a 12 mol% Ce-TZP sample heat treated at 2050°C.
- Figure 7.** A  $\langle 111 \rangle$  zone axis selected area diffraction (SAD) pattern of a regular 12 mol% Ce-TZP  $t'$ -phase sample.
- Figure 8.** Dark field electron micrograph revealing the antiphase boundaries in a 12 mol% Ce-TZP sample heat treated at 2050°C.
- Figure 9.** Nomarski interference-contrast optical micrograph showing surface uplift of a 12 mol% CeO<sub>2</sub>  $t'$  phase sample that was subjected to a unidirectional compressive stress of 800MPa.
- Figure 10.** A  $\langle 111 \rangle$  zone axis selected area diffraction pattern of a 12 mol% Ce-TZP  $t'$  phase sample after unidirectional compression testing. Note that one set of 112 spots has become very weak.

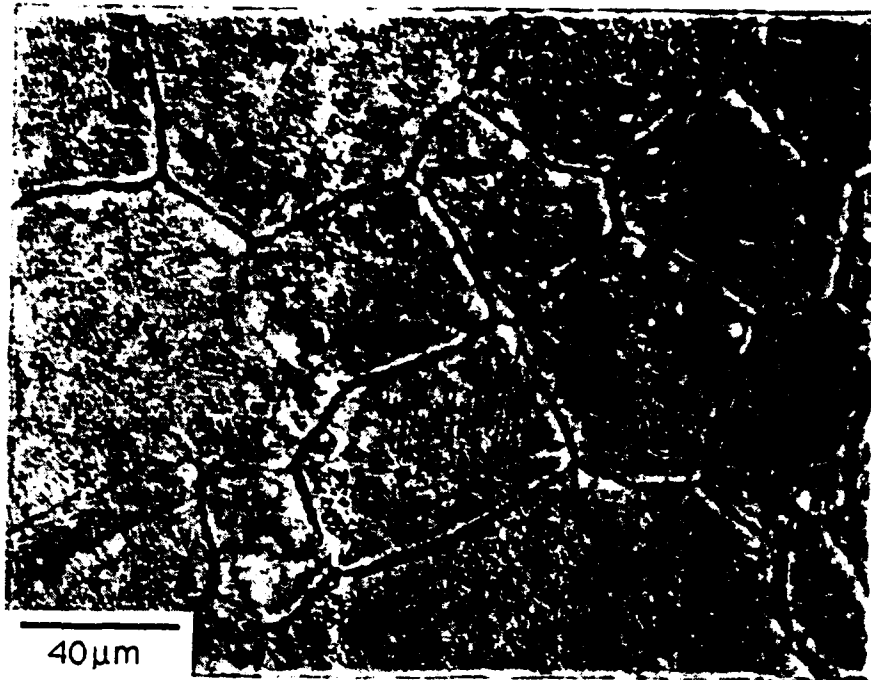


Figure 1

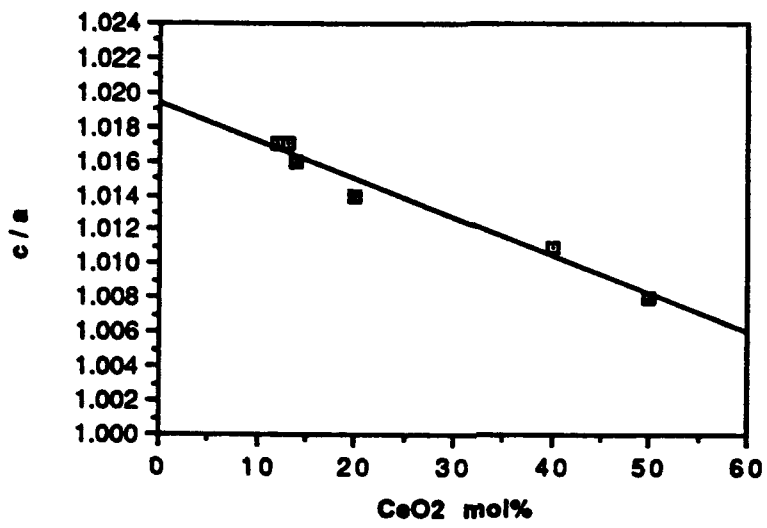


Figure 2

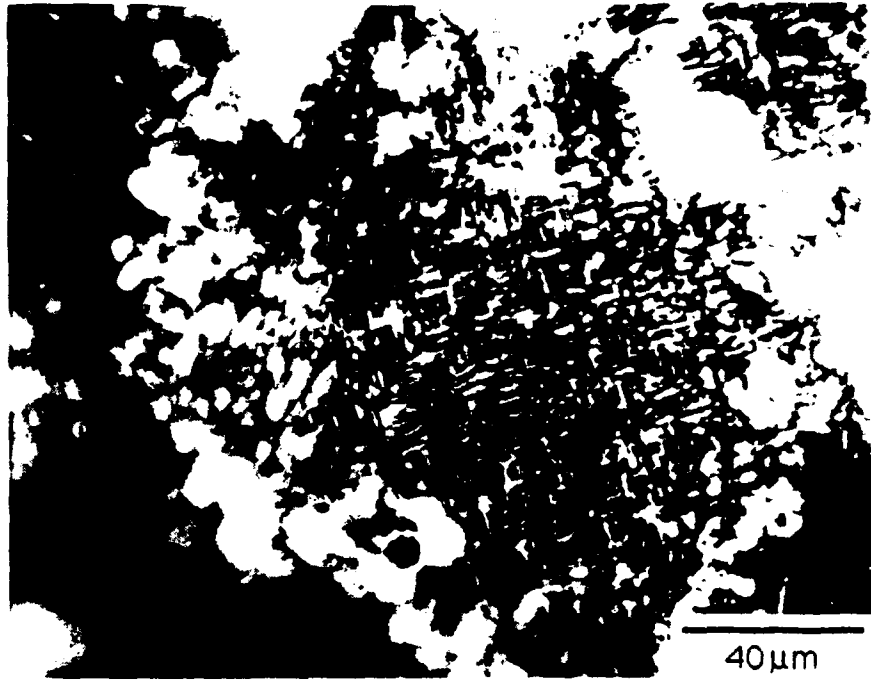


Figure 3

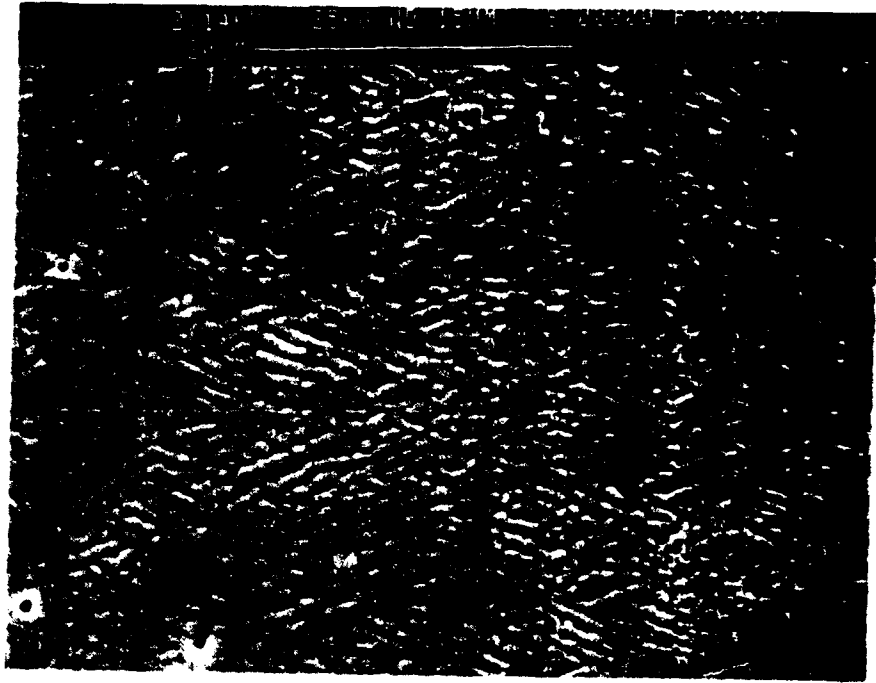


Figure 4



Figure 5

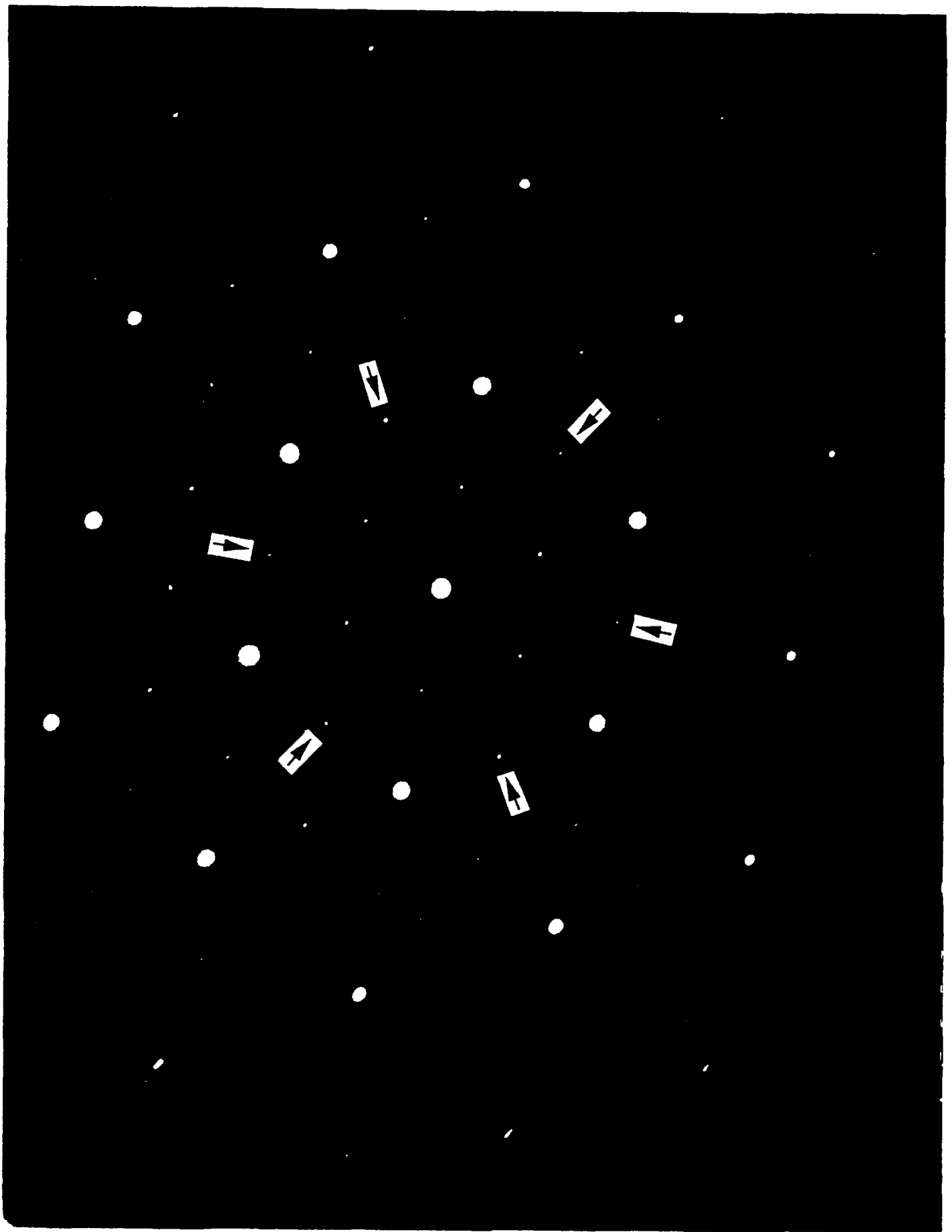


Figure 6

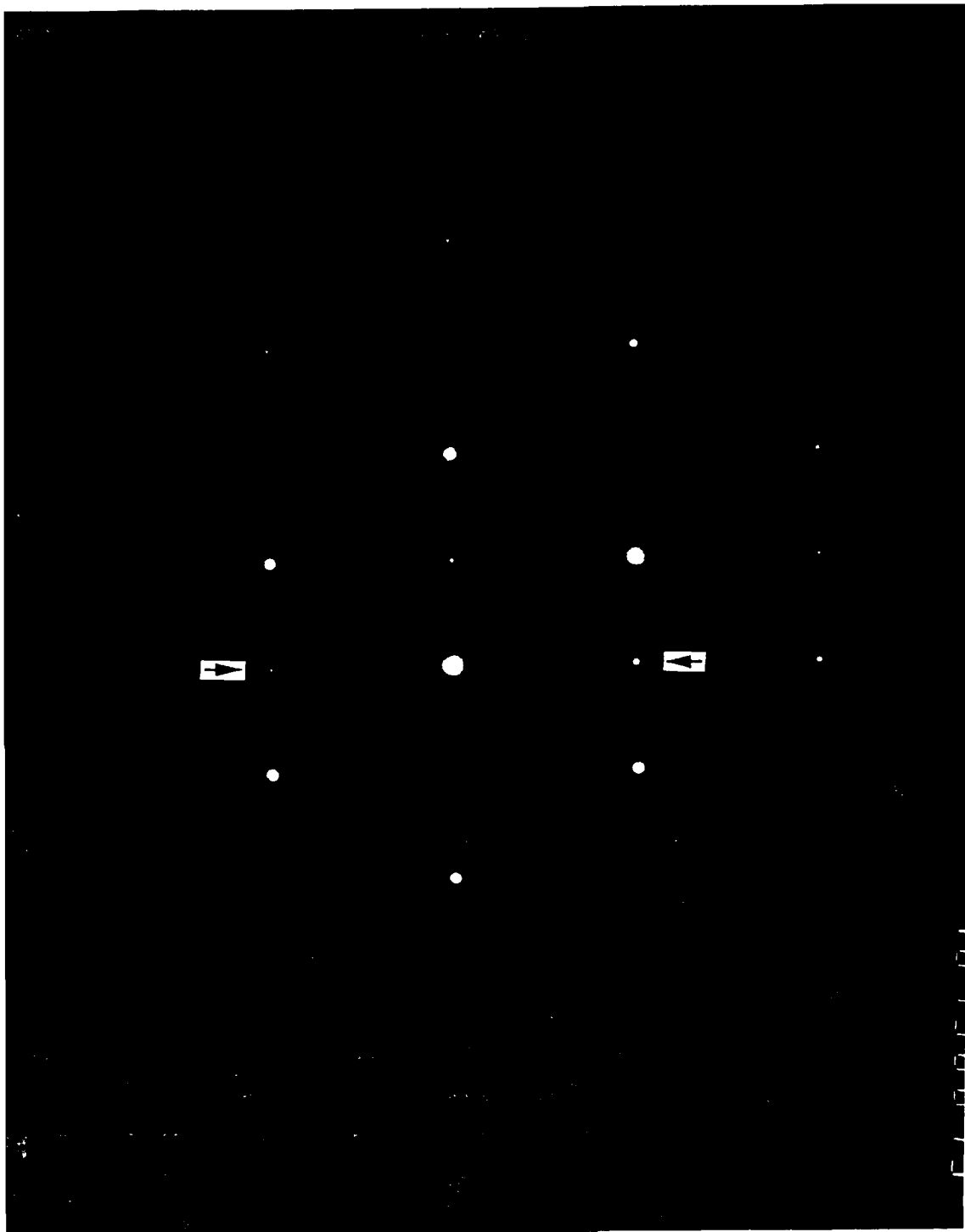
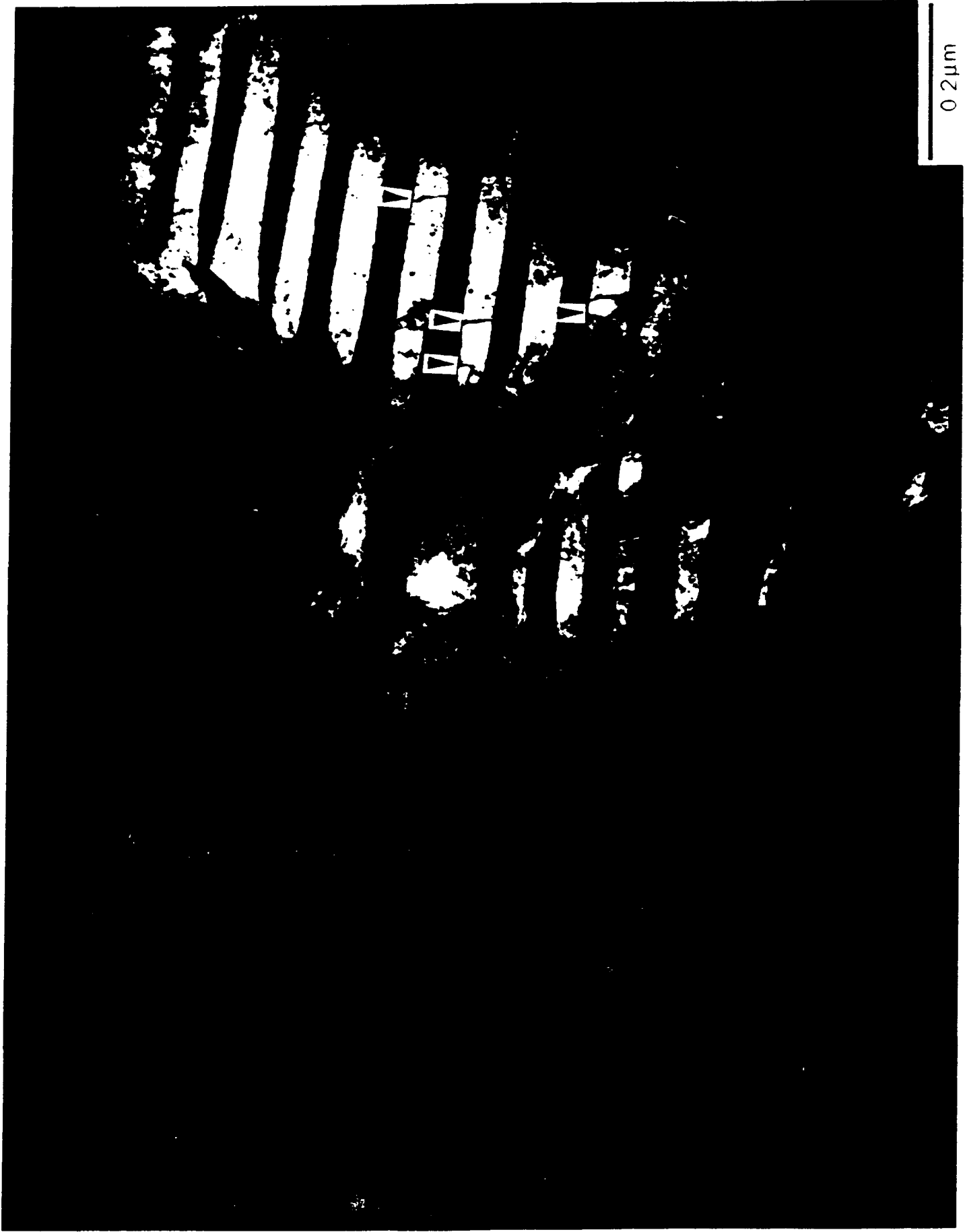


Figure 7

FIGURE CAPTIONS

Figure 1(a): An optical microscopy of a sample sintered at 2225°C for 10 minutes.



0.2  $\mu$ m



Figure 9

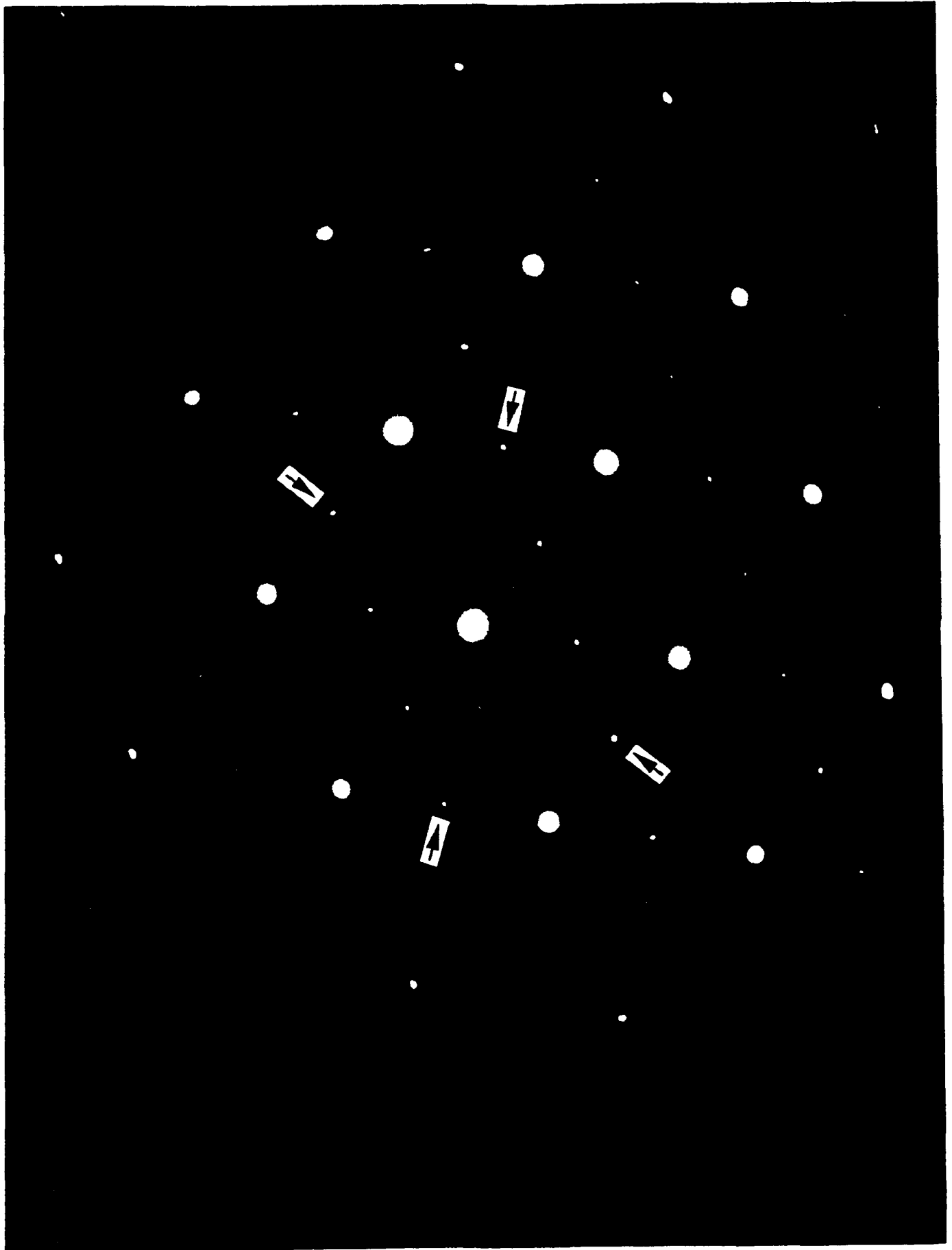


Figure 10

# Polycrystalline Polydomain Monoclinic Zirconia

Jong Chen and Anil V. Virkar  
Department of Materials Science, University of Utah, Salt Lake City, Utah  
84112

and

Raymond A. Cutler  
Ceramatec, Inc. Salt Lake City, Utah 84119

## ABSTRACT

Monoclinic zirconia samples without stabilizer were sintered from 1600° to 2225°C in Ar.  $ZrO_{2-x}$  sintered in the cubic stability regime could withstand the shape and volume change associated with the  $t \rightarrow m$  transformation, whereas samples sintered in the tetragonal stability field macrocracked upon cooling through the  $t \rightarrow m$  transformation. Twelve variants exist in the polycrystalline polydomain monoclinic  $ZrO_2$  cooled from the cubic phase field whereas only four variants result from the  $t \rightarrow m$  transformation. The larger number of variants in coarse-grained polycrystalline  $ZrO_{2-x}$  cooled from high temperatures allows stress accommodation so that macrocracking due to the shape and volume change is eliminated.

## I. INTRODUCTION

Zirconia is one of the most refractory oxide materials with a melting point of  $\approx 2700^\circ C$ [1].  $ZrO_2$  exists as three polymorphs: cubic (c) above  $\approx 2370^\circ C$ , tetragonal (t) between  $\approx 2370^\circ C$  and  $\approx 1050^\circ C$ , and monoclinic (m) below  $\approx 950^\circ C$ [2]. Upon heating, the  $m \rightarrow t$  temperature is  $\approx 1180^\circ C$ [2]. The  $t \rightarrow m$  transformation is a martensitic transformation and has generated great interest due to transformation toughening in a wide variety of ceramic systems containing  $ZrO_2$ [3]. Both the  $c \rightarrow t$  and the  $t \rightarrow m$  transformations are ferroelastic and as such twinning can accommodate stress associated with phase changes[4]. Virkar, et al.[5] have shown that toughening is possible due to ferroelastic phase transformations in a number of ceramic systems including partially stabilized zirconias. Despite its high melting point, monoclinic  $ZrO_2$  has not found use as an engineering material due to its large change in volume ( $\approx 4.5\%$ ) and shape ( $\approx 7\%$ ) during the  $t \rightarrow m$  transformation which causes cracking upon cooling. Cutler, et al.[6] suggested that monoclinic  $ZrO_2$  if cooled from the cubic stability regime could survive the  $t \rightarrow m$

transformations since domain formation accommodated stress. They showed that such samples could be cycled through  $m \leftrightarrow t$  transformations similar to polydomain single crystals formed by skull melting[7].

While it has been known for some time[8] that the  $c \rightarrow t$  transformation is displacive, Scott[9] showed that when arc-melted  $ZrO_2$ - $Y_2O_3$  alloys containing  $\approx 2$ -7 mol. %  $Y_2O_3$  were quenched rapidly the material was tetragonal and did not easily transform to monoclinic. These "non-transformable" tetragonal zirconias were designated  $t'$  to distinguish them from transformable  $t$ - $ZrO_2$ [10]. Distinguishing features of  $t'$ - $ZrO_2$  alloys in TEM are the three orthogonal variants which arise as a result of the diffusionless and displacive  $c \rightarrow t'$  transformation[11,12]. Jue and Virkar[13,14] showed that transmission optical microscopy (TOM) could reveal the orthogonal variants in coarse-grained  $t'$ - $ZrO_2$  although TEM was required to reveal the domain size. As expected, the  $t'$ - $ZrO_2$  can be transformed if the domains grow above a critical size[15]. Domain size, not grain size, controls  $t \rightarrow m$  transformation in  $t'$ - $ZrO_2$  alloys in contrast to conventional  $ZrO_2$  alloys which have monovariant grains.

Monovariant  $t$  grains give rise to monoclinic grains having four variants[16]. Orientation relationships for twinning are well established[17,18]. The space group, point group, and point group symmetry order for different phases of zirconia are listed in Table 1. Based on group theory, three (48/16) possible orientation states have been identified for the  $c \rightarrow t$  transformation leading to the three tetragonal variants. Twelve (48/4) possible orientation states can be predicted for cubic  $\rightarrow$  monoclinic transformation. In essence, each of the three tetragonal domains can give rise to four monoclinic variants.

Muddle and Hannink[19] observed 12 different monoclinic orientations in Mg-PSZ solution treated in the cubic phase region and rapidly cooled to room temperature before annealing in the cubic and tetragonal phase field. The tetragonal phase precipitated out from the cubic matrix during annealing and subsequently transformed to monoclinic upon cooling. Each  $t$  precipitate gave rise to four  $m$  variants. The cubic matrix phase was used as a reference and the orientation relationship between cubic and tetragonal phases was assumed to be identical between the principle axes. The selected area electron diffraction (SAD) pattern coincided with that expected for the 12 permitted monoclinic orientations[19]. Domain formation can also occur due to the stress-assisted transformation[3].

Hayakawa et al.[20,21] studied arc melted  $t'$   $ZrO_2$ -2 mol. %  $Y_2O_3$  alloy. The monoclinic phase was introduced by annealing at 540 K. TEM showed that the  $t \rightarrow m$  transformation comprises four variants of martensite plates having the common  $c_m$ -axis.

The purpose of the present communication is to compare microstructures of monoclinic  $ZrO_2$  prepared in two different ways: 1)  $t \rightarrow m$ , and 2)  $c \rightarrow t' \rightarrow m$  in order to

explain the structural integrity of materials made by the latter approach[6] in comparison to m-ZrO<sub>2</sub> which macrocracks when sintered in the t regime and cooled through the t-->m transformation.

## II. EXPERIMENTAL PROCEDURE

Samples were prepared from monoclinic ZrO<sub>2</sub> powder (TOSOH Grade TZ-0) by uniaxially pressing  $\approx$ 12 mm diameter x 20 mm rods at 35 MPa followed and isostatic pressing at  $\approx$ 200 MPa. The rods were packed in the same powder and sealed in a graphite crucible before heating in Ar atmosphere inside a laboratory-designed graphite foil resistance-heated furnace. The samples were sintered in the range 1600° to 2225°C for times of 10 minutes to 16 hours. After sintering, the samples were rapidly cooled to room temperature. The samples used for x-ray diffraction and microscopy were cut off from the center part of the rods.

XRD traces were obtained using CuK $\alpha$  radiation with a scanning speed of 2° per minute covering a range of 2 $\theta$  between 15° and 70°. Samples which did not macrocrack were polished with diamond paste to a 1  $\mu$ m finish and viewed in reflected light. Samples for TEM work were prepared by dimple grinding thin disks followed by ion-milling to perforation. The perforated samples were coated with a thin ( $\sim$ 50 Å) layer of carbon to prevent charging in TEM. Bright Field (BF) images were taken for the microstructure studies.

SAD was applied to identify the orientation of the monoclinic variants. (010) and (001) reflections are forbidden, but (100) is not. Considering the appearance of (100) reflection, the difference of d-spacing for (200), (020), and (002) reflections, and the angle between a and c axis, every diffraction spot in the electron diffraction pattern can be indexed. Therefore, the corresponding diffraction zone axis for the diffraction pattern can be determined.

## III. RESULTS

For the samples sintered above 2000°C, no macroscopic cracks could be detected. Figure 1(a) shows an optical microscopy of a sample sintered at 2225°C. The microstructure was similar to that observed by Cutler, et al.[6] with a thin Zr or ZrC region between grains. For samples sintered below 1950°C, extensive cracking always occurred. In Figure 1(b), an optical microscopy of a sample sintered at  $\approx$ 1600°C for 10 hours is shown.

XRD traces of all the samples with different sintering temperatures exhibited patterns corresponding to a single phase with monoclinic crystal structure. From XRD file, the lattice parameters for monoclinic phase are  $a = 5.1477 \text{ \AA}$ ,  $b = 5.2030 \text{ \AA}$ ,  $c = 5.3156 \text{ \AA}$ , and  $\beta = 99.38^\circ$ . X-ray diffraction patterns were similar to those shown by Cutler, et al. in Figure 11 of ref. 6. Zr or ZrC at grain boundaries were below the detection limits from the XRD patterns. No difference in lattice parameters for m-ZrO<sub>2</sub> was observed for samples heated at various temperatures in accord with the earlier work of Cutler, et al.[6].

TEM SAD patterns were taken from  $\langle 100 \rangle_m$  zone axes. With a large selected-area aperture, the diffraction pattern looked very complicated. However, using the smallest aperture ( $\approx 0.8 \text{ \mu m}$  diameter area), SAD patterns showed the diffractions with different orientation and twin pattern corresponding to the twin colonies in the bright field images.

Figure 2(a) is a bright field image of a sample sintered at 2225°C and Figure 2(b) is the corresponding electron diffraction pattern. In Figure 2(a), the BF micrograph showed twin colonies with different orientation and some microcracks between the colonies with different orientation. The appearance of microcracks is very similar to the presence of kinks in metal systems to accommodate the twinning shear[22]. The regions of twin colonies with different orientation or morphology were labeled as A, B and C. SAD was applied on region A, B and C in Figure 2(a) with the corresponding SAD patterns shown in Figure 3(a), 3(b) and 3(c), respectively. Area A contains  $[010]$  and  $[0\bar{1}0]$  zone axes as well as the  $[\bar{1}00]$  or  $[100]$  zone axis. However, the diffraction patterns from the  $[\bar{1}00]$  or  $[100]$  zone axis are the same. From crystal symmetry, it can be expected that both zone axes could appear simultaneously. The indexed schematics of  $[010]$ ,  $[0\bar{1}0]$ ,  $[\bar{1}00]$  and  $[100]$  zone axes are shown in Figure 4(a).

Region B (see Fig. 3(b)) contains  $[001]$  or  $[00\bar{1}]$  zone axis diffraction patterns and the same patterns with 90° rotation about  $[001]$ . However, the diffraction patterns from  $[00\bar{1}]$  or  $[001]$  zone axis are the same. From crystal symmetry, it can be expected that both zone axes could appear simultaneously. The indexed schematics of  $[00\bar{1}]$  or  $[001]$  zone axes are shown in Figure 5(b). In area C, the diffractions are exactly the same as those in area A with 90° rotation about  $[010]$  axis.

From the above analysis, eight variants (4 variants from  $[010]$  and  $[0\bar{1}0]$  axes, 2 variants from  $[100]$  axis, and 2 variants from  $[001]$  axis) were found directly from the SAD patterns. Another four variants (2 variants from  $[\bar{1}00]$  axis and 2 variants from  $[00\bar{1}]$  axis) are expected from crystal symmetry. Totally, twelve variants exist in the examined grain.

For the sample sintered at  $\approx 1600^\circ\text{C}$  for 10 hours, the bright field micrograph and the corresponding electron diffraction pattern are shown in Figure 5(a) and 5(b). Both micrographs and diffraction patterns are generally similar to those of the sample sintered at

2225°C. However, some significant differences can be pointed out. From BF micrographs, continuous cracks along grain boundaries were present in the sample sintered at 1600°C but not in the sample sintered at 2225°C. From SAD, fewer domain orientation can be found from one grain in the sample sintered at 1600°C than the sample sintered at 2225°C. At most, 8 domains can be expected in the sample sintered and annealed in the t phase field whereas 12 domains exist in the cooled from the c stability field.

#### IV. DISCUSSION

The present results, in accordance with the earlier work of Sense[23] and Cutler, et al.[6], show that samples sintered at lower temperatures macrocrack extensively whereas samples sintered higher temperature do not. These results will be considered to be related to phase transformation. As expected samples sintered below  $\approx 1950^\circ\text{C}$  extensively cracked due to the t $\rightarrow$ m transition with its large shape and volume change. However, ZrO<sub>2</sub> sintered above 2000°C did not macrocrack. As discussed by Cutler, et al.[6] this is not related to metal or carbide phase formation at grain boundaries but is rather related to ferroelasticity.

As discussed recently by Rice[24], it is well known that while the c $\rightarrow$ t transformation temperature is well established for ambient conditions, it is highly dependent on oxygen vacancy concentration in ZrO<sub>2-x</sub> in reducing conditions. Phase diagrams[25-27] for ZrO<sub>2-x</sub>, show an extremely rapid drop in the c $\rightarrow$ t phase boundary as ZrO<sub>2</sub> is reduced to  $\approx\text{ZrO}_{1.98}$ . Since oxygen stoichiometry in a graphite furnace is a function of atmosphere and reduction kinetics, it is not surprising that there is no fixed temperature where crack-free samples are obtained and hence the temperature variations between the present work ( $>2000^\circ\text{C}$ ) and previous investigators ( $>2250^\circ\text{C}$ [23], and  $>2300^\circ\text{C}$ [6]). The advantage of the furnace used in the present work was that rapid heating was possible reducing the total time at high temperatures. In the present work, macrocracking suggests that in samples heated above 2000°C were in the cubic region whereas below 1950°C the samples were sintered in the tetragonal phase field.

For phase transformation from c $\rightarrow$ t', three variants can be expected based on the group theory. Because the original phase is cubic, it can be expected that the domains from phase transformation with different variant (or orientation) will distribute evenly in one grain. The geometric change of the grain can also be expected to be close to an isotropic condition.

Comparing with the earlier work of Muddle and Hannink[19], the SAD results are very similar. However, the origin for the formation of monoclinic phase is very different.

In work on PSZ[19], the tetragonal phase precipitated out from the cubic matrix then transformed into monoclinic phase. Each t precipitate gave rise to four monoclinic variants. In the present work, however, the phase transformations are accomplished by diffusionless transformation as  $c \rightarrow t'$  so that each grain is composed of all 12 variants. In an air environment, there would not be any need for fast cooling since there is no two phase t+c phase field to enter with monoclinic  $ZrO_2$ . Hence, coarse-grained materials can be made which withstand the  $t' \rightarrow m$  transformation due to domain formation accommodating the shape and volume changes.

For phase transformation from tetragonal to monoclinic, four variants can be expected based on the group theory. It means that in a tetragonal phase with unique direction (or single domain), four correlated monoclinic phase domains can be produced through phase transformation. Therefore, from cubic to monoclinic, totally twelve variants can be expected. For the sample sintered above  $2000^\circ C$  and rapidly cooled, each  $t'$  grain has multiple domains[5, 11-15] which in turn transform into monoclinic domains with four possible variants. Because the monoclinic domains result from the tetragonal domains, the monoclinic domain size may be smaller than tetragonal domain size. The present TEM results did not differentiate any difference in domain size.

All grains should be evenly distributed to accommodate stress. However, for the samples sintered below  $1950^\circ C$ , each grain is a single tetragonal domain. Through the phase transformation from tetragonal to monoclinic, cracks can be expected since some strains can not be accommodated by the four monoclinic variants resulting in both intergranular and intragranular microcracks and macrocracks.

Based solely on crystallography, up to 24 variants are possible for the  $t \rightarrow m$  transformation[28]. However, only low shear solutions occur in practice. The variants, resulting in larger strains, are not favored from the point of view of elastic strain energy. From group theory, only 4 variants can be predicted for the  $t \rightarrow m$  transformation. However, the  $t \rightarrow m$  phase transition is also ferroelastic[4] and it is therefore possible to get additional variants due to stress-induced domain switching. This explains why more than 4 variants may be observed, as in the present study, for materials sintered in the tetragonal stability field. However, the stress induced domain switching will not result in an even distribution for the domain orientation, but will depending on the direction of applied stress[13-15]. The strongest evidence for increased domain formation for samples sintered at high temperatures is the ability of such samples to withstand repeated cycling through the  $m \leftrightarrow t$  transition temperatures[6].

## V. SUMMARY

Polycrystalline monoclinic  $ZrO_2$  samples sintered in the tetragonal phase field exhibit extensive macrocracking when cooled below the t $\rightarrow$ m transformation, in sharp contrast to samples sintered in the tetragonal stability field and then annealed in the cubic phase field and subsequently cooled. All materials have similar lattice parameters and only show monoclinic phase based on x-ray diffraction. From selected area electron diffraction,  $ZrO_{2-x}$  grains heated to 2225°C have more variants than the monoclinic zirconia sintered at 1600°C. The number of variants experimental determined for materials cooled from the cubic stability regime is consistent with the prediction from group theory. Ferroelastic domain formation and switching allows polycrystalline monoclinic zirconia to be fabricated without macrocracking when cooled from the cubic stability regime.

Acknowledgements: This work was supported by DARPA through AFOSR under Contract No. F49620-89-C-0054 to Ceramatec.

## REFERENCES

1. M. Yoshimura, "Phase Stability of Zirconia," *Am. Ceram. Soc. Bull.*, **67**[12] 1950-55 (1988).
2. J. W. Adams, H. N. Nakamura, R. P. Ingel and R. W. Rice, "Thermal Expansion Behavior of Single-Crystal Zirconia," *J. Am. Ceram. Soc.*, **68**[9] C-228-C-231 (1985).
3. D. J. Green, R. H. J. Hannink and M. V. Swain, *Transformation Toughening of Ceramics*. CRC Press, Boca Raton, FL, 1989.
4. V. K. Wadhawan, "Ferroelasticity and Related Properties of Crystals," *Phase Transitions*, **3**, 3-103 (1982).
5. A. V. Virkar, J. F. Jue, P. Smith, K. Mehta and K. Prettyman, "The Role of Ferroelastic Toughening of Brittle Materials," *Phase Transitions*, **35**, 27-46 (1991).
6. R. A. Cutler, J. R. Reynolds, and A. Jones, "Sintering and Characterization of Polycrystalline Monoclinic, Tetragonal, and Cubic Zirconia," *J. Am. Ceram. Soc.*, **75**[8] 2173-83 (1992).
7. R. P. Ingel, P. A. Willging, B. A. Bender and T. W. Coyle, "The Physical and Thermomechanical Properties of Monoclinic Single Crystals," pp. 459-69 in *Advances in Ceramics*, Vol. 24, *Science and Technology of Zirconia III*. Edited by S. Somiya, N. Yamamoto, and H. Yanigida. American Ceramic Society, Westerville, OH, 1988.
8. G. M. Wolten, "Diffusionless Phase Transformations in Zirconia and Hafnia," *J. Am. Ceram. Soc.*, **46** [9] 418-22 (1963).
9. H. G. Scott, "Phase Relationships in the Zirconia-Yttria System," *J. Mater. Sci.*, **10**, 1527-35 (1975).

10. R. A. Miller, J. L. Smialek, and R. A. Garlick, "Phase Stability in Plasma-Sprayed, Partially Stabilized Zirconia-Yttria," pp. 241-53 in *Advances in Ceramics, Vol. 3, Science and Technology of Zirconia*. Edited by A. H. Heuer and L. W. Hobbs. American Ceramic Society, Westerville, OH, 1981.
11. A. H. Heuer, R. Chaim, and V. Lanteri, "The Displacive Cubic  $\rightarrow$  Tetragonal Transformation in  $ZrO_2$  Alloys," *Acta Metall.*, **35**[3] 661-66, (1987).
12. V. Lanteri, R. Chaim, and A. H. Heuer, "On the Microstructures Resulting from the Diffusionless Cubic  $\rightarrow$  Tetragonal Transformation in  $ZrO_2$ - $Y_2O_3$  Alloys," *J. Am. Ceram. Soc.*, **69**[10] C-258-C-261 (1986).
13. J. F. Jue and A. V. Virkar, "Fabrication, Microstructural Characterization, and Mechanical Properties of Polycrystalline t'-Zirconia," *J. Am. Ceram. Soc.*, **74**[12] 3650-57 (1990).
14. J. F. Jue, J. Chen and A. V. Virkar, "Characterization of t' Phase in Ce-TZP Materials," unpublished work.
15. J. F. Jue, J. Chen, and A. V. Virkar, "Low Temperature Phase Stability of t' Zirconia," *J. Am. Ceram. Soc.*, **74**[7] 1745-50 (1991).
16. S. K Chan, "Theory of the Energetics and Nonclassical Nucleation for the Tetragonal-Monoclinic Transformation of Zirconia," pp. 983-95 in *Advances in Ceramics, Vol. 24, Science and Technology of Zirconia III*. Edited by S. Somiya, N. Yamamoto, and H. Yanigida. American Ceramic Society, Westerville, OH, 1988.
17. D. K. Smith and H. W. Newkirk, "The Crystal Structure of Baddeleyite (Monoclinic  $ZrO_2$ ) and its Relation to the Polymorphism of  $ZrO_2$ ," *Acta Cryst.*, **18** 983-91, (1965).
18. E. Bischoff and M. Ruhle, "Twin Boundaries in Monoclinic  $ZrO_2$  Particles Confined in a Mullite Matrix," *J. Am. Ceram. Soc.*, **66**[2] 123-27 (1983).
19. B. C. Muddle and R. H. J. Hannink, "Crystallography of the Tetragonal to Monoclinic Transformation in MgO-Partial-Stabilized Zirconia," *J. Am. Ceram. Soc.*, **69**[7] 547-55 (1986).
20. M. Hayakawa, N. Kuntani and M. Oka, "Structural Study on the Tetragonal to Monoclinic Transformation in Arc-Melted  $ZrO_2$ -2 mol. %  $Y_2O_3$  Alloy," *Acta Metall. Mater.*, **37**[8], 2223-28, (1989).
21. M. Hayakawa, K. Adachi and M. Oka, "Crystallographic Analysis of the Monoclinic Herringbone Structure in an Arc-Melted  $ZrO_2$ -2 mol. %  $Y_2O_3$  Alloy," *Acta Metall. Mater.*, **38**[9], 1753-59, (1990).
22. Reference about kinks in metal systems
23. K. A. Sense, "A Method for Producing Very Dense  $ZrO_2$ ," *J. Am. Ceram. Soc.*, **44**[9] 465 (1961).
24. R. W. Rice, "Comment on "Black Color in Partially Stabilized Zirconia," *J. Am. Ceram. Soc.*, **74**[7] 1745-46 (1991).

25. E. G. Rauh and S. P. Garg, "The  $ZrO_{2-x}$  (cubic)- $ZrO_{2-x}$  (cubic+tetragonal) Phase Boundary," *J. Am. Ceram. Soc.*, **63**[3-4] 239-40 (1980).
26. R. Ruh and H. J. Garrett, "Nonstoichiometry of  $ZrO_2$  and Its Relation to Tetragonal-Cubic Inversion in  $ZrO_2$ ," *J. Am. Ceram. Soc.*, **50**[5] 257-61 (1967).
27. E. Gebhardt, H. D. Seghezzi, and W. Duerrschnabel, "Investigation of the Zirconium-Oxygen System: II," *J. Nucl. Mater.*, **4**[3] 255-68 (1961).
28. P. M. Kelly and C. J. Ball, "Crystallography of Stress-Induced Martensitic Transformations in Partially Stabilized Zirconia," *J. Am. Ceram. Soc.*, **69**[3] 259-64 (1986)

Table 1: Space group, point group and symmetry order of zirconia with different crystal structure.

Crystal System	Space Group	Point Group	Symmetry Order
Cubic	Fm3m	m3m	48
Tetragonal	P4 <sub>2</sub> /nmc	4/mmm	16
Monoclinic	P2 <sub>1</sub> /c	2/m	4

## FIGURE CAPTIONS

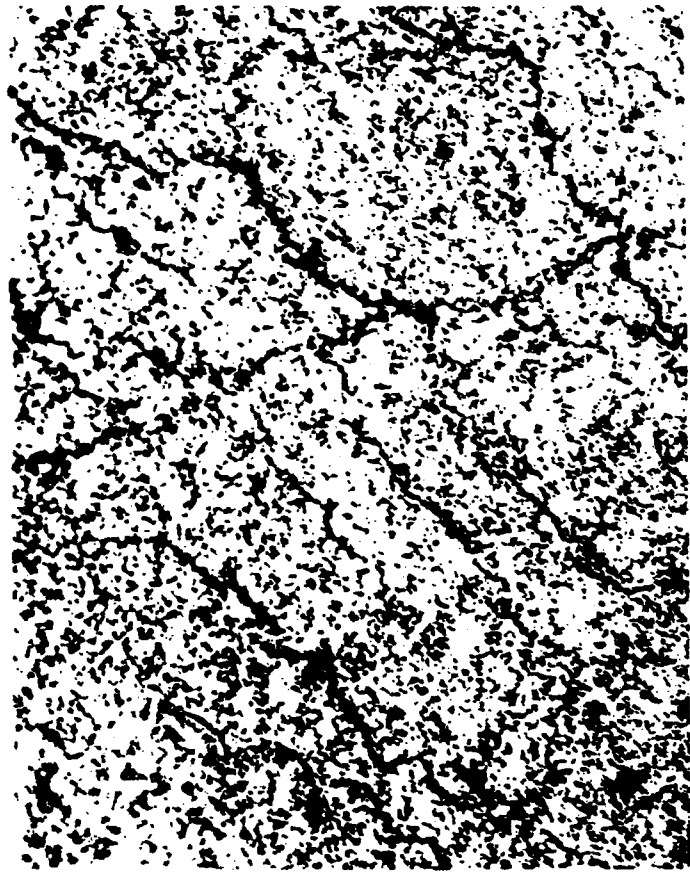
- Figure 1(a): An optical microscopy of a sample sintered at 2225°C for 10 minutes.
- Figure 1(b): An optical microscopy of a sample sintered at  $\approx 1600^\circ\text{C}$  for 10 hours, extensive crack can be found.
- Figure 2(a): A bright field TEM image of a sample sintered at 2225°C showing very complicated microstructure labeled as region A, B and C.
- Figure 2(b): The corresponding electron diffraction pattern from the most part in Figure 2(a).
- Figure 3(a): The Selected-Area-Diffraction pattern corresponds to the region A in Figure 2(a).
- Figure 3(b): The Selected-Area-Diffraction pattern corresponds to the region B in Figure 2(a).
- Figure 3(c): The Selected-Area-Diffraction pattern corresponds to the region C in Figure 2(a).
- Figure 4(a): The indexed schematics of electron diffraction patterns corresponding to  $[010]$ ,  $[0\bar{1}0]$ ,  $[\bar{1}00]$  and  $[100]$  zone axes.
- Figure 4(b): The indexed schematics of electron diffraction patterns corresponding to  $[00\bar{1}]$  or  $[001]$  zone axes.
- Figure 5(a): A bright field TEM image of a sample sintered at 1600°C.
- Figure 5(b): The corresponding electron diffraction pattern for the micrograph shown in Figure #6(a).



100  $\mu\text{m}$

ZrO<sub>2</sub> 2200°C 10 min 200X  
in Ar

Figure # 1 (a)



100  $\mu$ m

ZrO<sub>2</sub> 15% 1000°C

Figure # 1 (b)



600 mm

A

B

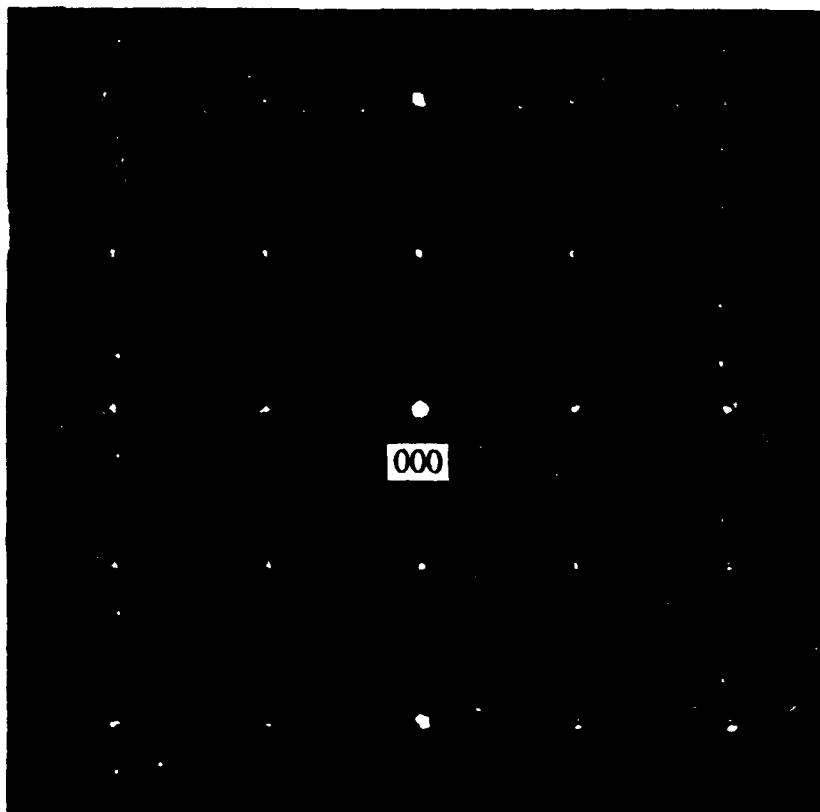


Figure # 2 (b)

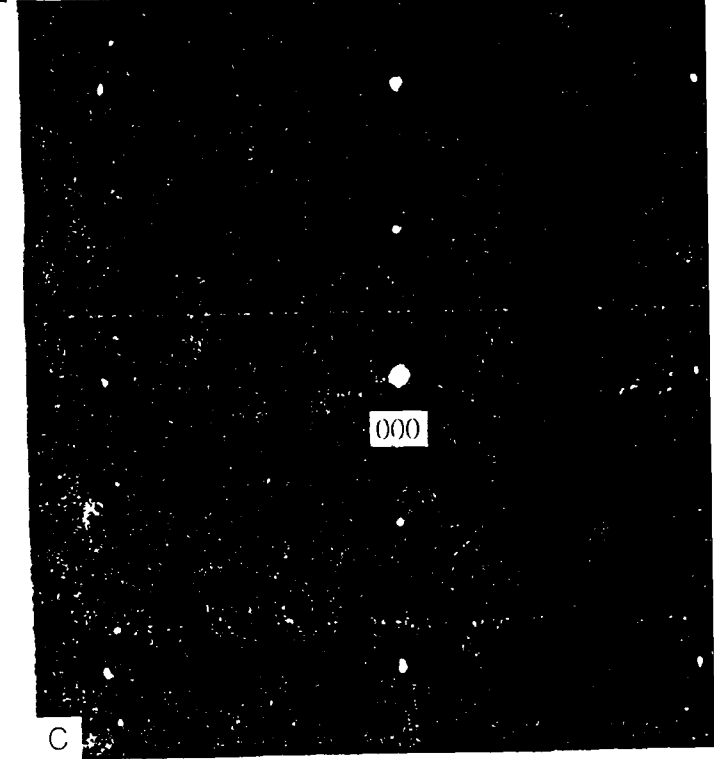
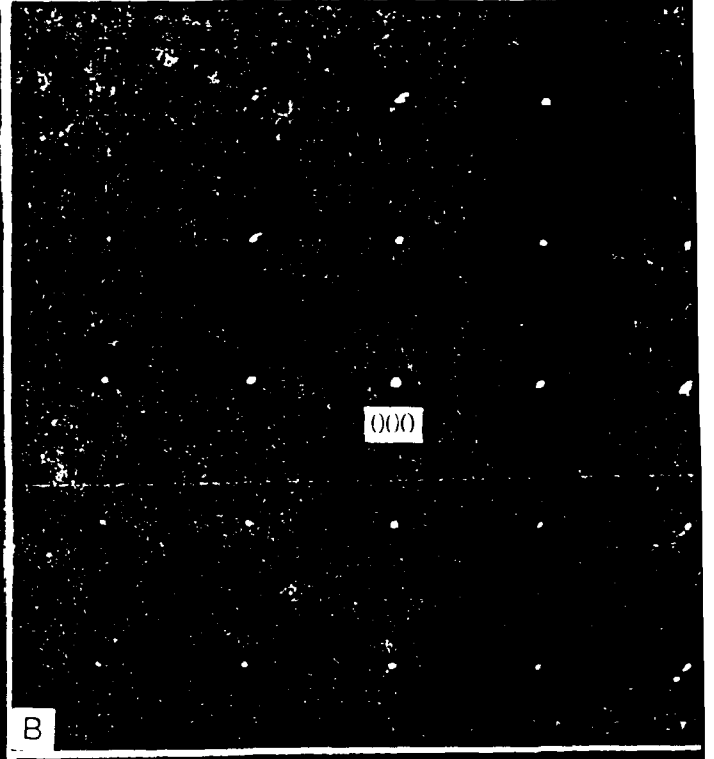
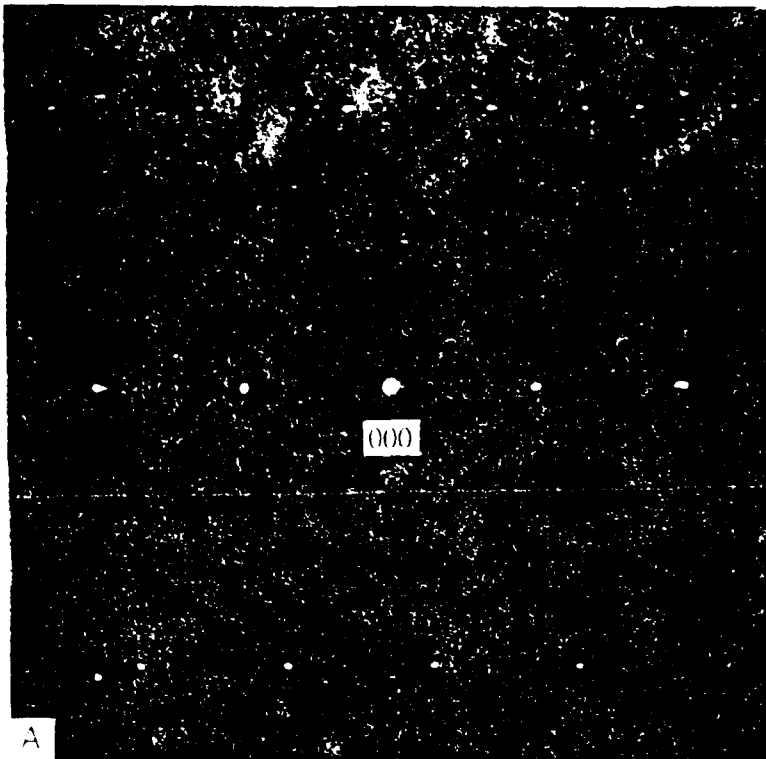


Figure # 3 a, 3 b, 3 c

e diffraction pattern for a 2D lattice

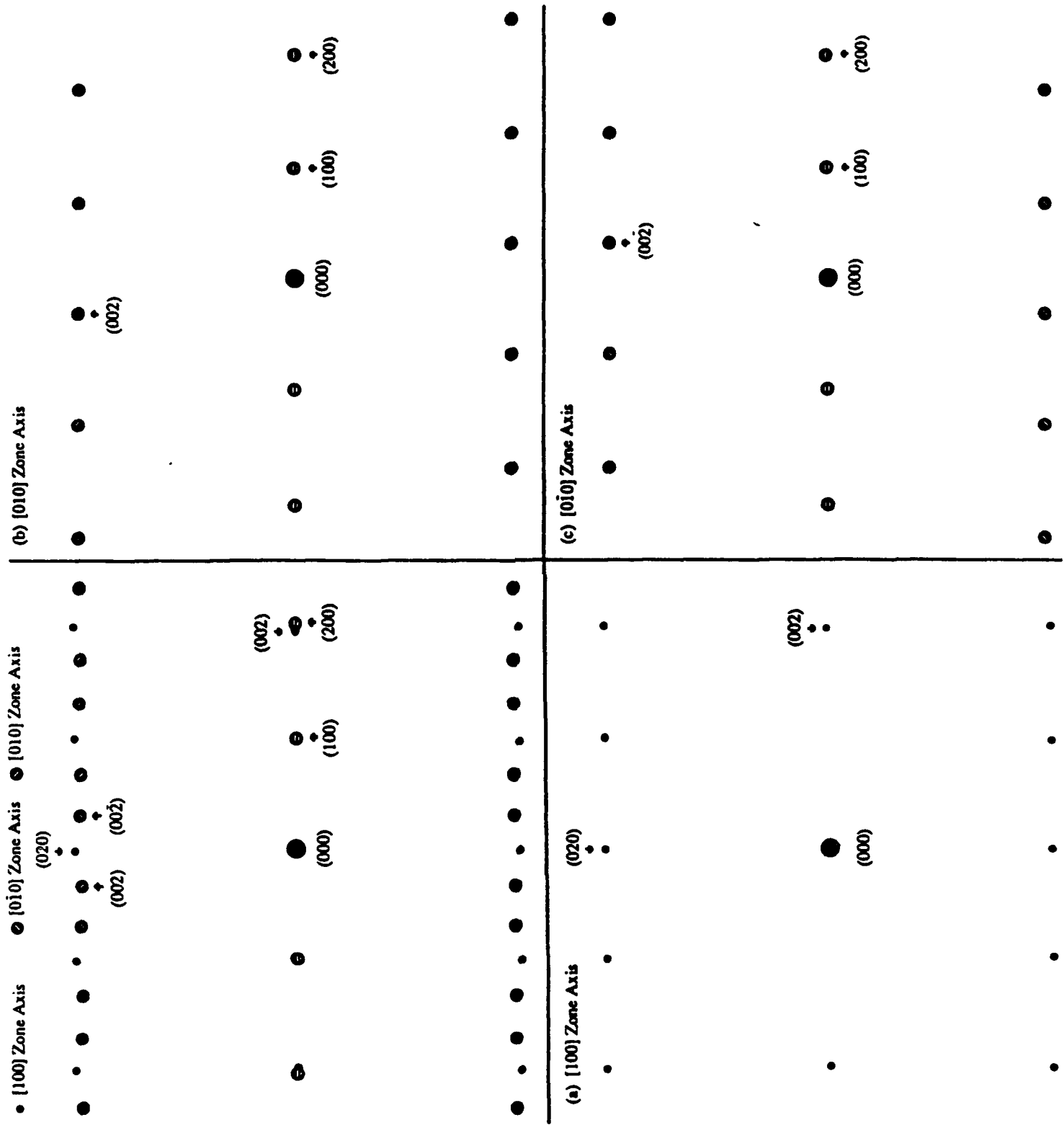
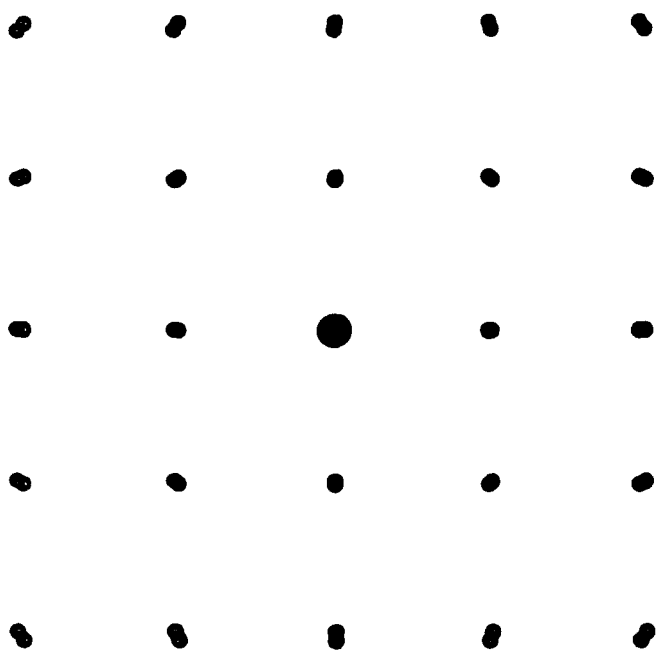


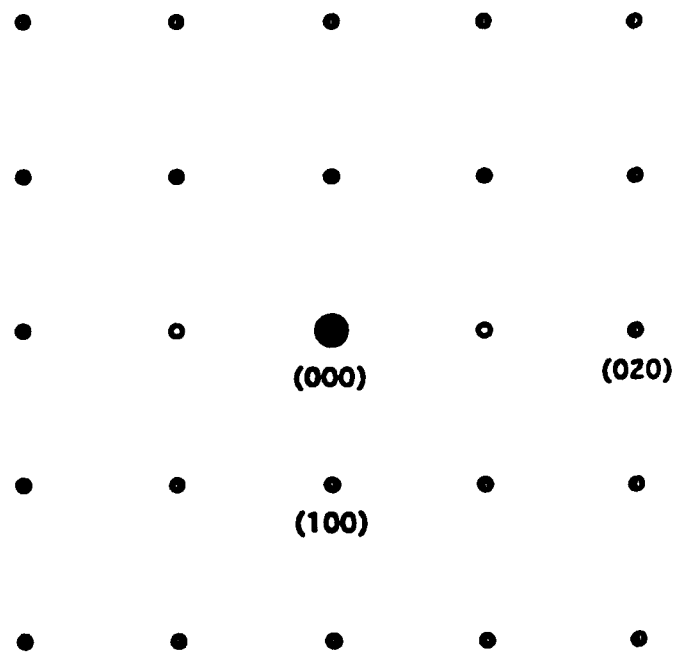
Figure # 4(a)

e diffraction pattern for B area

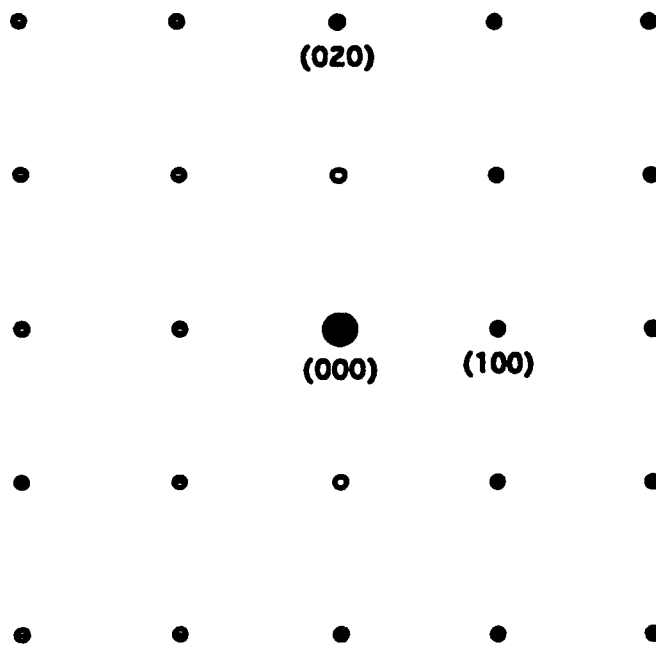
[001] Zone Axis with Twin Structure



(b)



(a)



(O's indicate forbidden reflections that may show up as a result of double diffraction)

Figure # 4(b)



Figure # 5(a)



Figure # 5 (b)